SYNTHESIS AND PROPERTIES OF MANISYL-SUBSTITUTED PYRIDYL-1,10-PHENANTHROLINES AND THE CHEMICAL TOPOLOGY OF INTERLOCKING RINGS

Dissertation zur Erlangung
der naturwissenschaftlichen Doktorwürde
(Dr. sc. nat.)

vorgelegt der
Mathematisch-naturwissenschaftlichen Fakultät
der Universität Zürich

Jeremy K. Klosterman
USA

Promotionskomitee:
Prof. Dr. Jay S. Siegel (Vorsitz)
Prof. Dr. Oliver Zerbe
Prof. Dr. Reto Dorta

UNIVERSITÄT ZÜRICH
2007

Die vorliegende Arbeit wurde von

der Mathematisch-naturwissenschaftlichen Fakultät

der Universität Zürich im Februar 2007

als Dissertation angenommen.

Promotionskomitee:

Jay S. Siegel, Vorsitz

Prof. Oliver Zerbe

Prof. Dr. Reto Dorta

Universität Zürich
Zürich, Switzerland 2007

For my parents,

Keith and Caren Klosterman

TABLE OF CONTENTS

Signature Page	iii
Dedication	iv
Table of Contents	v
List of Figures	viii
List of Schemes	xvi
List of Tables	xix
Acknowledgements	xxii
Curriculum Vitae	xxiii
Abstract of the Dissertation	xxv
Zusammanfassung	xxvii
Chapter 1. Chemical Topology	1
1.1 Introduction	2
1.1.1. Knot Theory and Topology	5
1.1.2 Stereochemistry and Topology	7
1.1.3 Chirality and Topological Chirality	9
1.1.4 Non-planar Graphs	11
1.1.5 Topological Stereochemistry of Links	13
1.1.6 Techniques for Identifying Links and Topological Chirality	15
1.2. Initial Strategies for the Synthesis of Interlocking Rings	17
1.2.1 Statistical Methods	19
1.2.2 Directed Methods	20
1.2.3 Möbius Strips and Ladders	22
1.3 Templated Synthesis of Topological Graphs	26
1.3.1 Metal Ion Templates	26
1.3.2 π-Donor π-Acceptor Templates	30
1.3.3 Hydrogen Bonding Templates	31
1.4 Thesis Objectives	35
1.5 References	37
Chapter 2. Synthesis of 2-Pyridyl-[1,10]phenanthrolines	43
2.1 Introduction	44
2.1.1 Condensation Methods	45

2.1.2 Nucleophilic Additions 48
2.1.3 Palladium Catalyzed Cross Coupling 50
2.2 Current Work 55
2.2.1 Introduction 55
2.2.2 Retrosynthesis 56
2.2.3 Synthesis 58
2.2.4 Results and Discussions 61
2.2.5 Conclusions 66
2.3 Experimental 67
2.4 Crystal Structure Data 88
2.5 References 91
Chapter 3 Photophysics of 2-Pyridyl-[1,10]phenanthrolines 95
3.1 Introduction 96
3.1.1 Photophysical Processes 97
3.1.2 The Franck-Condon Principle 101
3.1.4 Intramolecular Charge Transfer 103
3.1.4 Photophysics of Polypyridines 106
3.2 Current Work 114
3.2.1 Introduction 114
3.2.2 Results 116
3.2.3 Discussion 137
3.2.4 Conclusions 140
3.3 Experimental 142
3.4 References 144
Chapter 4 Coordination Chemistry of 2-Pyridyl-[1,10]phenanthrolines 148
4.1 Introduction 149
4.1.1 Ruthenium(II) and (III) Complexes 151
4.1.2 Copper(I) and (II) Complexes 156
4.1.3 Palladium(II) complexes 158
4.1.4 Platinum(II) and other metal complexes 159
4.2 Current Work 163
4.2.1 Introduction 163
4.2.2 Synthesis 163

4.2.3 Results and Discussion 169
4.2.4 Conclusions 217
4.3 Experimental 219
4.4 Crystal Structure Data 240
4.5 References 258
Chapter 5 The Borromean Link 265
5.1 Introduction 266
5.1.1 The Borromean Rings throughout History 267
5.1.2 Topology of Borromean Rings 270
5.1.3 Molecules containing the Borromean Topology 271
5.2 Current Work 278
5.2.1 Introduction 278
5.2.2 Retrosynthetic analysis 278
5.2.3 Synthesis and Results 280
5.2.4 Discussion and Outlook 299
5.2.5 Conclusions 304
5.3 Experimental 306
5.4 Crystal Structure Data 332
5.5 References 346

LIST OF FIGURES

Figure 1.1	Kekulé's dream.	2
Figure 1.2	Depictions of ethanol by (a) Kekule; (b) Couper; (c)Crum Brown; and (d) modern chemists.	3
Figure 1.3	Optical isomers of tartaric acids; van't Hoff's (a) d-form (b) l-form (c)meso-form and (d) the modern version	4
Figure 1.4	Topologically equivalent shapes.	5
Figure 1.5	Simple knots and links; (a) the unknot, 0_1^1, (b) the trefoil knot, 3_1, (c) the Hopf link 2_1^2.	5
Figure 1.6	Three embeddings of the figure-eight knot	6
Figure 1.7	A complicated embedding of an unknot.	6
Figure 1.8	Reidemeister moves	7
Figure 1.9	Constitutional isomers	7
Figure 1.10	Stereoisomers	8
Figure 1.11	Topological stereoisomers	8
Figure 1.12	Interconversion of enantiomers.	10
Figure 1.13	A deformation of a figure eight knot to its mirror image.	10
Figure 1.14	A rigidly achiral embedding of the figure eight knot	11
Figure 1.15	Molecular graphs of (a) alkanes up four carbons and (b) stilbene.	11
Figure 1.16	Planar embeddings of (a) (-)-(R,R,R,R)-[6]chochin[44] and (b) buckminsterfullerene.	12
Figure 1.17	Two examples of molecules with non-planar graphs; (a) The Simmons-Paquette Molecule,[41,43] and (b) Siegel's Kuratowski cyclophane.	12
Figure 1.18	The Kuratowski graphs, K_5 and $K_{3,3}$	13
Figure 1.19	Topologically chiral links: (a) The oriented Hopf Link, 2_1^2, (b) link 4_1^2, (c) the Whitehead link 5_1^2.	14
Figure 1.20	Three-Links; (a) Composite link $2_1^2 \# 2_1^2$, (b) Torus link 6_1^3, (c) Link 12_1^3, (d) The Borromean link 6_2^3.	15
Figure 1.21	Positive and negative crossings.	16

Figure 1.22	Relationships between geometrical, chemical, and topological chirality and achirality.	17
Figure 1.23	M.C. Escher's famous interpretation of a Möbius band.	22
Figure 1.24	A Möbius strip and its graph, a Möbius ladder.	23
Figure 1.25	Organometallic catenanes of Fujita and Bickelhaupt	29
Figure 1.26	Pseudorotaxane host-guest complex of bis-*p*-phenylene-34-crown-10 and paraquat.	30
Figure 1.27	Complexation of *p*-benzoquinone by host **34**	31
Figure 1.28	Leigh-type amide [2]-catenane.	33
Figure 1.29	Vögtle's "knotane", a molecular trefoil knot.	34
Figure 1.30	Busch's ammonium-type hydrogen bond template.	35
Figure 2.1	Metal Templated Synthesis of a chiral Hopf link.	44
Figure 2.2	Chemical (a) and schematic (b) representations of terpy **45** and pherpy **46** with the alpha (red), beta (green), and gamma (blue) positions highlighted.	45
Figure 2.3	Retrosynthetic analysis and common building blocks	56
Figure 2.4	Manisyl pyridyl-phenanthrolines.	57
Figure 2.5	Crystal structures of pyridyl-phenanthrolines **111** and **114**	64
Figure 3.1	Orbital level energy diagram of absorption, (A) and (B), and emission, (C) and (D), processes.	98
Figure 3.2	A simplified Jablonski energy state diagram illustrating key photophysical transitions.	98
Figure 3.3	(a) Sharp absorption and emission spectra from gas phase atoms; (b) absorption and emission spectra with vibrational structure from molecules in the gas-phase; and (c) broad, structureless absorption and emission from molecules in solution.	101
Figure 3.4	The Franck Condon principle.	103
Figure 3.5	Scheme of the photoinduced electron transfer between nearly non-interacting D and A. Regardless of whether excitation occurs into the D or A LE* state, the same CT* state forms.	103

Figure 3.6	a) Rotation around a single bond between the excited state donor ($D^{\bullet+}$) and acceptor ($A^{\bullet-}$). b) TICT model of DMABN, where B* (normal) is the locally excited state and A* (abnormal) is the excited charge transfer state.	104
Figure 3.7	Solvent effects on emission spectral wavelength for a fluorophore with an ICT excited state.	104
Figure 3.8	Unoccupied low-lying $b_1(\psi)$ and $a_2(\chi)$ orbitals of phenanthrolines	109
Figure 3.9	3 × 3 Pyridyl-phenanthroline matrix.	116
Figure 3.10	Absorption spectra of manisyl-substituted pyridyl-phenanthrolines **111 – 119**.	117
Figure 3.11	Solvent dependence of the absorption maxima for the first transition.	121
Figure 3.12	Emission spectra of manisyl-substituted pyridyl-phenanthrolines **111 – 119**.	123
Figure 3.13	Fluorescent quantum yields and their dependence on manisyl position; alpha-, beta- and gamma- relative to the phenanthroline or pyridine nitrogens; and solvent.	125
Figure 3.14	Dependence of fluorescence quantum yield on solvent polarity.	126
Figure 3.15	Plot of emission energy (in wave numbers, $cm^{-1} \times 10^{-3}$) against solvent $E_T(N)$ values.	128
Figure 3.16	Excitation spectra of manisyl-substituted pyridyl-phenanthrolines **111 – 119**	129
Figure 3.17	Plot of mean fluorescence lifetimes against solvent polarity $E_T(N)$ values.	132
Figure 3.18	Plot of radiative rate constants k_f against solvent polarity $E_T(N)$ values.	132
Figure 3.19	Fluorescence lifetime dependence on wavelength of **116** in ethanol	133
Figure 3.20	Calculated energies for the frontier orbitals of 1,10-phenanthroline (phen) **126,** terpyridine (terpy) **45**, and 2-pyridyl-phenanthroline (pherpy) **46**.	134
Figure 3.21	HOMO and LUMO MO diagrams of a)phenanthroline; b) terpyridine; and c) pyridyl-phenanthroline.	135

Figure 3.22	HOMO and LUMO MO orbitals of pyridyl-phenanthrolines a) **112**; b) **115**, and c) **118**.	137
Figure 3.23	Simplified energy diagram showing dual emission due to solvent stabilization of the charge-transfer (CT*) state	138
Figure 4.1	Changes in terpyridine conformation upon binding.	150
Figure 4.2	Complexation as a bidentate phenanthroline analogue **146** or terdentate terpyridine analogue **147**.	152
Figure 4.3	Saturated and unsaturated bridged terpyridine analogues.	153
Figure 4.4	ORTEP diagram of Ru(**154**-*N,N',N''*)(**154**-*N,N'*)Cl.	154
Figure 4.5	Copper(I) pyridyl-phenanthroline complex **164** and ORTEP diagram.	157
Figure 4.6	Copper(II) pyridyl-phenanthroline complex **165** and ORTEP diagram.	158
Figure 4.7	CPK representations of pyridyl-phenanthroline complexes **173** – **179**	170
Figure 4.8	Ortep diagram of $Fe(pherpy)_2$-$2PF_6$ **173** showing the squeezing and spreading of manisyl groups.	174
Figure 4.9	Crystal packing of $Fe(pherpy)_2$-$2PF_6$ **173** with a) the view perpendicular to the right-handed double helix and b) the view showing the intra-molecular π-stacking interactions between adjacent ligands within a single strand of the double helix.	175
Figure 4.10	Crystal packing of $Fe(pherpy)_2$-$2PF_6$ **173** showing a) intra-strand π-stacking and b) close-up view showing offset.	176
Figure 4.11	Crystal packing structure of $Fe(pherpy)_2$-$2PF_6$ **173** highlighting a) alternating double-helix strands and b) inter-strand interactions.	177
Figure 4.12	Crystal packing of $Fe(pherpy)_2$-$2PF_6$ **173** showing a) top- and b) side- views of double helix sheets.	177
Figure 4.13	Crystal packing of $Zn(pherpy)_2$-$2PF_6$ **177** with a) the view perpendicular to the right-handed double helix and b) the view showing the intra-molecular π-stacking interactions between adjacent ligands within a single strand of the double helix.	178

Figure 4.14	Crystal packing of Zn(pherpy) $_2$-2PF_6 **177**; a)intra-strand π-stacking and b) close-up view showing offset.	179
Figure 4.15	Crystal packing structure of Zn(pherpy) $_2$-2PF_6 **177** highlighting a) alternating double-helix strands and b) inter-strand interactions.	180
Figure 4.16	Crystal packing of Zn(pherpy) $_2$-2PF_6 **177** showing a) top- and b) side- views of double helix sheets.	180
Figure 4.17	CPK representations of terpyridine complexes **181** – **187**	182
Figure 4.18	Ortep diagram of Fe(terpy)$_2$-2PF_6 **181** showing the squeezing and spreading of manisyl groups.	185
Figure 4.19	Crystal packing of Fe(terpy) $_2$-2PF_6 **181** showing a) the view perpendicular to the right-handed double helix and b) the view showing the intra-molecular π-stacking interactions between adjacent ligands within a single strand of the double helix.	187
Figure 4.20	Crystal packing of Fe(terpy) $_2$-2PF_6 **181** showing a) intra-strand π-stacking and b) close-up view showing offset.	188
Figure 4.21	Crystal packing structure of Fe(terpy)$_2$-2PF_6 **181** highlighting a) alternating double-helix strands and b) inter-strand interactions.	189
Figure 4.22	Crystal packing of Fe(terpy) $_2$-2PF_6 **181** showing a) top- and b) side-views of double helix sheets.	189
Figure 4.23	Crystal packing of Zn(terpy) $_2$-2PF_6 **185** showing a) the view perpendicular to the right-handed double helix and b) the view showing the intra-molecular π-stacking interactions between adjacent ligands within a single strand of the double helix.	190
Figure 4.24	Crystal packing of Zn(terpy) $_2$-2PF_6 **185** showing a)π-stacking of independent dications in the unit cell and b) close-up view showing offset.	190
Figure 4.25	Crystal packing structure of Zn(terpy) $_2$-2PF_6 **185** highlighting a) alternating double-helix strands and b) inter-strand interactions.	191
Figure 4.26	Crystal packing of Zn(terpy) $_2$-2PF_6 **185** showing a) top- and b) side-views of double helix sheets.	191
Figure 4.27	Crystal packing of non-solvated Fe(pherpy)$_2$-2PF_6 **173** highlighting a)alternating double helix strands and b) intra-strand π-stacking.	193

Figure 4.28	Crystal packing of non-solvated $Fe(terpy)_2$-$2PF_6$-H_2O **181** highlighting a) alternating double helix strands and b) intra-strand π-stacking.	193
Figure 4.29	Crystal packing of non-solvated $Fe(pherpy)_2$-$2PF_6$ **173** showing a) top- and b) side- views of double helix sheets.	194
Figure 4.30	Crystal packing of non-solvated $Fe(terpy)_2$-$2PF_6$-H_2O **181** showing a) top- and b) side- views of double helix sheets.	194
Figure 4.31	600 MHz ^1H NMR spectrum of a CD_3CN solution of **174** $Co(pherpy)_2$-$2PF_6$.	197
Figure 4.32	600 MHz ^1H NMR spectrum of a CD_3CN solution of **182** $Co(terpy)_2$-$2PF_6$.	201
Figure 4.33	^1H NMR of pyridyl-phenanthroline **114** in $CDCl_3$ and its Ru(II) complex **189** in CD_2Cl_2.	202
Figure 4.34	UV-Vis absorption spectra of $M(pherpy)_2^{2+}$ in CH_2Cl_2.	204
Figure 4.35	UV-Vis absorption spectra of $M(terpy)_2^{2+}$ in CH_2Cl_2.	205
Figure 4.36	Normalized emission spectra of $M(pherpy)_2^{2+}$ in CH_2Cl_2	207
Figure 4.37	Normalized emission spectra of $M(terpy)_2^{2+}$ in CH_2Cl_2.	208
Figure 4.38	Normalized excitation spectra of (a) $M(pherpy)_2^{2+}$ and (b) $M(terpy)_2^{2+}$in CH_2Cl_2.	209
Figure 4.39	Normalized emission spectra of $Os(pherpy)_2^{2+}$ **179** (-blue-) and $Os(terpy)_2^{2+}$ **187** (-red-) in CH_2Cl_2.	210
Figure 4.40	Normalized emission spectra of $Os(pherpy)_2^{2+}$ **179** (-blue-) and $Os(terpy)_2^{2+}$ **187** (-red-) in CH_2Cl_2.	210
Figure 4.41	^1H-NMR titration of **178** in CD_2Cl_2 with $[NH_2Me_2][\Delta$-BINPHAT] in acetone-d_6.	212
Figure 4.42	^1H-NMR titration of **178** with $[n\text{-}Bu_3NH][\Lambda$-TRISPHAT] in CD_2Cl_2.	213
Figure 4.43	^1H-NMR titration of racemic **189** with $[n\text{-}Bu_3NH][\Delta$-TRISPHAT] in CD_2Cl_2.	214
Figure 4.44	400 MHz ^1H-NMR of **178**$[\Delta\text{-TRISPHAT}]_2$ in acetone-d_6.	215
Figure 4.45	Representation of **178**$[\Delta\text{-TRISPHAT}]_2$ showing the π-π stacking (d = 3.65 Å) and C-H $\cdots\pi$ interactions (d = 2.81).	216

Figure 4.46	Resolved topologically chiral catenands with C_2 symmetry.	217
Figure 4.47	ORTEP diagram of 5,6"-bis-(4-methoxy-2,6-dimethyl-phenyl)-[2,2':6',2"]terpyridine **190**.	256
Figure 5.1	The Borromean link.	266
Figure 5.2	van Gulick's construction of the Borromean link via a 3-braid.	267
Figure 5.3	(a) The Borromean Family crest and (b) the Ballantine Brewery logo.	268
Figure 5.4	The earliest known representation of the Trinity as the Borromean link.	269
Figure 5.5	The Valknut or Hrungnir's Heart with (a) Borromean and (b) trefoil topology.	269
Figure 5.6	Various presentations of the Borromean knot: (a) The Venn rings; (b) chain rings; and (c) orthogonal rings	270
Figure 5.7	Equivalent mirror images of a Borromean link with all three ring oriented.	271
Figure 5.8	Crystal structure of bipyridine 2-ring structure **200**. a) front view showing transoid bipyridines and b) side view showing compression of ring one and space available for threading.	274
Figure 5.9	Self-assembly of a nano-scale Borromeate.	276
Figure 5.10	Self-assembly of a chiral Borromeate.	276
Figure 5.11	Interpenetrating (6,3) layer containing the Borromean topology and reliant on (a) RCOO-Ni(II) coordination (b) Au-Au bonds, and (c) Ag-Ag bonds.	277
Figure 5.12	Formation of the three component supramolecular complexes through potassium cryptation by K.2.2.2. and I^-…I–C XB	277
Figure 5.13	(A) Ball-and-stick view of an infinite Borromean weave defined by ⋯ I^- ⋯ I–$(CF2CF2)_n$–I ⋯ interactions in the crystal structure of K.2.2.2, 1,8-diiiodoperfluorooctane, and potassium iodide; and (B) a space-filling representation of a single Borromean link from interwoven sheets.	277
Figure 5.14	ESI-MS of the new terpyridine two-ring complex **205**.	281
Figure 5.15	15 ESI-Spectra of unsuccessful attempts to thread a third ring precursor of the Borromean link using Ru(terpy)Cl_3 at 6 h.	282

Figure 5.16	ESI-mass spectra of four metal two-ring complexes **207** – **209**.	285
Figure 5.17	Geometrical changes upon metal complexation.	286
Figure 5.18	Crystal structure of fully compressed ring one **213**.	287
Figure 5.19	Crystal structure of [**197**][$Zn(OTf)_2]_2$.	289
Figure 5.20	Crystal structure of the threaded two-ring precursor **199**.	290
Figure 5.21	Linear hydrogen bonding motif of **199**.	291
Figure 5.22	Complementary CH $\cdots$ π interactions of a) neighboring cations and b) linear hydrogen bond networks, creating 2-D sheets.	292
Figure 5.23	Crystal structure of terpyridine two-ring **205**	293
Figure 5.24	Circumference of the second ring from (a) **205**, containing a terpyridine; and from (b) **200** containing a bipyridine.	299
Figure 5.25	Expansion of ring one complexes a) **213**; b) **214**; c)**199**; d) **200**; and e) **205**.	301
Figure 5.26	Off-set of ring one complexes a) **213**; b) **214**; c)**199**; d) **200**; and e) **205**.	301
Figure 5.27	Potential heteroleptic pre-complexes with large pocket depths.	304
Figure 5.28	ORTEP diagram of [Zn(5,5'-bis-(4-methoxy-2,6-dimethyl-phenyl)-2,2'-bipyridine)$_3$][$PF_6]_2$ **212**	337
Figure 5.29	ORTEP diagram of 4,4"-bis-(4-(4-methoxyphenyl)-2,6-dimethyl-phenyl)-2,2':6',2"-terpyridine **218**	343
Figure 5.30	ORTEP diagram of Ru[(4,4"-bis-(2,6-dimethyl-(4-hydroxyphenyl)-phenyl)-2,2':6',2"-terpyridine)(5,5"-dibromo-2,2':6',2"-terpyridine)][$PF_6]_2$ **224a**.	345

LIST OF SCHEMES

Scheme 1.1	Lüttringhaus's theoretical pathways towards catenane synthesis.	18
Scheme 1.2	The Wasserman catenane synthesis	20
Scheme 1.3	Schill's directed synthesis strategy.	21
Scheme 1.4	The Schill-Lüttringhaus catenane synthesis.	21
Scheme 1.5	Graphs resulting from the scission of *n* half-twisted Möbius ladders.	23
Scheme 1.6	Wolovsky's and Wasserman's Möbius metathesis method of making catenanes.	24
Scheme 1.7	Key steps in Walba's synthesis of a topologically chiral Möbius Strip.	25
Scheme 1.8	(a) Potassium ion templated synthesis of 18-crown-6 and the use of nickel(II) to template tetraazamacrocycles by (b) Curtis and (c) Busch.	27
Scheme 1.9	Synthetic strategies based on a three-dimensional transition metal template.	28
Scheme 1.10	Sauvage's transition metal templated catenane synthesis.	29
Scheme 1.11	Stoddart's first π-donor π-acceptor catenane.	31
Scheme 1.12	Hunter-Vögtle synthesis of [2]-catenanes.	32
Scheme 2.1	Possible (a) Skraup[6] and (b) Kröhnke syntheses of pyridyl-phenanthroline.	45
Scheme 2.2	Thummel's Friedländer synthesis of pyridyl-phenanthroline **46**	46
Scheme 2.3	Synthesis of 8-amino-7-quinolinecarbaldehyde **51**.	46
Scheme 2.4	Synthesis of benzoannulated pyridyl-phenanthrolinee **60**.	47
Scheme 2.5	Jahng's Kröhnke-Michael addition synthesis.	47
Scheme 2.6	The Chichibabin Reaction	48
Scheme 2.7	Nucleophilic aromatic substitution of pyridine with phenyl lithium	49
Scheme 2.8	Synthesis of 2-[5-methylpyridyn-2-yl]-9-[4-methoxyphenyl]-1,10-phenanthroline.	50
Scheme 2.9	Goto's failed synthesis of pyridyl-phenanthroline.	51
Scheme 2.10	Schlüter's bipyridine and terpyridine syntheses	52

Scheme 2.11	Siegel's synthesis of alpha and beta di-substituted terpyridines.	52
Scheme 2.12	Synthesis of manisyl substituted polypyridine ligands.	54
Scheme 2.13	Synthesis of 2,7-dibromo-phenanthroline	58
Scheme 2.14	Ortho-lithiation of 4-manisyl pyridine	59
Scheme 2.15	Unsuccessful synthesis of mixed 2,7-dihalophenanthrolines	60
Scheme 2.16	Formation of exo- and endo-topic metal complexes	65
Scheme 3.1	Sequence of states for emission from the locally excited (LE*) or charge transfer (CT*) state.	140
Scheme 4.1	Possible mechanisms for formation of $Ru(terpy)_2^{2+}$.	154
Scheme 4.2	Insertion of carbon monoxide and norbornadiene into carbon-palladium bonds of rigid, terdentate complexes.	159
Scheme 4.3	Synthesis of bis- pyridyl-phenanthroline osmium(II) complex **179**.	164
Scheme 4.4	Synthesis of bis- pyridyl-phenanthroline ruthenium(II) complex **189**.	166
Scheme 4.5	Synthesis of the chiral, bis-manisyl –terpyridine ruthenium(II) complex **191**.	167
Scheme 4.6	Synthesis of diastereomeric (-)menthyl-formate pyridyl-phenanthroline ruthenium(II) complex **193**.	168
Scheme 5.1	(Top) Substitution of crossings with double helices and deformation. (Bottom) Seeman's synthesis of DNA Borromean rings.	272
Scheme 5.2	Strategy for the step-wise synthesis of an orthogonal Borromean link.	273
Scheme 5.3	Loren's and Yoshizawa's synthesis of a bipyridine two-ring structure.	274
Scheme 5.4	Synthesis of phenanthroline 2-ring structure **202**.	275
Scheme 5.5	Route B. Synthetic strategy relying on preformed hetereoleptic complex **J**.	279
Scheme 5.6	Synthesis of terpyridine 2-ring structure **205**.	280
Scheme 5.7	Unsuccessful attempts to thread a third ring precursor of the Borromean link using $Ru(terpy)Cl_3$.	281

Scheme 5.8	Unsuccessful attempts to thread a third ring precursor of the Borromean link using zinc(II).	282
Scheme 5.9	Coordination chemistry of the two-ring complex **205**.	283
Scheme 5.10	Unsuccessful attempts to thread terpyridine ligands into Ru(II)2Ru(III)2 two-ring complex **208**.	285
Scheme 5.11	Extraction of Zn(II) from Zn_2Ru_2 two-ring **205** by bipyridine **206**.	285
Scheme 5.12	Synthesis of Ru[**197**][PF_6]$_2$	287
Scheme 5.13	Synthesis of one ring complex **214**.	289
Scheme 5.14	Unsuccessful ring-closure with 5,5”-bisethynyl terpyridine **204**.	294
Scheme 5.15	Unsuccessful ring-closure with 5,5”-dibromo terpyridine **216**.	295
Scheme 5.16	Synthesis of terpyridine two-ring structure **217**.	295
Scheme 5.17	Unsuccessful attempts to thread a third ring precursor of the Borromean link using terpy$RuCl_3$.	296
Scheme 5.18	Unsuccessful attempts to thread a third ring precursor of the Borromean link using terpyridine **210a** and $FeCl_2$.	296
Scheme 5.19	Synthesis of bisbromomethyl-terpyridine heteroleptic precomplex **220**.	297
Scheme 5.20	Unsuccessful synthesis of TIPS protected heteroleptic complex.	298
Scheme 5.21	Synthesis of 5,5”-dibromoterpyridine heteroleptic complexes.	298
Scheme 5.22	Unsuccessful synthesis of capping of propargyl thread one ring **199d** with heteroleptic complex **224b**.	298
Scheme 5.23	Control of pocket depth by lengthening of the alkynyl chain.	303

LIST OF TABLES

Table 2.1	Negishi couplings of halo-pyridyl-phenanthrolines	59
Table 2.2	Pd-catalyzed Coupling of Pherpys	61
Table 2.3	Chemical shifts of mono and dihalo-phenanthrolines	63
Table 2.4	$\Delta\ \delta$ of mono halophenanthrolines.	63
Table 2.5	Crystallographic Data for **111**	89
Table 2.6	Crystallographic Data for **114**	90
Table 3.1	Photophysical properties of conjugated phenanthrolines **127a – 127d** in acetonitrile.	107
Table 3.2	Photophysical properties of manisyl-phenanthrolines and bipyridines in acetonitrile.	108
Table 3.3	Photophysics of terpyridines **45** and **128** and in acetonitrile.	110
Table 3.4	Photophysical properties of phenyl-substituted terpyridines in dichloromethane.	111
Table 3.5	Photophysical properties of 4-substituted 4-phenylterpyridines in dichloromethane.	111
Table 3.6	Photophysical properties of amino-terpyridines in methylene chloride.	112
Table 3.7	Photophysics of manisyl-substituted terpyridines in acetonitrile.	113
Table 3.8a	Absorption data for pyridyl-phenanthrolines **111 – 113**.	118
Table 3.8b	Absorption data for pyridyl-phenanthrolines **114 – 116**.	119
Table 3.8c	Absorption data for pyridyl-phenanthrolines **117 – 119.**	120
Table 3.9	Emission data for pyridyl-phenanthrolines **111 – 119**	124
Table 3.10	Experimental lifetimes and radiative rates of pyridyl-phenanthrolines.	131
Table 3.11	Fluorescence lifetime dependence on wavelength of **116**.	133
Table 4.1	Emission data for $[Pt(pherpy)Cl]^+$ and derivatives in dichloromethane at room temperature.	160
Table 4.2	Synthesis of pyridyl-phenanthroline complexes	164
Table 4.3	Synthesis of terpyridine complexes	165
Table 4.4	Crystallographic data for first row pyridyl-phenanthroline complexes **173 –179**.	171
Table 4.5	Selected bond lengths (Å) and angles (deg) of pyridyl-phenanthroline complexes **173 – 179**.	174

Table 4.6	Crystallographic data of terpyridine complexes **36** – **40**.	183
Table 4.7	Selected bond distances (Å) and angles (deg) of terpyridine complexes **181** – **187**.	186
Table 4.8	Crystal data of "solvent-free" iron(II) pyridyl-phenanthroline and terpyridine complexes **173** and **181**.	192
Table 4.9	Comparison of ^{1}H NMR shifts of **115** in $CDCl_3$ and $M(pherpy)_2$-$2PF_6$ complexes **173**, **177** – **179** in CD_3CN.	196
Table 4.10	Manisyl region of the ^{1}H NMR spectra of CD_3CN solutions of $M(pherpy)_2$-$2PF_6$ complexes **173** – **179**.	198
Table 4.11	^{1}H NMR spectroscopic data for $M(terpy)_2$-$2PF_6$ complexes **181**, **185** – **187**.	200
Table 4.12	Manisyl region of the ^{1}H NMR spectra of $M(terpy)_2$-$2PF_6$ complexes **181** – **187**.	201
Table 4.13	UV-Vis absorption properties of $M(pherpy)_2$-$2PF_6$ **173 – 179** in methylene chloride.	204
Table 4.14	UV-Vis absorption properties of $M(terpy)_2$-$2PF_6$ in methylene chloride	205
Table 4.15	Emissive properties of $M(pherpy)_2$-$2PF_6$ **173 – 179** in methylene chloride.	207
Table 4.16	Emissive properties of $M(terpy)_2$-$2PF_6$ **181 – 187** in methylene chloride.	208
Table 4.17	MLCT emission data of $Os(pherpy)_2$-$2PF_6$ **179** and $Os(terpy)_2$-$2PF_6$ **187** in methylene chloride.	210
Table 4.18	Crystallographic Data for **173**	241
Table 4.19	Crystallographic Data for **174**	242
Table 4.20	Crystallographic Data for **175**	243
Table 4.21	Crystallographic Data for **176**	244
Table 4.22	Crystallographic Data for **177**	245
Table 4.23	Crystallographic Data for **178**	246
Table 4.24	Crystallographic Data for **179**	247
Table 4.25	Crystallographic Data for **181**	248
Table 4.26	Crystallographic Data for **182**	249
Table 4.27	Crystallographic Data for **183**	250
Table 4.28	Crystallographic Data for **184**.	251

Table 4.29	Crystallographic Data for **185**	252
Table 4.30	Crystallographic Data for **186**	253
Table 4.31	Crystallographic Data for **187**	254
Table 4.32	Crystallographic Data for **190**	255
Table 4.33	Crystallographic Data for **178**[Δ-TRISPHAT]$_2$	257
Table 5.1	Crystallographic Data for **199**	333
Table 5.2	Crystallographic Data for **205**	335
Table 5.3	Crystallographic Data for **212**	336
Table 5.4	Crystallographic Data for **213**	338
Table 5.5	Crystallographic Data for **214**	340
Table 5.6	Crystallographic Data for **218**	342
Table 5.7	Crystallographic Data for **224a**.	344

ACKNOWLEDGEMENTS

– the ringmaster –

Prof. Dr. Jay S. Siegel

Prof. Dr. Nat Finney

Prof. Dr. Kim Baldridge

Prof. Dr. Anthony Linden

The Swiss Light Source and the Paul Scherrer Institute

Nadja Bross, Simon Jurt, and the UNIZH NMR Facility

Prof. Dr. Laurent Bigler and the UNIZH MS Facility

Dr. Ivana Pesic and the LPF HPLC Facility

The Borromean Rings Team

Dr. Jon C. Loren

Dr. Michael DeClue

Karla Arias

Arif Karim

Simon Duttwyler

Ashley Sullivan

and

all Siegel and Baldridge Group members past and present

CURRICULUM VITAE

Jeremy K. Klosterman
USA

EDUCATION:

UNIVERSITÄT ZÜRICH, ZÜRICH, SWITZERLAND

Ph.D., Physical Organic Chemistry (2007)
Advisor: Professor Jay S. Siegel
Thesis: "*Synthesis and Properties of Manisyl-substituted Pyridyl-1,10-phenanthrolines and The Chemical Topology of Interlocking Rings*"

UNIVERSITY OF CALIFORNIA, SAN DIEGO, LA JOLLA, CALIFORNIA

M.Sc. Physical Organic Chemistry (June 2002)

NORTHWEST NAZARENE UNIVESITY, NAMPA, IDAHO

B.Sc, Chemistry (June 2000)
Advisor: Professor Daniel F. Nogales
Thesis: "*Molecular Recognition: Molecular Tweezers; a Versatile Synthetic Host"*

PROFESSIONAL EXPERIENCE:

Doctoral Research Associate, Universität Zürich	2003-2006
Doctoral Research Associate, University of California San Diego	2000-2003
Undergraduate Research Associate, Northwest Nazarene University	1998-1999
NMR Assistant, NMR staff, Universität Zürich	2005-2006
Teaching Assistant, Universität Zürich	2003-2004
Organisch-chemische Praktikum	
Teaching Assistant, University of California, San Diego	2000-2002
Honors Organic Chemistry	
Organic Chemistry	
Organic Chemistry Laboratory	

PUBLICATIONS:

Klosterman, Jeremy K., Linden, Anthony, Siegel, J.S., **Synthesis of Aryl-substituted 2-Pyridyl-[1,10]phenanthrolines; An Array of Oriented Terpyridine Analogues***, manuscript in preparation.*

Klosterman, J.K.; Baldridge, K.; Siegel, J.S. **Photophysics of Manisyl-Substituted 2-Pyridyl-[1,10]phenanthrolines.** *manuscript in preparation.*

Klosterman, J.K.; Linden, T.; Siegel, J.S. **Transition Metal Complexes of Manisyl-substituted Terpyridines and Pyridyl-phenathrolines: Photophysics, Isostructural and Isomorphous Crystals**, *manuscript in preparation.*

Klosterman, J.K.; Yasui, Y.; Loepfe, M.; Zysman-Colman, E.; Reingold, D.; Linden, A.; Siegel, J.S., **Ring-in-Ring Structures: A 2-ring Structure with Two Free Binding Sites**. *manuscript in preparation.*

PRESENTATIONS:

"Catenated and Interlocked Structures of Polypyridyl Complexes" Klosterman, J.K., Linden, A., Siegel, J.S.; poster presented at *Dorothy Crowfoot Hodgkin Symposium 2006* (Zürich, Switzerland, May 2006)

"Photophysical Properties of Aryl-Substituted 2-Pyridyl-[1,10]Phenanthrolines and Their Transition Metal Complexes" Klosterman, J.K., Linden, A., Siegel, J.S.; poster presented at *Swiss Chemical Society Fall Meeting 2005* (Lausanne, Switzerland, October 2005)

"Chemical Topology of Interlocking Rings" Klosterman, J.K., Yasui, Y., Loepfe, M., Zysman-Coleman, E., Reingold, D., Linden, A., Siegel, J.S.; oral presentation given at *Swiss Chemical Society Fall Meeting 2004* (Lucerne, Switzerland, October 2004)

"Chemical Topology of Interlocking Rings" Klosterman, J.K., Reingold, D., Yasui, Y., Zysman-Colman, E., Loepfe, M., Linden, A., Siegel, J.S.; poster presented at *European Research Conference on "Chemistry and Physics of Multifunctional Materials"*(Tomar, Portugal, September 2004)

"Chemical Topology and Interlocking Rings" Klosterman, J.K., Siegel, J.S.; oral presentation given at *UNIZH Organisch-chemisches Institüt Doktoranden Tag* (Zürich, Switzerland, June 2004)

"Synthesis, Properties, and Topologically Chiral Structures of Manisyl Substituted Pyridyl-[1,10]Phenanthrolines" Klosterman, J., and Siegel, J.S.; poster presented at *XVth FECHEM Conference on Organometallic Chemistry* (Zürich, Switzerland, August 2003)

"Synthesis of Aryl Substituted 1,10-Phenanthrolines" Klosterman, J., and Siegel, J.S.; poster presented at *Maria Goeppert-Mayer Interdisciplinary Symposium,* (San Diego, CA, USA March 2002)

"Synthesis of Aryl Substituted 1,10-Phenanthrolines" Klosterman, J., and Siegel, J.S.; poster presented at *The 10th International Symposium on Novel Aromatics* (San Diego, CA, USA August 2001)

"Synthesis of Aryl Substituted 1,10-Phenanthrolines" Klosterman, J., and Siegel, J.S., poster presented at *2001 Gordon Research Conference on Physical Organic Chemistry* (Manchester, NH, USA July 2001)

"Molecular Recognition: Molecular Tweezers; a Versatile Synthetic Host" Klosterman, J., and Nogales D.F.; poster presented at *217th American Chemical Society National Meeting*, Anaheim, CA (March 1999)

"Molecular Recognition: Molecular Tweezers; a Versatile Synthetic Host" Klosterman, J., and Nogales D.F.; poster presented at *41st Idaho Academy of Sciences* (Couer d'Alene, ID, USA April 1999)

"Molecular Recognition: Molecular Tweezers; a Versatile Synthetic Host" Klosterman, J., and Nogales D.F.; oral presentation given at *8th Murdock Foundation Regional Conference* (McMinnville, OR, USA 1999)

"**Molecular Recognition: Molecular Tweezers; a Versatile Synthetic Host**" Klosterman, J., and Nogales D.F.*;* poster presented at *7th Murdock Foundation Regional Conference* (Nampa, ID, USA 1998)

HONORS AND AWARDS:

Teaching Excellence Award, Department of Chemistry and Biochemistry,
University of California, San Diego (2002)

ABSTRACT OF THE DISSERTATION

SYNTHESIS AND PROPERTIES OF MANISYL-SUBSTITUTED PYRIDYL-1,10-PHENANTHROLINES AND THE CHEMICAL TOPOLOGY OF INTERLOCKING RINGS

Jeremy K. Klosterman
Doctor of Philosophy in Chemistry
Universität Zürich, 2007
Jay S. Siegel, Chair

Inspired by the beauty and complexity of topological graphs, the goal of my thesis work has been the molecular realization of such synthetically challenging structures and the investigation of their photophysical properties.

In order to achieve topologically chiral 2-catenanes via octahedral transition metal templates, a modular palladium catalyzed cross coupling procedure was developed and a 3 × 3 array of aryl substituted 2-pyridyl-[1,10]phenanthrolines (pherpy) was synthesized. The systematic variation of substitution pattern of such oriented terpyridine (terpy) analogues provides a valuable control over photophysical and electronic properties as well as the specific spatial orientation of the resulting metal complexes.

Fluorescence investigations revealed that pherpys can display from low to high quantum yields (Φ_f = 0.03-0.60) depending on the placement of aryl substituents. Further photophysical studies elucidated the duality of emissive states: a weakly emissive locally excited state, similar to the $^1\pi,\pi^*$ state of phenanthroline; and a strongly

emissive charge transfer state, dependent on manisyl regiochemistry and solvent polarity. MO calculations in collaboration with the Baldridge group (UZH) underscore the similarities in the electronic structures of phenanthroline and pyridyl-phenanthrolines rather than between terpyridine and pyridyl-phenanthroline.

A series of ML_2 coordination compounds of pherpys and terpys with Fe(II), Co(II), Ni(II), Cu(II), Zn(II), Ru(II), and Os(II), were synthesized. In the solid state, pyridyl-phenanthroline complexes are isomorphous (space group *Pcca*), except for the zinc complex, which is isostructural but not isomorphous (space group $P2_{1/c}$). Terpyridine complexes are isostructural but divided into two isomorphous subgroups (*Pnma* and *C2/c*). Within the crystal lattice the dications arrange into sheets of alternating left- and right- handed double-helixes via CH $\cdots\pi$ and π–π interactions. All of the complexes exhibit weak ligand-centered emission at room temperature and the osmium complexes possess an emissive metal-ligand charge-transfer state. Pyridyl-phenanthroline complexes are C_2 symmetric and their chirality was confirmed by ^{1}H-NMR titrations with Δ-TRISPHAT as a chiral counter-ion. Attempts at resolution by chromatography, crystallization, and HPLC were inconclusive.

En route to the Borromean Link, two new ring-in-ring structures with open terpyridine binding sites were synthesized. The two-ring structures are capable of complexing two equivalents of Ru(III), Zn(II), or Pt(II) but attempts to thread two terpyridine or bipyridine ligands were inconclusive. A systematic crystallographic investigation of single and two ring structures illuminated the flexibility of ring one and emphasized the difficulty of predicting the geometries and conformations of very large macrocycles. A new strategy relying on heteroleptic Ru(II) complexes as organometallic building blocks was developed to avoid the complexity of threading two-ring structures.

the meeting of two personalities

is like the contact

of two chemical substances:

if there is any reaction,

both are transformed.

-Jung

Chapter 1

Chemical Topology

1.1 Introduction

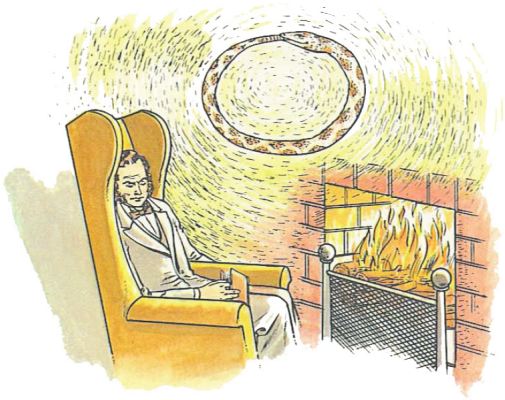

Figure 1.1 Kekulé's dream[1]

At the turn of the nineteenth century, chemists were searching for ways to categorize and understand the periodicity of the elements. The future Lord Kelvin, Sir William Thompson, theorized that the elements were merely vortex rings and knots in the ether[2]. His collaborator, Scottish physicist Peter Guthrie Tait, so inspired by this idea, attempted to tabulate all of the possible knots and thus generate a table of the elements.[3-5] Kelvin's theorem was proven incorrect and chemists soon thereafter lost interest in enumerating knots and links. Fortunately, mathematicians followed up on Tait's ideas and the field of knot theory was formed.

The possibility of molecules consisting of knotted and interlocked rings continued to spark the imagination of chemists.[6-8] The history of chemistry is filled with dreamers who, not content to merely replicate the work of Mother Nature, have looked outside the world of natural products for inspiration and new challenges,[9] and from Kekulé's dreams of Oroboros (Figure 1.1) to the prescient Zürich Lectures of Nobel prize winner Richard Willstätter,[10] rings and interlocked rings have repeatedly resurfaced in a Jungian manner.[11] Indeed, knotted structures possess an inherent beauty that touches humanity's soul and, like the intricately knotted illustrations decorating the Book of Kells, endow a sense of otherworldliness. The symmetry and

complexity of knots have long since captivated mathematicians, but the concepts of topology are impacting fields from nuclear physics and statistical mechanics to biology and chemistry. The reconnection of chemistry and topology is not obvious and until fifty years ago there was no need to integrate the two. The emergence and development of chemical structural theory was necessary for this link to reappear.[12]

The concept of structure and connectivity, so elegantly communicated through our modern symbolic sketches, did not come easily to chemists. Until the mid 1860's, chemists could measure the types and ratios of elements in a compound, called the empirical formula, and, when the correct atomic weights were used, derive the actual number of atoms with a molecule, the molecular ratio. The French chemist Gerhardt noticed that certain groups of atoms were replaced as a group and developed the "type" theory.[13] Subsequently, August Kekulé[14] and Archibald Couper[15] correctly deduced the tetravalency of carbon and explained existence of constitutional isomers, distinct molecules containing the same molecular formula yet different connections. In 1861, the Russian chemist, A.M. Butlerov, published his theory of chemical structure and defined it as "the type and manner of the mutual binding of the atoms in a compound substance."[16] The exact nature of the atoms and bonds remained unclear and were depicted in various forms (Figure 1.2). Nevertheless, the majority of the chemical community accepted the structural formula.

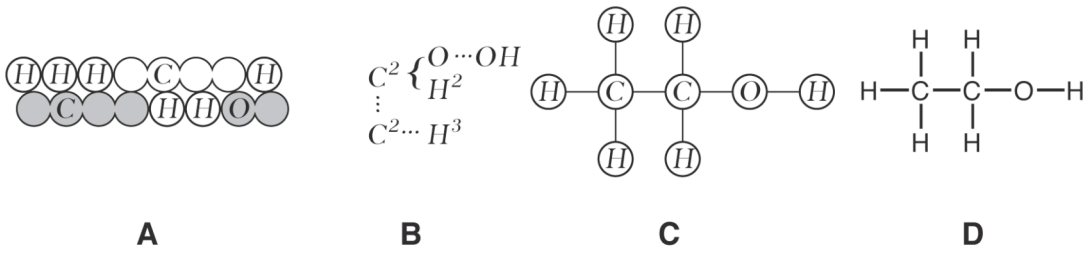

Figure 1.2 Depictions of ethanol by (a) Kekule;[17] (b) Couper;[15] (c)Crum Brown;[18] and (d) modern chemists.

Early advocates of the structural formula, such as Crum Brown,[18] made it very clear that these formulae described only the connectivity of atoms and did not convey the spatial distribution of the atoms. Fifty years later, the sheer wealth of molecules displaying "optical isomerism", such as tartaric acid (Figure 1.3), convinced chemists to grudgingly accept van't Hoff's[19] and Le Bel's[20] tetrahedral carbon and move confidently into three dimensions. Stereochemistry is the study of the three-dimensional structure of molecules and is an essential aspect of modern chemistry.

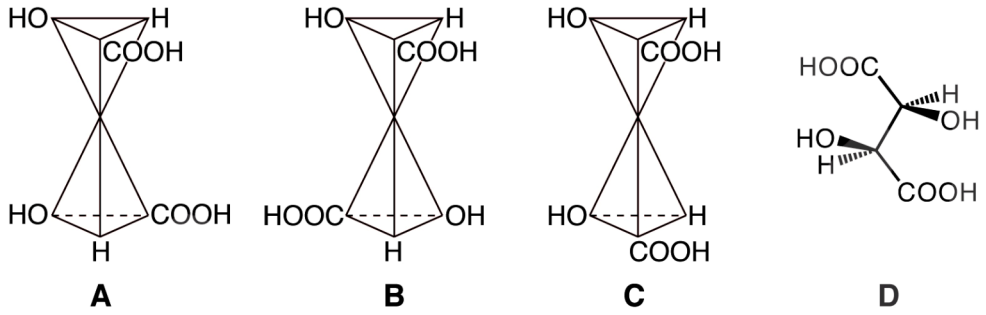

Figure 1.3 Optical isomers of tartaric acids; van't Hoff's (a) d-form (b) l-form (c)meso-form and (d) the modern version.

Topology and stereochemistry are commonly considered independent. That is, the stereochemistry of a molecule is not derived from the connections within a molecule, but rather from the geometrical properties of the molecular structure. For most molecules, this is true, but the stereochemistry of molecules consisting of interlocked rings and knots depends on their topology in addition to their geometry and in the 1950's chemists began synthesizing knotted and linked molecules[6] and molecular biologists have also found knotted and linked DNA strands existing in nature.[21-23] This juxtaposition of stereochemistry and topology has been termed *chemical topology*[24] or *topological stereochemistry.*[25] Once the realm of topologists, new chemical methodologies have enabled an explosive growth in this field,[26] benefiting both chemists and topologists.

This chapter introduces some simple theorems of knot theory and topology, their stereochemical implications, and the key strategies employed for the synthesis of topologically complex molecules.

1.1.1. Knot Theory and Topology

Knot theory is a subfield of topology.[27-30] Topology studies the properties of geometric shapes under continuous deformation. Triangles, squares, and circles (Figure 1.4) are quite distinct under normal (Euclidean) geometrical constraints, but are *isotopic* or topologically equivalent because, in topology, geometrical shapes are completely flexible and can be deformed (by twisting, pulling, etc.) into the next.

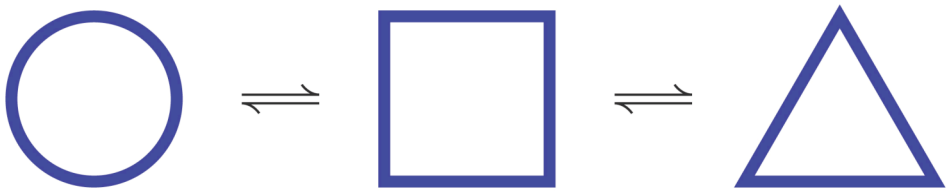

Figure 1.4 Topologically equivalent shapes.

A *knot* is a closed loop in three-dimensional space that does not intersect itself;[29] the simplest knot being a circle, called the unknot (Figure 1.5a), followed by the trefoil knot (Figure 1.5b). A *link* is a set of interlocked knots and the simplest link, consisting of two rings, is called the Hopf link, for the topologist Heinz Hopf (Figure 1.5c). The terms knot and link are interchangeable.

Figure 1.5 Simple knots and Links; (a) the unknot, 0_1^1, (b) the trefoil knot, 3_1, (c) the Hopf link 2_1^2.

Originally, tables of knots were organized by the number of crossings or overlaps and each knot or link was identified by K_x^n, where K is the crossing number and n is the number of loops and x is an arbitrary numerical index.[28] The trefoil knot is labeled 3_1 and the Hopf Link is 2_1^2 (Figure 1.5). However, just like a knotted loop of string, knots are flexible and can adopt a variety of complex forms. For example, the figure-eight knot can be drawn in many different forms (Figure 1.6), and each different representation of a knot is a different *projection* or *embedding* of the knot into three-dimensions.[30] A large portion of knot theory is identifying different knots or determining if the projection is a knot at all (Figure 1.7).

Figure 1.6 Three embedding of the figure-eight knot.[29]

Figure 1.7 A complicated embedding of an unknot.[29]

The first methods used to identify knots were empirical; including trial and error manipulations of models and drawings, and a good bit of intuition. Each move or deformation of the knot through three-dimensional space that does not pass the loop through itself is called an *ambient isotopy*. In 1926 Kurt Reidemeister[27] categorized the three types of ambient isotopies that would allow the interconversion of two projections of the same knot (Figure 1.8). If there exists a series of Reidemeister moves

that convert from one projection to another, then the two knots have the same topology. That is, they are *isotopic* and identical. On the contrary, if a series of moves cannot be identified, it does not prove that a there is no set of moves, merely that that they have not be found. Proving that two knots are not identical is much more difficult and requires the use of polynomials.

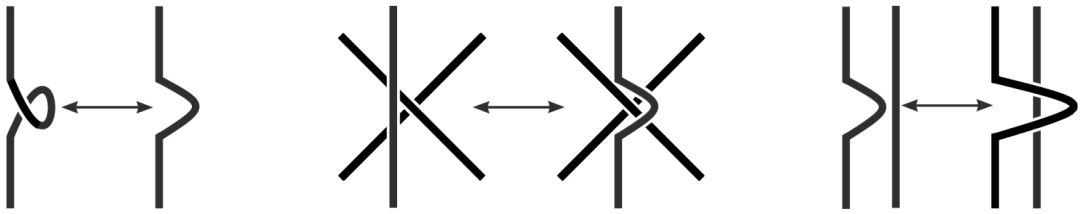

Figure 1.8 Reidemeister moves.

1.1.2 Stereochemistry and Topology

Many molecules posses the same empirical and molecular formulas and are called *isomers*. Stereochemistry is the branch of modern structural chemistry concerned with classifying and distinguishing molecular isomers. There are three classes of isomers that unambiguously identify a molecule:

(1.) *Constitutional isomers* have the same molecular formula but different connectivity. For example, a molecule possessing the molecular formula C_4H_{10} has two possible topologies; *n*-butane and *iso*-butane(Figure 1.9). They have different topologies and connectivity and in topological terms, they are not *isotopic* and not *homeomorphic*.

Figure 1.9 Constitutional isomers

(2.) *Stereoisomers* possess the same molecular formula and the same connectivity but differ in the spatial arrangement of atoms. For example, the rigid geometrical constraints of a E,Z-isomers of alkenes or a tetrahedron result in distinct stereoisomers (Figure 1.10). The strength and type of molecular rigidity varies significantly, allowing some stereoisomers to interconvert, whereas many can never interconvert. In topological terms, stereoisomers are isotopic and homeomorphic.

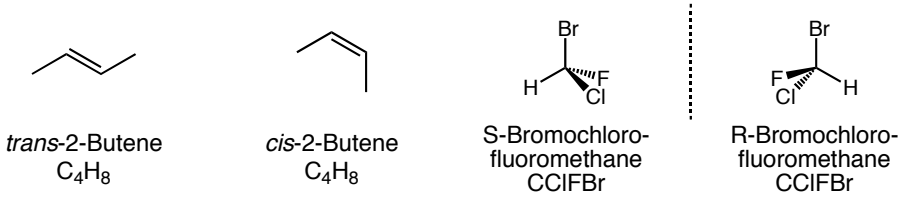

trans-2-Butene C_4H_8 | *cis*-2-Butene C_4H_8 | S-Bromochloro-fluoromethane CClFBr | R-Bromochloro-fluoromethane CClFBr

Figure 1.10 Stereoisomers

(3) *Topological stereoisomers* are a subclass of stereoisomers that do not depend on any rigidity to remain distinct. They possess the same connectivity but cannot be deformed into one another without breaking a bond. As such, they are homeomorphic but not isotopic. The prototypical example is the trefoil knot and the unknot (Figure 1.11).

Figure 1.11 Topological stereoisomers

1.1.3 Chirality and Topological Chirality

Essential to stereochemistry is the concept of chirality. A molecule is said to be *chiral* (from the Greek word, *χειρ*, for hand) when it cannot be superimposed onto its mirror image.[31] The prototypical example of chirality is a pair of hands. The left hand is the mirror image of the right but the two can never be interconverted by rigid

motions. If a molecule can be superimposed upon its mirror image, it is *achiral*. In symmetry terms, a chiral molecule must be dissymmetric, containing no mirror planes and thus be of C_n or D_n symmetry.[32] Stereoisomers that are mirror images are *enantiomers*. A classic example of a chiral molecule is Bromochlorofluoromethane (Figure 1.10). *Diastereomers* are stereoisomers not related by any symmetry, exemplified by *cis*- and *trans*-2-butene (Figure 1.10).

The most discernible property of a chiral substance is its optical activity. When polarized light, which is racemic, passes through a solution containing a single enantiomer the light vector shifts to the left or to the right. The opposite enantiomer will rotate the light in the opposite direction. Solutions of achiral substances or equimolar mixtures of the two enantiomers of a chiral molecule are optically inactive and will not rotate light in either direction.

Most stereoisomers are a result of molecular rigidity and Euclidean geometry.[25] For example, [6]helicene[33] (Figure 1.12a) exists as two stable enantiomers at room temperature in solution. At high temperatures, it is possible to distort the normally rigid benzene cores and equilibrate between the two enantiomers. Similarly, one could imagine converting between the two enantiomers of bromochlorofluoromethane via a planar transition state (Figure 1.12b). However, the energy required for this transformation is too high (~250 kcal)[34] and physically impossible to achieve without destroying the molecule.

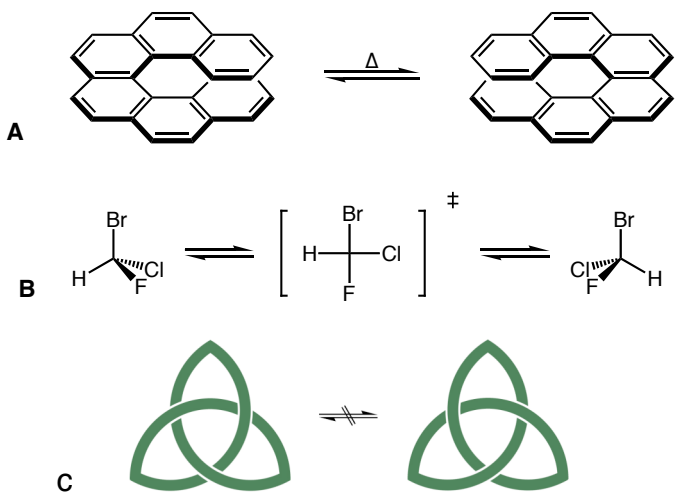

Figure 1.12 Interconversion of enantiomers.

A molecule, or knot, is *topologically chiral* if it cannot be converted into its mirror image by continuous deformation.[25] The trefoil knot is topologically chiral (Figure 1.12c). When two enantiomers are interconvertable, the molecule is *topologically achiral*. [6]Helicene and bromochlorofluormethane exhibit *Euclidean chirality* and are chemically chiral, but are topologically achiral. The figure-eight knot is topologically achiral and can be deformed to its mirror image (Figure 1.13). There also exists a rigidly achiral presentation (Figure 1.14).[30] As every planar projection contains a mirror plane, only knots, links, and molecules with non-planar graphs can be topologically chiral.

Figure 1.13 A deformation of a figure eight knot to its mirror image.[30]

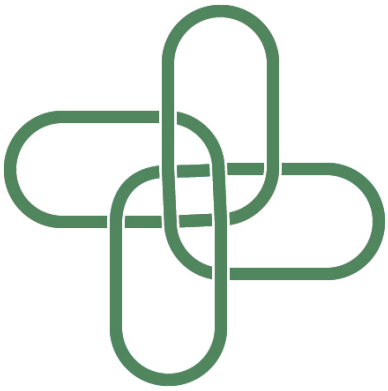

Figure 1.14 A rigidly achiral embedding of the figure eight knot.[30]

1.1.4 Non-planar Graphs

A graph is simply a set of points and their neighboring relationships defined by connecting lines. The points are called vertices and the lines, edges. First introduced by Euler in 1736,[35] graph theory has been deeply connected to topology and knots are typically represented as graphs. Chemistry too, has profited from graph theory.[36] Shortly after the advent of structural formulae, mathematicians Cayley and Sylvester recognized their character as topological graphs.[37] Treating carbon atoms as vertices and bonds as an edges (Figure 1.15), Cayley was able to calculate the number of structural isomers for alkanes containing up to thirteen carbons.[38]

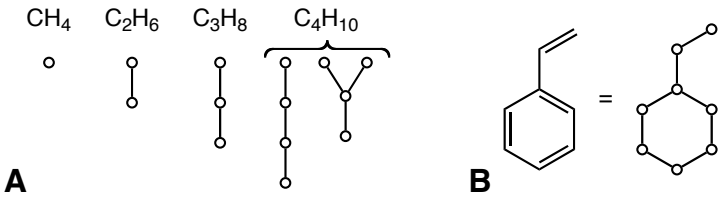

Figure 1.15 Molecular graphs of (a) alkanes up four carbons and (b) stilbene.

A graph that cannot be drawn lying in a plane without any crossings is said to be *non-planar*. In organic chemistry, molecules with non-planar graphs are very rare.[39,40]

Even large and complex molecules can be drawn as planar graphs (Figure 1.16). Nevertheless, molecules containing non-planar graphs have been synthesized (Figure 1.17); sometimes with the respective author's awareness[41,42] and sometimes without.[43]

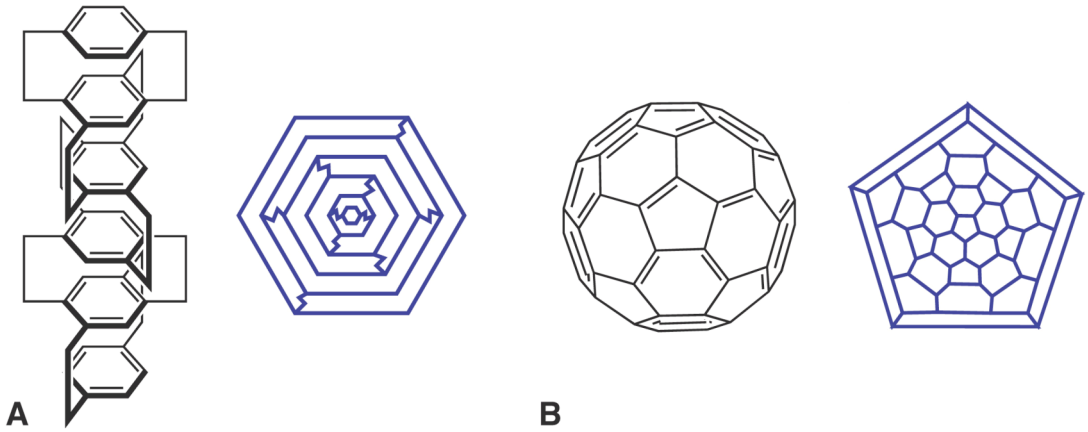

Figure 1.16 Planar embeddings of (a) (-)-(R,R,R,R)-[6]chochin[44] and (b) buckminsterfullerene.[45]

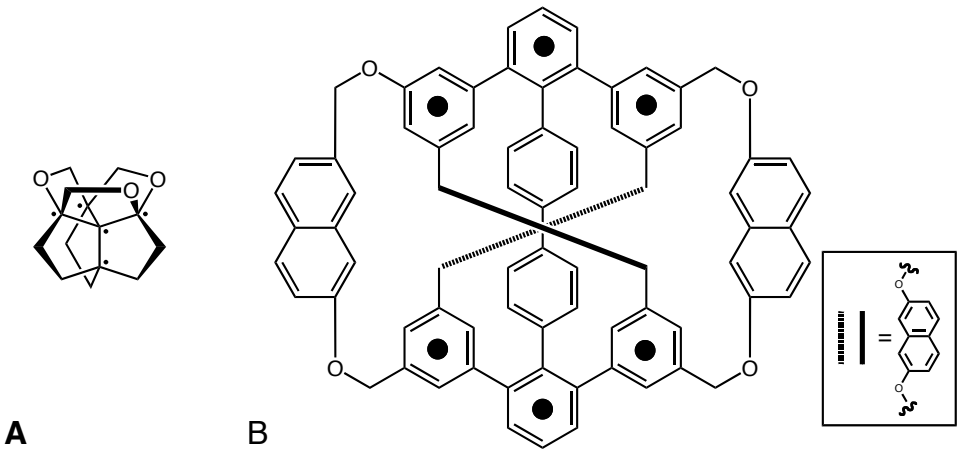

Figure 1.17 Two examples of molecules with non-planar graphs; (a) The Simmons-Paquette Molecule,[41,43] and (b) Siegel's Kuratowski cyclophane.[42]

In 1930, the Polish topologist, Kazimir Kuratowski demonstrated that all intrinsically non-planar graphs contain at least one of two graphs,[46] $K_{3,3}$ or K_5 as a sub-graph (Figure 1.18). The molecular graph of Simmons-Paquette molecule, contains graph K_5. The Kuratowski cyclophane possesses graph $K_{3,3}$ when the benzene rings are

considered vertices, called a Loschmidt replacement[47] (the key vertices are labeled in Figure 1.17). To date, the number of molecules recognized to contain $K_{3,3}$ or K_5 is small.

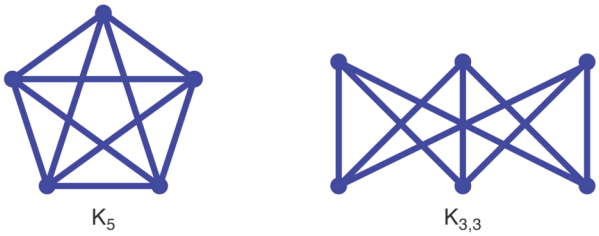

Figure 1.18 The Kuratowski graphs, K_5 and $K_{3,3}$

Knots and links are also non-planar, but do not contain a Kuratowski subgraph. They are specific non-planar embeddings of a planar *abstract graph*, a graph that is independent of any three-dimensional embedding. For example, every knot is merely a different way to draw a circle. Each knot contains the same abstract graph, the unknot. The unknot is planar, so knots (and links) are intrinsically non-planar, however, because of their specific embedding they are *extrinsically* non-planar.[30]

1.1.5 Topological Stereochemistry of Links

The Hopf link, 2_1^2, has an extrinsically non-planar graph and is achiral (Figure 1.5c).[48] Orienting the rings by adding directionality to both rings will break the mirror planes of both rings and result in a chiral Hopf Link (Figure 1.19a). There are also links that exhibit unconditional topological chirality, i.e., independent of any orientation. For example, links 4_1^2 and the Whitehead link, 5_1^2, are both topologically chiral (Figure 1.19b & c).,

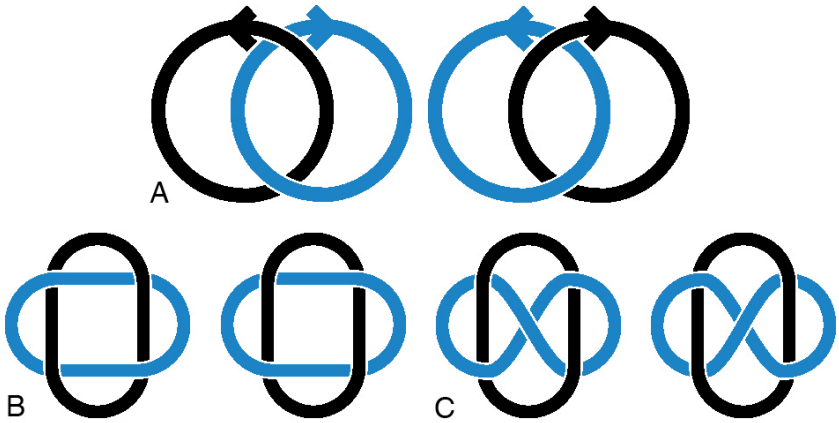

Figure 1.19 Topologically chiral links: (a) The oriented Hopf Link, 2_1^2, (b) link 4_1^2, (c) the Whitehead link 5_1^2.

Links containing three or more rings are organized into composite and prime links. *Composite links* are divisible into smaller non-trivial links. A linear 3-link (Figure 1.20a)[29] can be divided into two different Hopf links and is labeled as their sum, $2_1^2 \# 2_1^2$. *Prime links* are indivisible into smaller links other than the trivial unknot, i.e, the Torus link, 6_1^3, and link 12_1^3 (Figure 1.20b & c).

One of the most fascinating embeddings of a 3-link is the Borromean Link, link 6_2^3 (Figure 1.20d). It belongs to a family of links called Brunnian Links[49], in which no two rings are concatenated and the removal of one ring will cause the others to fall apart. A most interesting property of the Borromean link 6_2^3 is that upon orienting all three rings, the link remains achiral.[50]

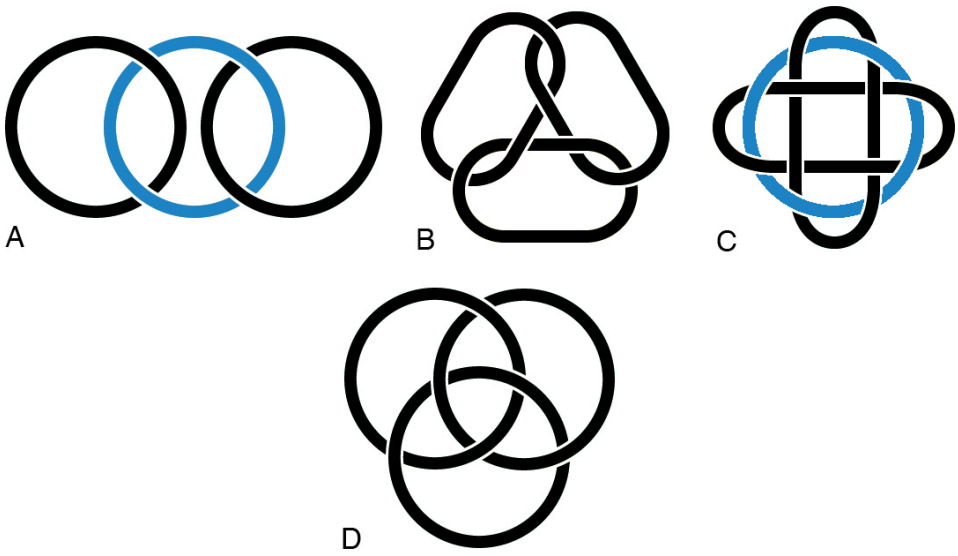

Figure 1.20 Three-Links; (a) Composite link $2_1^2\#2_1^2$, (b) Torus link 6_1^3, (c) Link 12_1^3, (d) The Borromean link 6_2^3.

The examples given so far are comparatively straightforward, but it is readily apparent that working with knots and links is complex. The flexibility required by topology enables links to adopt a continuum of shapes in three-dimensions. Identifying distinct links becomes increasingly difficult, let alone confirming topological chirality. Topologists search for properties that do not depend on specific presentations of an embedding. These properties are called *invariants*[51] and are used to identify link types and the presence or absence of chirality.

1.1.6 Techniques for Identifying Links and Topological Chirality

Many invariants of knots and links have been found,[29,30] but one of the most important and useful is called the *writhe*. To find the writhe, an embedding of a given knot is chosen (typically the embedding with a minimum number of crossings) and then oriented. Each crossing is assigned a positive or negative value, according to its right handed or left handed twist, respectively (Figure 1.21). The summation of

positive and negative crossings is the *writhe*.[49] Link polynomials are calculated from the writhe as well as several other more complex writhe invariants.

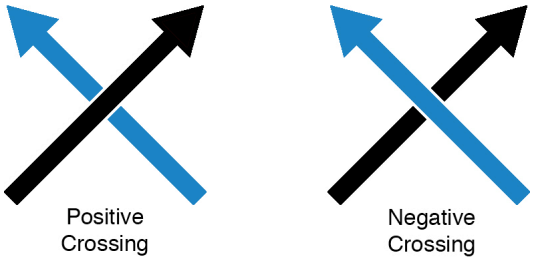

Figure 1.21 Positive and negative crossings.

There are several link polynomials available, foremost among them are the Jones polynomial, $V(t)$,[52] the HOMFLY polynomial of Hoste, Ocneau, Millet, Freyd, Lickorish, and Yetter, $P(l,m)$,[53] and the Kaufmann polynomial, $F(a,z)$.[54] The mathematics is beyond the scope of this thesis, but, in short, if the polynomial of two knots are different, the knots are different. If the polynomials are the same, the two knots are merely different embeddings of the same knot. If the polynomial of a knot and its mirror image differ, the knot is topologically chiral. All of the methods mentioned are capable of detecting topological chirality but none of them are yet *complete*, that is, capable of differentiating all classes of knot.[51] For each polynomial method there exists certain kinds of links called mutants that, while different, result in the same polynomial. Recently, Vassiliev[55] created a new class of knot invariants and has conjectured that they are *complete*. However, this has yet to be proven or disproved, nor have they been successfully applied to links.

Topologists can prove a graph to be topologically chiral but there are no confirmatory physical observables. However, as chiral substances can display a measurable optical activity, chemists are in the unique position of collaborating with topologists to confirm their predictions. Once the topological chirality of a knot or link

has been mathematically proven, it then follows that the molecule possessing the same graph will be chemically chiral as well, and if correct, the molecule will exist as two optically active enantiomers.[5657] A topologically achiral graph, however, does not imply that the molecule will be chemically achiral. Geometrical and chemical rigidity can generate chirality even if the graph is topologically achiral. The relationships between geometrical (Euclidean), chemical (molecular rigidity), and topological chirality and achirality are illustrated in Figure 1.22.

Figure 1.22 Relationships between geometrical, chemical, and topological chirality and achirality.

1.2. Initial Strategies for the Synthesis of Interlocking Rings

Motivated by the inherent aesthetics, synthetic challenge, and the possibility of discovering molecules with new and useful properties, chemists actively pursue molecular targets from the vast array of topologically interesting graphs. Though the idea of linked and knotted rings had been around since the turn of the century, it wasn't until the 1950's, after the problem of macrocyclization was addressed by the fundamental work of Ziegler[58], Hansley[59], Prelog[60] and Stoll[61], that chemists were able to address the synthesis of these molecules.

In 1957 Lüttringhaus[62] laid out a set of potential pathways (Scheme 1.1) for the synthesis of linked macrocycles called *catenanes*[63,64](from the Latin, *catena*, meaning chain). All of these are based on the presupposition that one could thread an open

chain through a pre-formed macrocyclic ring. Pathway A relies on the statistical probability that, in a solution of macrocycle, some open chain will be threaded at the time of cyclization. Pathway B relies upon an "auxiliary linkage", indicated by the dotted line, that brings the macrocycle and open chain together. Upon cleavage of the auxiliary linkage, free catenanes or macrocycles are achieved. Pathway C involves the linking of two functionalized open chains that upon cyclization result in a mixture of bound macrocycles, catenanes, and large macrocycle.

Pathway A

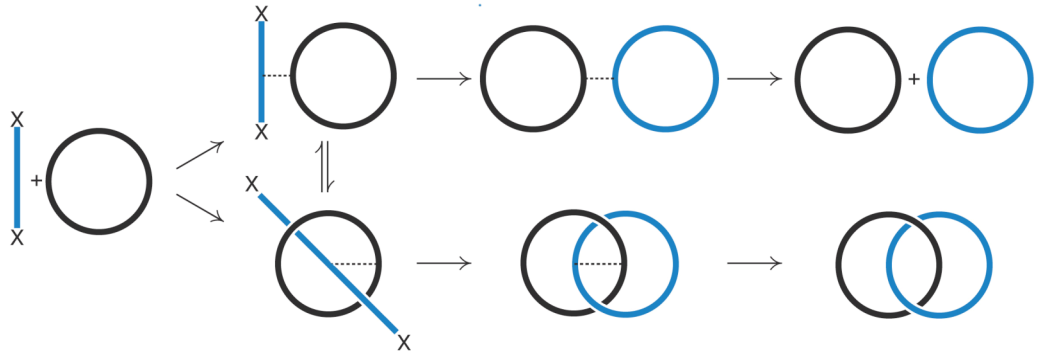

Pathway B

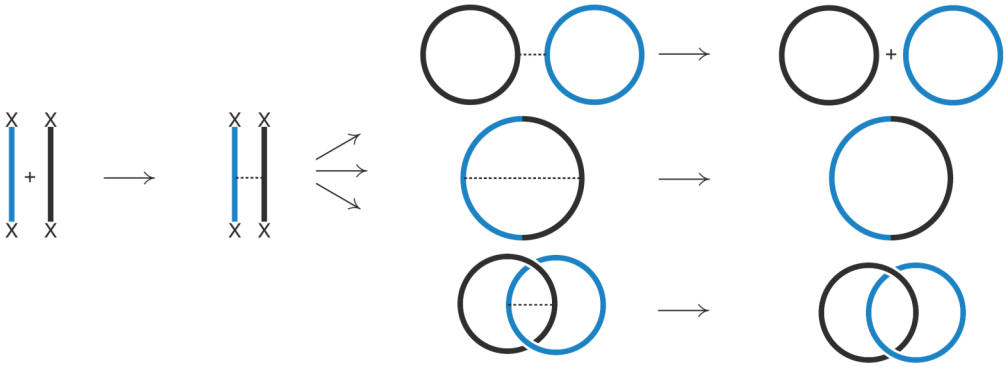

Pathway C

Scheme 1.1 Lüttringhaus's theoretical pathways towards catenane synthesis.

The majority of modern catenane syntheses can be mapped onto one of these three pathways. Initial strategies for catenane synthesis utilized statistical methods, directed methods, and Möbius strips. The following section highlights the key syntheses and describes the variety of synthetic methodologies and their contribution to current methods.

1.2.1 Statistical Methods

Statistical methods rely on the random threading of a preformed ring by an open strand (Pathway A in Scheme 1.1) and are governed by the laws of statistics. The determining factors are the size and structure of the starting materials, available conformations and sterics.[6] Around 1957, Edel Wasserman began manipulating space-filling models and found that a hydrocarbon ring containing twenty-four carbons was just large enough to thread through a polymethylene chain.[10] The difficulty was not the macrocyclization, the methodology was well established, but in providing convincing evidence that the product was truly concatenated. As shown in Scheme 1.2, starting with diethyltetratriacontanedioate **1,** containing thirty-four carbons, the cyclization via an acyloin condensation in the presence of an equimolar amount of penta-deuterated macrocycle **2** (derived from **4**) resulted in a mixture of free macrocycles **2** and **4**, and catenated material **3**. After chromatographic removal of starting macrocycle **2**, the remaining acyloin material, containing **3** and **4**, still showed carbon-deuterium stretches by IR spectroscopy. Cleavage of the acyloin functionality gave the diacid **4** and deuterated macrocycle **1** in approximately 0.001% yield.[64,65]

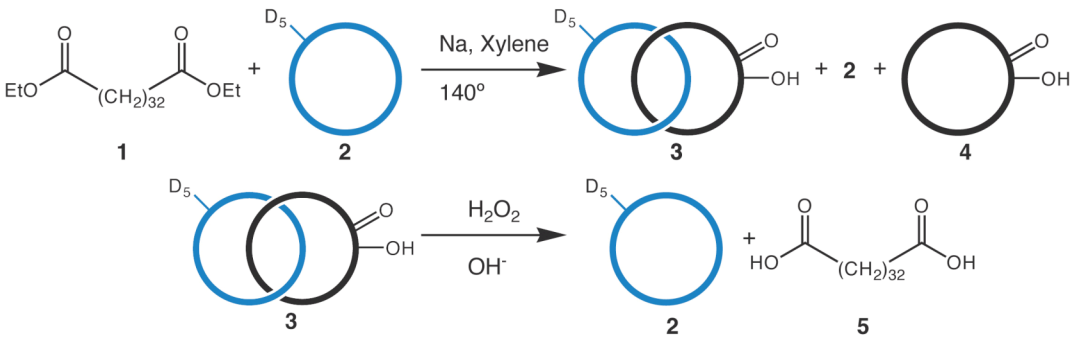

Scheme 1.2 The Wasserman catenane synthesis

In a seminal follow-up paper,[24] Frisch and Wasserman defined and laid the foundations for the field of chemical topology. Several other groups attempted catenane synthesis via statistical methods,[66-70] but given the low yields, newer higher yielding methodologies were pursued.

1.2.2 Directed Methods

A directed synthesis seeks to enforce a steric arrangement such that ring closure can only occur in the desired topology. In 1965 one of Lüttringhaus's students, Gottfried Schill, outlined a general strategy[71] for a directed strategy (Scheme 1.3). A planar ring containing substituents **A** and **D** as well as two floppy chains **R** is linked to another open chain with a group **B** so that the chain is held perpendicular to the planar ring. The **C** groups are chosen so that they cannot react with one another, but only with group **D**. Specific cyclization of the **R** groups followed by connecting both **C** moieties with group **D** results in a pre-catenane structure which, after cleavage of the planar ring, produces the final catenane structure.

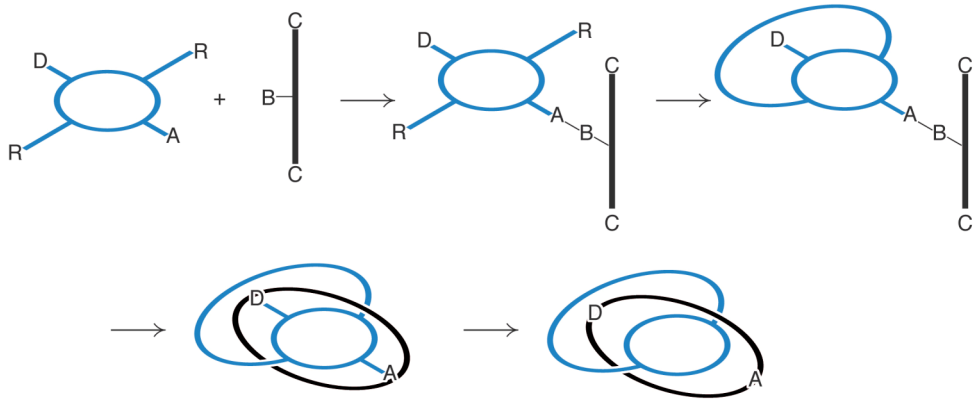

Scheme 1.3 Schill's directed synthesis strategy.[6]

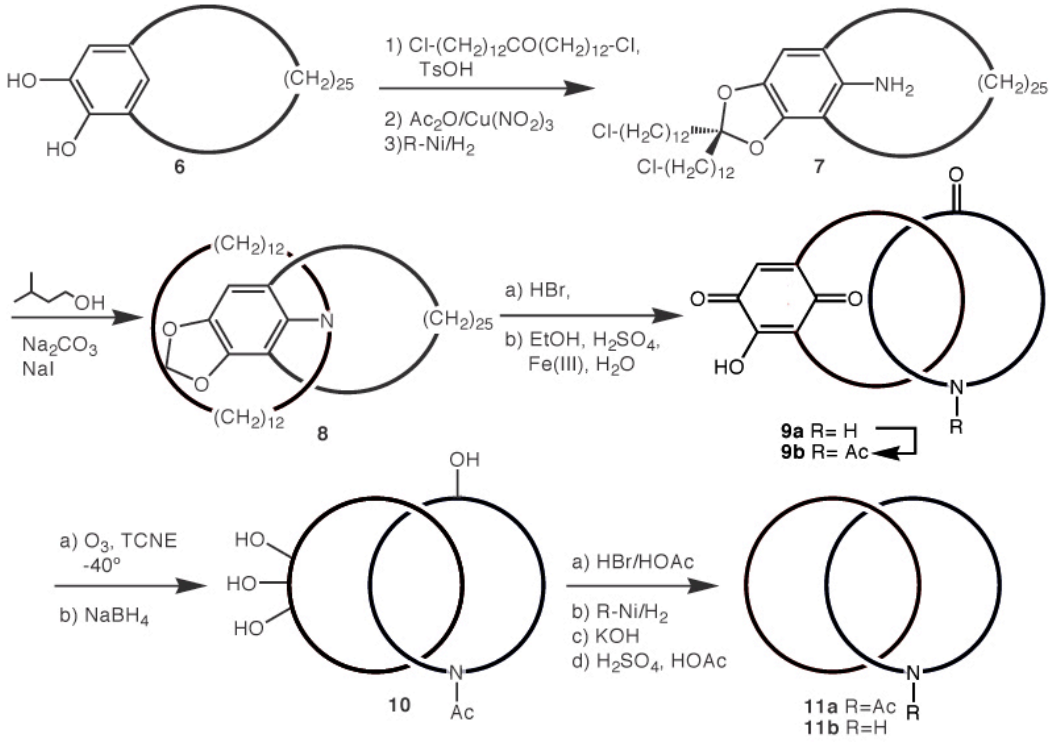

Scheme 1.4 The Schill-Lüttringhaus catenane synthesis.

Lüttringhaus, Schill, and coworkers successfully synthesized and characterized several catenanes via directed methods using di- and tri-ansa compounds. (Scheme 1.4)[6] Starting from the readily accessible catechol **6**, standard ketalization conditions with a dichloro-ketone, followed by nitration and reduction, gives the amino ketal **7**.

Macrocyclization results in the pre-catenane tertiary amine **8**. Hydrolysis of the ketal and oxidation of the aromatic nucleus gives the catenane **9a** (~76% yield from **6**), which is then protected as the amide. This catenane was fully characterized and its structure confirmed by elemental analysis, IR, NMR, and the fragmentation pattern of the mass spectrum.[71] Oxidative degradation of the aromatic ring followed by reduction of the crude product gives the tetra-ol **10**. A halogenation-hydrogenation-hydrolysis procedure results in the crystalline catenane **11a**. Deprotection results in the final catenane **11b**.[72-75] Schill and coworkers later applied this strategy to the synthesis of a trefoil knot but were unsuccessful.

The directed synthesis resulted in a drastically improved yield but the tedious and time consuming synthesis was not generally applicable. Nonetheless, the idea of using a template to control the conformation of the pre-catenane was a major step forward and would have a significant impact on the use of chemical templates to enhance catenane synthesis.

1.2.3 Möbius Strips and Ladders

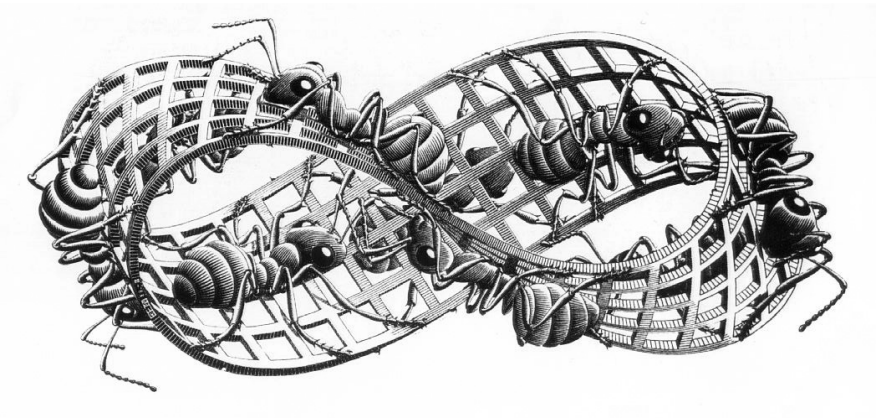

Figure 1.23 M.C. Escher's famous interpretation of a Möbius band.[76]

In the late 1950's, van Gulick recognized the inherent limitations of the statistical methods and proposed a completely different approach to topologically complex molecules via Möbius strips. The infinite surface of a Möbius band (Figure 1.23) is constructed by twisting a strip of paper once and connecting the two ends together. The topological graph of a Möbius strip is called a Möbius ladder (Figure 1.24).[77] When a strip with two half-twists is cut in half, two linked rings are obtained. Additionally, adding further half-twists results in a variety of complex topological graphs after scission (Scheme 1.5).

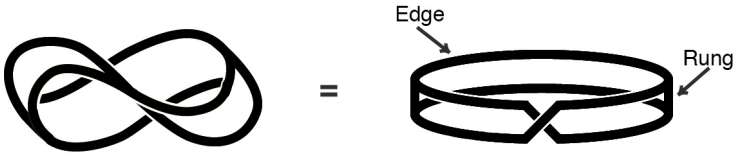

Figure 1.24 A Möbius strip and its graph, a Möbius ladder.

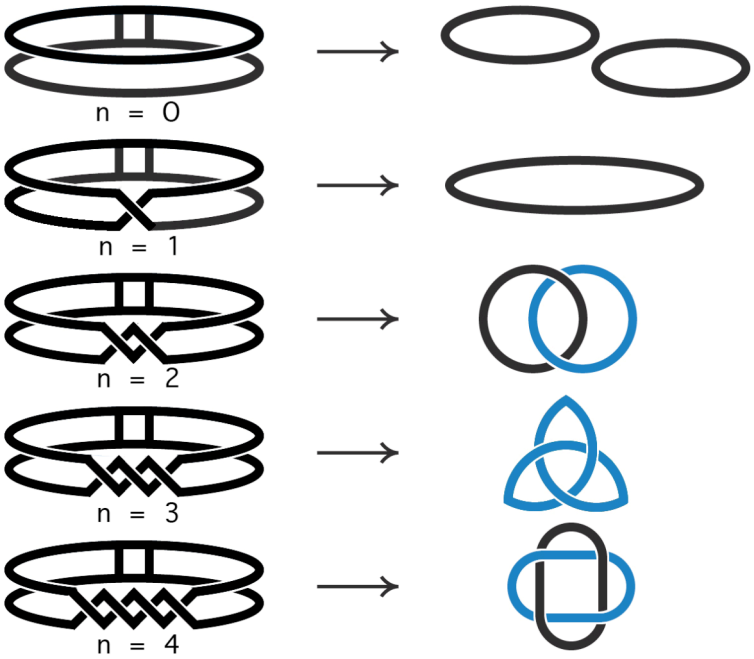

Scheme 1.5 Graphs resulting from the scission of *n* half-twisted Möbius ladders.

Wolovsky[78] and Wasserman[79] were able to independently demonstrate mass spectrum evidence of catenane formation in a Möbius strip approach using the olefin metathesis of cyclododecene (Scheme 1.6) , but further isolation and characterization proved impossible.

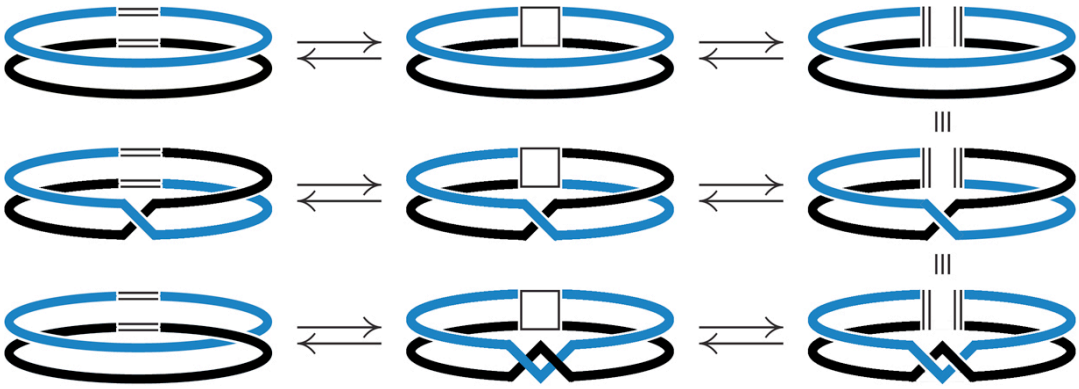

Scheme 1.6 Wolovsky's and Wasserman's Möbius metathesis method of making catenanes.

Walba was able to synthesize a Möbius ladder in molecular form (Scheme 1.7);[80] the long polyether chains represent the edges and the double bonds represent the rungs. Under high-dilution conditions, cyclization of the flexible tetramethylethylene (THYME)[81] ether **12** resulted in the untwisted **13**, and the Möbius ladder **14** (Scheme 1.7). Further evidence of the molecular topology was revealed upon ozonolysis of **13** and **14**, resulting in the macrocyclic triketone **15** and hexaketone **16**, respectively.[82]

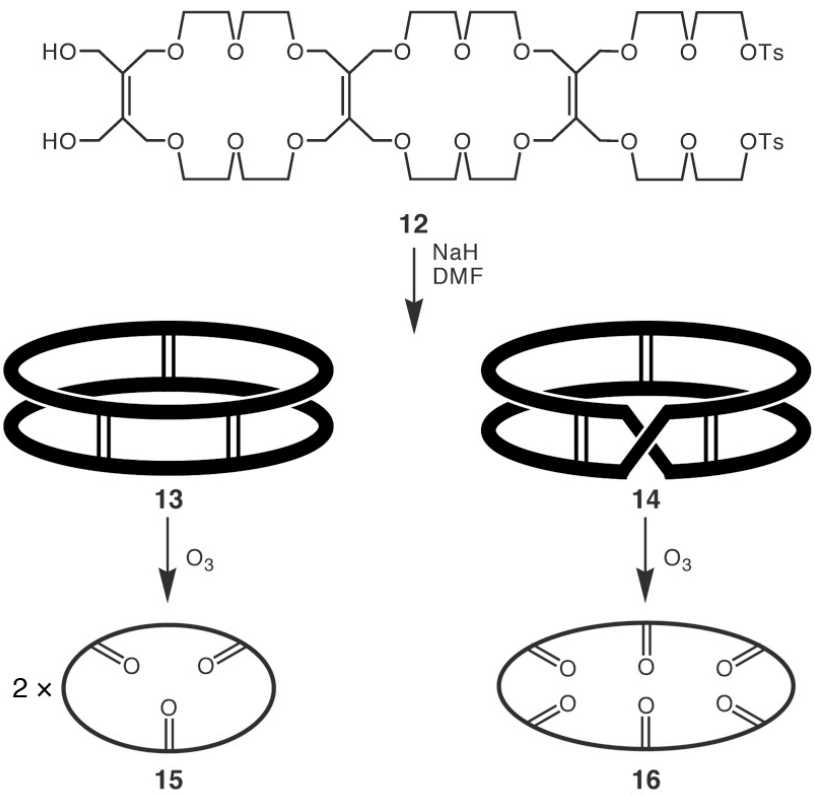

Scheme 1.7 Key steps in Walba's synthesis of a topologically chiral Möbius Strip.[82]

The three-rung Möbius strip **14** is a fascinating topological object. The graph of a three-rung Möbius ladder is non-planar and contains $K_{3,3}$ as a sub-graph. Though NMR titration experiments confirmed that **14** is chiral,[80] chemical chirality depends on rigidity and does not imply topological chirality. This intrigued Jon Simon, a topologist, and he proved that Möbius ladders with three rungs are topologically chiral, *if* the rungs and edges are differentiated.[83] It turns out that all Möbius ladders with an odd number of rungs greater than three are topologically chiral.[84]

Although successfully synthesizing Möbius ladders, Walba was never able to isolate any catenanes or knots via the Möbius strip approach. Ultimately, the Möbius strip approach suffers from a reliance on molecular flexibility and random twisting, and again, the problems lie not within macrocyclization, but in topological control.

1.3 Templated Synthesis of Topological Graphs

Modern syntheses of topological isomers rely heavily on molecular templates to enforce topological control. Templates are ubiquitous in nature but have only been consciously applied to chemical synthesis in the last fifty years.[85] Pederson[86] first noticed the templating effect of alkali metals in the synthesis of crown ethers, but it was Busch[87,88] who first deliberately employed them in organic synthesis. Busch defined a chemical template in the following manner: "A chemical template organizes an assembly of atoms with respect to one or more geometric loci, in order to achieve a particular linking of atoms."[89] The directed syntheses of Schill and Lüttringhaus meet this general definition but are lengthy and inefficient. In 1983, Sauvage and coworkers[90] were able to synthesize efficiently a [2]-catenane using a transition metal as a template. Several other template approaches relying on the principles of supramolecular chemistry[91] have since been effectively applied to the synthesis of topologically complex molecules. The most important and successful of these have used (i) metal-ion, (ii) hydrogen bonding, and (iii.) donor/acceptor interactions as templates.

1.3.1 Metal Ion Templates

The metal ion can be called the archetypal chemical template,[92] and provides a single anchor point around which to construct the desired molecule. The role of metal ion templates in macrocycle synthesis cannot be overemphasized. For example, in Pederson's famous synthesis of 18-crown-6 **17**, a potassium ion brings together the nucleophile and electrophile (Scheme 1.8a).[93] Equally important, Curtis[94] and Busch[87,88] used nickel to template macrocycle formation in high yields (Scheme 1.8b and c).

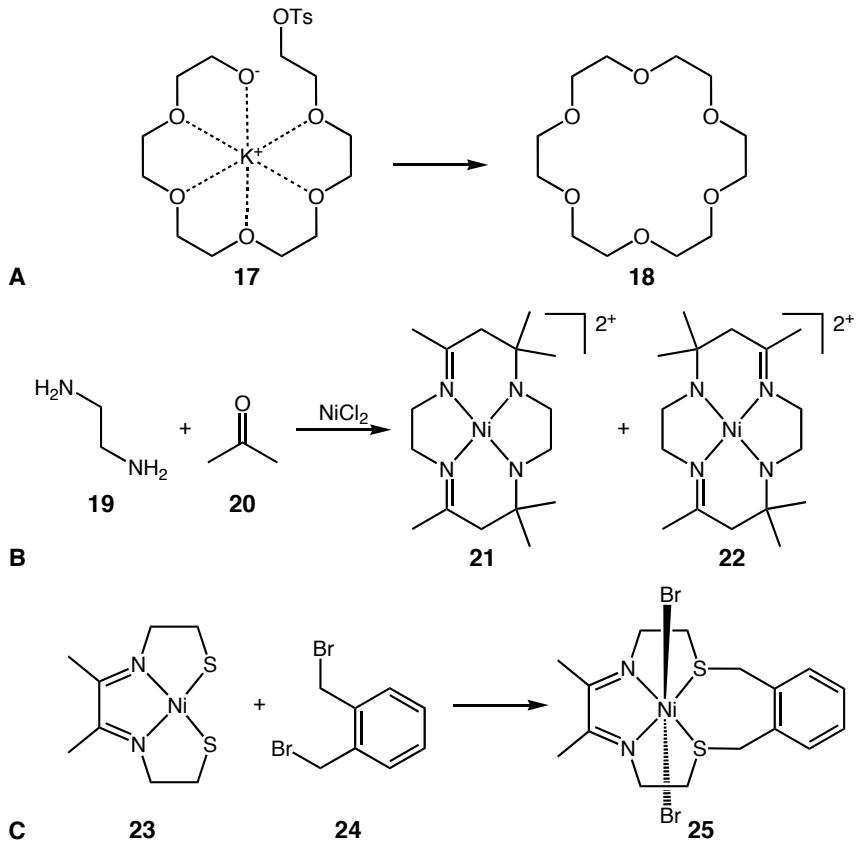

Scheme 1.8 (a) Potassium ion templated synthesis of 18-crown-6 and the use of nickel(II) to template tetraazamacrocycles by (b) Curtis and (c) Busch.

Wasserman[24] and Sokolov[95] envisaged that the predictable three-dimensional geometry of a transition metal would lend itself to the synthesis of catenanes and knots, but the use of metal ions templates, with a few exceptions,[96] remained in two-dimensional space. It wasn't until Sauvage first took full advantage of the three-dimensional geometry of transition metal ions to synthesize topologically complex molecular graphs.

Sauvage and coworkers envisaged two potential routes were for the construction of a [2]-catenane (Scheme 1.9). [26] In route (a), the two halves are brought together around the metal center before a double macrocyclization occurs. Route (b) requires the synthesis of a macrocycle first and the threading a second half-ring before the final cyclization. Note that route (a) can be mapped on to pathway (c) and route (b) onto pathway (b) of Lüttringhaus (Figure 1.3).

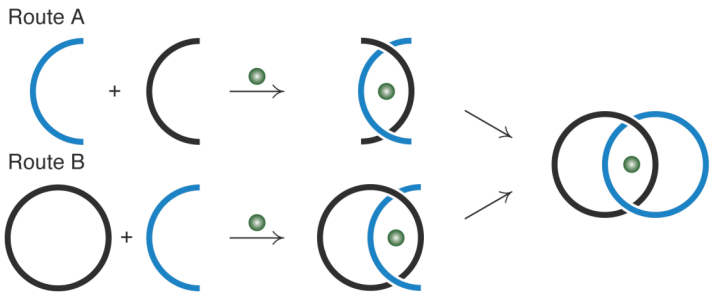

Scheme 1.9 Synthetic strategies based on a three-dimensional transition metal template.

Initially choosing route (b), Sauvage and coworkers employed the tetrahedral geometry of copper(I) with an appropriately substituted phenanthroline ligand to enforce the correct conformation (Scheme 1.10). Pre-catenane complex **28** is quantitatively formed by mixing phenanthroline macrocycle **26** and copper(I) before adding ligand **27**. Treatment of **28** with diiodohexaethylene glycol under basic conditions gave the catenand **29** in 42% yield. Route (a) was subsequently applied, but resulted in lower yields, 27%, of catenand **29**. Sauvage and many others have applied metal templates with much success and have achieved the molecular realization of a wealth of topological target including knots,[97,98] catenanes,[26,99] polycatenanes,[100,101] dumbbell shaped molecules called rotaxanes,[102] racks,[103] grids,[104] and helicates.[105]

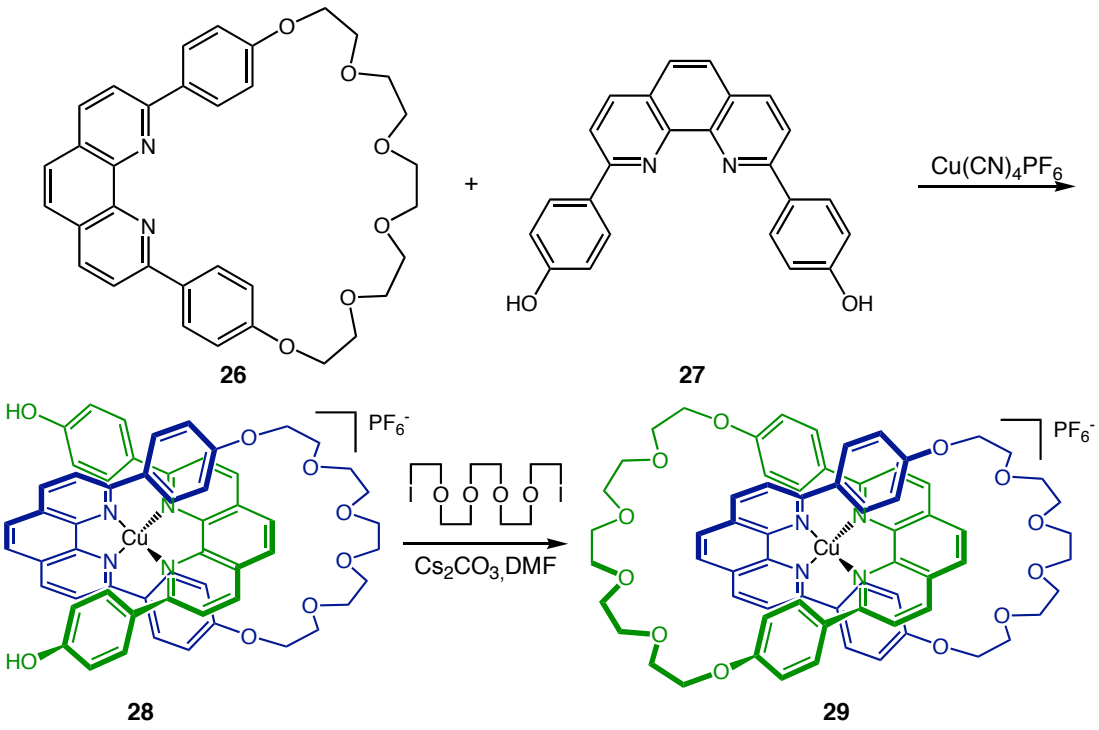

Scheme 1.10 Sauvage's transition metal templated catenane synthesis.[26]

Metal ions have also been used to facilitate the self-assembly of organometallic interlocked structures such as the catenanes of Fujita,[106] **30**, and Bickelhaupt,[107] **31** (Figure 1.25). In these intriguing applications of coordination chemistry, the templating metal ions are now an integrated part of the structural whole.[89]

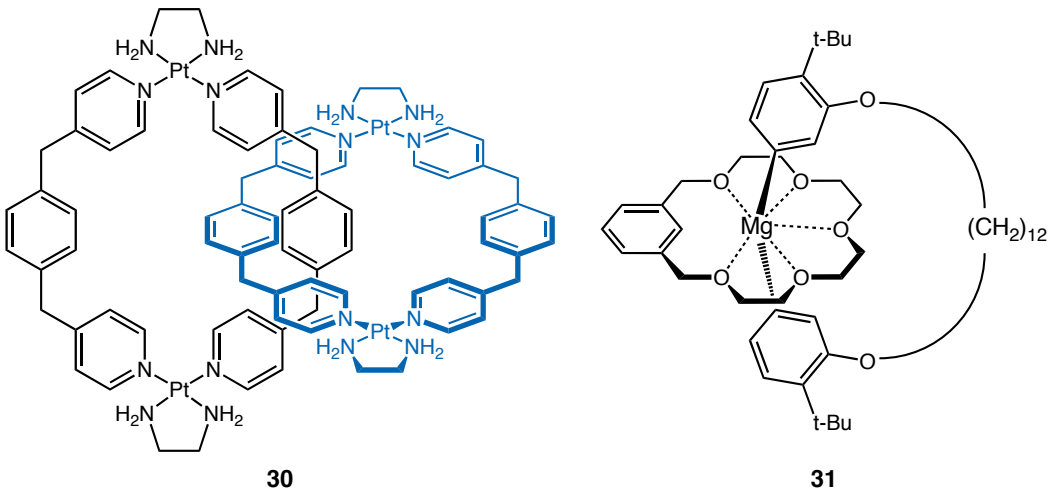

Figure 1.25 Organometallic catenanes of Fujita[106] and Bickelhaupt[107]

1.3.2 π-Donor π-Acceptor Templates

When designing a synthetic receptor for the electron deficient herbicides, diquat and paraquat, Stoddart and coworkers choose to combine π-electron rich dioxy-aromatics and macrocyclic polyethers.[108] The resulting pseudorotaxane-like host-guest complex **31** (Figure 1.26) inspired the first donor-acceptor catenane **35** (Scheme 1.11).[109]

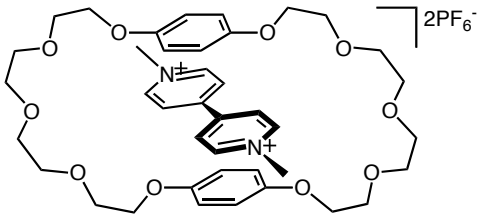

31

Figure 1.26 Pseudorotaxane host-guest complex of bis-*p*-phenylene-34-crown-10 and paraquat.

The dicationic **32**, prepared from *p*-xylylene dibromide **33** and excess 4,4'-biypyridine, is stirred with **33** and excess of the electron rich macrocyclic polyether **34**, and after two days, a 70% yield of the [2]-catenane **35** is isolated as the PF_6^- salt. The templating π-π interactions are revealed in the crystal structure. Not only are the aromatic rings within the catenane at optimal π-stacking distances, but the stacking interactions are propagated along a crystallographic axis between separate molecules. In the solution state, the interactions are weak and the rings can circumrotate freely at room temperature.[110] The Stoddart group and its collaborators are proliferate in applying this template to catenanes,[108] polycatenanes,[111] rotaxanes,[108] with an special emphasis on the design of molecular machines.[112]

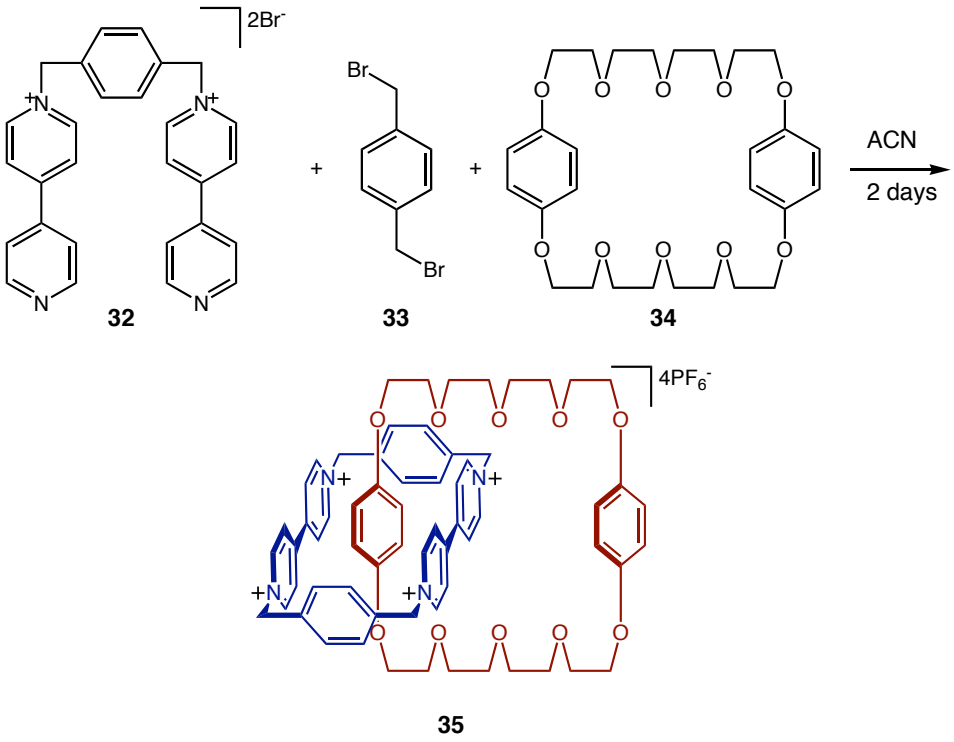

Scheme 1.11 Stoddart's first π-donor π-acceptor catenane.

1.3.3 Hydrogen Bonding Templates

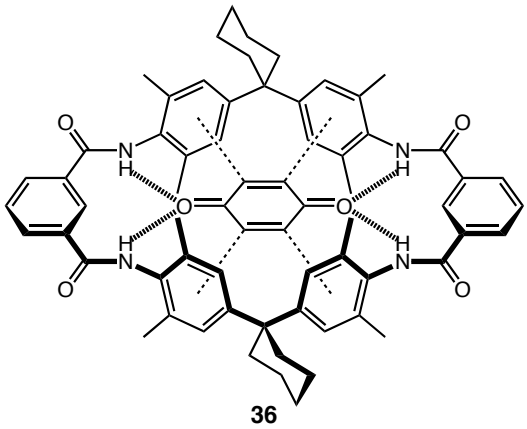

Figure 1.27 Complexation of *p*-benzoquinone by host **34.**[113]

In 1991, Hunter set out to create a receptor for benzoquinone and, relying hydrogen bonding and π-π interactions, designed macrocyclic host **36** (Figure 1.27).[113]

Host **36** was obtained in 10% yield from the reaction of diamine **37** and isophthaloyl dichloride **38**. When the synthesis was modified to a two-step procedure, the yield was increased to 51%, and two new products were isolated: the cyclic tetramer and the serendipitous new [2]-catenane **39** (Scheme 1.12). Later X-ray crystal structures confirmed these results and elucidated the hydrogen bond network holding the catenane together.[114]

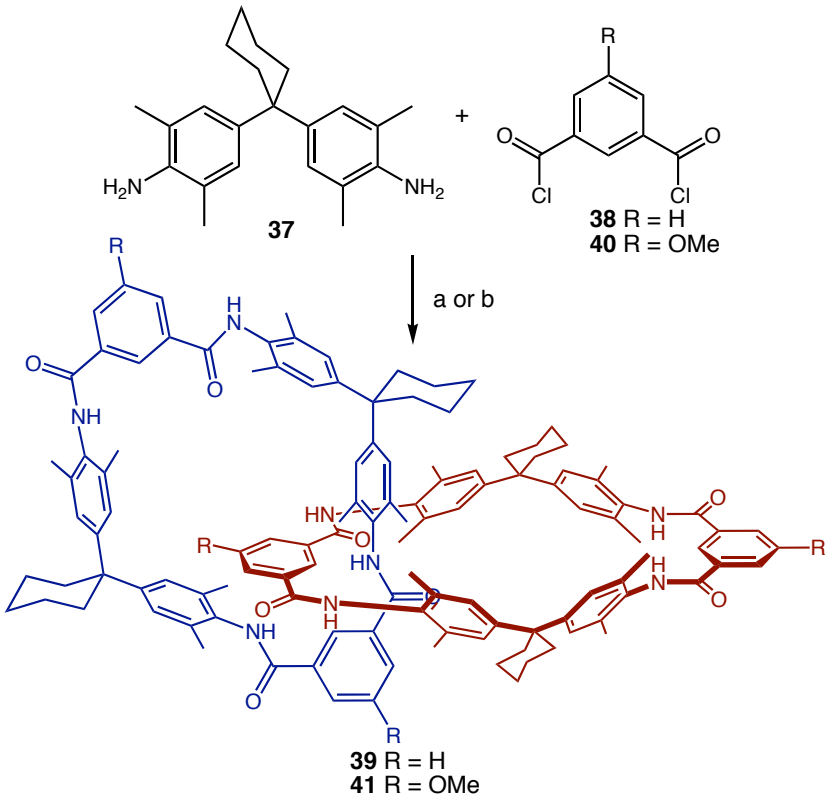

Scheme 1.12 Hunter-Vögtle synthesis of [2]-catenanes.

Concurrently, while en route to basket-shaped molecules, the Vögtle group reacted diamine **37** with 5-methoxyisophthaloyl dichloride **40** and obtained the desired tetrameric macrocycle in 10% yield as well as the [2]-catenane **41** in 8% yield (Scheme

1.11).[115] Further mechanistic investigations found that the macrocycle **36** (and derivatives) were the key intermediate in catenane formation.[116]

In 1995 Leigh et. al. reported a simple and general catenane synthesis from the readily available isophthaloyl dichloride and 1,4-bis(aminomethyl)benzene (Figure 1.28).[117,118] A variety of diamines and diacid chlorides are tolerated and, unlike the more hindered Vögtle-Hunter catenanes, the rings have free circumrotation.[119] The Leigh and Vögtle groups have continued to employ the amide-based hydrogen template to synthesis catenanes,[120] rotaxanes,[120] and knots,[121] the most impressive of which is the one pot synthesis and subsequent resolution of the molecular trefoil knot **43** (Figure 1.29).[122]

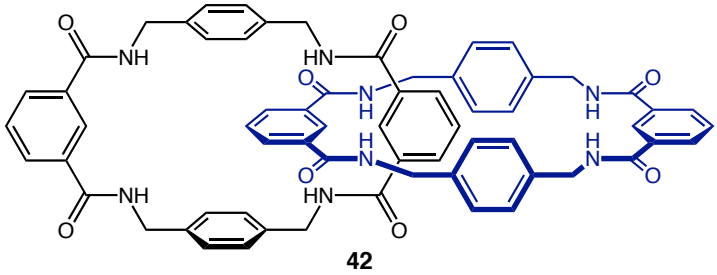

42

Figure 1.28 Leigh-type amide [2]-catenane.

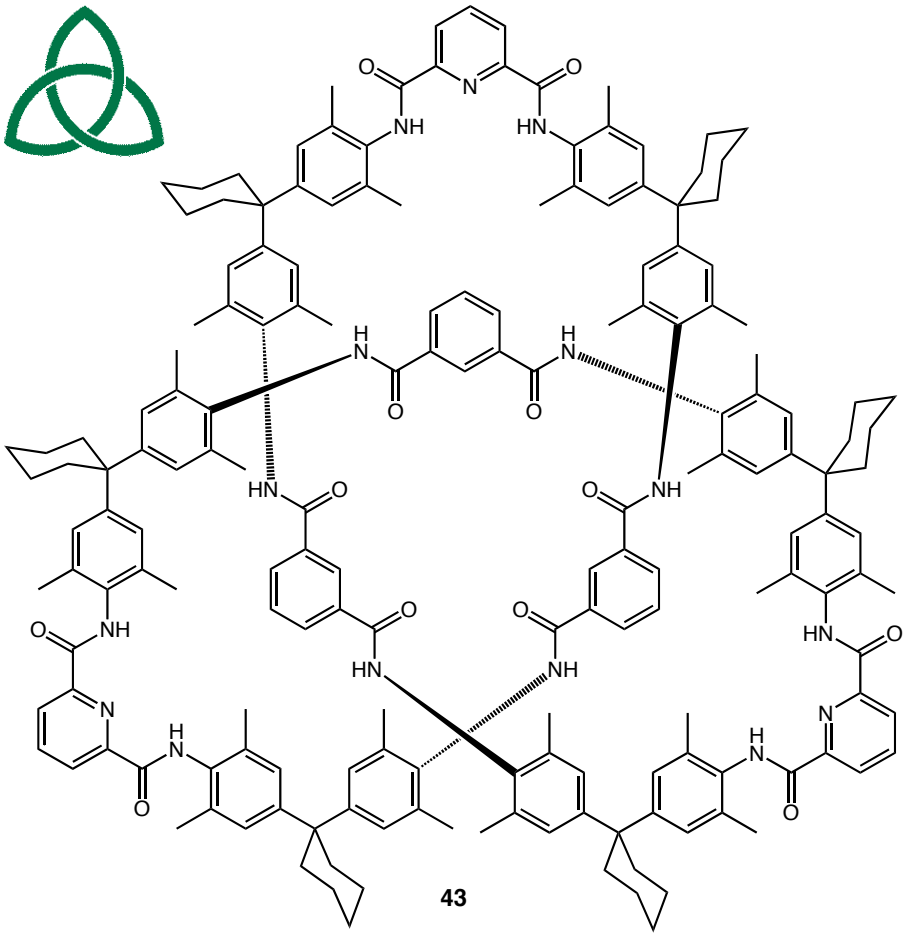

Figure 1.29 Vögtle's "knotane", a molecular trefoil knot.

The Busch[123] and Stoddart[124] groups have independently investigated an alternative hydrogen bond template, based on secondary ammonium ions and crown ethers. To date, only rotaxanes, such as **44** (Figure 1.30), and pseudorotaxanes have been synthesized.

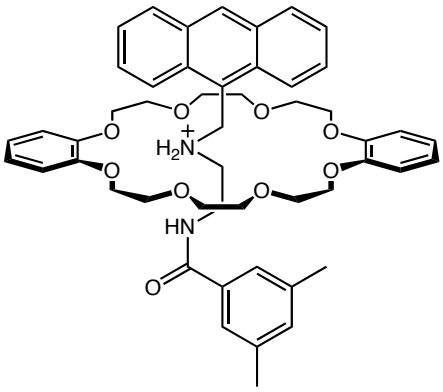

44

Figure 1.30 Busch's ammonium-type hydrogen bond template.[123]

1.4 Thesis Objectives

Initially an intellectual challenge, topology is showing an increasingly significant role in biomolecules and nanotechnology. The elementary topological concepts presented here have inspired a variety of new synthetic methodologies specifically designed to address the control of topology. The complicated structures of topologically complex graphs ensure that no plan is prescient of the variety of complications inherent to the conformational flexibility of large macrocycles.

Given the success and synthetic versatility of transition metal templates, the goal of this thesis is to apply this strategy to synthesis of interlocked rings and to gain a better understanding of the influence of topology on the structure and properties of chemical links. The subsequent chapter describes the synthesis of an array of manisyl-substituted 2-pyridyl-[1,10]phenanthrolines; a series of oriented terpyridine analogues.

The third chapter and fourth chapter detail their intriguing photophysical properties and coordination chemistry. The Borromean link is a fascinating embedding of a three link and recent advances towards a kinetic synthesis based on manisyl-substituted terpyridines will be described in chapter five.

1.5 References

(1) Brent, R. *The Golden Book of Chemistry Experiments*; Golden Press: New York, 1960, p 112.

(2) Thomson, W. H. *Trans. R. Soc. Edinburgh* **1869**, *25*, 217-260.

(3) Tait, P. G. *Trans. R. Soc. Edinburgh* **1876**.

(4) Tait, P. G. *Trans. R. Soc. Edinburgh* **1884**.

(5) Tait, P. G. *Trans. R. Soc. Edinburgh* **1885**.

(6) Schill, G. *Catenanes, Rotaxanes, and Knots*; Academic Press: New York, 1971; Vol. 22, p 192.

(7) *Molecular Catenanes, Rotaxanes, and Knots: A journey through the world of molecular topology*; Sauvage, J.-P.; Dietrich-Buchecker, C., Eds.; Wiley-VCH: Weinheim, 1999, p 368.

(8) Schill, G.; Zuercher, C. *Naturwiss.* **1971**, *58*, 40-45.

(9) Lehn, J.-M. *Angew. Chem., Int. Ed. Engl.* **1988**, *27*, 89-112.

(10) Wasserman, E. In *Molecular Catenanes, Rotaxanes and Knots: A Journey Through the World of Molecular Topology*; Sauvage, J.-P., Dietrich-Buchecker, C., Eds.; Wiley-VCH: Weinheim, 1999, pp 1-6.

(11) Jung, C. *Man and His Symbols*, 1974.

(12) Dmitriev, I. S. *Molecules Without Chemical Bonds*; Mir Publishers: Moscow, 1981, p 155.

(13) Partington, J. R. *A Short History of Chemistry*; 3 ed.; Dover: New York, 1989, p 415.

(14) Kekulé, A. *Bulletin de la Société Chimique Francais* **1865**, 98-110.

(15) Couper, A. S. *Philos. Mag.* **1858**, *16*, 104-116.

(16) Butlerov, A. M. *Zeitschrift für Chemie und Pharmacie* **1861**, *4*, 546-549.

(17) Kekulé, A. *Annalen der Chemie und Pharmacie* **1858**, *106*, 129-159.

(18) Crum Brown, A. *Proc. R. Soc. Edinburgh* **1864**, *23*, 428-.

(19) Van't Hoff, J. H. *Neerlandaises des Sciences Exactes et Naturelles* **1874**, *9*, 445-454.

(20) Le Bel, J. A. *Bull. Soc. Chim. Fr.* **1874**, *22*, 337.

(21) Clayton, D. A.; Vinograd, J. *Nature* **1967**, *216*, 652-657.

(22) Hudson, B. J.; Vinograd, J. *Nature* **1967**, *216*, 647-652.

(23) Liu, L. L.; Depew, R. E.; Wang, J. C. *Journal of Molecular Biology* **1976**, *106*, 439-452.

(24) Frisch, H. L.; Wasserman, E. *J. Am. Chem. Soc.* **1961**, *83*, 3789-3795.

(25) Walba, D. M. *Tetrahedron* **1985**, *41*, 3161-3212.

(26) Dietrich-Buchecker, C.; Sauvage, J.-P. *Chem. Rev.* **1987**, *87*, 795-810.

(27) Reidemeister, K. *Knotentheorie*; Springer: Berlin, 1932.

(28) Rolfsen, D. *Knots and Links*; Publish or Perish: Berkeley, 1976.

(29) Adams, C. C. *The Knot Book*; W.H. Freeman and Co.: New York, 1994, p 306.

(30) Flapan, E. *When Topology Meets Chemistry: A Topological Look at Molecular Chirality*; Cambridge University: Cambridge, 2000, p 241.

(31) Thomson, W. H. *J. Oxford Univ. Junior Scientific Club* **1894**, *18*, 25-.

(32) Mislow, K. *Introduction to Stereochemistry*; Dover: Mineola, 2002, p 193.

(33) Martin, R. H. *Angew. Chem., Int. Ed. Engl.* **1974**, *13*, 649-660.

(34) Monkhorst, H. J. *Chem. Commun.* **1968**, 1111-1112.

(35) Euler, L. *Acad. Sci. Imp. Petropol.* **1736**, *8*, 128-140.

(36) Trinajstc, N. *Chemical Graph Theory*; CRC Press: Boca Raton, 1992, p 352.

(37) Rouvray, D. H. *Journal of Molecular Structure: THEOCHEM* **1989**, *185*, 1-14.

(38) Cayley, A. *Philos. Mag.* **1877**, *3*, 34-35.

(39) Rücker, C.; Meringer, M. *Communications in Mathematical and in Computer Chemistry* **2002**, *45*, 153-172.

(40) Chambron, J.-C.; Dietrich-Buchecker, C.; Sauvage, J.-P. *Top. Curr. Chem.* **1993**, *165*, 131-162.

(41) Simmons III, H. E.; Maggio, J. E. *Tetrahedron Lett.* **1981**, *22*, 187-290.

(42) Chen, C.-T.; Gantzel, P.; Siegel, J. S.; Baldridge, K. K.; English, R. B.; Ho, D. M. *Angew. Chem., Int. Ed. Engl.* **1996**, *34*, 2657-2660.

(43) Paquette, L. A.; Vazeux, M. *Tetrahedron Lett.* **1981**, *22*, 291-294.

(44) Nakazaki, M.; Yamamoto, K.; Tanaka, S.; Kametani, H. *J. Org. Chem.* **1977**, *77*, 287-291.

(45) Aldersey-Williams, H. *The Most Beautiful Molecule: The Discovery of the Buckyball*; John Wiley & Sons, 1995, p 340.

(46) Kuratowski, K. *Fund. Math.* **1930**, *15*, 271-283.

(47) Sritana-Anant, Y.; Seiders, T. J.; Siegel, J. S. *Top. Curr. Chem.* **1998**, *196*, 1-43.

(48) Liang, C.; Mislow, K. *J. Math. Chem.* **1995**, *18*, 1-24.

(49) Livingston, C. *Knot Theory*; Math. Assoc. Amer.: Washington D.C., 1993.

(50) Tauber, S. J. *J. Res. Natl. Bur. Stand. A* **1963**, *67A*, 591-599.

(51) Cerf, C. In *Chemical Topology: Applications and Techniques*; Bochev, D., Rouvray, D. H., Eds.; Gordon and Breach: Amsterdam, 2000; Vol. 6, pp 1-35.

(52) Jones, V. F. R. *Bull. Am. Math. Soc.* **1985**, *89*, 103-111.

(53) Freyd, P.; Yetter, D.; Hoste, J.; Lickorish, W.; Millet, K.; Ocneanu, A. *Bull. Am. Math. Soc.* **1985**, *12*, 239-246.

(54) Kaufmann, L. *Topology* **1987**, *26*, 395-407.

(55) Vassiliev, V. A. In *Theory of Singularities and its Applications*; Arnold, V. I., Ed.; Am. Math. Soc.: Providence, R.I., 1990, pp 9-69.

(56) The existence of enantiomers does not ensure a measurable optical activity. Firstly, the two enantiomers must be separable or it must be possible to achieve a mixture enriched in one enantiomer. Secondly, the optical activity of an enantiopure solution can still fall below the detection threshold. See the following reference for an interesting discussion by Mislow and Bickart on cryptochirality and the fuzziness inherent in any observable.

(57) Mislow, K.; Bickart, P. *Israel Journal of Chemistry* **1977**, *15*, 1-6.

(58) Ziegler, K.; Eberle, H.; Ohlinger, H. *Liebigs Ann. Chem.* **1933**, *504*, 94-130.

(59) Hansley, V. L. *J. Am. Chem. Soc.* **1935**, *57*, 2303-2305.

(60) Prelog, V.; Frenkiel, L.; Kobelt, M.; Barman, P. *Helv. Chim. Acta* **1947**, *30*, 1741-1749.

(61) Stoll, M.; Hulstkamp, J. *Helv. Chim. Acta* **1947**, *30*, 1815-1821.

(62) Lüttringhaus, A.; Cramer, F.; Prinzbach, H. *Angewandte Chemie* **1957**, *60*, 137.

(63) van Gulick, N. *N. J. Chem.* **1993**, *17*, 619-625.

(64) Wasserman, E. *Sci. Am.* **1962**, *207*, 94-102.

(65) Wasserman, E. *J. Am. Chem. Soc.* **1960**, *82*, 4433-4434.

(66) Agam, G.; Graiver, D.; Zilkha, A. *J. Am. Chem. Soc.* **1976**, *98*, 5206-5214.

(67) Agam, G.; Zilkha, A. *J. Am. Chem. Soc.* **1976**, *98*, 5214-5216.

(68) Harrison, I. T. *J. Chem. Soc., Chem. Commun.* **1972**, 231-232.

(69) Harrison, I. T. *J. Chem. Soc., Perkins Trans. 1* **1974**, 301-304.

(70) Wang, J. C.; Schwartz, H. *Biopolymers* **1967**, *5*, 953-966.

(71) Schill, G. *Chem. Ber.* **1967**, *100*, 2021-2037.

(72) Schill, G.; Logemann, E.; Vetter, W. *Angew. Chem., Int. Ed. Engl.* **1972**, *11*, 1089-1090.

(73) Logemann, E.; Schill, G.; Vetter, W. *Chem. Ber.* **1978**, *111*, 2615-2629.

(74) Logemann, E.; Rissler, K.; Schill, G.; Fritz, H. *Chem. Ber.* **1981**, *114*, 2245-2260.

(75) Schill, G.; Rissler, K.; Fritz, H. *Chem. Ber.* **1983**, *116*, 1866-1872.

(76) *The World of M.C. Escher*; Locher, J. L., Ed.; Harry N. Abrams, Inc.: New York, 1988, p 263.

(77) Guy, R. K.; Harary, F. *Can. Math. Bull.* **1967**, *10*, 493.

(78) Wolovsky, R. *J. Am. Chem. Soc.* **1970**, *92*, 2132-2133.

(79) Ben-Efraim, D. A.; Batich, C.; Wasserman, E. *J. Am. Chem. Soc.* **1970**, *92*, 2133-2135.

(80) Walba, D. M.; Richards, R. M.; Haltiwanger, R. C. *J. Am. Chem. Soc.* **1982**, *104*, 3219-3221.

(81) Walba, D. M.; Richards, R. M.; Sherwood, S. P. *J. Am. Chem. Soc.* **1981**, *103*, 6213-6215.

(82) Walba, D. M.; Homan, T. C.; Richards, R. M.; Haltiwanger, R. C. *N. J. Chem.* **1993**, *17*, 661-681.

(83) Simon, J. *Topology* **1986**, *25*, 229-235.

(84) Flapan, E. *Math. Ann.* **1989**, *283*, 271-283.

(85) *Templated Organic Synthesis*; Diederich, F.; Stang, P. J., Eds.; Wiley-VCH: Weinheim, 2000, p 410.

(86) Pederson, C. J. *J. Am. Chem. Soc.* **1967**, *89*, 7017-7036.

(87) Busch, D. H.; Thompson, M. C. *J. Am. Chem. Soc.* **1962**, *84*, 1762-1763.

(88) Busch, D. H.; Thompson, M. C. *J. Am. Chem. Soc.* **1964**, *86*, 3651-3656.

(89) Busch, D. H.; Stephenson, N. A. *Coord. Chem. Rev.* **1990**, *100*, 119-154.

(90) Dietrich-Buchecker, C.; Sauvage, J.-P.; Kintzinger, J.-P. *Tetrahedron Lett.* **1983**, *24*, 5095-5098.

(91) *Comprehensive Supramolecular Chemistry*; Lehn, J.-M.; Atwood, J. L.; Davies, J. E. D.; Mac Nicol, D. D.; Vögtle, F., Eds.; Pergamon: Oxford, 1996, p 7660.

(92) Hubin, T. J.; Kolchinski, A. G.; Vance, A. L.; Busch, D. H. *Adv. Supramolec. Chem.* **1999**, *5*, 237-357.

(93) Greene, R. N. *Tetrahedron Lett.* **1972**, *13*, 1793-1796.

(94) Curtis, N. F. *Coord. Chem. Rev.* **1967**, *3*, 3-47.

(95) Sokolov, V. I. *Russ. Chem. Rev.* **1973**, *42*, 452-463.

(96) Creaser, I. I.; Harrowfield, J. M.; Herlt, A. J.; Sargeson, A. M.; Springborg, J.; Geue, R. J.; Snow, M. R. *J. Am. Chem. Soc.* **1977**, *99*, 3181-3182.

(97) Dietrich-Buchecker, C.; Rapenne, G.; Sauvage, J.-P. In *Molecular Catenanes, Rotaxanes and Knots: A Journey Through the World of Molecular Topology*; Sauvage, J.-P.,

Dietrich-Buchecker, C., Rapenne, G., Eds.; Wiley-VCH: Weinheim, 1999, pp 107-142.

(98) Dietrich-Buchecker, C.; Colasson, B. X.; Sauvage, J.-P. *Top. Curr. Chem.* **2005**, *249*, 261-283.

(99) Nierengarten, J. F.; Dietrich-Buchecker, C.; Sauvage, J.-P. *J. Am. Chem. Soc.* **1994**, *116*, 375-376.

(100) Dietrich-Buchecker, C.; Khemiss, A. K.; Sauvage, J.-P. *J. Chem. Soc., Chem. Commun.* **1986**, 1376-1378.

(101) Dietrich-Buchecker, C.; Hemmert, C.; Khemiss, A. K.; Sauvage, J.-P. *J. Am. Chem. Soc.* **1990**, *112*, 8002-8008.

(102) Blanco, M.-J.; Chambron, J.-C.; Jimenez, M. C.; Sauvage, J.-P. *Top. Stereochem.* **2003**, *23*, 125-173.

(103) Hanan, G. S.; Arana, C. R.; Lehn, J.-M.; Fenske, D. *Angew. Chem., Int. Ed. Engl.* **1995**, *34*, 1122-1124.

(104) Ruben, M.; Rojo, J.; Romero-Salguero, F. J.; Uppadine, L. H.; Lehn, J.-M. *Angewandte Chemie, International Edition* **2004**, 3644-3662.

(105) Piguet, C.; Bernardinelli, G.; Hopfgartner, G. *Chem. Rev.* **1997**, *97*, 2005-2062.

(106) Fujita, M. In *Molecular Catenanes, Rotaxanes, and Knots: A Journey Through the World of Molecular Topology*; Sauvage, J.-P., Dietrich-Buchecker, C., Eds.; Wiley-VCH: Weinheim, 1999, pp 368.

(107) Gruter, G.-J.; de Kanter, F. J. J.; Markies, P. R.; Nomoto, T.; Akkerman, O. S.; Bickelhaupt, F. *J. Am. Chem. Soc.* **1993**, *115*, 12179-12180.

(108) Amabilino, D. B.; Stoddart, J. F. *Chem. Rev.* **1995**, *95*, 2725-2828.

(109) Ashton, P. R.; Goodnow, T. T.; Kaifer, A. E.; Reddington, M. V.; Slawin, A. M. Z.; Spencer, N.; Stoddart, J. F.; Vicent, C.; Williams, D. J. *Angew. Chem., Int. Ed. Engl.* **1989**, *28*, 1396-1399.

(110) Anelli, P. L.; Ashton, P. R.; Ballardini, R.; Balzani, V.; Delgado, M.; Gandolfi, M. T.; Goodnow, T. T.; Kaifer, A. E.; Philp, D.; Pietraszkiewicz, M.; Prodi, L.; Reddington, M. V.; Slawin, A. M. Z.; Spencer, N.; Stoddart, J. F.; Vicent, C.; Williams, D. J. *J. Am. Chem. Soc.* **1992**, *114*, 193-218.

(111) Raymo, F. M.; Stoddart, J. F. *Chem. Rev.* **1999**, *99*, 1643-1663.

(112) Balzani, V.; Credi, A.; Raymo, F. M.; Stoll, M. *Angew. Chem. Int. Ed.* **2000**, *39*, 3349-3391.

(113) Hunter, C. A. *J. Chem. Soc., Chem. Commun.* **1991**, 749-751.

(114) Adams, H.; Carver, F. J.; Hunter, C. A. *J. Chem. Soc., Chem. Commun.* **1995**, 809-810.

(115) Vögtle, F. *Angew. Chem., Int. Ed. Engl.* **1992**, *31*, 1619-1622.

(116) Ottens-Hildebrandt, S.; Meier, S.; Schmidt, W.; Vögtle, F. *Angew. Chem., Int. Ed. Engl.* **1994**, *33*, 1767-.

(117) Johnston, A. G.; Leigh, D. A.; Pritchard, R. J.; Deegan, M. D. *Angew. Chem., Int. Ed. Engl.* **1995**, *34*, 1209-1212.

(118) Johnston, A. G.; Leigh, D. A.; Nezhat, L.; Smart, J. P.; Deegan, M. D. *Angew. Chem., Int. Ed. Engl.* **1995**, *34*, 1212-1216.

(119) Heim, C.; Udelhofen, D.; Vogtle, F. In *Molecular Catenanes, Rotaxanes and Knots*; Sauvage, J.-P., Dietrich-Buchecker, C., Eds.; Wiley-VCH: Weinheim, 1999, pp 177-222.

(120) Heim, C.; Udelhofen, D.; Vogtle, F. In *Molecular Catenanes, Rotaxanes and Knots: A Journey Through the World of Molecular Topology*; Sauvage, J.-P., Dietrich-Buchecker, C., Eds.; Wiley-VCH: Weinheim, 1999, pp 177-222.

(121) Lukin, O.; Vögtle, F. *Angew. Chem. Int. Ed.* **2005**, *44*, 2-23.

(122) Vögtle, F.; Hünten, A.; Vogel, E.; Buschbeck, S.; Safarowsky, O.; Recker, J.; Parham, A.-H.; Knott, M.; Müller, W. M.; Müller, U.; Okamoto, Y.; Kubota, T.; Lindner, W.; Francotte, E.; Grimme, S. *Angew. Chem. Int. Ed.* **2001**, *40*, 2468-2471.

(123) Kolchinski, A. G.; Busch, D. H.; Alcock, N. W. *J. Chem. Soc., Chem. Commun.* **1995**, 1289-1291.

(124) Ashton, P. R.; Campbell, P. J.; Chrystal, E. J. T.; Glink, P. T.; Menzer, S.; Philip, D.; Spencer, N.; Stoddart, J. F.; Tasker, P. A.; Williams, D. J. *Angew. Chem., Int. Ed. Engl.* **1995**, *34*, 1865.

CHAPTER 2

SYNTHESIS OF 2-PYRIDYL-1,10-PHENANTHROLINES

2.0 Abstract

In order to achieve topologically chiral 2-catenanes via octahedral transition metal templates, a modular palladium catalyzed cross coupling procedure was developed and a 3 × 3 array of aryl substituted 2-pyridyl-1,10-phenanthrolines (pherpy) was synthesized. The systematic variation of the substitution pattern of such oriented terpyridine (terpy) analogues provides valuable control over photo and electronic properties as well as the specific spatial orientation of the resulting metal complexes.

2.1 Introduction

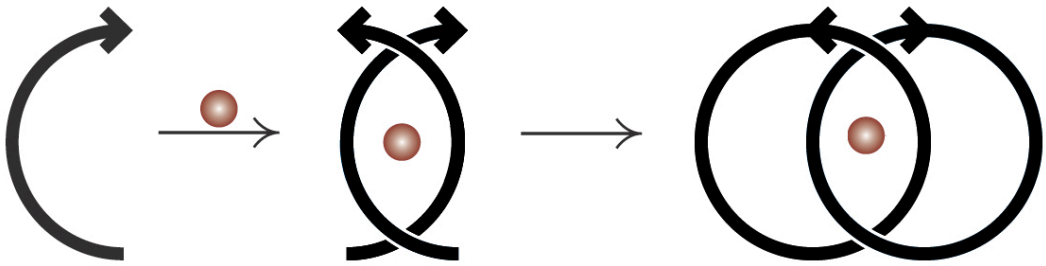

Figure 2.1 Metal Templated Synthesis of a chiral Hopf link.

The synthesis of an oriented, and thus chiral, Hopf link using a metal template strategy requires a suitably oriented ligand (Figure 2.1). The terdentate 2,2':6',2''-terpyridine (terpy) **45** has been used extensively for the formation of octahedral transition metal complexes,[1] and a wealth of symmetrical derivatives have been prepared,[2] including bridged[3] and chiral examples.[4] Only a limited number of unsymmetrical analogues are known,[5] of which 2-(pyrid-2-yl)-1,10-phenanthroline (pherpy) **46** presents a unique juxtaposition of the 1,10-phenanthroline (phen) backbone upon a terpyridine (Figure 2.2). The extra double bond of the pherpy differentiates the left and right side and, when schematically represented, provides the pherpy with an orientation that the terpyridine lacks (Figure 2.1b). As such, pyridyl-

phenanthrolines are useful building blocks for oriented topological isomers via octahedral transition metal templates. However, the limited synthetic access to functionalized derivatives, in addition to the poor solubility of the parent heterocycle, restrict the study of this family of compounds. In the following chapter, the scope of early methodologies are discussed and a new, general synthesis of diaryl pherpy derivatives capable of addressing the alpha, beta, and gamma positions relative to the nitrogens is reported.

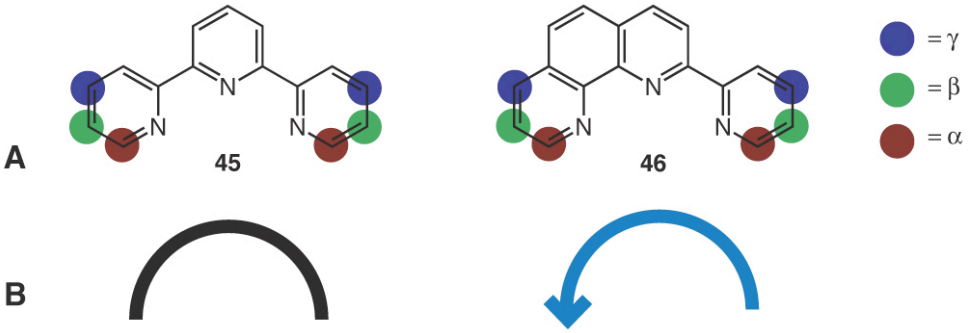

Figure 2.2 Chemical (a) and schematic (b) representations of terpy **45** and pherpy **46** with the alpha (red), beta (green), and gamma (blue) positions highlighted.

2.1.1 Condensation Methods

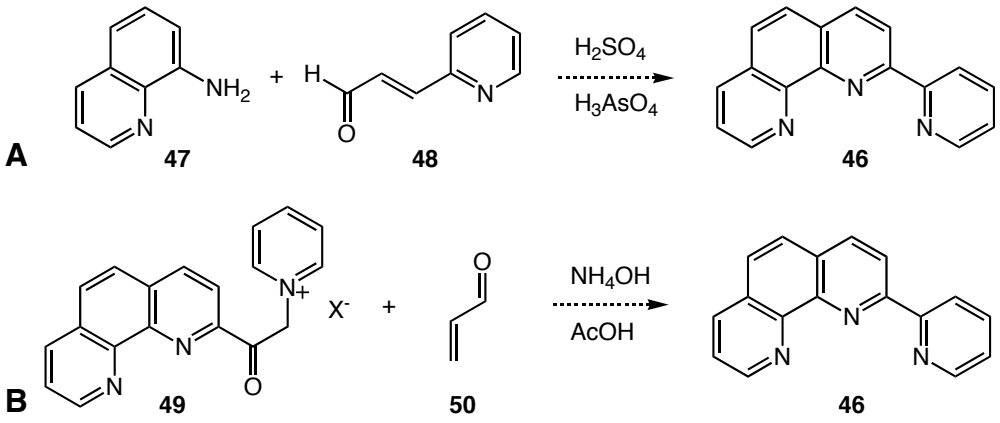

Scheme 2.1 Possible (a) Skraup[6] and (b) Kröhnke[7] syntheses of pyridyl-phenanthroline.

Although traditional Skraup[8] and Kröhnke[7] conditions (Scheme 2.1), are sufficient for pherpy synthesis, Thummel and coworkers[9] reported the first synthesis of

the parent pyridyl-phenanthroline using classical Friedländer[10] condensation methodologies (Scheme 2.2). Condensation of 8-amino-7-quinolinecarbaldehyde **51** and 2-acetylpyridine **52** in ethanolic KOH at reflux overnight gives pyridyl-phenanthroline **46** in good yield.

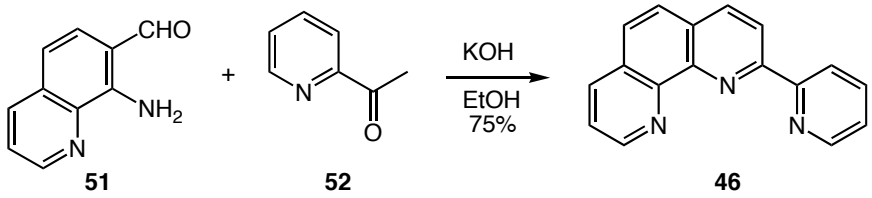

Scheme 2.2 Thummel's Friedländer synthesis of pyridyl-phenanthroline **46**.

The prerequisite **51** is not easily accessible and requires synthesis from 8-hydroxy quinoline **53** (Scheme 2.3).[9,11] The yields are acceptable, but the extra synthesis is tedious and not easily adapted to give a wide variety of pyridyl-phenanthroline derivatives. Nevertheless, Thummel and coworkers have used the Friedländer condensation of **51** to install the phenanthroline binding unit in a wealth of bridged ligands.[11-14]

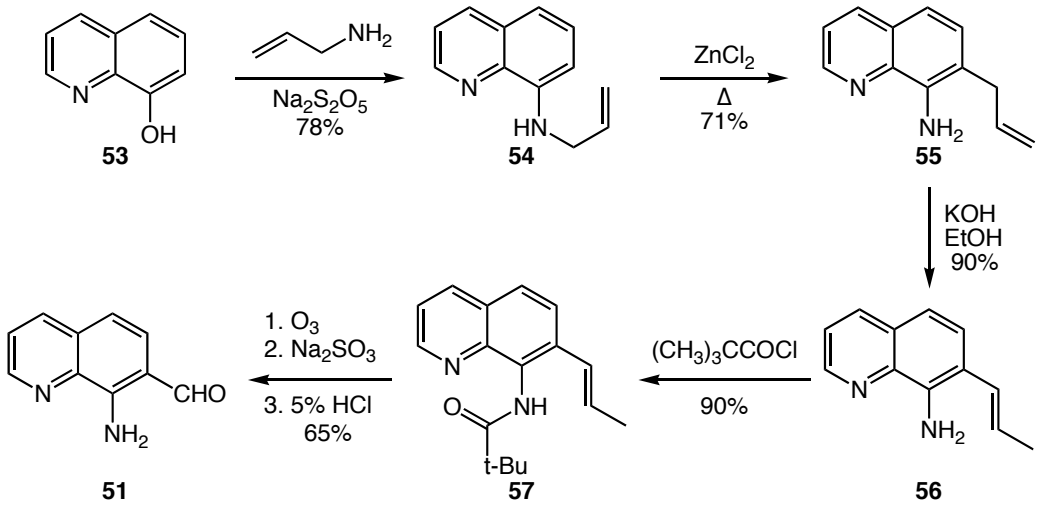

Scheme 2.3 Synthesis of 8-amino-7-quinolinecarbaldehyde **51**.

In a similar Friedländer condensation, Thummel's student, Jahng, later reversed the order of reactivity and condensed 2-acetyl-phenathroline **59** with 3-amino-2-napthaldehyde **58** to achieve the benzoannulated analogue **60** (Scheme 2.4).[15] Jahng also utilized a Michael addition of enamine **62** onto enaminone **61** to achieve the bridged analogue **63** (Scheme 2.5).[16]

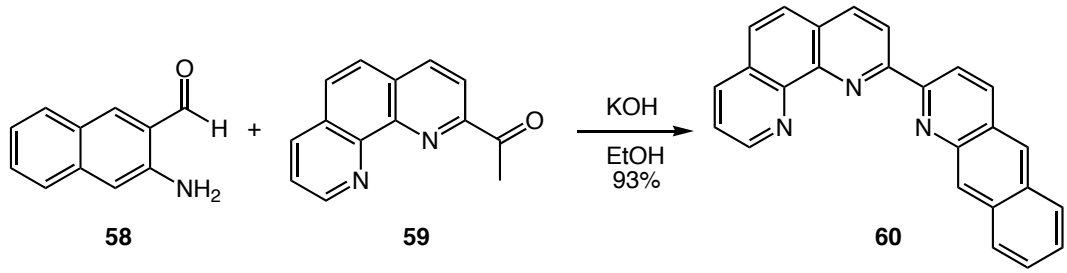

58 **59** **60**

Scheme 2.4 Synthesis of benzoannulated pyridyl-phenanthrolinee **60**.

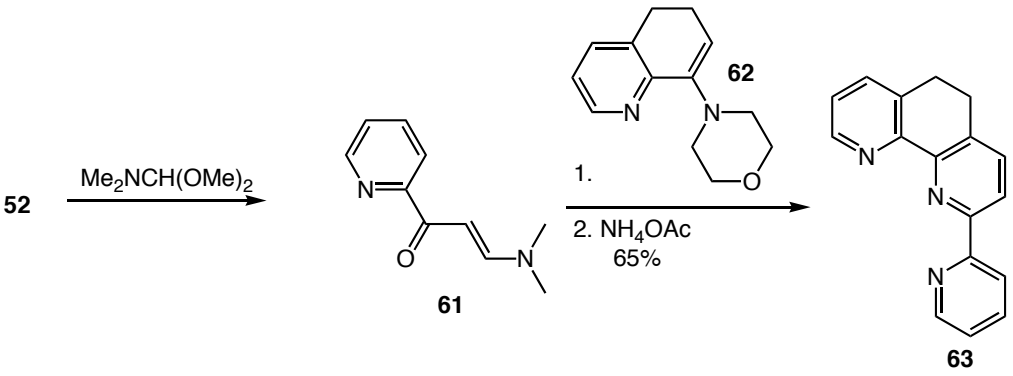

Scheme 2.5 Jahng's Kröhnke-Michael addition synthesis.

Traditional condensation methods gave the first successful synthesis of the pyridyl-phenanthroline core as well as several bridged and benzoannulated derivatives. However, the syntheses are often lengthy as each fragment must be individually synthesized, and self-condensation of amino-aldehydes is frequently a significant problem. To date, no attempts to synthesize functionalized pyridyl-phenanthroline derivatives, enabling further structural elaboration and potential tuning of electro- or photo- physical properties, have been made.

2.1.2 Nucleophilic Additions

Nitrogen containing heterocycles such as pyridine and quinoline undergo nucleophilic attack from metal amides to give amine derivatives.[17] In the Chichibabin reaction,[18] quinoline **64** is converted to 2-aminoquinoline **65** using sodium amide (Scheme 2.6).

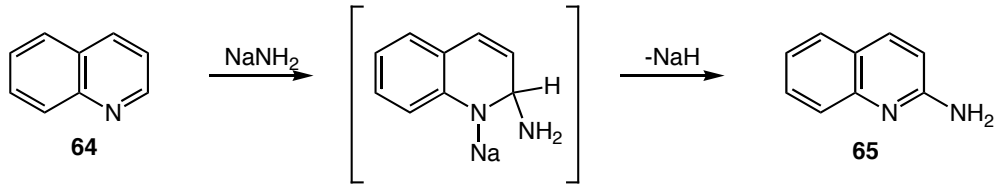

Scheme 2.6 The Chichibabin Reaction

Evans and Allen[19]demonstrated that aryl lithiates are also useful and reacted phenyl lithium with pyridine (Scheme 2.7). Unlike the synthesis of amino-pyridines, Chichababin reactions forming phenyl pyridines need oxidative conditions to regain aromaticity.

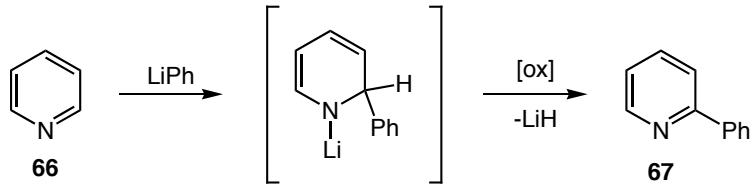

Scheme 2.7 Nucleophilic aromatic substitution of pyridine with phenyl lithium

The addition of aryl lithiates has been successfully applied to bipyridines,[20] phenanthrolines,[21,22] and with lesser success to terpyridines.[22] Due to its more electrophilic nature,[23] phenanthroline Chichibabin reactions have been explored extensively.

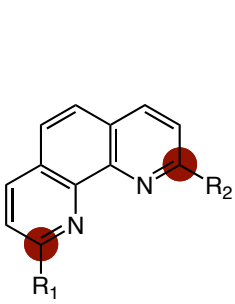

68a R_1 = Ph R_2 = H
68b R_1 = R_2 = Ph

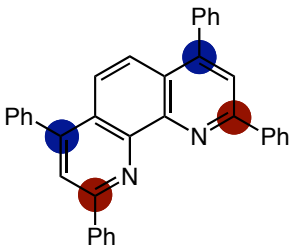

69

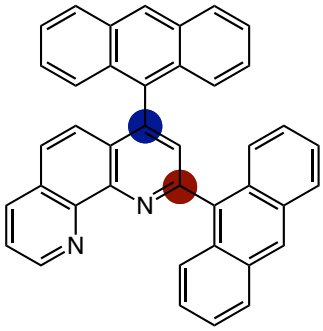

70

The Chichibabin reaction of aryl-lithiates is typically limited to the alpha (red) positions and gives mono- or di- substituted derivatives **68a** and **68b** depending on the conditions.[22,24] On rare occasions, the gamma (blue) position reacts to give the tetra substituted **69**[21] or sterically blocked **70**.[25] Dissymetric substitutions are possible with stepwise additions of different aryl lithiates.[25-27] A range of sterically hindered aryl lithiates are reactive, including mesityl, duryl, napthyl, anthryl, *o,o'*-dimethoxyphenyl.[25,28-30] The reaction also tolerates heterocyclic lithiates, as demonstrated in 1997 by Sauvage and coworkers,[26] who combined 2-anisyl-1,10-phenathroline **71** with the lithiated pyridine **72** to achieve the pyridyl-phenanthroline derivative **73** in acceptable yield (Scheme 2.8). McMillin and coworkers also used Sauvage's methodology to synthesize the parent pyridyl-phenanthroline, **46**, as well as several methylated derivates **74a–d** from the corresponding methyl phenanthrolines.

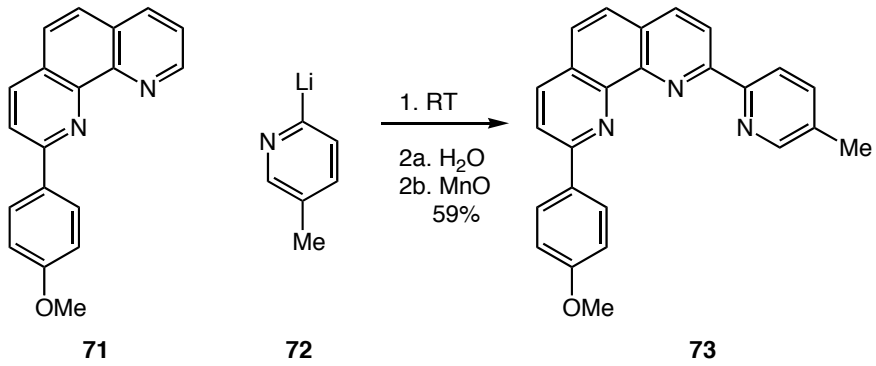

71 **72** **73**

Scheme 2.8 Synthesis of 2-[5-methylpyridyn-2-yl]-9-[4-methoxyphenyl]-1,10-phenanthroline.

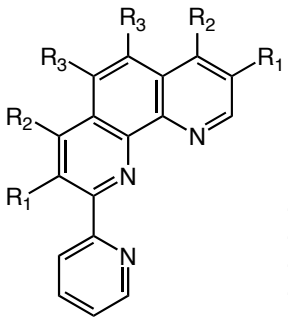

74a R_1 = H R_2 = Me R_3 = H
74b R_1 = H R_2 = H R_3 = Me
74c R_1 = Me R_2 = Me R_3 = H
74d R_1 = Me R_2 = H R_3 = Me

In short, nucleophilic additions of pyridyl lithiates to phenanthrolines are a succinct, direct route to pyridyl-phenanthrolines, but are limited to the alpha positions of phenanthroline. The stability of the pyridyl lithiates is frequently also a problem and restricts the general applicability of the Chichibabin reaction towards functionalized pyridyl-phenanthroline derivatives.

2.1.3 Palladium Catalyzed Cross Coupling

The importance of polypyridine ligands as potential supramolecular building blocks has encouraged many groups to find simple and general methodologies. Transition metal catalyzed coupling reactions are concise and convenient, and as such have been applied to polypyridine ligand synthesis with varying degrees of success.

In the beginning, harsh reaction conditions were necessary for the metal catalyzed coupling of pyridines. The classical Ullmann reaction,[30] as well as nickel[31] and other copper[32,33] catalyzed reactions gave bipyridines in acceptable yields, but functional group intolerance and tendency towards homocoupling led groups to look further. Phase transfer conditions using palladium on carbon was also a successful method for synthesizing bipyridines.[34,35] In 1974 Goto and coworkers attempted to synthesize mixed heterocyclic polypyridine ligands, including the parent pyridyl-phenanthroline, using phase transfer conditions (Scheme 2.9).[36] When pyridine N-oxide **76** was reacted with phenanthroline monohydrate **75** at high temperatures in the presence of platinated palladium-carbon only homocoupled phenanthroline was recovered in poor yield. When the reactants were reversed and phenanthroline N-oxide was reacted with pyridine, no products were isolated. The poor yields were ascribed to catalyst poisoning by the phenanthroline ligand.

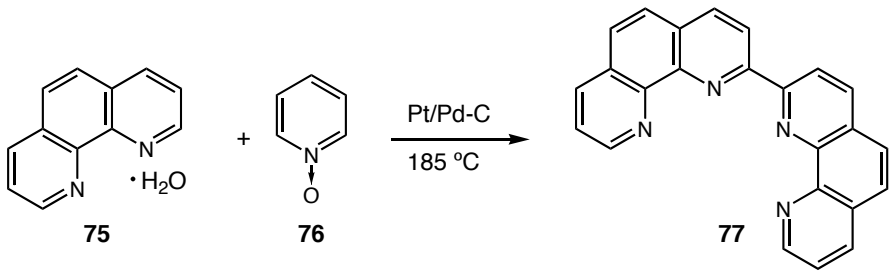

Scheme 2.9 Goto's failed synthesis of pyridyl-phenanthroline.

Recent work by many groups has shown that palladium catalyzed cross coupling of polypyridine ligands is a general and efficient method.[37] Schlüter and coworkers have developed a general procedure using Stille[38] and Suzuki-Miyuara[39] couplings for the synthesis of aryl-substituted bipyridine[40] and terpyridine[40] macrocycles, using easily accessible pyridyl stannanes **78** and **81**[41,42] as the synthetic cornerstones (Scheme 2.10).

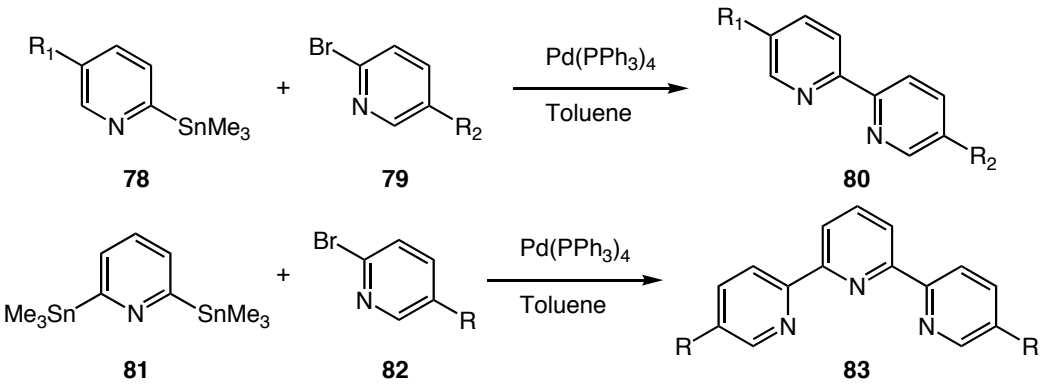

Scheme 2.10 Schlüter's bipyridine and terpyridine syntheses.

Whereas Schlüter's work has focused on substitution in the beta position, Siegel and coworkers[43] have successfully addressed both the alpha and beta position of bipyridines and terpyridines using similar Stille conditions. Treatment of halopyridine **84** or **88** with hexamethyldistannane[44] gives pyridylstannanes **85** and **89**. Coupling with 2,6-diiodopyridine **86** with palladium(II) gives the alpha, alpha- and beta, beta-terpyridines **87** and **90** (Scheme 2.11).

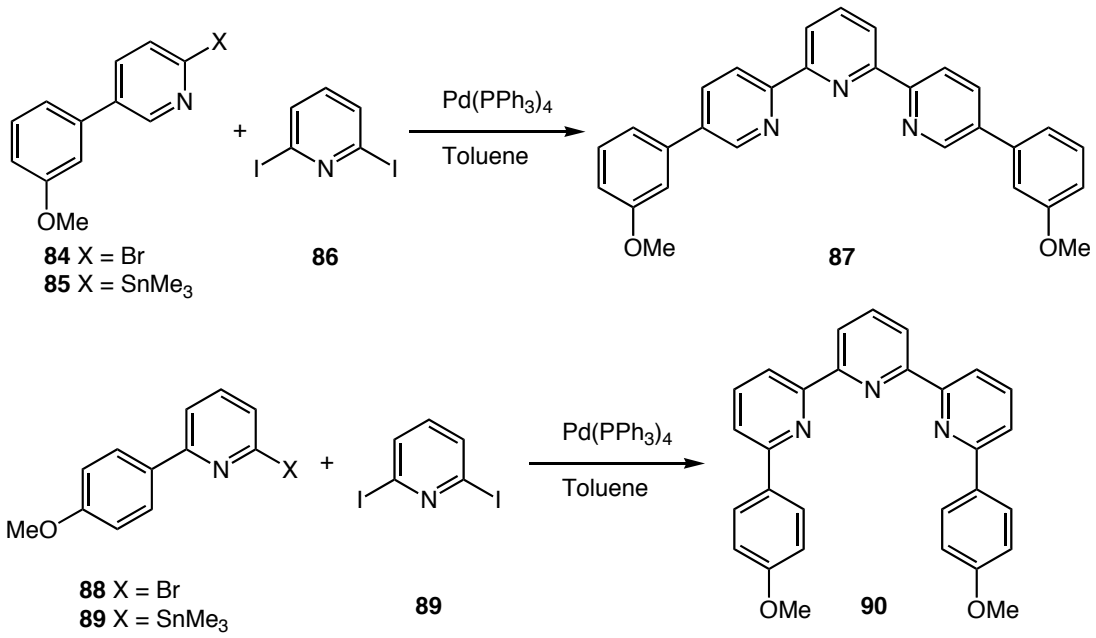

Scheme 2.11 Siegel's synthesis of alpha and beta di-substituted terpyridines.

The Suzuki-Miyuara[39] coupling conditions are simple, robust, and functional group tolerant. Many aryl-boronic acids have been successfully coupled to halo-pyridines and oligopyridines[45-47] though the availability and instability of pyridyl boronic acids[48] restricts their use to pyridin-3-yl boronic acid. Recent work by Rault and coworkers[49-52] demonstates that halo-pyridyl boronic acids and esters, even the highly unstable pyridin-2-yl boronic acid, are stable and suitable partners in Suzuki-Miyuara coupling.

Loren et. al.[53] applied Negishi[54] conditions to the synthesis of polypyridine ligand with great success. Highlighting the versatility of this approach was the combinatorial synthesis of broad library of bipyridines, phenanthrolines, terpyridines, and pyridyl-phenanthroline **110** (Scheme 2.12)

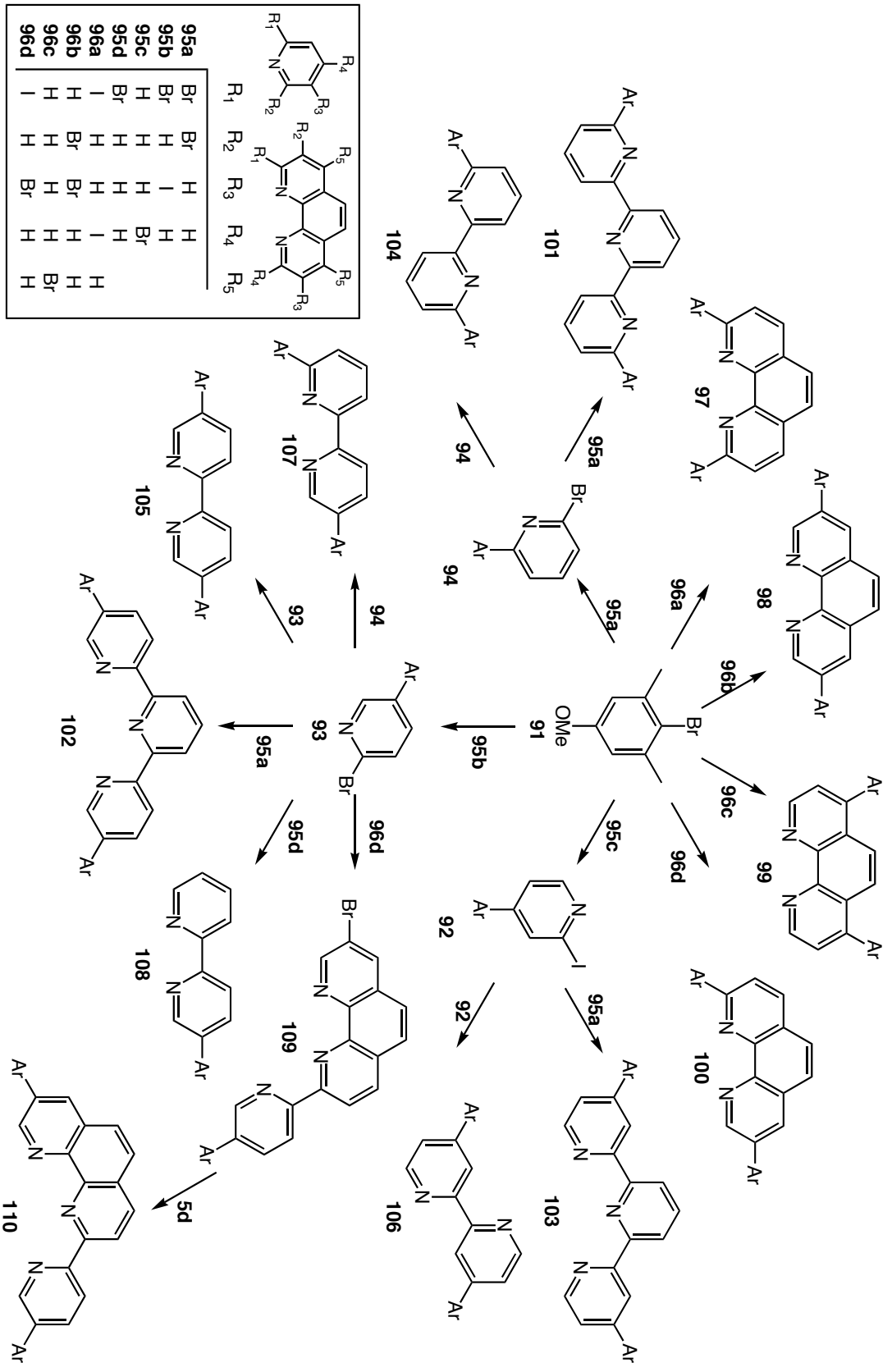

Scheme 2.12 Synthesis of manisyl substituted polypyridine ligands.[53]

Synthesis of key halopyridines **92**, **93**, and **94** enable each position; alpha (red), beta (blue), and gamma (green), to be addressed in a modular fashion creating a potential library of over 300 constituents if the phenyl substituents were permuted according to the Hammet series; R = F, H, Me, OTf, OMe, OH, NMe_2.

Ultimately, palladium catalyzed cross-couplings have emerged as successful and essential synthetic route to polypyridine ligands. The variety of coupling methodologies enable one to address the various substitution patterns and incorporate a wide range of useful functionalities.

2.2 Current Work

2.2.1 Introduction

Cross coupling methodologies, mentioned above, are all capable of generating the parent pyridyl-phenanthroline, but to date there has not yet been a serious attempt to develop a general synthesis capable of addressing the possible substitution patterns and functionalities of pyridyl-phenanthrolines. In order to design a versatile class of oriented ligands suitable for the synthesis of topologically challenging molecular targets, a general modular synthesis is desirable. As the Negishi-type coupling strategy employed by Loren et al. provides a succinct and practical route, we decided to expand this approach to prepare pyridyl-phenanthrolines.

2.2.2 Retrosynthesis

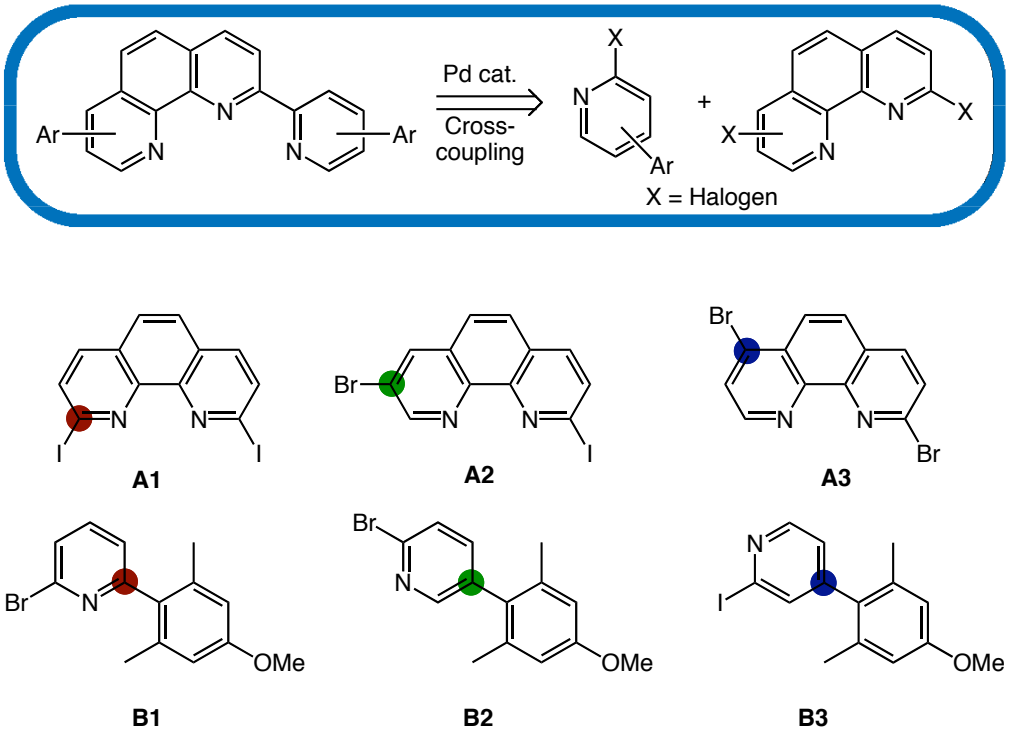

Figure 2.3 Retrosynthetic analysis and common building blocks.

Assuming the generality of this modular approach, a retrosynthetic strategy arises where an array of pherpy derivatives stem from combinatorial coupling of an elementary set of halophenanthrolines and halopyridines. Focusing on the positions alpha (red), beta (green), and gamma (blue), relative to the nitrogens reveals that dihalo-phenanthrolines **A1**–**A3**, aryl pyridines **B1**–**B3**, and aryl halide **91**[55] (Figure 2.3) suffice to synthesize a 3 × 3 matrix of pyridyl-phenanthrolines (Figure 2.4).

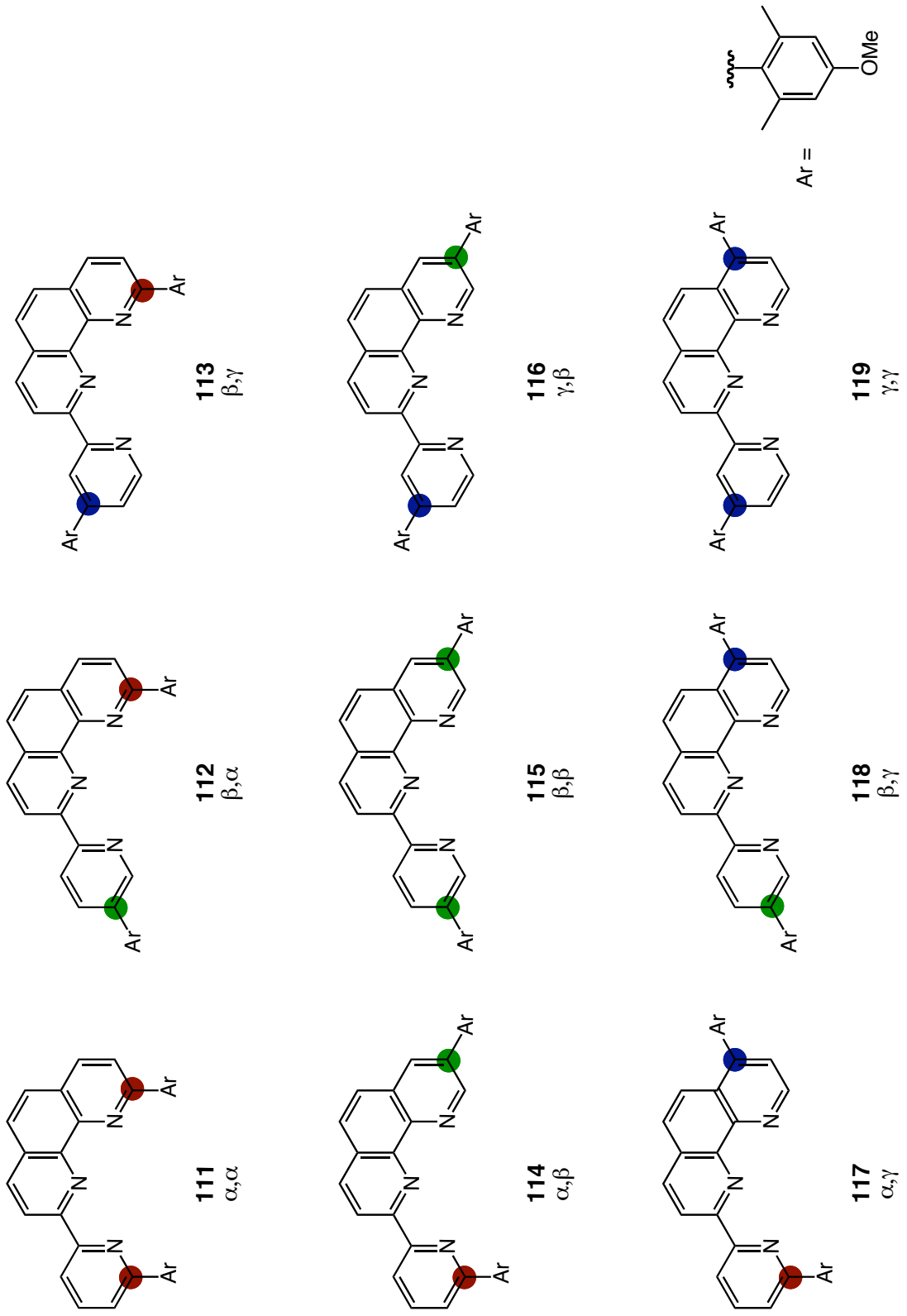

Figure 2.4 Manisyl pyridyl-phenanthrolines.

2.2.2 Synthesis

Diiodo-phenanthroline **A1** and 3-bromo-9-iodo-phenanthroline **A2** were prepared according to literature procedures.[56] The previously unknown 2,7-dibromo-phenanthroline **A3** was prepared by methylation of 4-bromo-phenanthroline **120**[57,58] with dimethylsulfate, giving a 2:1 mixture of **121a** and **121b**. Subsequent oxidation of the mixture gave the desired **122a** and its regioisomer **122b** (Scheme 2.13).[59] After chromatographic separation, treatment of **122a** with phosphoryl bromide gave 2,7-dibromo-phenanthroline **A3**.

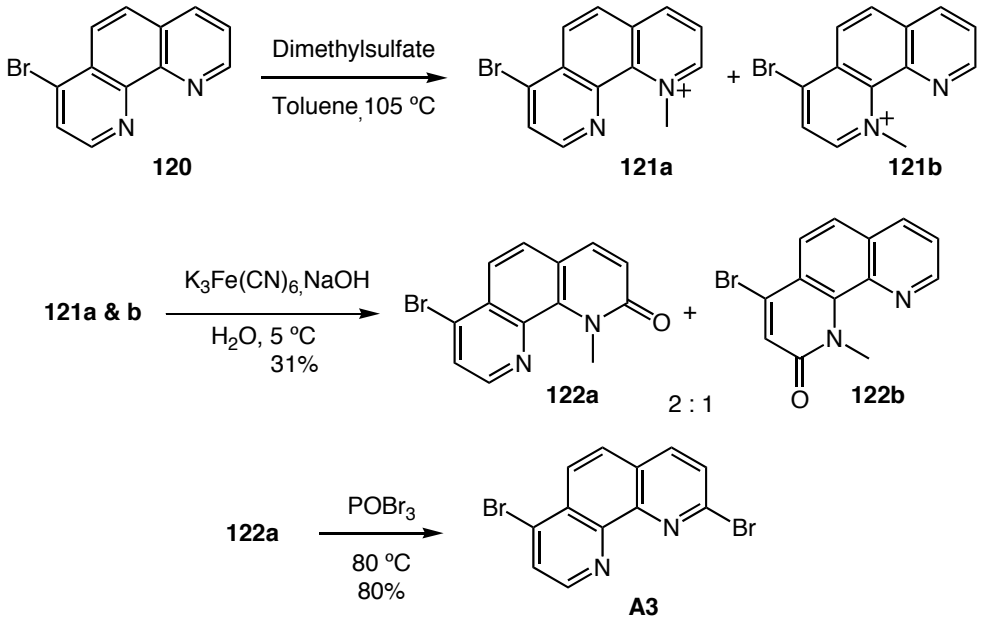

Scheme 2.13 Synthesis of 2,7-dibromo-phenanthroline

Aryl pyridines **B1** and **B2** were also prepared according to literature procedures.[53] 2-Iodo-4-manisyl pyridine **B3** was made from 4-manisylpyridine **123**[53] via directed ortho metalation using lithium di-*tert*-butyltetramethylpiperidinozincate (LiTMP-Zn^tBu_2)[60] as the base (Scheme 2.14).

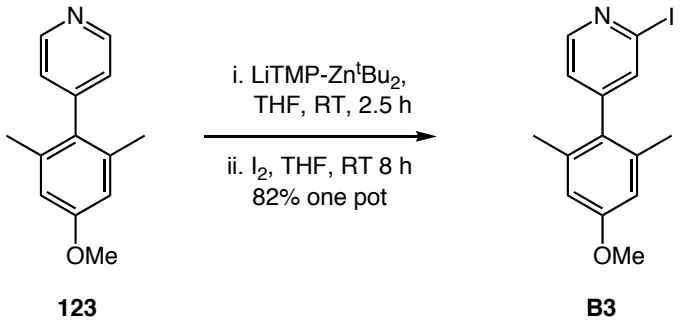

123 **B3**

Scheme 2.14 Ortho-lithiation of 4-manisyl pyridine.

The Negishi cross-coupling protocol[54] was chosen because the resulting terdentate ligands can precipitate from the reaction mixture after complexing the residual zinc chloride, thereby reducing catalyst poisoning and simplifying purification. Manisyl-pyridines **B1**–**B3** were converted into the organozinc reagents and coupled to the appropriate dihalo-phenanthroline to produce the corresponding halo-pyridyl-phenanthrolines **C1**–**C6** in good yields (Table 2.1).

Table 2.1 Negishi couplings of halo-pyridyl-phenanthrolines.

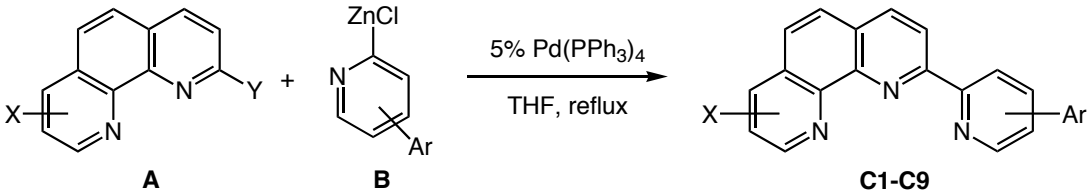

A **B** **C1-C9**

Halo-pyridine	Halo-phen	Product	Yield %
B1	**A1**	**C1**	52
B2	**A1**	**C2**	74
B3	**A1**	**C3**	26
B1	**A2**	**C4**	86
B2	**A2**	**C5**	60
B3	**A2**	**C6**	52
B1	**A3**	**C7**	18
B2	**A3**	**C8**	18[a]
B3	**A3**	**C9**	20

[a]DME

Lower yields of **C7–C9** were obtained due to unselective reactivity of the bromines in **A3**. Coupling of **A3** with **B1** or **B3** results in a regioisomeric mixture of mono-coupled products from which the desired halo-pherpy precipitated as the zinc salt. Coupling of **A3** and **B2** gives only the di-coupled product in THF; in DME a 2:1 mixture of mono and dicoupled material was obtained and separated by chromotography. Attempts to improve regio-selectivity by synthesizing mixed halophenanthrolines, 2-chloro-7-bromophenanthroline and 2-bromo-7-chlorophenanthroline from 4-bromophenanthroline and 4-chlorophenanthroline[57] were unsuccessful. Treatment of the respective halo-phenanthroline **122a** or **124a** with phosphoryl chloride or bromide gave the 2,7-dichloro or dibromophenanthroline (Scheme 2.15).

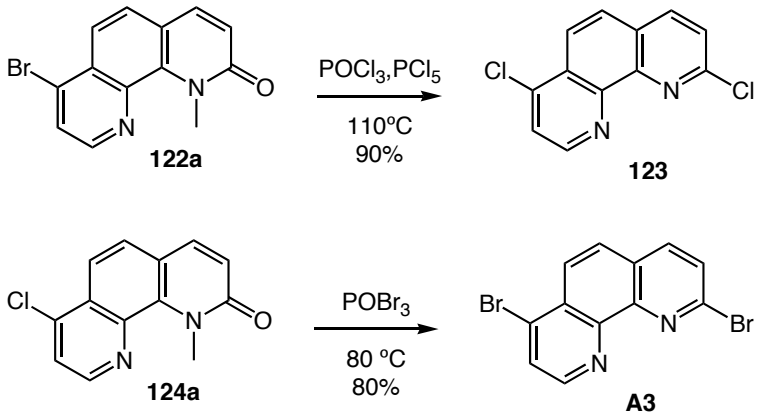

Scheme 2.15 Unsuccessful synthesis of mixed 2,7-dihalophenanthrolines

The submission of halo-pherpys **C2** and **C4** to Negishi conditions cleanly gave product in good yield, while **C1** and **C5** gave mixtures of product and starting material. Negishi reactions of **C7** and **C8** did not couple and only starting material was recovered. The halo-pherpys also contain the terdentate binding unit and can

precipitate from the reaction mixture as the zinc salt, thereby preventing the reaction from reaching completion.

In order to avoid inhibition due to precipitation of the zinc complex, the Suzuki-Miyaura cross-coupling procedure[39] was utilized. Halo-pyridyl-phenanthrolines **C3**, **C4**, and **C7**–**C9** gave the desired manisyl-pyridyl-phenanthrolines in good yields (Table 2.2).

Table 2.2 Pd-catalyzed Coupling of Pherpys.

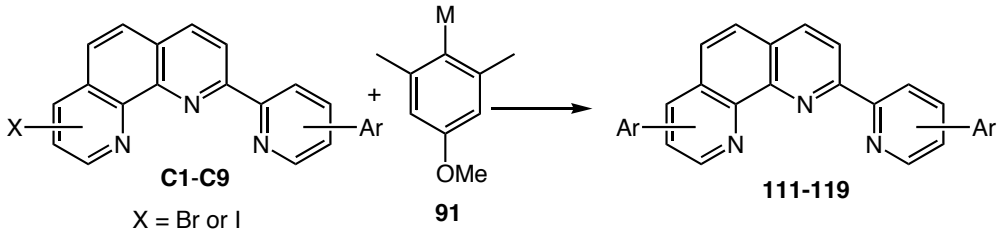

Halo-pherpy	Method	Product	Yield
C1	A	**111**	40
C2	A	**112**	74
C3	B	**113**	74
C4	A	**114**	79
C5	B	**115**	65
C6	B	**116**	90
C7	B	**117**	84
C8	A	**118**	12
C9	B	**119**	84

Reaction conditions: Method A) M = ZnCl, 5% $Pd(PPh_3)_4$, THF, reflux. Method B) M = $B(OH)_2$, $Ba(OH)_2$, 5-10% $Pd(PPh_3)_4$, DME/H_2O, 90 °C.

2.2.4 Results and Discussions

The utility of phenanthroline and its coordination complexes as supramolecular building blocks[29,61-63] is limited only by the often tedious and harsh conditions employed in constructing the phenanthroline core.[8] Given the utility of halogenated phenanthrolines under palladium catalyzed cross-coupling conditions, several groups, including our own, have focused on their synthesis. Their syntheses are surprisingly problematic, and although the 2,9-,[56,64] 3,8-,[65,66] 4,7-,[57,58] and 5,6-[58] positions have been

addressed, unsymmetrical dihalo-phenanthrolines are rare.[56] The novel 2,7-dihalophenanthroline, necessary for the synthesis of the pyridyl-phenanthroline array, contains a new and unsymmetrical substitution pattern and extends the versatility of functional phenanthrolines as key building blocks for the construction of supramolecular architectures with specific spatial orientations.

The wide range of dihalo-phenanthrolines employed in this work possess distinctive ^{1}H-NMR shifts and patterns enabling quick visual confirmation of regiochemistry and halogen identity as indicated in Table 2.3. As expected, substitution by chlorine results in very small proton shifts whereas the influence of bromine and iodine are more significant. The data also indicates that the electronic perturbation of each pyridine ring is relatively independent. Various additivity rules for heterocycles have been proposed,[67] but are limited within a series of similar compounds. Chemical shifts of halo-substituted heterocycles have been shown to be additive in select cases. The data here indicate that the chemical shifts of halo-phenanthrolines are additive and that one can subsequently predict the chemical shifts of dihalo phenanthrolines by determining the $\Delta\,\delta$ of each mono halo-phenanthroline (Table 2.4) and adding the terms together. The ^{13}C-NMR chemical shifts were also tabulated (See experimental) but are not additive.

Table 2.3 Chemical shifts of mono and dihalo-phenanthrolines

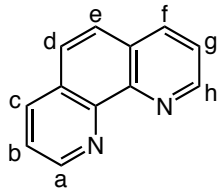

	a	b	c	d	e	f	g	h
phen	9.18	7.63	8.25	7.79	7.79	8.25	7.63	9.18
2-Cl-	Cl	7.65	8.21	7.84	7.80	8.27	7.68	9.23
2-Br-	Br	7.78	8.09	7.84	7.78	8.26	7.66	9.23
2-I-	I	7.85	8.02	7.84	7.75	8.25	7.66	9.24
3-Br-[68]	9.19	Br	8.42	7.85	7.73	8.27	7.67	9.20
4-Cl-	9.03	7.70	Cl	8.23	7.89	8.26	7.65	9.19
4-Br-	8.95	7.93	Br	8.23	7.90	8.29	7.68	9.22
4-I-	8.73	8.21	I	8.07	7.88	8.29	7.68	9.22
2,9-Di-Cl-	Cl	7.66	8.21	7.83	7.83	8.21	7.66	Cl
2,9-Di-Br-	Br	7.79	8.09	7.82	7.82	8.09	7.79	Br
2,9-Di-I-	I	7.83	8.02	7.79	7.79	8.02	7.83	I
2-Cl-9-I[68]	Cl	7.65	8.21	7.86	7.79	8.03	7.84	I
2-Cl-, 8-Br-	Cl	7.66	8.21	7.75	7.83	8.42	Br	9.21
2-I-, 8-Br-	I	7.85	8.04	7.76	7.80	8.41	Br	9.22
2,7-Di-Cl-	Cl	7.69	8.25	7.91	8.29	Cl	7.75	9.10
2,7-Di-Br-	Br	7.83	8.13	7.89	8.27	Br	7.95	8.99
2,7-Di-I-	I	7.88	8.05	7.84	8.10	I	8.22	8.77
3,8-Di-Br[65]	9.20	Br	8.44	7.78	7.78	8.44	Br	9.20
4,7-Di-Cl	9.06	7.75	Cl	8.35	8.35	Cl	7.75	9.06
4,7-Di-Br	8.95	7.94	Br	8.29	8.29	Br	7.94	8.95
4,7-Di-I	8.73	8.22	I	8.12	8.12	I	8.22	8.73

Table 2.4 $\Delta\ \delta$ of mono halophenanthrolines.

	a	b	c	d	e	f	g	h
phen	0.00	0.00	0.00	0.00	0.00	0.00	0.00	0.00
2-Cl-	Cl	0.02	-0.04	0.05	0.01	0.02	0.05	0.05
2-Br-	Br	0.15	-0.16	0.05	-0.01	0.01	0.03	0.05
2-I-	I	0.22	-0.23	0.05	-0.04	0.00	0.03	0.06
3-Br-[68]	0.01	Br	0.17	0.06	-0.06	0.02	0.04	0.02
4-Cl-	-0.15	0.07	Cl	0.44	0.10	0.01	0.02	0.01
4-Br-	-0.23	0.30	Br	0.44	0.11	0.04	0.05	0.04
4-I-	-0.45	0.58	I	0.28	0.09	0.04	0.05	0.04

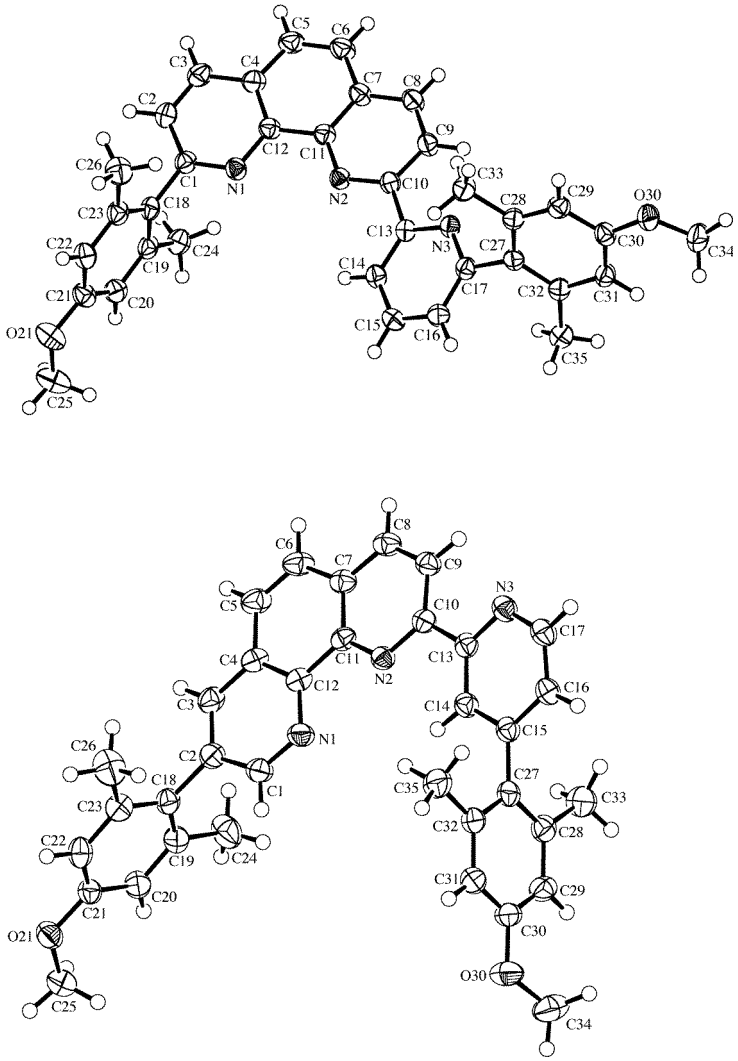

Figure 2.5 Crystal structures of pyridyl-phenanthrolines **111** and **114**.

The crystal structures of representative pyridyl-phenanthrolines **111** and **114** were determined (Figure 2.5).[69] The phenanthroline core is nearly planar, with torsion angles of 6.25(7)° and 3.62(11)° between rings containing N1 and N2 of **111** and **114**, respectively. The manisyl substituents of **114** adopt an orthogonal conformation relative to the adjacent pyridyl plane, 88.22° (11) and 86.05° (11), effectively minimizing orbital overlap. In **111**, however, the manisyl group in the pyridyl alpha-position approaches orthogonality (82.29(8)°), but the manisyl group alpha to the phenanthroline nitrogen deviates significantly from orthogonality (60.30(7)°) and orbital

overlap increases. The free pyridyl ring adopts a transoid conformation (with torsion angles of 22.62(7)° and 10.07(11)° between rings containing N2 and N3 of **111** and **114**, respectively). Upon terdentate metal coordination, the cis conformation will be adopted and the geometry of the ligand will alter significantly, resulting in exotopic and endotopic metal complexes (Scheme 2.15). Lehn and coworkers have recently exploited this geometry change to develop a nano-mechanical tweezers.[70,71]

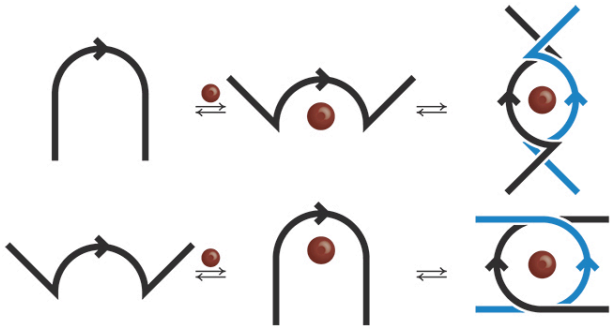

Scheme 2.15 Formation of exo- and endo-topic metal complexes.

Typically, Stille or Suzuki-Miyuara conditions are the methods of choice for the synthesis of polypyridines. This is surprising given the known instability of pyridyl boronic acids and the toxicity of stannanes. Negishi coupling conditions, on the other hand, utilize pyridyl zincates, which are easily accessible from the many commercially available halopyridines and ready to use without any extra isolation steps. Also, as emphasized by Loren et. al.,[53] terdentate oligopyridines can precipitate from the reaction mixtures as the zinc complexes, greatly simplifying purification. However, if both adduct and product contain the terdentate moieties, as the synthetic route to pyridyl-phenanthrolines required, the edduct can also complex to zinc salts, precipitate out, and retard the reaction. In several cases, it was necessary to employ Suzuki-Miyuara coupling procedures to prevent insoluble complexes. Nevertheless, the

Negishi procedure is suitable for the synthesis of halo pyridyl-phenanthrolines and most aryl-substituted pyridyl-phenanthrolines.

2.2.5 Conclusions

In conclusion, the syntheses of the pyridyl-phenanthrolines (pherpys) reported here demonstrate a general method based on palladium-catalyzed cross-coupling. The combination of readily accessible heterocyclic building blocks is a simple strategy that allows for systematic variation of new and useful substitution patterns of unsymmetrical oligopyridines. Due to their directionality, pyridyl-phenanthrolines are versatile starting points for the formation of chiral octahedral ML_2 complexes and the subsequent metal templated syntheses of topologically interesting molecules.[72] The following chapters highlight the structure-activity relationship of the intriguing photophysical properties revealed within the initial 3 × 3 matrix of manisyl pherpys and describe the coordination chemistry of select pyridyl-phenanthrolines.

2.3 Experimental

Materials and Methods

^{1}H- and ^{13}C NMR spectra were recorded on Varian (Mercury 300/400 MHz and Unity 500 MHz) spectrometers and were referenced to residual $CHCl_3$ at 7.26 ppm for proton spectra and 77.00 ppm for carbon spectra. High-resolution mass spectral (HRMS) analyses were performed by the University of California, Riverside mass spectrometry facility in EI mode. All experiments were carried out under argon in freshly distilled anhydrous solvents unless otherwise noted. Commercial chemicals were used as supplied from Aldrich or Acros Chemical Co. Column chromatography was performed on neutral aluminum oxide (Brockmann III) and silica gel (230-425 mesh). Melting points are uncorrected and recorded on a Mel-Temp Laboratory Device. 2,9-Diiodo-1,10-phenanthroline, 2-iodo-8-bromo-1,10-phenanthroline, 1H-1,10-phenanthrolin-4-one, 4-(4-methoxy-2,6-dimethylphenyl)pyridine, 2-bromo-5-(4-methoxy-2,6-dimethylphenyl)pyridine, and 2-bromo-6-(4-methoxy-2,6-dimethylphenyl)pyridine were all prepared according to literature procedures.[53,56,57]

Synthetic Procedures

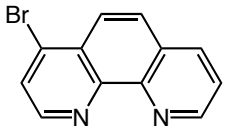

120

4-Bromo-1,10-phenanthroline

1H-1,10-phenanthrolin-4-one (5.00 g, 25.50 mmol) was placed in a dry 100 mL round-bottom flask under argon. Phosphorous oxybromide (18.00 g, 63.80 mmol) was added and the neat mixture was placed in a hot oil bath at 105 ºC and stirred overnight. The

solution was cooled to room temperature and quenched with aqueous ammonium hydroxide until strongly basic. The brown precipitate was filtered and washed with water. The solid was dissolved in warm chloroform, and washed three times with water. The organic layer was separated, dried over magnesium sulfate, filtered, and evaporated to afford a white solid (5.21 g, 79%, yield). m.p. 148-150 ºC; ^{1}H NMR (400 MHz, $CDCl_3$, δ): 9.21 (1H, dd, *J* = 4.4, 1.6 Hz), 8.94 (1H, d, *J* = 4.4) Hz, 8.28 (1H, dd, *J* = 8.0, 1.6 Hz), 8.21 (1H, d, *J* = 9.2 Hz), 7.92 (1H, d, *J* = 4.4 Hz), 7.89 (1H, d, *J* = 9.2 Hz), 7.67 (1H, dd, *J* = 8.0, 4.4 Hz); (75Mhz, $CDCl_3$, δ): 150.75, 149.72, 147.09, 145.65, 136.14, 134.02, 128.58, 128.16, 127.73, 127.11, 124.87, 123.60; HRMS m/z: calc. for $C_{12}H_7N_2Br$: 257.979259: found 257.978540.

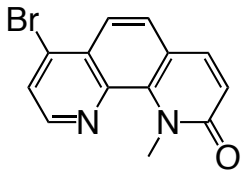

122a

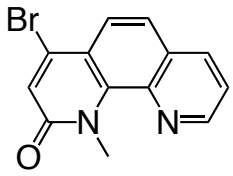

122b

7-Bromo-1-methyl-1-H-1,10-phenanthrolin-2-one(122a)

4-Bromo-1-methyl-1-H-1,10-phenanthrolin-2-one(122b)

4-Bromo-1,10-phenanthroline (3.43 g, 12.50 mmol) was dissolved in toluene (30 mL) and heated to reflux. Dimethyl sulfate (1.55 mL, 16.30 mmol) was dissolved in toluene (12 mL) and slowly added over 30 min. After an additional 1 h at reflux, the excess toluene was decanted. The residual tan solid was rinsed three times with toluene and dried under hi-vacuum overnight. The phenanthrolinum salt was dissolved in cold water (45 mL) and slowly added dropwise into a solution of $K_3Fe(CN)_6$ (10.28 g, 31.30 mmol) in water (35 mL) at 0 ºC. Simultaneously, NaOH (11.35 g, 284 mmol) in water (40 mL) was also added dropwise into the reaction flask. The mixture was stirred for 1 h at 0 ºC and warmed to room temperature, affording a yellow solution with a green suspension. The precipitate was filtered and washed with water. The green solid was

dissolved in methylene chloride, and washed three times with water. The organic layer was separated, dried with magnesium sulfate, filtered, and after evaporation, placed under hi-vacuum overnight to give a mixture of A, B, and starting material (5:2:1) as a green solid. Column chromatography on neutral alumina with methylene chloride gave two products; A (1.301 g, 36%), and B (0.493 g, 13%) as white solids. **A**: m.p. 176-180 ºC; ^{1}H NMR (300 MHz, $CDCl_3$, δ): 8.70 (1H, d, *J* = 4.8 Hz), 8.03 (1H, d, *J* = 9.0 Hz), 7.82 (1H, d, *J* = 4.5 Hz), 7.81 (1H, d, *J* = 9.3 Hz), 7.68 (1H, d, *J* = 8.7 Hz), 6.95 (1H, d, *J* = 9.3 Hz), 4.42 (3H, s); ^{13}C NMR (75Mhz, CDCl3, δ): 164.26, 146.27, 140.87, 138.78, 138.08, 133.84, 129.44, 127.92, 126.07, 123.17, 121.07, 120.97, 38.34; HRMS m/z: calc. for: $C_{13}H_9BrN_2O$: 287.98983 found 287.98950. **B**: m.p. 180-183 ºC; ^{1}H NMR (300 MHz, $CDCl_3$, δ): 8.98 (1H, dd, *J* = 4.2, 1.8 Hz), 8.22 (1H, dd, *J* = 8.1, 1.5 Hz), 8.11 (1H, d, *J* = 8.1 Hz), 7.64 (1H, d, *J* = 9.0 Hz), 7.55 (1H, dd, *J* = 8.1, 3.9 Hz), 7.35 (1H, s), 4.42 (3H, s); (75Mhz, CDCl3, δ): 162.45, 147.35, 139.77, 138.15, 135.94, 135.77, 130.28, 125.77, 125.56, 125.65, 122.42, 119.52, 38.62; HRMS m/z: calc. for: $C_{13}H_9BrN_2O$: 287.98983 found 287.98913.

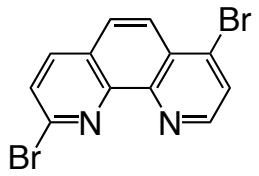

A3

2,7-Dibromo-1,10-phenanthroline

7-Bromo-1-methyl-1-H-1,10-phenanthrolin-2-one (0.76 g, 2.63 mmol) was placed in a dry 50 mL round-bottom flask under argon. Phosphorous oxybromide (1.95 g, 6.57 mmol) was added and the mixture placed in a hot oil bath at 105 ºC and stirred overnight. The solution was cooled to room temperature and quenched with aqueous ammonium hydroxide until strongly basic. The brown precipitate was filtered and washed with water. The solid was dissolved in warm chloroform, and washed three

times with water. The organic layer was separated, dried over magnesium sulfate, filtered, and evaporated to afford a brown solid (0.790 g, 90%). Column chromatography on neutral alumina with chloroform: hexanes (7:3 to 1:0) as eluant gave a white solid (0.450 g, 50%). m.p. 218-221 ºC; ^{1}H NMR (300 MHz, $CDCl_3$, δ): 8.99 (1H, d, *J* = 4.8 Hz), 8.27 (1H, d, *J* = 9.0 Hz), 8.12 (1H, d, *J* = 8.4 Hz), 7.94 (1H, d, *J* = 4.5 Hz) 7.89 (1H, d, *J* = 9.0), 7.83 (1H, d, *J* = 8.4 Hz); ^{13}C NMR (125 MHz, $CDCl_3$, δ): 150.15, 146.09, 145.85, 142.98, 138.07, 133.98, 128.51, 128.42, 127.42, 126.97, 125.45, 125.45; HRMS m/z: calc. for [M^+] $C_{12}H_6N_2Br_2$: 335.889770 found 335.889380.

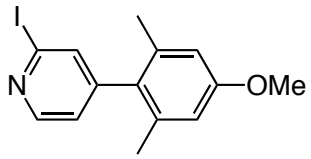

B3

2-Iodo-4-(4-methoxy-2,6-dimethylphenyl)-pyridine

Using Schlenk techniques, 2,2,6,6-tetramethylpiperdine (TMP) (6.62 g, 46.94 mmol) was added to THF (125 mL) and cooled to -78 ºC. n-BuLi (20.98 mL of a 2.35 M sol in hexanes, 49.30 mmol) was added dropwise and the solution stirred for 30 min at 0 ºC. A THF solution (100 mL) of di-t-butylzinc at 0 ºC prepared from $ZnCl_2$ (6.70 g, 49.30 mmol) and t-BuLi (57.99 mL of a 1.7 M sol in pentane, 98.57 mmol) was cannulated into the LiTMP solution at -78 ºC. The solution was warmed to room temperature and stirred for 45 mins. 4-Manisyl pyridine (5.00 g, 23.47 mmol) was dissolved in THF and cannulated into the solution of LiTMP-Zn^{t}Bu$_2$. After stirring at room temperature for 2.5 h, a solution of iodine (59.61 g, 235 mmol) in THF (250 mL) was slowly added dropwise and stirred overnight. The solvent was removed on a rotary evaporator and the reaction quenched with aqueous sodium thiosulfate. The mixture was extracted with methylene chloride and washed with aqueous sodium thiosulfate and water. The organic layer was separated, dried over magnesium sulfate, filtered, and

evaporated to afford a brown solid. Recrystallization from hot hexanes gave off-white crystals (6.52 g, 82%). Physical and spectral data matched literature. Mp = 100 - 102 °C. ^{1}H NMR (400 MHz, $CDCl_3$, δ): 8.41 (1H, d, *J* = 4.8 Hz), 7.57 (1H, d, *J* = 2.0 Hz), 7.09 (1H, dd, *J* = 4.8, 2.0 Hz), 6.65 (2H, s), 3.82 (3H, s), 2.02 (6H, s). C NMR (100 MHz, $CDCl_3$, δ): 158.95, 151.22, 150.44, 136.46, 135.86, 129.87, 124.56, 118.41, 112.91, 55.20, 21.05.

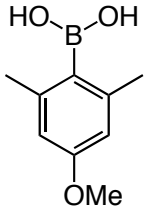

91

4-Methoxy-2,6-dimethylphenylboronic acid

A solution of Bromo-manisyl (0.50 g, 2.33 mmol) in THF (50 mL) was cooled to -78 ºC and n-BuLi (1.02 mL of a 2.5M sol in hexanes, 2.56 mmol) was added slowly via syringe. The resulting white solution was stirred for 20 min at -78 ºC before trimethoxy borate (0.42 g, 4.08 mmol) was added dropwise. The clear solution was stirred overnight at room temperature. The reaction was quenched and hydrolyzed with 10% hydrochloric acid (1 mL) and water (1 mL) and stirred 6 h at room temperature. The solution was diluted with diethyl ether and washed with water. The organic layer was separated, dried over magnesium sulfate, filtered, and evaporated to give a white solid (0.305 g, 73%). m.p. 110-175 ºC; ^{1}H NMR (400 MHz, CDCl3, δ): 6.55 (2H,s), 4.57 (2H,bs), 3.77 (3H, s), 2.37(6H, s); ^{13}C NMR (100 MHz, CDCl3, δ): 160.13, 141.56, 112.17, 109.98, 55.00, 22.39; HRMS m/z: calc. for [M^+] $C_9H_{13}BO_3$: 180.095775 found 180.095428.

General Procedure for Negishi Cross-Couplings

A THF solution of pyridyl halide (1.05 molar equiv. at 1 M) was cooled to -78 ºC and n-BuLi (1.1 molar equiv. of a 2.5 M sol in hexanes) was added and stirred for 5 min. To this was cannulated a THF solution of $ZnCl_2$ (1.1 molar equiv. at 1 M). The solution was stirred, allowed to warm to room temperature, and then cannulated into a THF solution of halo- phenanthroline or pyridyl phenanthroline (1.0 molar equiv at 0.5 M) and $Pd(PPh_3)_4$ (0.05 molar equiv). The resulting solution was heated at reflux overnight. After cooling to room temperature, any precipitate was filtered and washed with cold THF before drying. The precipitate was dissolved in chloroform and extracted with a saturated aqueous EDTA solution basified with sodium bicarbonate. The organic layer was separated, dried over magnesium sulfate, filtered, and evaporated. The crude was then purified on silica or alumina oxide plug as indicated for each compound.

General Procedure for Suzuki-Miyuara Cross-Couplings

Manisylboronic acid **91** (1.5 molar equiv.), halo pyridyl-phenanthroline (1.0 molar equiv.), $Pd(PPh_3)_4$ (0.05 molar equiv.), and $Ba(OH)_2 \bullet 8H_2O$ (2.0 molar equiv.) were placed in a 10 mL round bottom flask. After the addition of DME / water (6 : 1), the flask was placed in an oil bath at 90 ºC and stirred overnight. The gray precipitate was filtered and discarded, and the filtrate was diluted in chloroform and extracted with a saturated aqueous EDTA solution basified with sodium bicarbonate. The organic layer was separated, dried over magnesium sulfate, filtered, and evaporated. Residual Ph_3PO

was removed by trituration with diethyl ether and purification on silica or alumina oxide for each compound as indicated.

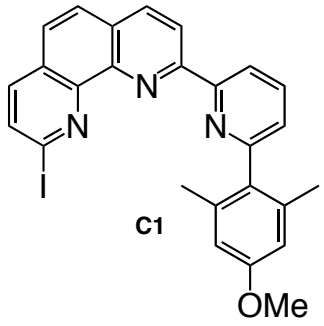

C1

9-Iodo-2-[6-(4-methoxy-2,6-dimethylphenyl)-pyridin-2-yl]-1,10-phenanthroline

Prepared using general Negishi coupling procedures. Column chromatography on silica with chloroform: methanol (1:0 then 99:1) as eluant gave a white film (0.135 g, 52%). m.p. 130-133 ºC; ^{1}H NMR (400 MHz, $CDCl_3$, δ): 8.90 (1H, d, *J* = 8.0 Hz), 8.82 (1H, d, *J* = 8.4 Hz), 8.30 (1H, d, *J* = 8.4 Hz), 8.01 (1H, d, *J* = 8.4 Hz), 7.99 (1H, t, *J* = 7.6 Hz), 7.86 (1H, d, *J* = 8.4 Hz), 7.84 (1H, d, *J* = 8.4 Hz), 7.74 (1H, d, *J* = 8.4 Hz), 7.32 (1H, d, *J* = 7.6 Hz), 6.72 (2H, s), 3.85 (3H, s), 2.14 (6H, s); ^{13}C NMR (100 MHz, $CDCl_3$, δ): 158.70, 158.69, 156.93, 155.71, 147.41, 144.27, 137.46, 137.09, 136.94, 136.69, 134.08, 133.48, 128.71, 127.92, 127.19, 125.94, 125.57, 121.72, 120.48, 119.25, 112.96, 55.26, 20.92; HRMS(DEI) m/z: calc. for [M^+] $C_{26}H_{20}N_3OI$: 517.06511: found 517.064292.

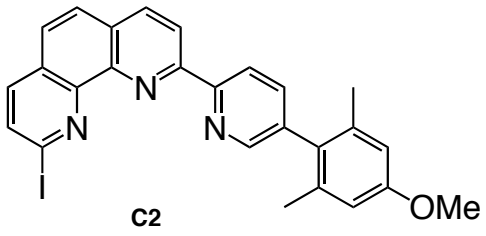

C2

9-Iodo-2-[5-(4-methoxy-2,6-dimethylphenyl)- pyridin-2-yl]-1,10-phenanthroline

Prepared using general Negishi coupling procedures. Column chromatography on neutral alumina with methylene chloride: hexanes (4:1 then 1:0) as eluant gave a white

film (0.288 g, 74%). m.p. 227-230 ºC; ^{1}H NMR (300 MHz, $CDCl_3$, δ): 9.04 (1H, d, *J* = 7.5 Hz), 8.87 (1H, d, *J* = 8.4 Hz), 8.55 (1H, d, *J* = 1.5 Hz), 8.41, (1H, d, *J* = 8.4 Hz), 8.04, (1H, d, *J* = 8.1 Hz), 7.91 (1H, d, *J* = 9.3 Hz), 7.88 (1H, d, *J* = 8.4 Hz), 7.79 (1H, d, *J* = 8.7 Hz), 7.77 (1H, dd, *J* = 7.8 Hz, 2.0 Hz), 6.74 (2H, s), 3.85 (3H, s), 2.10 (6H, s); ^{13}C NMR (100 MHz, $CDCl_3$, δ): 158.72, 156.36, 154.14, 149.68, 147.34, 144.34, 138.50, 137.72, 137.13, 136.93, 136.90, 134.13, 130.24, 128.68, 127.95, 127.14, 126.03, 122.40, 120.99, 119.27, 112.86, 55.23, 21.38; HRMS m/z: calc. for $[M]^+$ $C_{26}H_{20}N_3OI$: 517.065114: found 517.066198.

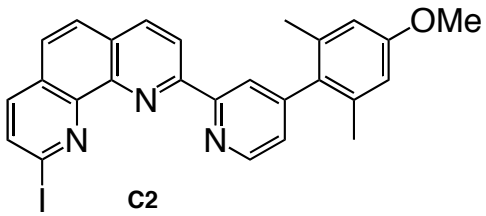

C2

9-Iodo-2-[4-(4-methoxy-2,6-dimethylphenyl)-pyridin-2-yl]-1,10-phenanthroline

Prepared using general Negishi coupling procedures. Trituration with cold methylene chloride gave a white solid (0.092 g, 26%). m.p. 271-274 ºC; ^{1}H NMR (400 MHz, $CDCl_3$, δ): 8.89 (1H, d, *J* = 8.4 Hz), 8.78 (1H, d, *J* = 4.8 Hz), 8.71 (1H, s), 8.39 (1H, d, *J* = 8.4 Hz), 7.99 (1H, d, *J* = 8.8 Hz), 7.88 (1H, d, *J* = 8.8 Hz), 7.84 (1H, d, *J* = 8.4 Hz), 7.76 (1H, d, *J* = 8.8 Hz), 7.21 (1H, dd, *J* = 4.8 Hz, 2.0 Hz), 6.71 (2H, s), 3.85 (3H, s), 2.13 (6H, s); ^{13}C NMR (125 MHz, $CDCl_3$, δ): 158.97, 157.06, 156.39, 150.70, 149.243, 147.65, 144.67, 137.05, 137.00, 136.95, 134.32, 132.04, 128.97, 128.15, 127.32, 126.23, 125.95, 123.84, 121.69, 119.26, 113.06, 55.13, 21.12; HRMS(DEI) m/z: calc. for $[M\text{-}H^+]$ $C_{26}H_{19}N_3OI$: 516.057289: found 516.058552.

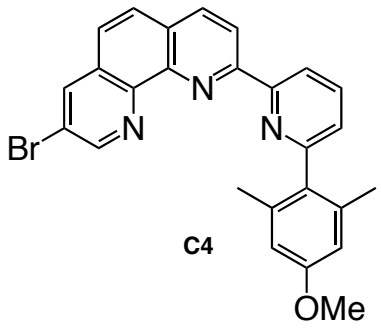

C4

8-Bromo-2-[6-(4-methoxy-2,6-dimethylphenyl)-pyridin-2-yl]-1,10-phenanthroline

Prepared using general Negishi coupling procedures. Off-white solid (0.419 g, 86%). m.p. 174-177 ºC; ^{1}H NMR (400 MHz, $CDCl_3$, δ): 9.24 (1H, d, *J* = 3.0 Hz), 8.83 (1H, d, *J* = 8.0 Hz), 8.80 (1H, d, *J* = 8.0 Hz), 8.43 (1H, d, *J* = 2.0 Hz), 8.32 (1H, d, *J* = 8.0 Hz), 7.97 (1H, t, *J* = 8.0 Hz), 7.88 (1H, d, *J* = 9.0 Hz), 7.73 (1H, d, *J* = 9.0 Hz), 7.32 (1H, d, *J* = 1.0 Hz), 6.72 (2H, s), 3.85 (3H, s), 2.14 (6H, s); ^{13}C NMR (100 MHz, $CDCl_3$, δ): 158.79, 158.70, 157.04, 155.78, 150.99, 145.25, 144.42, 137.42, 137.07, 136.75, 136.75, 133.42, 129.88, 128.53, 127.89, 125.50, 125.36, 121.73, 120.52, 119.58, 112.94, 55.25, 20.91; HRMS (DEI) m/z: calc. for $C_{26}H_{19}N_3O$: 468.071149; found: 468.070224.

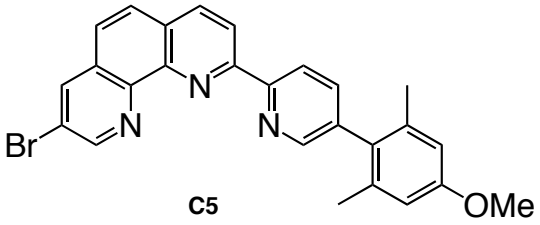

C5

8-Bromo-2-[5-(4-methoxy-2,6-dimethylphenyl)-pyridin-2-yl]-1,10-phenanthroline

Prepared using general Negishi coupling procedures. Off-white solid (0.401 g, 60%). ^{1}H NMR, ^{13}C NMR, and mass spectrum matched literature.[53] m. p. 114 - 117 °C. ^{1}H NMR (400 MHz, $CDCl_3$, δ): 8.20 (1H, d, *J* = 2.5 Hz), 8.95 (1H, d, *J* = 8.0 Hz), 8.81 (1H, d, *J* = 8.0 Hz), 8.53 (1H, d, *J* = 2.0 Hz), 8.39 (1H, d, *J* = 2.5 Hz), 8.37 (1H, d, *J* = 8.0 Hz), 7.86 (1H, d, *J* = 8.0 Hz), 7.72 (1H, dd, *J* = 8.0, 2.0 Hz), 7.70 (1H, d, *J* = 8.0 Hz), 6.70 (2H, s), 3.82 (3H, s), 2.06 (6H, s). ^{13}C NMR (100

MHz, $CDCl_3$, δ): 158.72, 156.50, 154.21, 151.01, 149.75, 145.32, 144.36, 138.48, 137.69, 137.41, 137.07, 136.94, 130.18, 129.91, 128.50, 127.84, 125.44, 122.41, 121.02, 119.63, 112.86, 55.23, 21.37.

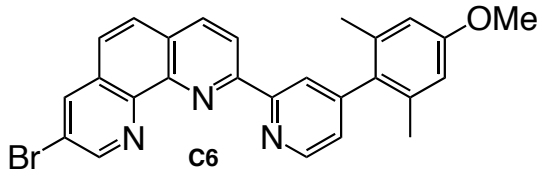

C6

8-Bromo-2-[4-(4-methoxy-2,6-dimethylphenyl)-pyridin-2-yl]-1,10-phenanthroline

Prepared using general Negishi coupling procedures. Column chromatography on neutral alumina with methylene chloride as eluant gave a white solid (0.132 g, 52%). m.p. 224-226 ºC; ^{1}H NMR (400 MHz, $CDCl_3$, δ): 9.15 (1H, d, *J* = 2.4 Hz), 8.90 (1H, d, *J* = 8.4 Hz), 8.79 (1H, d, *J* = 4.8 Hz), 8.74 (1H, s), 8.41 (1H, d, *J* = 2.4 Hz), 8.40 (1H, d, *J* = 8.8 Hz), 7.88 (1H, d, *J* = 8.8 Hz), 7.72 (1H, d, *J* = 8.8 Hz), 7.20 (1H, dd, *J* = 5.2, 1.2 Hz), 6.72 (2H, s), 3.85 (3H, s), 2.10 (6H, s); ^{13}C NMR (100 MHz, $CDCl_3$, δ): 158.67, 156.62, 156.12, 150.85, 150.40, 149.10, 145.32, 144.37, 137.34, 136.84, 136.74, 131.79, 129.88, 128.59, 127.82, 125.66, 125.47, 123.44, 121.31, 119.57, 112.81, 55.21, 21.28; HRMS(DEI) m/z: calc. for [M-H$^+$] $C_{26}H_{19}N_3OBr$: 468.071149: found 468.071740.

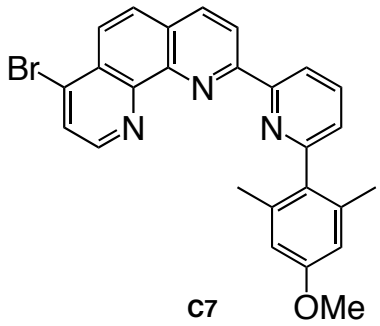

C7

7-Bromo-2-[6-(4-methoxy-2,6-dimethylphenyl)-pyridin-2-yl]-1,10-phenanthroline

Prepared using general Negishi coupling procedures. Column chromatography on neutral alumina with methylene chloride: hexanes (2:1 then 1:0) as eluant gave a white

solid (0.052 g, 18%). m.p. decomposes >330 ºC; ^{1}H NMR (400 MHz, $CDCl_3$, δ): 9.00 (1H, d, *J* = 4.4 Hz), 8.85 (1H, d, *J* = 8.4 Hz), 8.82 (1H, d, *J* = 8.4 Hz), 8.35 (1H, d, *J* = 8.4 Hz), 8.24 (1H, d, *J* = 9.2 Hz), 7.98 (1H, t, *J* = 8.0 Hz), 7.94 (1H, d, *J* = 9.2 Hz), 7.31 (1H, dd, *J* = 7.6, 1.0 Hz), 6.72 (2H, s), 3.85 (3H, s), 2.14 (6H, s); ^{13}C NMR (100 MHz, $CDCl_3$, δ): 158.79, 158.70, 157.17, 155.76, 149.60, 147.22, 145.07, 137.43, 137.06, 136.75, 134.07, 133.42, 128.56, 128.36, 126.96, 126.86, 125.53, 124.81, 122.00, 120.57, 112.94, 55.25, 20.90; HRMS m/z: calc. for $[M-H]^+$ $C_{26}H_{19}N_3OBr$: 468.071149: found 468.073072.

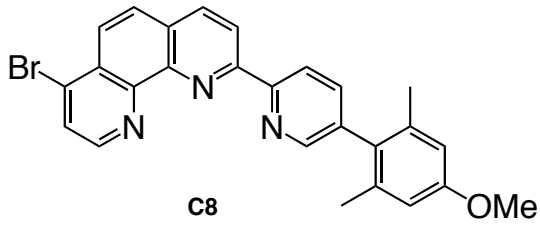

C8

7-Bromo-2-[5-(4-methoxy-2,6-dimethylphenyl)-pyridin-2-yl]-1,10-phenanthroline

Prepared using general Negishi coupling procedures substituting DME for THF. Column chromatography on neutral alumina with methylene chloride as eluant followed by radial chromatography on silica with chloroform: methanol (1:0 then 97:3) gave a white solid (0.065 g, 18%). m.p. 240-242 ºC; ^{1}H NMR (400 MHz, $CDCl_3$, δ): 9.00 (1H, d, *J* = 4.4 Hz), 9.00 (1H, d, *J* = 9.2 Hz), 8.85 (1H, d, *J* = 8.4 Hz), 8.55 (1H, d, *J* = 2.0 Hz), 8.43 (1H, d, *J* = 8.4 Hz), 8.24 (1H, d, *J* = 9.2 Hz), 7.96 (1H, d, *J* = 9.2 Hz), 7.94 (1H, d, *J* = 4.4 Hz), 7.74 (1H, dd, *J* = 8.0 Hz, 2.0 Hz), 6.72 (2H, s), 3.84 (3H, s), 2.08 (6H, s); ^{13}C NMR (100 MHz, $CDCl_3$, δ): 158.79, 156.68, 154.24, 149.78, 149.63, 147.23, 145.20, 138.47, 137.70, 137.12, 136.92, 134.06, 130.23, 128.54, 128.43, 127.70, 126.91, 124.90, 122.46, 121.32, 112.91, 55.25, 21.35; HRMS(DEI) m/z: calc. for $[M^+]$ $C_{26}H_{20}N_3OBr$: 469.078974; found 469.080195.

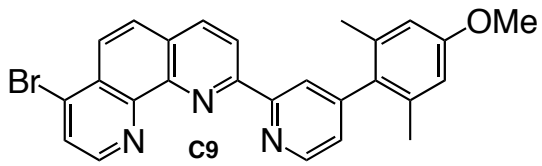

C9

7-Bromo-2-[4-(4-methoxy-2,6-dimethylphenyl)-pyridin-2-yl]-1,10-phenanthroline

Prepared using general Negishi coupling procedures. Column chromatography on neutral alumina with methylene chloride as eluant gave a white solid (0.059 g, 20%). m.p. 255-257 ºC; ^{1}H NMR (400 MHz, $CDCl_3$, δ): 8.91 (1H, d, *J* = 4.8 Hz), 8.90 (1H, d, *J* = 8.4 Hz), 8.80 (1H, d, *J* = 4.8 Hz), 8.74 (1H, d, *J* = 0.8 Hz), 8.43 (1H, d, *J* = 8.4 Hz), 8.24 (1H, d, *J* = 8.8 Hz), 7.95 (1H, d, *J* = 9.2 Hz), 7.91 (1H, d, *J* = 4.8 Hz), 7.21 (1H, dd, *J* = 4.8 Hz, 1.6 Hz), 6.72 (2H, s), 3.85 (3H, s), 2.10 (6H, s); ^{13}C NMR (100 MHz, $CDCl_3$, δ): 158.67, 156.81, 156.14, 150.48, 149.55, 149.49, 149.15, 147.21, 145.18, 136.88, 136.80, 134.01, 131.83, 128.64, 127.70, 126.88, 125.71, 124.96, 123.52, 121.66, 112.80, 55.25, 21.31; HRMS(DEI) m/z: calc. for $C_{26}H_{19}BrN_3O$ 468.071149; found 468.069385.

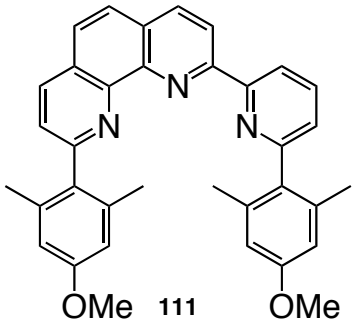

111

2-(4-methoxy-2,6-dimethyl-phenyl)-9-[6-(4-methoxy-2,6-dimethylphenyl)-pyridin-2-yl]-1,10-phenanthroline

Prepared using general Negishi coupling procedures. Column chromatography on Silica with methylene chloride: methanol (97:3) as eluant gave a white film (0.470 g, 40%). m.p. 201-204 ºC; ^{1}H NMR (400 MHz, $CDCl_3$, δ): 8.83 (1H, dd, *J* = 8.0, 0.8 Hz), 8.77 (1H, d, *J* = 8.4 Hz), 8.31 (1H, d, *J* = 8.0 Hz), 8.29 (1H, d, *J* = 8.4 Hz), 7.92 (1H, t, *J* = 7.6 Hz), 7.84 (2H, s), 7.61 (1H, d, *J* = 8.4 Hz), 7.25 (1H, dd, *J* =7.6, 0.8 Hz), 6.77 (2H, s), 6.71 (2H, s), 3.88 (3H, s), 3.84 (3H, s), 2.29 (6H, s), 2.13 (6H, s); ^{13}C NMR (100 MHz, $CDCl_3$, δ): 159.36, 158.78, 158.64, 158.45, 156.38, 156.22, 145.89, 145.66, 137.97, 137.44, 136.98, 136.47, 135.62, 133.57, 133.53, 128.69, 126.93, 126.29, 126.09, 125.19, 125.12, 121.11, 120.53, 113.07, 112.92, 55.22, 55.22, 21.41, 20.90; HRMS(DEI) m/z: calc. for [M-H$^+$] $C_{35}H_{30}N_3O_2$: 524.233803; found: 524.231953.

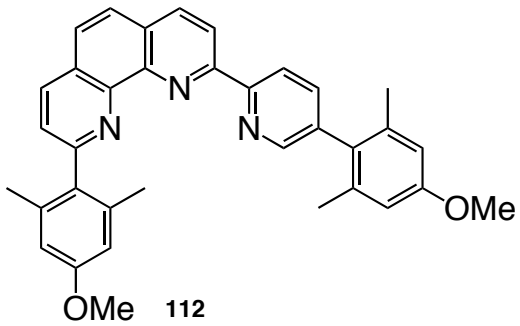

112

2-(4-methoxy-2,6-dimethyl-phenyl)-9-[5-(4-methoxy-2,6-dimethylphenyl)-pyridin-2-yl]-1,10-phenanthroline

Prepared using general Negishi coupling procedures. Column chromatography on neutral alumina with methylene chloride: hexanes (1:1 then 1:0) as eluant gave a white film (0.130 g, 74%). m.p. 125-130 ºC; ^{1}H NMR (300 MHz, $CDCl_3$, δ): 8.92 (1H, d, *J* = 8.1 Hz), 8.81 (1H, d, *J* = 8.4 Hz), 8.51 (1H, d, *J* = 1.8 Hz), 8.41 (1H, d, *J* = 8.7 Hz), 8.29 (1H, d, *J* = 8.4 Hz), 7.86 (2H), 7.69 (1H, dd, *J* = 8.1, 2.1 Hz), 7.62 (1H, d, *J* = 8.4 Hz), 6.75 (2H, s), 6.72 (2H, s), 3.86 (3H, s), 3.84 (3H, s), 2.31 (6H, s), 2.07 (6H, s); ^{13}C NMR (100 MHz, $CDCl_3$, δ): 159.41, 158.75, 158.66, 155.77, 154.72, 149.49, 145.87, 145.81, 138.38, 138.01, 137.75, 136.69, 135.523, 133.54, 130.38, 128.68, 126.95, 126.43, 126.02, 125.25, 125.25, 122.46, 120.32, 113.09, 112.82, 55.22, 55.22, 21.49, 21.27; HRMS(DEI) m/z: calc. for [M-H$^+$] $C_{35}H_{30}N_3O_2$: 524.233803; found: 524.232151.

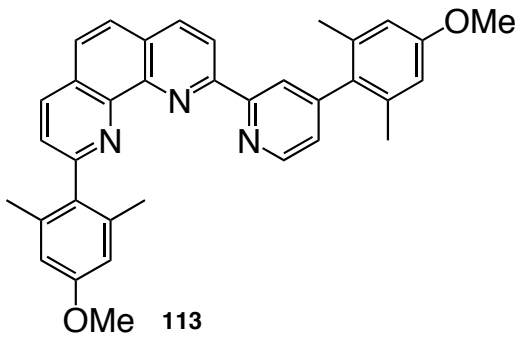

113

2-(4-methoxy-2,6-dimethyl-phenyl)-9-[4-(4-methoxy-2,6-dimethylphenyl)-pyridin-2-yl]-1,10-phenanthroline

Prepared using general Suzuki-Miyuara coupling procedures. Residual Ph_3PO was removed by trituration with diethyl ether and column chromatography on neutral alumina with methylene chloride as eluant gave a white film (0.028 g, 74%). m.p. 258-260 ºC; ^{1}H NMR (400 MHz, $CDCl_3$, δ): 8.79 (1H, d, *J* = 8.4 Hz), 8.76 (1H, d, *J* = 4.8 Hz), 8.66 (1H, d, *J* = 0.8 Hz), 8.39 (1H, d, *J* = 8.4 Hz), 8.27 (1H, d, *J* = 8.0 Hz), 7.84 (2H, s), 7.58 (1H, d, *J* = 8.0 Hz), 7.16 (1H, dd, *J* = 4.8, 1.6 Hz), 6.69 (2H, s), 6.68 (2H, s), 3.85 (3H, s), 3.84 (3H, s), 2.23 (6H, s), 2.09 (6H, s); ^{13}C NMR (100 MHz, $CDCl_3$, δ): 159.35, 158.72, 158.57, 156.45, 155.96, 150.02, 150.02, 148.87, 145.84, 138.01, 136.81, 136.63, 135.46, 133.29, 131.86, 128.74, 126.92, 126.47, 126.00, 125.50, 125.30, 124.00, 120.70, 113.16, 112.85, 55.21, 55.17, 21.42, 21.25; HRMS(DEI) m/z: calc. for [M-H$^+$] $C_{35}H_{30}N_3O_2$: 524.233803; found: 524.232834

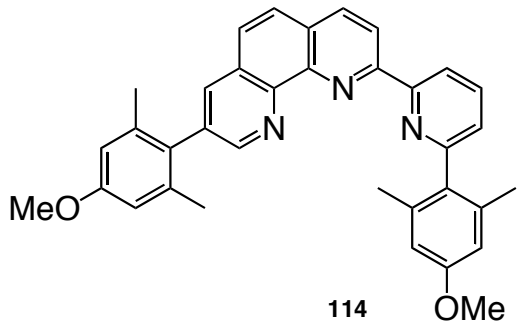

114

8-(4-methoxy-2,6-dimethyl-phenyl)-2-[6-(4-methoxy-2,6-dimethylphenyl)-pyridin-2-yl]-1,10-phenanthroline

Prepared using general Negishi coupling procedures. Column chromatography on neutral alumina with methylene chloride: hexanes (2:1 then 3:1) as eluant gave a white film (0.176 g, 79%). m.p. 223-225 ºC; ^{1}H NMR (400 MHz, $CDCl_3$, δ): 9.08 (1H, d, *J* = 2.4 Hz), 8.92 (1H, dd, *J* = 7.6, 0.8 Hz), 8.80 (1H, d, *J* = 8.4 Hz), 8.34 (1H, d, *J* = 8.4 Hz), 8.07 (1H, d, *J* = 2.4 Hz), 7.97 (1H, t, *J* = 8.0 Hz) 7.86 (1H, d, *J* = 8.8 Hz), 7.81 (1H, d, *J* = 8.8 Hz), 7.30 (1H, dd, *J* =7.6, 0.8 Hz), 6.76 (2H, s), 6.72 (2H, s), 3.86 (3H, s), 3.84 (3H, s), 2.15 (6H, s), 2.07 (6H, s); ^{13}C NMR (100 MHz, $CDCl_3$, δ): 158.86, 158.65, 158.63, 156.67, 155.92, 151.75, 145.42, 144.72, 137.83, 137.39, 136.90, 136.65, 136.36, 135.76, 133.49, 130.06, 128.59, 128.49, 126.62, 126.49, 125.33, 121.24, 120.49, 112.90, 112.90, 55.22, 55.19, 21.42, 20.86; HRMS(DEI) m/z: calc. for [M-H$^+$] $C_{35}H_{30}N_3O_2$: 524.233803; found: 524.2323842

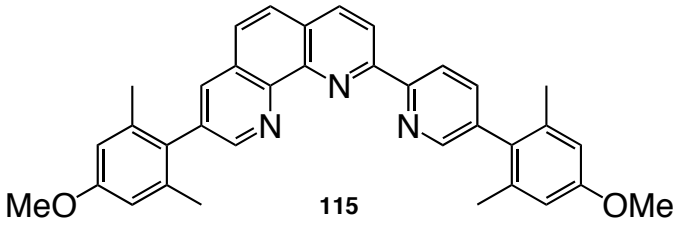

115

8-(4-methoxy-2,6-dimethyl-phenyl)-9-[5-(4-methoxy-2,6-dimethylphenyl)-pyridin-2-yl]-1,10-phenanthroline

Prepared using general Suzuki-Miyuara coupling procedures. Residual Ph_3PO was removed by column chromatography on neutral alumina with methylene chloride : hexanes (2 : 1) as eluant gave a white film (0.042 g, 65%). ^{1}H NMR, ^{13}C NMR, and mass spectrum matched literature.[53] m.p. 132 - 135 °C. ^{1}H NMR (500 MHz, $CDCl^3$, δ): 9.08 (1H, d, *J* = 2.0 Hz), 9.07 (1H, d, *J* = 8.0 Hz), 8.87 (1H, d, *J* = 8.5 Hz), 8.57 (1H, d, *J* = 2.0 Hz), 8.44 (1H, d, *J* = 8.5 Hz), 8.09 (1H, d, *J* = 2.0 Hz), 7.91 (1H, d, *J* = 9.0 Hz), 7.84 (1H, d, *J* = 9.0 Hz), 7.75 (1H, dd, *J* = 8.0, 2.0 Hz), 6.77 (2H, s), 6.74 (2H, s), 3.87 (3H, s), 3.85 (3H, s), 2.10 (6H, s), 2.08 (6H, s). ^{13}C NMR (125 MHz, $CDCl_3$, δ): 159.19, 159.01, 156.46, 154.68, 152.11, 149.91, 145.80, 144.95, 138.61, 138.08, 137.92, 137.14, 137.11, 136.63, 136.07, 130.47, 130.24, 128.86, 128.71, 126.82, 126.80, 122.61, 120.74, 113.05, 112.99, 55.19, 55.16, 21.27, 21.18.

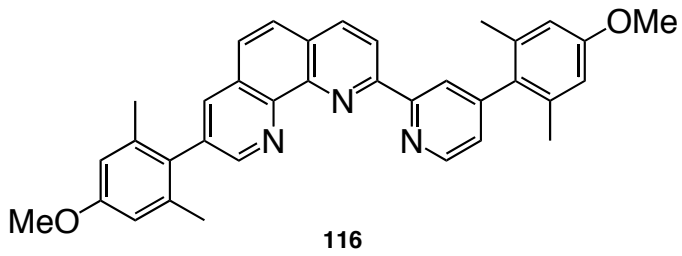

116

8-(4-methoxy-2,6-dimethyl-phenyl)-9-[4-(4-methoxy-2,6-dimethylphenyl)-pyridin-2-yl]-1,10-phenanthroline

Prepared using general Suzuki-Miyuara coupling procedures. Residual Ph_3PO was removed by trituration with diethyl ether and column chromatography on neutral alumina with methylene chloride as eluant gave a white film (0.064 g, 90%). m.p. 228-230 ºC; ^{1}H NMR (400 MHz, $CDCl_3$, δ): 8.98 (1H, d, *J* = 2.4 Hz), 8.90 (1H, d, *J* = 8.4 Hz), 8.80 (1H, d, *J* = 4.8 Hz), 8.79 (1H, s), 8.43 (1H, d, *J* = 8.4 Hz), 8.05 (1H, d, *J* = 2.0 Hz), 7.89 (1H, d, *J* = 8.8 Hz), 7.82 (1H, d, *J* = 8.4 Hz), 7.20 (1H, d, *J* = 8,4 Hz), 6.74 (2H, s), 6.70 (2H, s), 3.85 (3H, s), 3.84 (3H, s), 2.10 (6H, s), 2.04 (6H, s); ^{13}C NMR (100 MHz, $CDCl_3$, δ): 158.85, 158.59, 156.33, 156.28, 151.64, 150.47, 149.05, 145.51, 144.69, 137.85, 136.85, 136.74, 136.45, 135.82, 131.84, 130.01, 128.68, 128.64, 126.68, 126.66, 125.56, 123.37, 120.98, 112.86, 112.70, 55.23, 55.19, 21.42, 21.29; HRMS(DEI) m/z: calc. for [M-H$^+$] $C_{35}H_{30}N_3O_2$: 524.233803; found: 524.232201.

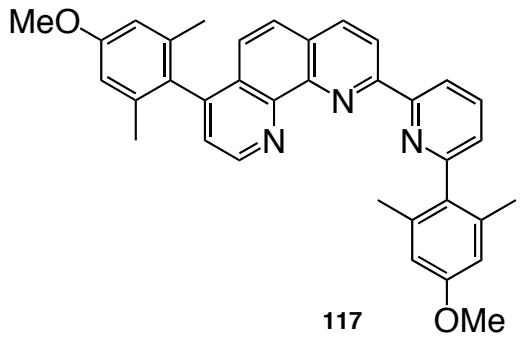

117

7-(4-methoxy-2,6-dimethyl-phenyl)-9-[6-(4-methoxy-2,6-dimethylphenyl)-pyridin-2-yl]-1,10-phenanthroline

Prepared using general Suzuki-Miyuara coupling procedures. Column chromatography on neutral alumina with methylene chloride as eluant gave a white film (0.047 g, 84%). m.p. 257-260 ºC; ^{1}H NMR (500 MHz, $CDCl_3$, δ): 9.29 (1H, d, *J* = 4.5 Hz), 8.90 (1H, d, *J* = 7.5 Hz), 8.77 (1H, d, *J* = 8.5 Hz), 8.30 (1H, d, *J* = 8.0 Hz), 7.98 (1H, t, *J* = 8.0 Hz), 7.71 (1H, d, *J* = 9.5 Hz), 7.46 (1H, d, *J* = 4.5 Hz), 7.41 (1H, d, *J* = 9.0 Hz), 7.30 (1H, d, *J* = 7.5 Hz), 6.78 (2H, s), 6.72 (2H, s) 3.89 (3H, s), 3.85 (3H, s), 2.15 (6H, s), 1.93 (6H, s); ^{13}C NMR (125 MHz, $CDCl_3$, δ): 159.04, 158.66, 158.65, 156.65, 156.09, 150.08, 147.85, 146.60, 145.77, 137.43, 137.34, 136.99, 136.55, 136.55, 133.51, 129.38, 128.46, 126.43, 125.31, 123.99, 123.84, 121.43, 120.57, 112.93, 112.86, 55.25, 55.23, 20.91, 20.78; HRMS(DEI) m/z: calc. for [M-H$^+$] $C_{35}H_{30}N_3O_2$: 524.233803; found: 524.233015.

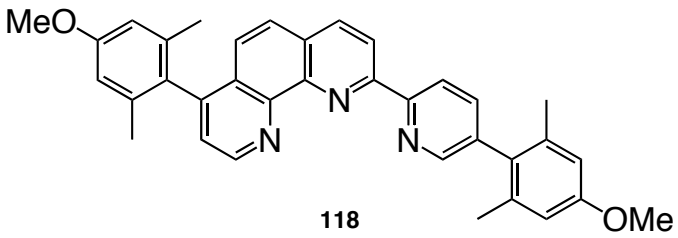

118

7-(4-methoxy-2,6-dimethyl-phenyl)-2-[5-(4-methoxy-2,6-dimethylphenyl)-pyridin-2-yl]-1,10-phenanthroline

Prepared using general Negishi coupling procedures. Column chromatography on silica with methylene chloride: methanol (97:3) as eluant gave a white film. Residual Ph_3PO was removed by trituration with ethyl ether to give a white solid (0.011 g, 12%). m.p. 300-301 ºC; ^{1}H NMR (400 MHz, $CDCl_3$, δ): 9.28 (1H, d, *J* = 4.2 Hz), 9.05 (1H, d, *J* = 7.8 Hz), 8.82 (1H, d, *J* = 8.4 Hz), 8.56 (1H, d, *J* = 2.1 Hz), 8.39 (1H, d, *J* = 8.7 Hz), 7.76 (1H, dd, *J* = 8.1, 2.1 Hz), 7.74 (1H, d, *J* = 9.0 Hz), 7.46 (1H, d, *J* = 4.5 Hz), 7.43 (1H, d, *J* = 9.3 Hz), 6.78 (2H, s), 6.73 (2H, s) 3.89 (3H, s), 3.85 (3H, s), 2.15 (6H, s), 1.92 (6H, s); ^{13}C NMR (125 MHz, $CDCl_3$, δ): 159.11, 158.77, 156.15, 154.57, 150.16, 149.72, 147.99, 145.92, 138.50, 137.80, 137.40, 136.94, 136.83, 130.33, 129.39, 128.52, 128.22, 126.47, 126.47, 124.11, 124.01, 122.50, 120.77, 112.89, 112.89, 55.26, 55.26, 21.38, 20.78; HRMS(DEI) m/z: calc. for [M^+] $C_{35}H_{31}N_3O2$: 525.241628; found: 525.240412.

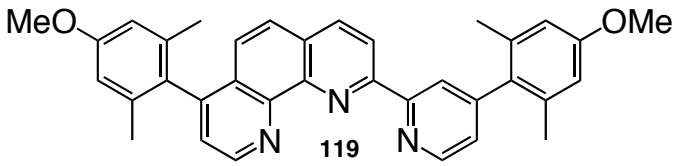

119

7-(4-methoxy-2,6-dimethyl-phenyl)-9-[4-(4-methoxy-2,6-dimethylphenyl)-pyridin-2-yl]-1,10-phenanthroline

Prepared using general Suzuki-Miyuara coupling procedures. Column chromatography on neutral alumina with methylene chloride as eluant gave a white film (0.052 g, 84%). m.p. 213-217 ºC; ^{1}H NMR (500 MHz, $CDCl_3$, δ): 9.20 (1H, d, *J* = 4.5 Hz), 8.90 (1H, d, *J* = 9.0 Hz), 8.84 (1H, s), 8.80 (1H, d, *J* = 5.0 Hz), 8.37 (1H, d, *J* = 8.0 Hz), 7.72 (1H, d, *J* = 8.5 Hz), 7.43 (1H, d, *J* = 4.5 Hz), 7.41 (1H, d, *J* = 9.0 Hz), 7.20 (1H, dd, *J* = 4.5, 1.5 Hz), 6.77 (2H, s), 6.73 (2H, s), 3.88 (3H, s), 3.86 (3H, s), 2.12 (6H, s), 1.89 (6H, s); ^{13}C NMR (125 MHz, $CDCl_3$, δ): 159.26, 158.84, 156.56, 156.39, 150.61, 150.15, 149.23, 148.06, 146.71, 145.98, 137.47, 136.94, 136.86, 132.07, 129.49, 128.72, 128.28, 126.55, 125.66, 124.12, 124.11, 123.51, 121.11, 112.95, 112.84, 55.19, 55,17, 21.16, 20.58; HRMS(DEI) m/z: calc. for [M-H$^+$] $C_{35}H_{30}N_3O2$: 524.233803; found: 524.232151.

2.4 Crystal Structure Data

Methods and Materials

All measurements were made on a *Nonius KappaCCD* area-detector diffractometer[73] using graphite-monochromated Mo *K*a radiation (l = 0.71073 Å) and an *Oxford Cryosystems Cryostream 700* cooler. Data reduction was performed with *HKL Denzo* and *Scalepack*[74]. The intensities were corrected for Lorentz and polarization effects, but not for absorption. The structures were solved by direct methods using *SIR92*,[75] which revealed the positions of all non-hydrogen atoms. The non-hydrogen atoms were refined anisotropically. All of the H-atoms were placed in geometrically calculated positions and refined using a riding model where each H-atom was assigned a fixed isotropic displacement parameter with a value equal to $1.2U_{eq}$ of its parent atom ($1.5U_{eq}$ for the methyl groups). Refinement of the structure was carried out on F^2 by using full-matrix least-squares procedures, which minimized the function $Sw(F_o^2 - F_c^2)^2$. The weighting scheme was based on counting statistics and included a factor to downweight the intense reflections. Neutral atom scattering factors for non-hydrogen atoms were taken from Maslen, Fox and O'Keefe[76], and the scattering factors for H-atoms were taken from Stewart, Davidson and Simpson[77]. Anomalous dispersion effects were included in F_c[78]; the values for f' and f'' were those of Creagh and McAuley[79]. The values of the mass attenuation coefficients are those of Creagh and Hubbel[80]. All calculations were performed using the *SHELXL97*[81] program.

Table 2.5 Crystallographic Data for **111**

Crystallised from		EtOH
Empirical formula		$C_{35}H_{31}N_3O_2$
Formula weight [g mol^{-1}]		525.65
Crystal color, habit		yellow, prism
Crystal dimensions [mm]		0.20 ´ 0.25 ´ 0.32
Temperature [K]		160(1)
Crystal system		triclinic
Space group		$P\bar{1}$ (#2)
Z		4
Reflections for cell determination		12429
2q range for cell determination [°]		4–55
Unit cell parameters	a [Å] = 11.6696(3)	α [°] = 101.922(1)
	b [Å] = 13.9357(3)	β [°] = 98.081(1)
	c [Å]= 17.5533(3)	γ [°] = 95.146(1)
V [Å^3]	2744.4(1)	
F(000)		1112
D_X [g cm^{-3}]		1.272
μ(Mo $K\alpha$) [mm^{-1}]		0.0795
Scan type		ϕ and ω
2θ(max) [°]		55
Total reflections measured		65806
Symmetry independent reflections		12568
R_{int}		0.057
Reflections with $I > 2\sigma(I)$		8333
Reflections used in refinement		12558
Parameters refined; restraints		828; 300
Final $R(F)$ [$I > 2\sigma(I)$ reflections]		0.0551
$wR(F^2)$ (all data)		0.1498
Weights: $w = [\sigma^2(F_o^2) + (0.0743P)^2 + 0.1952P]^{-1}$ where $P = (F_o^2 + 2F_c^2)/3$		
Goodness of fit		1.051
Secondary extinction coefficient		0.006(1)
Final Δ_{max}/σ		0.001
$\Delta\rho$ (max; min) [e Å^{-3}]		0.27; -0.20
σ(d(C–C)) [Å]		0.002–0.005

See attached CIF file for atomic coordinates.

Table 2.6 Crystallographic Data for **114**

Crystallised from	EtOH
Empirical formula	$C_{35}H_{31}N_3O_2$
Formula weight [g mol^{-1}]	525.65
Crystal colour, habit	pale yellow, prism
Crystal dimensions [mm]	0.35 ´ 0.38 ´ 0.50
Temperature [K]	160(1)
Crystal system	orthorhombic
Space group	$P2_12_12_1$ (#19)
Z	4
Reflections for cell determination	3646
$2q$ range for cell determination [°]	4–55
Unit cell parameters a [Å] = 12.2155(3)	α [°] = 90
b [Å] = 14.8014(4)	β [°] = 90
c [Å] = 15.6657(4)	γ [°] = 90
V [Å^3] = 2832.5(1)	
F(000)	1112
D_x [g cm^{-3}]	1.233
μ(Mo $K\alpha$) [mm^{-1}]	0.0770
Scan type	ϕ and ω
$2\theta_{(max)}$ [°]	55
Total reflections measured	39502
Symmetry independent reflections	3623
R_{int}	0.073
Reflections with $I > 2\sigma(I)$	2778
Reflections used in refinement	3622
Parameters refined	368
Final $R(F)$ [$I > 2\sigma(I)$ reflections]	0.0456
$wR(F^2)$ (all data)	0.1193
Weights: $w = [\sigma^2(F_o^2) + (0.0679P)^2 + 0.0809P]^{-1}$ where $P = (F_o^2 + 2F_c^2)/3$	
Goodness of fit	1.056
Secondary extinction coefficient	0.011(2)
Final Δ_{max}/σ	0.001
$\Delta\rho$ (max; min) [e Å^{-3}]	0.20; -0.19
$\sigma(d_{(C-C)})$ [Å]	0.003–0.004

See attached CIF file for atomic coordinates.

2.5 References

(1) Constable, E. C. *Adv. Inorg. Chem. Radiochem.* **1986**, *30*, 69-.

(2) Thompson, A. M. W. C. *Coord. Chem. Rev.* **1997**, *160*, 1-52.

(3) Thummel, R. P.; Jahng, Y. *J. Org. Chem.* **1985**, *50*, 2407-2412.

(4) Chelucci, G.; Thummel, R. P. *Chem. Rev.* **2002**, *102*, 3129-3170.

(5) Kelly, T. R. *J. Org. Chem.* **2002**, *67*, 2197-2205.

(6) Yale, H. L.; Bernstein, J. *J. Amer. Chem. Soc.* **1948**, *70*, 254.

(7) Kröhnke, F. *Synthesis* **1976**, 1-24.

(8) Manske, R. H. F. *Organic Reactions*; John Wiley and Sons: New York, 1953; Vol. 7, p 80-99.

(9) Hung, C.-Y.; Wang, T.-L.; Shi, Z.; Thummel, R. P. *Tetrahedron* **1994**, *50*, 10685-10692.

(10) Cheng, C.-C.; Yan, S.-J. *Organic Reactions*; John Wiley and Sons: New York, 1982; Vol. 28, p 37.

(11) Riesgo, E. C.; Jin, X.; Thummel, R. P. *J. Org. Chem.* **1996**, *61*, 3017-3022.

(12) Hung, C.-Y.; Wang, T.-L.; Jang, Y.; Kim, W. Y.; Schmehl, R. H.; Thummel, R. P. *Inorg. Chem.* **1996**, *35*, 5953-5956.

(13) Brown, D.; Muranjan, S.; Jang, Y.; Thummel, R. P. *Org. Lett.* **2002**, *4*, 1253-1256.

(14) Zong, R.; Wang, D.; Hammit, R.; Thummel, R. P. *J. Org. Chem.* **2006**, *71*, 167-175.

(15) Jahng, Y.; Park, J. G.; Kim, H. H. *Kor. J. Med. Chem.* **1998**, *8*, 22-29.

(16) Park, J. G.; Jahng, Y. *Bull. Kor. Chem. Soc.* **1998**, *19*, 436-439.

(17) Leffler, M. T. In *Organic Reactions*; Adams, R., Ed.; VCH Wiley: Weinheim, 1942; Vol. 1, pp 91-104.

(18) Chichibabin; Seide *J. Russ. Phys. Chem.* **1914**, *46*, 1216.

(19) Evans, J. C. W.; Allen, C. F. H. In *Organic Synthesis*; Blatt, A. H., Ed.; John Wiley and Sons: New York, 1943; Vol. 2, pp 517.

(20) Geissman, T. A.; Schlatter, M. J.; Webb, I. D.; Roberts, J. D. *J. Org. Chem.* **1946**, *11*, 741-750.

(21) Case, F. H.; Sasin, R. *Journal of Organic Chemistry* **1951**, *20*, 1330-1336.

(22) Dietrich-Buchecker, C. O.; Marnot, P. A.; Sauvage, J. P. *Tetrahedron Lett.* **1982**, *23*, 5291-5294.

(23) Kauffmann, T.; König, J.; Körber, D.; Lexy, H.; Streitberger, H. J.; Vahrenhorst, A. *Tetrahedron Lett.* **1977**, 389.

(24) Dietrich-Buchecker, C. O.; Nierengarten, J. F.; Sauvage, J. P.; Armaroli, N.; Balzani, V.; De Cola, L. *Journal of the American Chemical Society* **1993**, *115*, 11237-11244.

(25) Schmittel, M.; Michel, C.; Liu, S.-X.; Schildbach, D.; Fenske, D. *Eur. J. Inorg. Chem.* **2001**, 1155-1166.

(26) Collin, J.-P.; Gavina, P.; Sauvage, J.-P.; De Cian, A.; Fischer, J. *Aust. J. Chem.* **1997**, *50*, 951-957.

(27) Miller, M. T.; Gantzle, P. K.; Karpishin, T. B. *Inorg. Chem.* **1999**, *38*, 3414-3422.

(28) Lüning, U.; Müller, M. *Chem. Ber.* **1990**, *123*, 643-645.

(29) Schmittel, M.; Ganz, A. *J. Chem. Soc., Chem. Commun.* **1997**, 999-1000.

(30) Schmittel, M.; Ganz, A.; Fenske, D.; Herderich, M. *J. Chem. Soc., Dalton Trans* **2000**, 353-359.

(31) Tiecco, M.; Testaferri, L.; Tingoli, M.; Chianelli, D.; Montanucci, M. *Synthesis* **1984**, 736-738.

(32) Fanta, P. E. *Synthesis* **1974**, 9-21.

(33) Malmberg, H.; Nilsson, M. *Tetrahedron* **1986**, *14*, 3981-3986.

(34) Bamfield, P.; Quan, P. M. *Synthesis* **1978**, 537-538.

(35) Newkome, G. R.; Puckett, W. E.; Kiefer, G. E.; Gupta, V. D.; Xia, Y.; Coreil, M.; Hackney, M. A. *J. Org. Chem.* **1982**, *47*, 4116-4120.

(36) Haginiwa, J.; Higuchi, Y.; Kawashima, T.; Goto, T. *Yakugaku Zasshi* **1975**, *95*, 204-210.

(37) Li, J. J.; Gribble, G. *Palladium in Heterocyclic Chemistry*; Pergamon: New York, 2000; Vol. 20, p 432.

(38) Stille, J. K. *Angew. Chem. Int. Ed., Eng.* **1986**, *25*, 508-524.

(39) Miyuara, N.; Suzuki, A. *Chem. Rev.* **1995**, *95*, 2457-2483.

(40) Schlüter, A. D.; Opris, D., M.; Franke, P. *Eur. J. Org. Chem.* **2005**, 822-837.

(41) Yamamoto, Y.; Yanagi, A. *Chem. Pharm. Bull.* **1982**, *30*, 1731-.

(42) Schubert, U. S.; Eschbaumer, C. *Org. Lett.* **1999**, *1*, 1027-1029.

(43) Benaglia, M.; Ponzini, F.; Woods, C. R.; Siegel, J. S. *Org. Lett.* **2001**, *3*, 967-969.

(44) Benaglia, M.; Toyota, S.; Woods, C. R.; Siegel, J. S. *Tetrahedron Lett.* **1997**, *38*, 4737-4740.

(45) Thompson, A. E.; Hughes, G.; Batsanov, A. S.; Bryce, M. R.; Parry, P. R.; Tarbit, B. *J. Org. Chem.* **2004**, *70*, 388-390.

(46) Barder, T. E.; Walker, S. D.; Martinelli, J. R.; Buchwald, S. L. *J. Amer. Chem. Soc.* **2005**, *127*, 4685-4696.

(47) Kudo, N.; Perseghini, M.; Fu, G. C. *Angew. Chem. Int. Ed., Eng.* **2006**, *45*, 1282-1284.

(48) Fischer, F. C.; Havinga, E. *Rec. Trav. Chim. Pays-Bas* **1974**, *93*, 21-24.

(49) Bouillon, A.; Lancelot, J.-C.; Collot, V.; Bovy, P. R.; Rault, S. *Tetrahedron* **2002**, *58*, 2885-2890.

(50) Bouillon, A.; Lancelot, J.-C.; Collot, V.; Bovy, P. R.; Rault, S. *Tetrahedron* **2002**, *58*, 3323-3328.

(51) Bouillon, A.; Lancelot, J.-C.; Collot, V.; Bovy, P. R.; Rault, S. *Tetrahedron* **2002**, *58*, 4369-4373.

(52) Bouillon, A.; Lancelot, J.-C.; Santos, J. S. d. O.; Collot, V.; Bovy, P. R.; Rault, S. *Tetrahedron* **2003**, *59*, 10043-10049.

(53) Loren, J. C.; Siegel, J. S. *Angew. Chem. Int. Ed.* **2001**, *40*, 754-757.

(54) Negishi, E.-i. *Acc. Chem. Res.* **1982**, *15*, 340-348.

(55) 4-Methoxy-2,6-dimethylphenyl (manisyl) was chosen as the model aryl substituent to enhance solubility and demonstrate the potential for further structural elaboration. However, many aryl substituents work equally well.

(56) Toyota, S.; Woods, C. R.; Benaglia, M.; Siegel, J. S. *Tetrahedron Lett.* **1998**, *39*, 2697-2700.

(57) Snyder, H. R.; Freier, H. E. *J. Amer. Chem. Soc.* **1946**, *68*, 1320-1322.

(58) Case, F. H. *J. Org. Chem.* **1951**, *16*, 941-945.

(59) The relative nucleophilicity of the two nitrogen remained similiar even when 4-chlorophenanathroline was used.

(60) Kondo, Y.; Shilai, M.; Uchiyama, M.; Sakamoto, T. *J. Org. Chem.* **1999**, *121*, 3539-3540.

(61) Sammes, P. G.; Yahioglu, G. *Chem. Soc. Rev.* **1994**, *23*, 327-334.

(62) Chambron, J.-C.; Dietrich-Buchecker, C. O.; Sauvage, J.-P. In *Comprehensive Supramolecular Chemistry*; Sauvage, J.-P., Hosseini, M. W., Eds.; Pergamon: 1996; Vol. 9, pp 43-84.

(63) Tor, Y. *Synlett* **2002**, *7*, 1043-1054.

(64) Yamada, M.; Nakamura, Y.; Kuroda, S.; Shimao, I. *Bull. Chem. Soc. Jpn.* **1990**, *63*, 2710-2712.

(65) Tzalis, D.; Tor, Y.; Failla, S.; Siegel, J. S. *Tetrahedron Lett.* **1995**, *36*, 3489-3490.

(66) Saitoh, Y.; Koizumi, T.-a.; Osakada, K.; Yamamoto, T. *Can. J. Chem.* **1997**, *75*, 1336-1337.

(67) Batterman, T. J. *NMR Spectra of Simple Heterocycles*; John Wiley and Sons: New York, 1972, p 540.

(68) Woods, C. R. Electronic, University of California, San Diego, 1998.

(69) The asymmetric unit of **111** contains two molecules. Only molecule A is considered here. See the crystal structure data in the experimental section for the CIF files.

(70) Petitjean, A.; Khoury, R. G.; Kyritsakas, N.; Lehn, J.-M. *J. Amer. Chem. Soc.* **2004**, *126*, 6637-6647.

(71) Linke-Schaetzel, M.; Anson, C. E.; Powell, A. K.; Buth, G.; Palomares, E.; Durrant, J. D.; Balaban, T. S.; Lehn, J.-M. *Chem.--Eur. J.* **2006**, *12*, 1931-1940.

(72) Loren, J. C.; Gantzel, P.; Linden, A.; Siegel, J. S. *Org. Bio. Chem.* **2005**, *3*, 3105-3116.

(73) Hooft, R. *KappaCCD Collect Software* Delft, The Netherlands, 1999, p Nonius BV.

(74) Otwinowski, Z.; Minor, W. In *Methods in Crystallography*; Carter, C. W., Sweet, R. M., Eds.; Academic Press: New York, 1997; Vol. 276, pp 307-326.

(75) Altomare, A.; Cascarano, G.; Giacovazza, C.; Guagliardi, A.; Burla, M. C.; Polidori, G.; Carmalli, M. *J. Appl. Crystallogr.* **1994**, *27*, 435.

(76) Maslen, E. N.; Fox, A. G.; O'Keefe, M. A. In *International Tables for Crystallography*; Wilson, A. J. C., Ed.; Kluwer Academic Publishers: Dordrecht, 1992; Vol. C, pp 477-486.

(77) Stewart, R. F.; Davidson, E. R.; Simpson, W. T. *J. Chem. Phys.* **1965**, *42*, 3175-3187.

(78) Ibers, J. A.; Hamilton, W. C. *Acta Crystallogr.* **1964**, *17*, 781-782.

(79) Creagh, D. C.; Auley, W. J. In *International Tables for Crystallography*; Wilson, A. J. C., Ed.; Kluwer Academic Publishers: Dordrecht, 1992; Vol. C, pp 219-222.

(80) Creagh, D. C.; Hubbell, J. H. In *International Tables for Crystallography*; Wilson, A. J. C., Ed.; Kluwer Academic Publishers: Dordrecht, 1992; Vol. C, pp 200-206.

(81) Sheldrick, G. M.; University of Göttingen, Germany: Göttingen, 1997.

CHAPTER 3

PHOTOPHYSICS OF 2-PYRIDYL-1,10-PHENANTHROLINES

3.0 Abstract

Fluorescence investigations revealed that pherpys can display from low to high quantum yields (Φ_f = 0.03-0.60) depending on the placement of aryl substituents. Further photophysical studies elucidated the duality of emissive states: a weakly emissive locally excited state, similar to the $^1\pi,\pi^*$ state of phenanthroline; and a strongly emissive charge transfer state, dependent on manisyl regiochemistry and solvent polarity. MO calculations in collaboration with the Baldridge group (UZH) underscore the similarities in the electronic structures of phenanthroline and pyridyl-phenanthrolines rather than between terpyridine and pyridyl-phenanthroline.

3.1 Introduction

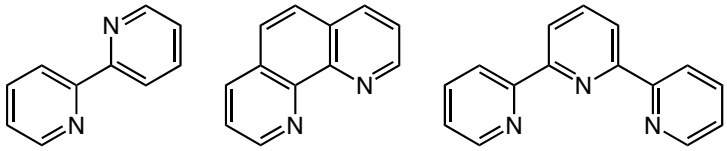

125 **126** **45**

The polypyridines 2,2'-bipyridine **125** (bipyridine), 1,10-phenanthroline **126** (phenanthroline), and 2,2';6',2"-terpyridine **45** (terpyridine) are among the most important and widely used ligands in coordination chemistry.[1-3] In particular, the photophysical and electrochemical properties of their metal complexes are especially interesting[4] and are being actively investigated for potential applications in artificial photosynthesis,[5-7] photo-induced electron transfer,[8,9] and molecular electronics.[10,11] A thorough understanding of the ligand photophysics is essential for the design of luminescent metal complexes and, ideally, the ability to tune the properties of a modular family of ligands to suit the purpose at hand is desired.[12]

This chapter provides background on radiative and non-radiative photophysical processes, as well as an overview of the current state of polypyridyl photophysics and

photochemistry before discussing the photophysical properties of aryl-substituted 2-pyridyl-phenanthrolines.

3.1.1 Photophysical Processes

When molecules absorb a photon of light, an electron is excited from a low energy orbital (ψ) into an unoccupied higher energy orbital (ψ^*); typically from the highest occupied molecular orbital (HOMO) into the lowest unoccupied orbital (LUMO) (Figure 3.1).[13] There are two possible excited electronic states, depending on the configuration of the electrons. When the spins of the two electrons are paired (antiparallel), the new excited state is called a *singlet state* (Figure 3.1a). When the two spins are unpaired (parallel), the excited state is called a *triplet state* (Figure 3.1b). The initial, ground state configuration is also a singlet state and written as S_0.[14] The lowest energy excited singlet state is S_1 and the next lowest is S_2. The lowest energy excited triplet state is T_1 and so forth. The photophysical processes of absorption (excitation) and emission (fluorescence and phosphorescence) can be individually visualized (Figure 3.1) but are more concisely described in a state energy diagram, called a Jablonksi diagram (Figure 3.2).[15]

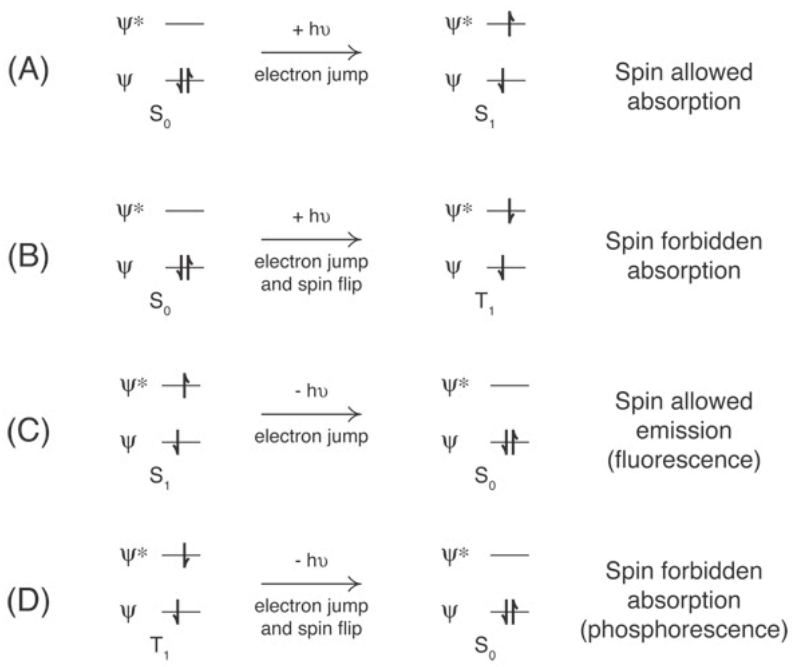

Figure 3.1 Orbital level energy diagram of absorption, (A) and (B), and emission, (C) and (D), processes.

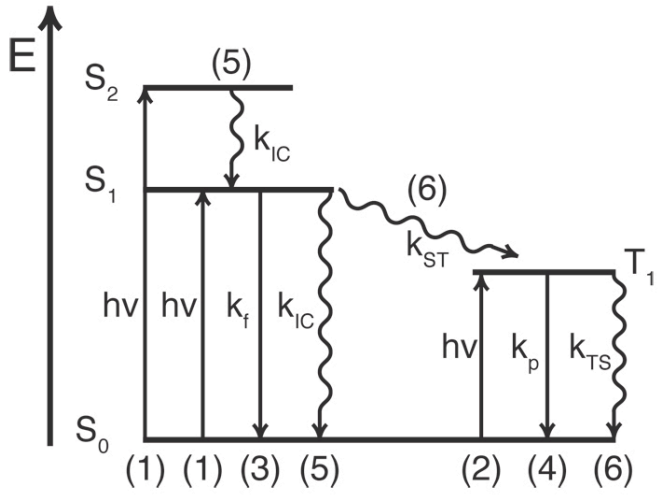

Figure 3.2 A simplified Jablonski energy state diagram illustrating key photophysical transitions.[13]

A *photophysical process* is any transition that interconverts between excited states and the ground state or between excited states,[13] and may be categorized as *radiative* or *non-radiative* processes. Transitions between states of different spin require electron spin inversion and are called "forbidden." The term "forbidden" is not absolute but

indicates a lower probability of a transition occurring. The important photophysical *radiative* processes are:[13] (1) "Allowed" absorption from the singlet ground state to a singlet excited state; typically $S_0 \rightarrow S_1$, experimentally quantified by the extinction coefficient ε; (2) "Forbidden" absorption from the singlet ground state to a triplet excited state; typically $S_0 \rightarrow T_1$, also experimentally quantified by the extinction coefficient ε; (3) *Fluorescence:* "Allowed" emission from a singlet excited state to the ground state, typically $S_1 \rightarrow S_0$, described by the fluorescence rate constant k_f; (4) *Phosphorescence*: "Forbidden" emission from a triplet excited state to the ground state, typically $T_1 \rightarrow S_0$, described by the phosphorescence rate constant k_p. Electrons can be excited into any of the higher level excited states (S_2, S_3…; T_2, T_3…) but usually only transitions into S_1 and S_2 are observed. Based on these observations, Kasha postulated that fluorescence occurs from the S_1 state, and phosphorescence from the T_1 state, regardless of into which level the initial excitation took place.[16]

The important *non-radiative* processes are:[16] (5) *Internal Conversion*: "Allowed" non-radiative transitions between states of the same spin; e.g., $S_2 \rightarrow S_1$ or $S_1 \rightarrow S_0$, described by the rate constant k_{IC}; (6) *Intersystem Crossing*: "Forbidden" non-radiative transitions between states of different spin; e.g., $S_1 \rightarrow T_1$ or $T_1 \rightarrow S_0$, characterized by the rate constants k_{ST} and k_{TS}.

The efficiency of a photophysical process is described by its *quantum yield* (**Φ**), which is simply the number of photophysical events per number of absorbed photons (Eq. 3.1).

$$\Phi = \frac{\text{number of events}}{\text{number of photons absorbed}} \tag{3.1}$$

The fluorescence quantum yield, Φ_f, is then the number of photons emitted (from S_1) per photons absorbed. Non-radiative processes, governed by the rate constants k_{IC} and

k_{ST}, depopulate the excited state, competitive with fluorescence, so the fluorescent quantum yield can be viewed as:

$$\Phi_f = \frac{k_f}{k_{IC} + k_{ST} + k_f} = k_f \tau_f \tag{3.2}$$

where the observed fluorescence lifetime, τ_f, equals $(k_{IC} + k_{ST})^{-1}$. The phosphorescence quantum yield, Φ_p, is the number of photons emitted (from T_1) per photons absorbed and in terms of competing processes, can be described by:

$$\Phi_p = \frac{k_p}{k_{TS} + k_p} \times \frac{k_{ST}}{k_{IC} + k_{ST} + k_f} = k_p \tau_p \Phi_{ST} \tag{3.3}$$

where the observed phosphorescence lifetime, τ_p, equals $(k_{TS} + k_p)^{-1}$, and the quantum yield for intersystem crossing, Φ_{ST}, is given by:

$$\Phi_{ST} = \frac{k_{ST}}{k_{IC} + k_{ST} + k_f} = k_{ST} \tau_f \tag{3.4}$$

Typically, fluorescence is fast ($\tau_f \sim 10^{-8}$ sec) and phosphorescence lifetimes are relatively long ($\tau_p \sim 10^{-4}$ sec).[17] The sum of radiative and non-radiative (Φ_{NR}) quantum yields is the total quantum yield (Φ_T) and equals unity, by definition (Eq. 3.5).

$$\Phi_f + \Phi_p + \sum \Phi_{NR} \equiv 1 \tag{3.5}$$

If the simplified Jablonski diagram (Figure 3.2) were sufficient, the excitation and relaxation of an electron by a single photon of the appropriate energy ($\Delta E = h\nu$) would result in spectra of "sharp" transition lines (Figure 3.3a). This is not the usual case and only the spectra of atoms in the gas phase exhibit distinct, well-defined transitions. The electronic states of molecules are affected by the motions (vibrations, rotations, etc.) of the nuclei relative to each other. Transitions between the vibrational levels of electronic states in molecules can sometimes be observed at in the gas phase at low pressures (Figure 3.3b). In solution, these vibrational levels are often partially or

completely unresolved and broad bands corresponding to an average of the vibrational levels of the two electronic states in a transition are observed (Figure 3.3).[13]

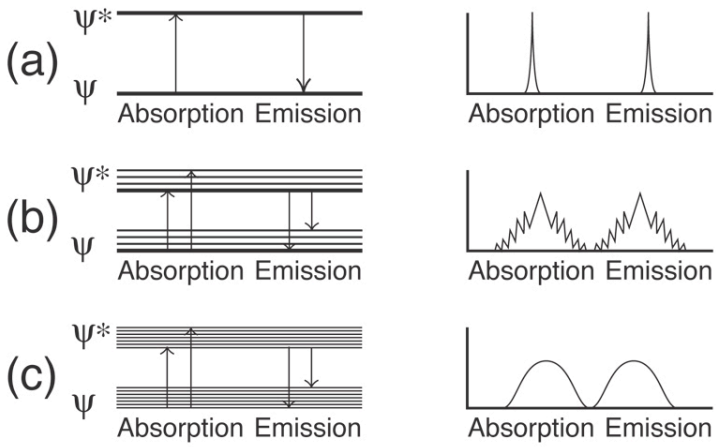

Figure 3.3 (a) Sharp absorption and emission spectra from gas phase atoms; (b) absorption and emission spectra with vibrational structure from molecules in the gas-phase; and (c) broad, structureless absorption and emission from molecules in solution.[13]

3.1.2 The Franck-Condon Principle

The relative intensity of a given transition indicates its probability and is governed by the Franck-Condon principle.[17] As the time required for the absorption (or emission) of a photon of light is very fast (10^{-15} sec) compared to the speed of nuclear motion (10^{-13} sec), the principle states that, during an electronic transition, the nuclei remain fixed in space. After the transition, the molecule is in a new energetic state and the nuclei can relax (through vibrations, rotations, etc.) into their new equilibrium positions. The stasis of nuclei is indicated by vertical lines, representing the primary electronic transitions, connecting two potential energy surfaces (Figure 3.4).

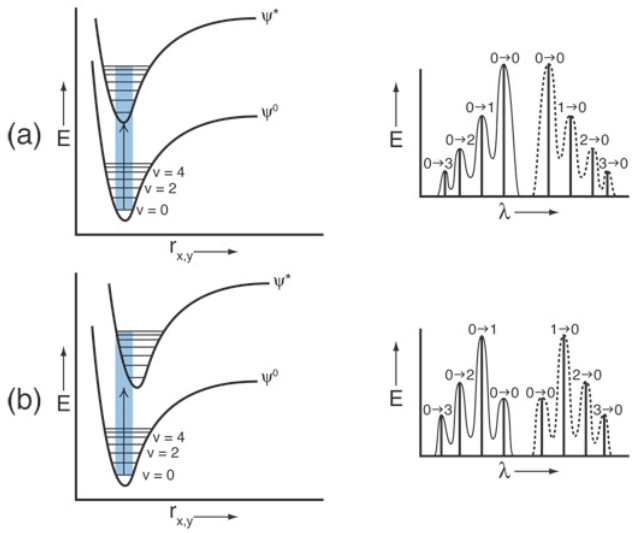

Figure 3.4 The Franck Condon principle. Potential energy curves and absorption (solid) and emission (dotted) spectra for transitions with (a) similar and (b) different excited state geometries. Shaded regions on the potential energy surfaces represent Franck-Condon overlap and correspond to spectral transitions with large intensity.[13]

At room temperature, most molecules exist in the ground vibronic state (ψ^0, $v = 0$) and vertical excitation occurs into primarily the $v = 0$ and $v = 1$ vibrational levels of the excited state ψ^* (Figure 3.4a). This occurs when the equilibrium bonding and geometries in ψ^0 and ψ^* are similar, e.g., rigid aromatic hydrocarbons. When the equilibrium bonding and geometries of ψ^0 and ψ^* are not similar, the potential energy curve of ψ^* is displaced relative to ψ^0 and vertical excitation occurs into the higher vibrational levels of ψ^* (Figure 3.4b).

The Franck-Condon principle holds true for emission as well and when the emissive excited state is the same as the absorptive excited state, the absorption and emission spectra will be mirror images (Figure 3.4). However, due to vibrational loss of energy, emissive processes shift to longer wavelengths (*red-shift*). This is called the *Stokes* shift after Irish physicist George G. Stokes, who first observed this difference in 1852.[18]

3.1.4 Intramolecular Charge Transfer

Organic molecules containing electron donating (D) and electron withdrawing (or accepting, A) groups can exhibit a photo-induced charge transfer (PCS) states called an internal (or intramolecular) charge transfer (ICT) state when the donor and acceptor groups are connected.[19,20] Assuming the donor and acceptor are non-interacting in the ground state, after photo-excitation of the donor (D) or acceptor moiety to a localized or locally excited state (LE*), electron transfer occurs and the new charge transfer (CT*) excited state is formed (Figure 3.5). Emission then occurs from the newly formed CT* state. When the donor and acceptor are conjugated in the ground state, the excitation usually occurs directly into the CT* state. Due to this conjugation, full charge separation is unattainable, but there is a growing class of molecules in which the donor and acceptor groups can adopt (or are held in) an orthogonal geometry and orbital overlap is severed, allowing full charge separation to occur.[20]

Excitation most often occurs into a non-polar Franck-Condon LE* state that thermally equilibrates via nuclear motions into the CT* states. The archetypical example is 4-N,N'-dimethylaminobenzonitrile (DMABN). Twisting dimethyl-amino orthogonal to the plane of the benzene ring allows full charge separation and results in a polar twisted intramolecular charge transfer (TICT) state (Figure 3.6).[21]

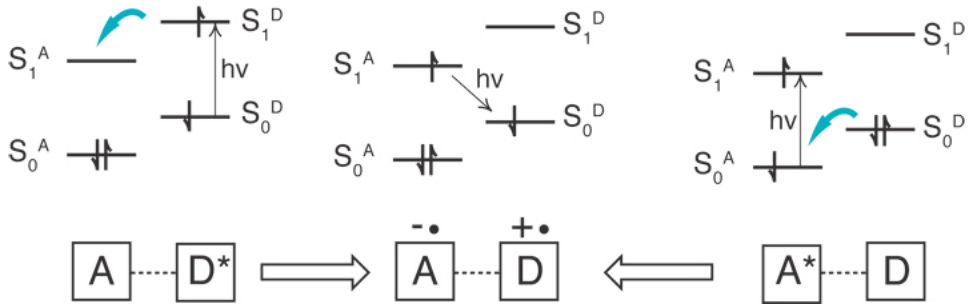

Figure 3.5 Scheme of the photoinduced electron transfer between nearly non-interacting D and A. Regardless of whether excitation occurs into the D or A LE* state, the same CT* state forms.

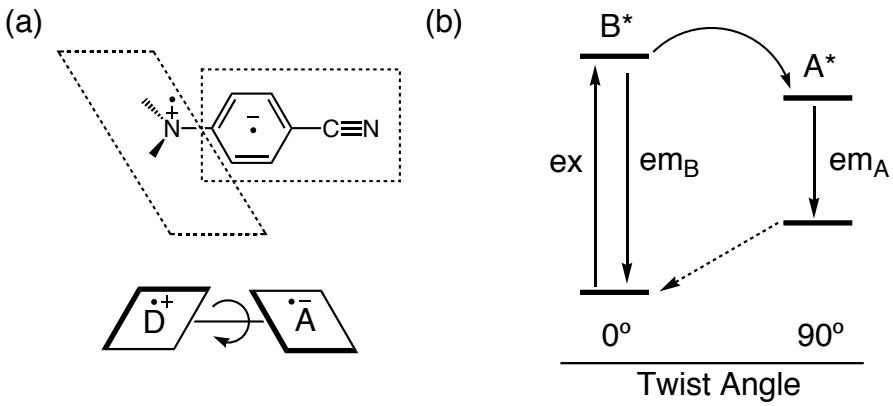

Figure 3.6 a) Rotation around a single bond between the excited state donor ($D^{\bullet+}$) and acceptor ($A^{\bullet-}$). b) TICT model of DMABN, where B* (normal) is the locally excited state and A* (abnormal) is the excited charge transfer state. The ground state at the 90° twist corresponds to the top of a potential barrier to internal rotation. The barrier between the B* and A* states reflects the thermal effects on the kinetics, originally thought to correspond to an avoided state crossing.[20]

Typically, the permanent dipole moment of the new CT* state is much larger than in the ground state. As a result, the emission energy will be significantly affected by the polarity of the medium. To illustrate, the absorption of light occurs from the thermally equilibrated ground state to the Franck-Condon excited state (Figure 3.7). The non-polar ground state remains unaffected by solvent polarity, but increasing solvent polarity stabilizes the polar excited state. After the CT* state reaches thermal equilibrium, emission occurs into the Franck-Condon ground state.

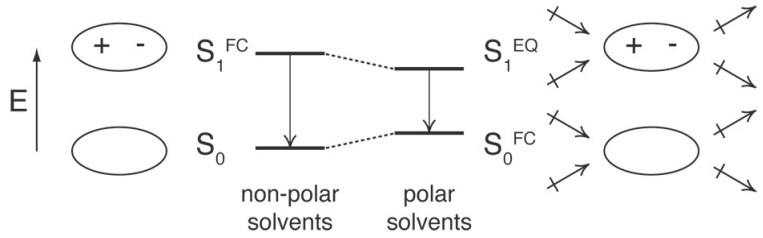

Figure 3.7 Solvent effects on emission spectral wavelength for a fluorophore with an ICT excited state. FC indicates a Franck-Condon state and EQ represents a thermally equilibrated electronic excited state.

The solvent-dependence of emission wavelength is characteristic of polarized CT* states and solvatochromatic[22] measurements can be used to determine the ground and excited state permanent dipole moments. In 1955, Mataga[23] and Lippert[24] demonstrated that the effect of the solvent polarity on the Stokes shift was related to the difference in the ground and excited states dipole moments by:

$$hc(\tilde{\nu}_a - \tilde{\nu}_f) = hc(\tilde{\nu}_a^0 - \tilde{\nu}_f^0) + \frac{2(\vec{\mu}_e - \vec{\mu}_g)}{a_0^3}\left[\frac{\varepsilon - 1}{2\varepsilon - 1} - \frac{n^2 - 1}{2n^2 + 1}\right] \tag{3.6}$$

where h is Planck's constant, c is the speed of light, $\tilde{\nu}_a$ is the energy of absorption in wave numbers (cm^{-1}), $\tilde{\nu}_f$ is the energy of emission, the superscript (^{0}) indicates the absence of solvent, $\vec{\mu}_g$ and $\vec{\mu}_e$ are the dipole moments of the ground and excited states, respectively, a_0 is the radius of the Onsager cavity,[25] ε is the solvent static dielectric constant,[26] and n is the solvent index of refraction. In cases where the absorption and emission transitions have different orbital origins, it is advisable to just use the fluorescence shift:[20]

$$hc\tilde{\nu}_f = hc\tilde{\nu}_f^0 - \frac{2\mu_e(\vec{\mu}_e - \vec{\mu}_g)}{a_0^3}\left[\frac{\varepsilon - 1}{2\varepsilon - 1} - \frac{1}{2}\left(\frac{n^2 - 1}{2n^2 + 1}\right)\right] \tag{3.7}$$

where the constants are the same as in Eq. 3.6. The solvent term in Eq. 3.6:

$$\Delta f = \left[\frac{\varepsilon - 1}{2\varepsilon - 1} - \frac{n^2 - 1}{2n^2 + 1}\right] \tag{3.8}$$

is called the Lippert-Mataga function and is useful for discussing the effects of solvent polarity on electronic transitions. Regardless of technique[27,28] employed, the excited state dipole moment of DMABN corresponds to a full electron transfer from the amino nitrogen to the benzene ring. It is important to note that the dipole moments are approximately solvent independent in strongly polar solvent, meaning that polarizability effects of the charge-separated structure is small.

3.1.4 Photophysics of Polypyridines

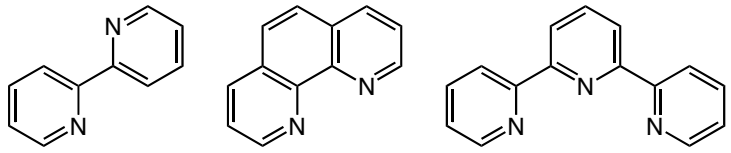

125 **126** **45**

The transition metal complexes of polypyridines play an essential role in the design of photo-active metal complexes,[8,9,29] but the parent ligands are basically non-emissive. The very poor fluorescence quantum yields and short lifetimes (bipyridine **125**: $\Phi_f = 5 \times 10^{-4}$, τ_f = 160 ps (3-methylpentane);[30] phenanthroline **126**: $\Phi_f = 1 \times 10^{-3}$, τ_f < 1.0 μs (cyclohexane);[31] and terpyridine **45**: $\Phi_f = 4 \times 10^{-3}$, τ_f = 2.7 ns (methylcyclohexane)[32]) are due to an efficient intersystem crossing from the $S_{(n,\pi^*)}$ into a nearby non-emissive $T_{(\pi,\pi^*)}$ excited state. The photophysics of aza-aromatics are often complicated by the out-of-plane vibronic coupling between the two close-lying $S_{(n,\pi^*)}$ and $S_{(\pi,\pi^*)}$ excited states, called the "proximity effect".[33] The energy gap between the two states can be tuned by solvent polarity (affecting the energy of $S_{(n,\pi^*)}$) or increasing the conjugation (lowering $S_{(\pi,\pi^*)}$).

As bipyridine and phenanthroline have intense electronic transitions along the long axis,[34] Tor and coworkers hypothesized that increasing the conjugation along this axis would lead to emissive phenanthroline derivatives with useful photophysical properties and series of 3,8-bis(4-substituted-phenylethynyl)-phenanthrolines **127a** – **127d** were synthesized. [12] The parent bis-phenylethynyl phenanthroline **127a** exhibits similar (slightly red-shifted) absorption and emission transitions as phenanthroline but the quantum yield increases to 0.41. Additional electron-donating groups increase the

quantum yields and further red-shift the transitions (Table 3.1). Raising the solvent polarity has little influence on the absorption maxima of substituted phenanthrolines **127a** – **127d** but causes large red-shifts in their emission spectra whereas phenanthroline emission blue-shifts,[31] indicating the charge transfer nature of the strongly emissive π-π* state as compared to the weakly emissive n,π* state of phenanthroline. Furthermore, the ligands are responsive to both Zn(II) and protons, resulting in drastic red-shifts and quenched fluorescence.

Table 3.1 Photophysical properties of conjugated phenanthrolines **127a** – **127d** in acetonitrile.[12]

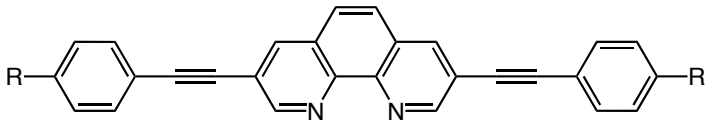

	R =	abs λ_{max} (nm)	em λ_{max} (nm)	Φ_f	τ (ns)
127a	H	342	375, 392	0.41	2.93
127b	Me	345	383, 396	1.0	1.50
127c	OCH_3	350	441	0.64	1.71
127d	$N(Me)_2$	402	587	§	§

§not determined

The importance of extending the conjugation in the long axis of phenanthroline and bipyridine is particularly evident in the work of Siegel and coworkers.[35-37] Systematic variation of 2,6-dimethylanisole (manisyl) α, β, and γ relative to the nitrogens in bipyridine and phenanthroline resulted in the phenanthrolines **97** – **100** and bipyridines **104** – **107** (Table 3.2).[36] It is readily apparent that substitution in the 3,8- and 5,5'-positions of phenanthroline and bipyridine, respectively, bestows extremely high quantum yields. The effect is more pronounced in bipyridine compared to phenanthroline and the minimal bipyridine chromophore is **104**. Further derivatives incorporating donating and accepting moieties in addition to solvatachromatic studies have revealed the intramolecular charge transfer (ICT) of the emissive state[37] and the

Siegel[38] and Kozhevnikov[39] labs are currently investigating symmetrical and unsymmetrical donor-accepter bipyridines.

Table 3.2 Photophysical properties of manisyl-phenanthrolines and bipyridines in acetonitrile.[35]

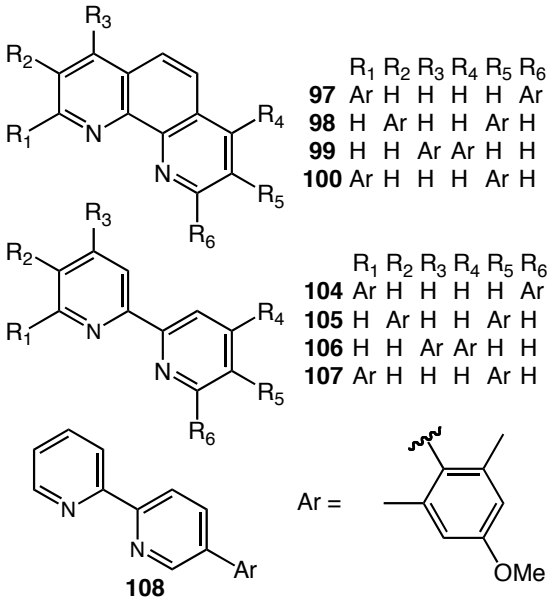

	abs λ_{max} (nm)	em λ_{max} (nm)	Φ_f
97	266	380	0.02
98	270	405	0.27
99	267	412	0.06
100	270	383	0.04
104	282	408	0.02
105	296	408	0.87
106	282	414	0.15
107	290	409	0.48
108	286	410	0.78

Although unaddressed, it interesting to note that the quantum yield of dissymmetrical bipyridine **107** is ~60% of **105** (or **108**). Furthermore, the quantum yield of 3,8-bis-manisyl phenanthroline **98** is significantly greater than dissymmetrical phenanthroline **100**, containing only one manisyl in the β-position. Phenanthroline ligands are rather exceptional in that the LUMO and LUMO+1 orbitals, called $b_1(\psi)$ and $a_2(\chi)$ to indicate their symmetry, are very close in energy (Figure 3.8).[40-42] In phenanthroline, the $a_2(\chi)$ orbital is lowest and is polarized along the short axis,[43] whereas $b_1(\psi)$ is slightly higher in energy and polarized along the long axis. It has been shown that alkyl substituents can invert the order of the orbitals[44] and it is possible a similar affect occurs in manisyl substituted phenanthrolines.

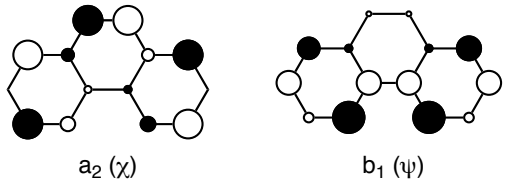

Figure 3.8 Unoccupied low-lying $b_1(\psi)$ and $a_2(\chi)$ orbitals of phenanthrolines.[40]

Whereas the photophysics of bipyridine[30,45] and phenanthroline[31,46] have been thoroughly investigated, there have only been a few reports of terpyridine ligand fluorescence[32,47,48] and even fewer systematic studies of terpyridine derivatives.[36,49,50] Sarkar and Chakravorti reported the first luminescence studies on the parent terpyridine **45** in 1994.[32] They reported that in acidic medium (Φ_f = 0.61 in 0.1 N H_2SO_4) the fluorescence quantum yield increases and the emission is red-shifted and ascribe the emission to a doubly protonated terpyridine.[51] The singly and triply protonated species were not detected. A covalent hydrate is invoked to explain the increased quantum yield in basic and neutral aqueous solution, similar to an anomalous emission in aqueous bipyridine and phenanthroline[46,52] that was later attributed trace residual Zn(II).[45]

Constable and coworkers reported the enhanced fluorescence of 4-(9-anthryl)-terpyridine **128** in 1998.[48] Titration of terpyridine and **128** methylene chloride solutions with trifluoroacetic acid causes significant changes (Table 3.3). The first protonation of terpyridine causes a red-shift in emission maximum and an slight increase in quantum yield, but the second protonation causes a blue-shift in the emission maximum and significantly raises the quantum yield. Upon the second protonation of **128** the fluorescence of displays a red-shift and is completely quenched. Mono-protonated **128H$^+$** was not detected. It is known that coordination of polypyridines to zinc(II) results in spectral changes similar to protonation.[53] The absorption and emission

spectra of **Zn(45)$_2^{2+}$** and **Zn(128)$_2^{2+}$** are similar to that of **45H$_2^{2+}$** and **128H$_2^{2+}$** and the solvatochromic nature of the emission from **Zn(128)$_2^{2+}$** indicates an intramolecular charge transfer (ICT) excited state.

Table 3.3 Photophysics of terpyridines **45** and **128** and in acetonitrile.[48]

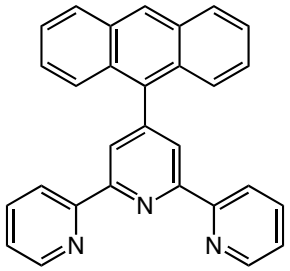

128

	abs λ_{max} (nm)	Φ_f	τ (ns)
45	338	0.003	
45H$^+$	410	0.17	3.0
45H^{2+}	360	0.71	2.7
Zn(45)$_2^{2+}$	353	0.65	
128	422	0.5	4.4
128H$^+$			
128H^{2+}	532	$<10^{-4}$	
Zn(128)$_2^{2+}$	575	0.04	3.8

In 2001, Araki and coworkers[50] noted that the emission intensity of the Ru(II) complex of 4-phenyl-terpyridine is enhanced relative to the parent Ru(II) terpyridine complex[54] and theorized that there would be similar enhancement of the parent ligand photophysics. A series of phenyl-substituted terpyridines was synthesized, **129** – **133**, and although the electronic transition energetics are similar, the quantum yields of 4-phenyl-terpyridine **130** and 6,6"-diphenyl-terpyridine **133** increase markedly (Table 3.4).

Electron donating and withdrawing substituents were introduced into the *para*-position of the phenyl group, **134** – **140**. The π-π^* transitions of **134** – **138** are similar to that of terpyridine **45**, however the amino- **139** and dimethylamino- terpyridine **140** absorptions are red-shifted 50-70 nm (Table 3.5). Similar trends were observed for the emission. The only exception is nitro-terpyridine **134**, which is non-emissive because of efficient n/π orbital coupling. The Stokes shift of **130** is independent of solvent polarity whereas terpyridine **139** and **140** showed considerable solvatochromic behavior, indicating an ICT process.

Semi-empirical molecular orbital calculations (MOPAC/AM1) performed on **130** showed that both the π- character HOMO and LUMO were localized exclusively on the terpyridine moiety and were denoted π_{terpy} and π^*_{terpy}. The second highest occupied molecular orbital (HOMO-1) state is localized on the phenyl moiety (π_{Ph}) and in the case of **140** (and **139**), the energy level of π_{Ph} is raised above π_{terpy} and the π-π* transition changes from a LE (π_{terpy},π^*_{terpy}) to a ICT transition (π_{Ph} and π^*_{terpy}). Subsequent work by Goodall and Williams showed that 4'-(4-*N*,*N*-diphenylamino)-terpyridine displays similar absorption and emission as 4'-(4-*N*,*N*-dimethylamino)-terpyridine **140** but is not quenched in protic solvents.[47]

Table 3.4 Photophysical properties of phenyl-substituted terpyridines in dichloromethane.[50]

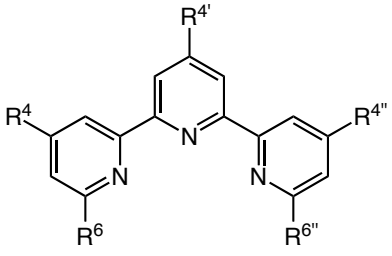

	R4	R6	R4'	R4'- R6"
45	H	H	H	H H
129	Ph	H	H	H H
130	H	H	Ph	H H
131	Ph	H	H	Ph H
132	H	Ph	H	H H
133	H	Ph	H	H Ph

	abs λ_{max} (nm)	em λ_{max} (nm)	Φ_f
45	280	337	0.02
129	262	344	0.02
130	278	340	0.33
131	301	342	0.05
131	278	341	0.07
133	306	344	0.16

Table 3.5 Photophysical properties of 4-substituted 4-phenylterpyridines in dichloromethane.[50]

	abs λ_{max} (nm)	em λ_{max} (nm)	Φ_f
134	283		
135	278	355	0.22
136	278	356	0.40
137	279	352	0.33
138	285	373	0.28
139	288	450	0.13
140	291	469	0.23

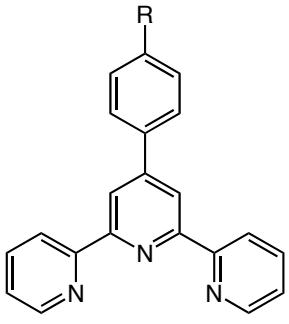

	R
134	NO_2
135	Br
136	Cl
137	CH_3
138	OCH_3
139	NH_2
140	NMe_2

2-Aminopyridine[55] and 6-amino-bipyridine[56] are known fluorophores and in their follow-up study, Araki and coworkers theorized that the addition of amino-functionalities onto the terpyridine core would also increase fluorescence.[49] Addition of amino groups to the 6- and 6"- positions, **141** and **142**, resulted in the appearance of a new absorption band (~320 nm) and the decrease of the band at 280 nm. Substitution in the 4'-position **143** had no affect on the absorption spectra. The emission data revealed that 6-aminoterpyridine **141** displays a strong blue fluorescence and that, in contrast, emission of 4-aminoterpyridine **143** resembles the parent terpyridine. Modulating the electron donating abilities of the amino group increases intersystem crossing and lowers the fluorescence quantum yield and comparison to *ortho*-amino-pyridines and bipyridines combined with MO calculations revealed that the minimal fluorescent chromophore was 6-amino-bipyridine. No explanation has been provided for the decrease in quantum efficiency resulting from the addition of a second amino group.

Table 3.6 Photophysical properties of amino-terpyridines in methylene chloride.[49]

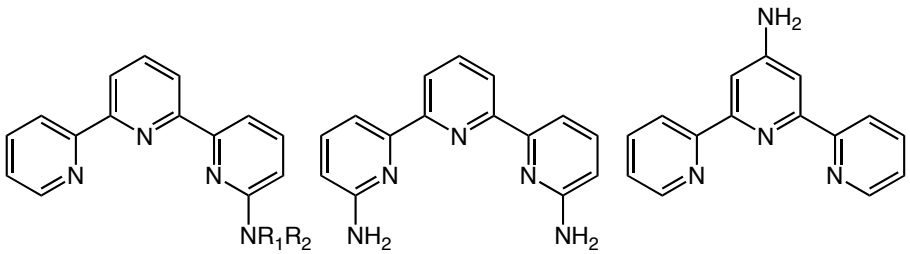

141 $R_1 = R_2 = H$ **142** **143**
144 $R_1 = R_2 = Me$
145 $R_1 = H$, $R_2 = COOEt$

	abs λ_{max} (nm)	em λ_{max} (nm)	Φ_f
141	284, 319	384	0.70
142	327	386	0.48
143	278	368	0.02
144	278, 354	427	0.57
145	289, 306	345	0.05

While investigating the photophysics of manisyl-substituted polypyridines, Loren et. al. reported that the addition of manisyl groups to terpyridines enhances quantum efficiency with specific regiochemistry.[36] Symmetrical di-substitution in positions β to the nitrogens, **102**, bestows extremely high quantum efficiency, whereas substitution in the α- or γ- positions gives manisyl-terpyridines, **101** and **103** respectively, with nearly identical emission maxima as **102** but with poor quantum efficiency (Table 3.7). The minimal fluorescent chromophore is again the substituted bipyridine **108** displaying a unique ICT emission that is currently under investigation.[37,57] Included in the photophysical study was manisyl-substituted 2-pyridyl-phenanthroline **110** as bridged terpyridine derivative. Compared to the parent terpyridine **102**, the addition of a single ethynylene bridge reduced the quantum yield by half.

Table 3.7 Photophysics of manisyl-substituted terpyridines in acetonitrile.[36]

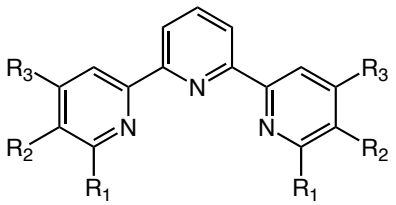

	R_1	R_2	R_3
101	Ar	H	H
102	H	Ar	H
103	H	H	Ar

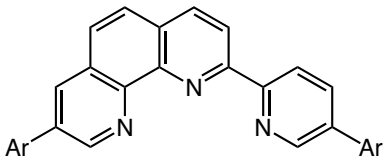

110

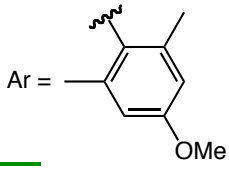

	abs λ_{max} (nm)	em λ_{max} (nm)	Φ_f
101	284	412	0.08
102	286	408	0.85
103	279	417	0.02
110	296	443	0.44

3.2 Current Work

3.2.1 Introduction

The importance of polypyridine ligands and their metal complexes cannot be overstated[1-3] The photophysical and electrochemical properties of polypyridyl metal complexes are well-suited to a variety of applications,[58,59] and are highly dependent on the nature of the ligand. A thorough understanding of the ligand photophysics is essential for the design of luminescent metal complexes and, ideally, the ability to tune the properties of a modular family of ligands to suit the purpose at hand is desired.[12]

Recent work by Loren et. al.[36] has shown that manisyl substituted bipyridines, phenanthrolines, and terpyridines can exhibit a highly emissive solvatochromic charge-transfer state and preliminary investigations of pyridyl-phenanthrolines revealed a similar high fluorescence dependent on solvent polarity. With a 3 × 3 pyridyl-phenanthroline matrix in hand, a systematic investigation of the structure fluorescence relationship and its solvatachromatism was undertaken.

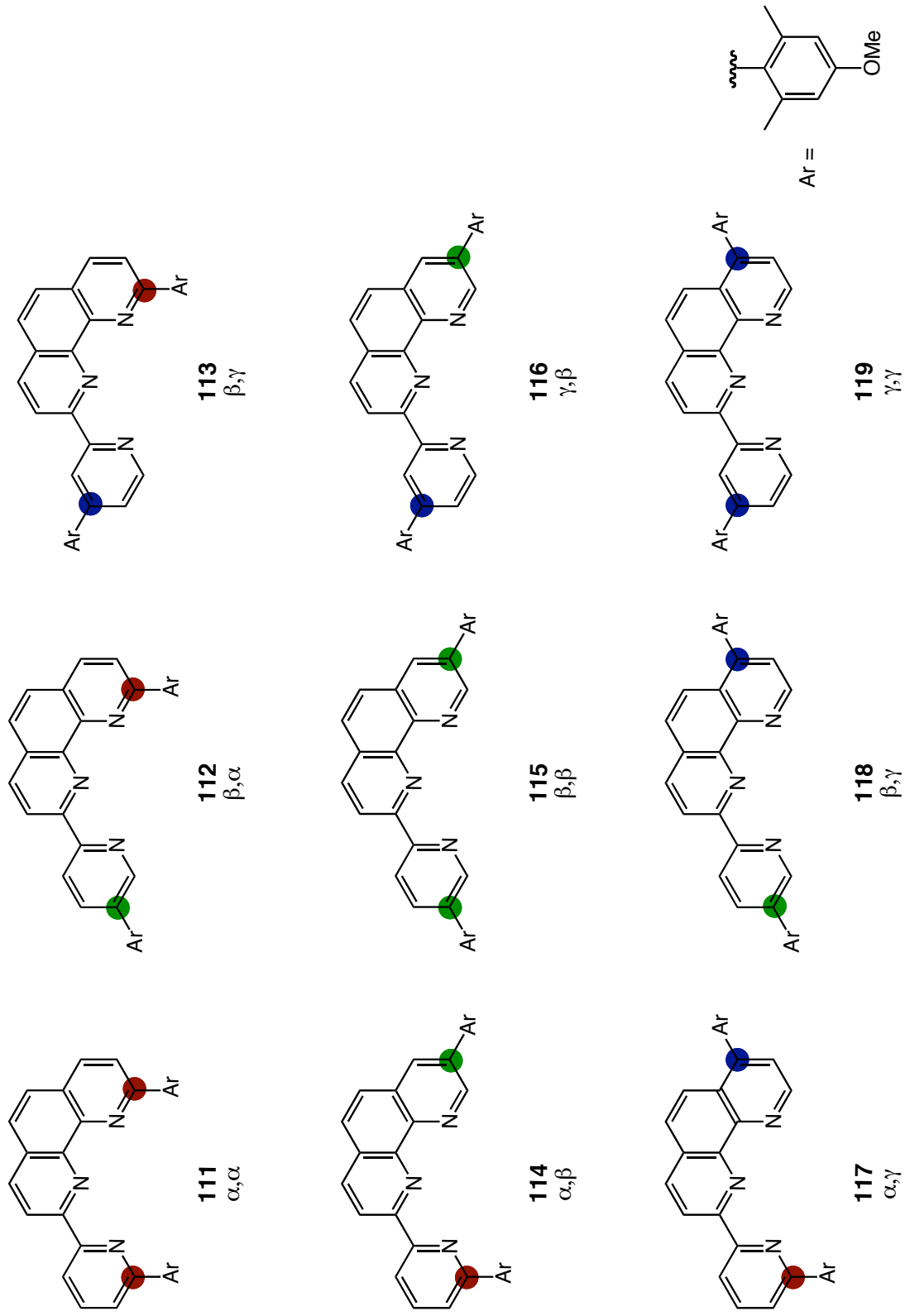

Figure 3.9 3 × 3 Pyridyl-phenanthroline matrix.

3.2.2 Results

Absorption. The room temperature absorption spectra of pyridyl-phenanthrolines **111** – **119** in ethanol (EtOH), acetonitrile (ACN), methylene chloride (CH_2Cl_2), diethyl ether (Et_2O), and cyclohexane (CH) are shown in Figure 3.6. The spectra are remarkably similar in shape and energy, and display one or two intense bands around 290 nm and a weak band at 350 nm. Examination of the 3 × 3 pyridyl-phenanthroline grid (Figure 3.6) reveals that the band shape depends on the position of the manisyl group relative to the phenanthroline nitrogen, but not the pyridyl nitrogen.

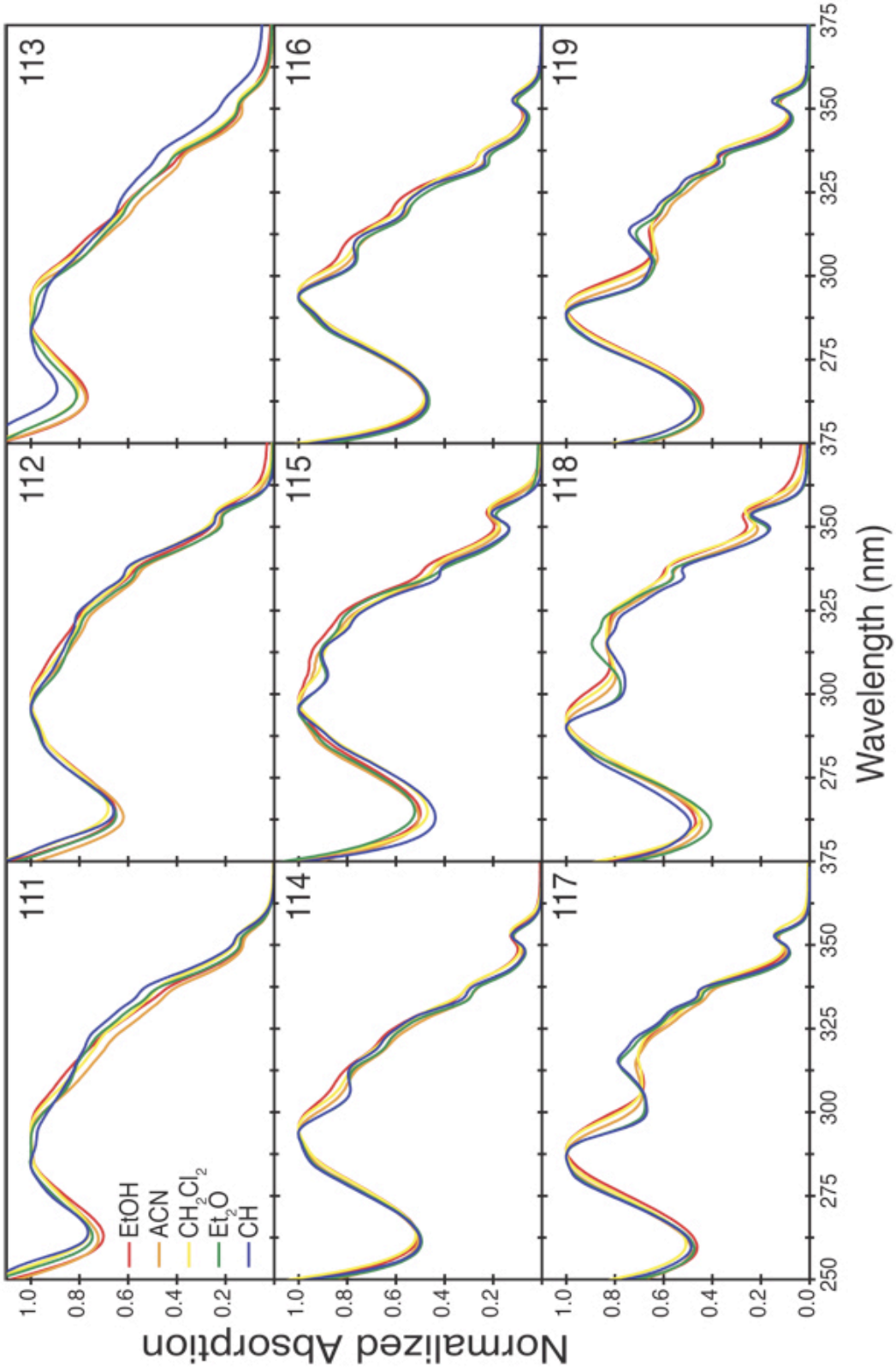

Figure 3.10 Absorption spectra of manisyl-substituted pyridyl-phenanthrolines **111** – **119** in ethanol (red), acetonitrile (orange), methylene chloride (yellow), diethyl ether (green), and cyclohexane (blue) at room temperature.

According to their structure and absorptive behavior, pyridyl-phenanthrolines can be divided into the following three classes: (i) 9-manisyl-(manisyl-pyrid-2-yl)-phenanthrolines (α-phen) **111** – **113**; (ii) 8-manisyl-(manisyl-pyrid-2-yl)-phenanthrolines (β-phen) **114** – **116**; (iii) 7-manisyl-(manisyl-pyrid-2-yl)-phenanthrolines (γ-phen) **117** – **119**.

α-Phens **111** – **113** are distinguished by a strong, broad absorption (ε ~33,000 for **111** and **112** but 15,000 for **113**) at ~290 nm (Table 3.8a). In non-polar solvents, i.e., cyclohexane or diethyl ether, weak vibrational structures are apparent ($\Delta\nu$ ~ 1300 cm^{-1}). In polar solvents, ethanol or acetonitrile, the vibrational features are muted as the spectra broaden and undergo a very slight red shift (~500 – 1000 cm^{-1}). Weak (ε ~5,000) transitions at 350 nm appear as a pre-band shoulder due to overlap.

Table 3.8a Absorption data for pyridyl-phenanthrolines **111** – **113**.

	Solvent	λ_{max} nm	ε_{max}	λ_{max} (nm)	ε_{max}
111	EtOH	293	32600	351	4300
111	CH_3CN	293	31800	351	4000
111	CH_2Cl_2	294	32600	352	5100
111	Et_2O	285	31800	352	4300
111	CH	284	26000	352	4100
112	EtOH	299	32400	353	7800
112	CH_3CN	296	33300	354	7000
112	CH_2Cl_2	298	33200	354	8100
112	Et_2O	295	35100	353	7500
112	CH	296	31900	353	7700
113	EtOH	287	16300	352	2300
113	CH_3CN	291	14900	352	1900
113	CH_2Cl_2	286	19000	352	2800
113	Et_2O	284	16200	351	2400
113	CH	283	10900	351	2400

(ii) The absorption spectra of β-phens **114 – 116** also display an intense (ε ~40,000), structured transition at ~295 nm. In cyclohexane and diethyl ether, a second band at ~310 nm appears. Further vibrational features are present in non-polar and polar solvents ($\Delta\nu$ ~ 1300 cm^{-1}). The lowest energy transitions at 353 nm are clearly resolved and no longer overlapped by the broad higher energy bands. The position and intensity of the absorption maxima are virtually independent of solvent polarity (Table 3.8b), and significant broadening occurs in polar solvents.

Table 3.8b Absorption data for pyridyl-phenanthrolines **114 – 116**.

	Solvent	λ_{max} (nm)	ε_{max}	λ_{max} (nm)	ε_{max}	λ_{max} (nm)	ε_{max}
114	EtOH	295	31200			353	4000
114	CH_3CN	294	45800	310	36115	353	5300
114	CH_2Cl_2	295	39400	310	36115	354	5100
114	Et_2O	294	44400	312	34778	353	5200
114	CH	293	20300	312	16117	353	2500
115	EtOH	298	37800	313	35663	354	8500
115	CH_3CN	297	39200	311	36240	354	8500
115	CH_2Cl_2	298	42100		37573	355	9200
115	Et_2O	295	44400	313	40389	354	8300
115	CH	296	37700	313	33950	353	7800
116	EtOH	295	38100	309	31005	353	4300
116	CH_3CN	294	38600	308	29346	353	4000
116	CH_2Cl_2	295	38600	309	29846	353	4300
116	Et_2O	293	39500	309	29765	352	4000
116	CH	294	37500	309	28974	353	4000

(iii) The absorption spectra of γ-phens **117** – **119** display two intense (ε ~30,000 – 40,000 and 20,000 – 30,000) transitions at ~290 nm and ~315 nm. The higher energy transitions are broad and unstructured and undergo a slight red-shift as solvent polarity increases (Table 3.8c). The lower energy transitions are more structured and show vibrational structure ($\Delta\nu$ ~500 – 1000 cm^{-1}). The position and intensity of the second absorption maxima are independent of solvent polarity (Table 3.8c), and significant broadening occurs in polar solvents. The lowest energy transitions at ~352 nm are clearly resolved.

Table 3.8c Absorption data for pyridyl-phenanthrolines **117** – **119**.

	Solvent	λ_{max} (nm)	ε_{max}	λ_{max} (nm)	ε_{max}	λ_{max} (nm)	ε_{max}
117	EtOH	289	36300	316	25600	352	4400
117	CH_3CN	287	36700	314	26300	352	4700
117	CH_2Cl_2	288	33600	317	23700	352	4800
117	Et_2O	287	35400	315	27600	353	4800
117	CH	287	33700	315	26600	352	4900
118	EtOH	293	18100	316	15000	353	4900
118	CH_3CN	291	29700	315	24900	353	4900
118	CH_2Cl_2	293	26400	319	22000	353	7500
118	Et_2O	290	30900	315	27600	355	6900
118	CH	290	22900	315	19000	353	7500
119	EtOH	291	36900	313	24400	354	5400
119	CH_3CN	288	37900	312	24500	352	4500
119	CH_2Cl_2	290	36500	315	23800	352	4800
119	Et_2O	288	38200	313	27200	353	5100
119	CH	288	31100	313	23000	352	5100

Taken as a whole, the absorptive properties of manisyl-substituted pyridyl-phenanthrolines are very similar, given the significant changes in structure. On the one hand, this is intuitive as the phenanthroline moiety is the largest intact chromophore present, and dominates the energetic transitions. The steric interactions of the 2,6-methyl groups hold the manisyl substituents orthogonal to the phenanthroline and pyridine planes, effectively destroying conjugation. Thus, variation of the point of

attachment should have no significant effect on the HOMO – LUMO energy gap. However, manisyl position influences the intensity and vibrational structure of absorption bands.

As a result of the similarity in the semi-autonomous chromophores, the absorptive electronic transitions are complex and a quantitative interpretation is difficult without deconvolution. Nevertheless, several qualitative conclusions can be drawn from the available data. Pyridyl-phenanthrolines possess three main absorptive transitions. The first transition at ~290 nm, similar to that of aryl-substituted phenanthrolines,[12,60,61] is strongly allowed, independent of manisyl position, and shows a slight red-shift with increasing solvent polarity (Figure 3.11) and can be assigned to a π – π* transition in the pyridyl-phenanthroline chromophore.

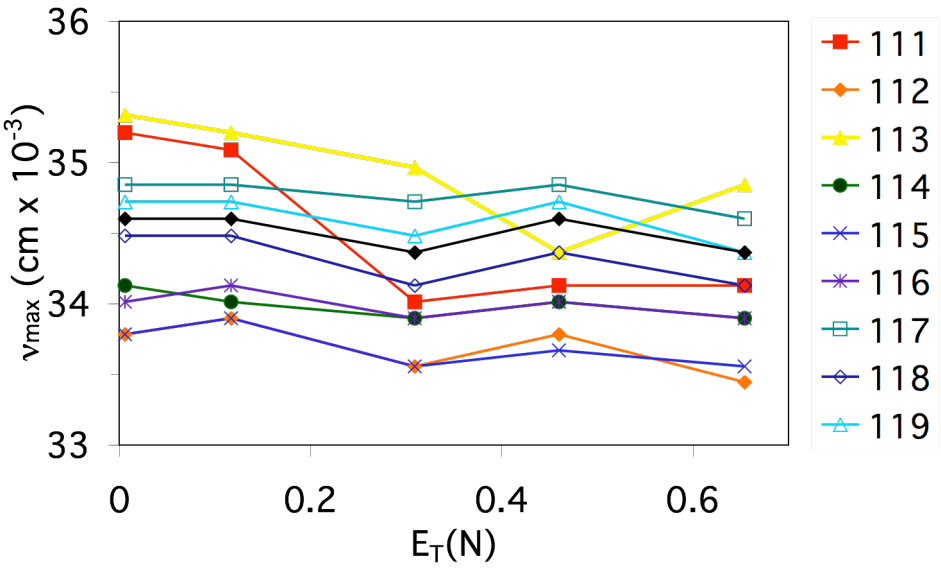

Figure 3.11 Solvent dependence of the absorption maxima for the first transition.

The second transition, at ~310 is also strongly allowed and nearly independent of solvent polarity but is sensitive to the position of the manisyl substituents on the

phenanthroline core. This transition is broad and unresolved for α-phen compounds, but is partially resolved for β- and γ-phens. Due to the intensity and solvent independence, this transition can be also assigned to an allowed π – π* transition. The third distinct transition, at ~350 cm^{-1}, is weak and practically unaffected by solvent polarity. Significant overlapping obscures this band in α-phens but the band is resolved as it moves to consecutively longer wavelengths in β- and γ-phens. Based on the absence of solvent sensitivity and significantly lower intensity, this band can be assigned to a partially allowed π – π* transition.[62]

Emission. The room temperature emission spectra of pyridyl-phenanthrolines **111 – 119** in ethanol, acetonitrile, methylene chloride, diethyl ether, and cyclohexane are shown in Figure 3.12. Degassing the dilute solutions with nitrogen has no appreciable effect on the emissive properties and all spectra were then collected by excitation at the λ_{max} (~290 nm) in the presence of molecular oxygen. Pyridyl-phenanthrolines exhibit a dual fluorescence that depends on solvent polarity and manisyl position. In non-polar solvents, i.e., cyclohexane and ether, the dominant emission is structured, short-lived, and weakly emissive (Table 3.9). With maxima at ~360, 380, and 400 nm, the emission can be directly superimposed upon the emission of phenanthroline, and can be assigned to the lowest singlet $^1\pi\pi^*$ state of the phenanthroline core. For simplicity, this will be called the locally excited (LE*) state.[31,52,60] In polar solvents, i.e., ethanol and acetonitrile, the dominant emission is broad, unstructured, longer lived, and strongly emissive (Table 3.9). These features are highly indicative of a intramolecular charge transfer (ICT) state and will be referred to as the CT* state.[13,20,63]

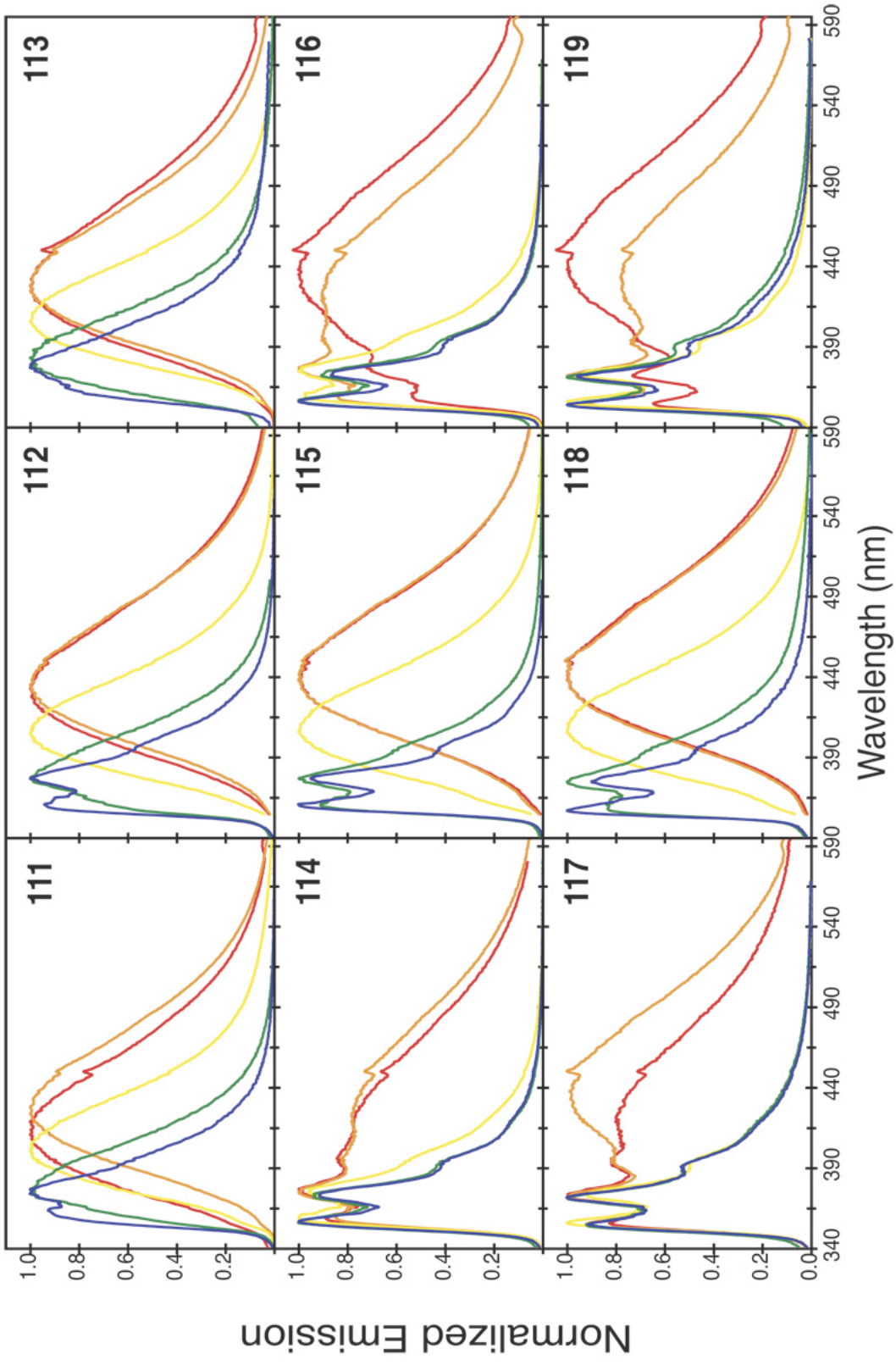

Figure 3.12 Emission spectra of manisyl-substituted pyridyl-phenanthrolines **111** – **119** in ethanol (red), acetonitrile (orange), methylene chloride (yellow), diethyl ether (green), and cyclohexane (blue) at room temperature.

Table 3.9 Emission data for pyridyl-phenanthrolines **111** – **119**.

Ligand	Solvent	λ_{max} (nm)	Φ_f
111	EtOH	411	0.047
111	CH_3CN	424	0.175
111	CH_2Cl_2	401	0.095
111	Et_2O	377	0.0096
111	CH	364, 374*	0.0052
112	EtOH	433	0.188
112	CH_3CN	435	0.408
112	CH_2Cl_2	405	0.257
112	Et_2O	377	0.019
112	CH	360, 377*	0.012
113	EtOH	428	0.083
113	CH_3CN	428	0.083
113	CH_2Cl_2	406	0.089
113	Et_2O	383	0.0082
113	CH	377	0.0078
114	EtOH	359, 377*, 396, 417	0.029
114	CH_3CN	360, 375*, 395, 422	0.07
114	CH_2Cl_2	359*, 376, 394sh	0.08
114	Et_2O	357*, 372, 392sh	0.012
114	CH	356*, 373, 393sh	0.012
115	EtOH	438	0.509
115	CH_3CN	438	0.623
115	CH_2Cl_2	406	0.454
115	Et_2O	360, 377*, 394sh	0.054
115	CH	361*, 377, 395sh	0.022
116	EtOH	360, 377, 435*	0.094
116	CH_3CN	359, 375*, 396, 438	0.07
116	CH_2Cl_2	356, 375*, 394sh	0.072
116	Et_2O	357*, 373, 392sh	0.012
116	CH	356*, 373, 392sh	0.012
117	EtOH	356, 372*, 394, 435	0.022
117	CH_3CN	355, 372*, 394, 423	0.026
117	CH_2Cl_2	356*, 373, 393	0.043
117	Et_2O	357, 372*, 391	0.007
117	CH	356, 372*, 391	0.007
118	EtOH	438	0.356
118	CH_3CN	443	0.607
118	CH_2Cl_2	406	0.48
118	Et_2O	360, 375*, 393sh	0.034
118	CH	357*, 375, 393sh	0.015
119	EtOH	355, 372, 438*	0.054
119	CH_3CN	354, 372*, 393, 430	0.038
119	CH_2Cl_2	356*, 372, 390,	0.034
119	Et_2O	354, 371*, 389	0.009
119	CH	354*, 372, 390	0.007

*Absolute maximum

Examination of the emission spectra grid (Figure 3.12) and fluorescence quantum yields (Figure 3.13) reveals the delicate interplay of structure and emissive states. Pyridyl-phenanthrolines with manisyl groups in the beta position relative to the *pyridyl* nitrogen (β-pyr), **112**, **115**, and **118**, show a highly emissive, "pure" CT* state in polar solvents, as indicated by the high quantum yields (Φ_f = 0.20 – 0.60) and broad band shape. In non-polar solvents, the CT* state disappears and the LE* state becomes more prevalent and is comparable to the other pyridyl-phenanthrolines (Figure 3.12). Pyridyl-phenanthrolines with manisyl groups in the alpha-position on the *phenanthroline* core (α-phen) also display "pure" CT* emissions in polar solvents but are not as emissive. In non-polar solvents, the LE* state is broadened and featureless. The remaining four pyridyl-phenanthrolines, exhibit dual emission in polar solvents, dominated by the weakly emissive LE* state and fully switch to LE* emission in non-polar solvents.

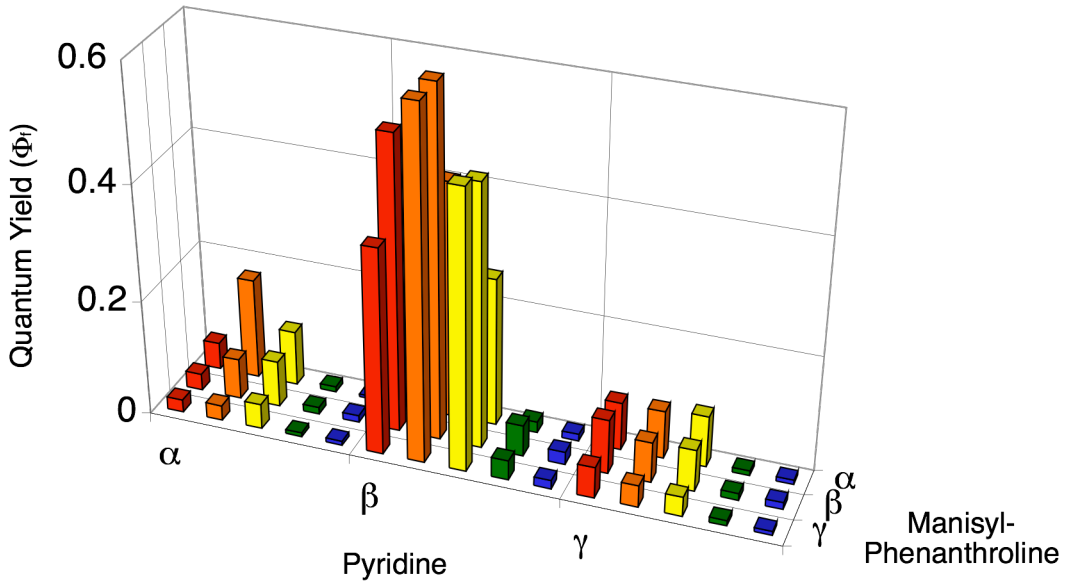

Figure 3.13 Fluorescent quantum yields and their dependence on manisyl position; alpha-, beta- and gamma- relative to the phenanthroline or pyridine nitrogens; and solvent; ethanol (red), acetonitrile (orange), methylene chloride (yellow), diethyl-ether (green), and cyclohexane (blue).

Solvent polarity has only a minor influence on the absorptive properties of pyridyl-phenanthrolines, but the emission behavior is highly solvatachromatic. The fluorescence quantum yields increase with increasing solvent polarity (Figure 3.14). The quantum yields of **111**, **112**, **115**, and **118** show the largest increase with increasing solvent polarity, indicating a highly polar emissive state, but decrease in ethanol, most likely due to protic solvent-solute interactions.[62]

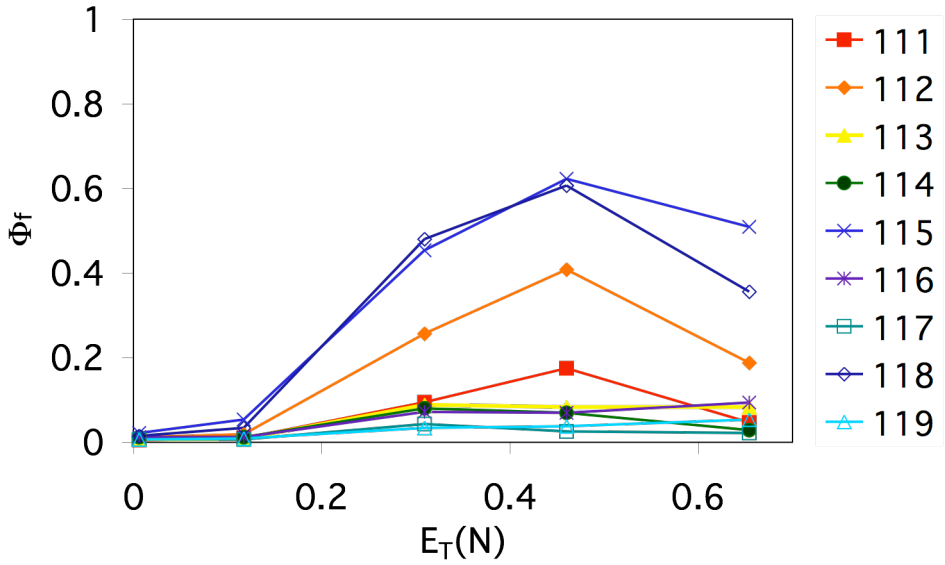

Figure 3.14 Dependence of fluorescence quantum yield on solvent polarity.

The highest energy transition in an emission spectrum corresponds to the 0,0 transition (Figure 3.4). Plotting the energy of the 0,0 transitions, in wave numbers, against Reichardt's $E_T(N)$ normalized solvent polarity scale[6426,65] reveals the energy differences of the LE* and CT* states, relative to the ground state (Figure 3.15). The 0,0 transition of pyridyl-phenanthrolines **114**, **116**, **118**, and **119** originates from the LE* state, substantiated by the small Stokes shift, and is independent of solvent polarity. Emission from the phenanthroline $^1\pi,\pi^*$ state shifts to shorter wavelength with increasing solvent polarity[31] and is attributed to the close proximity of the non-emissive

^{1}n,π* state. The fact that the LE* emission of pyridyl-phenanthrolines is independent of solvent polarity suggests that the emitting state is a non-polar ^{1}π,π* state.[66] The 0,0 transitions of pyridyl-phenanthrolines exhibiting CT* emission are solvent-sensitive and shift to lower wavelengths with increasing solvent polarity. The red-shift to lower energies is indicative of a polarized emitting state stabilized by increasing solvent polarity, and typical of excited states with enlarged dipoles and charge-transfer character.[20] The solvent-induced stabilization of the CT* state levels off at acetonitrile and increased solvent polarity incurs no further charge-separation or stabilization. The transition from the non-polar LE* to the polar CT* state depends on the location of manisyl group on the phenanthroline core. The LE* state of β-pyrs **115** and **118** dominates in both cyclohexane and ether and is insensitive to solvent polarity. In methylene chloride, the CT* state becomes the emissive state and is further stabilized in acetonitrile and ethanol. On the contrary, the LE* state of α-phens **111** – **113** is sensitive to solvent polarity and shows a smooth transition from the LE* to CT* emitting states. The solvent sensitivity and broadened emission structure of α-phens suggests there is significant mixing of the LE* and CT* states when the manisyl group is placed alpha to the phenanthroline nitrogen.

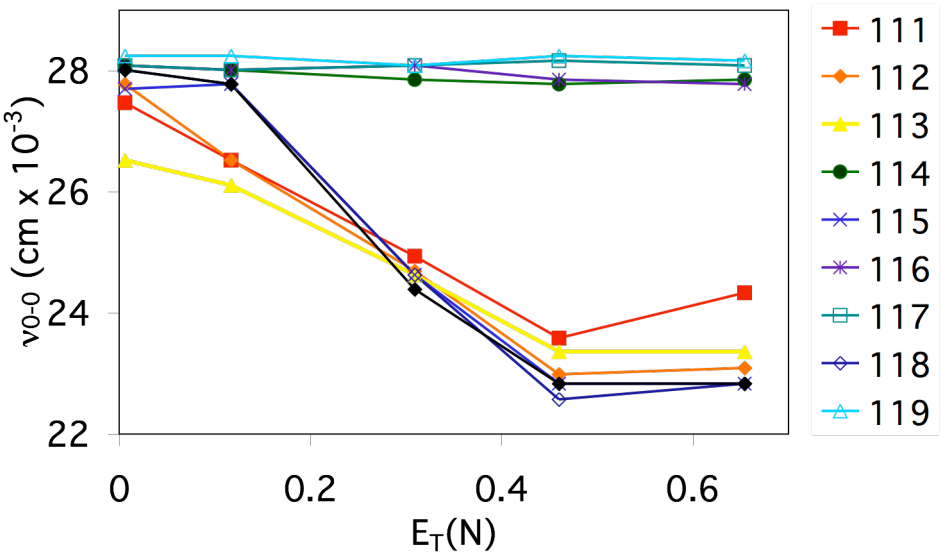

Figure 3.15 Plot of emission energy (in wave numbers, $cm^{-1} \times 10^{-3}$) against solvent $E_T(N)$ values.

The solvent and substituent induced switching from a LE* to CT* emissive state is supported by the excitation spectra (Figure 3.16). The shape and intensities of the excitation spectra recorded at the emission λ_{max} are independent of emission wavelength. The excitation spectra of β-pyrs **112**, **115**, and **118** show an increased intensity for the partially allowed absorptive transitions at ~350 nm, indicating that these are the key absorptive transitions for accessing the CT* emissive state. Pyridyl-phenanthrolines exhibiting predominately LE* emission (**114**, **116**, **117**, and **119**), show an excitation maxima at 380 nm. The solvent independent excitation maxima of phenanthroline is 261 nm[46] and supports the assignment of the pyridyl-phenanthroline LE* state to the $^1\pi,\pi^*$ state of phenanthroline. The excitation spectra of the remaining α-phens supports mixed LE* and CT* emitting states. The excitation maxima of **111** is ~350 nm, even in the non-polar cyclohexane and diethyl-ether, whereas the maxima of **113** switches to ~290 nm in cyclohexane. The excitation maxima of **111** and **113** switch to 290 nm in ethanol, but the emission spectra remains purely CT* in nature.

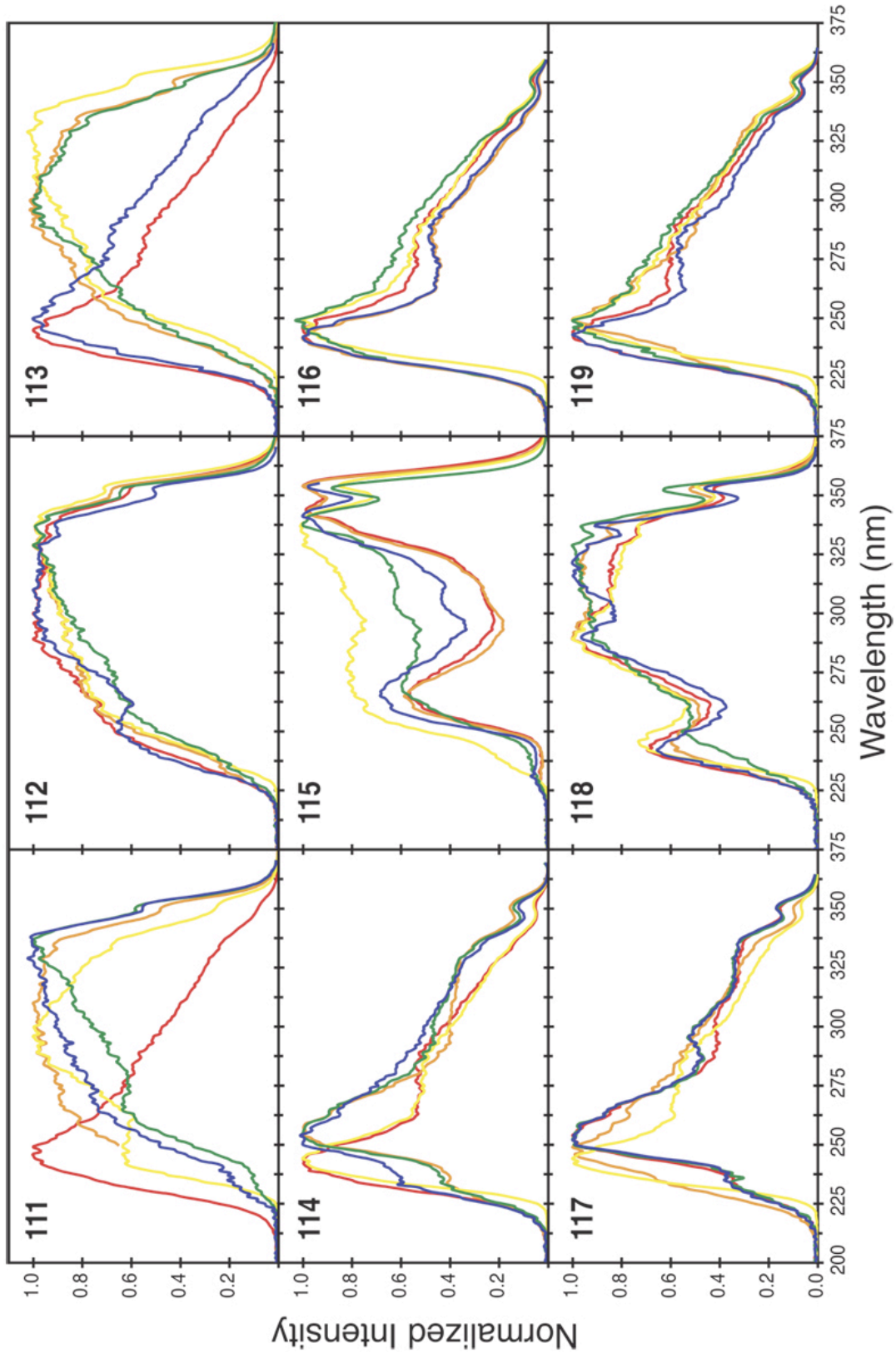

Figure 3.16 Excitation spectra of manisyl-substituted pyridyl-phenanthrolines **111** – **119** in ethanol (red), acetonitrile (orange), methylene chloride (yellow), diethyl ether (green), and cyclohexane (blue) at room temperature.

The emission decays and lifetimes of phenanthroline derivatives are often non-trivial.[61,67] Pyridyl-phenanthrolines also display complex fluorescence decays that do not fit single exponential fits but require biexponential fits (Table 3.10). Although calculation of radiative rate constants from a nonexponential decay is impossibly complex, using the mean fluorescence lifetime $\langle\tau\rangle$ allows one to derive approximate rates that are quite informative. The influence of solvent on the lifetime is clarified when the mean fluorescence lifetimes and single exponential lifetimes are plotted against the solvent polarity (Figure 3.17). In non-polar solvents, cyclohexane and diethyl ether, where the LE* state is the dominant state, the lifetimes are less than one nanosecond and comparable to those of phenanthroline (τ < 1.0 ns in cyclohexane).[31] As the solvent polarity is increased, most lifetimes reach their maximum length in acetonitrile before shortening in ethanol. Protic solvents, like ethanol, are known to induce fluorescence quenching through non-radiative pathways via hydrogen bonding.[20] When compared to the lifetime of phenanthroline in polar solvents (τ = 2.10 ns in ethanol), only the lifetimes of **115** and **118** stand out. Both contain manisyl groups beta to the pyridyl nitrogen (β-pyr) and access the emissive CT* state to the greatest extent as evidenced by the large fluorescent quantum yields. This trend is repeated when the approximate radiative rates are plotted against solvent polarity (Figure 3.17). The radiative rates of all three β-pyr **112**, **115**, and **118** are enhanced relative to the other pyridyl-phenanthrolines and reach a maximum in methylene chloride.

Table 3.10 Experimental lifetimes and radiative rates of pyridyl-phenanthrolines.[a]

Ligand	Solvent	τ_1 ns (%)	τ_2 ns (%)	$\langle\tau\rangle^b$ ns	k_f (ns^{-1})^b	k_{nr}(ns^{-1})^b	χ^2
111	EtOH	0.52 (0.95)	2.09 (0.05)	0.54	0.09	1.76	0.603
111	CH_3CN	1.82			0.10	0.45	0.809
111	CH_2Cl_2	0.71			0.13	1.27	0.979
111	Et_2O	0.35 (0.94)	2.24 (0.06)	0.36	0.03	2.73	0.653
111	CH	0.57	4.08 (0.05)	0.60	0.01	1.67	0.817
112	EtOH	1.68			0.11	0.48	0.437
112	CH_3CN	2.34			0.17	0.25	0.496
112	CH_2Cl_2	0.60 (0.6)	1.22 (0.40)	0.75	0.34	0.99	0.393
112	Et_2O	0.36 (0.9)	2.13 (0.10)	0.39	0.05	2.50	0.522
112	CH	0.46			0.03	2.15	0.545
113	EtOH	1.37 (0.95)	4.26 (0.05)	1.42	0.06	0.65	0.697
113	CH_3CN	1.75 (0.89)	9.17 (0.11)	1.92	0.04	0.48	1.140
113	CH_2Cl_2	0.66 (0.90)	5.64 (0.10)	0.72	0.12	1.26	0.870
113	Et_2O	0.58 (0.85)	4.12 (0.15)	0.66	0.01	1.49	0.940
113	CH	0.35 (0.91)	1.66 (0.09)	0.38	0.02	2.60	1.089
114	EtOH	0.54			0.05	1.80	0.430
114	CH_3CN	2.32			0.03	0.40	0.845
114	CH_2Cl_2	0.65 (0.85)	1.20 (0.15)	0.70	0.11	1.32	0.474
114	Et_2O	0.27 (0.93)	1.65 (0.07)	0.29	0.04	3.45	0.777
114	CH	0.29	1.55 (0.07)	0.31	0.04	3.21	0.951
115	EtOH	3.38			0.15	0.15	0.589
115	CH_3CN	2.84			0.22	0.13	0.738
115	CH_2Cl_2	1.62			0.28	0.34	0.692
115	Et_2O	0.73 (0.93)	3.13 (0.07)	0.77	0.07	1.23	0.931
115	CH	0.35 (0.91)	1.66 (0.09)	0.37	0.06	2.63	1.089
116	EtOH	0.67 (0.59)	3.82 (0.41)	1.01	0.09	0.90	0.430
116	CH_3CN	1.41 (0.14)	2.45 (0.86)	2.22	0.03	0.42	0.413
116	CH_2Cl_2	0.79 (0.99)	3.41 (0.01)	0.80	0.09	1.17	0.673
116	Et_2O	0.28 (0.92)	2.10 (0.08)	0.30	0.04	3.28	0.773
116	CH	0.29 (0.94)	1.56 (0.06)	0.30	0.04	3.24	0.385
117	EtOH	0.44 (0.87)	1.30 (0.13)	0.48	0.05	2.05	0.594
117	CH_3CN	2.00			0.01	0.49	0.725
117	CH_2Cl_2	0.51 (0.96)	2.23 (0.04)	0.53	0.08	1.82	0.802
117	Et_2O	0.27 (0.92)	2.02 (0.08)	0.29	0.02	3.42	0.829
117	CH	0.26 (0.94)	1.52 (0.06)	0.27	0.03	3.63	0.723
118	EtOH	3.02			0.12	0.21	0.487
118	CH_3CN	2.81			0.22	0.14	1.199
118	CH_2Cl_2	1.29			0.37	0.40	0.340
118	Et_2O	0.84 (0.95)	2.96 (0.05)	0.87	0.04	1.11	1.261
118	CH	0.87 (0.92)	2.41 (0.08)	0.92	0.02	1.07	0.854
119	EtOH	0.52 (0.62)	4.18 (0.38)	0.78	0.07	1.21	0.474
119	CH_3CN	0.64 (0.46)	2.02 (0.54)	1.01	0.04	0.95	0.385
119	CH_2Cl_2	0.39 (0.94)	1.79 (0.06)	0.41	0.08	2.36	0.814
119	Et_2O	0.26 (0.86)	2.23 (0.14)	0.30	0.03	3.34	0.792
119	CH	0.29 (0.95)	1.98 (0.05)	0.30	0.02	3.28	0.855

[a] excitation at 295 nm and recorded at λ_{max}

[b] $\langle\tau\rangle$, k_f, and k_{nr} are weighted means from the biexponential fits: $\langle\tau\rangle = 1/(\%_{\tau 1}/\tau_1 + \%_{\tau 2}/\tau_2)$, $k_f = \phi_f/\langle\tau\rangle$, and $k_{nr} = (1-\phi_f)/\langle\tau\rangle$.[68]

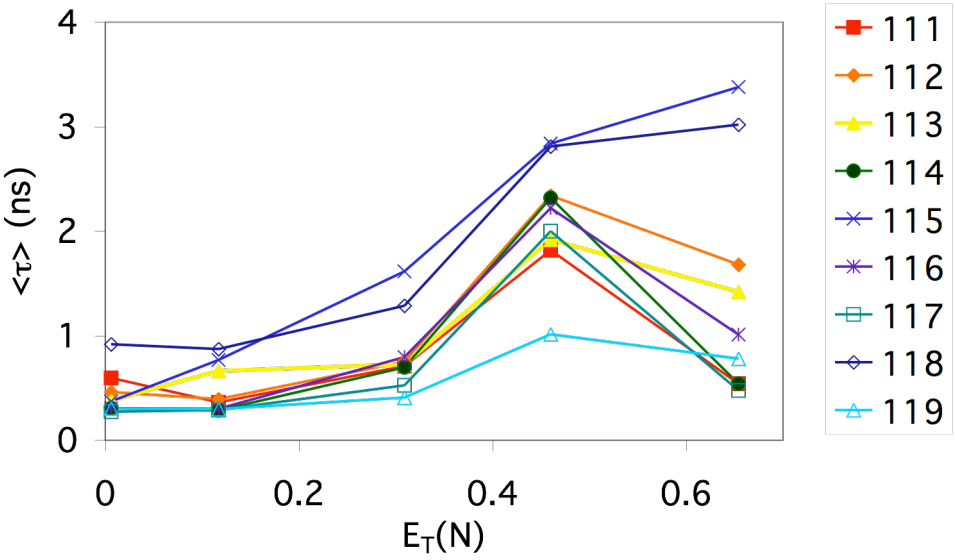

Figure 3.17 Plot of mean fluorescence lifetimes against solvent polarity $E_T(N)$ values.

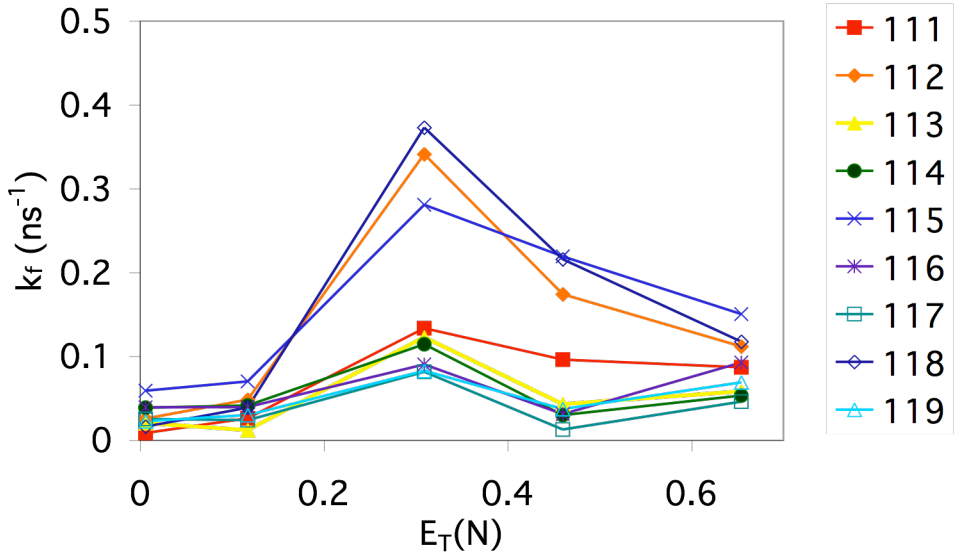

Figure 3.18 Plot of radiative rate constants k_f against solvent polarity $E_T(N)$ values.

When biexponential fluorescence kinetics are present, the value of τ_1 and τ_2 remained consistent, but the relative contribution of the two lifetimes varies according to the observed wavelength. Lifetime data were collected at each emission maxima for pyridyl-phenanthroline **116**[69] in each solvent displaying biexponential decays (Table

3.11). In ethanol, for example, the relative contribution of the longer lifetime (arbitrarily designated τ_2) increases from 41% to 72% as the observed wavelength increases (Figure 3.19). The shorter lifetime, τ_1, lengthens with increasing polarity as does the lifetime of the $^1\pi,\pi^*$ state of phenanthroline.

Table 3.11 Fluorescence lifetime dependence on wavelength of **116**.

EtOH	τ_1	τ_2	τ_1(%)	τ_2(%)	χ^2
360 nm	0.67 ns	3.82 ns	0.59	0.41	0.43
377 nm	0.78 ns	3.87 ns	0.38	0.62	0.45
390 nm	0.97 ns	3.93 ns	0.35	0.65	0.429
430 nm	1.12 ns	3.96 ns	0.28	0.72	0.532
ACN					
377 nm	1.12 ns	2.52 ns	0.13	0.87	0.413
430 nm	1.41 ns	2.45 ns	14	86	0.436
Et_2O					
355 nm	0.25 ns	1.89 ns	0.91	0.09	0.868
375 nm	0.28 ns	2.10 ns	0.92	0.08	0.773
390 nm	0.29 ns	2.37 ns	0.89	0.11	0.814

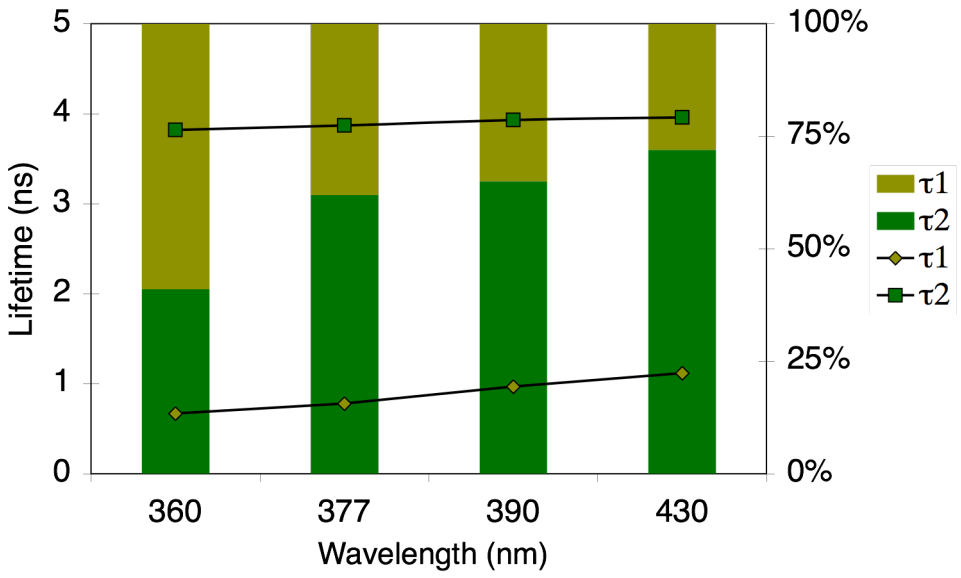

Figure 3.19 Fluorescence lifetime dependence on wavelength of **116** in ethanol: τ_1 (green squares); t_2 (brown diamonds).

MO Calculations. The geometries of phenanthroline **126**, terpyridine **45**, and pyridyl-phenanthroline **46** were optimized using B3LYP/DZV(d,p)[70] and the frontier orbitals optimized at the Moller-Plesset (MP2)[71] level of theory using the DZV(d,p) basis set and correlate well with previous work by McMillin.[72] Pyridyl-phenanthroline has the lowest energy LUMO and the highest energy HOMO resulting in the smallest HOMO-LUMO gap of the three ligands (Figure 3.20). Comparison of the frontier orbital diagrams emphasizes that pyridyl-phenanthroline **46** resembles a pyridyl substituted phenanthroline rather than a bridged terpyridine.

The impact of substituents depends on the orbital amplitude at the point of substitution[54] and in this regard, pyridyl-phenanthroline behaves as a hybrid (Figure 3.21). The phenanthroline portion of **46** has nodes in the beta position (relative to the phenanthroline nitrogens), whereas the pyridyl fragment has nodes in the alpha- and beta-positions. Importantly, the HOMO and LUMO of **46** has appreciable orbital density on the central nitrogen atom where **45** does not. This will result in different photophysical properties of their transition metal complexes as the strength of metal-ligand charge-transfer (MLCT) absorption depends on the orbital density of the nitrogen atoms in polypyridines.[73,74]

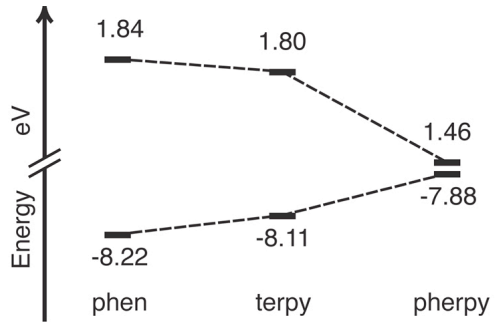

Figure 3.20 Calculated energies for the frontier orbitals of 1,10-phenanthroline (phen) **126,** terpyridine (terpy) **45**, and 2-pyridyl-phenanthroline (pherpy) **46**. The LUMO orbitals have positive energies while the energies are negative for the HOMO orbitals.

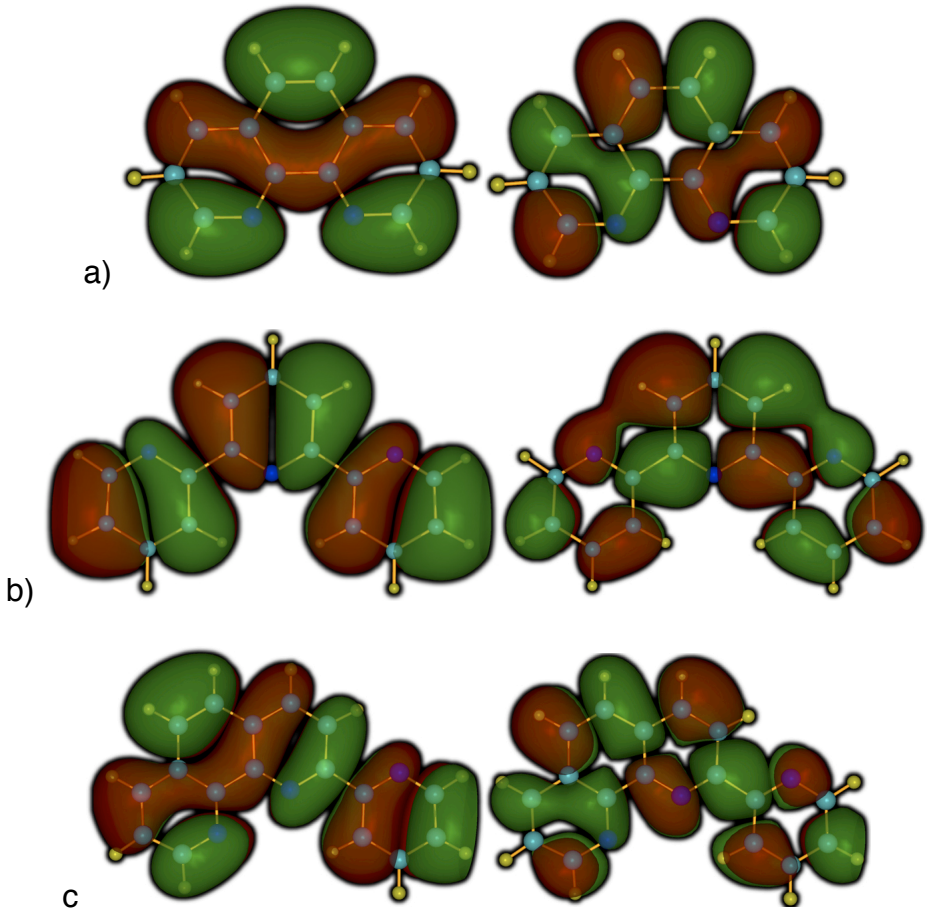

Figure 3.21 HOMO and LUMO MO diagrams of a)phenanthroline; b) terpyridine; and c) pyridyl-phenanthroline.

To understand the effects of manisyl-substitution better, MO diagrams were calculated for β-pyrs **112**, **115**, and **118** (Figure 3.22). In all three structures, the pyridine rings are flat and conjugated with the phenanthroline. The orientation of the manisyl groups, however, depends on the regiochemistry. Manisyl groups in the beta- and gamma- positions (relative to the phenanthroline) are almost perfectly orthogonal (~90º) to the phenanthroline ring and have no electron density in the HOMOs or LUMOs. When the manisyl group is in the alpha position, it is no longer perfectly orthogonal (~70º) and conjugates with the phenanthroline moiety, as evidenced by orbital density in the HOMO and the larger change in HOMO-LUMO gap (Figure 3.22a). Thus, the effect of manisyl substituents on the photophysics of pyridyl-

phenanthrolines is dictated by the existence of orbital nodes at the attachment points. On the pyridine ring, there are nodes at the alpha- and gamma- positions and manisyl substituents there have no noticeable impact. There is, however, orbital density at the beta- position of the pyridine and the manisyl groups of β-pyrs **112**, **115**, and **118** can interact with the pyridyl-phenanthroline LE* and access the CT* state. On the phenanthroline ring, there is a node at the β-position and the CT* is inaccessible. Manisyl groups in the gamma- position are also unable to access the CT* state. However, the manisyl substituents in α-phens **111 – 113** are no longer held orthogonal, mostly due to lesser steric crowding, and able to form a similar CT* state, albeit with reduced efficiency.

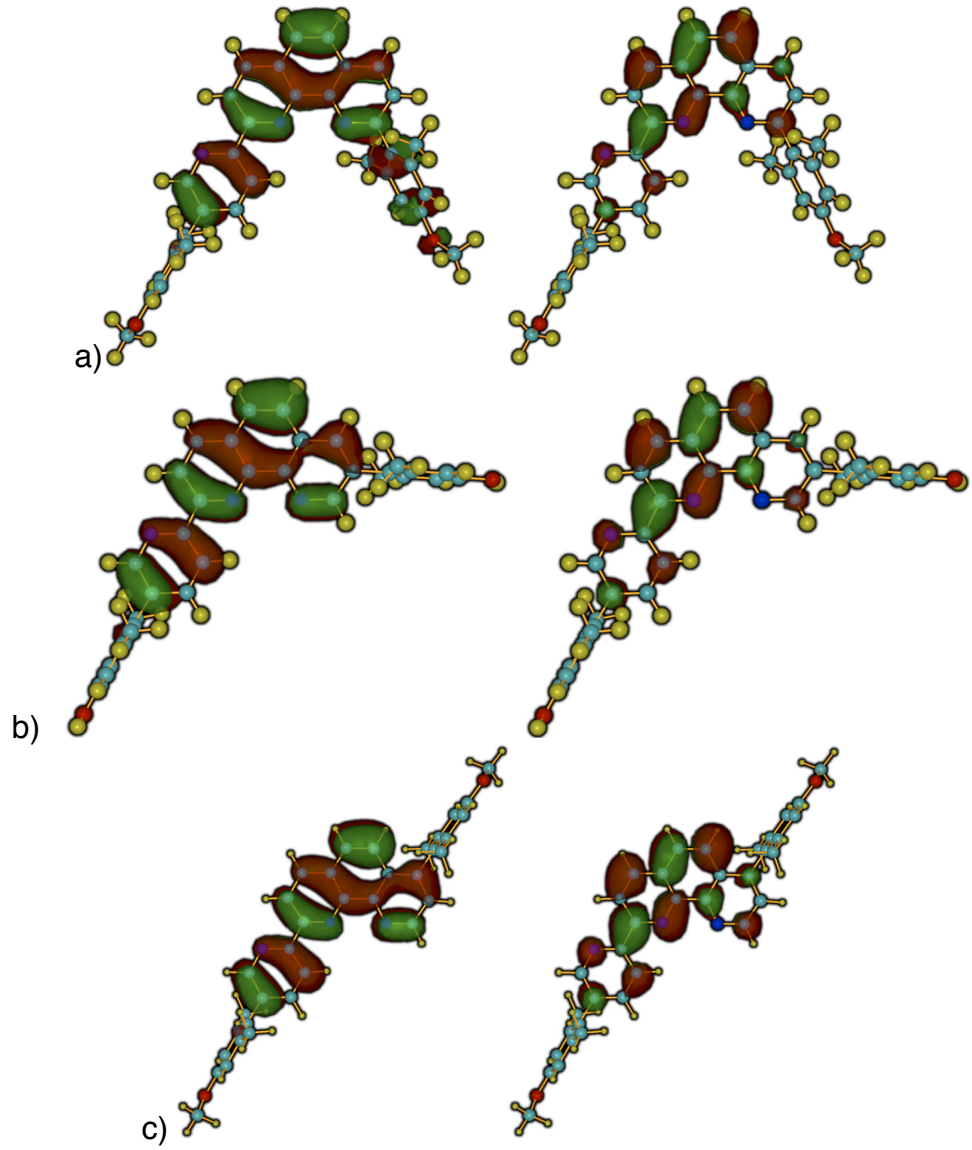

Figure 3.22 HOMO and LUMO MO orbitals of pyridyl-phenanthrolines a) **112**; b) **115**, and c) **118**.

3.2.3 Discussion

Manisyl-substituted pyridyl-phenanthrolines exhibit two fluorescent states that differ in their response to substituent position and solvent polarity (Figure 3.23). The predominant emission in nonpolar solvents is independent of solvent polarity and can be attributed to a nonpolar locally excited LE* state similar to the $^1\pi,\pi^*$ state of phenanthroline. In polar solvents, the predominant excited state is stabilized by increasing solvent polarity and can be attributed to an excited state with CT* character.

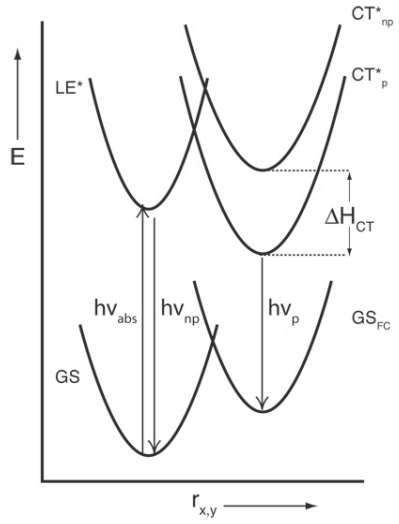

Figure 3.23 Simplified energy diagram showing dual emission due to solvent stabilization of the charge-transfer (CT*) state: GS is the ground state; GS_{FC} is the Franck-Condon Ground state; LE* is the locally excited state; CT^*_{np} and CT^*_{p} are the charge-transfer excited state in non-polar and polar solvents, respectively; hv_{abs} is the absorption from the GS to the LE*, hv_{np} and hv_{p} are the dominant fluorescence in non-polar and polar solvent respectively.

The position of manisyl substitution controls the accessibility of the CT* state. Pyridyl-phenanthrolines with manisyl groups β to the pyridine nitrogen, β-pyrs **112**, **115**, and **118**, have good orbital overlap and can best access the CT* state. Pyridyl-phenanthrolines with manisyl groups in the pyridine α- or γ- position have very poor orbital overlap and do not readily access the CT* state. Pyridyl-phenanthrolines with manisyl groups in the phenanthroline α- position display a mixed LE*/CT* emissive state in non-polar solvents, resulting from a deviation from orthogonality and increased conjugation with the phenanthroline core. When the manisyl is β to the phenanthroline nitrogen, the CT* state is not accessible, even though phenanthrolines can display an intense electronic transition polarized along the long axis.[12] In phenanthroline, the short axis, $a_2(\chi)$, and long axis, $b_1(\psi)$, states (Figure 3.8) are almost degenerate, but in pyridyl-phenanthroline the phenanthroline-like $a_2(\chi)$ orbital has been stabilized relative to the $b_1(\psi)$ orbital and the node at the beta- position prevents access

to a CT* state. (Figure 3.22). Manisyl groups in the phenanthroline gamma- position also show restricted access to the CT* in spite of increased orbital density at the *ipso*-carbon atom.

The dependence of the CT* state quantum yield on manisyl position reinforces the role of the electron rich manisyl as the donor in the CT* state. One can infer that, similar to previous manisyl substituted bipyridines and terpyridines, the base fluorophore is again a 4-manisyl-2,2'-bipyridine **108**.[36] As the MO calculations show (Figure 3.22), the manisyl group is orthogonal to the pyridine plane for beta-manisyl pyridines. The absorption data indicates that the manisyl group is independent and is not influenced by the ground state pyridyl-phenanthroline π-system. In the CT* state the manisyl acts as a donor moiety and TICT state[20] is probable.[35-37]

In a TICT system, the degree of orbital overlap is a function of the dihedral angle of the bridging carbons. When there is free rotation, as in DMABN, the amino group can twist to a 90º angle after excitation and electron transfer to achieve charge separation. In systems where the donor and acceptor are held orthogonal, i.e., pre-twisted systems,[75] only a small deviation from orthogonality is needed for electron transfer. After transfer, orthogonality is regained and charge-separation is achieved. Further deviations, then allow orbital overlap to reappear and emission and charge resolution is possible. Thus for manisyl-substituted phenanthrolines, only small deviations are necessary to allow the CT* state to form. Although it is possible to excite directly into the CT* state, the relative independence of the absorption spectra from solvent polarity and manisyl position leads to the following sequence of states (Scheme 3.1). Upon absorption, an electron is first raised from the ground state (GS) into the locally excited state (LE*), where, in non-polar solvents, weak emission occurs.

In polar solvents, a second electron transfer creates a twisted intramolecular charge transfer (simply labeled CT*) state that is strongly emissive.

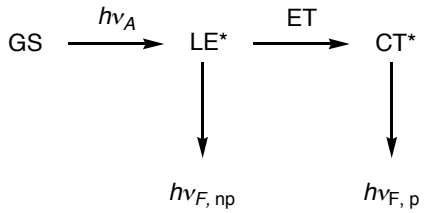

Scheme 3.1 Sequence of states for emission from the locally excited (LE*) or charge transfer (CT*) state. GS is the ground state, $h\nu_{F,\,np}$ and $h\nu_{F,\,p}$ are fluorescence in non-polar and polar solvents, respectively.

3.2.4 Conclusions

The photophysics of pyridyl-phenanthrolines are surprisingly complex relative to their bipyridine and terpyridine analogues. Access to the series of pyridyl-phenanthrolines with systematic structural variation has allowed, in combination with solvatachromatic studies, the establishment of new class of molecules possessing dual emission. The study of organic molecules displaying dual emission is an active area of physical organic chemistry[76] and controlling the switching of molecular electronic states is the focus of many chemosensors. Whereas the nature of the states can be assigned to a singlet excited state, similar to the $^1\pi,\pi^*$ state of phenanthroline, and a singlet twisted intramolecular charge transfer state involving donation of electron density from the orthogonal manisyl rings, the photophysical processes governing the thermodynamics and interconversion of the two states is still open for debate. Further studies examining the temperature dependence of the LE* and CT* states would better clarify the energetics and interconversion of the two states. Additionally, transient absorption spectra (flash spectroscopy)[13,63] can help clarify the sequence of states and provide structural insights. Continued computational calculation collaboration with the

Baldridge group has already borne fruit and will continue to impart a deeper understanding of the photophysics of pyridyl-phenanthroline as well as provide a challenging new system with which to check the validity of computational methods.

3.3 Experimental

All spectra were recorded in spectroscopic grade solvents and are uncorrected. UV-Vis absorption spectra were recorded on Perkin-Elmer UV-Vis Lambda 19 spectrometer at concentrations of 10^{-5} M. Emission measurements were made on the identical samples using an Edinburgh FLSP920 combined steady state, fluorescence and phosphorescence spectrometer. Emission and excitation spectra were collected using the Xe900 – 450W steady state xenon lamp (ozone free) with computer controlled excitation shutter with excitation and observation at each wavelength maximum. Reported emission spectra were recorded at the global absorption maximum (~295 nm) for each compound. Reported excitation spectra were recorded at the emission maximum of the LE* (355 nm) or CT* (405 or 430 nm) state. Lifetime decays were then measured using time-correlated single photon counting (TCSPC) with the nF900 nanosecond flash-lamp. The same samples were then diluted to optical transparency (Abs = 0.05 – 0.04) and the emission rerecorded. The integrated intensity was compared to an iso-absorptive standard of 9,10-diphenylanthracene (DPA) in degassed ethanol using the method of Demas and Crosby (Eq. 3.9):[77]

$$\Phi_{unk} = \Phi_{std}\left(\frac{A_{std}}{I_{std}}\right)\left(\frac{I_{unk}}{A_{unk}}\right)\left(\frac{\eta_{unk}}{\eta_{std}}\right)^2 \tag{3.9}$$

where Φ_{unk} is the fluorescence quantum yield of the unknown, Φ_{std} is the quantum yield of the standard ($\Phi_{DPA} = 0.91$),[77] A_{unk}, A_{std}, I_{unk}, and I_{std} are the respective absorption and the integrated fluorescence intensities of the unknown and standard, and η is the index of refraction of the solvent used for the unknown and standard. Multiple measurements indicate a 5 % precision for Φ_f determined by this method.

Computations: B3LYP[70] and MP2[71] methods were employed, using GAMESS.[78] Ground state geometries of terpy (*C*2V), 1,10-phenanthroline (*C*2V), and pyridyl-

phenanthroline (*C*2V) were optimized with B3LYP and used to calculate the HOMO and LUMO energies with MP2 using the DZV(d,p)[79] basis set.

3.4 References

(1) Kaes, C.; Katz, A.; Hosseini, M. W. *Chem. Rev.* **2000**, *100*, 3553-3590.

(2) Sammes, P. G.; Yahioglu, G. *Chem. Soc. Rev.* **1994**, *23*, 327-334.

(3) Thompson, A. M. W. C. *Coord. Chem. Rev.* **1997**, *160*, 1-52.

(4) Crosby, G. A. *Acc. Chem. Res.* **1975**, *8*, 231-238.

(5) Alstrum-Acevedo, J. H.; Brennaman, M. K.; Meyer, T. J. *Inorg. Chem.* **2005**, *44*, 6802-6827.

(6) Gust, D.; Moore, T. A.; Moore, A. L. *Acc. Chem. Res.* **2001**, *34*, 40-48.

(7) Meyer, T. J. *Pure Appl. Chem.* **1986**, *58*, 1193-1206.

(8) Balzani, V.; Juris, A.; Venturi, M.; Campagna, S.; Serroni, S. *Chem. Rev.* **1996**, *96*, 759-833.

(9) Juris, A.; Balzani, V.; Barigelletti, F.; Campagna, S.; Belser, P.; Von Zelewsky, A. *Coordination Chemistry Reveiws* **1988**, *84*, 85-277.

(10) Barigelletti, F.; Flamigni, L. *Chem. Soc. Rev.* **2000**, *29*, 1-12.

(11) Jortner, J.; Ratner, M. *Molecular Electronics*; Blackwell Science: London, 1997.

(12) Joshi, H. S.; Jamshidi, R.; Tor, Y. *Angew. Chem. Int. Ed.* **1999**, *38*, 2721-2725.

(13) Turro, N. J. *Modern Molecular Photochemistry*; University Science Books: Sausalito, 1991, p 628.

(14) While there exist molecules possessing a triplet ground state, e.g., molecular oxygen, they are the exception and not common.

(15) Jablonski, A. *Z. Physik* **1935**, *94*, 38.

(16) Kasha, M. *Faraday Discuss.* **1950**, *9*, 14-19.

(17) Kopecky, J. *Organic Photochemistry: A Visual Approach*; VCH Publishers, Inc.: New York, 1992, p 285.

(18) Stokes, G. G. *Mathematical and Physical Papers*; Cambridge University Press: Cambridge, 1880-1905; Vol. I-V.

(19) de Silva, A. P.; Gunaratne, H. Q. N.; Gunnlaugsson, T.; Huxley, A. J. M.; McCoy, C. P.; Rademacher, J. T.; Rice, T. E. *Chem. Rev.* **1997**, *97*, 1515-1566.

(20) Grabowksi, Z. R.; Rotkiewicz, K.; Rettig, W. *Chem. Rev.* **2003**, *103*, 3899-4031.

(21) Grabowksi, Z. R.; Rotkiewicz, K.; Siemiarczuk, A.; Cowley, D. J.; Baumann, W. *Nouv. J. Chim.* **1979**, *3*, 443-454.

(22) Liptay, W. *Z. Naturforsch.* **1965**, *20a*, 1441-1471.

(23) Mataga, N.; Kaifu, Y.; Koizumi, M. *Bull. Chem. Soc. Jpn.* **1956**, *29*, 465-470.

(24) Lippert, E. *Z. Naturforsch.* **1955**, *10a*, 541-545.

(25) Onsager, L. *J. Amer. Chem. Soc.* **1936**, *58*, 1486-1493.

(26) Reichardt, C. *Solvents and Solvent Effects in Organic Chemistry*; 2 ed.; VCH: Weinheim, 1990, p 534.

(27) Liptay, W. In *Excited States*; Lim, E. C., Ed.; Academic Press: New York, 1974, pp 129.

(28) Suppan, P. *J. Chem. Soc., Faraday Trans. 2* **1981**, *77*, 3546.

(29) Sauvage, J.-P.; Collin, J.-P.; Chambron, J.-C.; Guillerez, S.; Coudret, C.; Balzani, V.; Barigelletti, F.; De Cola, L.; Flamigni, L. *Chem. Rev.* **1994**, *94*, 993-1019.

(30) Castellucci, E.; Angeloni, L.; Marconi, G.; Venuti, E.; Baraldi, I. *J. Phys. Chem.* **1990**, *94*, 1740-1745.

(31) Bandyopadhyay, B. N.; Harriman, A. *J. Chem. Soc., Faraday Trans. 1* **1977**, *73*, 663-674.

(32) Sarkar, A.; Chakravorti, S. *J. Lumin.* **1995**, *63*, 143-148.

(33) Lim, E. C. In *Excited States*; Lim, E. C., Ed.; Academic Press: New York, 1982, pp 305.

(34) Bosnich, B. *Acc. Chem. Res.* **1969**, *2*, 266-273.

(35) Loren, J. C., University of California, San Diego, 2004.

(36) Loren, J. C.; Siegel, J. S. *Angew. Chem. Int. Ed.* **2001**, *40*, 754-757.

(37) Arias, K.; Barder, T.; Loren, J. C.; Zysman-Coleman, E.; Baldridge, K. K.; Siegel, J. S. *in preparation.*

(38) Active Masters and Ph.D. work in progress of Karla Arias. University of Zürich, Zürich, Switzerland.

(39) Kozhevnikov, D. N.; Shabunina, O. V.; Kopchuk, D. S.; Slepukhin, P. A.; Kozhevnikov, V. N. *Tetrahedron Lett.* **2006**, *47*, 7025-7029.

(40) Ernst, S.; Vogler, C.; Klein, A.; Kaim, W.; Zalis, S. *Inorg. Chem.* **1996**, *35*, 1295-1300.

(41) Casadonte, D. J.; McMillin, D. R. *J. Amer. Chem. Soc.* **1987**, *104*, 331.

(42) Honeyburne, C. L. *Mol. Phys.* **1971**, *21*, 1057-1066.

(43) Kaim, W. *J. Amer. Chem. Soc.* **1982**, *104*, 3833-3837.

(44) Klein, A.; Kaim, W.; Waldhör, E.; Hausen, H.-D. *J. Chem. Soc., Perkins Trans. 2* **1995**, 2121.

(45) Kotlicka, J.; Grabowksi, Z. R. *J. Photochem.* **1979**, *11*, 413-418.

(46) Henry, M. S.; Hoffman, M. Z. *J. Phys. Chem.* **1979**, *83*, 618-625.

(47) Goodall, W.; Williams, J. A. G. *Chem. Comm.* **2001**, 2514-2515.

(48) Albano, G.; Balzani, V.; Constable, E. C.; Maestri, M.; Smith, D. R. *Inorg. Chim. Acta* **1998**, *277*, 255-231.

(49) Mutai, T.; Cheon, J.-D.; Tsuchiya, G.; Araki, K. *J. Chem. Soc., Perkins Trans. 2* **2002**, 862-865.

(50) Mutai, T.; Cheon, J.-D.; Arita, S.; Araki, K. *J. Chem. Soc., Perkins Trans. 2* **2001**, 1045-1050.

(51) Martin, R. B.; Lissfelt, J. A. *J. Amer. Chem. Soc.* **1956**, *78*, 938-940.

(52) Henry, M. S.; Hoffman, M. Z. *J. Amer. Chem. Soc.* **1977**, *99*, 5201-5203.

(53) Ohno, T.; Kato, S. *Bull. Chem. Soc. Jpn.* **1974**, *47*, 2953.

(54) Maestri, M.; Armaroli, N.; Balzani, V.; Constable, E. C.; Thompson, A. M. W. C. *Inorg. Chem.* **1995**, *34*, 2759-2767.

(55) Weisstuch, A.; Ttesta, A. C. *J. Phys. Chem.* **1968**, *72*, 1982.

(56) Araki, K.; Mutai, T.; Shigemitsu, Y.; Yamada, M.; Nakajima, T.; Kuroda, S.; Shimao, I. *J. Chem. Soc., Perkins Trans. 2* **1996**, 613.

(57) Active Masters and Ph.D. work in progress of Karla Arias. University of Zürich, Zürich, Switzerland.

(58) Roundhill, D. M. *Photochemistry and Photophysics of Metal Complexes*; Plenum: New York, 1994.

(59) Kalyanasundaram, K. *Photochemistry of Polypyridine and Porphyrin Complexes*; Academic Press: London, 1992.

(60) Armaroli, N.; De Cola, L.; Balzani, V.; Sauvage, J.-P.; Dietrich-Buchecker, C. O.; Kern, J.-M. *J. Chem. Soc., Faraday Trans.* **1992**, *88*, 553-556.

(61) Birckner, E.; Grummt, U.-W.; Göller, A. H.; Pautzsch, T.; Egbe, D. A. M.; Al-Higari, M.; Klemm, E. *J. Phys. Chem. A* **2001**, *105*, 10307-10315.

(62) Badger, G. M.; Walker, I. S. *J. Chem. Soc.* **1956**, 122.

(63) Lakowicz, J. R. *Principles of Fluorescence Spectroscopy*; 2 ed.; Kluwer Academinc/Plenum: New York, 1999, p 698.

(64) Normalized ET(N) values, derived from the transition energy at RT of the long-wavelength absorption of a standard pyridinium-N-phenoxide betaine dye, ET(30). The ET(N) of Tetramethylsilane is set to 0.000 and water is 1.000.

(65) Reichardt, C. *Chem. Rev.* **1994**, *94*, 2319-2358.

(66) The assignment of the LE* emission to a singlet state is further supported by the insensitivity to molecular oxygen.

(67) Grummt, U.-W.; Birckner, E.; Al-Higari, M.; Egbe, D. A. M.; Klemm, E. *J. Fluoresc.* **2001**, *11*, 41-51.

(68) Calvert, J. G.; Pitts Jr., J. N. *Photochemistry*; John Wiley and Sons, Inc.: New York, 1966, p 899.

(69) Pyridyl-phenanthroline 116 was specifically chosen as it exhibits dual emission in polar solvents.

(70) Lee, C.; Yang, W.; Parr, R. G. *Phys. Rev.* **1988**, *B37*, 785-789.

(71) Moller, C.; Plesset, M. S. *Physics Review* **1934**, *46*, 618.

(72) Moore, J. J.; Nash, J. J.; Fanwick, P. E.; McMillin, D. R. *Inorg. Chem.* **2002**, *41*, 6387-6396.

(73) Ceulemans, A.; Vanquickenborne, L. G. *J. Amer. Chem. Soc.* **1981**, *103*, 2238-2241.

(74) Day, P.; Sanders, N. *J. Chem. Soc. A* **1967**, 1536-1541.

(75) Al-Hassan, K. A.; Azumi, T.; Rettig, W. *Chem. Phys. Lett.* **1993**, *206*, 25-29.

(76) Kosower, E. *Acc. Chem. Res.* **1982**, *15*, 259-266.

(77) Crosby, G. A.; Demas, J. N. *J. Phys. Chem.* **1971**, *75*, 991-1024.

(78) Schmidt, M. W.; Baldridge, K. K.; Boatz, J. A.; Elbert, S. T.; Gordon, M. S.; Jensen, J. H.; Koseki, S.; Matsunaga, N.; Nguyen, K. A.; Su, S.; Windus, T. L.; Elbert, S. T. *J. Comput. Chem.* **1993**, *14*, 1347-1395.

(79) Dunning, T. H.; Hay, P. J. In *Methods of Electronic Structure Theory*; Schaeffer, H. F., Ed.; Plenum: New York, 1977, pp Ch 1.

CHAPTER 4

COORDINATION CHEMISTRY OF 2-PYRIDYL-1,10-PHENANTHROLINES

4.0 Abstract

A series of ML_2 coordination complexes of pherpys and terpys with Fe(II), Co(II), Ni(II), Cu(II), Zn(II), Ru(II), and Os(II), were synthesized. In the solid state, pyridyl-phenanthroline complexes are isomorphous (space group *Pcca*), except for the zinc complex, which is isostructural but not isomorphous (space group $P2_{1/c}$). Terpyridine complexes are isostructural but divided into two isomorphous subgroups (*Pnna* and *C2/c*). Within the crystal lattice the dications arrange into sheets of alternating left and right handed double-helixes via CH $\cdots\pi$ and π-π interactions. All of the complexes exhibit weak LC emission at room temperature and the osmium complexes possess an emissive MLCT state. Pyridyl-phenanthroline complexes are C_2 symmetric and their chirality was confirmed by NMR titrations with Δ-TRISPHAT as a chiral counter-ion. Attempts at resolution by chromatography, crystallization, and HPLC were inconclusive.

4.1 Introduction

Since Morgan and Burstall first discovered the parent 2,2':6',2"-terpyridine (terpyridine) in 1932,[1] the coordination chemistry of terpyridines has been extensively explored.[2] In recent years, terpyridines have been key building blocks for the construction of metallosupramolecular architectures.[3-5] Commonly employed as a planar terdentate ligands, terpyridines typically form pseudo-octahedral complexes with metal to ligand ratios of 1:2 (ML_2) (Figure 4.1). In solid state and solution, terpyridines exist in the *trans, trans-* configuration but adopt the *cis,cis-* conformation upon metal complexation (Figure 4.1).[2,6] Terpyridines distort and bite down upon the metal-ion as well.[2] In spite of the increased ligand strain, the strong back donation from the d-orbitals of metals in low oxidation states into the electron poor π^* orbitals of the

pyridine rings combined with a strong chelate effect results in octahedral complexes that are quite stable.

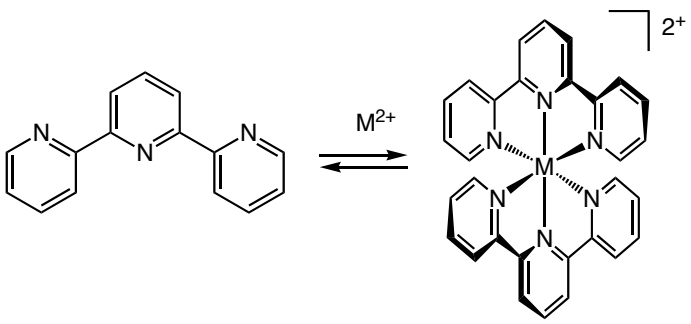

Figure 4.1 Changes in terpyridine conformation upon binding.

Polypyridine transition metal complexes possess unique photophysical and redox properties and are the focal point of research on artificial photosynthesis,[7-9] photo-induced electron transfer,[10,11] and molecular electronics.[12,13] The ML_3 ruthenium complexes of 2,2'-bipyridines (bipyridine) and 1,10-phenanthrolines (phenanthroline) are extensively used. The lowest triplet metal-to-ligand charge transfer (^{3}MLCT)[14] excited state of these chemically stable complexes exhibits long-lived (up to 1 μs), room temperature ^{3}MLCT luminescence with high quantum efficiency as well as strong oxidizing and reducing capabilities.[11] However, the different stereoisomers formed by asymmetrically substituted bipyridines and phenanthrolines[15,16] are problematic for the construction of supramolecular assemblies.[17,18] The simple, highly symmetrical geometry of ML_2, ruthenium bis-terpyridine complex is ideal for the construction of metallosupramolecular architectures but possesses a very short lifetime (0.25 ns) and is essentially non-luminescent in solution at room temperature. The contrast in photophysical properties is due to deactivation via non-radiative metal-centered triplet (^{3}MC) states of similar energy to the potentially emissive ^{3}MLCT state of $Ru(terpy)_2^{2+}$. Increasing the energy difference between the ^{3}MC and ^{3}MLCT states by modulating the

HOMO-LUMO gap of the terpyridine ligands can result in longer lifetimes and increased luminescence.[19-21]

The intriguing juxtaposition of a phenanthroline upon a terpyridine backbone found in 2-pyridyl-phenanthrolines forms chiral ML_2 complexes with C_2 symmetry. Pyridyl-phenanthroline coordination compounds are thus distinct from the diastereomeric mixes of substituted ML_3 complexes and achiral terpyridine ML_2 complexes. The smaller HOMO-LUMO gap and the ability to systematically vary substituents highlight their potential as coordination chemistry building blocks. This chapter reviews the known metal complexes of pyridyl-phenanthrolines before describing the synthesis and properties of a series of chiral transition metal complexes of manisyl substituted pyridyl-phenanthrolines in contrast to the analogous terpyridine series.

4.1.1 Ruthenium(II) and (III) Complexes

In the initial report concerning the synthesis of the parent 2-pyridyl-phenanthroline ligand,[22] **46**, Thummel and coworkers envisioned that, as a juxtaposition of phenanthroline and terpyridine, there were two possible binding modes when paired with an octahedral metal. Complexation as a bidentate 2-substituted phenanthroline would lead to ML_3^{2+} complex **146** whereas complexation as a terdentate terpyridine would lead to ML_2^{2+} complex **147**. When treated with $RuCl_3$ only complex **147** is formed.

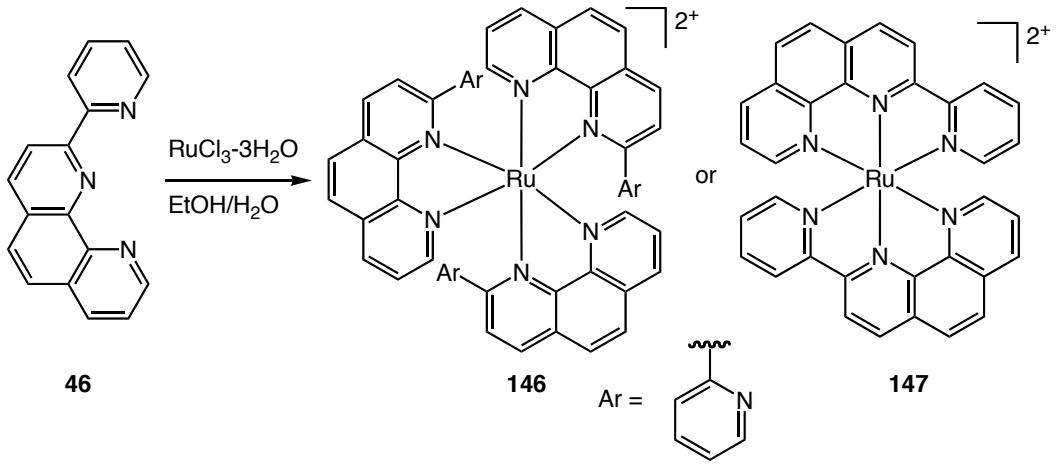

Figure 4.2 Complexation as a bidentate phenanthroline analogue **146** or terdentate terpyridine analogue **147**.

In the follow-up study, the photophysics of the ruthenium complexes of pyridyl-phenanthroline **46** and the fully bridged analogues **148–150** were investigated (Figure 4.3).[23] It was postulated that the increased delocalization would lower the energy of the ligand π^* without affecting the ligand field, thus widening the energy gap between the emissive ^{3}MLCT and non-emissive ^{3}MC states and increasing the lifetime and quantum yield at room temperature. Typically, lowering the energy gap between the ground and excited states increases non-radiative decay rates, [24-26] but increasing the delocalization can reduce excited state distortion and thus the non-radiative relaxation decay rates.[27,28] Although the electrochemical half-wave potentials of the ligands and complexes confirm increased ligand delocalization, all of the complexes are non-luminescent in solution at room temperature. At 77 K, the luminescence lifetimes and absorption maxima wavelength also lengthen as the unsaturation increases but the increased rigidity prevents the ligands from obtaining an optimal bite angle and leads to a weaker ligand field. The lack of room temperature emission is attributed to a concurrent lowering of ^{3}MC due to the weaker ligand field.

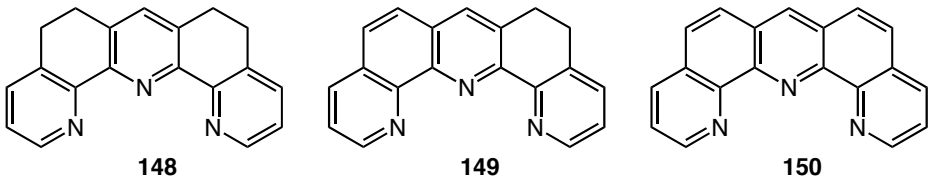

148 **149** **150**

Figure 4.3 Saturated and unsaturated bridged terpyridine analogues.

Thummel and coworkers then exploited the unsymmetrical nature of the 2-pyridyl-phenanthrolines to investigate the mechanism of ruthenium(II) complexes.[29] Assuming the first coordination of terpyridine to $RuCl_3$-$3H_2O$ is fast, there are two sites for nucleophilic attack by the second terpyridine onto intermediate **I** (Scheme 4.1). If the attack is equatorial, complex **II** will be formed whereas complex **III** will be the product of an axial attack. Under dark conditions, detection of compound **II** is possible, but it quickly transforms to complex **III** when the reaction is performed with terpyridine. The steric bulk of benzo-fused 2-pyridyl-phenanthroline **154** favors equatorial attack from the phenanthroline moiety and results in almost complete formation (~95%) of complex type **II** that does not convert to structure type **III**. Benzo-fused pyridyl-phenanthroline **155** is less encumbered and favors axial attack from the quinoline nitrogen and forms compound type **III** as the major product (~97%). Bridged ligand **156**, however, forms a 2:1 mixture of species **II** and **III**. Upon exposure to light, **II** will slowly isomerizes to **III**. The study highlights the fine balance of steric and electronic factors that control the formation of bis-terdentate ruthenium(II) complexes and emphasizes the importance of π-stacking between coordinating ligands. The benzo-pyridines of ligands **154** and **155** can rotate and adopt suitable π-stacking conformation (Figure 4.4) but are differentiated by sterics. The pyridyl of bridged ligand **156** cannot accommodate intraligand π-stacking and is less stable. Conversion of **II** to **III** for ligand **156** is not thermal and only occurs under

photochemical activation implying that photochemical dissociation of the chloride prior to or concerted with coordination of the quinoline nitrogen.

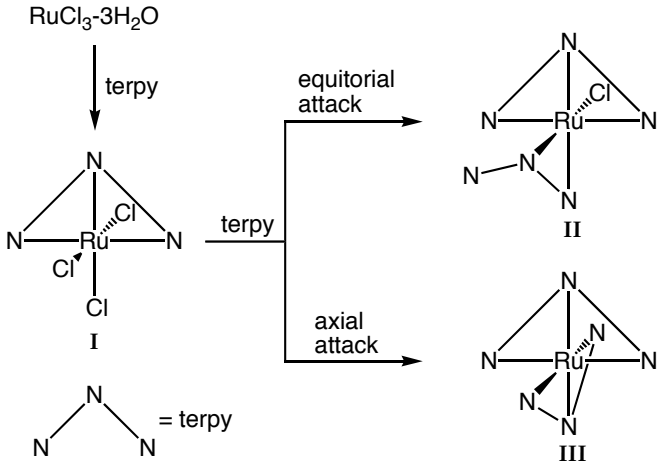

Scheme 4.1 Possible mechanisms for formation of $Ru(terpy)_2^{2+}$.[29]

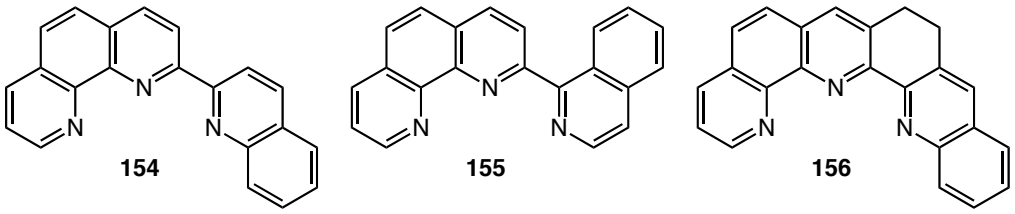

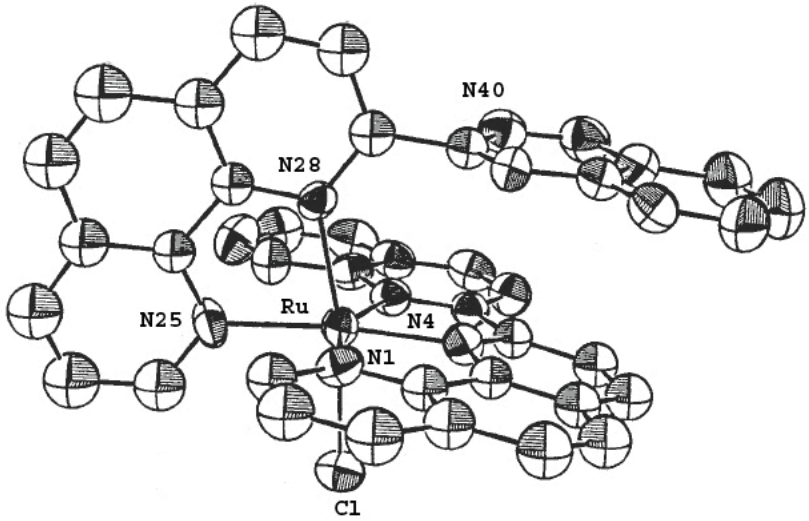

Figure 4.4 ORTEP diagram of Ru(**154**-*N,N',N''*)(**154**-*N,N'*)Cl.[29]

In 2000, Barigelletti and coworkers published a photophysical investigation of cyclometallated and non-cyclometallated ruthenium(II) complexes of sterically hindered phenanthrolines and terpyridines.[30] At 77 K in butyronitrile, all the ruthenium complexes are luminescent. Typical for terpyridine ruthenium complexes,[21] non-cyclometallated derivatives, including **157** and **158** are non-luminescent at room temperature. The distorted octahedral geometry of terpyridine complexes induce a weak ligand field and the energetically nearby non-radiative ^{3}MC states deactivate luminescence. Bulky substituents α to the nitrogen further distort the geometry and the ligand field. On the other hand, cyclometallated derivatives, e.g. **159**, are luminescent at room temperature with long-lived excited states (70 to 106 ns). Similar to other cyclometallated ruthenium complexes,[31] the strong ligand field induced by σ-donation from the carbon atom destabilizes the ^{3}MC state, stabilizes the ^{3}MLCT state and increases luminescence, contrary to the "energy-gap" law.[14,32]

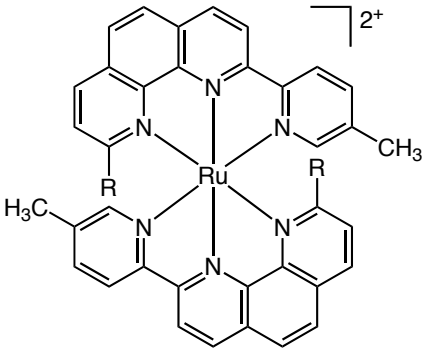

157

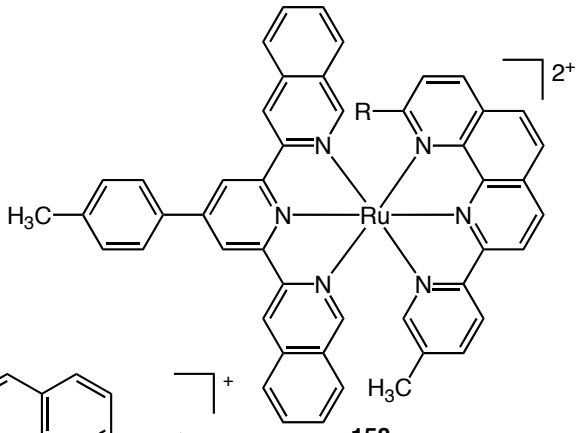

158

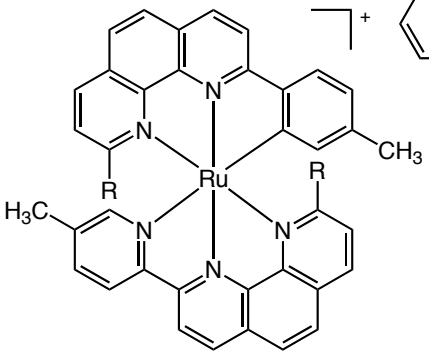

159

Given the importance of metal complexes in molecular biology and medicinal chemistry,[33] Jahng and coworkers investigated the *in vitro* cytotoxic activity of several pyridyl-phenanthrolines and their Ru(L-*N',N", N"'*)Cl_3 complexes, **160** – **162**.[34] Free pyridyl-phenanthrolines showed no appreciable cytotoxicity below 50 μg/mL, but terpyridine **45** showed potent toxicity at 0.01 – 0.001 μg/mL. All three of the unsymmetrical Ru(L-*N',N", N"'*)Cl_3 complexes are more toxic than the unsymmetrical Ru(terpy)Cl_3[35] complex in all six tested human cancer cell lines. The introduction of a single benzo-fused ring, **161**, slightly increases toxicity whereas the introduction of a second ring, **162**, decreases it. No rationalization of this observation was given, and no further investigations have been published.

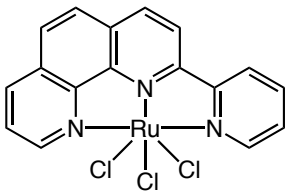

160

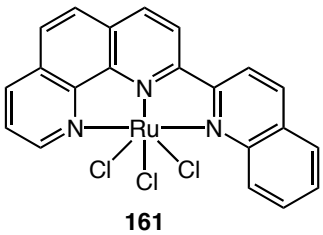

161

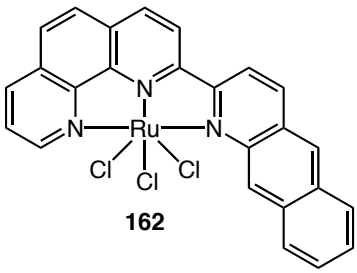

162

4.1.2 Copper(I) and (II) Complexes

In the field of molecular machines, generating and controlling large molecular motions is an appealing aspiration. Sauvage and coworkers reported a rotaxane[36] and a catenane[37-39] incorporating both terpyridine and phenanthroline units. Modulating the oxidation state of the bound copper ion induces significant structural rearrangement in both systems. Recognizing that pyridyl-phenanthroline **163**, can act as either a bidentate or terdentate ligand when paired with transition metals of the appropriate oxidation state, copper(I) and (II) complexes were made. When reacted with copper(I), the expected[40] tetrahedral geometry is revealed in the crystal structure (Figure 4.5).

Unexpectedly, one ligand binds through the phenanthroline moiety and the other ligand binds as a bipyridine.[41] The interaction of one electron rich methoxyphenyl (anisyl) group with the electron poor phenanthroline of the opposite ligand via π-stacking stabilizes this binding motif. The ^{1}H-NMR data, however shows only one set of chemical shifts and denotes a fast equilibrium as the two ligands interconvert in solution. The copper(II) adopts the normal octahedral geometry,[42] and is stabilized through donor-acceptor π-stacking interactions of both anisyl groups (Figure 4.6). The cyclic volatammograms (CV) of both compounds are identical, fully reversible and indicate that the structural rearrangement is fast on the CV time scale (>1 s^{-1}).

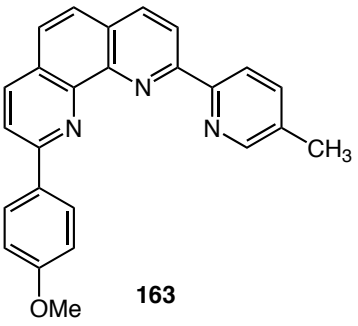

163

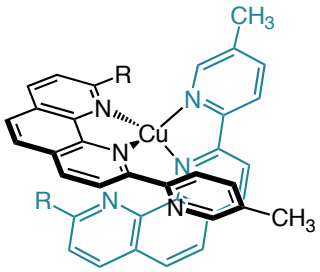

164

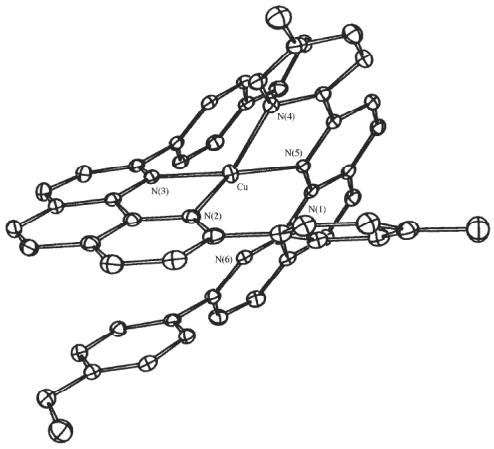

Figure 4.5 Copper(I) pyridyl-phenanthroline complex **164** and ORTEP diagram.

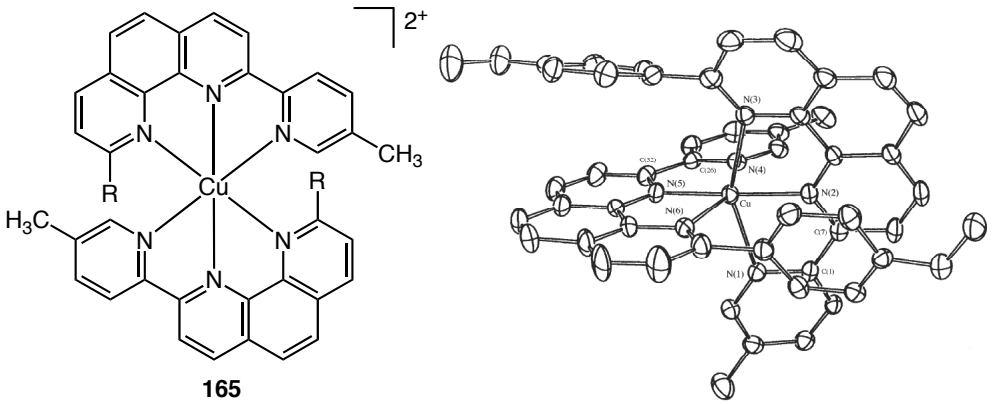

Figure 4.6 Copper(II) pyridyl-phenanthroline complex **165** and ORTEP diagram.

4.1.3 Palladium(II) complexes

The insertion of unsaturated molecules, e.g. carbon monoxide and alkenes, into a carbon-metal bond is essential to many palladium catalyzed reactions.[43,44] The mechanism of insertion depends on the nature of the ligands and their ability to dissociate.[43]

In 1990, Vrieze and coworkers reported the CO insertion into an ionic palladium-terpyridine complex [Pd(Me)terpy]Cl.[45,46] The initially proposed mechanism involved CO insertion to form an usual five-coordinate intermediate, due to the strong chelating effect of terpyridine, but given that terpyridine can also bind in a bidentate manner,[47] Vrieze collaborated with Thummel to investigate the properties of the rigid terdentate ligands **45**, **46**, **149**, **150**, and **166**.[48] Formation of palladium complexes **45a**, **46a**, **149a**, **150a**, and **66a** is straightforward and exposure to carbon monoxide results in the acetylpalladium complexes **45b**, **46b**, **149b**, **150b**, and **166b** within one minute (Scheme 4.2). Only strained alkenes, e.g., norbornene or norbornadiene, inserted into **45b**, **46b**, **149b**, **150b**, but not **166b**, to give complexes **45c**, **46c**, **149c**, and **150c**. Spectroscopic data indicate that the terdentate ligands bind in a bidentate fashion. The rate of norbornadiene insertion increases **45c** < **150c** < **46c** and is attributed to ligand

strain. Ligand **150** is unable to fully pinch onto the metal ion and thus easily disassociates. Ligands **45** and **46** can better distort to achieve more optimal palladium-nitrogen distances but can rotate the pendent pyridyl ring whereas ligand **150** cannot. The surprising results indicate that even rigid terdentate ligands can bind in a bidentate manner and that increasing rigidity can lead to increased strain, facilitating nitrogen dissociation.

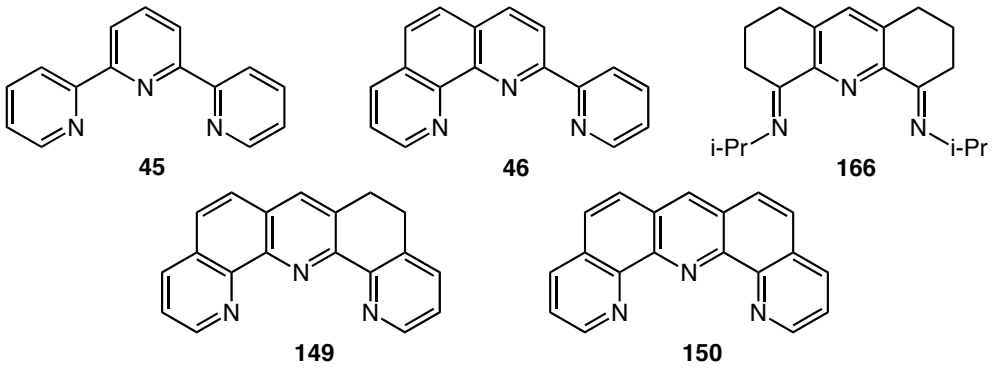

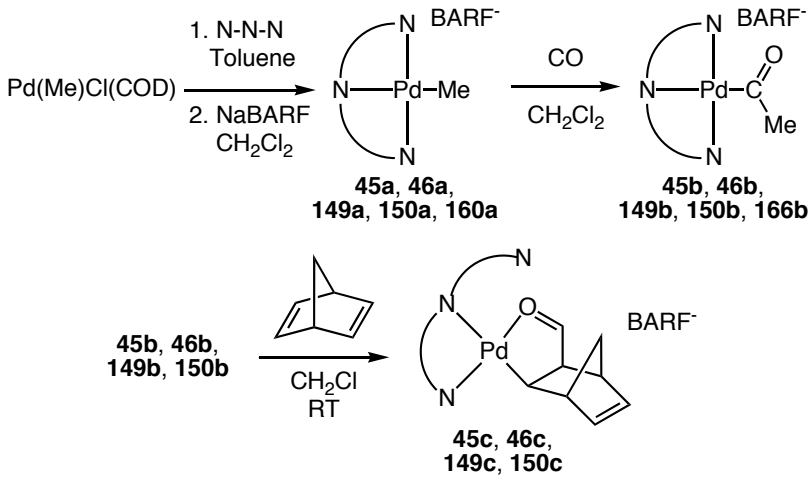

Scheme 4.2 Insertion of carbon monoxide and norbornadiene into carbon-palladium bonds of rigid, terdentate complexes.[48]

4.1.4 Platinum(II) and other metal complexes

While palladium complexes show useful catalytic activity, platinum(II) polypyridine complexes can display long-lived emissive MLCT states in solution.[49-51]

The $[Pt(terpy)Cl]^+$ system,[52,53] **167a**, is of particular interest is due to its ability to bind proteins via ligand substitution of the labile chloride ion by arginine or histidine residues,[54,55] as well as intercalating into double stranded DNA.[56,57] The parent complex is luminescent in the solid state and at low temperatures but is non-luminescent at room temperature in solution due to non-radiative decay via accessible MC excited states.[52] A variety of luminescent derivatives have been prepared via substitution of the chloride with other ligands[53], modulation of the electronic properties of the terpyridine ligands by incorporating electron-donating, electron-withdrawing,[58] or conjugating substituents, [59] and in 2002, McMillin and coworkers reported that the platinum chloride complexes of the parent pyridyl-phenanthroline and its methylated derivatives, **168a – 168e**, show enhanced luminescence (Table 4.1).[60]

Table 4.1 Emission data for $[Pt(pherpy)Cl]^+$ and derivatives in dichloromethane at room temperature.

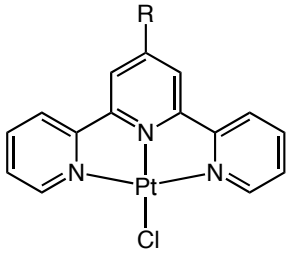

167a R = H
167b R = Ph

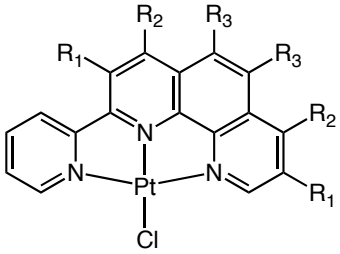

168a R_1 = H R_2 = H R_3 = H
168b R_1 = H R_2 = Me R_3 = H
168c R_1 = H R_2 = H R_3 = Me
168d R_1 = Me R_2 = Me R_3 = H
168e R_1 = Me R_2 = H R_3 = Me

Ligand	λ_{max}, nm	τ, μs	ϕ (10^2)	k_r, s^{-1}
167b[61]	535, 570, 608	0.085	0.21	2.5×10^4
168a	547, 591, 650	0.23	0.31	1.2×10^4
168b	553, 599, 653	1.5	1.6	1.1×10^4
168c	554, 601, 655	4.0	3.8	9.4×10^3
168d	563, 609, 673	5.0	2.6	5.3×10^3
168e	567, 611, 675	9.3	5.5	6.0×10^3

The electrochemistry of platinum complexes **168a – 168e**, as well as the pentacoordinate $ZnCl_2$ analogues **169a – 169e**, are similar to the analogous terpyridine complexes.[58,62] The two ligand based reduction waves are ~0.2 V more positive for coordinated pyridyl-phenanthrolines than for terpyridines and the addition of methyl groups induces small negative shifts in the reduction potential. Methyl groups in the 4, 7-positions exert a greater effect than substitution in the 3,8- or 5,6- positions. The UV-Vis absorption data of the platinum, **168a – 168e**, and zinc complexes, **169a – 169e** are also strikingly similar to, but at longer wavelengths than, the 4'-phenyl terpyridine complexes **157b** and **170**.[53] However, only methyl substitution at the 5,6-positions has any effect (lowering) on the energy of the MLCT absorption. The bis-iron complexes **171a – 171e** and **172** also display similar absorptive properties, but are more sensitive to methyl substitution. The MLCT absorption red shifts to longer wavelengths when methyl groups are in the 3,8- and 4,7- positions, but undergo a blue shift when placed in the 5,6- positions. At room temperature, only the pyridyl-phenanthroline platinum(II) complexes are luminescent. Addition of methyl substituents lowers the emission energy but increases the quantum yields and lifetimes seemingly independent of regiochemistry but with the greatest effect at the 5,6- positions (Table 4.1). In conjunction with MO calculations, the emissive properties of pyridyl-phenanthroline platinum(II) complexes were rationalized from the difference in HOMO-LUMO gaps between the parent terpyridine (~10.2 eV), 4'-phenyl-terpyridine (~9.9 eV) and pyridyl-phenanthroline (9.5 eV) ligands.

However, several questions remained: why is the pyridyl-phenanthroline platinum(II) complex **169a** luminescent whereas the ruthenium analogue **147** is not? Why does the methyl regiochemistry affect MLCT absorption of the $Fe(pherpy)_2^{2+}$ complexes, but not the $Pt(pherpy)Cl^+$ emission? Moreover, why do the lifetimes

increase as the emission energy decreases? To account for these discrepancies, McMillin and coworkers pointed out that even though the lowest energy absorptions are clearly of MLCT nature, the emissive states need not be the same. The lifetimes and radiative rate constants (Table 4.1) necessitate an emissive triplet excited state involving a heavy metal center, but could involve intraligand excited-states. Vibrational structure within the emission spectra indicates significant $^3\pi$-π^* character and a mixed ^{3}d-$\pi^*/^3\pi$-π^* excited state[63-65] was proposed to account for the unusual photophysical properties of pyridyl-phenanthrolines.

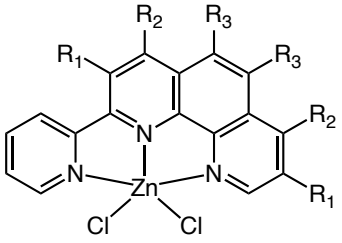

169a R_1 = H R_3 = H
169b R_1 = H R_3 = H
169c R_1 = H R_3 = Me
169d R_1 = Me R_3 = H
169e R_1 = Me R_3 = Me

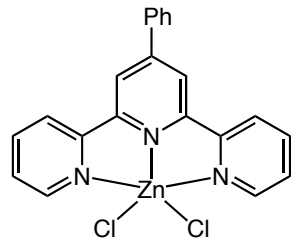

170

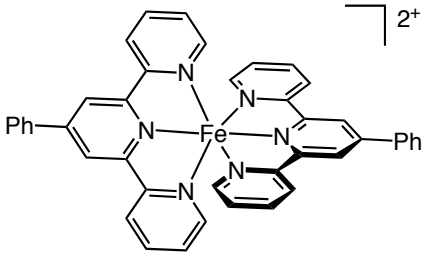

172

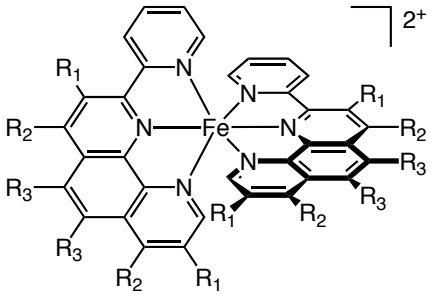

171a R_1 = H R_2 = H R_3 = H
171b R_1 = H R_2 = Me R_3 = H
171c R_1 = H R_2 = H R_3 = Me
171d R_1 = Me R_2 = Me R_3 = H
171e R_1 = Me R_2 = H R_3 = Me

At first glance, pyridyl-phenanthrolines are rigid, dissymmetric terpyridine analogues, but the few explorations into their coordination chemistry have revealed several important distinctions. The addition of an extra ethynylene bridge extends

conjugation and increases rigidity, resulting in a smaller HOMO-LUMO gap and weaker ligand field, respectively. A closer inspection reveals subtle but important differences in the nature and locations of the excited states (*Vida infra*). The influence of substituents depends on the orbital amplitude at the point of substitution,[66-68] and the difference between the two ligand families can result in very similar complexes with very different photophysical properties.[52]

4.2 Current Work

4.2.1 Introduction

In accordance with the goal of utilizing octahedral ML_2 complexes of 2-pyridyl-phenanthrolines as chiral building blocks for the templated synthesis of oriented links, we decided to prepare a range of pyridyl-phenanthroline metal complexes as model systems and to investigate their electrochemical and photophysical properties in comparison to the analogous terpyridine complexes.

4.2.2 Synthesis

Choosing 8-(4-methoxy-2,6-dimethyl-phenyl)-9-[5-(4-methoxy-2,6-dimethyl-phenyl)-pyridin-2-yl]-1,10-phenanthroline **115** as the model ligand, a wide range of different metal ions was chosen for complexation (Table 4.2). Conversion of **115** into its iron(II) complex **173** was achieved by reaction with ferrous sulfate in an acetone/water mixture.[69,70] For other first row transition metals, reaction of the metal acetate salts in methanol, methanol/water, and ethanol/water mixtures gave pyridyl-phenanthroline complexes **174** – **177** (Table 4.2).[71] Coordination of ligand **115** with ruthenium(II) to give **178** was achieved by reaction with $RuCl_2(DMSO)_4$ in refluxing ethylene glycol.[21,72] Reaction of **115** with osmium(IV) in a microwave reactor gave the

desired complex **179** as well as the mono demethylated product **180** in a 1:1 ratio (Scheme 4.3).[73,74]

Table 4.2 Synthesis of pyridyl-phenanthroline complexes.

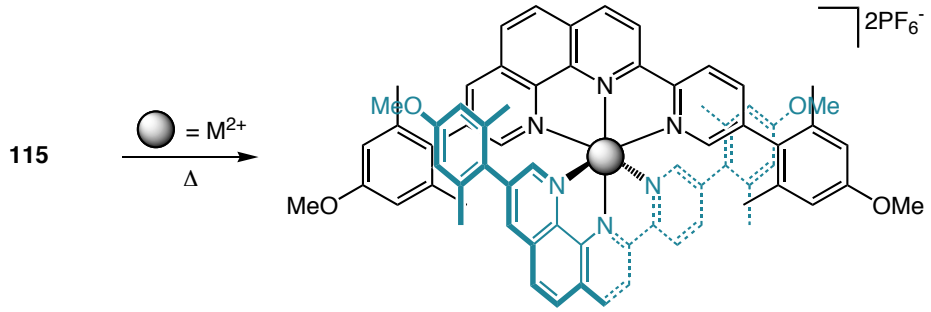

Ligand	Metal Salt	Solvent	Temperature	Time (hrs)	Product	Yield (%)
115	$FeSO_4$-$7H_2O$	Acetone/H_2O	55° C	1.5	**173**	90
115	$Co(OAc)_2$-$4H_2O$	MeOH	reflux	3	**174**	78
115	$Ni(OAc)_2$-$4H_2O$	EtOH/H_2O	75° C	overnight	**175**	88
115	$Cu(OAc)_2$-$1H_2O$	MeOH/H_2O	70° C	overnight	**176**	87
115	$Zn(OAc)_2$-$2H_2O$	MeOH	reflux	overnight	**177**	70
115	$RuCl_2(DMSO)_4$	Ethylene glycol	125° C	overnight	**178**	78
115	K_2OsCl_6	Ethylene glycol	225° C	10 min	**179**	28

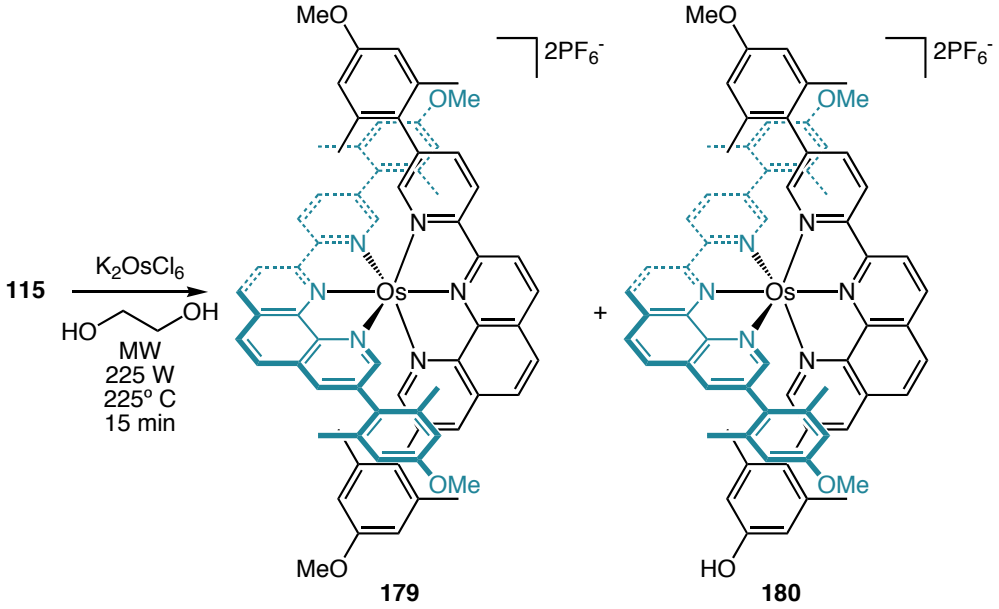

Scheme 4.3 Synthesis of bis- pyridyl-phenanthroline osmium(II) complex **179**.

The corresponding terpyridine complexes were also synthesized with 5,5”-(4-methoxy-2,6-dimethylphenyl)-2,2';6',2”-terpyridine **102** in similar yields (Table 4.3). Reaction with osmium(IV) in a microwave reactor again gave in a 1:1 mixture of the desired complex **187** as well as the mono demethylated product, which was removed by chromatography.

Aqueous workup of all resultant complexes with potassium hexafluorophosphate provided the complexes as the water insoluble hexafluorophosphate salts, simplifying isolation and suitable for photophysical work.[3] Subsequent cold diffusion of diethyl ether into acetonitrile solutions of the hexafluorophosphate salts yielded the complexes as crystalline materials.

Table 4.3 Synthesis of terpyridine complexes.

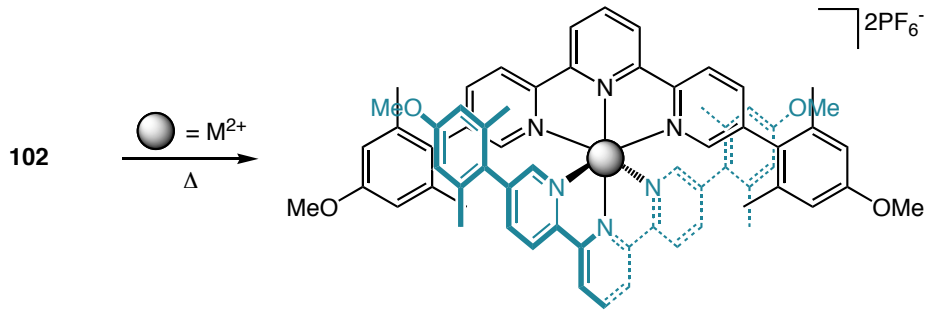

Ligand	Metal Salt	Solvent	Temperature	Time (hrs)	Product	Yield (%)
102	$FeSO_4$-$7H_2O$	Acetone/H_2O	55° C	overnight	**181**	92
102	$Co(OAc)_2$-$4H_2O$	MeOH	reflux	4	**182**	83
102	$Ni(OAc)_2$-$4H_2O$	EtOH/H_2O	75° C	5	**183**	83
102	$Cu(OAc)_2$-$1H_2O$	MeOH/H_2O	70° C	overnight	**184**	82
102	$Zn(OAc)_2$-$2H_2O$	MeOH	reflux	overnight	**185**	75
102	$RuCl_2(DMSO)_4$	Ethylene glycol	125° C	overnight	**186**	99
102	K_2OsCl_6	Ethylene glycol	190° C	15 min	**187**	25

Homoleptic ML_2 complexes of terpyridines containing 6,6”-bis aryl substituents are rare[75,76] due to steric reasons,[77,78] and Schmittel and coworkers have applied similar steric constraints to form heteroleptic copper and silver phenanthroline complexes

selectively.[79,80] Constable et. al. showed that introduction of phenyl substituents at both the 6, and 6' results in high-spin iron(II) complexes whereas a single phenyl substituent results in spin-crossover systems.[75] The sterically hindered pyridyl-phenanthroline **114**, containing a manisyl substituent alpha- to the pyridyl nitrogen, was chosen to further differentiate the phenanthroline and pyridine manisyl and facilitate chiral resolution of the ruthenium(II) complex.

Reaction of sterically-hindered pyridyl-phenanthrolines **114** with $RuCl_2(DMSO)_4$ in ethylene glycol for four hours gave the partially reacted complex **188** (Scheme 4.5). As expected, the ^{1}H-NMR spectrum of **188** is very complex due to the many possible constitutional, atropo- and stereo- isomers.[81] No further attempts were made to characterize the mixture and further heating for two days gave the final complexes **189** in good yields.[82]

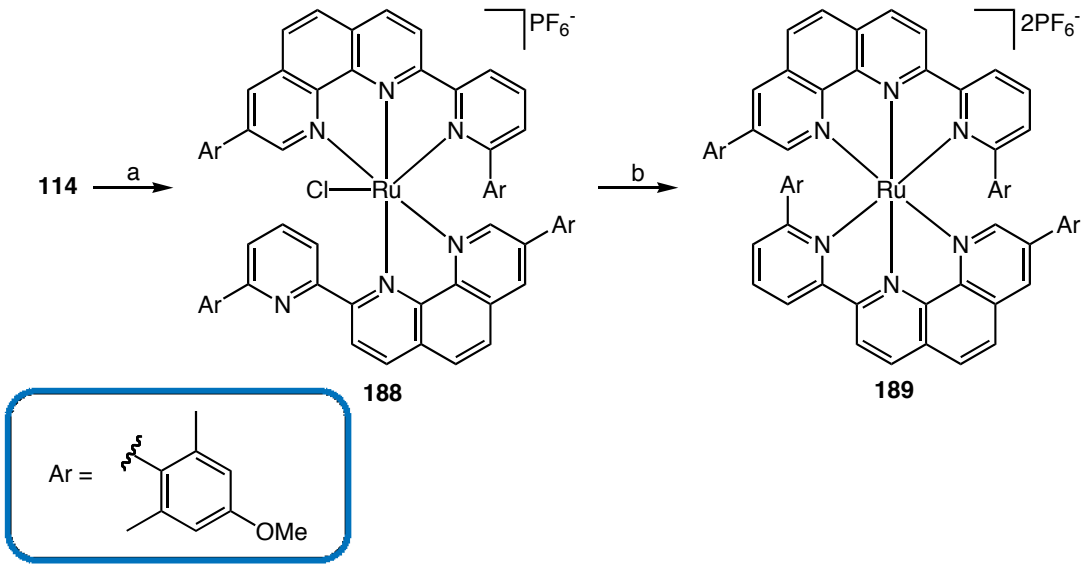

Scheme 4.4 Synthesis of bis- pyridyl-phenanthroline ruthenium(II) complex **189**. Reaction conditions: a) $RuCl_2(DMSO)_4$, ethylene glycol, 125° C, 4 h; b) ethylene glycol, 2 days.

Coordination of the novel, partially hindered, unsymmetrical terpyridine **190** with $RuCl_2(DMSO)_4$ to give **191** was clean and no intermediates were isolated (Scheme 4.5). Complex **191** possesses C_2 symmetry and is chiral.

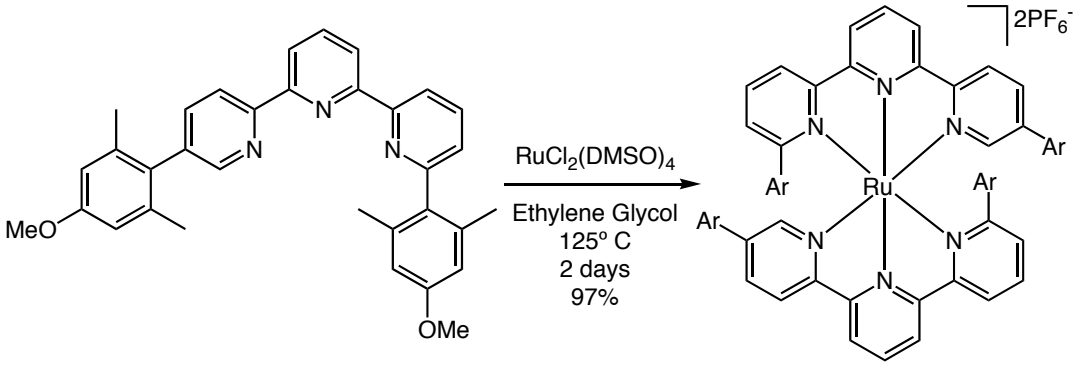

190 **191**

Scheme 4.5 Synthesis of the chiral, bis-manisyl –terpyridine ruthenium(II) complex **191**.

To aid in the resolution of pyridyl-phenanthroline complexes, ligand **115** was deprotected with molten pyrdine hydrochloride, giving pyridyl-phenanthroline **115b** in good yield (Scheme 4.6). Reaction of **115b** with $RuCl_2(DMSO)$ gives the tetra phenol ruthenium(II) complex **192**. Treatment of **192** with (-)-menthyl chloroformate results in diastereomeric complex **193** (Scheme 4.7).[83]

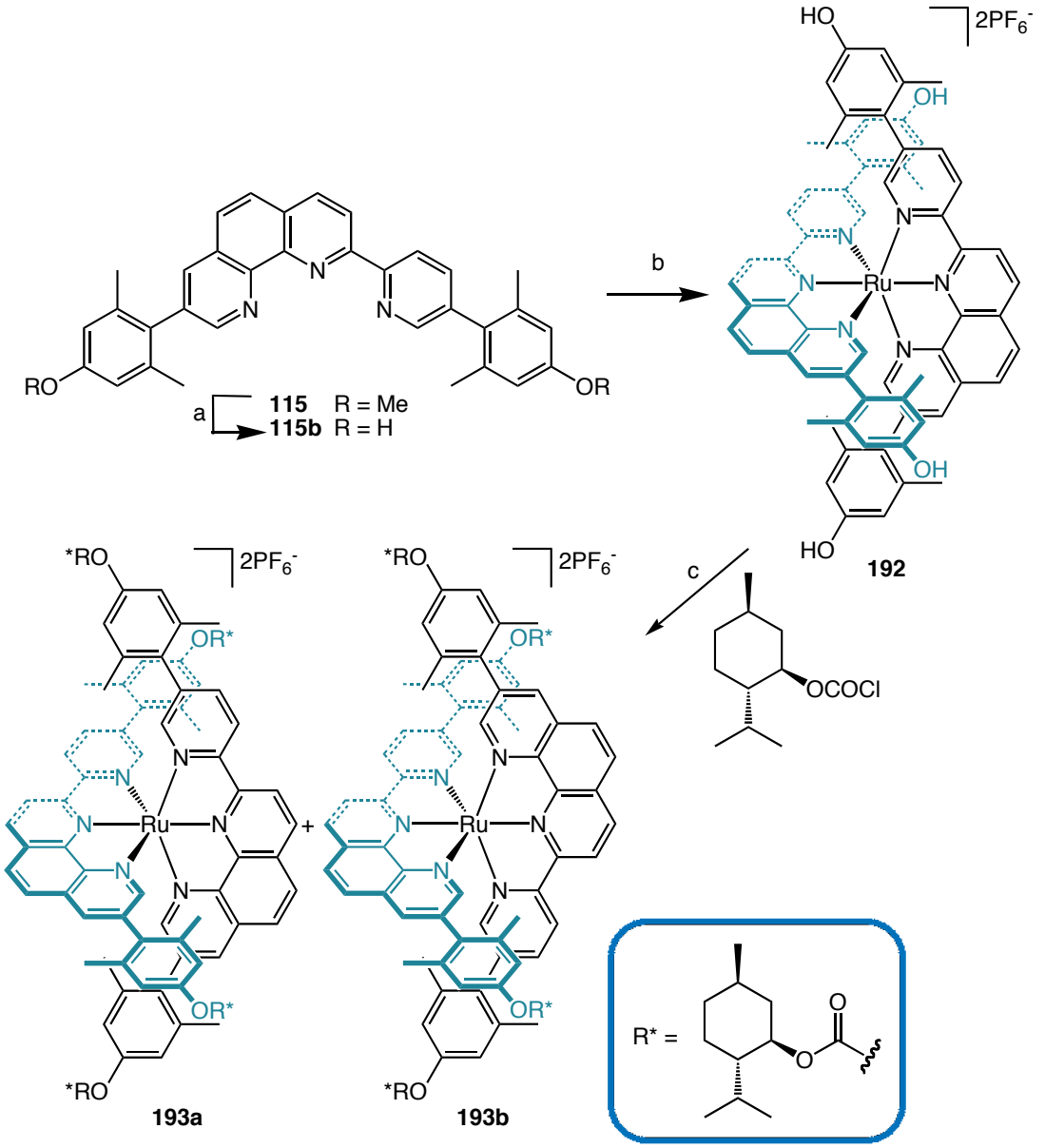

Scheme 4.7 Synthesis of diastereomeric (-)menthyl-formate pyridyl-phenanthroline ruthenium(II) complex **193**. Reaction conditions: a) pyridine-HCl, neat, 185 °C, 4h 90%; b) $RuCl_2(DMSO)_4$, ethylene glycol, 125 °C, 6 h, 70%; c) (-)-menthyl chloroformate, ACN, DIPEA, 78%.

4.2.3 Results and Discussion

Solid State Structures of $M(pherpy)_2$-$2PF_6$ and $M(terpy)_2$-$2PF_6$ complexes: Crystal structures of manisyl-substituted pyridyl-phenanthroline **173** – **179** and terpyridine complexes **181** – **187** were determined and detailed examination across the late first-row transition metals (Fe(II) – Zn(II)) and down the d^6 metals (Fe(II) – Os(II)) shows a remarkable interplay of ligand and metal. The structures of pyridyl-phenanthroline complexes **173** – **176**, **178**, and **179** are isomorphous and isostructural, possessing orthorhombic *Pcca* symmetry (Figure 4.7 and Table 4.4). The dication sits across a crystallographic two-fold axis, while the PF_6^- anion and an acetonitrile molecule are in general positions, giving a 1:2:2 dication : anion : solvent ratio. The structure of the Zn(II) complex **177** is monoclinic and belongs to the $P2_1/c$ space group; however the dimensions of the monoclinic unit cell are similar to those of the analogous structures. The dication does not possess any crystallographic symmetry and the asymmetric unit contains one entire dication, two disordered anions and three acetonitrile molecules.

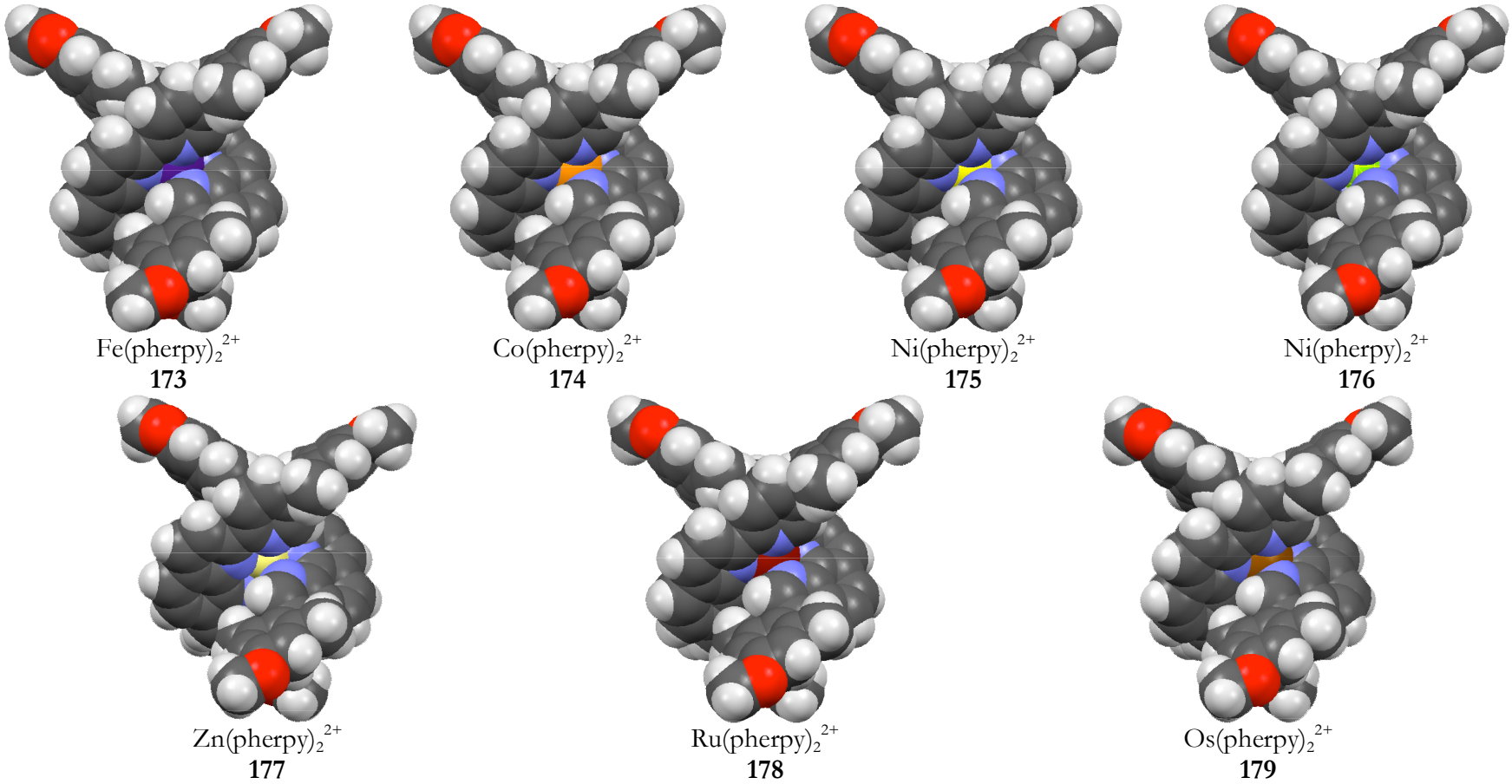

Figure 4.7 CPK representations of pyridyl-phenanthroline complexes **173 – 179** (from the crystal structures).[84]

Table 4.4 Crystallographic data for first row pyridyl-phenanthroline complexes **173 –179**.

	173	**174**	**175**	**176**	**177**	**178**	**179**
Formula	$Fe(pherpy)_2$-$2PF_6$-$2CH_3CN$	$Co(pherpy)_2$-$2PF_6$-$2CH_3CN$	$Ni(pherpy)_2$-$2PF_6$-$2CH_3CN$	$Cu(pherpy)_2$-$2PF_6$-$2CH_3CN$	$Zn(pherpy)_2$-$2PF_6$-$3CH_3CN$	$Ru(pherpy)_2$-$2PF_6$-$2CH_3CN$	$Os(pherpy)_2$-$2PF_6$-$2CH_3CN$
Formula weight	1479.17	1482.26	1482.03	1496.87	1474.46	1524.33	1613.53
Color	Purple	Orange-brown	Yellow	Lime-green	Light yellow	Red	Purple-brown
Crystal system	ortho-rhombic	ortho-rhombic	ortho-rhombic	ortho-rhombic	monoclinic	orthorhombic	orthorhombic
Space group	*Pcca*	*Pcca*	*Pcca*	*Pcca*	$P2_1/c$	*Pcca*	*Pcca*
Z	4	4	4	4	4	4	4
a [Å]	25.6038(5)	25.3072(4)	25.3094(4)	24.9866(3)	12.9177(1)	25.3777(5)	25.3861(5)
b [Å]	12.2125(2)	12.5642(1)	12.6402(2)	12.9263(2)	25.4666(3)	12.5601(3)	12.5157(3)
c [Å]	21.8379(3)	21.8238(3)	21.9538(3)	21.9263(3)	22.1526(3)	21.8678(4)	21.8136(4)
α [º]	90	90	90	90	90	90	90
β [º]	90	90	90	90	93.0097(8)	90	90
γ [º]	90	90	90	90	90	90	90
V[$Å^3$]	6828.4(2)	6939.2(2)	7023.4(2)	7081.9(2)	7277.5(1)	6970.3(3)	6930.7(2)

In all pyridyl-phenanthroline complexes, the metal dication is chelated by two terdentate ligands. The coordination geometry is pseudo-octahedral. The two central CH groups of the phenanthroline moiety are disordered over two sites, which effectively complete six-membered rings between all pyridine rings, so that the pyridine and phenanthroline moieties are essentially indistinguishable. This indicates that the ligand must be disordered through a 180° rotation about the central N-atom. Except for these two CH groups, all atoms in both conformations of the ligand occupy identical positions (within the resolution limit of X-ray diffraction), thus removing the need to model disorder for the entire ligand. The disordered CH groups are the only indication that the ligand lies in one direction in some molecules and in the opposite direction in other molecules. These two orientations are not present in equal quantities, there being a 68 – 76% occupation of the major conformation in the various crystal structures. As a result, the bond lengths and angles distinguishing the outer nitrogen atoms represent a weighted average of the two conformations (Table 4.5). As expected for terpyridine analogues, the central nitrogen-metal distances (M-N_2) are the shortest, and increase Fe(II) ~ Co(II) < Cu(II) < Ni(II) < Ru(II) ~ Os(II) < Zn(II), with distances of 1.878(3) Å and 2.045(6) Å for Fe(pherpy)$_2$-2PF$_6$ **173** and Zn(pherpy)$_2$-2PF$_6$ **177** respectively, and are comparable to similar terpyridine complexes.[2] The nitrogen-metal distances of the outer nitrogens (M-N_1 and M-N_3) are indistinguishable and no definitive comparison of the M-N_1 (pyridine) and M-N_3 (phenanthroline) distance can be made. The increase in metal ionic radius also affects the ligand bite angle (N_1-N_2-N_3), which plays a significant role in determining the topology of resultant supramolecular architectures.[69] The bite angles increase in the order of Fe(II) < Os(II) < Ru(II) < Co(II) ~ Ni(II) < Zn(II) ~ Cu(II) and range from N_1-N_2-N_3 = 103.9 ° and 110° for Fe(pherpy)$_2$-2PF$_6$ **173** and Cu(pherpy)$_2$-2PF$_6$ **176** respectively. The trend in

bite angle is supported by the distances between N_1 and N_3 as well as the distances between the oxygen atoms in the methoxy groups of the pendant manisyl groups (Table 4.5).

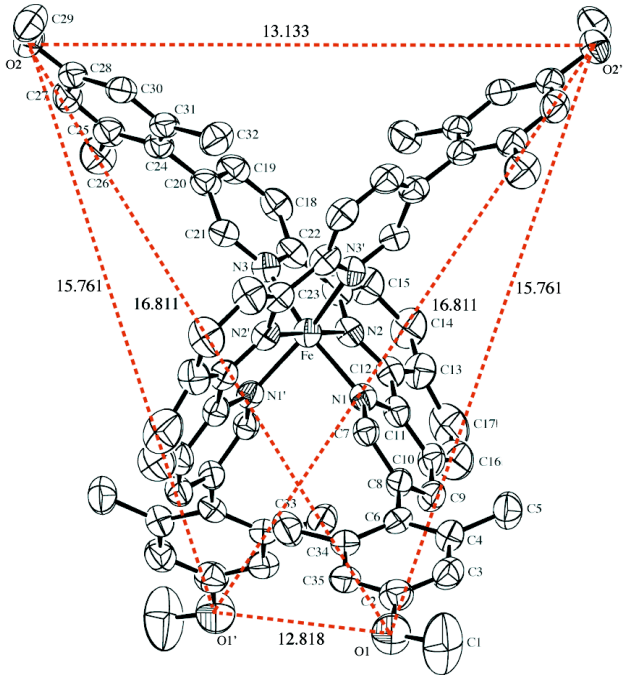

Figure 4.8 Ortep diagram of Fe(pherpy)$_2$-2PF$_6$ **173** showing the squeezing and spreading of manisyl groups.

Defining the plane of each ligand by the three nitrogens and central metal ion, the dihedral angle between the two planes, **Θ**, all pyridyl-phenanthroline complexes display similar deviations from the octahedral ideal of 90º (12º ± 1.0), and no particular Jahn-Teller effects are distinguishable.[42] The ligands of **173** – **176**, **178**, and **179** remain linear as indicated by the N2-M-N2' angles (~179º). Measuring the distances between the four terminal oxygens reveals that two manisyl groups of opposing ligands have been squeezed together whereas the other two manisyl groups have been further separated (Figure 4.8 and Table 4.5). One ligand of the Zn(II) complex **177** has slipped, as indicated by angle between the ligands, N_2-M-$N_{2'}$ = 171º, but is otherwise analogous..

Table 4.5 Selected bond lengths (Å) and angles (deg) of pyridyl-phenanthroline complexes **173 – 179**.

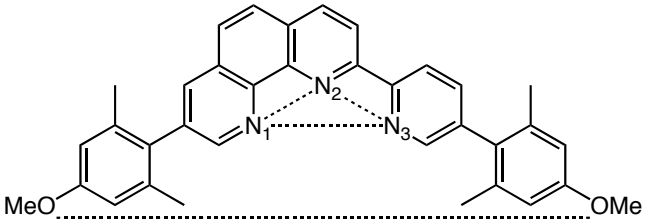

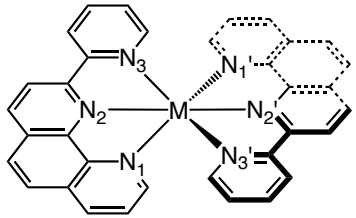

	173	**174**	**175**	**176**	**177**	**178**	**179**
Metal	Fe(II)	Co(II)	Ni(II)	Cu(II)	Zn(II)[a]	Ru(II)	Os(II)
Space group	*Pcca*	*Pcca*	*Pcca*	*Pcca*	$P2_1/c$	*Pcca*	*Pcca*
$M\text{-}N_1$	2.002(3)	2.086(3)	2.127(3)	2.186(3)	2.255(6)/2.196(5)	2.084(4)	2.077(7)
$M\text{-}N_2$	1.878(3)	1.879(3)	1.968(3)	1.937(3)	2.045(6)/2.032(5)	1.978(4)	1.980(6)
$M\text{-}N_3$	2.012(3)	2.105(3)	2.135(3)	2.198(3)	2.206(7)/2.211(5)	2.096(4)	2.088(7)
$N_1\text{-}M\text{-}N_3$[º]	161.2(1)	160.0(1)	156.6(1)	156.8(1)	152.8(2)/152.9(2)	157.4(2)	157.4(3)
$N_1\text{-}N_2\text{-}N_3$[º]	103.9	107.5	107.3	110.3	109.3/109.9	105.6	104.8
$N_1\text{-}N_3$	3.960	4.127	4.172	4.294	4.336/4.285	4.099	4.083
$O_1\text{-}O_2$	16.811	17.074	17.091	17.247	17.446/17.184	17.010	16.948
$O_1\text{-}O_1$'	12.848	12.574	12.502	12.293	12.558	12.521	12.541
$O_1\text{-}O_2$'	15.761	15.895	15.799	15.888	16.038	15.780	15.724
$O_2\text{-}O_1$'	15.761	15.895	15.799	15.888	15.347	15.780	15.724
$O_2\text{-}O_2$'	13.133	13.105	13.19	13.168	13.221	13.183	13.156
$N_2\text{-}M\text{-}N_2$'[º]	179.0(2)	179.2(2)	178.7(2)	179.1(1)	171.3(3)	179.3(2)	178.6(4)
Θ [º]	78.7	77.5	78.0	76.7	79.8	77.8	77.2

[a] The two ligands are non-equivalent.

The crystal packing provides some insight into the "flattening" of the octahedron. Taking Fe(pherpy)$_2$-2PF$_6$ **173** as the prototypical example, the dications align in a double helical strand, with a helical pitch of ~24.4 Å, along the crystallographic two-fold axis (Figure 4.9a). At first glance, it appears that the helices are propagated through π-π interactions of the manisyl groups, reminiscent of single and double helixes found in Ag^+ and Zn^{2+} terpyridine complexes,[85,86] but the centers of each ring are separated by ~4.9 Å, and the angle between the planes of each ring is ~24°. Closer examination reveals that above each manisyl ring, an aromatic hydrogen from the adjacent phenanthroline (or pyridine) is ~2.8 Å from the ring center, giving a total two interactions per strand of the double helix and four interactions per dication pair (Figure 4.9b). The intramolecular C-H···π interactions are responsible for the double helix formation and not any extended π-π interactions.[87]

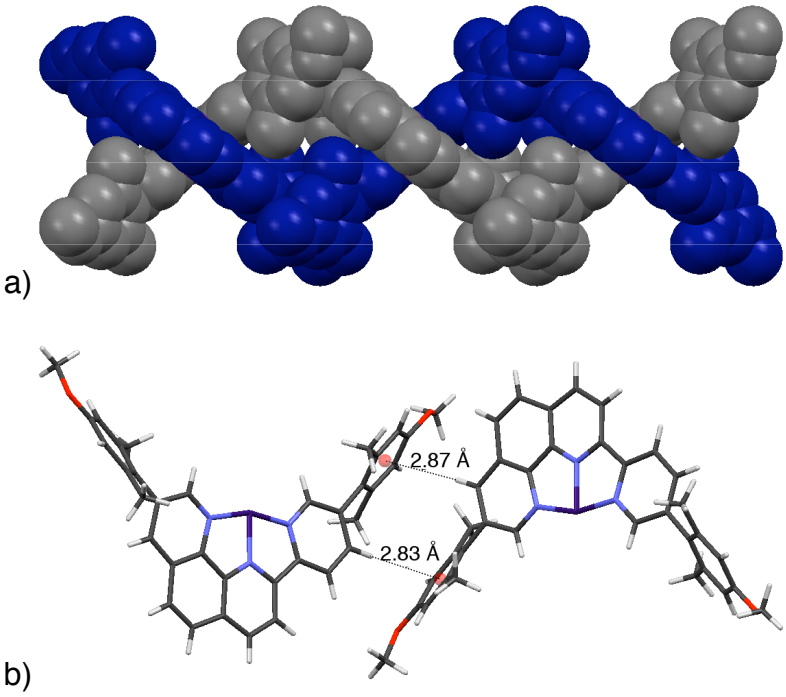

Figure 4.9 Crystal packing of Fe(pherpy)$_2$-2PF$_6$ **173** with a) the view perpendicular to the right-handed double helix and b) the view showing the intra-molecular π-stacking interactions between adjacent ligands within a single strand of the double helix.

Perpendicular to the helical axis, each dication also interacts with its neighbor in adjacent helices via offset face-face π-stacking interactions (Figure 4.10a). The manisyl groups are anti-parallel and separated by ~3.7 Å. A displacement angle of ~21° corresponds to a typical parallel displacement of ~1.3 Å (Figure 4.10b).[87]

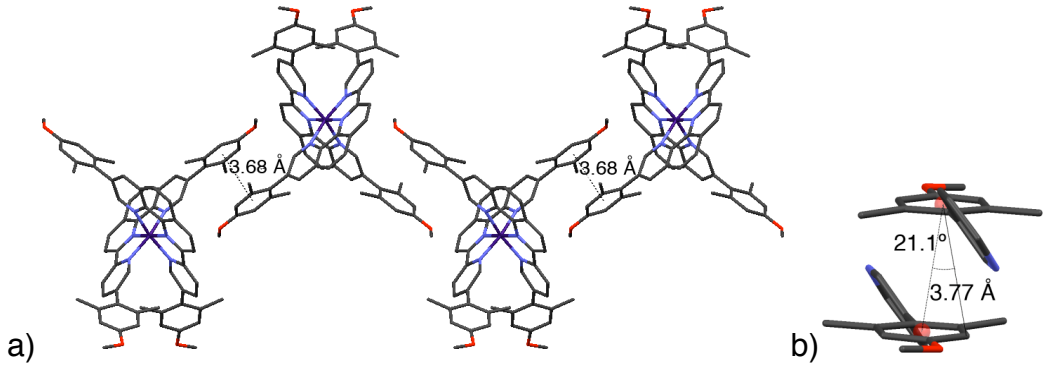

Figure 4.10 Crystal packing of Fe(pherpy)$_2$-2PF$_6$ **173** showing a) intra-strand π-stacking and b) close-up view showing offset.

The two motifs continue as 2-D sheets of interlocked double-helices (Figure 4.11). As a center of inversion exists between each helix, the helices arrange as alternating right- and left-helices (Figure 4.11a). Looking down the helical axis discloses that each sheet of helices is separated by a layer of seemingly disordered anions and solvent molecules (Figure 4.12a). Looking along the rows of double helical sheets reveals that adjacent dications in neighboring helices are related by another center of inversion. Though the acetonitrile molecules are disordered, they intercalate perfectly between manisyl groups of neighboring sheets (manisyl centroid-centroid distance ~6.9 Å), and thus propagate π-π stacking interactions between sheets (Figure 4.12b).

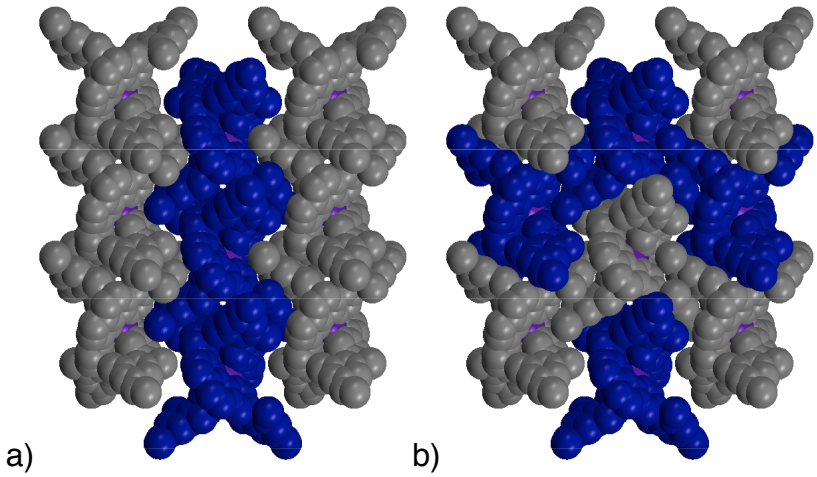

Figure 4.11 Crystal packing structure of Fe(pherpy)$_2$-2PF$_6$ **173** highlighting a) alternating double-helix strands and b) inter-strand interactions.

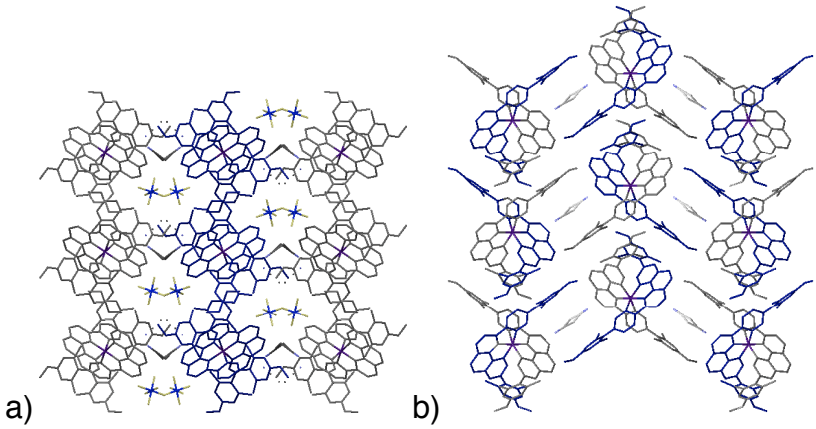

Figure 4.12 Crystal packing of Fe(pherpy)$_2$-2PF$_6$ **173** showing a) top- and b) side- views of double helix sheets.

Examination of the $Zn(pherpy)_2$-$2PF_6$ **177** crystal packing (space group $P2_1/c$) elucidates a similar lattice. The double helix motif is present (Figure 4.13a), but the manisyl groups are now closer together (~4.3 Å and ~4.7 Å) with angles of ~14° and ~20° between the planes of the rings. The intramolecular C-H···π distances have lengthened to ~3.3 Å (Figure 4.13b), lengthening the helical pitch, ~25.8 Å. The structural change is most likely due to the slipping of one non-equivalent pyridyl-phenanthroline ligand.

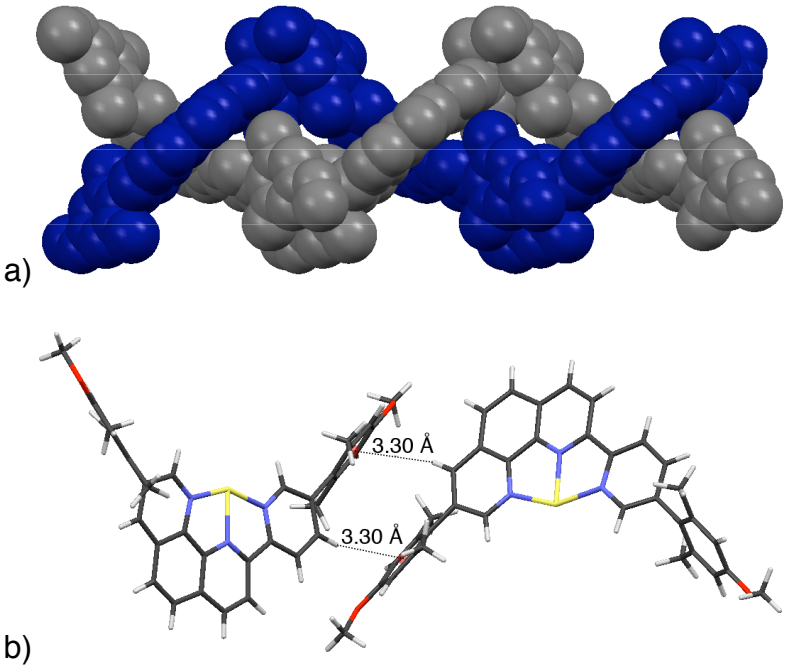

Figure 4.13 Crystal packing of $Zn(pherpy)_2$-$2PF_6$ **177** with a) the view perpendicular to the right-handed double helix and b) the view showing the intra-molecular π-stacking interactions between adjacent ligands within a single strand of the double helix.

Similar offset face-face π-stacking interactions exist between dications of neighboring helices(Figure 4.14a). The manisyl groups are anti-parallel, separated by ~3.8 Å, and parallel displaced ~1.3 Å (Figure 4.14b).

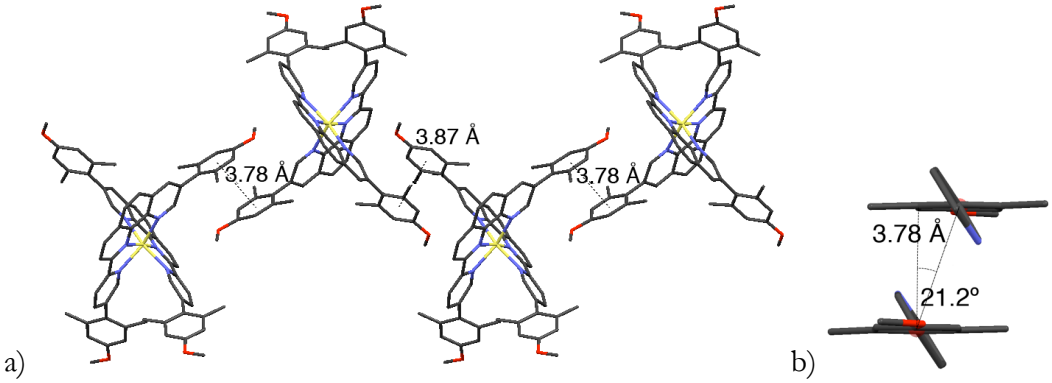

a) b)

Figure 4.14 Crystal packing of Zn(pherpy) $_2$-2PF$_6$ **177**; a)intra-strand π-stacking and b) close-up view showing offset.

The crystal lattice of Zn(pherpy)$_2$-2PF$_6$ **177** is similar to that of Fe(pherpy)$_2$-2PF$_6$ **173** and consists of sheets of interlocked double helices, but is slightly tilted due to the different space group (Figure 4.15). The helices arrange into alternating right- and left-helices (Figure 4.15a) that interact through π-stacking of the manisyl groups (Figure 4.15b). Each sheet of helices is separated by a similar (but not identical) layer of disordered anions and solvent molecules (Figure 4.16a) The acetonitrile molecules again intercalate perfectly between manisyl groups of neighboring double-helix sheets (manisyl centroid-centroid distance ~6.9 Å), and propagate π-π stacking interactions between sheets (Figure 4.16b).

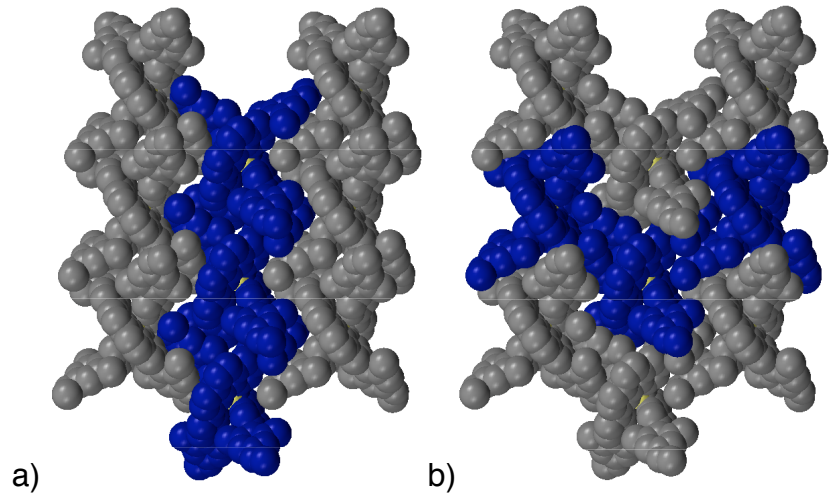

Figure 4.15 Crystal packing structure of Zn(pherpy)$_2$-2PF$_6$ **177** highlighting a) alternating double-helix strands and b) inter-strand interactions.

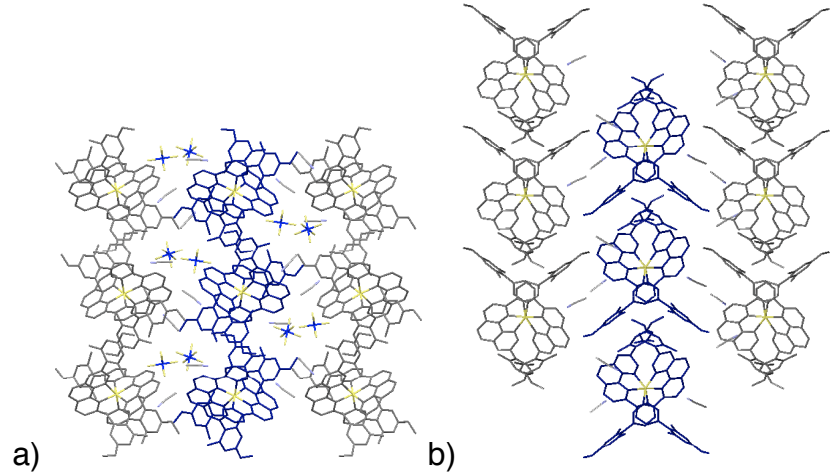

Figure 4.16 Crystal packing of Zn(pherpy)$_2$-2PF$_6$ **177** showing a) top- and b) side- views of double helix sheets.

Similar to the pyridyl-phenanthrolines, the solid-state structures of the manisyl substituted terpyridine complexes **181** – **187** partition into two isomorphous and isostructural groups (Figure 4.17 and Table 4.6). Terpyridine complexes **181**, **182**, **186**, and **187** are monoclinic and belong to space group C2/*c*. The dication sits across a crystallographic two-fold axis, while the anion is in a general position, thereby giving the required 1:2 dication : anion ratio. There are also three acetonitrile molecules in general positions, which lead to a 1:6 dication : acetonitrile ratio. The structures of terpyridine complexes **183** – **185** are orthorhombic and belong to space group *Pnna*. There are two symmetry-independent dications in each structure that sit across crystallographic two-fold axis. There are two symmetry-independent disordered PF_6^- anions in general positions, as well as six different sites for partially occupied and disordered acetonitrile molecules. Each dication is also slightly disordered. In one of the symmetry-independent dications, one methoxy group in each ligand is disordered by rotating the O–Me group about the C–OMe bond through about 180°. This results in slight disorder for the entire manisyl group to which the methoxy group is attached. In the second dication, the methoxy group and its parent manisyl group are similarly disordered, although the O–Me group in each conformation points in roughly the same direction, instead of being flipped by 180°. In each case, the major conformation exists in approximately 63 – 65% of the dications.

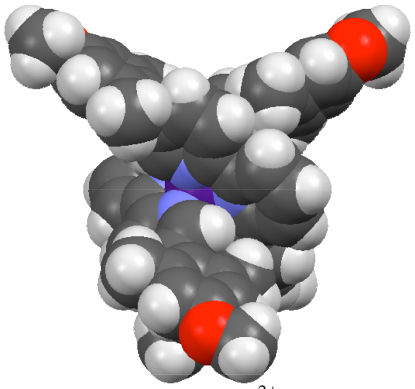

$Fe(terpy)_2^{2+}$
181

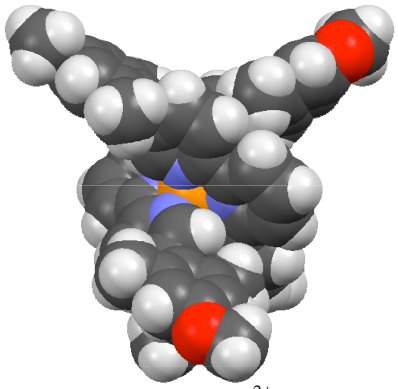

$Co(terpy)_2^{2+}$
182

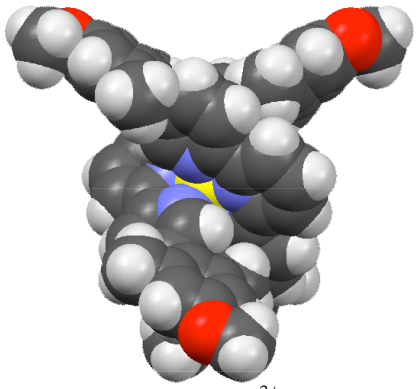

$Ni(terpy)_2^{2+}$
183

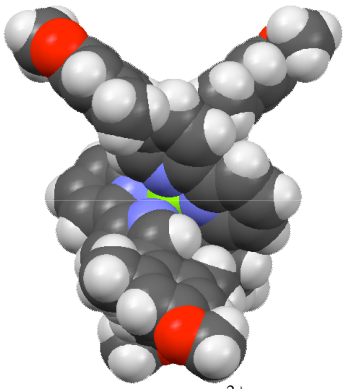

$Cu(terpy)_2^{2+}$
184

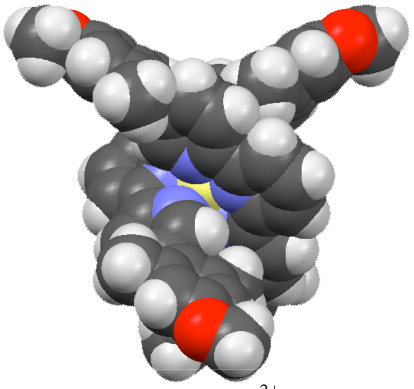

$Zn(terpy)_2^{2+}$
185

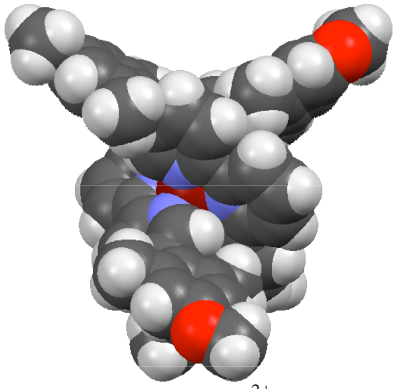

$Ru(terpy)_2^{2+}$
186

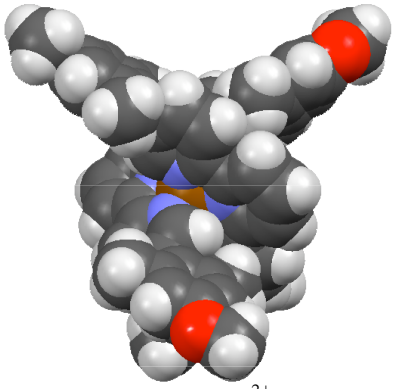

$Os(terpy)_2^{2+}$
187

Figure 4.17 CPK representations of terpyridine complexes **181 – 187** (from the crystal structures).[88]

Table 4.6 Crystallographic data of terpyridine complexes **36 – 40**.

	181	**182**	**183**	**184**	**185**	**186**	**187**
Formula	$Fe(terpy)_2$-$2PF_6$-$6CH_3CN$	$Co(terpy)_2$-$2PF_6$-$6CH_3CN$	$Ni(terpy)_2$-$2PF_6$-$3CH_3CN$	$Cu(terpy)_2$-$2PF_6$-$2.5CH_3CN$	$Zn(terpy)_2$-$2PF_6$-$2.82CH_3CN$	$Ru(terpy)_2$-$2PF_6$-$6CH_3CN$	$Os(terpy)_2$-$2PF_6$-$6CH_3CN$
Formula Weight	1595.33	1598.43	1475.04	1459.35	1474.46	1640.49	1729.69
Crystal system	monoclinic	monoclinic	ortho-rhombic	ortho-rhombic	ortho-rhombic	Red	Brown
Color	Purple	Orange-brown	Orange	Green	Colorless	monoclinic	monoclinic
Space Group	C2/*c*	C2/*c*	*Pnna*	*Pnna*	*Pnna*	C2/*c*	C2/*c*
Z	4	4	8	8	8	4	4
a [Å]	29.749(1)	29.5268(4)	22.0069(3)	22.0072(3)	22.0637(2)	29.4883(4)	29.4529(4)
b [Å]	11.4106(4)	11.7893(3)	25.2020(5)	24.9787(4)	25.1063(4)	11.8087(1)	11.8271(1)
c [Å]	22.7396(6)	22.4187(5)	24.8731(3)	25.1014(3)	25.1199(4)	22.4060(3)	22.4142(2)
α [º]	90	90	90	90	90	90	90
β [º]	90.062(2)	90.847(2)	90	90	90	90.9353(6)	90.9746(7)
γ [º]	90	90	90	90	90	90	90
V[$Å^3$]	7719.1(4)	7803.1(3)	13795.1(4)	13798.5(3)	13914.9(3)	7801.1(2)	7806.7(1)

The central nitrogen-metal distances (M-N_2) are the shortest, and increase Fe(II) ~ Co(II) < Cu(II) ~ Ru(II) < Ni(II) < Os(II) < Zn(II), with distances of 1.878 Å and 2.074 Å for Fe(terpy)$_2$-2PF_6 **181** and Zn(terpy)$_2$-2PF_6 **185** respectively, and are comparable to pyridyl-phenanthroline complexes (*Vida infra*) and other terpyridine complexes (Table 4.7).[2] The nitrogen-metal distances of the outer nitrogens (M-N_1 and M-N_3) are almost indistinguishable and indicate that any Jahn-Teller distortion is minor. The increase in metal ionic radius also affects the ligand bite angle (N_1-N_2-N_3).[69] The bite angles increase in the order of Fe(II) < Ru(II) ~ Os(II) < Co(II) < Ni(II) < Zn(II) < Cu(II) and range from N_1-N_2-N_3 = 102.2 ° to 108.9° for Fe(terpy)$_2$-2PF_6 **181** and Cu(terpy)$_2$-2PF_6 **184** respectively. The distances between N_1 and N_3, as well as the distances between the oxygen atoms in the methoxy groups of the pendant manisyl groups, corroborate the trend in bite angle (Table 4.7).

Defining the plane of each ligand by the three nitrogens and central metal ion, the dihedral angle between the two planes, **Θ**, all terpyridine complexes display similar deviations from the octahedral ideal of 90º (11.2º ± 0.9). The ligands of **181**, **182**, **186** and **187**, however, remain linear as indicated by the N_2-M-N_2' angles (~179º). The two independent dications of complexes **183** – **185** display dissimilar deviations. In the second dication (designated by * in Table 4.6), one ligand has slipped and the complex is no longer linear, as indicated by angle between the ligands, N_2-M-$N_{2'}$ = 175.1 – 176.9º. The effect is most pronounced in the Zn(terpy)$_2$-2PF_6 complex **185**, but is not as significant as the Zn(pherpy)$_2$-2PF_6 complex **177**. Again, two manisyl groups of opposing ligands have been squeezed together whereas the other two manisyl groups have been pushed apart (Figure 4.18 and Table 4.7).

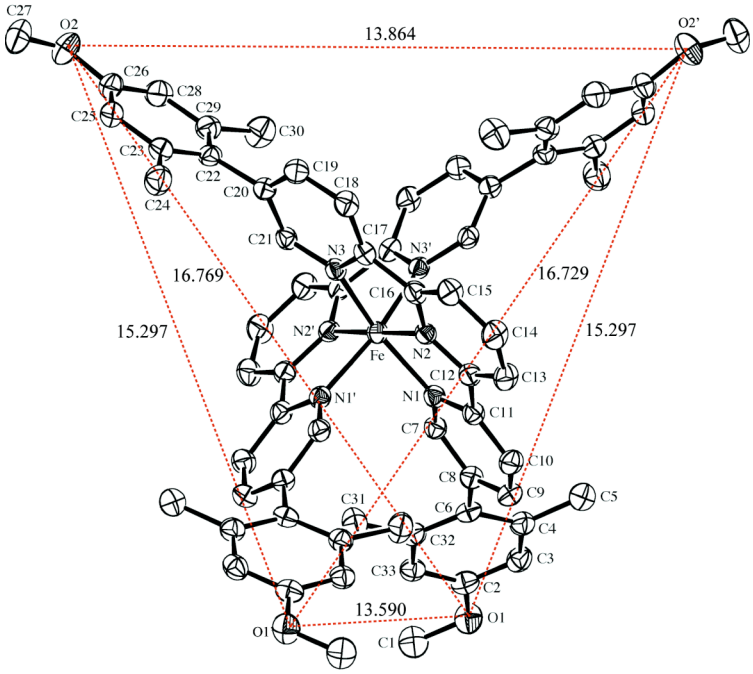

Figure 4.18 Ortep diagram of Fe(terpy)$_2$-2PF_6 **181** showing the squeezing and spreading of manisyl groups.

Table 4.7 Selected bond distances (Å) and angles (deg) of terpyridine complexes **181** – **187**.

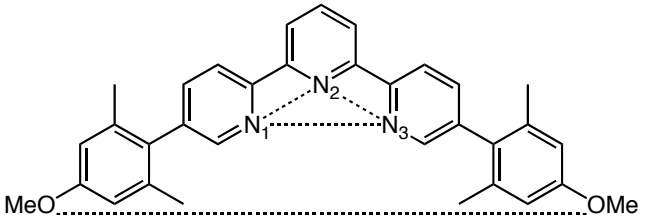

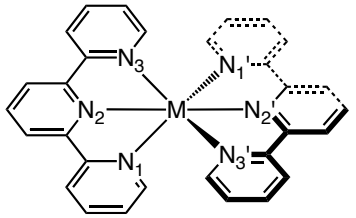

	181	**182**	**183**	**183***	**184**	**184***	**185**	**185***	**186**	**187**
Metal	Fe(II)	Co(II)	Ni(II)		Cu(II)		Zn(II)		Ru(II)	Os(II)
Point group	C2/c	C2/c	Pnna		Pnna		Pnna		C2/c	C2/c
$M-N_1$	1.971(2)	2.063(2)	2.122(3)	2.107(3)	2.167(4)	2.161(4)	2.186(4)	2.159(4)	2.060(2)	1.984(2)
$M-N_2$	1.878(2)	1.882(2)	1.983(3)	1.995(3)	1.964(4)	1.975(4)	2.061(4)	2.074(4)	1.972(2)	2.058(2)
$M-N_3$	1.975(2)	2.057(2)	2.113(3)	2.114(3)	2.177(4)	2.159(4)	2.170(4)	2.183(4)	2.060(2)	2.062(2)
N_1-M-N_3[º]	162.12(8)	160.92(9)	156.3(1)	156.3(1)	156.2(2)	155.8(2)	152.3(2)	151.7(2)	158.73º(6)	157.94º(9)
$N_1-N_2-N_3$[º]	102.24	105.65	106.36	105.8	108.85	108.41	107.71	107.45	103.63	103.65
N_1-N_3	3.898	4.063	4.146	4.131	4.251	4.223	4.230	4.120	4.049	4.044
O_1-O_2	16.769	16.952	17.501	17.037	17.587	16.957	17.495	16.978	16.947	16.83
O_1-O_1'	13.590	13.465	12.379	12.858	13.724	13.718	13.776	12.928	13.505	13.516
O_1-O_2'	15.297	15.405	15.644	15.566	15.717	15.491	15.529	15.434	15.343	15.341
O_2-O_1'	15.297	15.405	15.644	15.566	15.717	15.491	15.529	15.553	15.343	15.341
O_2-O_2'	13.864	13.769	13.362	13.563	12.244	12.808	12.330	13.324	13.682	13.618
N_2-M-N_2'[º]	179.8(1)	179.4(1)	178.7(2)	176.9(2)	178.6(2)	176.2(2)	177.9(2)	175.1(2)	179.34º(9)	179.4º(1)
Θ [º]	80.4	78.7	79.6	78.4	79.0	77.1	79.1	78.0	78.9	78.7

Taking Fe(terpy)$_2$-2PF$_6$ **181** as the prototypical example of terpyridine complexes with C2/*c* space group, the dications again align in a double helix, with a helical pitch of ~22.8 Å (Figure 4.19a). The manisyl groups are ~5.1 Å apart with angles of ~20º between the planes of the rings. Each ligand along a helix strand, interactions with the next ligand via intramolecular C-H···π distances of ~2.5 and ~2.7 Å giving a total four interactions per dication pair (Figure 4.19b).

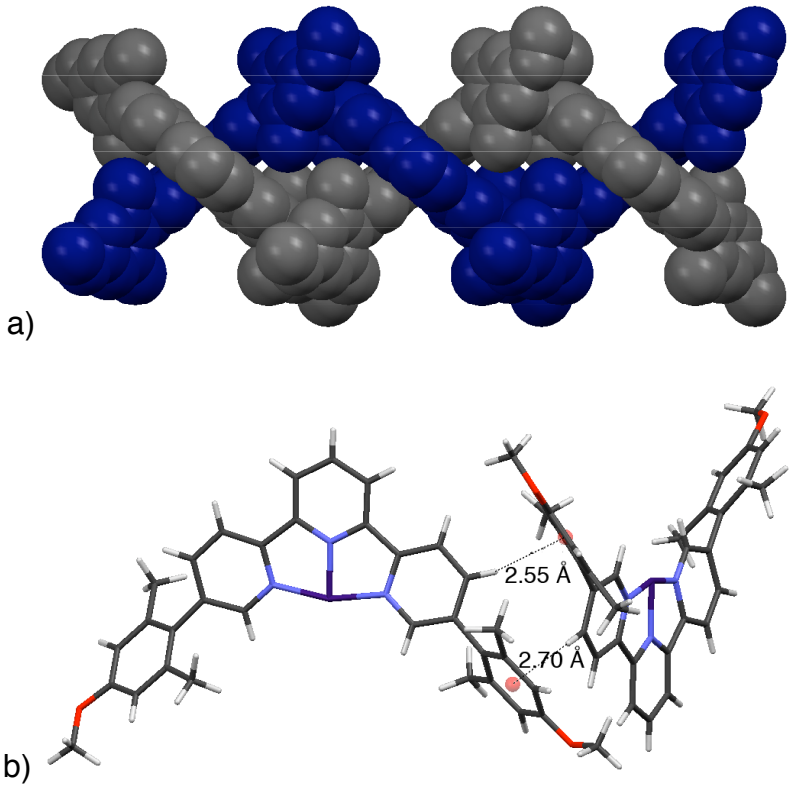

Figure 4.19 Crystal packing of Fe(terpy)$_2$-2PF$_6$ **181** showing a) the view perpendicular to the right-handed double helix and b) the view showing the intra-molecular π-stacking interactions between adjacent ligands within a single strand of the double helix.

Similar offset face-face π-stacking interactions exist between dications of neighboring helices (Figure 4.20a). The manisyl groups are anti-parallel, separated by ~3.5 Å, and parallel displaced ~1.3 Å (Figure 4.20b).

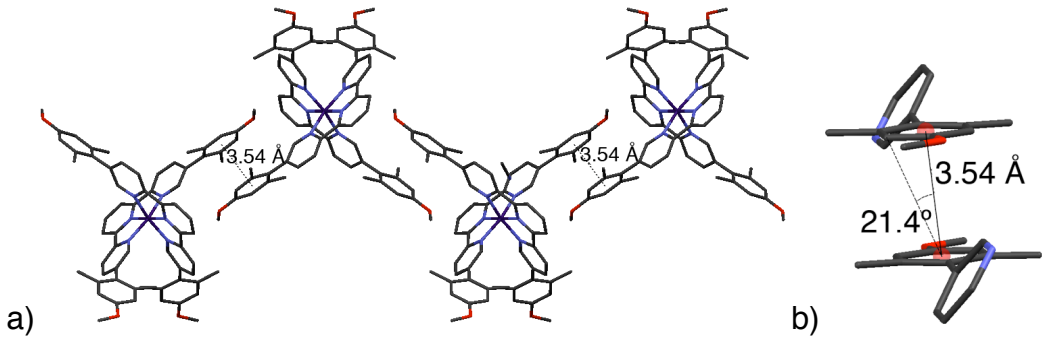

Figure 4.20 Crystal packing of Fe(terpy) $_2$-2PF$_6$ **181** showing a) intra-strand π-stacking and b) close-up view showing offset.

The crystal lattice of Fe(pherpy)$_2$-2PF$_6$ **181** is similar to that of Fe(pherpy)$_2$-2PF$_6$ **173** and consists of sheets of interlocked double-helices (Figure 4.21). The helices arrange as alternating right- and left-helixes (Figure 4.21a) that interact through π-stacking of the manisyl groups (Figure 4.21b). Each sheet of helices is separated by a thick layer of disordered anions and solvent molecules (Figure 4.22a). However, the acetonitrile molecules do not intercalate between neighboring double helix and unlike the pyridyl-phenanthroline complexes, the helices of neighboring sheets now exhibit the same handedness (Figure 4.22b).

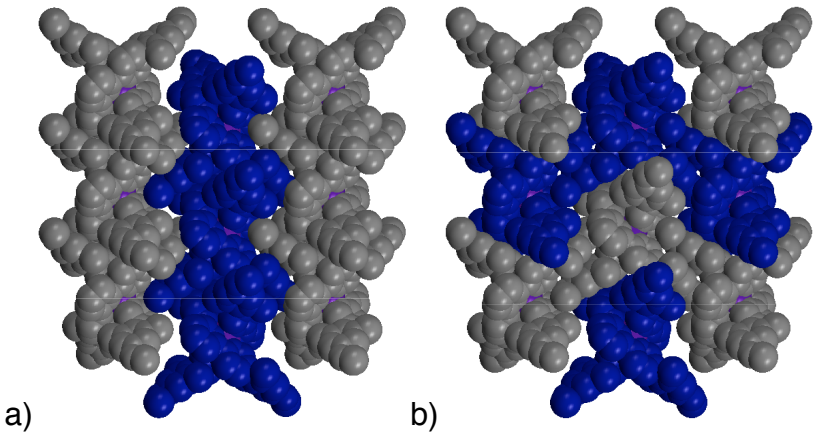

Figure 4.21 Crystal packing structure of Fe(terpy)$_2$-2PF$_6$ **181** highlighting a) alternating double-helix strands and b) inter-strand interactions.

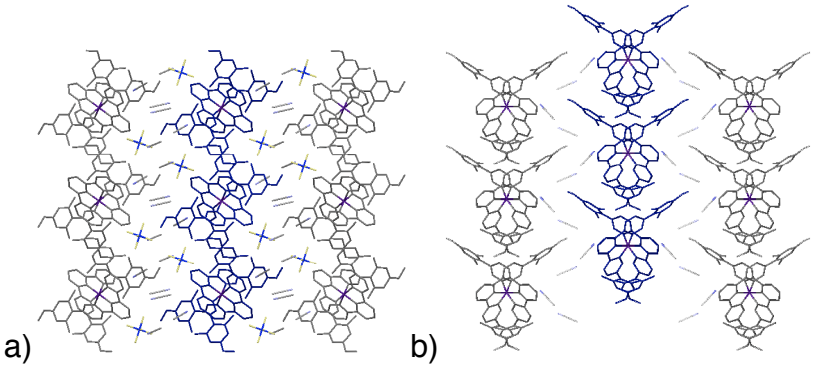

Figure 4.22 Crystal packing of Fe(terpy) $_2$-2PF$_6$ **181** showing a) top- and b) side- views of double helix sheets.

Exemplifying terpyridine complexes with space group *Pnna*, the dications of Zn(terpy)$_2$-2PF$_6$ **185** also align in double helices, with a helical pitch of ~25.1 Å (Figure 4.23a). Similar to pyridyl-phenanthrolines, the manisyl groups of the Zn(II) terpyridine complex are closer (~4.1 Å) than the corresponding Fe(II) complex (~5.1 Å) but maintain angles of ~20º between the planes of the rings. Each ligand along a helix strand, interactions with the next ligand via intramolecular C-H $\cdots\pi$ interactions of ~2.6 and ~2.7 Å (Figure 4.23b).

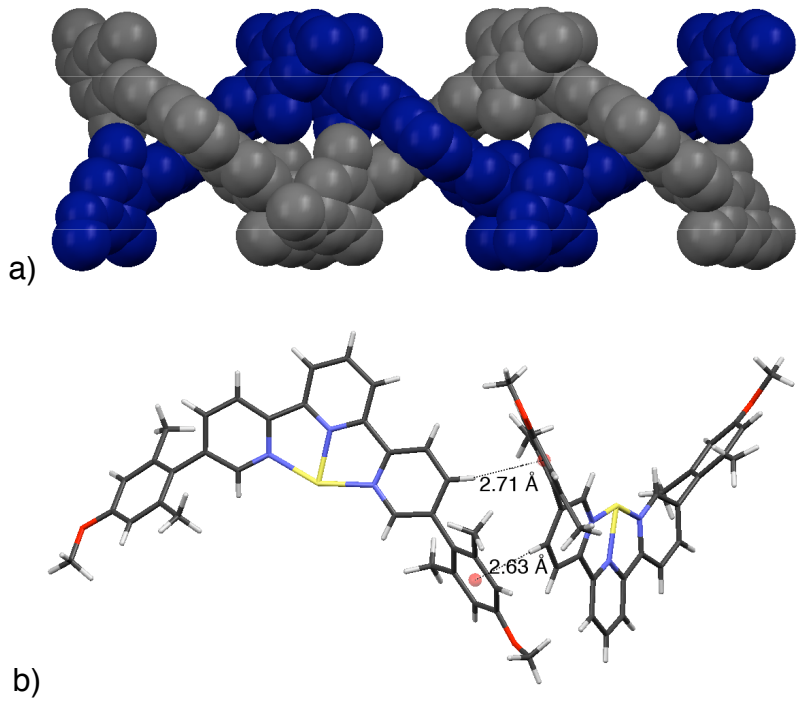

Figure 4.23 Crystal packing of Zn(terpy) $_2$-2PF$_6$ **185** showing a) the view perpendicular to the right-handed double helix and b) the view showing the intra-molecular π-stacking interactions between adjacent ligands within a single strand of the double helix.

Within the unit cell, the two independent dications interact via offset face-face π-stacking (Figure 4.24a). The manisyl groups are anti-parallel, separated by ~3.7 Å, and parallel displaced ~1.3 Å (Figure 4.24b). This interaction continues perpendicular to the helical axis and between each helix.

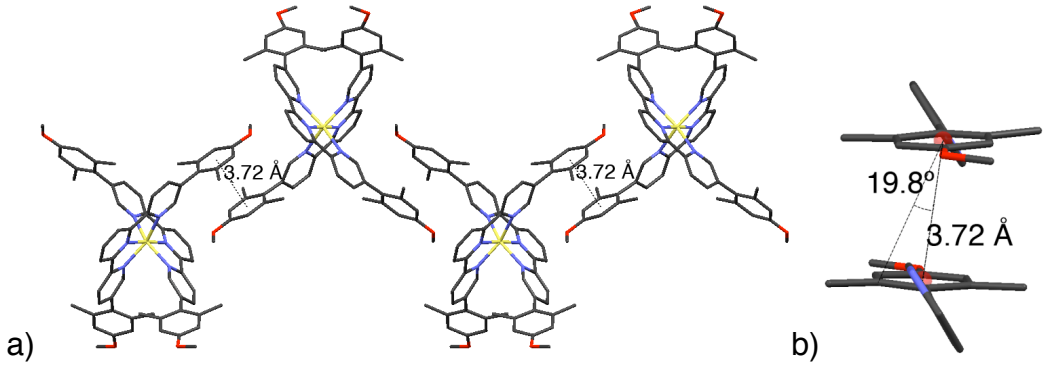

Figure 4.24 Crystal packing of Zn(terpy) $_2$-2PF$_6$ **185** showing a)π-stacking of independent dications in the unit cell and b) close-up view showing offset.

The crystal lattice of $Zn(terpy)_2$-$2PF_6$ **185** again consists of sheets of interlocked double-helices (Figure 4.25). The individual helices arrange into alternating right- and left-helixes (Figure 4.26a) and layers of disordered anions and solvent molecules separate sheets of helices (Figure 4.26a). Unlike the $Fe(terpy)_2$-2-PF_6 **181**, $Zn(terpy)_2$-$2PF_6$ **185** lattice resembles the pyridyl-phenanthrolines and acetonitrile molecules again intercalate perfectly between manisyl groups of neighboring double-helix sheets (manisyl centroid-centroid distance ~7.2 Å) (Figure 4.26b).

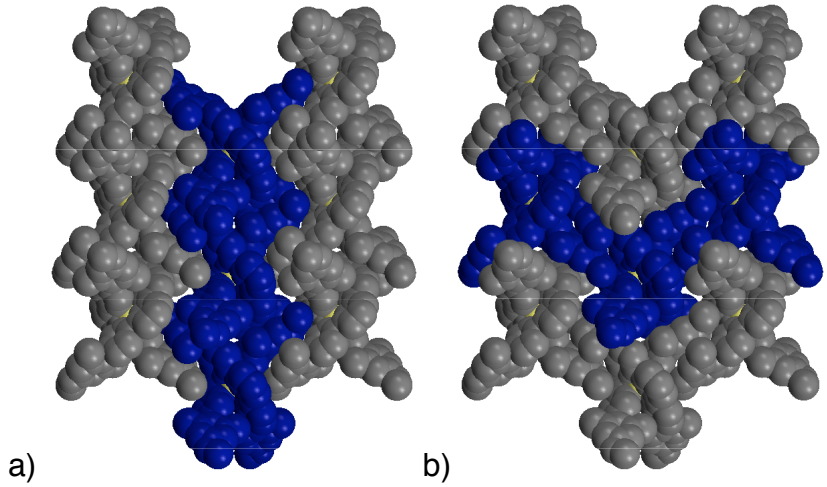

Figure 4.25 Crystal packing structure of $Zn(terpy)_2$-$2PF_6$ **185** highlighting a) alternating double-helix strands and b) inter-strand interactions.

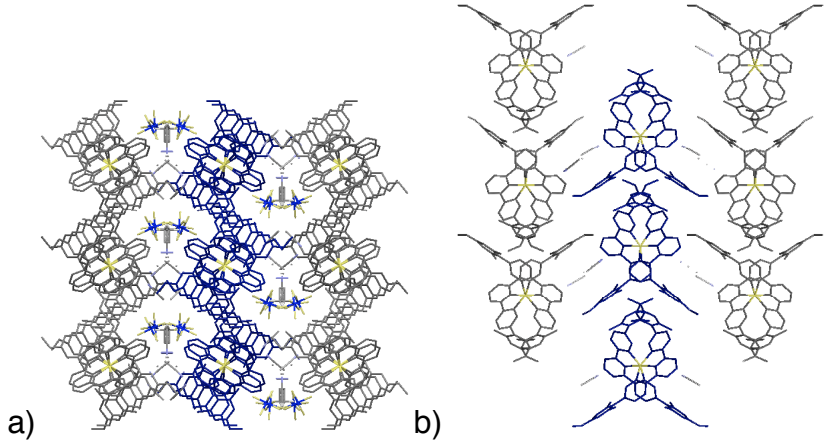

Figure 4.26 Crystal packing of $Zn(terpy)_2$-$2PF_6$ **185** showing a) top- and b) side- views of double helix sheets.

To understand the role of the solvent in the crystal lattice formation better, crystals of $Fe(pherpy)_2$-$2PF_6$ **173** and $Fe(terpy)_2$-$2PF_6$ **181** were grown from methylene chloride and the structures determined. The crystal lattice of **173** is solvent free whereas **181** contains one disordered water molecule. The unit cell volumes are reduced accordingly (Table 4.8). Even though the space group of both systems changed to *Pbcn*, the overall conformations, angles, and distances within each dication are almost the same as in the acetonitrile solvated analogue. One of the pyridyl-phenanthroline ligands of **173** is again disordered but now there is an 85% occupation of the major conformation

Table 4.8 Crystal data of "solvent-free" iron(II) pyridyl-phenanthroline and terpyridine complexes **173** and **181**.

	173	**181**
Formula	$Fe(pherpy)_2$-$2PF_6$	$Fe(terpy)_2$-$2PF_6$-H_2O
Formula Weight	1397.06	1367.04
Solvent	CH_2Cl_2/Et_2O	CH_2Cl_2/benzene
Crystal system	orthorhombic	orthorhombic
Color	Purple	Purple
Space Group	*Pbcn*	*Pbcn*
Z	4	4
a [Å]	23.8915(5)	23.3906(5)
b [Å]	11.6189(3)	11.4829(2)
c [Å]	23.1604(5)	23.2945(6)
α [º]	90	90
β [º]	90	90
γ [º]	90	90
V[Å^3]	6429.2(3)	6256.7(2)

The overall crystal packing of each dication is nearly identical to the solvated crystal. As expected, the dications align in sheets of alternating right- and left-handed helices (Figures 4.27a and 4.28a) and interlock through π-stacking of the manisyl groups (Figure 4.27b and Figure 4.28b). However, in the absence of acetonitrile, there are no

interactions between the sheets, and they compress into a staggered conformation, with each helix aligned in the same direction as its counterpart in the neighboring sheet (Figure 4.27 and 4.28).

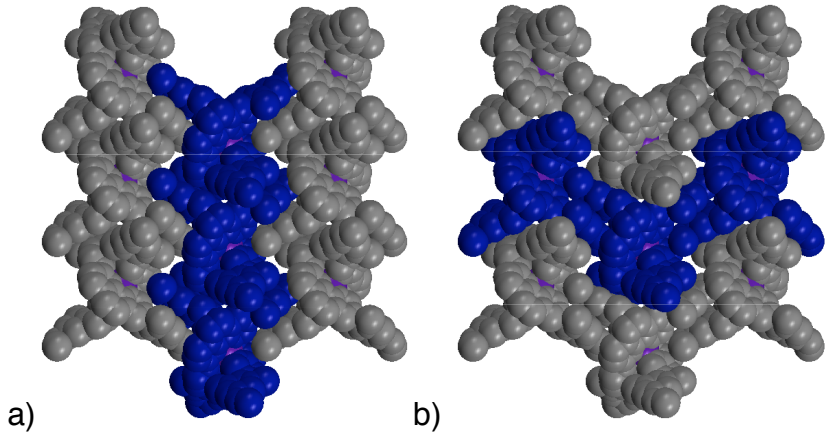

Figure 4.27 Crystal packing of non-solvated $Fe(pherpy)_2$-$2PF_6$ **173** highlighting a)alternating double helix strands and b) intra-strand π-stacking.

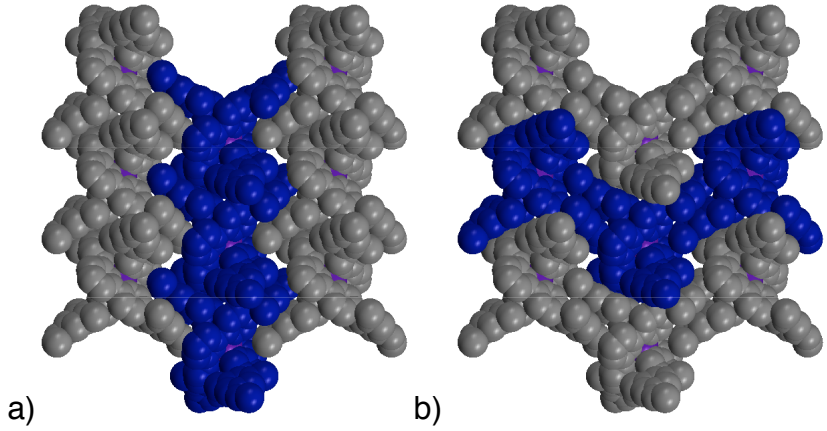

Figure 4.28 Crystal packing of non-solvated $Fe(terpy)_2$-$2PF_6$-H_2O **181** highlighting a) alternating double helix strands and b) intra-strand π-stacking.

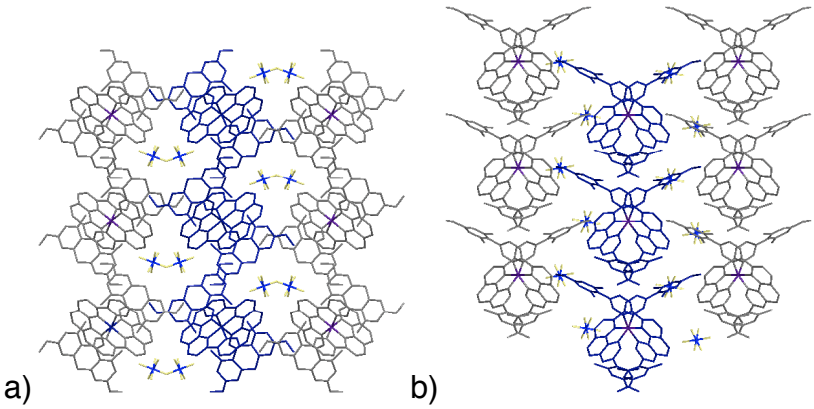

Figure 4.29 Crystal packing of non-solvated Fe(pherpy)$_2$-2PF$_6$ **173** showing a) top- and b) side- views of double helix sheets.

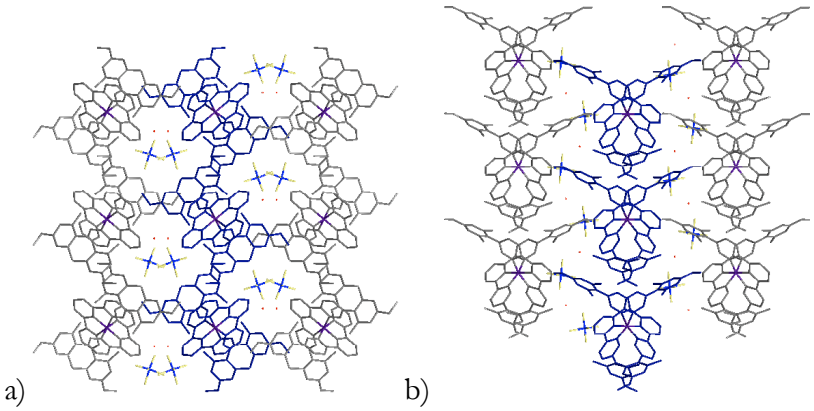

Figure 4.30 Crystal packing of non-solvated Fe(terpy)$_2$-2PF$_6$-H$_2$O **181** showing a) top- and b) side- views of double helix sheets.

Solution State Structures of $M(pherpy)_2$-$2PF_6$ and $M(terpy)_2$-$2PF_6$ complexes: Diamagnetic (Fe, Ru, Os, and Zn) and paramagnetic (Co, Ni, and Cu) complexes were characterized by ^{1}H-NMR and ^{13}C-NMR. The ^{1}H-NMR spectra of diamagnetic pyridyl-phenanthroline complexes **173, 177 – 179** are sharp and well resolved and were assigned with COSY, HSQC, and HMBC experiments (Table 4.9). Upon complexation, protons **d** and **1** are closest to the metal ion and undergo the largest shift ($\Delta\delta$ = ~1 – 2 ppm). The aromatic and methyl protons of the orthogonal manisyl groups are now diastereotopic and the respective pairs of singlets split into four (δ = ~6.7 and ~3.7 ppm). The manisyl methoxy protons are enantiotopic and thus remain as two singlets. The change in chemical shifts for the d^6 metal complexes (Fe(II), Ru(II), and Os(II)) are quite similar and only the chemical shifts of **h** varies according to metal identity.

Table 4.9 Comparison of ^{1}H NMR shifts of **115** in $CDCl_3$ and M(pherpy)$_2$-2PF$_6$ complexes **173**, **177** – **179** in CD_3CN.

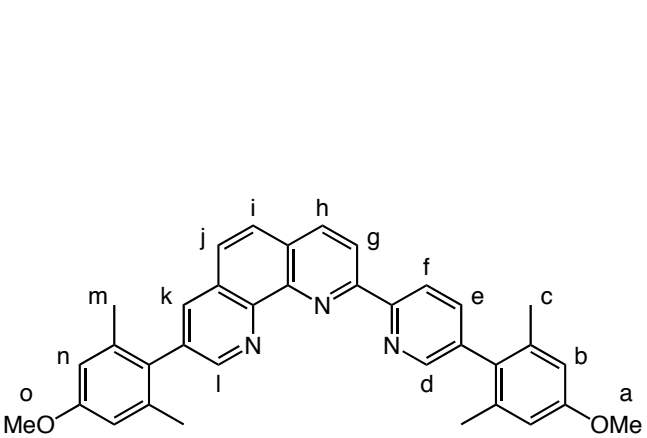

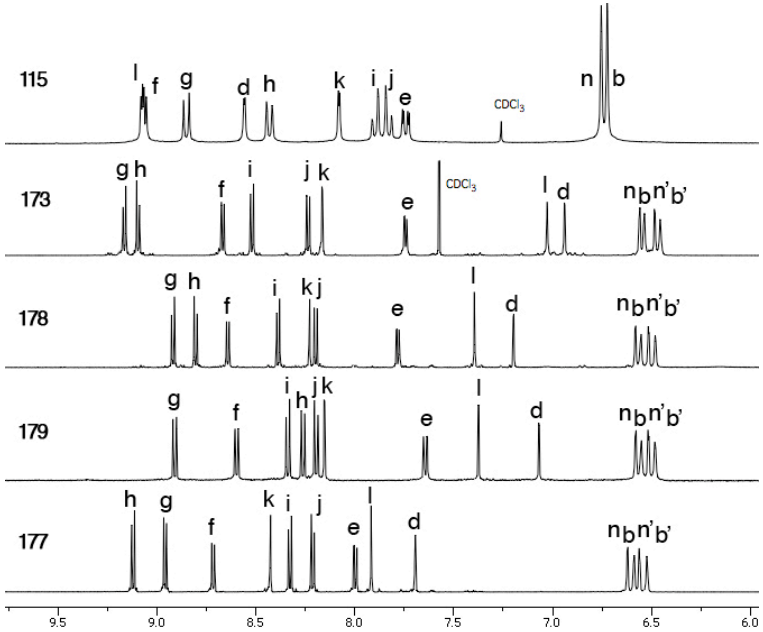

	a	b	b'	c	c'	d	e	f	g	h	i	j	k	l	m	m'	n	n'	o
115[a]	3.84	6.73		2.10		8.56	7.74	9.06	8.86	8.43	7.90	7.83	8.08	9.07	2.08		6.76		3.87
173[b] Fe(II)	-0.16	-0.19	-0.27	-0.61	-0.91	-1.62	+0.00	-0.39	+0.30	+0.67	+0.62	+0.41	+0.08	-2.04	-0.60	-0.88	-0.20	-0.28	-0.18
178[b] Ru(II)	-0.16	-0.18	-0.25	-0.53	-0.77	-1.36	+0.04	-0.42	+0.06	+0.37	+0.49	+0.37	+0.15	-1.68	-0.51	-0.72	-0.18	-0.25	-0.18
179[b] Os(II)	-0.17	-0.18	-0.25	-0.52	-0.72	-1.49	-0.09	-0.46	+0.05	-0.16	+0.44	+0.37	+0.08	-1.69	-0.51	-0.73	-0.18	-0.25	-0.18
177[b] Zn(II)	-0.15	-0.14	-0.21	-0.43	-0.62	-0.86	+0.26	-0.34	+0.10	+0.69	+0.43	+0.38	+0.35	-1.15	-0.42	-0.63	-0.14	-0.20	-0.16

[a] In $CDCl_3$, [b] $\Delta\delta$ = δ complex (CD_3CN) - δ free ligand ($CDCl_3$)

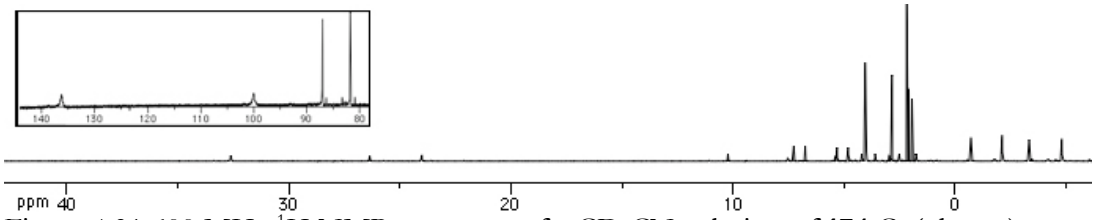

Figure 4.31 600 MHz ^{1}H NMR spectrum of a CD_3CN solution of **174** Co(pherpy)$_2$-2PF$_6$.

The ^{1}H-NMR spectra of paramagnetic pyridyl-phenanthrolines **174** – **176**, on the other hand, are drastically shifted and/or broadened (Figure 4.31).[89,90] Interaction of a nucleus and the unpaired electrons of paramagnetic coupling is called hyperfine coupling and occurs through direct contact and pseudo-contact mechanisms.[91] Direct contact requires the delocalization of unpaired electron spin density through the connected sigma or pi framework and significantly affects the chemical shifts of nuclei where unpaired spin density is located. Paramagnetic metal ions, such as Co(II), Ni(II), and Cu(II) also perturb the locally applied magnetic field and can affect the chemical shifts of local nuclei as a function of distance and orientation. This through-space interaction of a nucleus and an unpaired electron is called pseudo-contact and is a form of dipolar coupling. Broadening also results from coupling of the nuclear spin with the unpaired electron spin of the paramagnetic metal ion.[92] In all cases, the core pyridyl-phenanthroline hydrogen and carbon atoms undergo significant broadening and large downfield hyperfine shifts mostly likely due to a mixed contact coupling mechanism through the ligand sigma and pi framework. Electron spin delocalization purely through the ligand π-system would result in alternating upfield and downfield shifts.[91] Unfortunately, assignment of the proton resonances was not possible as the broadening is such that no coupling is observed.

The protons of the orthogonal manisyl groups also broaden slightly, but the shifts remain close to the reference values for the free ligand and diamagnetic complexes (Table 4.10). The manisyl carbons are also sharp and well defined in all ^{13}C

NMR spectra whereas the core pyridyl-phenanthroline carbons are broadened and usually missing for **174** – **176**. The orthogonality of the manisyl groups breaks conjugation, and inhibits efficient transfer of spin density from the paramagnetic metal through a direct contact mechanism.[92] The manisyl groups are close enough for a pseudo-contact coupling to occur as exemplified in the Co(II) spectra. The extreme broadness of the manisyl resonances of Ni(II) and Cu(II) complexes **175** and **176** is likely due to partial or full ligand dissociation.

Table 4.10 Manisyl region of the ^{1}H NMR spectra of CD_3CN solutions of $M(pherpy)_2$-$2PF_6$ complexes **173** – **179**.

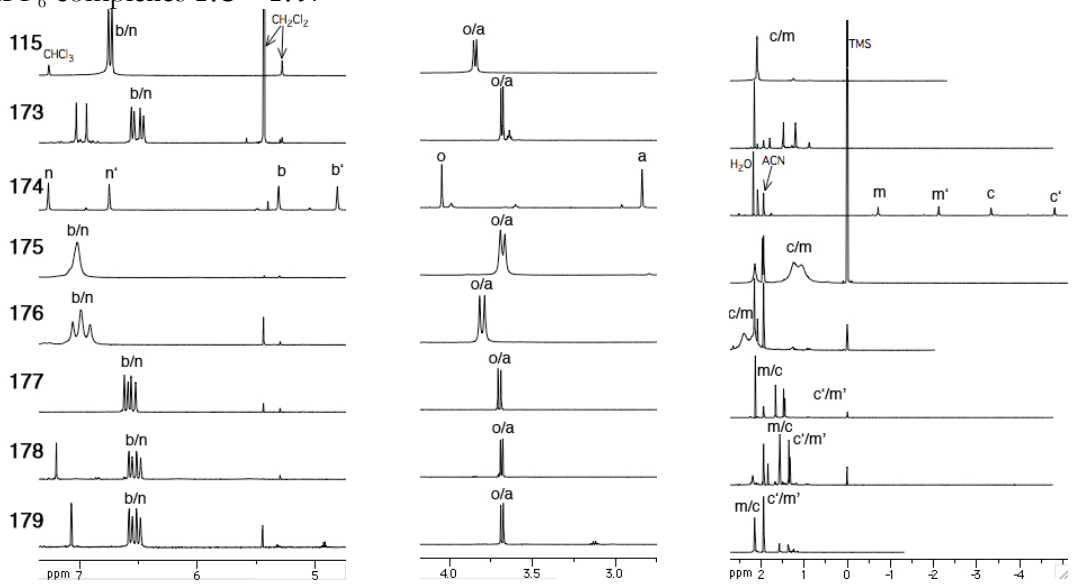

		a	b	b'	c	c'	m	m'	n	n'	o
115		3.84	6.73		2.10		2.08		6.76		3.87
173	Fe(II)	-0.16	-0.19	-0.27	-0.61	-0.91	-0.60	-0.88	-0.20	-0.28	-0.18
174	Co(II)	-1.00	-1.42	-1.92	-5.44	-6.91	-2.79	-4.20	+0.51	-0.01	+0.33
175	Ni(II)	-0.17	+0.29		-1.04		-0.83		+0.26		-0.18
176	Cu(II)	-0.05	+0.26	+0.18	-0.09		+0.31		+0.30	+0.23	-0.05
177	Zn(II)	-0.15	-0.14	-0.21	-0.43	-0.62	-0.42	-0.63	-0.14	-0.20	-0.16
178	Ru(II)	-0.16	-0.18	-0.25	-0.53	-0.77	-0.51	-0.72	-0.18	-0.25	-0.18
179	Os(II)	-0.17	-0.18	-0.25	-0.52	-0.72	-0.51	-0.73	-0.18	-0.25	-0.18

The ^{1}H-NMR spectra of diamagnetic terpyridine complexes **181**, **185** – **187** are also sharp and well resolved and can be assigned coupling patterns and constants (Table 4.11). Again, protons **d** are the closest to the metal ion and undergo the largest shift ($\Delta\delta$ = ~1 – 1.5 ppm). The change in chemical shifts for the d^6 metal complexes (Fe(II), Ru(II), and Os(II)) are quite similar and only the chemical shifts of **h** systematically varies according to metal identity. Similar to the paramagnetic pyridyl-phenanthroline complexes, chemical shifts of **182** – **184** range over ~100 ppm and the manisyl groups are shifted by pseudo-contact coupling(Figure 4.32 and Table 4.12). The resonances of the Ni(II) and Cu(II) complexes also broaden from partial or full ligand dissociation.

Table 4.11 ^{1}H NMR spectroscopic data for M(terpy)$_2$-2PF$_6$ complexes **181**, **185** – **187**.

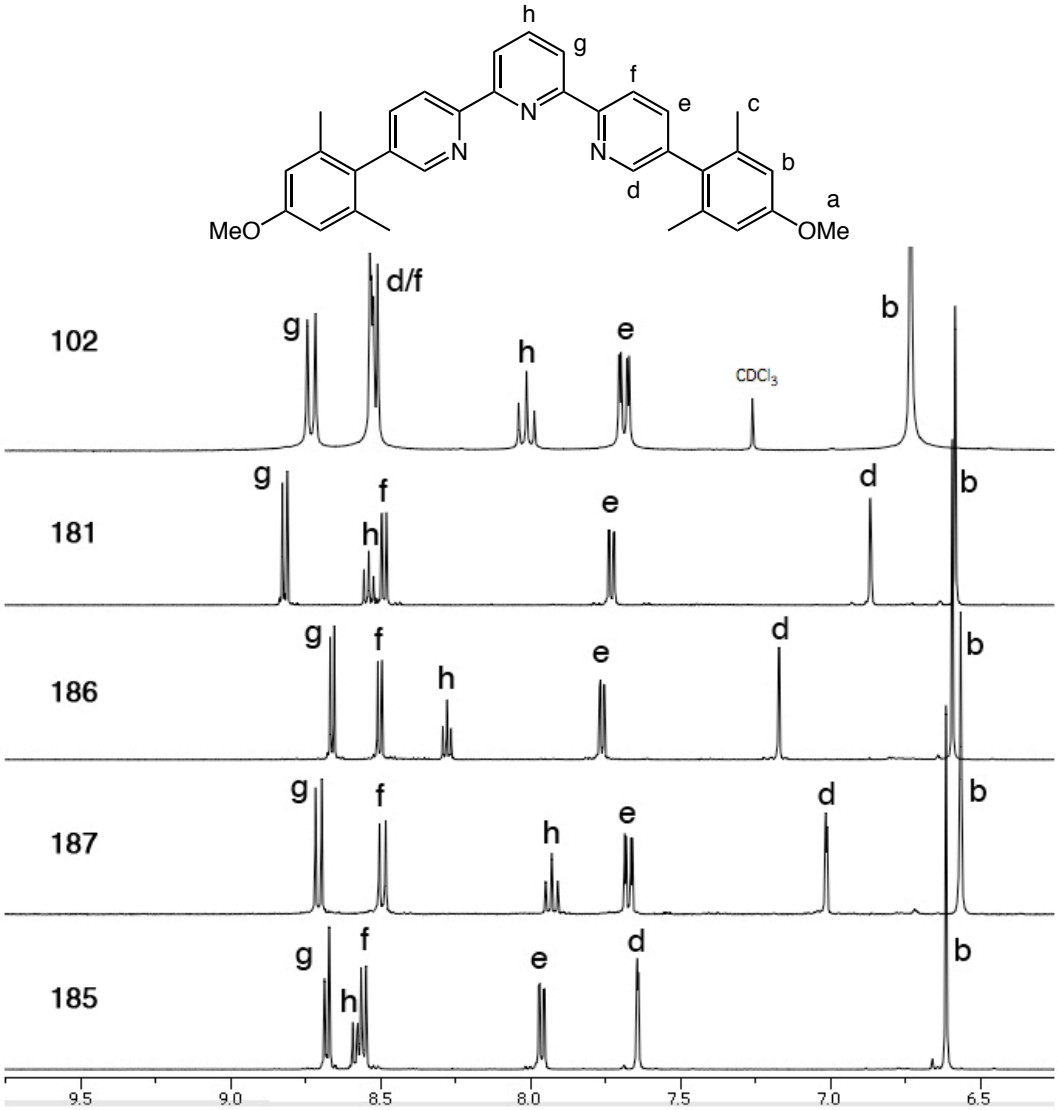

		a	b	c	d	e	f	g	h
102[a]		3.85	6.73	2.09	8.52	7.68	8.51	8.72	8.01
181[b]	Fe(II)	-0.13	-0.15	-0.60	-1.66	+0.05	-0.03	+0.10	+0.54
186[b]	Ru(II)	-0.13	-0.14	-0.52	-1.35	+0.08	-0.01	-0.06	+0.27
187[c]	Os(II)	-0.13	-0.16	-0.47	-1.51	-0.01	-0.02	-0.01	-0.08
185[b]	Zn(II)	-0.13	-0.12	-0.46	-0.88	+0.28	+0.05	-0.04	+0.57

[a] in CDCl3, [b]Δδ = δ complex (CD_3CN) - δ free ligand ($CDCl_3$), [c]Δδ = δ complex (CD_2Cl_2)- δ free ligand ($CDCl_3$)

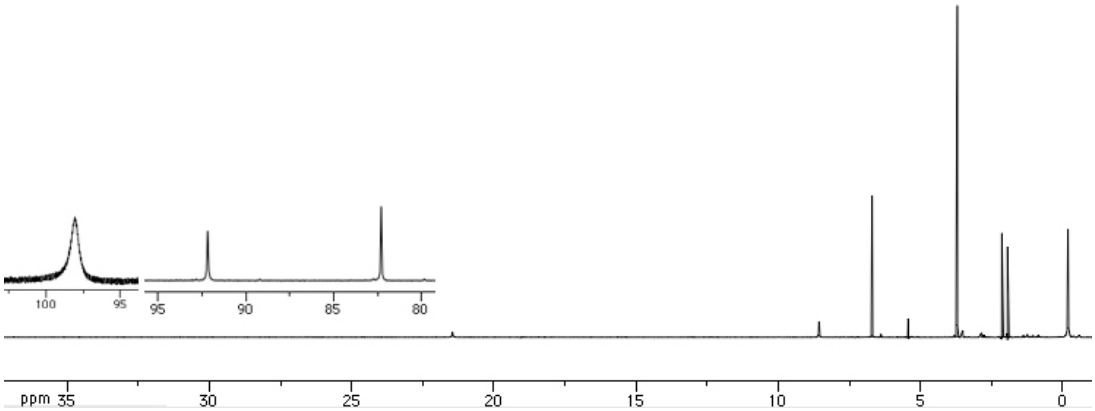

Figure 4.32 600 MHz ^{1}H NMR spectrum of a CD_3CN solution of **182** $Co(terpy)_2$-$2PF_6$.

Table 4.12 Manisyl region of the ^{1}H NMR spectra of $M(terpy)_2$-$2PF_6$ complexes **181** – **187**.

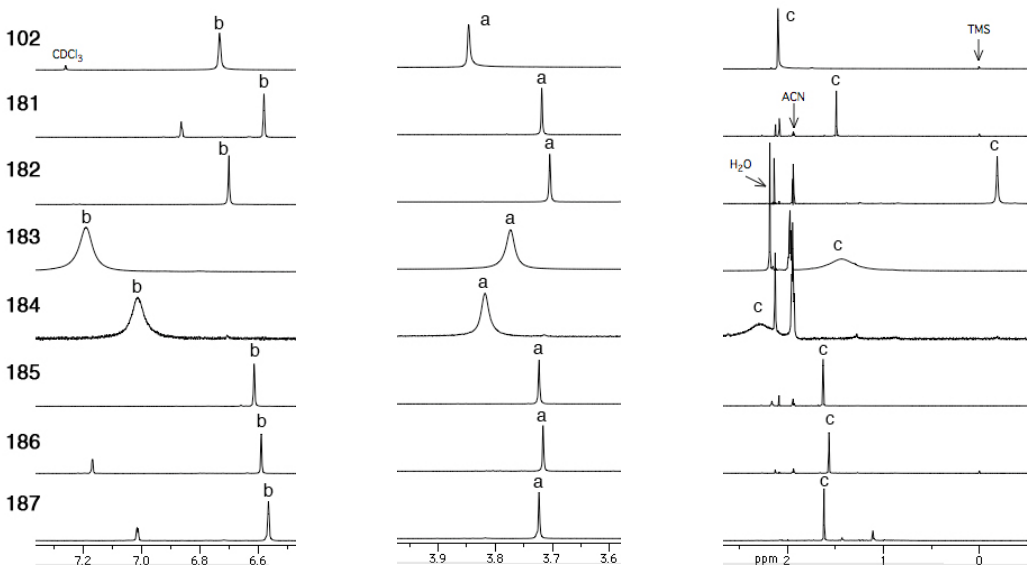

		a	b	c
102		3.85	6.73	2.09
181	Fe(terpy)	-0.13	-0.15	-0.60
182	Co(terpy)	-0.14	-0.03	-2.27
183	Ni(terpy)	-0.11	0.41	-0.67
184	Cu(terpy)	-0.04	0.28	0.18
185	Zn(terpy)	-0.13	-0.12	-0.46
186	Ru(terpy	-0.13	-0.14	-0.52
187	Os(terpy)	-0.13	-0.16	-0.47

The ^{1}H-NMR resonances of pyridyl-phenanthroline **114** shift upon binding to ruthenium (Figure 4.33). Manisyl protons **b**, **c**, **m**, and **n** are diastereotopic and split into two sets of signals. Coordination of alpha-substituted terpyridine derivatives can result in significant intraligand interactions (Figure 4.6),[75,93] and proton b' is likely near the π-electron clouds of the second ligand resulting in the large upfield shift.

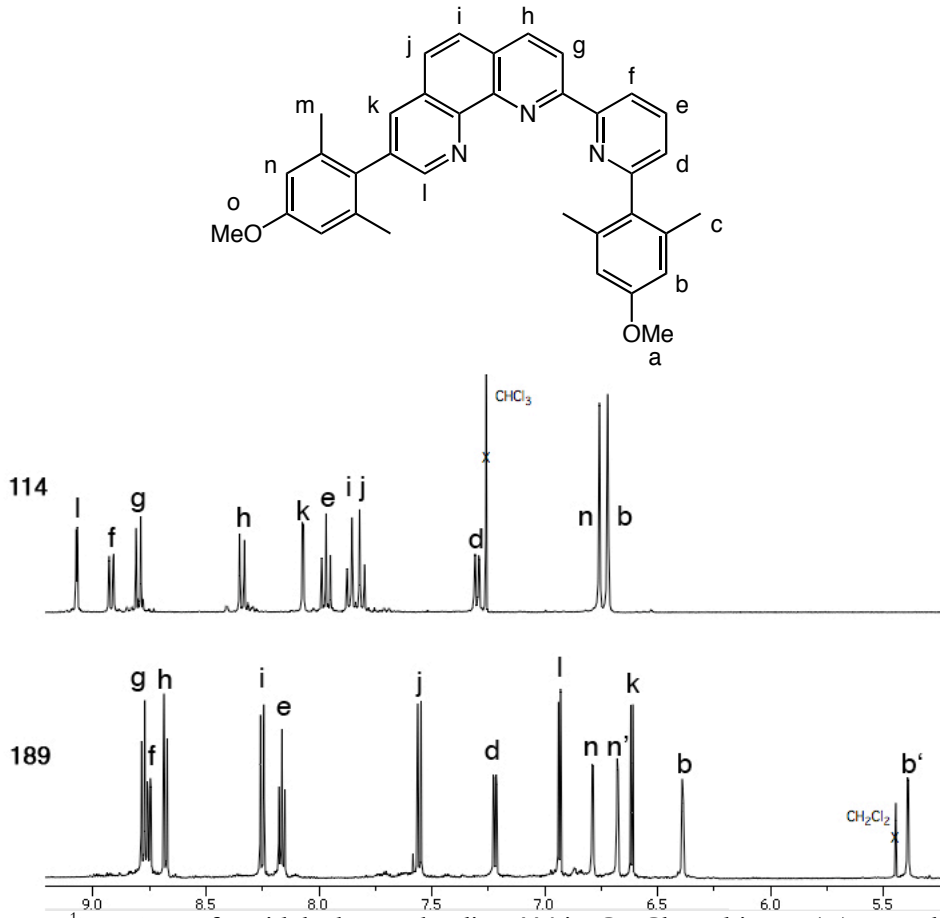

Figure 4.33 ^{1}H NMR of pyridyl-phenanthroline **114** in $CDCl_3$ and its Ru(II) complex **189** in CD_2Cl_2.

Absorption Spectra. The UV-vis spectra of $M(pherpy)_2$-$2PF_6$ complexes **173** – **179** and $M(terpy)_2$-$2PF_6$ complexes **181** –**187** exhibit two groups of ligand-centered (LC) transitions analogous to those observed for terpyridine and pyridyl-phenanthroline complexes.[23,60,71] The strength of the intense π-π* absorption of pyridyl-phenanthroline ligand **115** at 298 nm increases but is otherwise unaffected by complexation whereas the weakly allowed π-π* transition at 350 nm increases in intensity and is red-shifted ~20 nm (Figure 4.34 and Table 4.13). The increase in relative intensity for the second transition results from reduced spin-orbit coupling of the π-π* and nearby n-π* states as the nitrogen lone pairs are now bound to the metal ions.[94,95] Complexation affects the transitions of terpyridine ligand **102** to a greater extent. The intense π-π* absorptions at 287 and 305 nm increase in intensity but also red-shift 20 – 30 nm and another transition grows in at ~350 nm (Figure 4.35 and Table 4.14). The lower energy bands, located between 450 and 700 nm, of the iron, ruthenium, and osmium complexes are attributable to MLCT transitions.[96] The shapes of the terpyridine and pyridyl-phenanthroline MLCT bands are similar and the longer wavelength of the pyridyl-phenanthroline complex is due to the increased conjugation in the ligand backbone, stabilizing the LUMO and lowering the energy of the MLCT bands relative to the analogous terpyridine complex. The fine structure and shoulders present in the MLCT bands could be vibrational structure, a splitting of the dπ orbitals of the metal center,[97] and or, in the case of the pyridyl-phenanthroline, a dissymmetric MLCT state localized on the phenanthroline moiety.[23]

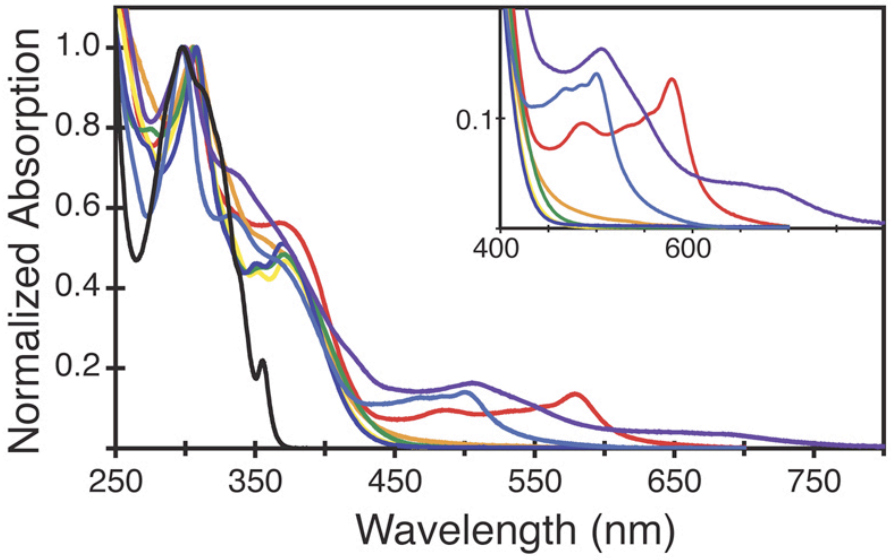

Figure 4.34 UV-Vis absorption spectra of $M(pherpy)_2^{2+}$ in CH_2Cl_2: $Fe(pherpy)_2$-$2PF_6$ (-red-), $Co(pherpy)_2$-$2PF_6$ (-orange-), $Ni(pherpy)_2$-$2PF_6$ (-yellow-), $Cu(pherpy)_2$-$2PF_6$ (-green-), $Zn(pherpy)_2$-$2PF_6$ (-blue-), $Ru(pherpy)_2$-$2PF_6$ (-indigo-), $Os(pherpy)_2$-$2PF_6$ (-violet-), and **115** (-black-).

Table 4.13 UV-Vis absorption properties of $M(pherpy)_2$-$2PF_6$ **173 – 179** in methylene chloride.

	λ_{max} (nm)	ε_{max}	$\lambda_{maxMLCT}$ (nm)	$\varepsilon_{maxMLCT}$
115	298*, 355	42100		
173	305*, 367	57,000	486, 579*	8,000
174	305*, 360sh	47,000		
175	307*, 351, 371	51,000		
176	306*, 354, 370	56,000		
177	308*, 351, 369	54,000		
178	298*, 333, 365sh	72,000	469, 485, 500*	10,000
179	299*, 337sh	578316	505*, 690	9321

*denotes λ_{max} and ε_{max} is given.

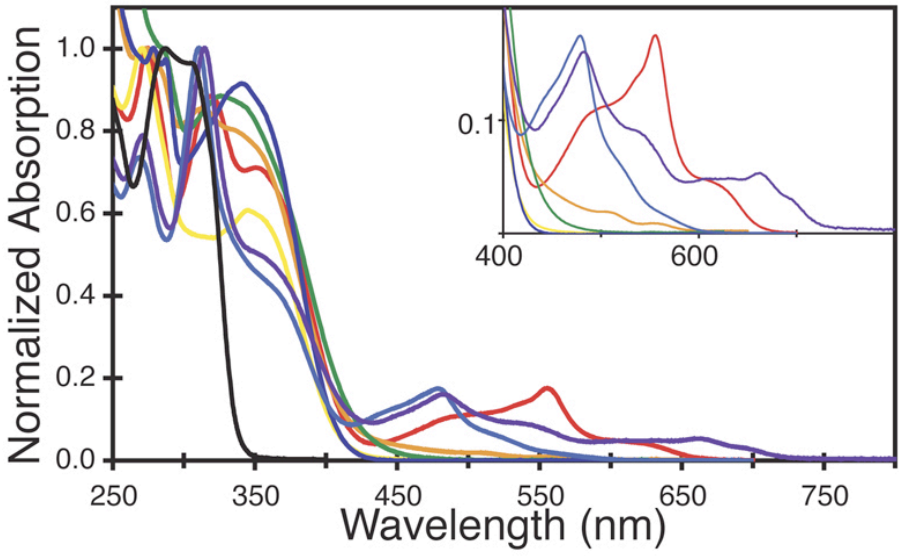

Figure 4.35 UV-Vis absorption spectra of $M(terpy)_2^{2+}$ in CH_2Cl_2: $Fe(terpy)_2$-$2PF_6$ (-red-), $Co(terpy)_2$-$2PF_6$ (-orange-), $Ni(terpy)_2$-$2PF_6$ (-yellow-), $Cu(terpy)_2$-$2PF_6$ (-green-), $Zn(terpy)_2$-$2PF_6$ (-blue-), $Ru(terpy)_2$-$2PF_6$ (-indigo-), $Os(terpy)_2$-$2PF_6$ (-violet-), **102** (-black).

Table 4.14 UV-Vis absorption properties of $M(terpy)_2$-$2PF_6$ in methylene chloride.

	λ_{max} (nm)	ε_{max}	$\lambda_{maxMLCT}$ (nm)	$\varepsilon_{maxMLCT}$
102	287*, 305	27,800		
181	275*, 319, 351	59,000	495sh, 555, 610sh	10,000
182	274*, 313, 335sh	52,000	503, 553	1,000
183	271*, 345	75,000		
184	285sh*, 326	45,000		
185	279*, 287, 341	34,000		
186	269, 311*, 360sh	69,000	479	12,000
187	315*, 356sh	69,600	485*, 537sh, 665, 694sh	11,100

*denotes λ_{max} and ε_{max} is given.

Emission: As the Ru(II) complexes of terpyridine are known to be virtually non-luminescent at room temperature in solution, it was surprising to find that $M(pherpy)_2$-$2PF_6$ complexes **173** – **179** and $M(terpy)_2$-$2PF_6$ complexes **181** – **187** exhibit a weak, but detectable emission centered 500 nm and 475 nm respectively (Figures 4.36 and 4.37, Tables 4.15 and 4.16).[98] Examination of the lifetimes (≤ 10 ns), excitation spectra (Figure 4.38) and comparison to protonated **115** reveals that the emission originates from an intraligand charge transfer (ILCT) state. In this case, the role of the metal ion, is that of Lewis acid and induces a red-shift of the ILCT transition.[99] The heavy-atom effect accounts for the loss of quantum yield for the complex relative to the free ligand. Zinc complexes **177** and **185**, however, retain appreciable luminescence, Φ_f = 0.11 and 0.24, respectively. Zinc, with its filled *d* sub shell, often behaves more like a proton, and can enhance the quantum yields of polypyridines.[100] Polypyridine ligands, such as bipyridine and terpyridine, are being actively applied toward zinc chemosensors[101,102] and the resultant zinc complexes are under investigation for non-linear optical (NLO) properties.[99,103] It is interesting to note that while lower than the parent ligands, the quantum yield of the zinc complexes are much higher than the protonated ligands and is mostly likely due to the increased rigidity of the zinc(II) complex, which reduces the efficacy of non-radiative pathways.

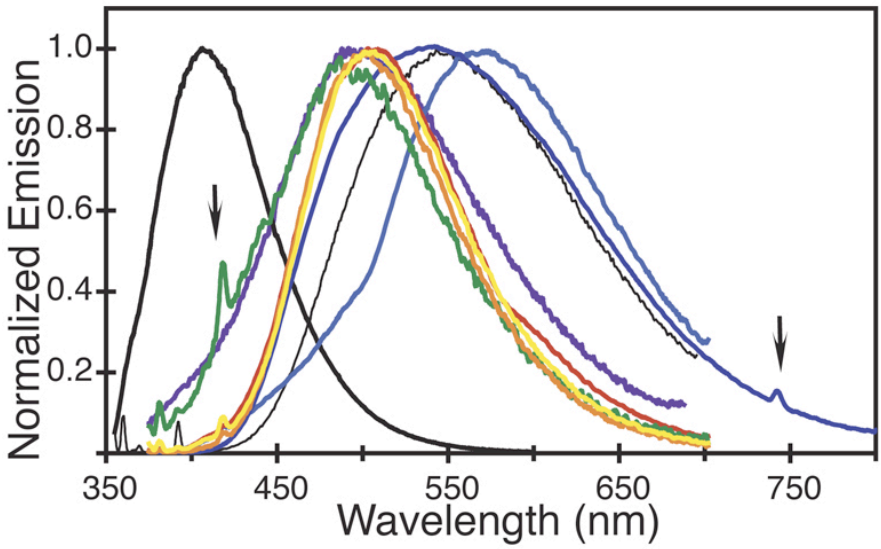

Figure 4.32 Normalized emission spectra of $M(pherpy)_2^{2+}$ in CH_2Cl_2: $Fe(pherpy)_2$-$2PF_6$ (-red-), $Co(pherpy)_2$-$2PF_6$ (-orange-), $Ni(pherpy)_2$-$2PF_6$ (-yellow-), $Cu(pherpy)_2$-$2PF_6$ (-green-), $Zn(pherpy)_2$-$2PF_6$ (-blue-), $Ru(pherpy)_2$-$2PF_6$ (-indigo-), $Os(pherpy)_2$-$2PF_6$ (-violet-), **115** (-thick black-), **115**[H^+] (-thin black-). Arrows indicate Raman scattering.

Table 4.15 Emissive properties of $M(pherpy)_2$-$2PF_6$ **173 – 179** in methylene chloride.[a]

	metal ion	λ_{max} (nm)	Φ_f[a)]	τ_1 ns (%)	τ_2 ns (%)
173	Fe(II)	505	0.004	6.34	
174	Co(II)	500	0.001	6.84	
175	Ni(II)	505	0.002	7.15	
176	Cu(II)	485	<0.001		
177	Zn(II)	540	0.109	3.02 (92%)	10.66 (8%)
178	Ru(II)	570	0.009	3.27 (93%)	8.624 (7%)
179	Os(II)	500	0.008	2.70 (81%)	6.40 (19%)
115		406	0.454	1.62	
115H$^{+b)}$	H^+	543	0.029	1.75 (94%)	8.06 (6%)

a) O_2 not removed a) relative to 9,10-DPA in EtOH[104] b)excess trifluoroacetic acid in methylene chloride.

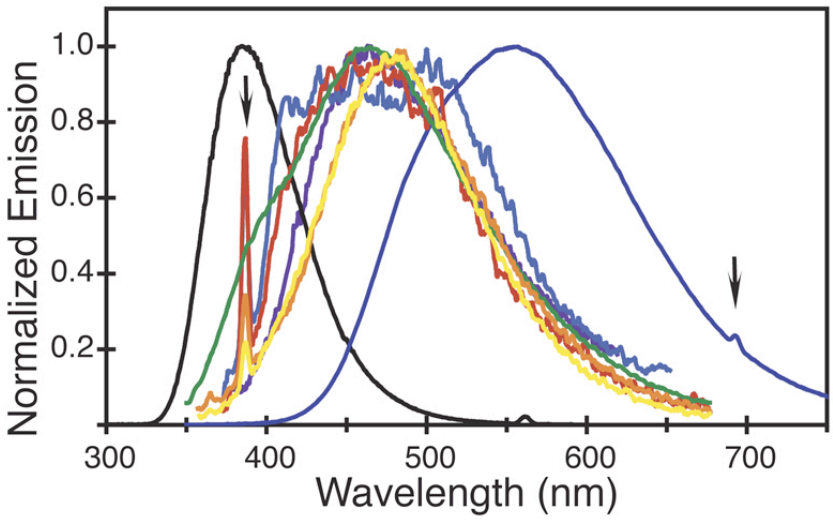

Figure 4.37 Normalized emission spectra of $M(terpy)_2^{2+}$ in CH_2Cl_2: $Fe(terpy)_2$-$2PF_6$ (-red-), $Co(terpy)_2$-$2PF_6$ (-orange-), $Ni(terpy)_2$-$2PF_6$ (-yellow-), $Cu(terpy)_2$-$2PF_6$ (-green-), $Zn(terpy)_2$-$2PF_6$ (-blue-), $Ru(terpy)_2$-$2PF_6$ (-indigo-), $Os(terpy)_2$-$2PF_6$ (-violet-), and **102** (-black-). Arrows indicate Raman scattering.

Table 4.16 Emissive properties of $M(terpy)_2$-$2PF_6$ **181 – 187** in methylene chloride.[a]

	metal ion	λ_{max} (nm)	Φ_f[b]	τ_1 ns (%)	τ_2 ns (%)
181	Fe(II)	465	<0.001		
182	Co(II)	480	0.001		
183	Ni(II)	480	0.001		
184	Cu(II)	465	0.005	2.61	
185	Zn(II)	555	0.237	7.04	
186	Ru(II)	500	<0.001		
187	Os(II)	465	0.005	1.35 (84%)	5.52 (16%)
102		385	0.375	0.91	
102H$^+$ [c]	H^+	535			

[a] O_2 not removed [b] relative to 9,10-DPA in EtOH[104] [c]excess methanesulfonic acid in acetonitrile.[105]

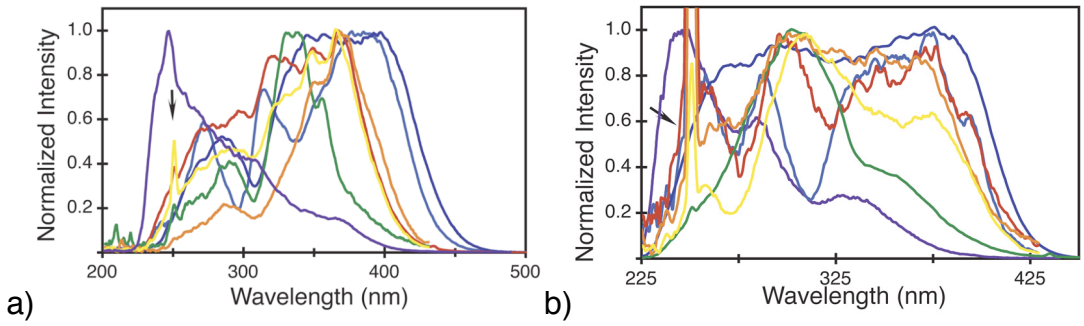

Figure 4.38 Normalized excitation spectra of (a) $M(pherpy)_2^{2+}$ and (b) $M(terpy)_2^{2+}$in CH_2Cl_2: $Fe(L)_2$-$2PF_6$ (-red-), $Co(L)_2$-$2PF_6$ (-orange-), $Ni(L)_2$-$2PF_6$ (-yellow-), $Cu(L)_2$-$2PF_6$ (-green-), $Zn(L)_2$-$2PF_6$ (-blue-), $Ru(L)_2$-$2PF_6$ (-indigo-), $Os(L)_2$-$2PF_6$ (-violet-).

No room temperature emission was observed from the MLCT states of the iron(II) or ruthenium(II) complexes, due to nearby non-emissive ^{3}MC states.[11] The ^{3}MC levels of osmium(II) are much higher in energy and cannot be populated at room temperature[21] and emission from the MLCT states of both **179** and **187** is observed at 775 and 715 nm, respectively (Figure 4.39). The low energy of the transitions means that the emission wavelengths are at the limit of the detector and quantum yields could not be determined with confidence for terpyridine **187**, or at all for pyridyl-phenanthroline **179**. The long lifetimes (≥290 ns) and excitation spectra confirm their assignment as emissive MLCT states (Table 4.16 and Figure 4.40). It is interesting to note that the lifetimes of the terpyridine complex **187** are much larger than the pyridyl-phenanthroline complex **179**. Meyer and coworkers have shown that increasing the delocalization of MLCT states reduces the excited state distortion and increase lifetimes.[27,28] However, given that the relative intensities of the ILCT and MLCT emissive states are approximately the same for pyridyl-phenanthroline complex **179**, but only the MLCT emissive state is appreciable for terpyridine complex **187**, there are several photophysical processes occurring and further work involving low-temperature studies should help elucidate the discrepancies.

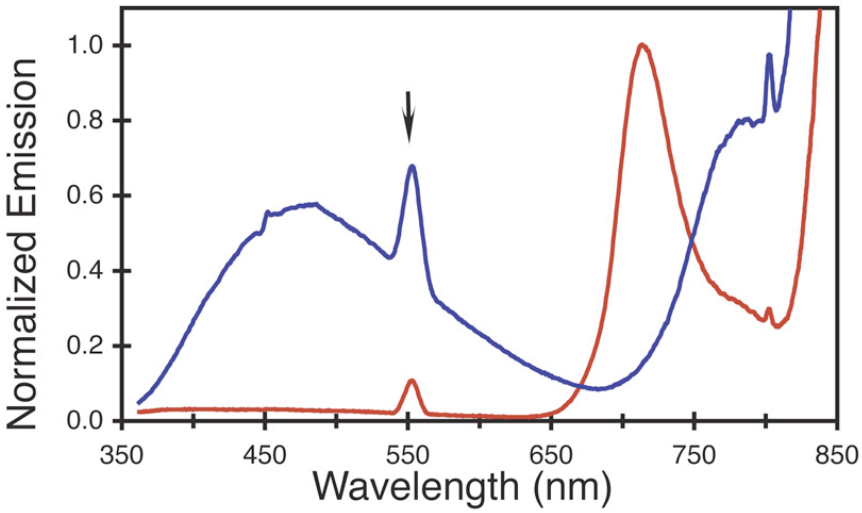

Figure 4.39 Normalized emission spectra of $Os(pherpy)_2^{2+}$ **179** (-blue-) and $Os(terpy)_2^{2+}$ **187** (-red-) in CH_2Cl_2. Arrows indicate twice the excitation wavelength.

Table 4.17 MLCT emission data of $Os(pherpy)_2$-$2PF_6$ **179** and $Os(terpy)_2$-$2PF_6$ **187** in methylene chloride.[a]

		λ_{max} (nm)	Φ_f^a	τ_1 (%)	τ_2 (%)
179	$Os(pherpy)_2^{2+}$	775		290.9 ns (78%)	7.31 ns (22%)
187	$Os(terpy)_2^{2+}$	715	0.036	540.3 ns (91%)	2256.2 ns (9%)

[a)]at room temperature in aerated solution [b)] relative to 9,10-DPA in EtOH[104]

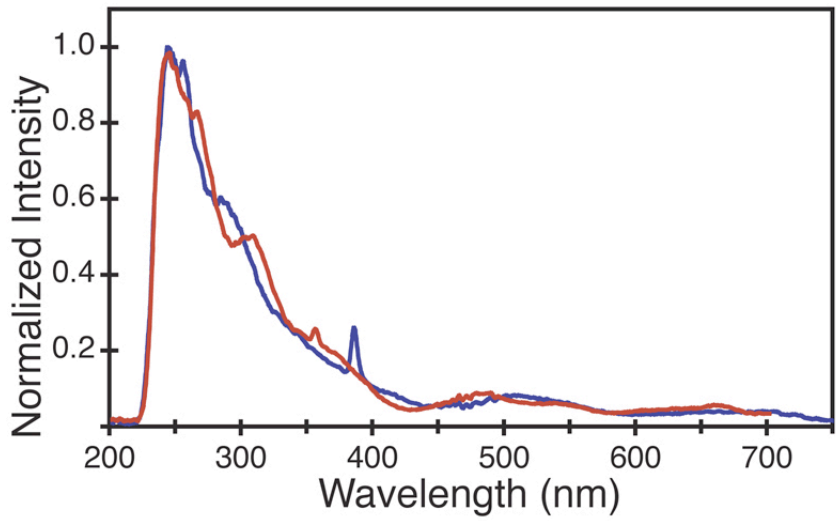

Figure 4.40 Normalized emission spectra of $Os(pherpy)_2^{2+}$ **179** (-blue-) and $Os(terpy)_2^{2+}$ **187** (-red-) in CH_2Cl_2.

Chirality of Ruthenium complexes: Recent work by Lacour and coworkers has demonstrated that tris(tetrachlorobenzendiolato) phosphate(V) (TRISPHAT)[106] **195** is an effective NMR chiral shift reagent and chiral auxiliary for the resolution of chiral dications by simple chromatography, extraction, and recrystalization.[107,108] The particular efficacy of TRISPHAT arises from the formation of highly lipophilic diastereomeric contact ion pairs. It was uncertain whether D_3-symmetric TRISPHAT would form strong enough diastereomeric ion pairs with C_2-symmetric pyridyl-phenanthroline complexes to enable resolution, so C_2-symmetric derivatives BINPHAT[109] and BFT[110] were also investigated.

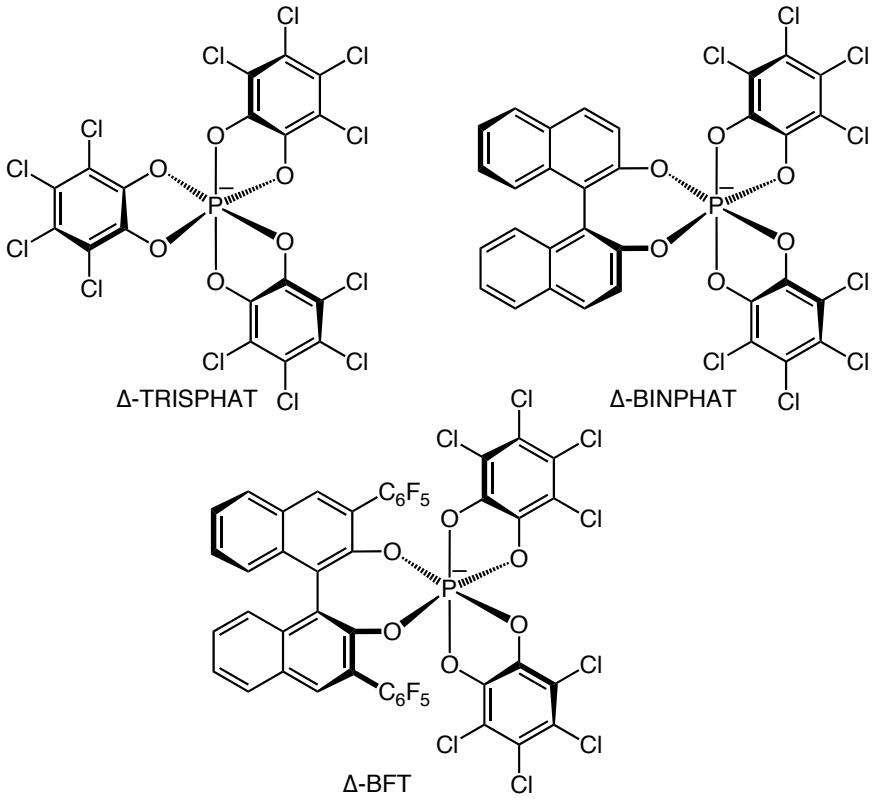

Our initial goal was to demonstrate the utility of hexacoordinated phosphate anions as chiral shift reagents to determine the enantiomeric purity of pyridyl-

phenanthrolines complexes. Titration of a concentrated d_6-acetone solution of $[NH_2Me_2][\Delta$-BINPHAT] into a CD_2Cl_2 solution of racemic ruthenium complex **178**, resulted in no splitting (Figure 4.41).

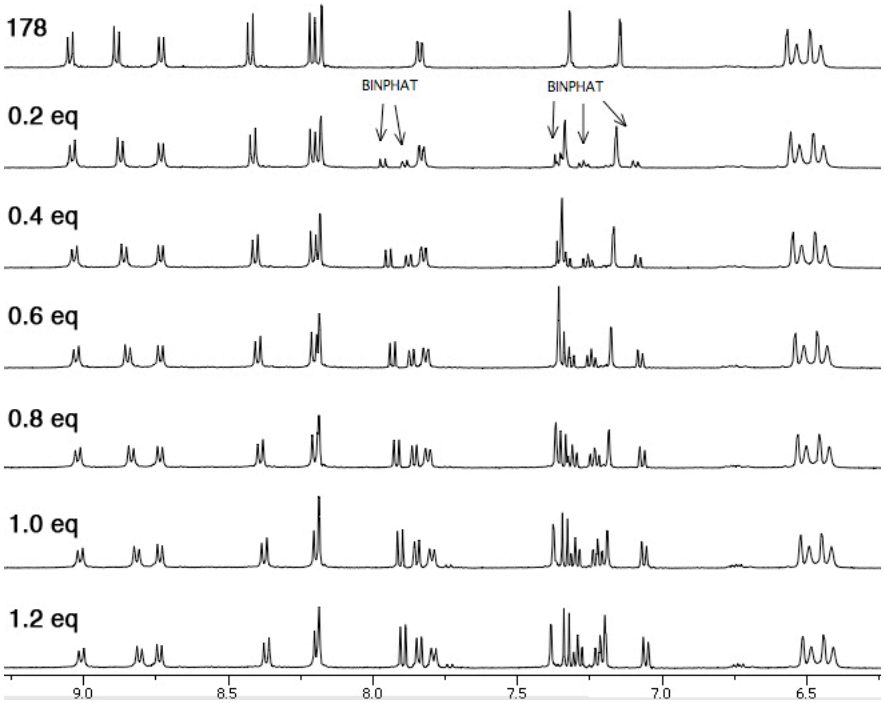

Figure 4.41 ^{1}H-NMR titration of **178** in CD_2Cl_2 with $[NH_2Me_2][\Delta$-BINPHAT] in acetone-d_6.

Upon titration of **178** with [n-Bu_3NH][**Λ**-TRISPHAT] in CD_2Cl_2, however, the two diastereomeric ion pairs are clearly distinguishable (Figure 4.42). At 0.75 equivalents, protons **d** and **l** of the two diastereomers are baseline separated, and maximal separation of occurs after the addition of one equivalent of anion. Why the protons **d** and **l** are the most affected is unclear as both protons are directed towards the metal ion and cannot directly interact with the TRISPHAT anion. At 1.5 equivalents, the spectra is broadened and poorly resolved due the formation of a red precipitate. The relative intensities of the diastereomeric protons do not significantly change and do not support the selective precipitation of one diastereomeric ion pair.

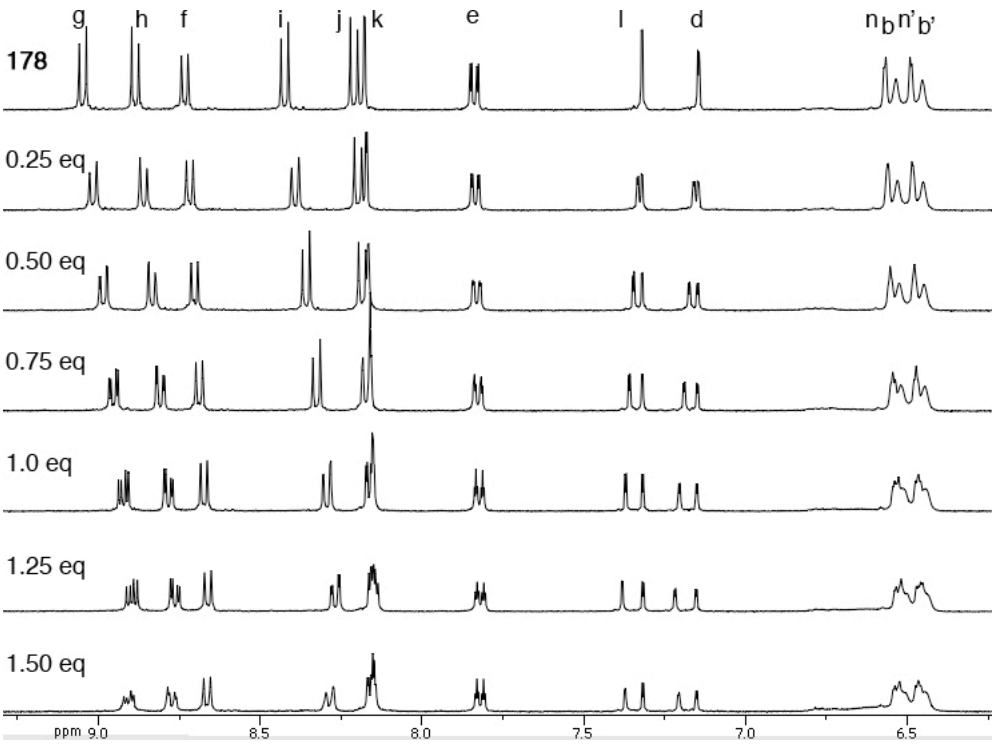

Figure 4.42 ^{1}H-NMR titration of **178** with [n-Bu_3NH][Λ-TRISPHAT] in CD_2Cl_2.

Titration of racemic **189** with [n-Bu_3NH][Δ-TRISPHAT] in CD_2Cl_2 also results in non-equivalency of the diastereomeric ion pairs (Figure 4.43). Protons **e** and **b** are the most sensitive to the presence of TRISPHAT and are baseline separated. Proton **e** and its counterpart clearly separate at one equivalent and sharpen with additional anion equivalents. Only after 2.0 equivalents are protons **b** of the two diastereomers baseline separated.[111] Proton **d** approaches clean separation with excess anion whereas the separations of protons **j** and **l** are reduced after two equivalents. Protons **b** – **f** are located on the manisyl pyridine section of the ligand and are affected to the greatest extent indicating that the one of the diastereomeric ion pair interaction occur at this site.

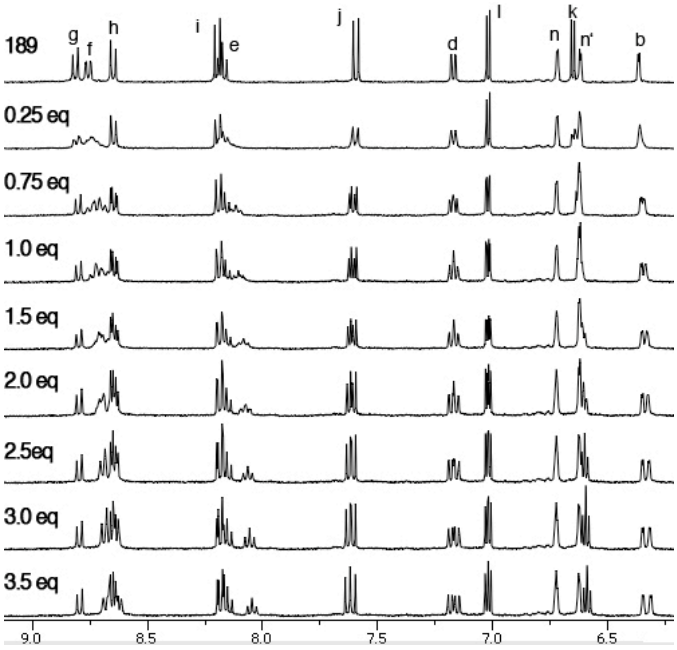

Figure 4.43 ^{1}H-NMR titration of racemic **189** with [n-Bu_3NH][Δ-TRISPHAT] in CD_2Cl_2.

Attempts towards resolution of the racemic **178** began with anion metathesis. Complex **178**$[PF6]_2$ with 2.1 equivalents of [cinchonidinium][Δ-TRISPHAT] in acetone was applied to a neutral alumina column and elution with methylene chloride resulted in a single red band and red baseline. Isolation of the first band gave a sparingly soluble red solid and the presence of Δ-TRISPHAT^{-} was confirmed by ESI-MS. The ^{1}H-NMR spectra in acetone-d_6 shows what appears to be a single set of resonances, but protons **d**, **e**, and **l** exhibit fine structure which could result from a solvent-weakened diastereomeric ion pair of racemic complex (Figure 4.44).

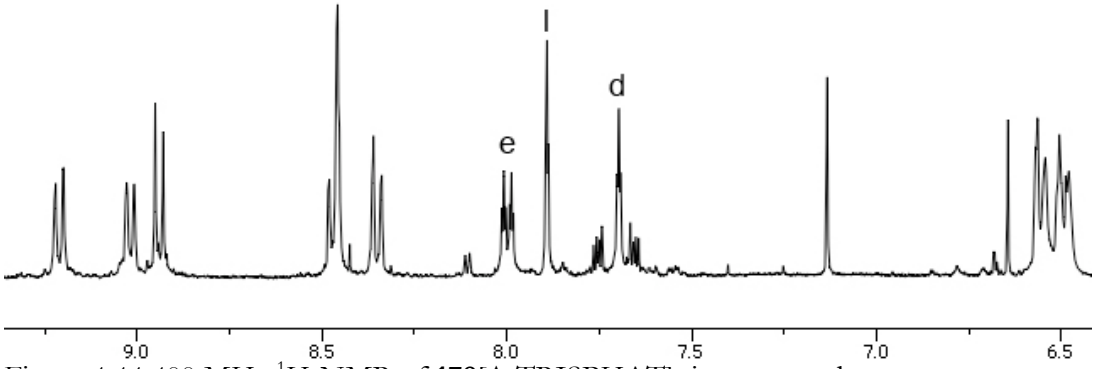

Figure 4.44 400 MHz ^{1}H-NMR of **178**[Δ-TRISPHAT]$_2$ in acetone-d$_6$.

X-ray quality crystals were obtained by slow evaporation and the structure determined. Complex 178[Δ-TRISPHAT]$_2$ crystallizes in the chiral $P2_12_12_1$ space group and is shown in Figure 4.45. The absolute configuration of the Δ-TRISPHAT anions were confirmed by refining the Flack parameter to 0.05(5). The configuration of the dication **178**, however, could not be confidently assigned as the ethynylene atoms in both phenanthroline bridges are again disordered, 54% and 76%, rendering the pyridine and phenanthroline moieties are indistinguishable. Nevertheless, the interactions of the dication and the Δ-TRISPHAT anions are quite remarkable. One of the two anions interacts through offset face-face π-π interaction with the electron rich manisyl ring (d ~ 3.65 Å, displacement angle = 22º). The dication is wedged in the cleft of the second anion and one of the phenanthroline protons is within the π-electron cloud of one of the tetrachlorocatechols. Recent work by Amouri and coworkers has identified similar supramolecular chiral recognition via π-π interactions between TRISPHAT and a chiral organometallic species in the solid state.[112,113] Further chromatographic resolutions using TRISPHAT and BFT were inconclusive as the chiral anions induce a chiral CD effect in the MLCT transition of racemic dication.

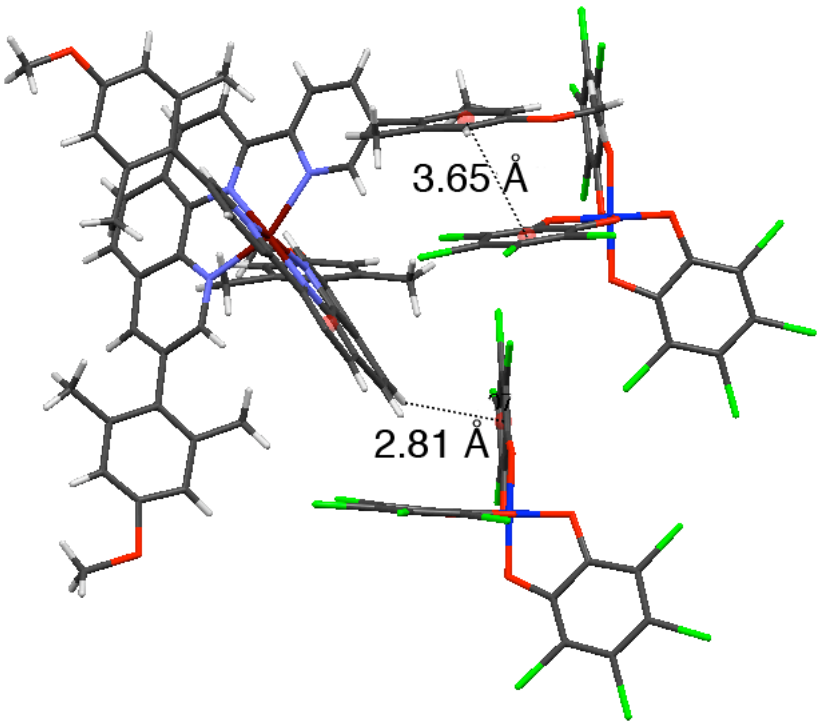

Figure 4.45 Representation of **178**[Δ-TRISPHAT]$_2$ showing the π-π stacking (d = 3.65 Å) and C-H···π interactions (d = 2.81) (from the crystal structure).

Numerous attempts to separate the PF_6^- salts of **178**, **189**, **192**, and **193** with chiral HPLC on normal and reverse phase were unsuccessful. To the best of our knowledge only one similar C_2 metal complex has been resolved by Sauvage and coworkers using a silica gel column coated with amylose tris (3,5-diphenylmethylcarbamate).[114]

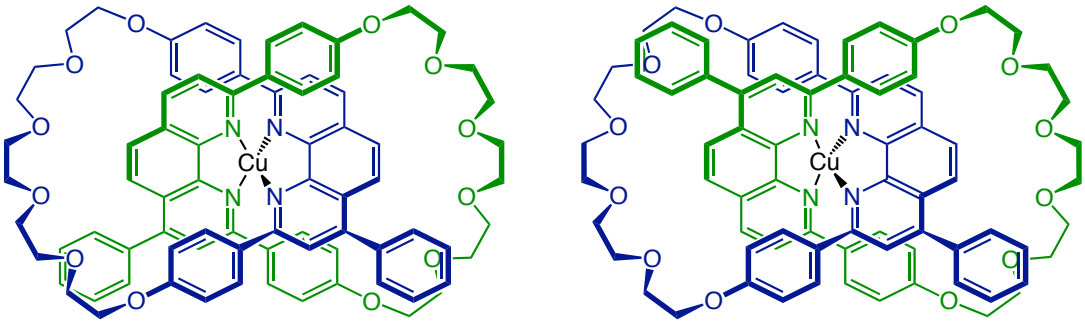

Figure 4.46 Resolved topologically chiral catenands with C_2 symmetry.[114]

4.2.4 Conclusions

The ML_2 complexes of manisyl-substituted pherpys and terpys provide a unique insight into the subtle effects of ligand modulation on the solid-state and electronic properties of coordination compound. The ligand structure and inter-ligand contacts determine the solid-state structure rather than the geometrical and electronic preferences of the metal ion. The manisyl group, originally chosen for solubility enhancement,[105] not only endows the ligands with desirable photophysical process[69,115] (*vida infra*), but, in the solid state, establishes specific π-π interaction motifs. The first, an intermolecular C-H···π interaction between a proton of the heterocyclic core and the π-electron cloud of the manisyl ring, aligns the dications in double helices along a crystallographic two-fold axis. The second, an anti-parallel, off-set, face-face, π-π interaction of manisyl rings, occurs at a center of inversion and arranges the helices into a sheet of alternating left and right handed helices. π-π interactions are important non-covalent forces, similar to hydrogen bonds,[116] found in self-assembly and molecular recognition events from large biological systems to simple small molecules.[117] Interactions between electron rich and electron poor aromatic rings have been exhaustively used for the formation of discrete supramolecular assemblies,[118] whereas their role in the formation of non-discrete supramolecular assemblies is not as well studied.[87] The role of hydrogen bonds, on the other hand, is better understood and is often pointed out as a packing motif but an understanding and incorporation of all non-covalent interactions is necessary for the tuning and prediction of crystal structure and material properties.[119,120] The formation of solvent separated sheets of helices of manisyl-substituted terpyridines and pyridyl-phenanthrolines illustrates the additive effects of these weak interactions and creates a scaffold capable of addressing the tuning and harnessing of aromatic interactions for the design of molecular assemblies.

The weak ligand-centered (LC) emission of manisyl-substituted terpyridine and pyridyl-phenanthroline complexes arises from the efficient TICT emissive state of the parent ligand. The LC emission is present in all of the complexes, but due to the heavy atom effect, only zinc complexes exhibit appreciable luminescence. Osmium complexes also possess an emissive MLCT state, but low temperature studies combined with further computations are necessary to better understand the complicated photophysical processes.

4.3 Experimental

Materials and Methods

^{1}H- and ^{13}C NMR spectra were recorded on Bruker 300, 400, 500, and 600 MHz spectrometers and were referenced to residual $CHCl_3$ (^{1}H-NMR: 7.26 ppm; and ^{13}C-NMR 77.00 ppm), CD_3CN (^{1}H-NMR: 1.94 ppm and ^{13}C-NMR: 1.39 ppm), $(CD_3)_2CO$ (^{1}H-NMR: 2.05 ppm and ^{13}C-NMR: 29.84 ppm), or CD_2Cl_2 (^{1}H-NMR: 5.31 ppm and ^{13}C-NMR: 54.00 ppm).[121] All experiments were carried out under normal atmosphere in reagent grade solvents unless otherwise noted. Commercial chemicals were used as supplied from Aldrich or Acros Chemical Co. Column chromatography was performed on neutral aluminum oxide (Brockmann III) and silica gel (230-425 mesh). Melting points are uncorrected and recorded on a Mel-Temp Laboratory Device. Dichlorotetrakis(dimethyl sulphoxide)ruthenium(II),[72] 5,5"-bis-(4-methoxy-2,6-dimethyl-phenyl)-[2,2':6',2"]terpyridine,[105] and Ru[8-(4-hydroxy-2,6-dimethyl-phenyl)-2-[5-(4-hydroxy-2,6-dimethylphenyl)-pyridin-2-yl]-1,10-phenanthroline]$_2$-2PF_6[69] were prepared according to literature procedures. All TRISPHAT, BINPHAT, and BFT salts were graciously provided by Richard Frantz from the Lacour group in Geneva.

Photophysical measurements: All spectra were recorded in spectroscopic grade dichloromethane and are uncorrected. UV-Vis absorption spectra were recorded on Perkin-Elmer UV-Vis Lambda 19 spectrometer at concentrations of 10^{-5} M. Emission measurements were made on the identical samples using an Edinburgh FLSP920 combined steady state, fluorescence and phosphorescence spectrometer. Emission and excitation spectra were collected using the Xe900 – 450W steady state xenon lamp (ozone free) with computer controlled excitation shutter with excitation and observation at each wavelength maximum. Reported emission spectra were

recorded at the global absorption maximum for each compound. Reported excitation spectra were recorded at the emission maximum. Lifetime decays were then measured using time-correlated single photon counting (TCSPC) with the nF900 nanosecond flash-lamp and analyzed with the included software package. The same samples were then diluted to optical transparency (Abs = 0.04 – 0.05) and the emission rerecorded. The integrated intensity was compared to an iso-absorptive standard of 9,10-diphenylanthracene (DPA) in degassed ethanol using the method of Demas and Crosby (Eq. 4.1):[104]

$$\Phi_{unk} = \Phi_{std}\left(\frac{A_{std}}{I_{std}}\right)\left(\frac{I_{unk}}{A_{unk}}\right)\left(\frac{\eta_{unk}}{\eta_{std}}\right)^2 \qquad (4.1)$$

where Φ_{unk} is the fluorescence quantum yield of the unknown, Φ_{std} is the quantum yield of the standard ($\Phi_{DPA} = 0.91$),[104] A_{unk}, A_{std}, I_{unk}, and I_{std} are the respective absorption and the integrated fluorescence intensities of the unknown and standard, and η is the index of refraction of the solvent used for the unknown and standard. Multiple measurements indicate a 5 % precision for Φ_f determined by this method.

Synthetic Procedures:

General procedure for coordination of metal acetates:

An aqueous solution of metal acetate (0.5 molar equiv.) was added drop-wise to an alcoholic solution of ligand (1.0 molar equiv.) at reflux. The resulting colored solution was heated at reflux overnight. After cooling to room temperature, a saturated aqueous solution of potassium hexafluorophosphate was added to induce precipitation. The precipitate was filtered over celite and washed with water and diethyl ether. The precipitate was dissolved in methylene chloride and dried over magnesium sulfate, filtered, and evaporated. Recrystallization from acetonitrile/diethyl ether gave x-ray quality crystals.

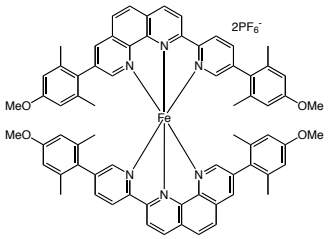

173

Fe[8-(4-methoxy-2,6-dimethyl-phenyl)-2-[5-(4-methoxy-2,6-dimethylphenyl)-pyridin-2-yl]-1,10-phenanthroline]$_2$-2PF$_6$

Pyridyl-phenanthroline **115** (0.049 g, 9.33 × 10^{-5} moles) was dissolved in degassed acetone (5 mL) and heated to 55 ºC. An aqueous solution (5 mL) of Fe(SO_4)-7H_2O (0.26 g, 9.33 × 10^{-5} moles) was added drop-wise over 30 min to cause a dark purple solution. The reaction was heated at 55 ºC for 1.5 hrs. The solution was cooled to room temperature and the acetone evaporated. A saturated aqueous solution of potassium hexafluorophosphate was added to induce precipitation. The precipitate was

filtered over celite and washed with water and diethyl ether. The precipitate was dissolved in methylene and dried over magnesium sulfate, filtered, and evaporated to afford a dark purple crystalline solid (0.057 g, 90%, yield). Recrystallization from acetonitrile/diethyl ether gave x-ray quality crystals. m.p. >350 ºC; ^{1}H NMR (600 MHz, CD_3CN, δ): 9.17 (2H, d, *J* = 8.4 Hz), 9.10 (2H, d, *J* = 8.4 Hz), 8.67 (2H, d, *J* = 8.4 Hz), 8.52 (2H, d, *J* = 9.6 Hz), 8.24 (2H, d, *J* = 9.0 Hz), 8.16 (2H, d, *J* = 1.8 Hz), 7.74 (2H, dd, *J* = 8.4, 1.8 Hz), 7.03 (2H, d, *J* = 1.2 Hz), 6.94 (2H, d, *J* = 1.2 Hz), 6.56 (2H, d, *J* = 1.2 Hz), 6.54 (2H, s), 6.48 (2H, d, *J* = 2.4 Hz), 6.46 (2H, s), 3.69 (6H, s), 3.68 (6H, s), 1.49 (6H, s), 1.48 (6H, s), 1.20 (6H, s), 1.19 (6H, s); ^{13}C NMR (150Mhz, CD_3CN, δ): 161.59, 160.51, 160.50, 157.80, 157.64, 156.08, 151.56, 148.48, 141.68, 141.29, 140.38, 138.84, 138.30, 138.17, 138.11, 137.98, 137.09, 130.82, 130.59, 130.00, 128.96, 128.79, 128.33, 125.20, 123.62, 114.02, 113.96, 55.79, 55.30, 20.83, 20.75, 20.50, 20.38; ESI-MS: *m/z* for $[M]^{2+}$ calc. 553.2, found 553.3; *m/z* for $[M + PF_6^-]^+$ calc. 1251.4, found 1251.2.

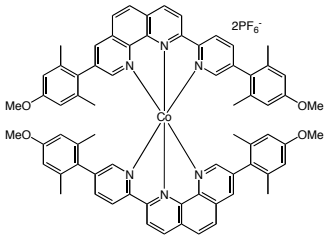

174

Co[8-(4-methoxy-2,6-dimethyl-phenyl)-2-[5-(4-methoxy-2,6-dimethylphenyl)-pyridin-2-yl]-1,10-phenanthroline]$_2$-2PF$_6$

Prepared using general coordination procedures for metal acetates with **115** (0.048 g, 9.14×10^{-5} moles) and $Co(OAc)_2$-$4H_2O$ (0.012 g, 5.03×10^{-5} moles). The precipitate was dissolved in methylene chloride and dried over magnesium sulfate, filtered, and evaporated to afford an orange brown crystalline solid (0.050 g, 78%, yield). Recrystallization from acetonitrile/diethyl ether gave x-ray quality crystals. m.p. >350 ºC; ^{1}H NMR (600 MHz, CD_3CN, δ): 136.00 (2H, s), 100.00 (2H, s), 87.02 (2H, s), 81.79

(2H, s), 32.62 (2H, s), 26.36 (2H, s), 24.01 (2H, s), 10.23 (2H, s), 7.27 (2H, s), 6.75 (2H, s), 5.31 (2H, s), 4.81 (2H, s), 4.20 (6H, s), 2.84 (6H, s), -0.71 (6H, s), -2.12 (6H, s), -3.34 (6H, s), -4.81 (6H, s); ^{13}C NMR (150Mhz, CD_3CN, δ): 187.05, 186.01, 181.73, 175.72, 174.64, 173.96, 163.48, 161.43, 155.91, 147.35, 147.03, 146.48, 146.01, 117.85, 114.18, 114.056, 111.70, 111.60, 56.15, 54.88, 17.37, 16.11, 14.41, 13.16; ESI-MS: m/z for $[M]^{2+}$ calc. 554.7, found 554.8; m/z for $[M + PF_6^-]^+$ calc. 1254.4, found 1254.3.

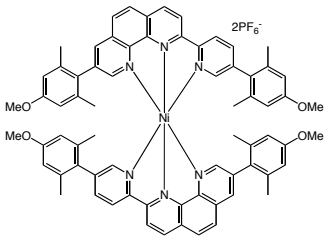

175

Ni[8-(4-methoxy-2,6-dimethyl-phenyl)-2-[5-(4-methoxy-2,6-dimethylphenyl)-pyridin-2-yl]-1,10-phenanthroline]$_2$-2PF$_6$

Prepared using general coordination procedures for metal acetates with **115** (0.047 g, 8.95×10^{-5} moles) and $Ni(OAc)_2$-$4H_2O$ (0.011 g, 4.48×10^{-5} moles). The precipitate was dissolved in methylene chloride and dried over magnesium sulfate, filtered, and evaporated to afford a yellow crystalline solid (0.055 g, 88%, yield). Recrystallization from acetonitrile/diethyl ether gave x-ray quality crystals. m.p. >350 ºC; ^{1}H NMR (600 MHz, CD_3CN, δ): 74.95 (2H, bs), 72.041 (2H, s), 30.68 (2H, s), 25.87 (2H, s), 20.34 (2H, s), 15.09 (2H, s), 12.20 (2H, s), 7.02 (8H, s), 3.69 (6H, s), 3.67 (6H, s), 1.25 (12H, s), 1.06 (12H, s); ^{13}C NMR (150Mhz, CD_3CN, δ): 181.16, 178.60, 163.51, 163.19, 150.90, 150.57, 149.30, 148.86, 114.27, 114.19, 114.04, 113.97, 55.85, 55.81, 18.78, 18.56, 18.42, 18.33; ESI-MS: m/z for $[M]^{2+}$ calc. 554.2, found 554.7; m/z for $[M + PF_6^-]^+$ calc. 1253.4, found 1253.8.

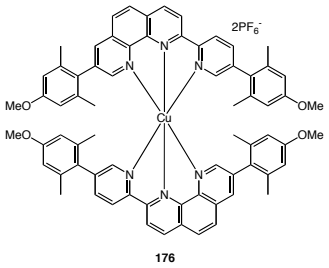

176

Cu[8-(4-methoxy-2,6-dimethyl-phenyl)-2-[5-(4-methoxy-2,6-dimethylphenyl)-pyridin-2-yl]-1,10-phenanthroline]$_2$-2PF$_6$

Prepared using general coordination procedures for metal acetates with **115** (0.058 g, 1.10×10^{-4} moles) and Cu(OAc)$_2$-H$_2$O (0.011 g, 5.50×10^{-5} moles). The precipitate was dissolved in methylene chloride and dried over magnesium sulfate, filtered, and evaporated to afford a dark lime green crystalline solid (0.067 g, 87%, yield). Recrystallization from acetonitrile/diethyl ether gave x-ray quality crystals. m.p. 335 ºC dec.; ^{1}H NMR (600 MHz, CD_3CN, δ): 15.58 (2H, bs), 13.52 (2H, bs), 10.51 (2H, s), 9.00 (2H, s), 7.06 (2H, s), 6.99 (4H, s), 6.91 (2H, s), 3.82 (6H, s), 3.79 (6H, s), 2.39 (12H, s), 2.01 (12H, s); ^{13}C NMR (150Mhz, CD_3CN, δ): 162.07, 161.87, 142.65, 142.62, 141.46, 141.36, 114.31, 114.25, 114.25, 114.21, 55.90, 55.88, 20.88, 20.83; ESI-MS: m/z for $[M]^{2+}$ calc. 556.7, found 556.7; m/z for $[M + PF_6^-]^+$ calc. 1258.4, found 1258.2.

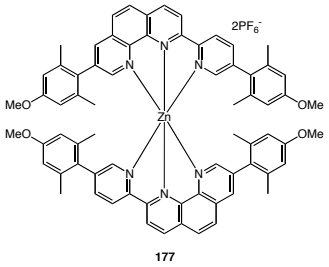

177

Zn[8-(4-methoxy-2,6-dimethyl-phenyl)-2-[5-(4-methoxy-2,6-dimethylphenyl)-pyridin-2-yl]-1,10-phenanthroline]$_2$-2PF$_6$

Prepared using general coordination procedures for metal acetates with **115** (0.046 g, 8.76×10^{-5} moles) and Zn(OAc)$_2$-2H$_2$O (0.01 g, 4.381×10^{-5} moles). The precipitate was dissolved in methylene chloride and dried over magnesium sulfate, filtered, and

evaporated to afford a fluorescent yellow crystalline solid (0.043 g, 70%, yield). Recrystallization from acetonitrile/diethyl ether gave x-ray quality crystals. m.p. 340 ºC dec.; ^{1}H NMR (600 MHz, CD_3CN, δ): 9.12 (2H, d, *J* = 8.4 Hz), 8.96 (2H, d, *J* = 9.0 Hz), 8.72 (2H, dd, *J* = 8.4, 0.6 Hz), 8.43 (2H, d, *J* = 8.4 Hz), 8.33 (2H, d, *J* = 1.8 Hz), 8.21 (2H, d, *J* = 9.0 Hz), 8.00 (2H, dd, *J* = 8.4, 2.4 Hz), 7.92 (2H, d, *J* = 1.8 Hz), 7.70 (2H, d, *J* = 1.8 Hz), 6.62 (2H, d, *J* = 2.4 Hz), 6.59 (2H, s), 6.56 (2H, d, *J* = 2.4 Hz), 6.53 (2H, s), 3.71 (6H, s), 3.69 (6H, s), 1.67 (6H, s), 1.66 (6H, s), 1.48 (6H, s), 1.45 (6H, s); ^{13}C NMR (150Mhz, CD_3CN, δ): 160.64, 160.62, 157.98, 156.04, 155.86, 155.06, 149.53, 147.15, 141.58, 140.84, 140.22, 138.50, 138.44, 138.36, 138.29, 138.23, 135.24, 131.85, 131.09, 130.04, 128.98, 128.89, 128.43, 125.71, 123.21, 114.35, 114.06, 114.01, 55.87, 55.87, 20.98, 20.88, 20.73, 20.60; ESI-MS: *m*/*z* for $[M]^{2+}$ calc. 557.2, found 557.2; *m*/*z* for $[M + PF_6^-]^+$ calc. 1259.4, found 1259.2.

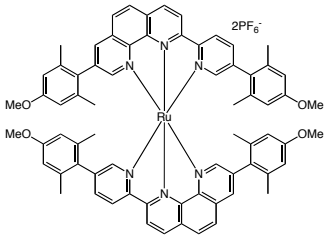

178

Ru[8-(4-methoxy-2,6-dimethyl-phenyl)-2-[5-(4-methoxy-2,6-dimethylphenyl)-pyridin-2-yl]-1,10-phenanthroline]$_2$-2PF$_6$

An ethylene glycol solution (20 mL) of ligand **115** (0.100 g, 1.91 × 10^{-4} moles) and $RuCl_2(DMSO)_4$ (0.046 g, 9.52 × 10^{-4} moles) was heated at 125 ºC overnight. The solution was cooled to room temperature and a saturated aqueous solution of potassium hexafluorophosphate was added to induce precipitation. The dark red precipitate was filtered over celite and washed with water and diethyl ether. The precipitate was dissolved in methylene chloride and dried over magnesium sulfate, filtered, and evaporated to afford a blood-red crystalline solid (0.107 g, 78%, yield).

Recrystallization from acetonitrile/diethyl ether gave x-ray quality crystals. m.p. >350 ºC; ^{1}H NMR (600 MHz, CD_3CN, δ): 8.92 (2H, d, *J* = 8.4 Hz), 8.80 (2H, d, *J* = 9.0 Hz), 8.64 (2H, d, *J* = 8.4 Hz), 8.39 (2H, d, *J* = 9.0 Hz), 8.23 (2H, d, *J* = 1.2 Hz), 8.20 (2H, d, *J* = 9 Hz), 7.78 (2H, dd, *J* = 7.80, 1.8 Hz), 7.40 (2H, d, *J* = 1.2 Hz), 7.20 (2H, d, *J* = 1.8 Hz), 6.58 (2H, d, *J* = 2.4 Hz), 6.55 (2H, s), 6.52 (2H, d, *J* = 2.4 Hz), 6.48 (2H, s), 3.69 (6H, s), 3.68 (6H, s), 1.57 (6H, s), 1.57 (6H, s), 1.36 (6H, s), 1.33 (6H, s); ^{13}C NMR (150Mhz, CD_3CN, δ): 160.63, 160.59, 151.31, 150.63, 150.25, 147.38, 143.74, 143.64, 141.80, 141.41, 141.30, 140.08, 140.02, 138.61, 138.57, 138.38, 138.33, 130.85, 130.62, 129.48, 129.10, 128.76, 127.98, 124.48, 123.13, 114.08, 114.05, 114.02, 55.88, 55.86, 21.10, 21.00, 20.88, 20.75; ESI-MS: *m*/*z* for $[M]^{2+}$ calc. 576.2, found 575.4; *m*/*z* for $[M + PF_6^-]^+$ calc. 1297.3, found 1297.2.

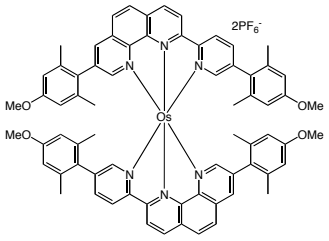

179

Os[8-(4-methoxy-2,6-dimethyl-phenyl)-2-[5-(4-methoxy-2,6-dimethylphenyl)-pyridin-2-yl]-1,10-phenanthroline]$_2$-2PF$_6$

An ethylene glycol solution (1.5 mL) of ligand **115** (0.053 g, 1.00 × 10^{-4} moles) and K_2OsCl_6 (0.024 g, 5.00 × 10^{-5} moles) was placed in a microwave reactor and the temperature raised to 225 ºC over 5 min at 225 W. The temperature was maintained for 10 min and then cooled to room temperature. The solution was poured into a saturated aqueous solution of potassium hexafluorophosphate to induce precipitation. The dark red-brown precipitate was filtered over celite and washed with water and diethyl ether. The precipitate was dissolved in methylene chloride and dried over magnesium sulfate, filtered, and evaporated. Column chromatography on neutral

aluminum oxide with a methylene chloride/methanol gradient (100/0, 99/1, 97/3) as eluant gave the product as a dark brown crystalline solid (0.021 g, 27%, yield). Recrystallization from acetonitrile/diethyl ether gave x-ray quality crystals. m.p. >350 ºC; ^{1}H NMR (600 MHz, CD_3CN, δ): 8.91 (2H, d, *J* = 9.0 Hz), 8.60 (2H, d, *J* = 7.8 Hz), 8.34 (2H, d, *J* = 9.0 Hz), 8.27 (2H, d, *J* = 9.0 Hz), 8.20 (2H, d, *J* = 9.0 Hz), 8.16 (2H, d, *J* = 1.2 Hz), 7.65 (2H, dd, *J* = 8.4, 1.8 Hz), 7.38 (2H, d, *J* = 1.2 Hz), 7.07 (2H, d, *J* = 1.2 Hz), 6.58 (2H, d, *J* = 1.8 Hz), 6.55 (2H, s), 6.51 (2H, d, *J* = 2.4 Hz), 6.48 (2H, s), 3.69 (6H, s), 3.67 (6H, s), 1.58 (6H, s), 1.57 (6H, s), 1.38 (6H, s), 1.36 (6H, s); ^{13}C NMR (150Mhz, CD_3CN, δ): 160.56, 160.54, 159.53, 155.47, 154.70, 154.57, 153.12, 146.80, 141.85, 140.59, 140.52, 138.54, 138.49, 138.38, 138.32, 137.19, 134.86, 132.20, 130.11, 129.58, 129.50, 128.72, 128.14, 125.96, 121.79, 113.98, 113.93, 55.82, 55.82, 20.96, 20.89, 20.74, 20.63; ESI-MS: *m*/*z* for $[M]^{2+}$ calc. 621.2, found 620.8; *m*/*z* for $[M + PF_6^-]^+$ calc. 1386.5, found 1385.6.

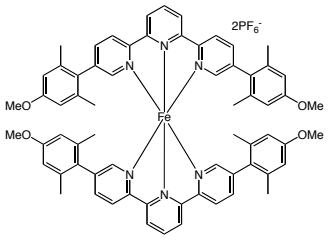

181

Fe[5,5''-bis-(4-methoxy-2,6-dimethyl-phenyl)-[2,2':6',2'']terpyridine]$_2$-2PF$_6$

Terpyridine **102** (0.116 g, 2.32 × 10^{-4} moles) was dissolved in degassed acetone (10 mL) and heated to 55 ºC. An aqueous solution (10 mL) of $Fe(SO_4)$-$7H_2O$ (0.064 g, 2.32 × 10^{-4} moles) was added drop-wise over 30 min to cause a dark purple solution. The reaction was heated at 55 ºC overnight. The solution was cooled to room temperature and the acetone evaporated. A saturated aqueous solution of potassium hexafluorophosphate was added to induce precipitation. The precipitate was filtered over celite and washed with water and diethyl ether. The precipitate was dissolved in

methylene and dried over magnesium sulfate, filtered, and evaporated to afford a dark purple crystalline solid (0.287 g, 92%, yield). Recrystallization from acetonitrile/diethyl ether gave x-ray quality crystals. m.p. >350 ºC; ^{1}H NMR (500 MHz, CD_3CN, δ): 8.82 (4H, d, J = 8.5 Hz), 8.54 (2H, t, J = 8.0 Hz), 8.49 (4H, dd, J = 8.5, 0.5 Hz), 7.73 (4H, dd, J = 8.0, 2.0 Hz), 6.86 (4H, d, J = 1.0 Hz), 6.58 (8H, s), 3.72 (12H, s), 1.49 (24H, s); (125Mhz, CD_3CN, δ): 161.15, 160.69, 157.29, 154.52, 141.58, 141.46, 139.26, 138.29, 128.56, 124.71, 124.50, 114.15, 55.91, 20.75; ESI-MS: m/z for $[M]^{2+}$ calc. 529.2, found 528.8; m/z for $[M + PF_6^-]^+$ calc. 1203.4, found 1203.6.

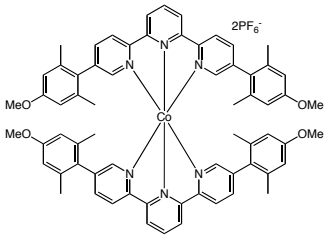

182

Co[5,5''-bis-(4-methoxy-2,6-dimethyl-phenyl)-[2,2':6',2'']terpyridine]$_2$-2PF$_6$

Prepared using general coordination procedures for metal acetates with **102** (0.050 g, 9.98×10^{-5} moles) and $Co(OAc)_2$-$4H_2O$ (0.012 g, 4.99×10^{-5} moles). The precipitate was dissolved in methylene chloride and dried over magnesium sulfate, filtered, and evaporated to afford a brown crystalline solid (0.056 g, 83%, yield). Recrystallization from acetonitrile/diethyl ether gave x-ray quality crystals. m.p. >350 ºC; ^{1}H NMR (600 MHz, CD_3CN, δ): 98.05 (4H, bs), 57.17 (4H, bs), 47.28 (4H, bs), 21.46 (2H, s), 8.57 (4H, s), 6.70 (8H, s), 3.71 (12H, s), -0.186 (24H, s); ^{13}C NMR (150 Mhz, CD_3CN, δ): 171.39, 162.57, 151.21, 146.33, 114.03, 55.89, 18.01; ESI-MS: m/z for $[M]^{2+}$ calc. 530.7, found 530.8; m/z for $[M + PF_6^-]^+$ calc. 1206.4, found 1206.1.

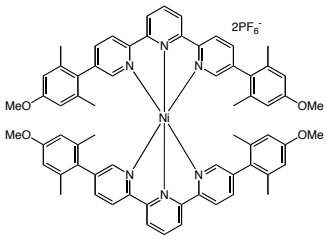

183

Ni[5,5''-bis-(4-methoxy-2,6-dimethyl-phenyl)-[2,2':6',2'']terpyridine]$_2$-2PF$_6$

Prepared using general coordination procedures for metal acetates with **102** (0.050 g, 1.00×10^{-4} moles) and Ni(OAc)$_2$-4H$_2$O (0.012 g, 5.00×10^{-5} moles). The precipitate was dissolved in methylene chloride and dried over magnesium sulfate, filtered, and evaporated to afford a yellow crystalline solid (0.056 g, 83%, yield). Recrystallization from acetonitrile/diethyl ether gave x-ray quality crystals. m.p. >350 ºC; ^{1}H NMR (300 MHz, CD$_3$CN, δ): 98.05 (4H, bs), 75.21 (4H, bs), 69.51 (4H, bs), 17.66 (2H, bs), 12.52 (4H, bs), 7.14 (8H, s), 3.74 (12H, s), 1.42 (24H, s); ^{13}C NMR (75 Mhz, CD$_3$CN, δ): 171.67, 163.36, 150.46, 132.03, 114.44, 55.96, 19.05; ESI-MS: m/z for $[M]^{2+}$ calc. 530.2, found 530.8; m/z for $[M + PF_6^-]^+$ calc. 1205.4, found 1206.1.

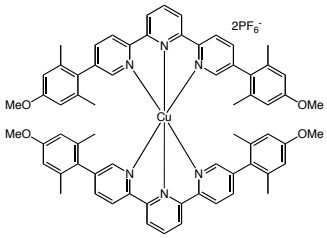

184

Cu[5,5''-bis-(4-methoxy-2,6-dimethyl-phenyl)-[2,2':6',2'']terpyridine]$_2$-2PF$_6$

Prepared using general coordination procedures for metal acetates with **102** (0.044 g, 8.782×10^{-5} moles) and Cu(OAc)$_2$-H$_2$O (0.009 g, 4.391×10^{-5} moles). The precipitate was dissolved in methylene chloride and dried over magnesium sulfate, filtered, and evaporated to afford a dark lime green crystalline solid (0.049 g, 82%, yield). Recrystallization from acetonitrile/diethyl ether gave x-ray quality crystals. m.p. 335 ºC dec.; ^{1}H NMR (300 MHz, CD$_3$CN, δ): 9.22 (4H, bs), 7.01 (8H, s), 3.81 (12H, s), 2.27

(24H, s); ^{13}C NMR (100 Mhz, CD_3CN, δ): 161.76, 141.59, 114.33, 55.82, 20.93; ESI-MS : m/z for $[M]^{2+}$ calc. 532.7, found 533.3; m/z for $[M + PF_6^-]^+$ calc. 1210.4, found 1211.6.

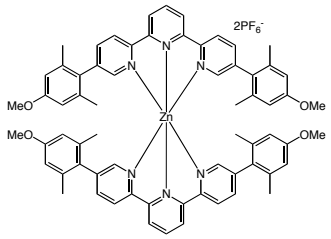

185

Zn[5,5''-bis-(4-methoxy-2,6-dimethyl-phenyl)-[2,2':6',2'']terpyridine]$_2$-2PF$_6$

Prepared using general coordination procedures for metal acetates with **102** (0.044 g, 8.78×10^{-5} moles) and $Zn(OAc)_2$-$2H_2O$ (0.009 g, 4.4×10^{-5} moles). The precipitate was dissolved in methylene chloride and dried over magnesium sulfate, filtered, and evaporated to afford a fluorescent yellow crystalline solid (0.049 g, 82%, yield). Recrystallization from acetonitrile/diethyl ether gave x-ray quality crystals. m.p. 340 ºC dec.; ^{1}H NMR (500 MHz, CD_3CN, δ): 8.68 (4H, d, J = 8.0 Hz), 8.58 (2H, t, J = 8.0 Hz), 8.56 (4H, dd, J = 8.0, 0.5 Hz), 7.96 (4H, dd, J = 8.0, 2.0 Hz), 7.64 (4H, dd, J = 1.5, 0.5 Hz), 6.62 (8H, s), 3.72 (12H, s), 1.63 (24H, s); ^{13}C NMR (125 Mhz, CD_3CN, δ): 160.64, 150.46, 149.68, 147.35, 145.39, 143.74, 141.57, 138.43, 128.80, 124.80, 123.92, 114.10, 55.90, 20.97; ESI-MS: m/z for $[M]^{2+}$ calc. 533.2, found 533.8; m/z for $[M + PF_6^-]^+$ calc. 1211.4, found 1212.1.

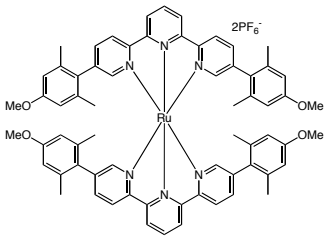

186

Ru[5,5''-bis-(4-methoxy-2,6-dimethyl-phenyl)-[2,2':6',2'']terpyridine]$_2$-2PF$_6$

An ethylene glycol solution (20 mL) of ligand **102** (0.050 g, 9.98 × 10^{-5} moles) and $RuCl_2(DMSO)_4$ (0.024 g, 4.99 × 10^{-5} moles) was heated at 125º overnight. The solution was cooled to room temperature and a saturated aqueous solution of potassium hexafluorophosphate was added to induce precipitation. The dark red precipitate was filtered over celite and washed with water and diethyl ether. The precipitate was dissolved in methylene chloride and dried over magnesium sulfate, filtered, and evaporated to afford a blood-red crystalline solid (0.055 g, 99% yield). Recrystallization from acetonitrile/diethyl ether gave x-ray quality crystals. m.p. >350 C; ^{1}H NMR (600 MHz, CD_3CN, δ): 8.66 (4H, d, *J* = 7.8 Hz), 8.50 (4H, d, *J* = 8.4 Hz), 8.28 (2H, t, *J* = 7.8 Hz), 7.76 (4H, dd, *J* = 8.4, 1.8 Hz), 7.17 (4H, d, *J* = 1.2 Hz), 6.59 (8H, s), 3.72 (12H, s), 1.57 (24H, s); ^{13}C NMR (150 Mhz, CD_3CN, δ): 160.69, 157.45, 156.21, 153.69, 141.60, 140.66, 138.35, 137.05, 128.51, 125.00, 124.80, 114.12, 55.91, 21.00; ESI-MS: *m*/*z* for $[M]^{2+}$ calc. 552.2, found 552.1; *m*/*z* for $[M + PF_6^-]^+$ calc. 1249.3, found 1249.3.

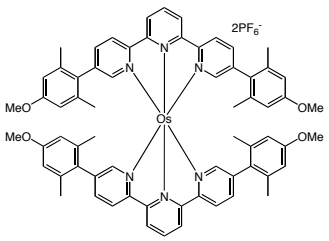

187

Os[5,5''-bis-(4-methoxy-2,6-dimethyl-phenyl)-[2,2':6',2'']terpyridine]$_2$-2PF$_6$

An ethylene glycol solution (1.5 mL) of ligand **102** (0.050 g, 1.00 × 10^{-4} moles) and K_2OsC_6 (0.024 g, 5.00 × 10^{-5} moles) was placed in a microwave reactor and the

temperature raised to 190 ºC over 5 min at 225 W. The temperature was maintained for 10 min and then cooled to room temperature. The solution was poured into a saturated aqueous solution of potassium hexafluorophosphate to induce precipitation. The dark brown precipitate was filtered over celite and washed with water and diethyl ether. The precipitate was dissolved in methylene chloride and dried over magnesium sulfate, filtered, and evaporated. Column chromatography on neutral aluminum oxide with a methylene chloride/methanol gradient (100/0, 99/1, 97/3) as eluant gave the product as a dark brown crystalline solid (0.018 g, 25%, yield). Recrystallization from acetonitrile/diethyl ether gave x-ray quality crystals. m.p. >350 ºC; ^{1}H NMR (400 MHz, CD_3CN, δ): 8.71 (4H, d, J = 8.4 Hz), 8.49 (4H, dd, J = 8.4, 0.4 Hz), 7.93 (2H, t, J = 8.4 Hz), 7.67 (4H, dd, J = 8.4, 2.0 Hz), 7.01 (4H, dd, J = 1.2, 0.4 Hz), 6.57 (8H, s), 3.72 (12H, s), 1.62 (24H, s); ^{13}C NMR (100 Mhz, CD_3CN, δ): 160.53, 158.12, 155.07, 152.97, 142.44, 140.87, 137.63, 137.06, 126.96, 124.93, 123.14, 114.12, 55.77, 21.03; ESI-MS: m/z for $[M]^{2+}$ calc. 597.2, found 597.2; m/z for $[M + PF_6^-]^+$ calc. 1339.4, found 1339.4.

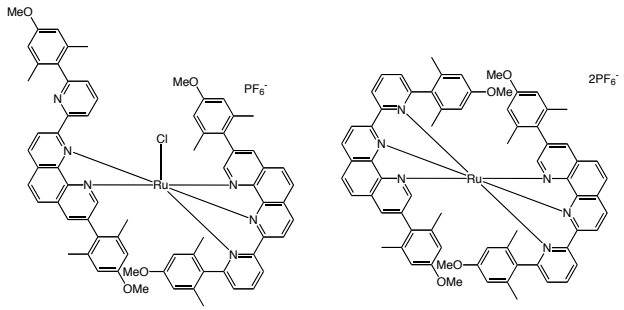

Ru[8-(4-methoxy-2,6-dimethyl-phenyl)-2-[6-(4-methoxy-2,6-dimethylphenyl)-pyridin-2-yl]-1,10-phenanthroline]$_2$Cl-PF$_6$

Ru[8-(4-methoxy-2,6-dimethyl-phenyl)-2-[6-(4-methoxy-2,6-dimethylphenyl)-pyridin-2-yl]-1,10-phenanthroline]$_2$-PF$_6$

An ethylene glycol solution (5 mL) of ligand **114** (0.038 g, 7.24×10^{-5} moles) and $RuCl_2(DMSO)_4$ (0.018 g, 3.62×10^{-5} moles) was heated at 125 ºC for 4 h. The solution was cooled to room temperature and a saturated aqueous solution of potassium hexafluorophosphate was added to induce precipitation. The dark reddish-brown precipitate was filtered over celite and washed with water and diethyl ether. The precipitate was dissolved in methylene chloride and dried over magnesium sulfate, filtered, and evaporated to afford a red-brown crystalline solid (0.041 g). Column chromatography on silica gel with a acetonitrile:water:sat. aq. KPF_6 (100:0:0; 97:3:0.3; 95:5:0.5) as eluant gave **188** as a red-brown solid (0.009 g, 20% yield) and **189** as a red crystalline solid (0.005 g, 10% yield). Complex **188** was not characterized but dissolved in a solution of ethylene glycol : dichloroethane : ethanol (1:1:0.5 mL) and heated to 150 ºC for 2 days. After precipitation with aq. KPF_6, only compound **189** (0.006 g) was isolated (0.011 g, 20% total yield). m.p. >350 ºC; ^{1}H NMR (600 MHz, CD_3CN, δ): 8.78 (2H, d, J = 9.0 Hz), 8.75 (2H, dd, J = 8.4, 1.2 Hz), 8.68 (2H, d, J = 8.4 Hz), 8.25 (2H, d, J = 9.0 Hz), 8.16 (2H, t, J = 7.8 Hz), 7.56 (2H, d, J = 9.0, Hz), 7.22 (2H, dd, J = 7.80,

1.2 Hz), 6.93 (2H, d, J = 5.4 Hz), 6.79 (2H, d, J = 2.4 Hz), 6.68 (2H, d, J = 2.4 Hz), 6.62 (2H, d, J = 6.0 Hz), 6.39 (2H, d, J = 2.4 Hz), 5.39 (2H, d, J = 1.8 Hz), 3.78 (6H, s), 3.77 (6H, s), 1.87 (6H, s), 1.27 (6H, s), 1.22 (6H, s), 0.18 (6H, s); ^{13}C NMR (150Mhz, CD_3CN, δ): 167.70, 161.15, 161.07, 160.35, 157.18, 153.60, 150.90, 149.91, 147.20, 140.52, 138.45, 138.19, 137.81, 137.27, 133.96, 131.69, 131.25, 131.06, 130.66, 129.30, 128.82, 127.68, 127.44, 125.54, 123.80, 114.28, 114.19, 114.08, 112.18, 55.97, 55.83, 21.05, 20.80, 19.95, 19.07; ESI-MS: m/z for $[M]^{2+}$ calc. 576.2, found 575.4; m/z for $[M + PF_6^-]^+$ calc. 1297.3, found 1297.2.

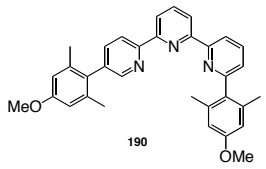

190

5,6''-bis-(4-methoxy-2,6-dimethyl-phenyl)-[2,2':6',2'']terpyridine

To a THF solution (25 mL) of 2-bromo-6-(4-methoxy-2,6-dimethylphenyl)pyridine **B1** (0.750 g 2.57 × 10^{-3} moles) at -78 ºC, was added n-BuLi (1.50 mL of a 2.5 M sol in hexanes) and stirred for 5 min. A THF solution (25 mL) of $ZnCl_2$ (0.37 g, 2.69 × 10^{-3} moles) was cannulated into the reaction flask. The solution was stirred, allowed to warm to room temperature, and then cannulated into a THF solution of 2,6-dibromopyridine (0.750 g, 3.18 × 10^{-3} moles)) and $Pd(PPh_3)_4$ (0.142 g, 1.22 × 10^{-4} moles). The resulting solution was heated at reflux overnight. The THF was removed by rotary evaporator and the residual solution diluted in methylene chloride. After extraction with a saturated aqueous EDTA solution basified with sodium bicarbonate, the organic layer was separated, dried over magnesium sulfate, filtered, and evaporated. The crude was then purified on silica gel with 10% ethyl acetate in hexanes to give a 6-bromo, 6'-(4-methoxy-2,6-dimethyl-phenyl)-2,2'-bipyridine as white solid (0.457 g, 48% yield). 6-bromo, 6'-(4-methoxy-2,6-dimethyl-phenyl)-2,2'-bipyridine (0.390 g, 1.06 × 10^{-}

^{3} moles) was dissolved in THF (25 mL) and cooled to -78°C. To this was added t-BuLi (0.97 mL of a 1.7 M sol in pentanes) and the solution stirred for 5 min. A THF solution (25 mL) of $ZnCl_2$ (0.223 g, 1.64×10^{-3} moles) was cannulated into the reaction flask. The solution was stirred, allowed to warm to room temperature, and then cannulated into a THF solution of 2-bromo-4-(4-methoxy-2,6-dimethylphenyl)pyridine **B2** (0.464 g, 1.59×10^{-3} moles) and $Pd(PPh_3)_4$ (0.061 g, 5.30×10^{-5} moles). The resulting solution was heated at reflux overnight. After cooling to room temperature, a tan precipitate was filtered and washed with cold THF before drying. The precipitate was dissolved in methylene chloride and extracted with a saturated aqueous EDTA solution basified with sodium bicarbonate. The organic layer was separated, dried over magnesium sulfate, filtered, and evaporated to give an off-white solid (0.285 g, 54% yield). m.p. 225 – 228 °C; ^{1}H NMR (400 MHz, $CDCl_3$, δ): 8.73 (1H, dd, *J* = 8.4, 0.8 Hz), 8.58 (1H, dd, *J* = 8.0, 1.2 Hz), 8.51 (1H, dd, *J* = 8.0, 1..2 Hz), 8.48 (2H, d, *J* = 7.6 Hz), 7.93 (1H, t, *J* = 7.6 Hz), 7.91 (1H, t, *J* = 7.6 Hz), 7.69 (1H, dd, *J* = 8.0, 2.0 Hz), 7.26 (1H, dd, *J* = 7.6, 1.2 Hz), 6.73 (2H, s), 6.72 (2H, s), 3.85 (6H, s), 2.15 (6H, s), 2.10 (6H,s); ^{13}C NMR (100Mhz, $CDCl_3$, δ): 158.99, 158.94, 158.90, 156.02, 155.72, 155.15, 154.63, 149.95, 138.27, 137.86, 137.85, 137.53, 136.61, 133.62, 130.41, 125.14, 121.40, 120.76, 120.73, 118.82, 113.04, 112.96, 55.15, 55.15, 21.21, 20.75; HRMS *m/z*: calc. for $C_{33}H_{31}N_3O_2$: 501.24163; found: 501.24103.

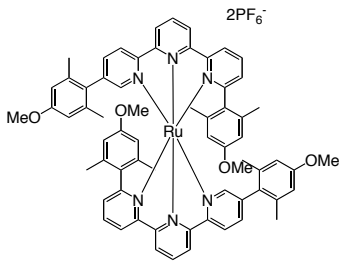

191

Ru[5,6''-bis-(4-methoxy-2,6-dimethyl-phenyl)-[2,2':6',2'']terpyridine]$_2$-2PF$_6$

An ethylene glycol solution (5 mL) of ligand **192** (0.100 g, 2.00 × 10^{-5} moles) and $RuCl_2(DMSO)_4$ (0.048 g, 5.00 × 10^{-5} moles) was heated at 150 ºC for 2 days. The solution was cooled to room temperature and a saturated aqueous solution of potassium hexafluorophosphate was added to induce precipitation. The dark red precipitate was filtered over celite and washed with water and diethyl ether. The precipitate was dissolved in methylene chloride and dried over magnesium sulfate, filtered, and evaporated to afford a blood-red crystalline solid (0.135 g, 97%, yield). m.p. 235 ºC dec.; ^{1}H NMR (600 MHz, CD_3CN, δ): 8.53 (2H, m, *J* = 9.0 Hz), 8.41 (6H, m, *J* = 8.4, 1.2 Hz), 8.12 (4H, m, *J* = 8.4 Hz), 7.68 (2H, dd, *J* = 8.0, 2.0 Hz), 7.16 (2H, d, *J* = 7.6, 0.8 Hz), 6.52 (4H, s), 6.41 (2H, s), 6.19 (2H, dd, *J* = 10.8, 1.2 Hz), 3.86 (6H, s), 3.70 (6H, s), 1.68 (6H, s), 1.37 (6H, s), 1.17 (6H, s), 0.62 (6H, s); ^{13}C NMR (100Mhz, CD_2Cl_2, δ): 167.21, 160.60, 160.36, 159.93, 157.30, 156.84, 154.55, 151.54, 142.00, 141.07, 140.21, 137.55, 137.43, 137.14, 136.66, 135.93, 132.54, 132.44, 130.76, 127.08, 124.70, 124.41, 124.28, 123.29, 114.26, 114.19, 114.04, 55.84, 55.71, 21.20, 20.85, 20.57, 19.08 ; ESI-MS: *m*/*z* for $[M]^{2+}$ calc. 552.2, found 552.1; *m*/*z* for $[M + PF_6^-]^+$ calc. 1249.3, found 1249.3.

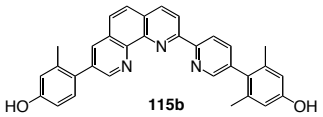

115b

8-(4-Hydroxy-2,6-dimethyl-phenyl)-2-[6-(4-hydroxy-2,6-dimethylphenyl)-pyridin-2-yl]-1,10-phenanthroline

Prepared according to literature procedures.[69] Tan solid (0.260 g, 97%). Spectra matched literature values. m.p. 263 – 266 ºC decomposes. ^{1}H NMR (500 MHz, DMSO-d_6, δ): 9.42 (1H, s), 9.37 (1H, bs), 8.96 (1H, d, *J* = 2.0 Hz), 8.91 (1H, d, *J* = 8.0 Hz), 8.81 (1H, d, *J* = 8.0 Hz), 8.66 (1H, d, *J* = 8.0 Hz, 1H), 8.54 (1H, d, *J* = 2.0 Hz), 8.35 (1H, d, *J* = 2.0 Hz), 8.09 (1H, d, *J* =9.0 Hz), 8.04 (1H, d, *J* = 9.0 Hz), 7.87 (1H, dd, *J* = 8.0, 2.0 Hz), 6.64 (2H, s), 6.60 (2H, s), 1.99 (6H, s), 1.98 (6H s). ^{13}C NMR (125 MHz, DMSO-d_6, δ): 156.98, 156.84, 155.14, 153.86, 151.42, 150.12, 145.06, 143.89, 138.92, 137.56, 137.26, 137.09, 137.04, 137.01, 135.84, 128.79, 128.59, 128.38, 128.26, 127.22, 126.83, 121.42, 119.95, 114.57, 114.51, 20.85, 20.77.

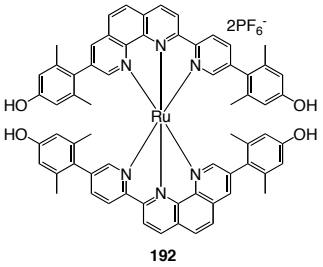

192

Ru[8-(4-hydroxy-2,6-dimethyl-phenyl)-2-[6-(4-hydroxy-2,6-dimethylphenyl)-pyridin-2-yl]-1,10-phenanthroline]$_2$-2PF$_6$

An ethylene glycol solution (20 mL) of ligand **115b** (0.086 g, 1.73 × 10^{-4} moles) and $RuCl_2(DMSO)_4$ (0.041 g, 8.65 × 10^{-4} moles) was heated at 125 ºC overnight. The solution was cooled to room temperature and a saturated aqueous solution of potassium hexafluorophosphate was added to induce precipitation. The dark red precipitate was filtered over celite and washed with water and diethyl ether. The precipitate was dissolved in acetonitrile, diluted with methylene chloride and dried over

magnesium sulfate, filtered, and evaporated to afford a blood-red crystalline solid (0.083 g, 70%, yield). m.p. > 350 ºC; ^{1}H NMR (400 MHz, $CDCl_3$, δ): 9.21 (1H, dd, *J* = 4.4, 1.6 Hz), 8.94 (1H, d, *J* = 4.8) Hz, 8.28 (1H, dd, *J* = 8.0, 1.6 Hz), 8.21 (1H, d, *J* = 9.2 Hz), 7.92 (1H, d, *J* = 4.4 Hz), 7.89 (1H, d, *J* = 9.2 Hz), 7.67 (1H, q, *J* = 4 Hz); ^{13}C NMR (75Mhz, $CDCl_3$, δ): 150.749, 149.715, 147.087, 145.645, 136.138, 134.022, 128.579, 128.159, 127.728, 127.114, 124.871, 123.596, 20.49; ESI-MS: *m*/*z* for $[M]^{2+}$ calc. 548.2, found 548.1; *m*/*z* for $[M + PF_6^-]^+$ calc. 1241.2, found 1241.2.

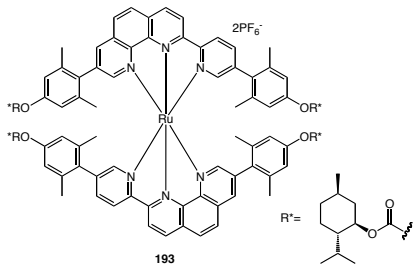

Ru[8-(4-(-)-(R)-(menthyl formate)-2,6-dimethyl-phenyl)-2-[6-(4-(-)-(R)-(menthyl formate) -2,6-dimethylphenyl)-pyridin-2-yl]-1,10-phenanthroline]$_2$-2PF$_6$

Complex **192** was dissolved in acetonitrile and DIPEA was added to cause a turbid solution. The solution was stirred for 10 min at room temperature and (-)-(R)-menthyl chloroformate was added and the solution stirred for 2 h. The reaction was quenched with water and extracted with methylene chloride. The organic layers was separated, dried over magnesium sulfate, filtered, and evaporated to afford a blood-red solid (0.059 g, 78% yield). m.p. 235 – 240 ºC; ^{1}H NMR (400 MHz, CD_3CN, δ): 8.95 (2H, d, *J* = 8.8 Hz), 8.83 (2H, d, *J* = 8.8) Hz, 8.69 (2H, d, *J* = 8.0 Hz), 8.41 (2H, d, *J* = 8.8 Hz), 8.28 (2H, d, *J* = 1.2 Hz), 8.22 (2H, d, *J* = 8.4 Hz), 7.83 (2H, dd, *J* = 8.4, 1.2 Hz), 7.45 (2H, d, *J* = 1.2 Hz), 7.27 (2H, d, *J* = 2.0 Hz), 6.85 (2H, s), 6.82 (2H, s), 6.78 (2H, s), 6.75 (2H, s), 4.55 (4H, m), 2.05 (4H, m), 1.71 (8H, m), 1.59 (12H, d, *J* = 2.0 Hz), 1.45 (10H, m), 1.40 (6H, d, *J* = 4.0 Hz), 1.38 (6H, d, *J* = 4.0 Hz), 1.10 (8H, m), 0.92 (30H, m), 0.80 (12H, dd, *J* = 6.8, 1.2 Hz); ^{13}C NMR (100Mhz, CD_3CN, δ): 158.49, 155.86,

155.53, 154.69, 154.31, 154.29, 152.06, 152.03, 149.88, 147.16, 140.73, 140.50, 139.32, 138.92, 138.88, 138.68, 138.64, 138.15, 135.34, 134.31, 133.85, 131.85, 131.37, 130.08, 129.14, 125.96, 123.49, 121.33, 121.32, 121.29, 80.49, 48.07, 41.28, 34.80, 32.24, 30.97, 27.28, 24.28, 22.31, 20.99, 20.81, 20.72, 20.59, 20.47; ESI-MS: m/z for $[M]^{2+}$ calc. 912.4, found 912.4.

4.4 Crystal Structure Data

Methods and Materials

All measurements were made on a *Nonius KappaCCD* area-detector diffractometer[122] using graphite-monochromated Mo *K*a radiation (λ = 0.71073 Å) and an *Oxford Cryosystems Cryostream 700* cooler. Data reduction was performed with *HKL Denzo* and *Scalepack*.[123] The intensities were corrected for Lorentz and polarization effects, but not for absorption. The structures were solved by direct methods using *SIR92*,[124] which revealed the positions of all non-hydrogen atoms. The non-hydrogen atoms were refined anisotropically. All of the H-atoms were placed in geometrically calculated positions and refined using a riding model where each H-atom was assigned a fixed isotropic displacement parameter with a value equal to $1.2U_{eq}$ of its parent atom ($1.5U_{eq}$ for the methyl groups). Refinement of the structure was carried out on F^2 by using full-matrix least-squares procedures, which minimized the function $Sw(F_o^2 - F_c^2)^2$. The weighting scheme was based on counting statistics and included a factor to downweight the intense reflections. Neutral atom scattering factors for non-hydrogen atoms were taken from Maslen, Fox and O'Keefe,[125] and the scattering factors for H-atoms were taken from Stewart, Davidson and Simpson.[126] Anomalous dispersion effects were included in F_c;[127] the values for f' and f'' were those of Creagh and McAuley.[128] The values of the mass attenuation coefficients are those of Creagh and Hubbel.[129] All calculations were performed using the *SHELXL97*[130] program.

Table 4.18 Crystallographic Data for **173**.

Crystallised from		CH_3CN / Et_2O
Empirical formula		$C_{74}H_{68}F_{12}FeN_8O_4P_2$
Formula weight [g mol^{-1}]		1479.17
Crystal colour, habit		purple, prism
Crystal dimensions [mm]		0.25 × 0.27 × 0.37
Temperature [K]		160 (1)
Crystal system		orthorhombic
Space group		*Pcca* (#54)
Z		4
Reflections for cell determination		106882
2θ range for cell determination [°]		4 – 50
Unit cell parameters	a [Å] = 25.6038(5)	α [°] = 90
	b [Å] = 12.2125(2)	β [°] = 90
	c [Å] = 21.8379(3)	γ [°] = 90
V [Å^3]	6828.4(2)	
F(000)		3056
D_x [g cm^{-3}]		1.439
μ(Mo $K\alpha$) [mm^{-1}]		0.358
Scan type		ϕ and ω
$2\theta_{(max)}$ [°]		50
Transmission factors (min; max)		0.817; 0.917
Total reflections measured		85406
Symmetry independent reflections		6034
R_{int}		0.085
Reflections with $I > 2\sigma(I)$		4164
Reflections used in refinement		6034
Parameters refined; restraints		640; 944
Final $R(F)$ [$I>2\sigma(I)$ reflections]		0.0663
$wR(F^2)$ (all data)		0.1991
Weights:	$w = [\sigma^2(F_o^2) + (0.1069P)^2 + 6.6299P]^{-1}$ where $P = (F_o^2 + 2F_c^2)/3$	
Goodness of fit		1.047
Secondary extinction coefficient		0.0027(4)
Final Δ_{max}/σ		0.001
$\Delta\rho$ (max; min) [e Å^{-3}]		1.04; -0.41
$\sigma(d_{(C-C)})$ [Å]		0.005 – 0.03

Table 4.19 Crystallographic Data for **174**.

Crystallised from		CH_3CN / Et_2O
Empirical formula		$C_{74}H_{68}CoF_{12}N_8O_4P_2$
Formula weight [g mol^{-1}]		1482.26
Crystal colour, habit		orange-brown, prism
Crystal dimensions [mm]		0.25 × 0.25 × 0.35
Temperature [K]		160 (1)
Crystal system		orthorhombic
Space group		*Pcca* (#54)
Z		4
Reflections for cell determination		88463
2θ range for cell determination [°]		4–50
Unit cell parameters	a [Å] = 25.3072(4)	α [°] = 90
	b [Å] = 12.5642(1)	β [°] = 90
	c [Å] = 21.8238(3)	γ [°] = 90
V [Å^3]	6939.2(2)	
F(000)		3060
D_x [g cm^{-3}]		1.419
μ(Mo $K\alpha$) [mm^{-1}]		0.382
Scan type		ϕ and ω
$2\theta_{(max)}$ [°]		50
Transmission factors (min; max)		0.834; 0.914
Total reflections measured		68072
Symmetry independent reflections		6108
R_{int}		0.075
Reflections with $I > 2\sigma(I)$		4150
Reflections used in refinement		6108
Parameters refined; restraints		637; 944
Final $R(F)$ [$I>2\sigma(I)$ reflections]		0.0587
$wR(F^2)$ (all data)		0.1839
Weights:	$w = [\sigma^2(F_o^2) + (0.1010P)^2 + 3.9221P]^{-1}$ where $P = (F_o^2 + 2F_c^2)/3$	
Goodness of fit		1.046
Final Δ_{max}/σ		0.002
$\Delta\rho$ (max; min) [e Å^{-3}]		0.93; -0.41
$\sigma(d_{(C-C)})$ [Å]		0.004–0.03

Table 4.20 Crystallographic Data for **175**.

Crystallised from		CH_3CN / Et_2O
Empirical formula		$C_{74}H_{68}F_{12}N_8NiO_4P_2$
Formula weight [g mol^{-1}]		1482.03
Crystal colour, habit		yellow, prism
Crystal dimensions [mm]		0.12 × 0.30 × 0.32
Temperature [K]		160 (1)
Crystal system		orthorhombic
Space group		*Pcca* (#54)
Z		4
Reflections for cell determination		99688
2θ range for cell determination [°]		4–55
Unit cell parameters	a [Å] = 25.3094(4)	α [°] = 90
	b [Å] = 12.6402(2)	β [°] = 90
	c [Å] = 21.9538(3)	γ [°] = 90
V [Å^3]	7023.4(2)	
F(000)		3064
D_x [g cm^{-3}]		1.401
μ(Mo $K\alpha$) [mm^{-1}]		0.409
Scan type		ϕ and ω
$2\theta_{(max)}$ [°]		55
Transmission factors (min; max)		0.885; 0.961
Total reflections measured		77907
Symmetry independent reflections		8070
R_{int}		0.062
Reflections with $I > 2\sigma(I)$		5148
Reflections used in refinement		8068
Parameters refined; restraints		639; 944
Final $R(F)$ [$I>2\sigma(I)$ reflections]		0.0737
$wR(F^2)$ (all data)		0.2276
Weights:	$w = [\sigma^2(F_o^2) + (0.1093P)^2 + 6.1409P]^{-1}$ where $P = (F_o^2 + 2F_c^2)/3$	
Goodness of fit		1.051
Final Δ_{max}/σ		0.001
$\Delta\rho$ (max; min) [e Å^{-3}]		1.09; -0.33
$\sigma(d_{(C-C)})$ [Å]		0.006–0.04

Table 4.21 Crystallographic Data for **176**.

Crystallised from	CH_3CN / Et_2O
Empirical formula	$C_{74}H_{68}CuF_{12}N_8O_4P_2$
Formula weight [g mol^{-1}]	1486.87
Crystal colour, habit	lime-green, prism
Crystal dimensions [mm]	0.15 × 0.17 × 0.27
Temperature [K]	160 (1)
Crystal system	orthorhombic
Space group	*Pcca* (#54)
Z	4
Reflections for cell determination	103896
2θ range for cell determination [°]	4 – 50
Unit cell parameters a [Å] = 24.9866(3)	α [°] = 90
b [Å] = 12.9263(2)	β [°] = 90
c [Å] = 21.9263(3)	γ [°] = 90
V [Å^3] = 7081.9(2)	
F(000)	3068
D_x [g cm^{-3}]	1.394
μ(Mo $K\alpha$) [mm^{-1}]	0.440
Scan type	ϕ and ω
$2\theta_{(max)}$ [°]	50
Transmission factors (min; max)	0.811; 0.940
Total reflections measured	71951
Symmetry independent reflections	6270
R_{int}	0.071
Reflections with $I > 2\sigma(I)$	4433
Reflections used in refinement	6269
Parameters refined; restraints	640; 944
Final $R(F)$ [$I>2\sigma(I)$ reflections]	0.0662
$wR(F^2)$ (all data)	0.1918
Weights: $w = [\sigma^2(F_o^2) + (0.0950P)^2 + 5.7769P]^{-1}$ where $P = (F_o^2 + 2F_c^2)/3$	
Goodness of fit	1.071
Secondary extinction coefficient	0.0053(6)
Final Δ_{max}/σ	0.001
$\Delta\rho$ (max; min) [e Å^{-3}]	0.92; -0.36
$\sigma(d_{(C-C)})$ [Å]	0.005 – 0.03

Table 4.22 Crystallographic Data for **177**.

Crystallised from		CH_3CN / Et_2O
Empirical formula		$C_{76}H_{71}F_{12}N_9O_4P_2Zn$
Formula weight [g mol^{-1}]		1529.76
Crystal colour, habit		yellow, prism
Crystal dimensions [mm]		0.25 × 0.30 × 0.38
Temperature [K]		160 (1)
Crystal system		monoclinic
Space group		$P2_1/c$ (#14)
Z		4
Reflections for cell determination		256696
2θ range for cell determination [°]		4–50
Unit cell parameters	a [Å] = 12.9177(1)	α [°] = 90
	b [Å] = 25.4666(3)	β [°] = 93.0097(8)
	c [Å] = 22.1526(3)	γ [°] = 90
V [Å^3]	7277.5(1)	
F(000)		3160
D_x [g cm^{-3}]		1.396
μ(Mo $K\alpha$) [mm^{-1}]		0.468
Scan type		ϕ and ω
$2\theta_{(max)}$ [°]		50
Transmission factors (min; max)		0.771; 0.895
Total reflections measured		110992
Symmetry independent reflections		12861
R_{int}		0.076
Reflections with $I > 2\sigma(I)$		8514
Reflections used in refinement		12858
Parameters refined; restraints		1119; 1780
Final $R(F)$ [$I>2\sigma(I)$ reflections]		0.1065
$wR(F^2)$ (all data)		0.2818
Weights:	$w = [\sigma^2(F_o^2) + (0.0956P)^2 + 23.8126P]^{-1}$ where $P = (F_o^2 + 2F_c^2)/3$	
Goodness of fit		1.069
Secondary extinction coefficient		0.0013(4)
Final Δ_{max}/σ		0.001
$\Delta\rho$ (max; min) [e Å^{-3}]		1.18; -0.97
$\sigma(d_{(C-C)})$ [Å]		0.006–0.01

Table 4.23 Crystallographic Data for **178**.

Crystallised from		CH_3CN / Et_2O
Empirical formula		$C_{74}H_{68}F_{12}N_8O_4P_2Ru$
Formula weight [g mol^{-1}]		1524.33
Crystal colour, habit		red, plate
Crystal dimensions [mm]		0.02 × 0.27 × 0.45
Temperature [K]		160 (1)
Crystal system		orthorhombic
Space group		*Pcca* (#54)
Z		4
Reflections for cell determination		140159
2θ range for cell determination [°]		4 – 50
Unit cell parameters	a [Å] = 25.3777(5)	α [°] = 90
	b [Å] = 12.5601(3)	β [°] = 90
	c [Å] = 21.8678(4)	γ [°] = 90
V [Å^3]	6970.3(3)	
F(000)		3128
D_x [g cm^{-3}]		1.452
μ(Mo $K\alpha$) [mm^{-1}]		0.359
Scan type		ϕ and ω
$2\theta_{(max)}$ [°]		50
Transmission factors (min; max)		0.617; 0.999
Total reflections measured		78747
Symmetry independent reflections		6150
R_{int}		0.142
Reflections with $I > 2\sigma(I)$		4026
Reflections used in refinement		6149
Parameters refined; restraints		639; 944
Final $R(F)$ [$I>2\sigma(I)$ reflections]		0.0647
$wR(F^2)$ (all data)		0.1984
Weights:	$w = [\sigma^2(F_o^2) + (0.0950P)^2 + 12.6316P]^{-1}$ where $P = (F_o^2 + 2F_c^2)/3$	
Goodness of fit		1.052
Final Δ_{max}/σ		0.002
$\Delta\rho$ (max; min) [e Å^{-3}]		1.11; -0.64
$\sigma(d_{(C-C)})$ [Å]		0.007 – 0.04

Table 4.24 Crystallographic Data for **179.**

Crystallised from		CH_3CN / Et_2O
Empirical formula		$C_{74}H_{68}F_{12}N_8O_4OsP_2$
Formula weight [g mol^{-1}]		1613.53
Crystal colour, habit		purple-brown, prism
Crystal dimensions [mm]		0.17 × 0.25 × 0.28
Temperature [K]		160(1)
Crystal system		orthorhombic
Space group		*Pcca* (#54)
Z		4
Reflections for cell determination		45814
2θ range for cell determination [°]		4 – 50
Unit cell parameters	a [Å] = 25.3861(5)	α [°] = 90
	b [Å] = 12.5157(3)	β [°] = 90
	c [Å] = 21.8136(4)	γ [°] = 90
V [Å^3]	6930.7(2)	
F(000)		3256
D_x [g cm^{-3}]		1.546
μ(Mo $K\alpha$) [mm^{-1}]		1.974
Scan type		ϕ and ω
$2\theta_{(max)}$ [°]		50
Transmission factors (min; max)		0.595; 0.712
Total reflections measured		70390
Symmetry independent reflections		6111
R_{int}		0.100
Reflections with $I > 2\sigma(I)$		3820
Reflections used in refinement		6107
Parameters refined; restraints		552; 577
Final $R(F)$ [$I > 2\sigma(I)$ reflections]		0.0616
$wR(F^2)$ (all data)		0.1822
Weights:	$w = [\sigma^2(F_o^2) + (0.0756P)^2 + 38.0393P]^{-1}$ where $P = (F_o^2 + 2F_c^2)/3$	
Goodness of fit		1.065
Secondary extinction coefficient		0.0039(3)
Final Δ_{max}/σ		0.001
$\Delta\rho$ (max; min) [e Å^{-3}]		1.11; -1.08
$\sigma(d_{(C-C)})$ [Å]		0.01 – 0.02

Table 4.25 Crystallographic Data for **181**.

Crystallised from		CH_3CN / Et_2O
Empirical formula		$C_{78}H_{80}F_{12}FeN_{12}O_4P_2$
Formula weight [g mol^{-1}]		1595.33
Crystal colour, habit		red, plate
Crystal dimensions [mm]		0.07 × 0.20 × 0.35
Temperature [K]		160 (1)
Crystal system		monoclinic
Space group		*C*2/*c* (#15)
Z		4
Reflections for cell determination		140202
2θ range for cell determination [°]		4 – 50
Unit cell parameters	*a* [Å]= 29.749(1)	α [°] = 90
	b [Å] = 11.4106(4)	β [°] = 90.062(2)
	c [Å] = 22.7396(6)	γ [°] = 90
V [Å^3]	7719.1(4)	
F(000)		3312
D_x [g cm^{-3}]		1.373
μ(Mo *K*α) [mm^{-1}]		0.323
Scan type		ϕ and ω
$2\theta_{(max)}$ [°]		50
Transmission factors (min; max)		0.743; 0.994
Total reflections measured		43088
Symmetry independent reflections		6783
R_{int}		0.068
Reflections with $I > 2\sigma(I)$		5116
Reflections used in refinement		6782
Parameters refined; restraints		566; 543
Final *R(F)* [$I>2\sigma(I)$ reflections]		0.0497
wR(F^2) (all data)		0.1255
Weights:	$w = [\sigma^2(F_o^2) + (0.0486P)^2 + 15.9333P]^{-1}$ where $P = (F_o^2 + 2F_c^2)/3$	
Goodness of fit		1.052
Secondary extinction coefficient		0.0007(1)
Final Δ_{max}/σ		0.002
$\Delta\rho$ (max; min) [e Å^{-3}]		0.48; -0.46
$\sigma(d_{(C-C)})$ [Å]		0.004 – 0.007

Table 4.26 Crystallographic Data for **182**.

Crystallised from		MeCN / Et_2O
Empirical formula		$C_{78}H_{80}CoF_{12}N_{12}O_4P_2$
Formula weight [g mol^{-1}]		1598.43
Crystal colour, habit		red, prism
Crystal dimensions [mm]		0.20 × 0.25 × 0.27
Temperature [K]		160 (1)
Crystal system		monoclinic
Space group		*C*2/*c* (#15)
Z		4
Reflections for cell determination		34748
2θ range for cell determination [°]		4–50
Unit cell parameters	*a* [Å] = 29.5268(4)	α [°] = 90
	b [Å] = 11.7893(3)	β [°] = 90.847(2)
	c [Å] = 22.4187(5)	γ [°] = 90
V [Å^3]	7803.1(3)	
F(000)		3316
D_x [g cm^{-3}]		1.361
μ(Mo *K*α) [mm^{-1}]		0.347
Scan type		ϕ and ω
$2\theta_{(max)}$ [°]		50
Transmission factors (min; max)		0.819; 0.937
Total reflections measured		62530
Symmetry independent reflections		6889
R_{int}		0.094
Reflections with $I > 2\sigma(I)$		4796
Reflections used in refinement		6887
Parameters refined; restraints		566; 555
Final *R(F)* [$I>2\sigma(I)$ reflections]		0.0506
wR(F^2) (all data)		0.1421
Weights:	$w = [\sigma^2(F_o^2) + (0.0765P)^2 + 6.11P]^{-1}$ where $P = (F_o^2 + 2F_c^2)/3$	
Goodness of fit		1.038
Secondary extinction coefficient		0.0006(2)
Final Δ_{max}/σ		0.001
$\Delta\rho$ (max; min) [e Å^{-3}]		0.47; -0.48
$\sigma(d_{(C-C)})$ [Å]		0.004–0.006

Table 4.27 Crystallographic Data for **183**

Crystallised from		MeCN / Et_2O
Empirical formula		$C_{72}H_{71}F_{12}N_9NiO_4P_2$
Formula weight [g mol^{-1}]		1475.04
Crystal colour, habit		orange, prism
Crystal dimensions [mm]		0.25 × 0.25 × 0.40
Temperature [K]		160(1)
Crystal system		orthorhombic
Space group		*Pnna* (#52)
Z		8
Reflections for cell determination		158471
2θ range for cell determination [°]		4 – 50
Unit cell parameters	a [Å] = 22.0069(3)	α [°] = 90
	b [Å] = 25.2020(5)	β [°] = 90
	c [Å] = 24.8731(3)	γ [°] = 90
V [Å^3]	13795.1(4)	
F(000)		6112
D_x [g cm^{-3}]		1.420
μ(Mo $K\alpha$) [mm^{-1}]		0.417
Scan type		ϕ and ω
$2\theta_{(max)}$ [°]		50
Transmission factors (min; max)		0.707; 0.893
Total reflections measured		128129
Symmetry independent reflections		12152
R_{int}		0.105
Reflections with $I > 2\sigma(I)$		7907
Reflections used in refinement		12148
Parameters refined; restraints		1125; 1091
Final $R(F)$ [$I > 2\sigma(I)$ reflections]		0.0563
$wR(F^2)$ (all data)		0.1440
Weights:	$w = [\sigma^2(F_o^2) + (0.0513P)^2 + 21.7030P]^{-1}$ where $P = (F_o^2 + 2F_c^2)/3$	
Goodness of fit		1.030
Secondary extinction coefficient		0.00026(6)
Final Δ_{max}/σ		0.001
$\Delta\rho$ (max; min) [e Å^{-3}]		0.60; -0.57
$\sigma(d_{(C-C)})$ [Å]		0.005 – 0.006

Table 4.28 Crystallographic Data for **184**.

Crystallised from		MeCN / Et_2O
Empirical formula		$C_{71}H_{69.50}CuF_{12}N_{8.50}O_4P_2$
Formula weight [g mol^{-1}]		1459.35
Crystal colour, habit		green, prism
Crystal dimensions [mm]		0.17 × 0.25 × 0.37
Temperature [K]		160 (1)
Crystal system		orthorhombic
Space group		*Pnna* (#52)
Z		8
Reflections for cell determination		219498
2θ range for cell determination [°]		4 – 50
Unit cell parameters	a [Å] = 22.0072(3)	α [°] = 90
	b [Å] = 24.9787(4)	β [°] = 90
	c [Å] = 25.1014(3)	γ [°] = 90
V [Å^3]	13798.5(3)	
F(000)		6032
D_x [g cm^{-3}]		1.405
μ(Mo $K\alpha$) [mm^{-1}]		0.451
Scan type		ϕ and ω
$2\theta_{(max)}$ [°]		50
Transmission factors (min; max)		0.747; 0.915
Total reflections measured		146815
Symmetry independent reflections		12190
R_{int}		0.092
Reflections with $I > 2\sigma(I)$		8865
Reflections used in refinement		12186
Parameters refined; restraints		1069; 2160
Final $R(F)$ [$I>2\sigma(I)$ reflections]		0.0984
$wR(F^2)$ (all data)		0.2595
Weights:	$w = [\sigma^2(F_o^2) + (0.1066P)^2 + 64.2448P]^{-1}$ where $P = (F_o^2 + 2F_c^2)/3$	
Goodness of fit		1.049
Secondary extinction coefficient		0.0010(1)
Final Δ_{max}/σ		0.004
$\Delta\rho$ (max; min) [e Å^{-3}]		1.39; -1.31
$\sigma(d_{(C-C)})$ [Å]		0.007 – 0.01

Table 4.29 Crystallographic Data for **185**.

Crystallised from		MeCN / Et_2O
Empirical formula		$C_{71.65}H_{70.47}F_{12}N_{8.82}O_4P_2Zn$
Formula weight [g mol^{-1}]		1474.46
Crystal colour, habit		colourless, prism
Crystal dimensions [mm]		0.10 × 0.27 × 0.32
Temperature [K]		160(1)
Crystal system		orthorhombic
Space group		*Pnna* (#52)
Z		8
Reflections for cell determination		77505
2θ range for cell determination [°]		4 – 52
Unit cell parameters	a [Å] = 22.0637(2)	α [°] = 90
	b [Å] = 25.1063(4)	β [°] = 90
	c [Å] = 25.1199(4)	γ [°] = 90
V [Å^3]	13914.9(3)	
F(000)		6096.88
D_x [g cm^{-3}]		1.408
μ(Mo $K\alpha$) [mm^{-1}]		0.487
Scan type		ϕ and ω
$2\theta_{(max)}$ [°]		52
Transmission factors (min; max)		0.851; 0.951
Total reflections measured		127617
Symmetry independent reflections		13714
R_{int}		0.095
Reflections with $I > 2\sigma(I)$		8677
Reflections used in refinement		13712
Parameters refined; restraints		1039; 1018
Final $R(F)$ [$I > 2\sigma(I)$ reflections]		0.0603
$wR(F^2)$ (all data)		0.1587
Weights:	$w = [\sigma^2(F_o^2) + (0.0582P)^2 + 26.1830P]^{-1}$ where $P = (F_o^2 + 2F_c^2)/3$	
Goodness of fit		1.018
Final Δ_{max}/σ		0.001
$\Delta\rho$ (max; min) [e Å^{-3}]		0.84; -0.63
$\sigma(d_{(C-C)})$ [Å]		0.007 – 0.009

Table 4.30 Crystallographic Data for **186**

Crystallised from		CH_3CN / Et_2O
Empirical formula		$C_{78}H_{80}F_{12}N_{12}O_4P_2Ru$
Formula weight [g mol^{-1}]		1640.49
Crystal colour, habit		red, prism
Crystal dimensions [mm]		0.22 × 0.30 × 0.40
Temperature [K]		160 (1)
Crystal system		monoclinic
Space group		*C*2/*c* (#15)
Z		4
Reflections for cell determination		103846
2θ range for cell determination [°]		4 – 60
Unit cell parameters	*a* [Å] = 29.4883(4)	α [°] = 90
	b [Å] = 11.8087(1)	β [°] = 90.9353(6)
	c [Å] = 22.4060(3)	γ [°] = 90
V [Å^3]	7801.1(2)	
F(000)		3384
D_x [g cm^{-3}]		1.397
μ(Mo *K*α) [mm^{-1}]		0.328
Scan type		ϕ and ω
2$\theta_{(max)}$ [°]		60
Transmission factors (min; max)		0.614; 0.885
Total reflections measured		94623
Symmetry independent reflections		11431
R_{int}		0.084
Reflections with $I > 2\sigma(I)$		8995
Reflections used in refinement		11428
Parameters refined; restraints		565; 561
Final *R(F)* [$I>2\sigma(I)$ reflections]		0.0440
wR(F^2) (all data)		0.1174
Weights:	$w = [\sigma^2(F_o^2) + (0.0549P)^2 + 9.1532P]^{-1}$ where $P = (F_o^2 + 2F_c^2)/3$	
Goodness of fit		1.034
Final Δ_{max}/σ		0.002
$\Delta\rho$ (max; min) [e Å^{-3}]		0.59; -0.82
$\sigma(d_{(C-C)})$ [Å]		0.003 – 0.005

Table 4.31 Crystallographic Data for **187**

Crystallised from		CH_3CN / Et_2O
Empirical formula		$C_{78}H_{80}F_{12}N_{12}O_4OsP_2$
Formula weight [g mol^{-1}]		1729.69
Crystal colour, habit		brown, tablet
Crystal dimensions [mm]		0.20 × 0.38 × 0.40
Temperature [K]		160(1)
Crystal system		monoclinic
Space group		*C*2/*c* (#15)
Z		4
Reflections for cell determination		159774
2θ range for cell determination [°]		4 – 56
Unit cell parameters	*a* [Å] = 29.4529(4)	α [°] = 90
	b [Å] = 11.8271(1)	β [°] = 90.9746(7)
	c [Å] = 22.4142(2)	γ [°] = 90
V [Å^3]	7806.7(1)	
F(000)		3512
D_x [g cm^{-3}]		1.472
μ(Mo *K*α) [mm^{-1}]		1.759
Scan type		ϕ and ω
$2\theta_{(max)}$ [°]		56
Transmission factors (min; max)		0.615; 0.712
Total reflections measured		81476
Symmetry independent reflections		9306
R_{int}		0.057
Reflections with $I > 2\sigma(I)$		8424
Reflections used in refinement		9302
Parameters refined; restraints		538; 415
Final *R(F)* [$I > 2\sigma(I)$ reflections]		0.0313
wR(F^2) (all data)		0.0767
Weights: $w = [\sigma^2(F_o^2) + (0.0375P)^2 + 16.4115P]^{-1}$ where $P = (F_o^2 + 2F_c^2)/3$		
Goodness of fit		1.058
Final Δ_{max}/σ		0.002
$\Delta\rho$ (max; min) [e Å^{-3}]		1.76; -1.18
$\sigma(d_{(C-C)})$ [Å]		0.003 – 0.007

Table 4.32 Crystallographic Data for **190**.

Crystallised from		$CHCl_3$ / cyclohexane
Empirical formula		$C_{33}H_{31}N_3O_2$
Formula weight [g mol^{-1}]		501.63
Crystal colour, habit		colourless, plate
Crystal dimensions [mm]		0.08 × 0.22 × 0.28
Temperature [K]		160(1)
Crystal system		triclinic
Space group		$P\bar{1}$ (#2)
Z		2
Reflections for cell determination		4531
2θ range for cell determination [°]		4 – 50
Unit cell parameters	a [Å] = 7.9821(7)	α [°] = 108.113(5)
	b [Å] = 11.812(1)	β [°] = 95.399(5)
	c [Å] = 14.988(1)	γ [°] = 95.831(5)
V [Å^3]	1324.2(2)	
F(000)		532
D_x [g cm^{-3}]		1.258
μ(Mo $K\alpha$) [mm^{-1}]		0.0789
Scan type		ω
$2\theta_{(max)}$ [°]		50
Total reflections measured		19113
Symmetry independent reflections		4667
R_{int}		0.086
Reflections with $I > 2\sigma(I)$		3261
Reflections used in refinement		4667
Parameters refined		349
Final $R(F)$ [$I > 2\sigma(I)$ reflections]		0.0693
$wR(F^2)$ (all data)		0.2075
Weights: $w = [\sigma^2(F_o^2) + (0.1115P)^2 + 0.6628P]^{-1}$ where $P = (F_o^2 + 2F_c^2)/3$		
Goodness of fit		1.027
Final Δ_{max}/σ		0.001
$\Delta\rho$ (max; min) [e Å^{-3}]		0.27; -0.24
$\sigma(d_{(C-C)})$ [Å]		0.003 – 0.004

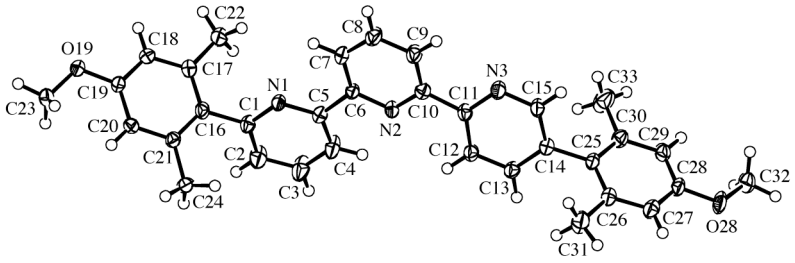

Figure 4.47 ORTEP diagram of 5,6”-bis-(4-methoxy-2,6-dimethyl-phenyl)-[2,2’:6’,2”]terpyridine **190**

Table 4.33 Crystallographic Data for **178**[Δ-TRISPHAT]$_2$.

Crystallised from		CD_3CN
Empirical formula		$C_{106}H_{62}Cl_{24}N_6O_{16}P_2Ru$
Formula weight [g mol^{-1}]		2689.58
Crystal colour, habit		red, plate
Crystal dimensions [mm]		0.08 × 0.17 × 0.20
Temperature [K]		160(1)
Crystal system		orthorhombic
Space group		$P2_12_12_1$ (#19)
Z		4
Reflections for cell determination		11674
2θ range for cell determination [°]		4–50
Unit cell parameters	a [Å] = 13.6607(3)	α [°] = 90
	b [Å] = 27.5108(5)	β [°] = 90
	c [Å] = 32.2583(7)	γ [°] = 90
V [Å^3]	12123.2(4)	
F(000)		5400
D_x [g cm^{-3}]		1.473
μ(Mo $K\alpha$) [mm^{-1}]		0.746
Scan type		ϕ and ω
$2\theta_{(max)}$ [°]		50
Total reflections measured		138485
Symmetry independent reflections		21452
R_{int}		0.170
Reflections with $I > 2\sigma(I)$		12609
Reflections used in refinement		21452
Parameters refined; restraints		1446; 754
Final $R(F)$ [$I > 2\sigma(I)$ reflections]		0.0950
$wR(F^2)$ (all data)		0.2137
Weights: $w = [\sigma^2(F_o^2) + (0.0893P)^2 + 18.5631P]^{-1}$ where $P = (F_o^2 + 2F_c^2)/3$		
Goodness of fit		1.052
Final Δ_{max}/σ		0.033
$\Delta\rho$ (max; min) [e Å^{-3}]		0.87; -0.61
$\sigma(d_{(C-C)})$ [Å]		0.009 – 0.02

4.5 References

(1) Morgan, G. T.; Burstall, F. H. *J. Chem. Soc.* **1931**, 20.

(2) Constable, E. C. *Adv. Inorg. Chem. Radiochem.* **1987**, *30*, 69-121.

(3) Hofmeier, H.; Schubert, U. S. *Chem. Soc. Rev.* **2004**, *33*, 373-399.

(4) Ruben, M.; Rojo, J.; Romero-Salguero, F. J.; Uppadine, L. H.; Lehn, J.-M. *Angew. Chem. Int. Ed., Eng.* **2004**, *43*, 3644-3662.

(5) Constable, E. C. *Progress in Inorganic Chemistry* **1994**, *42*, 67-138.

(6) Even though it can be misleading, coordination chemists often draw terpyridines in the cis,cis- conformation to emphasize the coordination geometry.

(7) Alstrum-Acevedo, J. H.; Brennaman, M. K.; Meyer, T. J. *Inorg. Chem.* **2005**, *44*, 6802-6827.

(8) Gust, D.; Moore, T. A.; Moore, A. L. *Acc. Chem. Res.* **2001**, *34*, 40-48.

(9) Meyer, T. J. *Acc. Chem. Res.* **1989**, *22*, 163-170.

(10) Balzani, V.; Juris, A.; Venturi, M.; Campagna, S.; Serroni, S. *Chem. Rev.* **1996**, *96*, 759-833.

(11) Juris, A.; Balzani, V.; Barigelletti, F.; Campagna, S.; Belser, P.; Von Zelewsky, A. *Coord. Chem. Rev.* **1988**, *84*, 85-277.

(12) Jortner, J.; Ratner, M. *Molecular Electronics*; Blackwell Science: London, 1997.

(13) Barigelletti, F.; Flamigni, L. *Chem. Soc. Rev.* **2000**, *29*, 1-12.

(14) Meyer, T. J. *Pure Appl. Chem.* **1986**, *58*, 1193-1206.

(15) Keene, F. R. *Coord. Chem. Rev.* **1997**, *166*, 121-159.

(16) Von Zelewsky, A. *Stereochemistry of Coordination Compounds*; Wiley: Chichester, UK, 1995.

(17) Lohmeier, B. G. G.; Schubert, U. S. *J. Polymer Sci. A.* **2003**, *41*, 1413-1427.

(18) Constable, E. C. In *Transition Metals in Supramolecular Chemistry*; Fabbrizzi, L., Poggi, A., Eds.; Kluwer Academic: Dordrecht, 1994, pp 81-99.

(19) Medleycott, E. A.; Hanan, G. S. *Chem. Soc. Rev.* **2005**, *34*, 133-142.

(20) Maestri, M.; Armaroli, N.; Balzani, V.; Constable, E. C.; Thompson, A. M. W. C. *Inorg. Chem.* **1995**, *34*, 2759-2767.

(21) Sauvage, J.-P.; Collin, J.-P.; Chambron, J.-C.; Guillerez, S.; Coudret, C.; Balzani, V.; Barigelletti, F.; De Cola, L.; Flamigni, L. *Chem. Rev.* **1994**, *94*, 993-1019.

(22) Hung, C.-Y.; Wang, T.-L.; Shi, Z.; Thummel, R. P. *Tetrahedron* **1994**, *50*, 10685-10692.

(23) Hung, C.-Y.; Wang, T.-L.; Jang, Y.; Kim, W. Y.; Schmehl, R. H.; Thummel, R. P. *Inorg. Chem.* **1996**, *35*, 5953-5956.

(24) Kober, E. M.; Caspar, J. V.; Lumpkin, R. S.; Meyer, T. J. *J. Phys. Chem.* **1986**, *90*, 3722-3734.

(25) Caspar, J. V.; Meyer, T. J. *J. Phys. Chem.* **1983**, *87*, 952-957.

(26) Caspar, J. V.; Kober, E. M.; Sullivan, B. P.; Meyer, T. J. *J. Amer. Chem. Soc.* **1982**, *104*, 630-632.

(27) Strouse, G. F.; Schoonover, J. R.; Duesing, R.; Boyde, S.; Jones, W. E., Jr.; Meyer, T. J. *Inorg. Chem.* **1995**, *34*, 473-487.

(28) Boyde, S.; Strouse, G. F.; Jones, W. E., Jr.; Meyer, T. J. *J. Amer. Chem. Soc.* **1990**, *112*, 7395-7396.

(29) Jahng, Y.; Thummel, R. P.; Bott, S. G. *Inorg. Chem.* **1997**, *36*, 3133-3138.

(30) Barigelletti, F.; Ventura, B.; Collin, J.-P.; Kayhanian, R.; Gaviña, P.; Sauvage, J.-P. *Eur. J. Org. Chem.* **2000**, 113-119.

(31) Collin, J.-P.; Beley, M.; Sauvage, J.-P.; Barigelletti, F. *Inorg. Chim. Acta* **1991**, *186*, 91-93.

(32) The Energy gap law states that`; as the energy gap between the excited state and ground state decreases, non-radiative pathways become more accessible and luminescence decreases.

(33) Bertini, I.; Gray, H. B.; Lippard, S. J.; Valentine, J. S. *Bioinorganic Chemistry*; University Science Books: Sausalito, 1994, p 612.

(34) Jahng, Y.; Park, J. G.; Kim, H. H. *Korean Journal of Medicinal Chemistry* **11998**, *8*, 22-29.

(35) van Vliet, P. M.; Toekimin, S., M. S.; Haasnoot, J. G.; Reedijk, J.; Novakova, O.; Vrana, O.; Brabec, V. *Inorg. Chim. Acta* **1995**, *231*, 57-64.

(36) Collin, J.-C.; Gaviña, P.; Sauvage, J.-P. *Chem. Comm.* **1996**, 2005-2006.

(37) Baumann, F.; Livoreil, A.; Kaim, W.; Sauvage, J.-P. *Chem. Comm.* **1997**, 35-36.

(38) Cardenas, D. J.; Livoreil, A.; Sauvage, J.-P. *J. Amer. Chem. Soc.* **1996**, *118*, 11980-11981.

(39) Livoreil, A.; Dietrich-Buchecker, C. O.; Sauvage, J.-P. *J. Amer. Chem. Soc.* **1994**, *116*, 9399-9400.

(40) Geoffroy, M.; Wermeille, M.; Dietrich-Buchecker, C. O.; Sauvage, J.-P.; Bernardinelli, G. *Inorg. Chim. Acta* **1990**, *167*, 157-164.

(41) The fully coordinated phenanthroline and bipyridine nitrogen atoms are ~2.0 – 2.1 Å from the copper atom. The partially coordinated nitrogen atom of the phenanthroline (N6) is 2.72 Å from the copper atom, indicating significant interaction.

(42) Allmann, R.; Henke, W.; Reinen, D. *Inorg. Chem.* **1978**, *17*, 378-382.

(43) Drent, E.; Budzelaar, P. H. M. *Chem. Rev.* **1996**, *96*, 663-681.

(44) Yamamoto, A. *Organotransition Metal Chemistry: Fundamental Concepts and Applications*; Wiley: New York, 1986, p 480.

(45) Rülke, R. E.; Han, I. M.; Elsevier, C. J.; Vrieze, K.; Van Leeuwe, P. W. N. M.; Roobeek, C. F.; Zoutberg, C.; Wang, Y. F.; Stam, C. H. *Inorg. Chim. Acta* **1990**, *169*, 5-8.

(46) Rülke, R. E.; Kaasjager, V. E.; Kliphuis, D.; Elsevier, C. J.; van Leeuwen, P. W. N. M.; Vrieze, K. *Organomet.* **1996**, *15*, 668-677.

(47) Constable, E. C.; Hannon, M. J.; Thompson, A. M. W. C.; Tocher, D. A.; Walker, J. *Supramol. Chem.* **1993**, *2*, 243.

(48) Groen, J.; de Zwart, A.; Vlaar, M. J. M.; Ernsting, J. M.; Van Leeuwen, P. W. N. M.; Vrieze, K.; Kooijman, H.; Smeets, W. J. J.; Spek, A. L.; Budzelaar, P. H. M.; Xiang, Q.; Thummel, R. P. *Eur. J. Inorg. Chem.* **1998**, 1129-1143.

(49) Michalec, J. F.; Bejune, S. A.; Cuttell, D. G.; Summerton, G. C.; Gertenbach, J. A.; Field, J. S.; Haines, R. J.; McMillin, D. R. *Inorganic Chemistry* **2001**, *40*, 2193.

(50) Hobert, S. E.; Carney, J. T.; Cummings, S. D. *Inorg. Chim. Acta* **2001**, *318*, 89-96.

(51) Neve, F.; Crispini, A.; Campagna, S. *Inorg. Chem.* **1997**, *36*, 6150-6156.

(52) McMillin, D. R.; Moore, J. J. *Coord. Chem. Rev.* **2002**, *229*, 113-121.

(53) Aldridge, T. K.; Stacy, E. M.; McMillin, D. R. *Inorg. Chem.* **1994**, *33*, 722-727.

(54) Ratilla, E. M. A.; Scott, B. K.; Moxness, M. S.; Kostic, N. M. *Inorg. Chem.* **1990**, *29*, 918-926.

(55) Ratilla, E. M. A.; Kostic, N. M. *J. Amer. Chem. Soc.* **1988**, *110*, 4427-4428.

(56) Jennette, K. W.; Gill, J. T.; Sadownick, J. A.; Lippard, S. J. *J. Amer. Chem. Soc.* **1976**, *98*, 6159-6168.

(57) Jennette, K. W.; Lippard, S. J.; Vassiliades, G. A.; Bauer, W. R. *Proceedings of the National Academy of Sciences of the United States of America* **1974**, *71*, 3839-3843.

(58) Crites, D. K.; Cunningham, C. T.; McMillin, D. R. *Inorg. Chim. Acta* **1998**, *273*, 346-353.

(59) Michalec, J. F.; Bejune, S. A.; Cuttell, D. G.; Summerton, G. C.; Gertenbach, J. A.; Field, J. S.; Haines, R. J.; McMillin, D. R. *Inorg. Chem.* **2001**, *40*, 2193-2200.

(60) Moore, J. J.; Nash, J. J.; Fanwick, P. E.; McMillin, D. R. *Inorg. Chem.* **2002**, *41*, 6387-6396.

(61) Michalec, J. F.; Bejune, S. A.; McMillin, D. R. *Inorg. Chem.* **2000**, *39*, 2708-2709.

(62) Hill, M. G.; Bailey, J. A.; Miskowski, V. M.; Gray, H. B. *Inorg. Chem.* **1996**, *35*, 4585-4590.

(63) Crosby, G. A. *Acc. Chem. Res.* **1975**, *8*, 231-238.

(64) Ayala, N. P.; Flynn, C. M.; Sacksteder, L.; Demas, J. N.; Degraff, B. A. *J. Amer. Chem. Soc.* **1990**, *110*, 3837-3844.

(65) Pierloot, K.; Ceulemans, A.; Merchan, M.; Serrano-Andres, L. *J. Phys. Chem. A* **2000**, *104*, 4374-4382.

(66) Farrell, I. R.; Hartl, F.; Zalis, S.; Mahabiersing, T.; Vlcek, A. *J. Chem. Soc., Dalton Trans* **2000**, 4323-4331.

(67) Klein, A.; Kaim, W.; Waldhor, E.; Hausen, H.-D. *J. Chem. Soc., Perkins Trans. 2* **1995**, 2121-2126.

(68) Gouterman, M. *J. Phys. Chem.* **1959**, *30*, 1139-1161.

(69) Loren, J. C.; Gantzel, P.; Linden, A.; Siegel, J. S. *Org. Bio. Chem.* **2005**, *3*, 3105-3116.

(70) Belfrekh, N.; Dietrich-Buchecker, C. O.; Sauvage, J.-P. *Inorg. Chem.* **2000**, *39*, 5169-5172.

(71) Schubert, U. S.; Eschbaumer, C.; Andres, P.; Hofmeier, H.; Weidl, C. H.; Herdtweck, E.; Dulkeith, E.; Morteani, A.; Hecker, N. E.; Feldman, J. *Syn. Met.* **2001**, *121*, 1249-1252.

(72) Evans, I. P.; Spencer, A.; Wilkinson, G. *J. Chem. Soc., Dalton Trans* **1973**, 204-209.

(73) No evidence of di-, tri-, or tetra-ol was found. Cleavage of ester (following reference) and ether (*Vida infra*) functional groups under the harsh reaction conditions most likely occurs with the assistance of ethylene glycol and will further addressed in Chapter 5. Reaction of **115** with RuCl3-3H2O under identical microwave conditions results in similar cleavage of methoxy ethers.

(74) Anderson, T. J.; Scott, J. R.; Millett, F.; Durham, B. *Inorg. Chem.* **2006**, *45*, 3843-3845.

(75) Constable, E. C.; Baum, G.; Bill, E.; Dyson, R.; van Eldik, R.; Fenske, D.; Kaderli, S.; Morris, D.; Neubrand, A.; Neuburger, M.; Smith, D. R.; Wieghardt, K.; Zehnder, M.; Zuberbühler, A. D. *Chem., Eur. J.* **1999**, *5*, 498-508.

(76) Kirchhoff, J. R.; McMillin, D. R.; Marnot, P. A.; Sauvage, J.-P. *J. Amer. Chem. Soc.* **1985**, *107*, 1138-1141.

(77) Benaglia, M.; Ponzini, F.; Woods, C. R.; Siegel, J. S. *Org. Lett.* **2001**, *3*, 967-969.

(78) Nakayama, Y.; Baba, Y.; Yasuda, H.; Kawakita, K.; Ueyama, N. *Macromolecules* **2003**, *36*, 7953-7958.

(79) Schmittel, M.; Michel, C.; Ganz, A.; Herderich, M. *J. Prakt. Chem.* **1999**, *341*, 228.

(80) Schmittel, M.; Ganz, A. *Chem. Comm.* **1997**, 999-1000.

(81) Only one enantiomer of each is shown for the sake of clarity

(82) The reaction was followed by TLC and ESI-MS.

(83) Li, Z.; Liang, X.; Wu, F.; Wan, B. *Tetrahedron: Asymmetry* **2004**, *15*, 665-669.

(84) Unless necessary, all counter-ions, solvent molecules, and disordered atoms have been removed for clarity.

(85) Hannon, M. J.; Painting, C. L.; Plummer, E. A.; Childs, L. J.; Alcock, N. W. *Chem., Eur. J.* **2002**, *8*, 2225-2238.

(86) Dumitru, F.; Petit, E.; van der Lee, A.; Barboiu, M. *Eur. J. Inorg. Chem.* **2005**, 4255-4262.

(87) Janiak, C. *J. Chem. Soc., Dalton Trans* **2000**, 3885-3896.

(88) For the sake of clarity, only one of the two independant cations of 38 - 40 is shown, and counter-ions, solvent molecules, and disordered atoms removed.

(89) Constable, E. C.; Kulke, T.; Neuburger, M.; Zehnder, M. *N. J. Chem.* **1997**, *21*, 1091-1102.

(90) Constable, E. C.; Davies, J. E.; Phillips, D.; Raithby, P. R. *Polyhedron* **1998**, *17*, 3989-3997.

(91) Bertini, I.; Luchinaut, C. *Coord. Chem. Rev.* **1996**, *150*, 1-292.

(92) *NMR of Paramagnetic Molecules: Principles and Applications*; La Mar, G. N.; Horrocks Jr., W. D.; Holm, R. H., Eds.; Academic Press: New York, 1973, p 678.

(93) Collin, J.-P.; Gaviña, P.; Sauvage, J.-P.; De Cian, A.; Fischer, J. *Aust. J. Chem.* **1997**, *50*, 951-957.

(94) Kalyanasundaram, K. *Photochemistry of Polypyridine and Porphyrin Complexes*; Academic Press: London, 1992, p 626.

(95) El-Sayed, M. A. *J. Chem. Phys.* **1963**, *38*, 2834-2838.

(96) Juris, A.; Balzani, V.; Barigelletti, F.; Campagna, S.; Belser, P.; Von Zelewsky, A. *Coordination Chemistry Reveiws* **1988**, *84*, 85-277.

(97) Ceulemans, A.; Vanquickenborne, L. G. *J. Amer. Chem. Soc.* **1981**, *103*, 2238-2241.

(98) When emission spectra were recorded in acetonitrile, ligand dissociation occurs and, due to its high quantum yield, obscures the weak complex emission.

(99) Maury, O.; Viau, L.; Sénéchal, K.; Corre, B.; Guégan, J.-P.; Renouard, T.; Ledoux, I.; Zyss, J.; Le Bozec, H. *Chem., Eur. J.* **2004**, *10*, 4454-4466.

(100) Ohno, T.; Kato, S. *Bull. Chem. Soc. Jpn.* **1974**, *47*, 2953-2957.

(101) Ajayaghosh, A.; Carol, P.; Sreejith, S. *J. Amer. Chem. Soc.* **2005**, *127*, 14962-14963.

(102) Goodall, W.; Williams, J. A. G. *Chem. Comm.* **2001**, 2514-2515.

(103) Sénéchal, K.; Maury, O.; Le Bozec, H.; Ledoux, I.; Zyss, J. *J. Amer. Chem. Soc.* **2002**, *124*, 4560.

(104) Crosby, G. A.; Demas, J. N. *J. Phys. Chem.* **1971**, *75*, 991-1024.

(105) Loren, J. C.; Siegel, J. S. *Angew. Chem. Int. Ed.* **2001**, *40*, 754-757.

(106) Lacour, J.; Ginglinger, C.; Grivet, C.; Bernardinelli, G. *Angew. Chem. Int. Ed.* **1997**, *36*, 608-610.

(107) Lacour, J.; Frantz, R. *Org. Bio. Chem.* **2004**, *3*, 15-19.

(108) Lacour, J. *Chimia* **2002**, *56*, 672-675.

(109) Lacour, J.; Londez, A.; Goujon-Gingliner, C.; Buss, V.; Bernardinelli, G. *Org. Lett.* **2000**, *2*, 4185-4188.

(110) Frantz, R.; Lacour, J. In *Unpublished Work* 2005.

(111) Proton b' overlaps the CH2Cl2 signal and cannot be clearly distinguished.

(112) Amouri, H.; Caspar, R.; Gruselle, M.; Guyard-Duhayon, C.; Boubekeur, K.; Lev, D. A.; Collins, L. S. B.; Grotjahn, D. *Organomet.* **2004**, *23*, 4338-4341.

(113) Mimassi, L.; Guyard-Duhayon, C.; Rager, M. N.; Amouri, H. *Inorg. Chem.* **2004**, *43*, 6644-6649.

(114) Kaida, Y.; Okamoto, Y.; Chambron, J.-C.; Mitchell, D. K.; Sauvage, J.-P. *Tetrahedron Lett.* **1993**, *34*, 1019-1022.

(115) Arias, K.; Barder, T.; Loren, J. C.; Zysman-Coleman, E.; Baldridge, K. K.; Siegel, J. S. *in preparation.*

(116) *Supramolecular Assembly via Hydrogen Bonds II*; Mingos, D. M. P., Ed.; Springer-Verlag: Berlin, 2004; Vol. 111, p 180.

(117) Hunter, C. A. *Chem. Soc. Rev.* **1994**.

(118) Amabilino, D. B.; Stoddart, J. F. *Chem. Rev.* **1995**, *95*, 2725-2828.

(119) *Structure Correlation*; Bürgi, H.-B.; Dunitz, J. D., Eds.; VCH: Weinheim, 1994; Vol. 2, p 888.

(120) Gavezzotti, A.; Filippini, G. *J. Amer. Chem. Soc.* **1996**, *118*, 7153-7157.

(121) Gottlieb, H. E.; Kotlyar, V.; Nudelman, A. *J. Org. Chem.* **1997**, *62*, 7512-7515.

(122) Hooft, R. *KappaCCD Collect Software* Delft, The Netherlands, 1999, p Nonius BV.

(123) Otwinowski, Z.; Minor, W. In *Methods in Crystallography*; Carter, C. W., Sweet, R. M., Eds.; Academic Press: New York, 1997; Vol. 276, pp 307-326.

(124) Altomare, A.; Cascarano, G.; Giacovazza, C.; Guagliardi, A.; Burla, M. C.; Polidori, G.; Carmalli, M. *Journal of Applied Crystallography* **1994**, *27*, 435.

(125) Maslen, E. N.; Fox, A. G.; O'Keefe, M. A. In *International Tables for Crystallography*; Wilson, A. J. C., Ed.; Kluwer Academic Publishers: Dordrecht, 1992; Vol. C, pp 477-486.

(126) Stewart, R. F.; Davidson, E. R.; Simpson, W. T. *J. Chem. Phys.* **1965**, *42*, 3175-3187.

(127) Ibers, J. A.; Hamilton, W. C. *Acta Crystal.* **1964**, *17*, 781-782.

(128) Creagh, D. C.; Auley, W. J. In *International Tables for Crystallography*; Wilson, A. J. C., Ed.; Kluwer Academic Publishers: Dordrecht, 1992; Vol. C, pp 219-222.

(129) Creagh, D. C.; Hubbell, J. H. In *International Tables for Crystallography*; Wilson, A. J. C., Ed.; Kluwer Academic Publishers: Dordrecht, 1992; Vol. C, pp 200-206.

(130) Sheldrick, G. M.; University of Göttingen, Germany: Göttingen, 1997.

CHAPTER 5

THE BORROMEAN LINK

5.1 Introduction

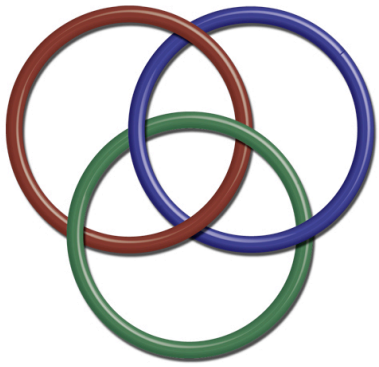

Figure 5.1 The Borromean link.

The complex topological graph called the Borromean link (Figure 5.1) has captivated humanity since the dawn of time.[1] Inseparable when united, the three independent rings are interlocked so that no two rings are concatenated, thus upon the breaking of any one ring, the other two fall apart.[2,3] The unifying symbolism found within this characteristic property ensures the link's continuous presence within all facets of human existence. From medieval art, theology, and heraldry to modern quantum mechanics,[4] particle physics[5,6] and magnetism,[7,8] the link has resurfaced as a Jungian landmark. To chemists, the daunting challenge of structural complexity has enshrined the Borromean link as the holly grail of the topology-inspired synthetic targets.[9,10]

When Wasserman reunited topology and chemistry in the early 1960's and laid the foundation of chemical topology, he postulated that a hydrocarbon ring containing the minimum of thirty carbon atoms would leave enough space for two more rings to interweave and adopt the correct Borromean topology.[11,12] Whereas Wasserman envisioned a synthesis relying on statistical threading, van Gulick speculated that the specific cyclization of a 3-braid could also lead to the correct topology (Figure 5.2).[13] Additional potential syntheses have been proposed and discussed, but the link remained

elusive.[14-18] Since the advent of supramolecular chemistry[19] and the concept of a chemical template,[20] molecules containing topologically complex molecular graphs such as catenanes and knots are now commonplace.[21-23] The intricate complexity of Borromean link topology, however, remains a significant challenge and only rare examples exist.

Figure 5.2 van Gulick's construction of the Borromean link via a 3-braid.[13]

The following chapter briefly discusses the history and properties of the Borromean link before presenting the various synthetic approaches and, finally, the application of manisyl-substituted polypyridine ligands towards the metal templated synthesis of the Borromean link.

5.1.1 The Borromean Rings throughout History

The name Borromean stems from the coat of arms of the Borromeo family, Renaissance nobility from Northern Italy (Figure 5.3). Although the rings are sometimes shown with diamonds or spikes, and often with varying topology,[2425] local legend claims that the three rings represent the Visconti, Sforza, and Borromeo families. The three families, often vicious foes, formed an "inseperable union" by intermarriage and choose interlocking rings to symbolize this union.[1] The rings can still be found in carvings and on buildings all over northern Italy. The terms "Borromean link" or "Borromean rings" were not in general usage until after the 1960's,[26] and early

papers in chemical topology refer to the symbol as the Ballantine rings or link, after the logo of a well-known brewer (Figure 5.3). Inspired by the wet ring marks left on the pub table by Peter Ballantine, the three rings represent "Purity, Body, and Flavor" and were used as the Ballantine logo from 1879.

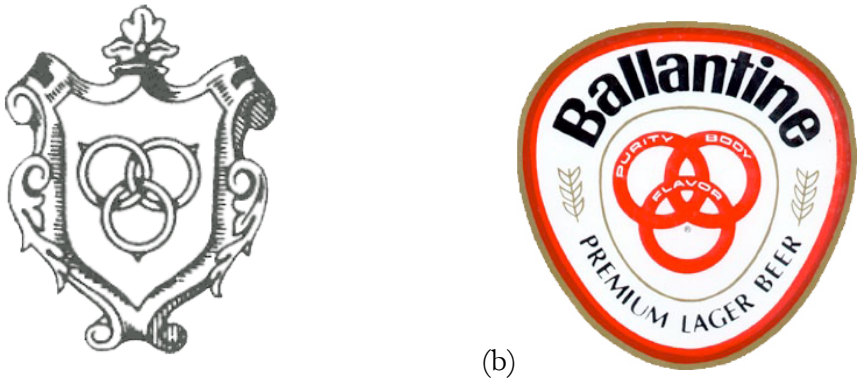

(a) (b)

Figure 5.3 (a) The Borromean Family crest and (b) the Ballantine Brewery logo.

The symbol itself is much older and can be found throughout history. In Christian theology, the mystery of the Holy Trinity was hotly debated at the Council of Nicea in 325 A.D. Though not unanimous, the views of Bishop Athanasius were in the majority and the Athanasian creed soon became church dogma.[27] The creed, which begins:

> Whosoever will be saved, before all things it is necessary that he hold the Catholic faith… And the Catholic faith is this, that we worship one God in Trinity and Trinity in Unity, neither confounding the Persons nor dividing the Substance. For there is one Person of the Father, another of the Son, and another of the Holy Ghost.

is a symbolic expression of the mystery of Christ's divinity and difficult to conceptualize. Geometric symbols, especially triangles and rings, become popular aids and three linked rings were common.[28] Not all the linked rings possessed the correct topology, but earliest known use of the Borromean topology was in a thirteenth-

century manuscript from Chartres, which contained four Borromean links (Figure 5.3).[29] Unfortunately the manuscript was lost in a 1944 fire.

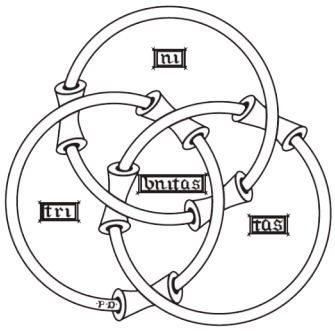

Figure 5.4 The earliest known representation of the Trinity as the Borromean link.

In Norse mythology, the valknut (old Norse, *valr*, slain warriors + *knut*, knot) consists of three interlocked triangles (Figure 5.5), and is thought to:

> symbolize the power of the god Odin to bind or unbind [a man's mind] ... so that men became helpless in battle, and he could also loosen the tensions of fear and strain by his gifts of battle-madness, intoxication, and inspiration.[30]

Also known as Odin's knot or Hrungnir's heart, the knot takes the Borromean or trefoil topology (Figure 5.5a and b). Hrungnir was a giant slain by the god Thor with his trusty hammer Mjollnir after losing a bet. "Hrungnir had, as is well known, a heart of stone, sharp and three-sided; just as the rune has since been risted that is called Hrungnir's heart."[31] The rune has been found on several important 7th and 8th century Viking stone pillars, usually associated with fallen warriors.

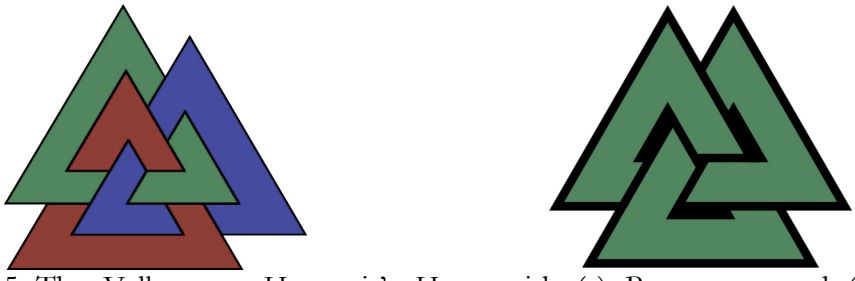

Figure 5.5 The Valknut or Hrungnir's Heart with (a) Borromean and (b) trefoil topology.[32]

5.1.2 Topology of Borromean Rings

The first appearance of link 6_2^3 in a mathematical context was in Tait's 1876 treatise on knot enumeration.[3] Hermann Brunn later studied the general class of links that become trivial upon the removal of any one component and such links, including the Borromean link, are called Brunnian links.[33] As before, in topology knots and links are considered flexible and as such the Borromean link can adopt many different embeddings (Figure 5.6). The first embedding is the most widespread and is often referred to as the Venn rings as they resemble a Venn Diagram. The three presentations shown have different symmetry, (S_6, D_{2d}, and T_h, respectively) but each is rigidly achiral and therefore the Borromean link is topologically achiral.[17] The Borromean link remains topologically achiral even after orienting all three rings (Figure5.7)![34]

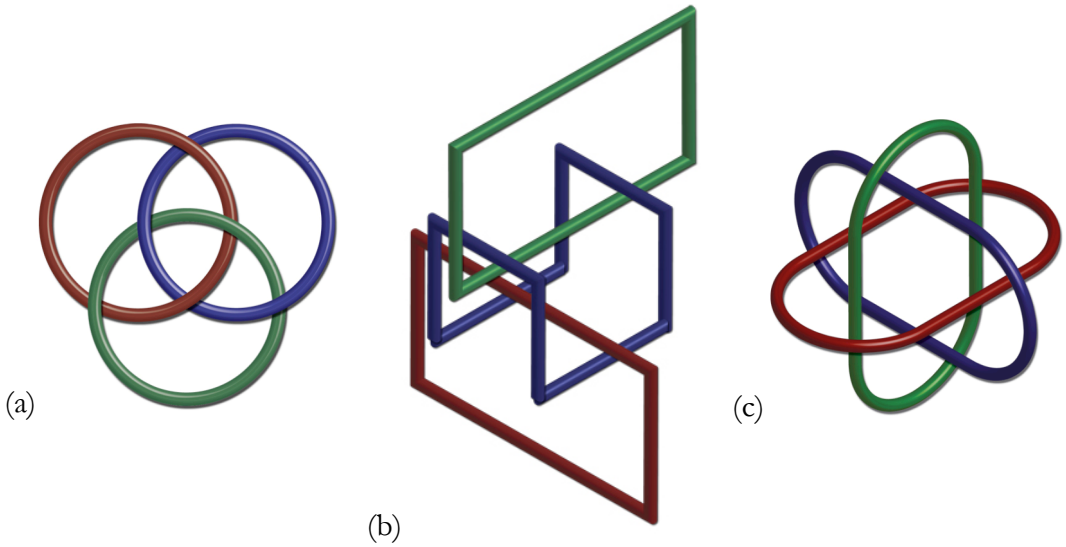

Figure 5.6 Various presentations of the Borromean knot: (a) The Venn rings; (b) chain rings; and (c) orthogonal rings.

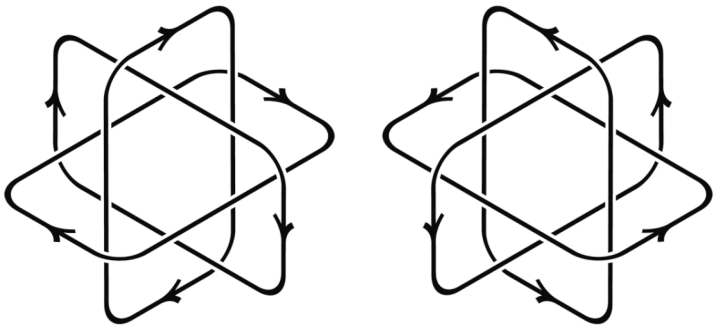

Figure 5.7 Equivalent mirror images of a Borromean link with all three ring oriented.[34]

5.1.3 Molecules containing the Borromean Topology

The first molecule containing Borromean topology was reported by Ned Seeman in 1997 (Scheme 5.1).[35] Exploiting the predictable hydrogen bonding between DNA and RNA base pairs as a templating mechanism, Seeman and coworkers are able to synthesize various knotted and catenated molecular nano-structures.[36,37] Replacing each of the crossings in the Venn rings (A) with one and a half turns of the appropriate double helix (the inner helix is right-handed and the outer left-handed), results in an embedding (B) that remains topologically equivalent (Scheme 5.1). Synthesis of DNA superstructure equivalent to (C) was achieved by the ligation of two, three-arm junctions (Scheme 5.1 Bottom).[35] Selective scission of any one ring gives topological proof of structure as it leaves the remaining two rings intact but results in the disassembly of structure, observable by gel-electrophoresis.

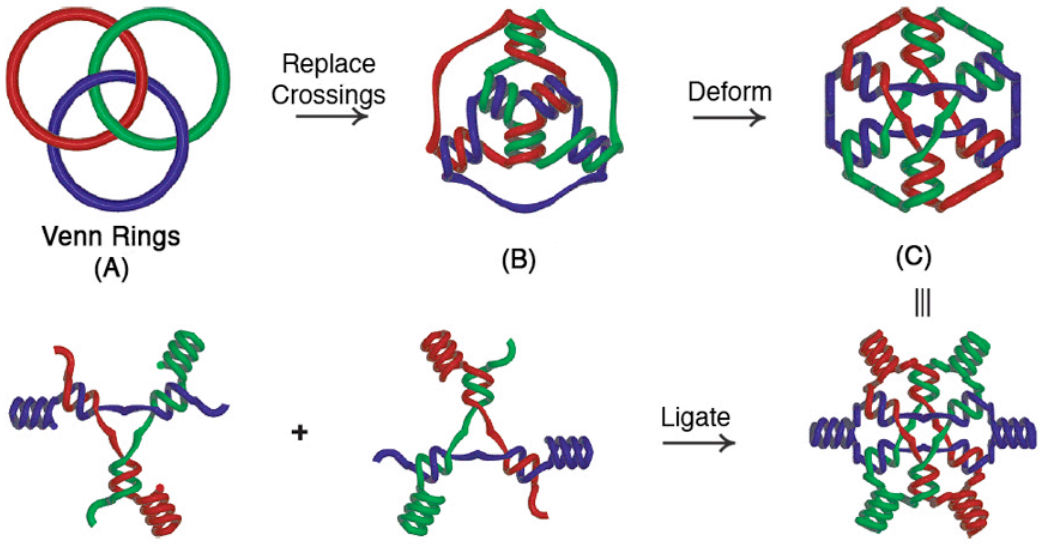

Scheme 5.1 (Top) Substitution of crossings with double helices and deformation. (Bottom) Seeman's synthesis of DNA Borromean rings.[35]

Though Seeman's synthesis of DNA Borromean link was indubitably a landmark in chemical topology, many continued to pursue a molecular Borromean link displaying the topology of the simple Venn or orthogonal rings. In 2003 Loren et. al. predicted a transition metal templated strategy for the sequential construction of an orthogonal Borromean link (Scheme 5.2).[383940] Starting with a large macrocycle (A) containing two endocyclic binding sites, the threading of two exo-topic ligands (B) establishes a doubly penentrated structure templating the formation of a ring-in-ring compound (E). When (D) incorporates an endocyclic binding unit, a second complexation and threading of ligand (F) would result in an orthogonal Borromean link (I) after ring-closure or "capping" with (H).

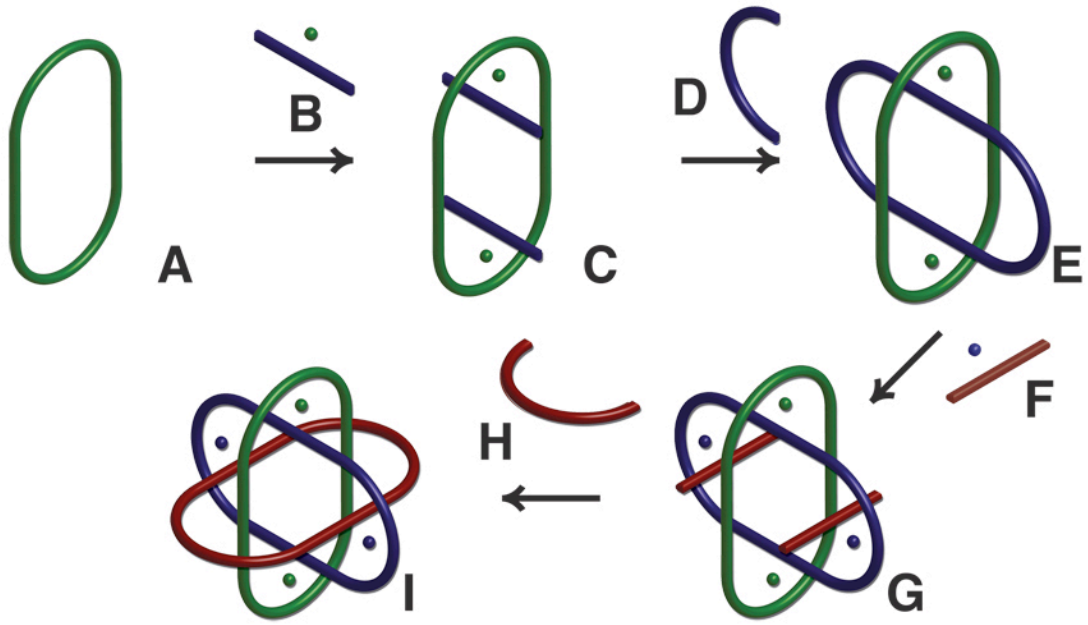

Scheme 5.2 Strategy for the step-wise synthesis of an orthogonal Borromean link.

Relying on the well-known coordination chemistry of poly-pyridines,[41] an advanced two-ring intermediate was synthesized in very good yield (Scheme 5.3).[38] Unfortunately, all attempts to thread of linear bipyridine ligands in the presence of copper(I) were unsuccessful. A thorough analysis of the three-dimensional structure utilizing x-ray crystallography was able to offer an explanation (Figure 5.8). The first ring is ~27 Å across (from central pyridine ring to central pyridine ring) and is bowed into a chair-like structure, with space (~8 Å diameter) for the threading of the third ring components (Figure 5.8b). The bridging bipyridine caps of ring two adopt the favored *transoid*- conformation, stretching ring two and compressing ring one. In order for metal complexation to occur, the bipyridines must first assume a *cisoid* conformation (disfavorable by ~25 kJ).[42] Thereby reducing the height of ring two and further compressing ring one. Loren conjectured that the ring one behaves as a loaded spring and further compression is energetically prohibitive.

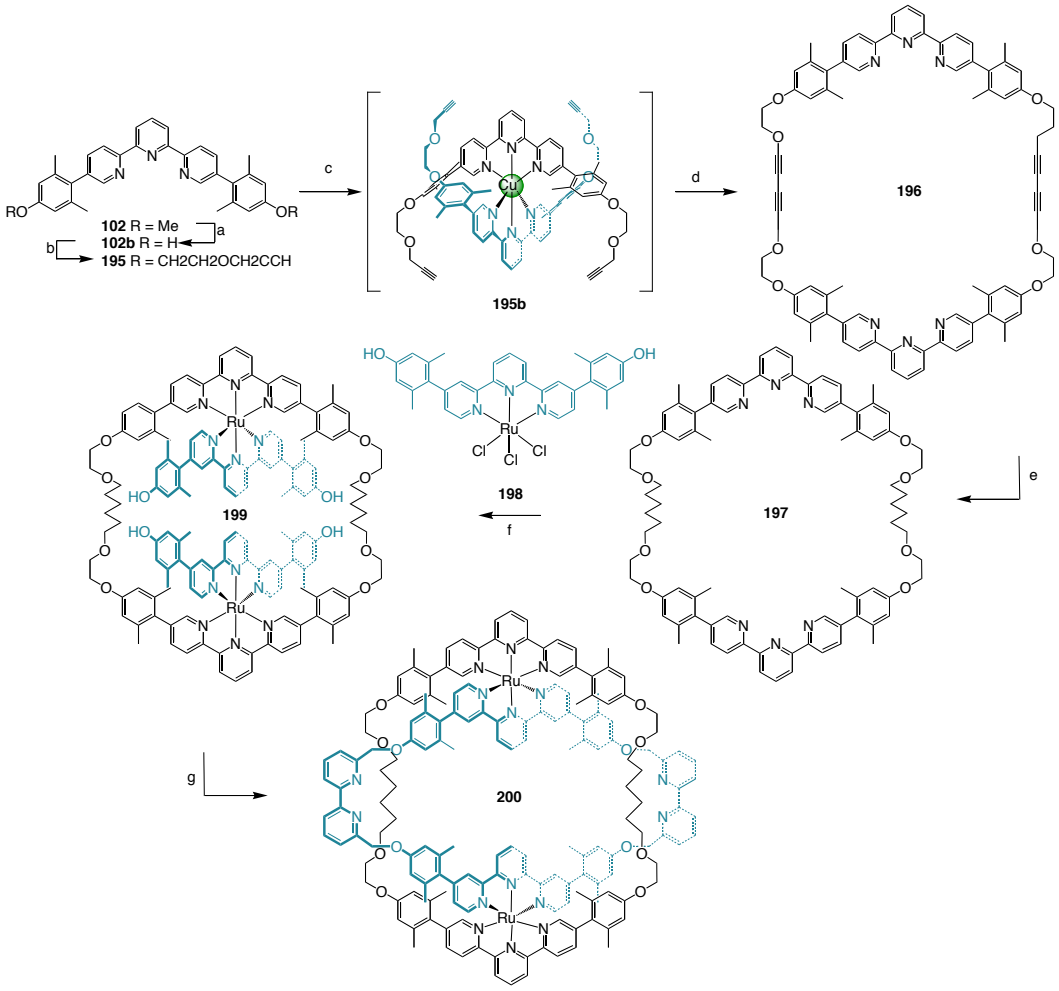

Scheme 5.3 Loren's and Yoshizawa's synthesis of a bipyridine two-ring structure. Reaction conditions: a) PyrHCl, 185 °C, 4 h, 97%. b) Cs_2CO_3, $TsO(CH_2)_2OCH_2CCH$ (2.2eq), DMF, 80 °C, 10h, 69%. c) $Cu(OAc)_2$-H_2O (0.5 eq), EtOH, RT, 1h. d) $Cu(OAc)_2$-H_20 (10.0 eq), EtOH (high dil.), Δ, 72 h, 91%. e) H_2, 80psi, 10% Pd-carbon, 1:1 EtOH:CH_2Cl_2, 6h, 91%. f) 198 (2.1 eq), 2:2:1 CH_2Cl_2:EtOH:ethylene glycol, Δ, 12 h, 65%. g) 6,6'-bisbromomethyl-2,2'-biypyridine (2.1 eq), Cs_2CO_3, ACN, Δ, 72 h, 49%.

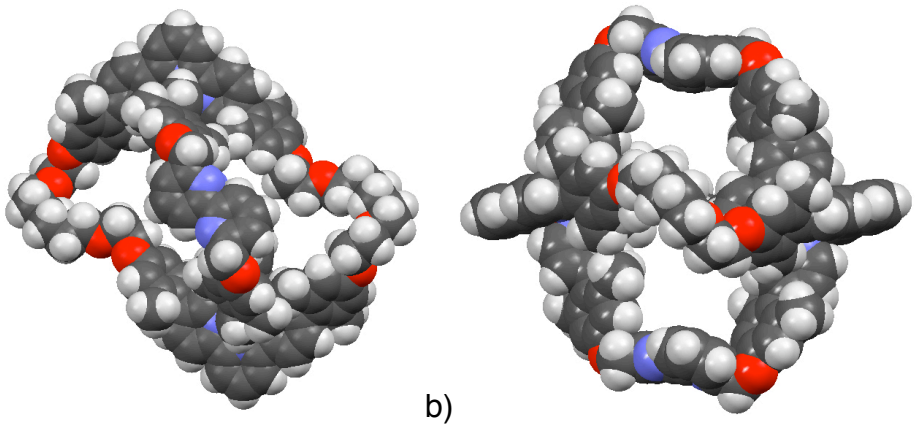

Figure 5.8 Crystal structure of bipyridine 2-ring structure **200**. a) front view showing transoid bipyridines and b) side view showing compression of ring one and space available for threading.[38]

Conversion of ring two precursor **199** into the triflate derivative **199b** allowed the synthesis of a rigidified phenanthroline two-ring structure **202**, identified by ^{1}H-NMR and ESI-MS (Scheme 5.4), but threading reactions were unsuccessful.[43]

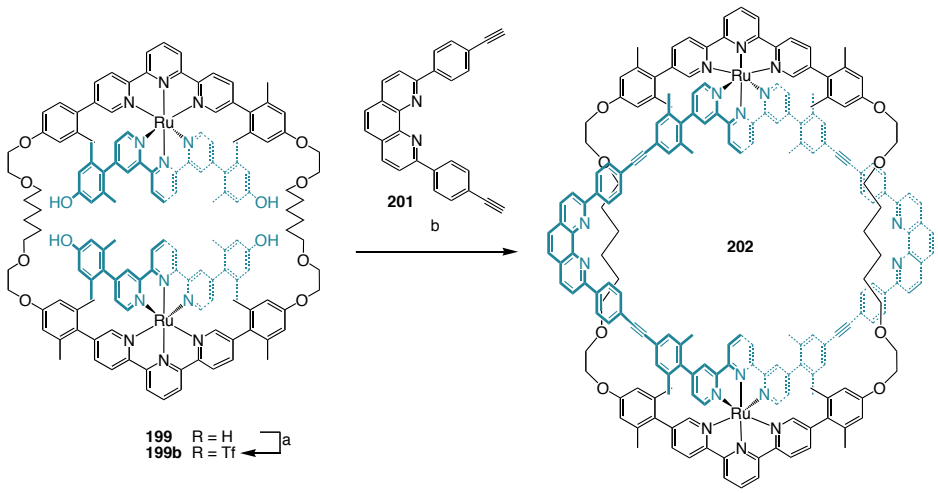

Scheme 5.4 Synthesis of phenanthroline 2-ring structure **202**. Reaction conditions: a) trifluoromethanesulfonic anhydride, CH_2Cl_2, pyridine, 0 ºC, 6h, 99%. b) **201**, DIA, $Pd(PPh_3)_4$, DMF, 80 ºC, 72 h, 31%.[43]

In completely different approach, the Stoddart group employed the principles of self-assembly[44-46] to synthesize a molecular Borromean link (Figure 5.9).[47] Combining the dynamic reversibility of imine bonds[48-51] with the templating influence of zinc ions, an elegant one-pot synthesis resulted in the thermodynamic formation of Borromean links, unambiguously confirmed by x-ray crystallography. In the solid state, the link is approximately 2.5 nm across and exhibits the S_6 symmetry of the Venn diagram rather than the T_h symmetry of the orthogonal presentation. Reduction of the imine bonds resulted in the metal free Borromeand[52] and the metal-free single macrocycles. Under the reductive conditions, ring cleavage occurs and the topology disassembles.[53] When enantiopure precursor ligand is used, a chiral Borromeates are acquired (Figure 5.10). By virtue of its symmetry, a Borromean link can never be topologically chiral. This does not exclude the existence of Euclidean chirality and Stoddart's chiral Borromeate

shows strong Cotton effects at λ_{min} = 224 nm ($\Delta\varepsilon$= 29.75 $m^{-1}cm^{-1}$) and λ_{max} = 239 nm ($\Delta\varepsilon$ = 49.0 $m^{-1}cm^{-1}$).

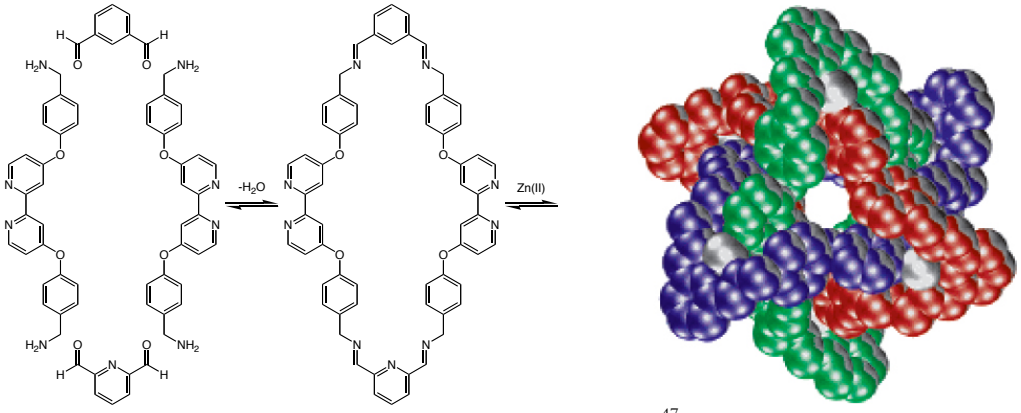

Figure 5.9 Self-assembly of a nano-scale Borromeate.[47]

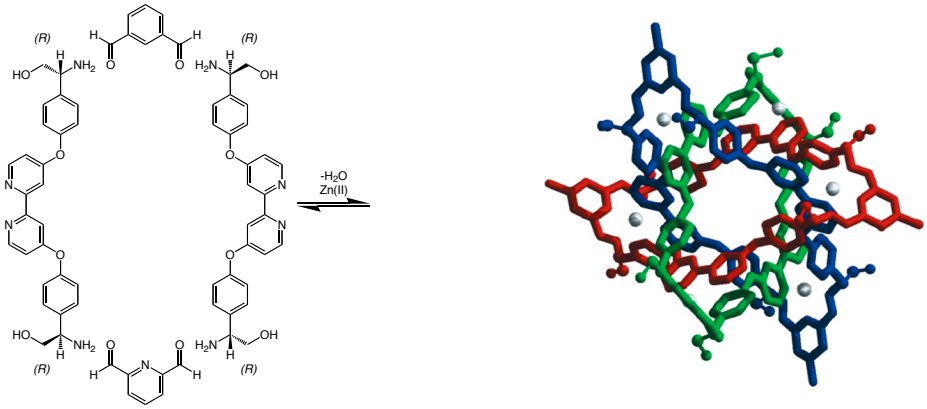

Figure 5.10 Self-assembly of a chiral Borromeate.[54]

A handful of coordination networks composed of three-entangled (6,3)layers, containing the correct Borromean topology, have been found in the last five years (Figure 5.11).[55-61] In 2003, Resnati and coworkers noticed that the non-covalent interactions of halogens with electron donors (Figure 5.12)[62] sometimes gives coordination networks with Borromean topology,[63] and in the follow-up work,[64] they modulated the alkyl chain length to program in the Borromean connectivity (Figure 5.13). Similar to the knotted and linked proteins of Liang and Mislow,[65,66] the topology of these network is dependant on which interactions are considered topologically

significant. Different topologies can be visualized depending on which interactions are considered in the network.

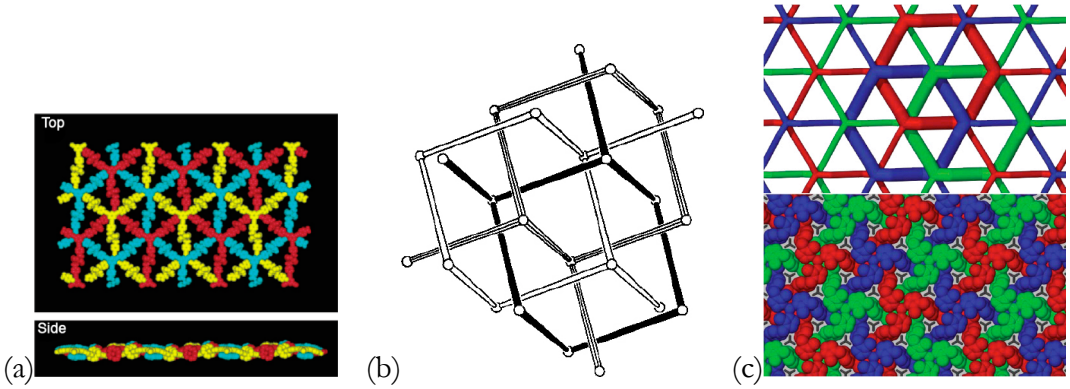

Figure 5.11 Interpenetrating (6,3) layer containing the Borromean topology and reliant on (a) RCOO-Ni(II) coordination[61] (b) Au-Au bonds,[59] and (c) Ag-Ag bonds.[55]

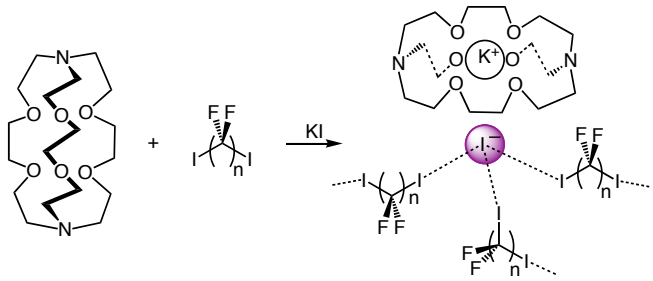

Figure 5.12 Formation of the three component supramolecular complexes through potassium cryptation by K.2.2.2. and I⁻…I–C XB

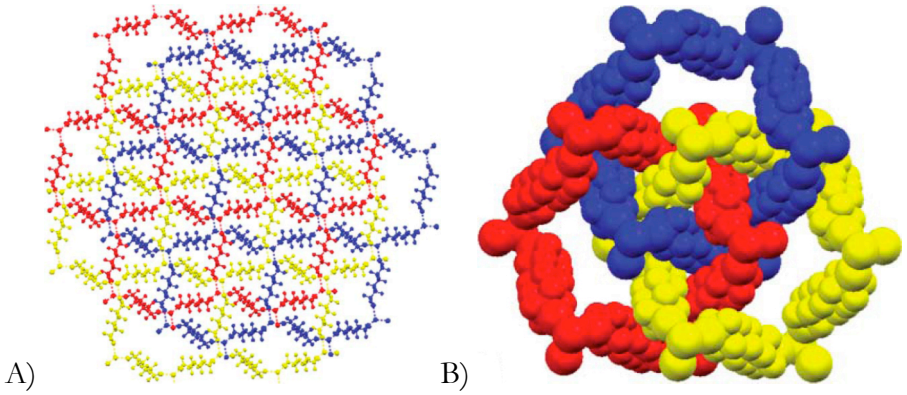

Figure 5.13 (A) Ball-and-stick view of an infinite Borromean weave defined by ···I⁻ ··· I–(CF2CF2)$_n$–I ··· interactions in the crystal structure of K.2.2.2, 1,8-diiiodoperfluorooctane, and potassium iodide; and (B) a space-filling representation of a single Borromean link from interwoven sheets.

5.2 Current Work

5.2.1 Introduction

Despite the stunning success of the Stoddart's thermodynamic self-assembly of a Borromean link, the sequential construction of a Borromean link under kinetic control offers a degree of control and specificity inaccessible by one-pot self assembly methodologies.[9] The thermodynamic and kinetic strategies are not divergent but rather, complementary and a full spectrum of available methodologies can only benefit future chemists and engineers in pursuit of the nanoscale.

5.2.2 Retrosynthetic analsyis

The efficient synthesis of a two-ring structure composed of differentiated rings by Loren et. al. established the foundation of a directed, stepwise approach. The difficulty of setting the third ring reveals the intricacy and inherent difficulty of engineering nano-scale architectures. The preference of bipyridine for the *transoid* conformation results in a large change in overall structure and prevents further complexation. The change to rigid phenanthroline cap **201** was predicted to prevent such conformational reorganization and to hold the pocket open for complexation, but was also unsuccessful. From the structural and conformational lessons of our forerunners, three hypotheses were drawn: (1) switching from a bidentate motif to an terdentate motif provides additional kinetic and thermodynamic stability, favoring the binding of an octahedral metal ion within the two-ring structure; (2) rigidity is essential, small conformational flexibility in the ligand can result large overall structural changes; and (3) the rigid terdentate ligand should extend the first ring, prevent compression, and create as large as a threading pocket as possible. Comparison with the successful bipyridine and phenanthroline ligands, and CPK modeling indicate that terpyridine

ligands **203** and **204** meet all size and rigidity requirements and as such, are potential caps.

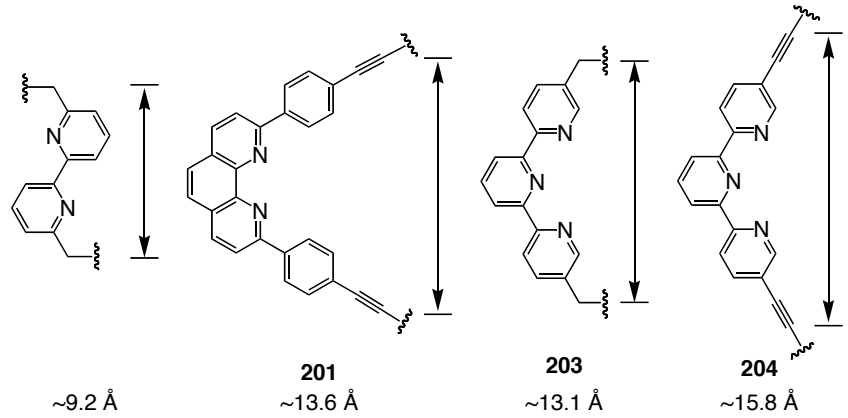

An additional advantage of switching to an terdentate ligand, such as terpyridine, is the availability to form robust and kinetically stabile ruthenium(II) complexes, opening another potential synthetic route (Scheme 5.5). Rather than capping the threaded ring two precursor (**C**) with an empty terpyridine unit (**D**), use of an appropriate heteroleptic ruthenium(II) complex (**J**) could directly result in a threaded two-ring structure (**G**), avoiding the conformation difficulties of threading.

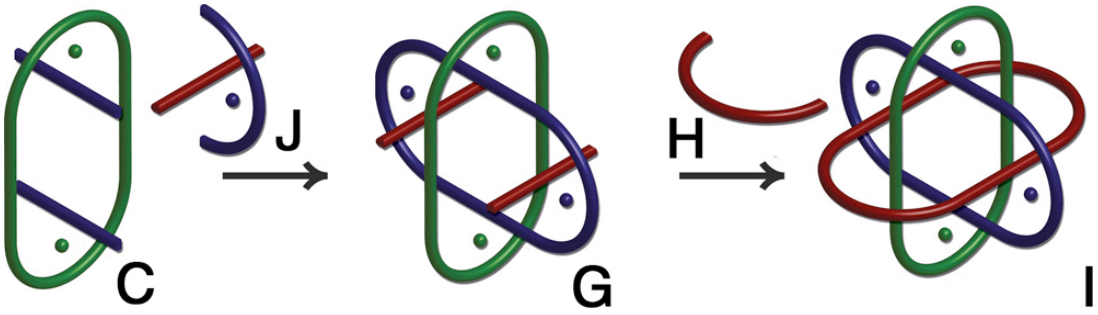

Scheme 5.5 Route B. Synthetic strategy relying on preformed hetereoleptic complex **J**.

5.2.3 Synthesis and Results

Route A: Sequential capping and threading. Renewed synthetic efforts towards the Borromean link commenced with the synthesis of a new two-ring structure incorporating empty terpyridine units (Scheme 5.6). Treatment of threaded two-ring precursor **199** with 5,5"-bis(bromomethyl)terpyridine under Williamson ether synthesis conditions gave the new ring-ring structure **205** in good yield (60%). Confirmation of structure was afforded by the expected D_{2h} symmetry in ^{1}H and ^{13}C NMR and the characteristic sequential loss of PF_6^- counter-ions in the mass spectrometry spectra (Figure 5.14)

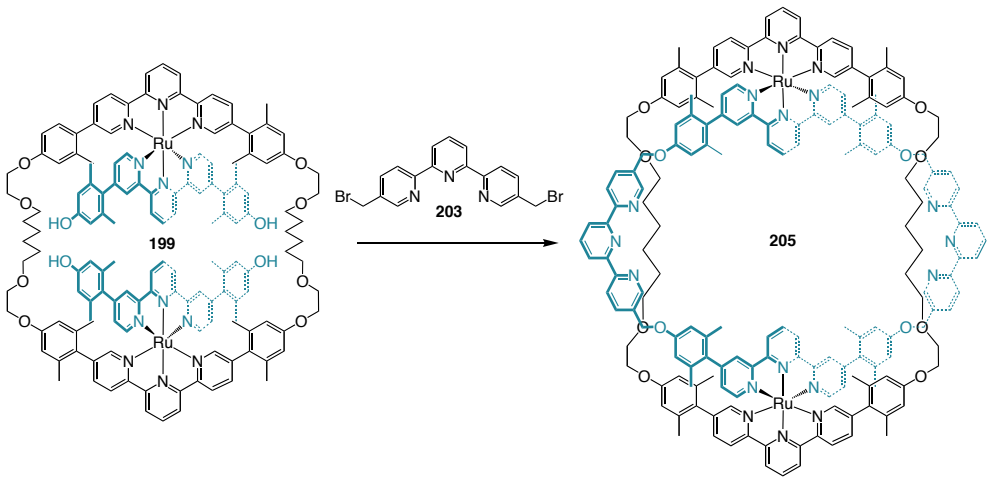

Scheme 5.6 Synthesis of terpyridine 2-ring structure **205**. Reaction conditions: **203**, Cs_2CO_3, ACN, Δ, 12 h, 60 %.

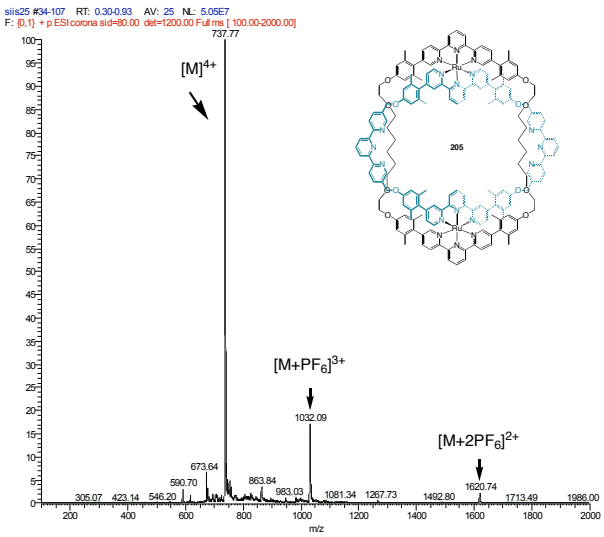

Figure 5.14 ESI-MS of the new terpyridine two-ring complex **205**.

Initial threading attempts utilized terpyridine ruthenium(III)trichloride complex **198** and were unsuccessful under a range of conditions. Monitoring the reaction by TLC and ESI-MS showed the disappearance of starting material and indicated the formation of a species with the mass of a mono-threaded species (Figure 5.15), but only reduced **198** was recovered.

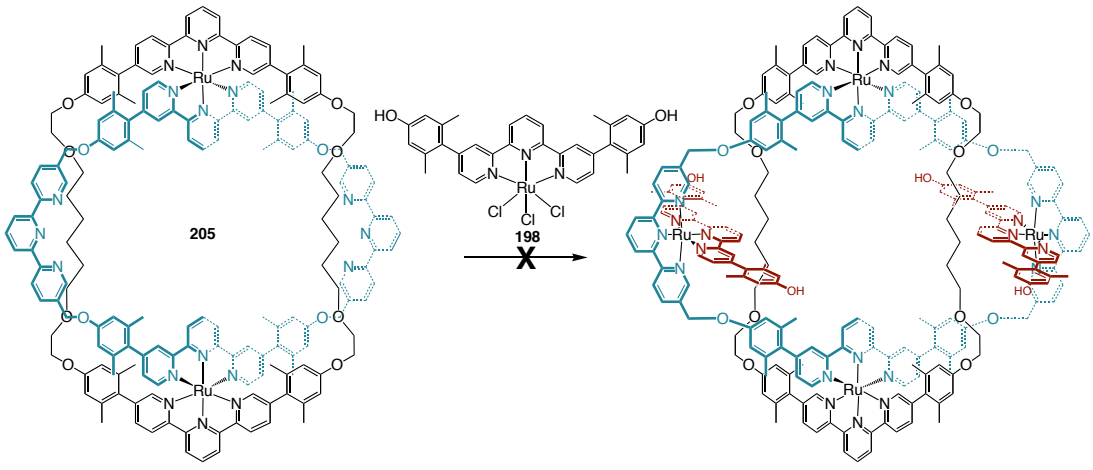

Scheme 5.7 Unsuccessful attempts to thread a third ring precursor of the Borromean link using Ru(terpy)Cl_3. Ring one is black, ring two is blue, and ring three is red. Reaction conditions: a) *N*-ethylmorpholine, EtOH, Δ, 2 days; b) ethylene glycol, 125 ºC, 3 - 5 days; c) 1:1 Ethylene glycol: DMSO, 125 ºC, 4 days.

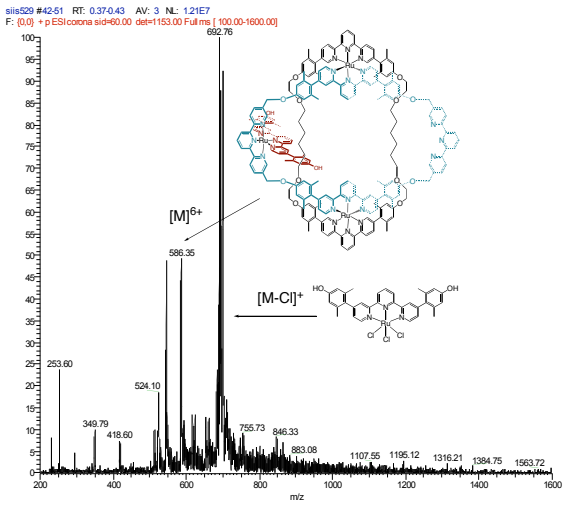

Figure 5.15 ESI-Spectra of unsuccessful attempts to thread a third ring precursor of the Borromean link using Ru(terpy)Cl_3 at 6 h. Further reaction times show degradation of the mono-threaded two-ring structure.

Zinc(II) can form hexacoordinate octahedral complexes, but because of the filled d subshell prefers a pentacoordinate trigonal biypyramidal geometry.[67] Zinc complexes are kinetically labile and it was hoped that treatment of **205** with zinc(II)acetate in the presence of linear bipyrdine thread **206** under equilibrium conditions would favor the heteroleptic mixed species (Scheme 5.8). However, only two-ring **205**, free ligand and Zn(**206**)$_3$[PF_6]$_2$ were observed by TLC and MS.

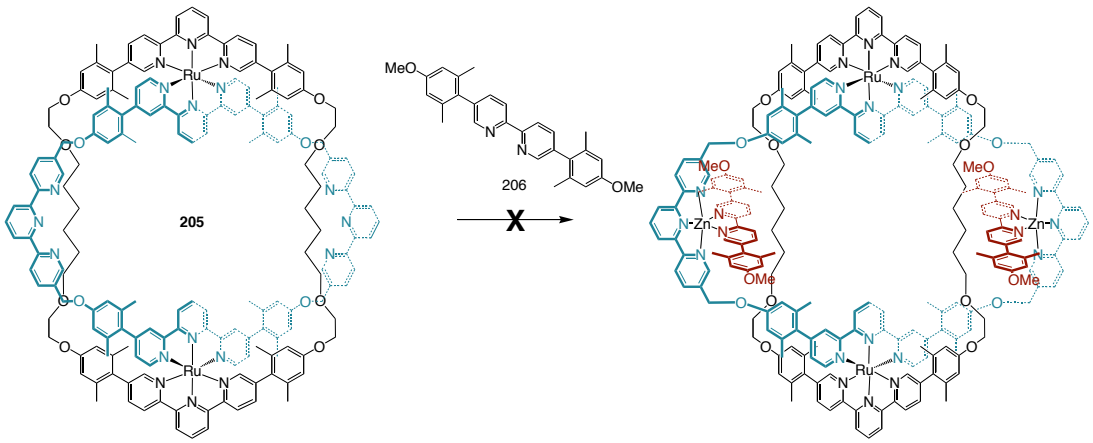

Scheme 5.8 Unsuccessful attempts to thread a third ring precursor of the Borromean link using zinc(II). Reaction conditions: **206**, Zn(OTf)$_2$, CH_2Cl_2, 35 ºC, overnight.

In order to ascertain whether the absence of threading was due to conformational issues inhibiting complexation or steric restrictions of the threading pocket, two-ring **205** was treated with zinc triflate (Scheme 5.9) and showed complexation of two equivalents of $Zn(OTf)_2$ (Figure 5.16a).

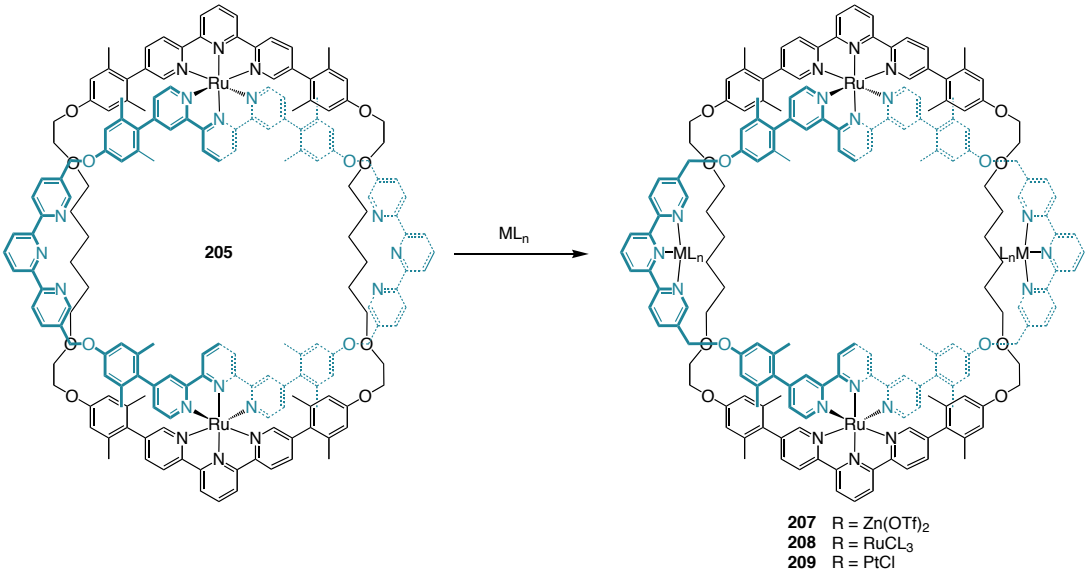

Scheme 5.9 Coordination chemistry of the two-ring complex **205**. Reaction conditions: 1) $Zn(OTf)_2$, ACN, RT, 3 h, quant. 2) $RuCl_3$, 1:1 EtOH:dichloroethane, 80 °C, overnight, quant. 3) $PtCl_2(COD)$, $AgBF_4$, ACN, RT, 30 min, 70 %.

Reaction of two-ring **205** with $RuCl_3$ in refluxing ethanol (Scheme 5.9) gave the $Ru(II)_2Ru(III)_2$ two ring complex **208** (Figure 5.16b). Platinum(II) is a diamagnetic d_{10} metal known to form tetracoordinate square planar complexes with terpyridines,[68] and treatment of **205** with platinum(II)dichloride cyclooctadiene[69,70] resulted in the immediate formation of the Pt_2Ru_2 two-ring **209** (Scheme 5.9 and Figure 5.16c).

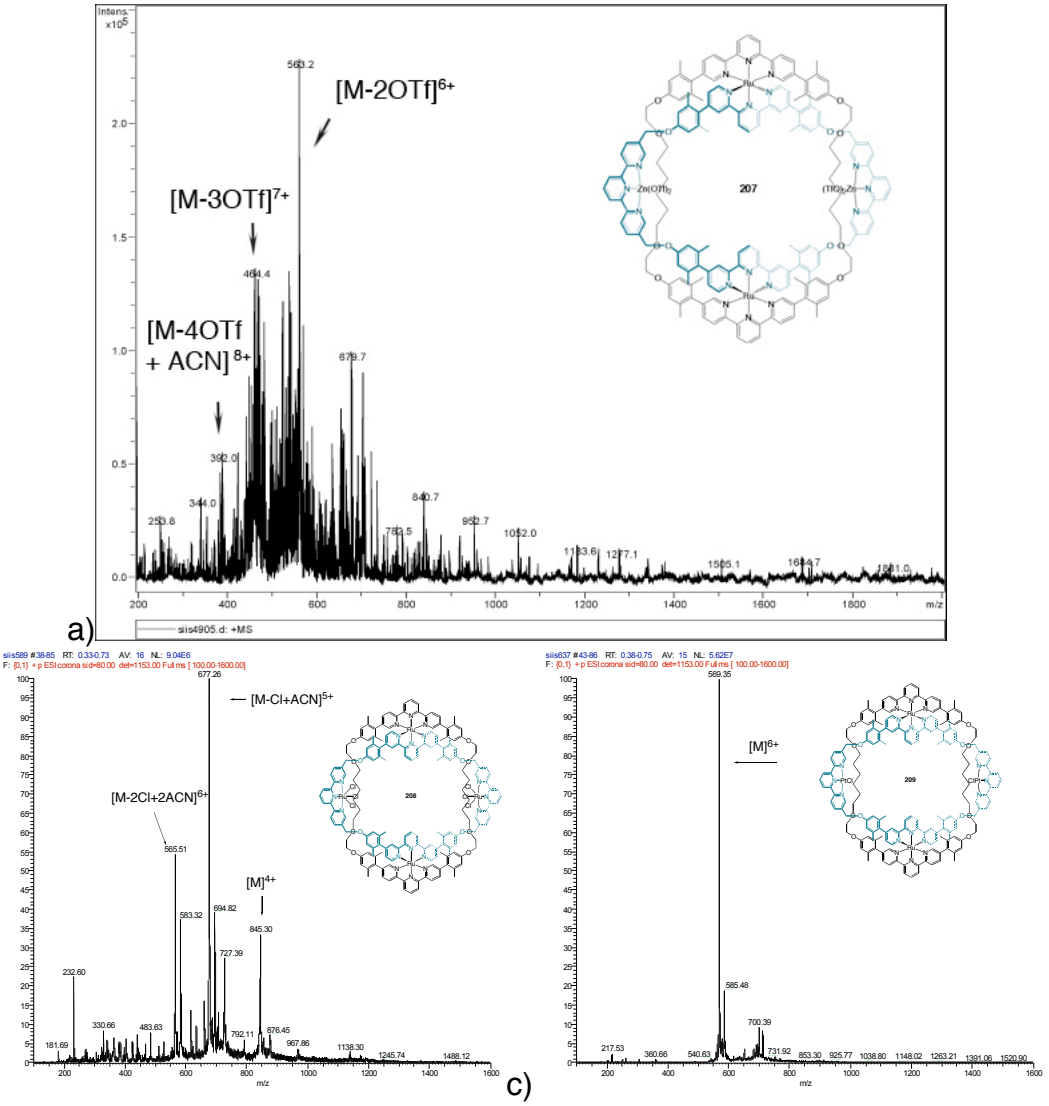

Figure 5.16 ESI-mass spectra of four metal two-ring complexes **207** – **209**; where M is the parent ion mass of the tetracation.[71]

Having established that the empty terpyridine units of ring two can bind two equivalents of metal-ion, threading was again attempted. Heating $Ru(II)_2Ru(III)_2$ two-ring complex **208** in the presence of the third ring precursor terpyridine **210** resulted in only decomposition of starting material (Scheme 5.10). When smaller terpyridine **211** is used, again no product was detected by ESI-MS and only decomposition was observed.

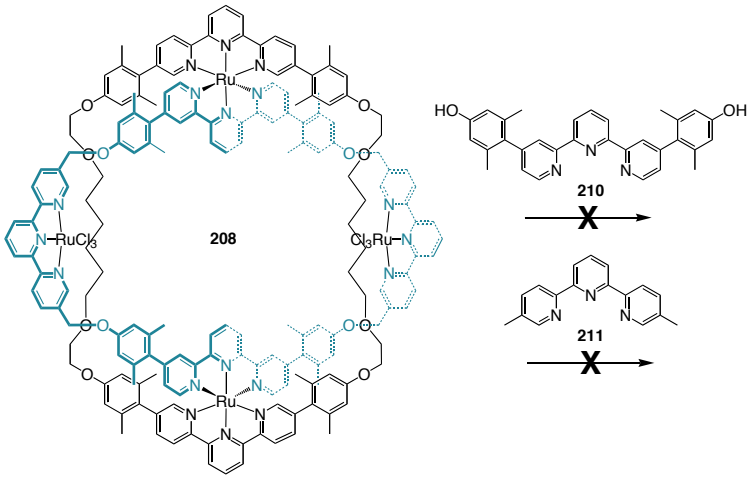

Scheme 5.10 Unsuccessful attempts to thread terpyridine ligands into Ru(II)2Ru(III)2 two-ring complex **208**. Reaction conditions: a) **210** or **211**, ethylene glycol, 125 °C, overnight, or b) 211, N-ethyl morpholine, EtOH, 80 °C, 2 days.

Adding bipyridine thread **206** to an acetonitrile solution of Zn_2Ru_2 two-ring **207** resulted in the extraction of zinc from the two ring complex and only zinc free **205** and Zn(**206**)3$[PF_6]_2$ were isolated (Scheme 5.11).

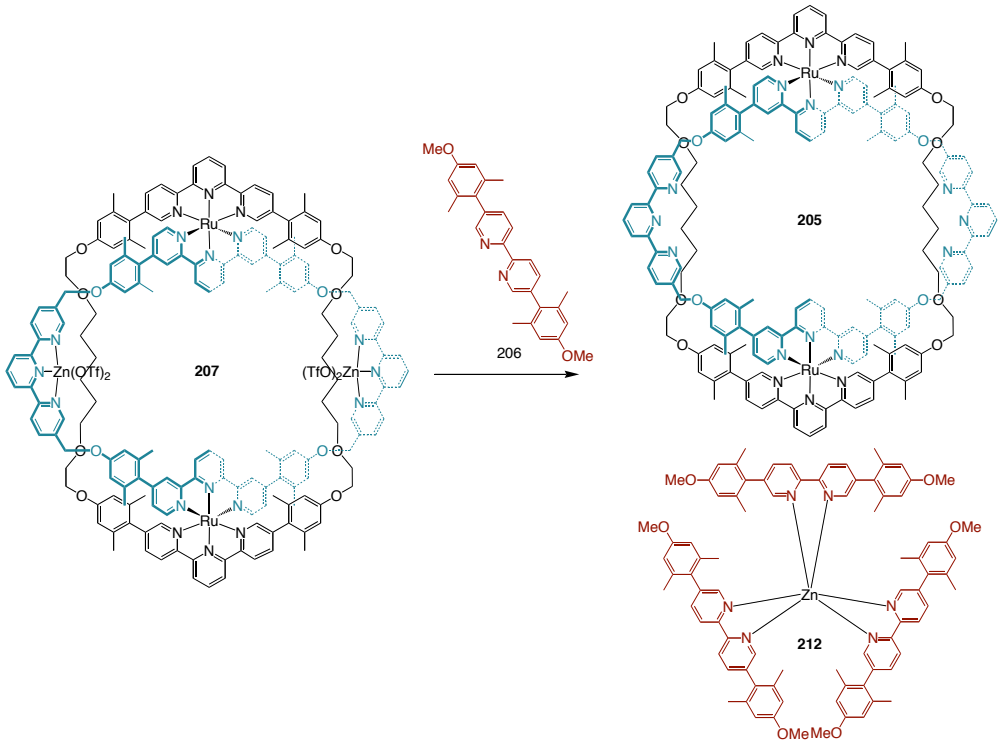

Scheme 5.11 Extraction of Zn(II) from Zn_2Ru_2 two-ring **205** by bipyridine **206**. Reaction Conditions: ACN, RT, 1 day.

Unlike the bipyridine two ring of Loren et. al., there is no significant geometry change in the terpyridine binding unit upon metal ion coordination (Figure 5.17). The empty terpyridines can and do freely rotate and bind metal ions without disturbing the tertiary structure of the complex. There may still be conformational issues that prevent the insertion of a large terpyridine ligand within the binding pocket. Additionally, the terpyridines have been drawn as an endocyclic binding pocket, but it is possible that an exocyclic motif exists. Ultimately, only solid state crystallography is capable of addressing the topology of two ring structures.

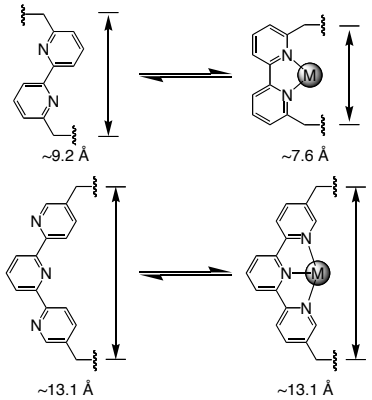

Figure 5.17 Geometrical changes upon metal complexation.

We hypothesized that the first ring acts as a cinch or a belt and controls the conformation of the second ring by contraction and dilation. In order to verify this hypothesis, a systematic crystallographic investigation of the first ring was undertaken. Coordination of one equivalent of ruthenium(II) under traditional conditions (Scheme 5.12) resulted in a fully compressed helical structure similar the proposed transition state **195b** (Scheme 5.3).

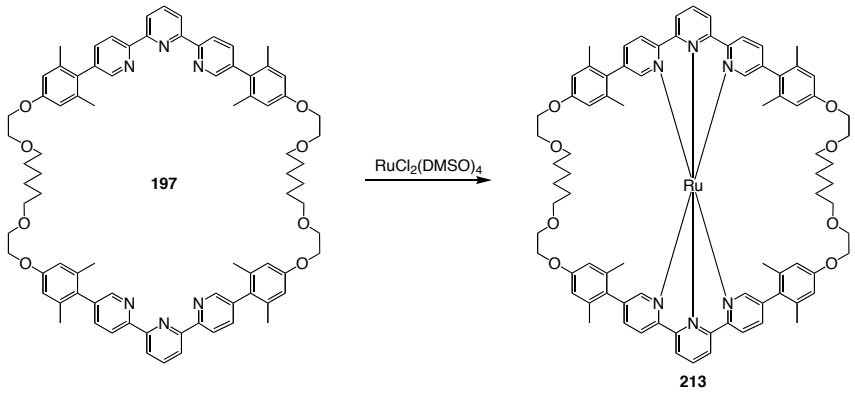

Scheme 5.12 Synthesis of Ru[**197**][PF_6]$_2$. Reaction conditions: 2:2:1 Ethylene glycol, dichloroethane, EtOH, 125 ºC, overnight, 96%.

Crystals of **213** were grown from the slow diffusion of diethyl ether into a saturated acetonitrile solution and the structure solved (Figure 5.18). The asymmetric unit contains one disordered cation, two highly disordered anions distributed over three partially occupied sites, and an estimated four acetonitrile molecules. The solvent molecules are disordered and could not be modelled adequately, so their contribution to the intensity data was removed by using the *SQUEEZE* routine of the *PLATON* program. In the cation, significant disorder is present in one of the alkyl ether chains and one of the immediately adjacent manisyl rings. The overall quality of the structure is quite low (R = 0.103), but the conformation of the cation is clearly discernable. The overall cation geometry is reminiscent of a helical bow tie (Figure 5.18a) and the bond angles and distances are similar to other manisyl-terpyridine structures (vida infra). Each cation interacts with adjacent bow-ties through anti-parallel offset π-stacking of manisyl groups (centroid-centroid distance ~3.7 Å, displacement angle ~21º) (Figure 5.18b) and with another neighboring bow-tie through two CH $\cdots$ π interactions of ~2.99 Å (Figure 5.18c).

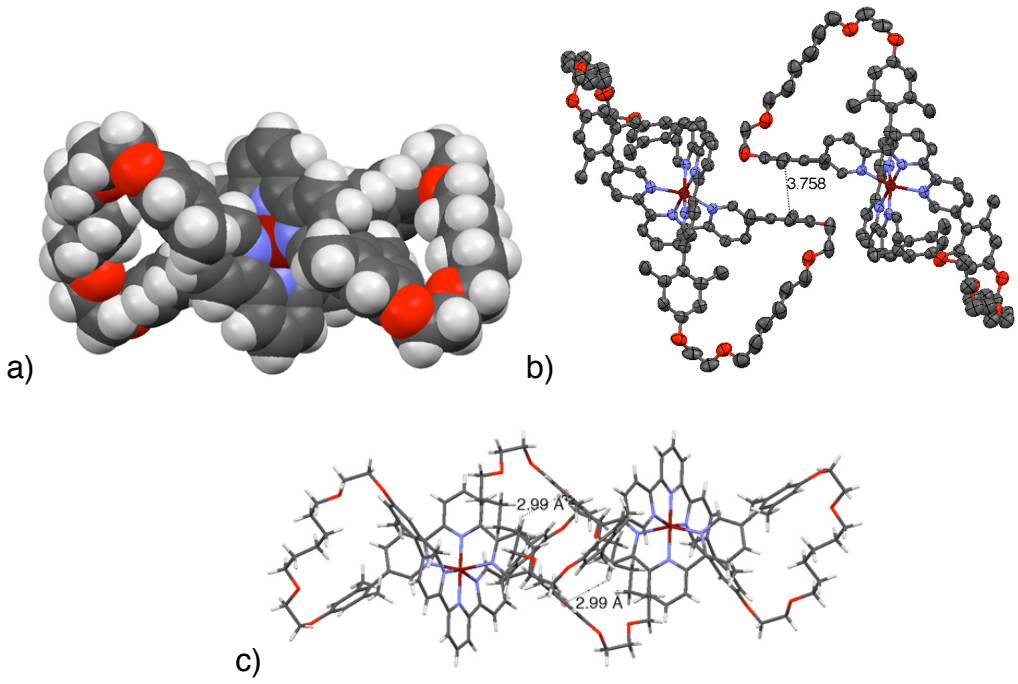

Figure 5.18 Crystal structure of fully compressed ring one **213**. a) Space filling side view; b) ORTEP diagram showing off-set π–stacking of manisyl groups between cations; and c) CH $\cdots$ π interactions between cations. Disordered atoms, anions, and solvent molecular have been removed for the sake of clarity.

Coordination of two equivalents of zinc(II) resulted in a partially compressed flat structure **214** (Scheme 5.13). Crystals of [**197**][$Zn(OTf)_2$]$_2$ were grown from the slow diffusion of diethyl ether into a saturated acetonitrile solution and the structure solved (Figure 5.19). In the cation, each zinc atom is coordinated by the terpyridine ligand, one disordered triflate anion and two water molecules. The cation sits across a crystallographic centre of inversion, while the asymmetric unit contains, in addition, one uncoordinated triflate anion in a general position, two acetonitrile molecules and one molecule of diethyl ether. At each zinc atom in the cation, one of the coordinated water molecules forms hydrogen bonds with an ether O-atom in the terpyridine ligand (almost on the opposite side of the ligand) and with an uncoordinated triflate anion. The other coordinated water molecule forms hydrogen bonds with the same uncoordinated triflate anion and the ether O-atom of a neighbouring diethyl ether

molecule. The macrocycle has collapsed upon itself and one manisyl group of each terpyridine interacts through anti-parallel offset π-stacking (centroid-centroid distance ~3.7 Å, displacement angle ~21°) (Figure 5.19b). The planes of each terpyridine unit, defined by the three nitrogen and the bound zinc atoms, are parallel but offset by ~3.0Å (Figure 5.19c). The macrocycles pack in a staggered fashion, separated by disordered solvent and the uncoordinated anion (Figure 5.21d).

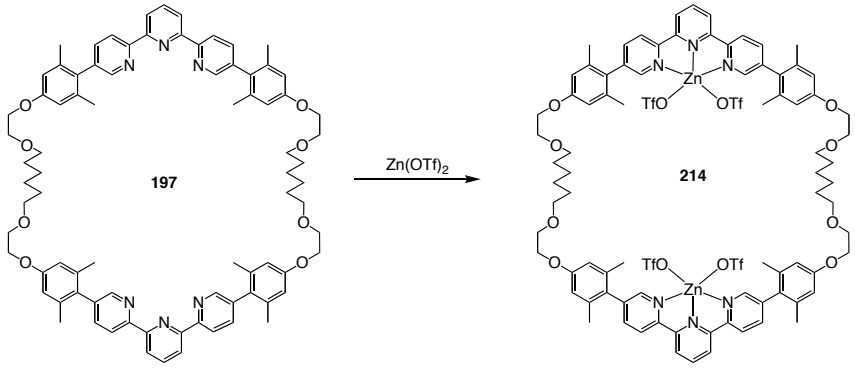

Scheme 5.13 Synthesis of one ring complex **214**. Reaction conditions: 1:1 Ethanol : CH_2Cl_2, RT, 5 h, quant.

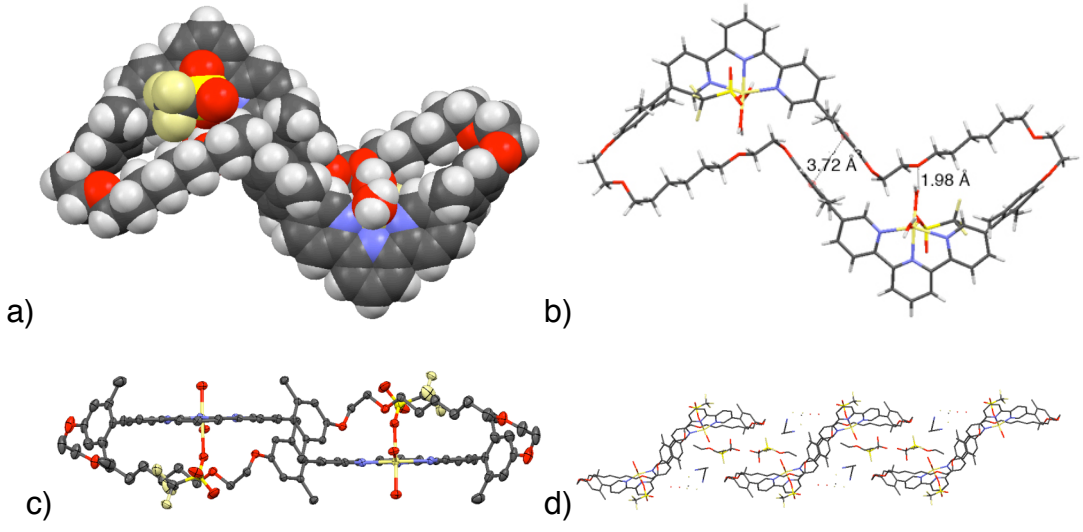

Figure 5.19 Crystal structure of [**197**][$Zn(OTf)_2]_2$: a) space filling side view; (b) side view showing interaction of manisyl groups; c) top view of the ORTEP diagram showing the offset of terpyridine planes; and d) staggered packing diagram.

X-ray quality crystals of the bis-threaded one-ring structure **199** were acquired by the slow diffusion of diethyl ether into a saturated methylene chloride solution and the structure solved (Figure 5.20). The cation sits across a crystallographic centre of inversion, while there are two PF_6^- anions in general positions, giving the required 1:4 cation : anion ratio, one of which is disordered. The asymmetric unit also contains sufficient space for several solvent molecules, but the disorder of the solvent molecules could not be modelled adequately. The disordered solvent molecules were omitted entirely from the subsequent refinement model, which gave better refinement results and there were no significant peaks of residual electron density to be found in the voids of the structure. This procedure leaves a single cavity of 1450 $Å^3$ per unit cell.

All bond distances and angles are comparable to similar heteroleptic terpyridine complexes. The two ruthenium(II) centres of bis-ruthenium complex **199** are separated by 13.35 Å. The planes of the penetrating terpyridine rings are off set by 3.21 Å (Figure 5.20b), and the phenol oxygen atoms of the terpyridine threads are separated by 8.27 Å (Figure 5.20a).

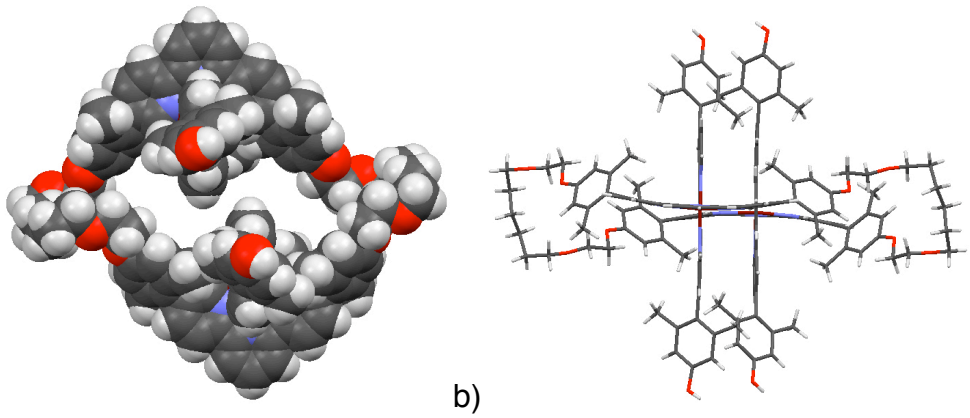

Figure 5.20 Crystal structure of the threaded two-ring precursor **199**. a) Side and b) top view. Disordered solvent and anion molecules removed for clarity.

The unit cell contains two cations connected by hydrogen bonding through one of the symmetry-independent hydroxy groups with one of the ether oxygen atoms in the adjacent cation (Figure 5.21). The corresponding hydroxy group in the same part of this second cation forms a corresponding hydrogen bond back to the original cation. However, the centro-symmetric nature of the cation means that each cation donates two hydrogen bonds of this type which then links the cations into a linear double-bridged hydrogen bond network.

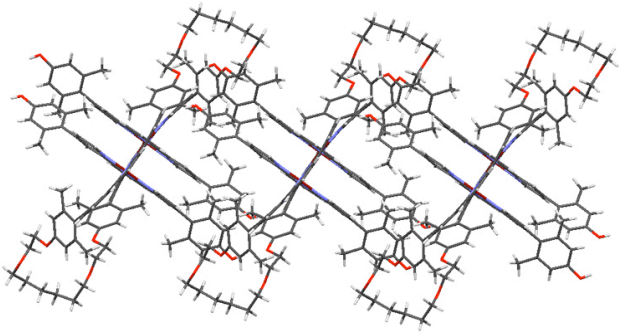

Figure 5.21 Linear hydrogen bonding motif of **199**.

Perpendicular to the linear hydrogen bonding chain, neighboring cations interact through complementary CH $\cdots \pi$ interactions (~2.75 Å) (Figure 5.22a) and create a 2-D sheet of hydrogen bonding and aromatic interactions (Figure 5.22b).

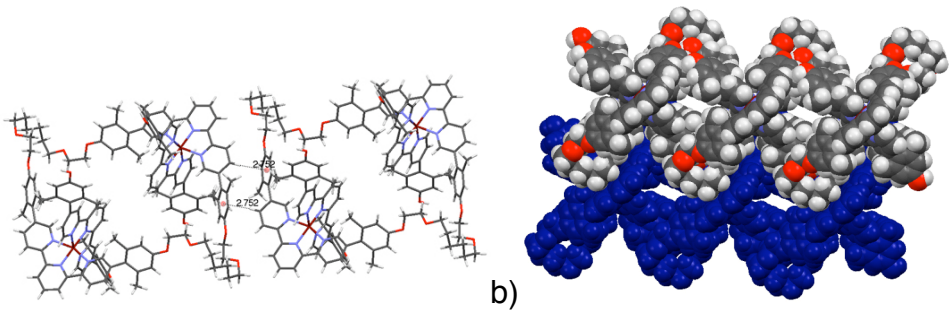

Figure 5.22 Complementary CH $\cdots \pi$ interactions of a) neighboring cations and b) linear hydrogen bond networks, creating 2-D sheets. One linear H-bond network is in black, and the other blue.

Single crystals of the terpyridine two ring structure **205** were grown from the slow diffusion of benzene vapors into a saturated benzonitrile solution. Although the crystals appeared to be of good enough quality, they did not diffract strongly enough for the in-house x-ray diffractor. When a synchrotron laser was used as the radiation source, the crystals diffracted enough for data collection. The overall data quality is poor and reflections are missing due to the diffractor set-up. Partial refinement of the data reveals the complete second ring (Figure 5.23). Both endocyclic terpyridines of the first ring are located but the alkyl linkers very disordered, most likely due to disorder or the missing reflections (Figure 5.23a).

Given the poor quality of data, care must be taken when analyzing the structure. Nevertheless, several important features deserve to be mentioned. First, the empty terpyridine units are endocyclic. The second ring is nearly planar, and, in spite of the structural rigidity of the second ring, distorted into a rhomboid shape. As a result, the first ring contracts and distorts so that the planes of the coordinated terpyridines in the first ring are off-set ~8.4 Å. The coordinating terpyridines in the second ring are also offset, but only ~3.8 Å because of rigidity (Figure 5.23b). The distortion of both rings brings the two ruthenium centers to a distance ~15.7 Å, comparable to, or smaller than, the 16.5 Å separation in the bipyridine two-ring structure **200** (Figure 5.8)! In fact, the increased size of ring two induces more distortion in both rings. Looking down on the plane of ring two (Figure 5.23c) reveals two large pockets (~8 Å diameter) that can easily accommodate the coordination of a metal ion. Referring to the crystal structure of $Ru(terpy)_2$ complex **186** (*vida infra)*, the distance from the central nitrogen atom of one ligand to the farthest opposite hydrogen on the second ligand is 7.62 Å. Thus, there should be just enough space for a coordinated terpyridine ligand within each pocket, but just barely. Whether or not the pockets are large enough to accommodate a

terpyridine ligand depends on the mechanism and geometry of coordination, but the chemical evidence, so far, is contrary.

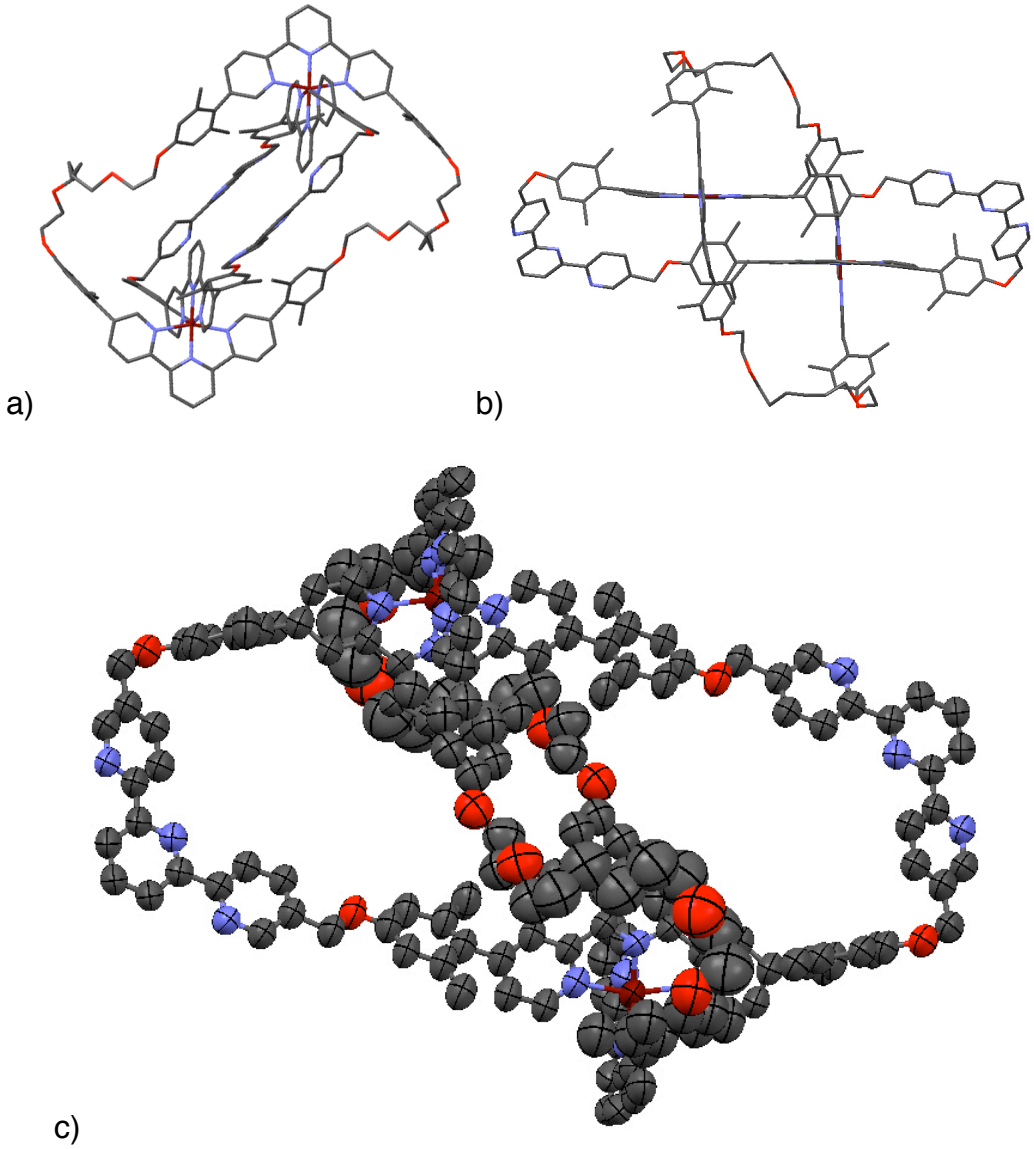

Figure 5.23 Crystal structure of terpyridine two-ring **205**, showing the a) side view, b) top view of ring one, and c) ORTEP diagram of the plane of the second ring Extremely disordered solvent and anion molecules removed for the sake of clarity.

In order to further rigidify ring two and simultaneously fully extend ring one, incorporation of 5,5"-bis-ethynyl terpyridine **204** into ring two was attempted. The reaction of the triflated threaded structure **199b** with terpyridine **204** under optimized Sonogashira conditions (Scheme 5.14) shows only consumption of starting material by

TLC and ESI-MS. In an alternate approach, the triflate **199b** reacts with trimethylsilylacetylene to give protected tetraalkynyl species **199c** (Scheme 5.15)**.** Deprotection and reaction with 5,5"-dibromoterpyridine **216** showed only the disappearance of starting material. The fact that bis-ruthenium threaded complexes **199b** and **199c** demonstrate the desired reactivity but macrocyclization with terpyridine **204** is never observed implies that ring one is unable to accommodate such a large ring two. According to the CPK models, ring one is just enough large enough to form the proposed two ring **215**. Both rings are strained and the ability to adopt the appropriate transition state geometry is unlikely.

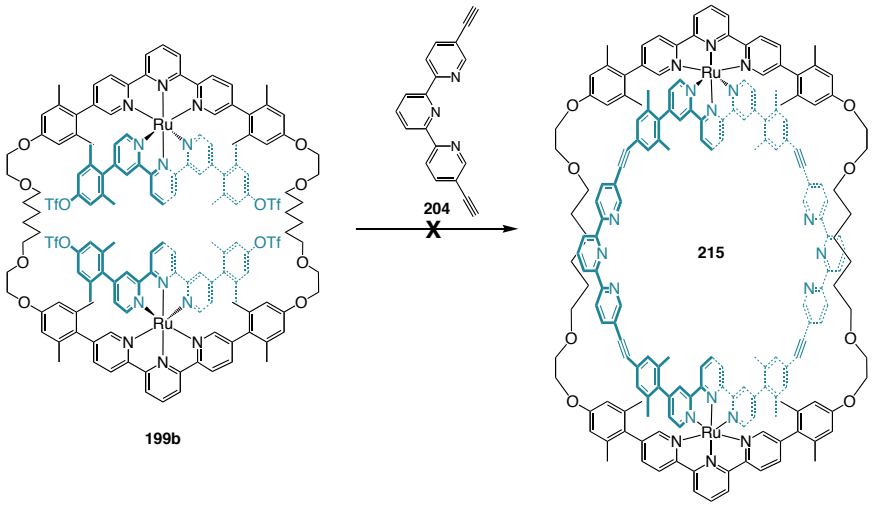

Scheme 5.14 Unsuccessful ring-closure with 5,5"-bisethynyl terpyridine **204**. Reaction conditions: $PdCl_2(dppf)$, CuI, DMF, Et_3N, 80 °C, 2 – 3 days.

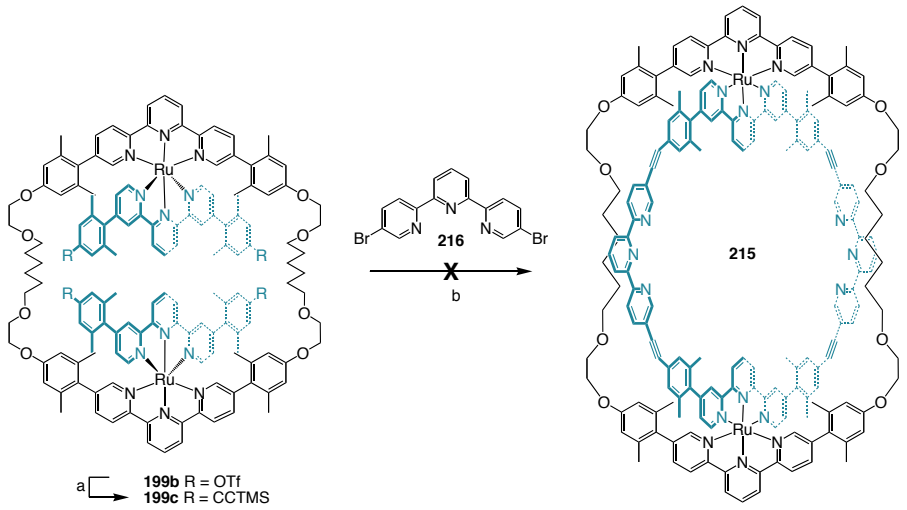

Scheme 5.15 Unsuccessful ring-closure with 5,5”-dibromo terpyridine **216**. Reaction conditions: a) (2-trimethylsilyl-ethynyl)tributylstannane, $PdCl_2$dppf, DMF, 90 %. b) $PdCl_2$(dppf), CuI, DMF, Et_3N, 80 ºC, 2 – 3 days.

Two ring **199e**, however, is more flexible and Sonagashira reaction with 5,5”-dibromoterpyridine results in the new two ring structure **217** (Scheme 5.16). To date, threading reactions involving Ru(III), and Fe(II) complexes of have been unsuccessful, and decomposition of two-ring **217** during threading is a significant problem (Scheme 5.17 and 5.18).

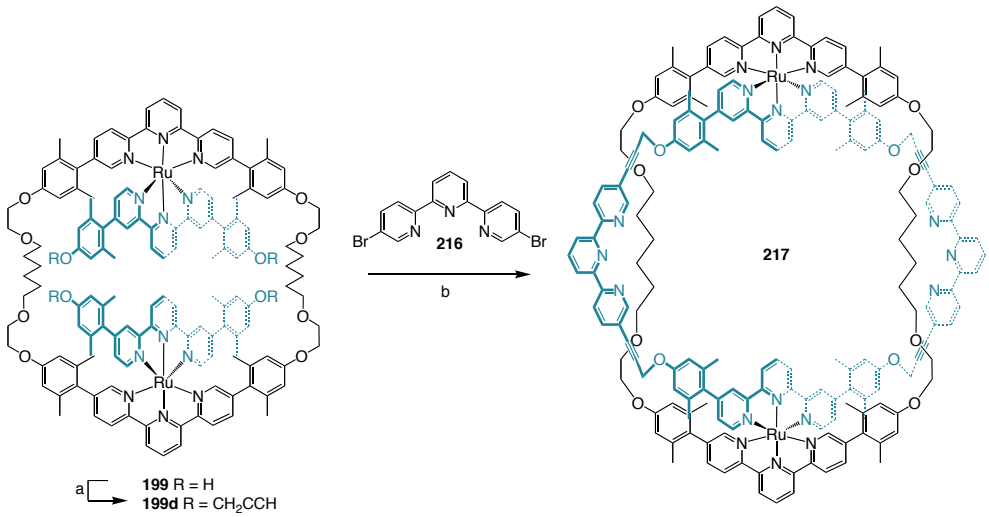

Scheme 5.16 Synthesis of terpyridine two-ring structure **217**. Reaction conditions: a) propargyl bromide, Cs_2CO_3, DMF, 80 ºC, overnight, 89%. b) **216**, $Pd(PPh_3)_4$, DMF, Et_3N, 80 ºC, 2 days, 75%.

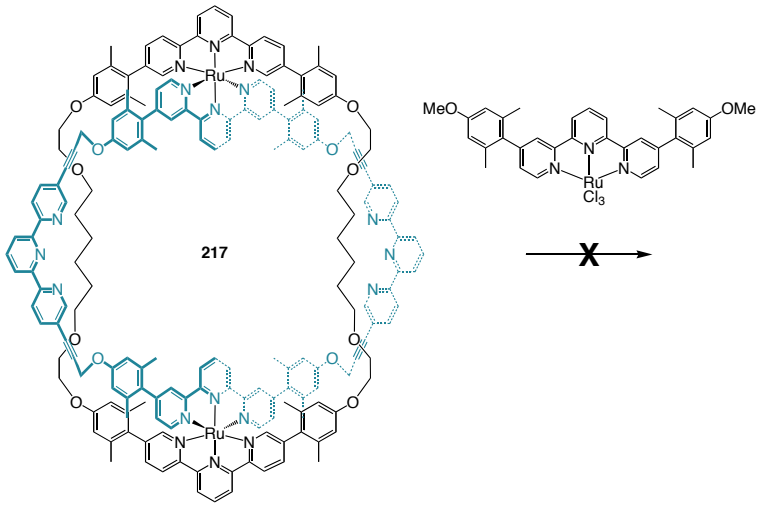

Scheme 5.17 Unsuccessful attempts to thread a third ring precursor of the Borromean link using terpyRuCl_3. Reaction conditions: a) *N*-ethylmorpholine, EtOH, 80 °C.

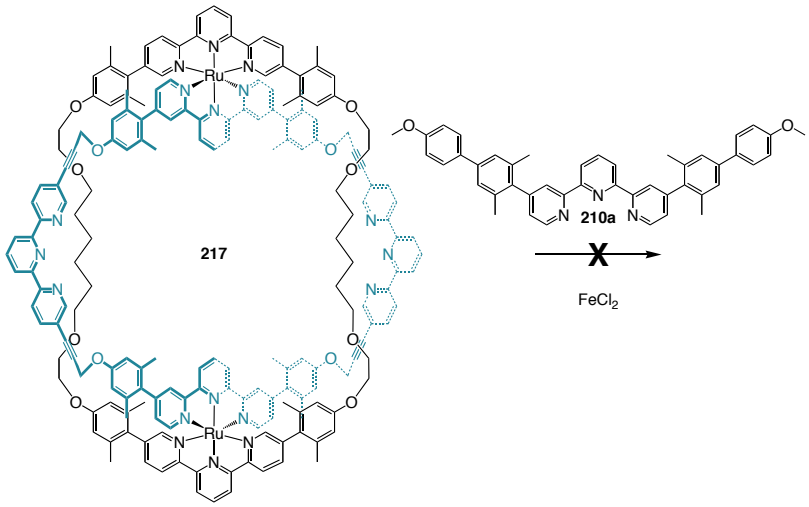

Scheme 5.18 Unsuccessful attempts to thread a third ring precursor of the Borromean link using terpyridine **210a** and $FeCl_2$. Reaction conditions: 1.) **210a** and $FeCl_2$, ACN, RT, 2 h; 2.) **199d**, ACN, 6 h, 50 °C.

Route B. Preformed heteroleptic complexes. In order to circumvent the difficulties of threading a large terpyridine ligand into the distorted pockets of the new two-ring structures **205** and **217**, an alternative approach was investigated. An appropriately functionalized, preformed heteroleptic ruthenium(II) complex could directly result in a threaded two-ring structure when used instead of an empty terpyridine cap (Scheme 5.5). Efforts to synthesize heteroleptic complexes based on

terpyridines **203** and **216**, both capable of forming two-ring complexes, were undertaken (Scheme 5.19). Reaction of **203** with the extended terpyridine Ru(II)Cl_3 complex **218** in ethylene glycol gave the heteroleptic complex **219**, where the "benzylic" bromides have been cleanly displaced by ethylene glycol. Gentler conditions, i.e., N-ethyl morpholine and ethanol also resulted in displacement. Fortunately, treatment with boron tribromide returned the benzylic bromides but cleaved the methoxy protecting groups as well. Unprotected heteroleptic complex **220** did not react with **205** to form any threaded two-ring complex, but gave only insoluble red material. Attempts to reprotect the diphenol **220** failed as the benzylic bromides are very reactive and were displaced by typically non-nucleophilic bases, i.e. imidazole or triethyl amine, used for the introduction of a variety of protecting groups.

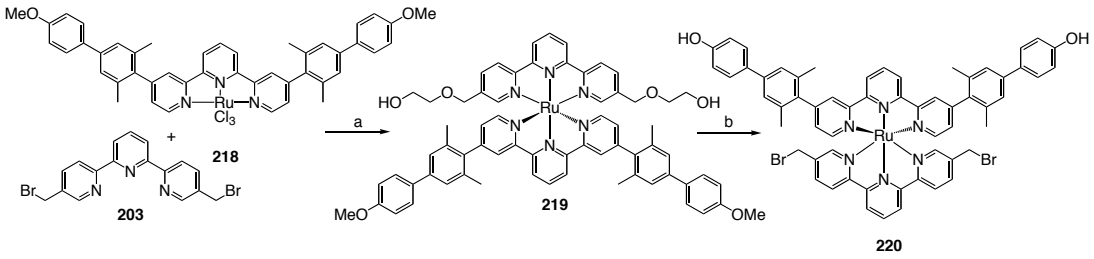

Scheme 5.19 Synthesis of bisbromomethyl-terpyridine heteroleptic precomplex **220**. Reaction conditions: a) ethylene glycol, 125 ºC, 16 h (90%); b) BBr_3, CH_2Cl_2, -78 ºC, 16 h, 94%.

Switching the solvent to benzyl alcohol gave the TIPS protected benzylic ether heteroleptic complex **222** (Scheme 5.20). Removal of the benzyl protecting groups by hydrogenation was incomplete and extended reaction times and increased pressure reduced selectivity and resulted in a mixture of products.

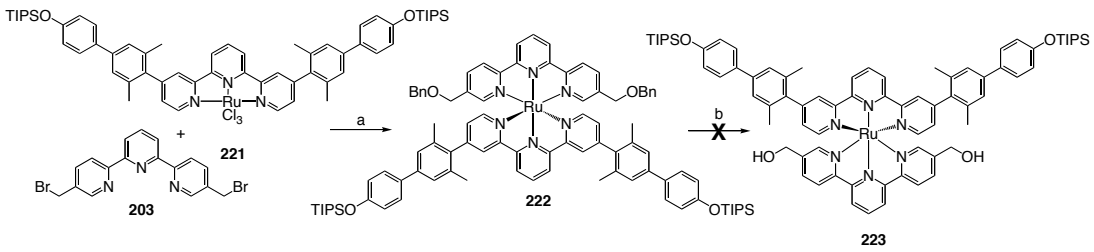

Scheme 5.20 Unsuccessful synthesis of TIPS protected heteroleptic complex. Reaction conditions: a) benzylic alcohol, 125 ºC, overnight, 87%. b) H_2, palladium on carbon, 1:1 EtOH : CH_2Cl_2, 1 atm.

To avoid the problem of protecting groups, heteroleptic complexes were prepared from 5,5"-dibromo terpyridine **216** and the corresponding terpyridine $RuCl_3$ (Scheme 5.21). Unfortunately, all macrocyclization attempts were unsuccessful (Scheme 5.22).

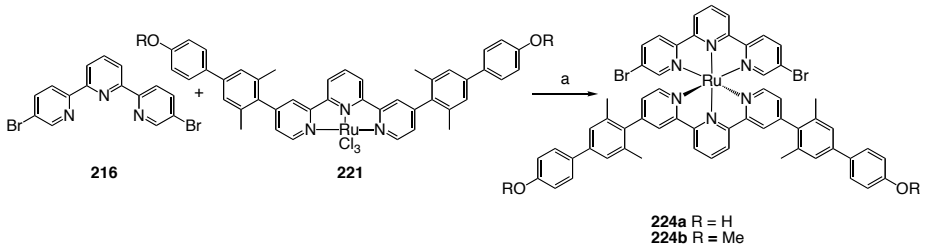

Scheme 5.21 Synthesis of 5,5"-dibromoterpyridine heteroleptic complexes. Reaction conditions: ethylene glycol, 125º, 10 h, **224a**: 53%, **224b**: 89%.

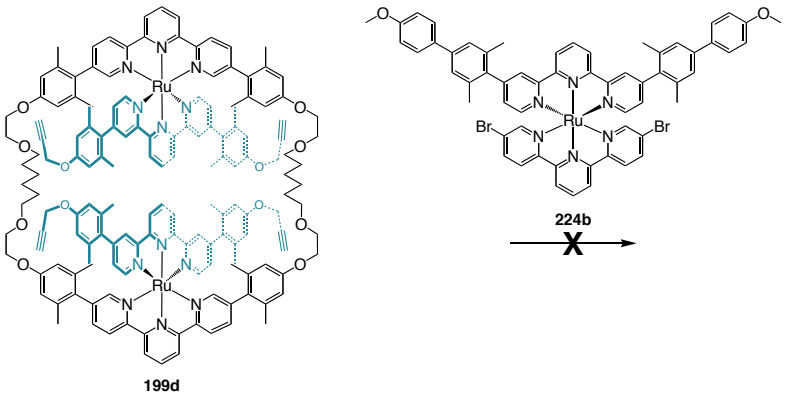

Scheme 5.22 Unsuccessful synthesis of capping of propargyl thread one ring **199d** with heteroleptic complex **224b**. Reaction conditions: $Pd(PPh_3)_4$, DMF, Et_3N, 80 ºC, 2 days.

5.2.4 Discussion and Outlook

Switching to a terdentate terpyridine "cap" was an important adjustment that endows the two-ring system with an essential features; the ability to coordinate two equivalents of metal ions. The *transoid* to *cisoid* conformational change of bipyridines upon metal coordination requires gross structural reorganization and is unfavorable. Terpyridines undergo the same configuration *transoid-cisoid* changes but the overall ligand and two-ring geometry remains constant. The partial crystal structure of two-ring **205** confirms the desired topology but reveals a severe rhombozoid distortion. As result, the height of the new terpyridine two-ring structure is smaller than Loren's bipyrdine even though the circumference is larger (64 atoms versus 54 atoms) (Figure 5.24). The free terpyridines are able to freely rotate and coordinate metal ions, but the distorted structure prevents setting of the third ring.

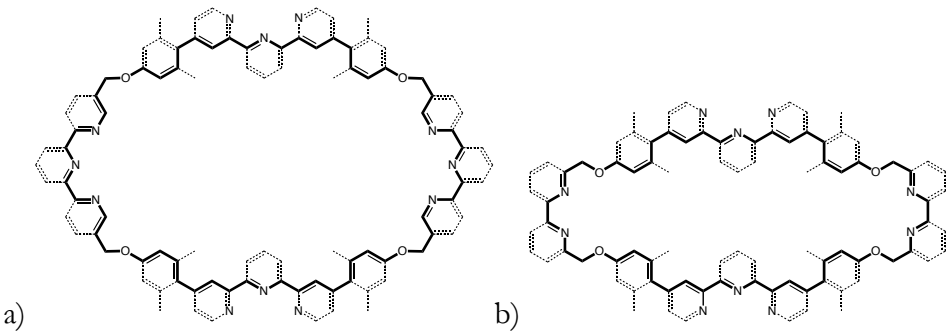

Figure 5.24 Circumference of the second ring from (a) **205**, containing a terpyridine; and from (b) **200** containing a bipyridine.

The conformational and size restrictions imposed by the first ring were examined in the solid state by x-ray crystallography (Figure 5.25 and 5.26). One can infer that, in the solid state, rather than acting as a loaded spring and preventing further compression, the first ring is flexible and adapts to constraints of the second ring. First, comparison of **214** and **199** shows the different pocket depths necessary for

coordinating a simple metal ion, **214**, versus the larger volume of a coordinated terpyridine thread, **199**. The distance from central nitrogen atom of ring one to the furthest hydrogen of the opposing terpyridine is ~7.6 Å in **199**, **200**, and **205** (Figure 5.27a). Whereas the distance from the same nitrogen atom to the opposing oxygen of the coordinated water in **214** is ~4.0 Å (Figure 5.27b). In fact, a quick survey of the N-M-X distance in Ru(II), Zn(II), and Pt(II) terpyridine complexes shows an average distance ~4.0 Å.[41] So the fact that the pockets of the new terpyridine two ring structure (~8 Å deep) can coordinate metal ions with small *trans*- ligands (Cl or OH) but cannot accommodate a large terpyridine ligand without major structural changes, thus rendering the second pocket inactive, is not unreasonable.

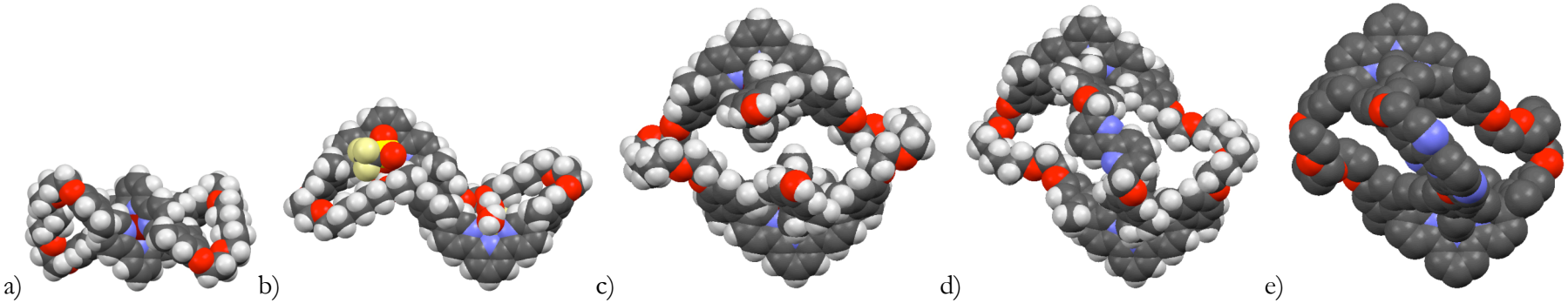

Figure 5.25 Expansion of ring one complexes a) **213**; b) **214**; c)**199**; d) **200**[38]; and e) **205**.

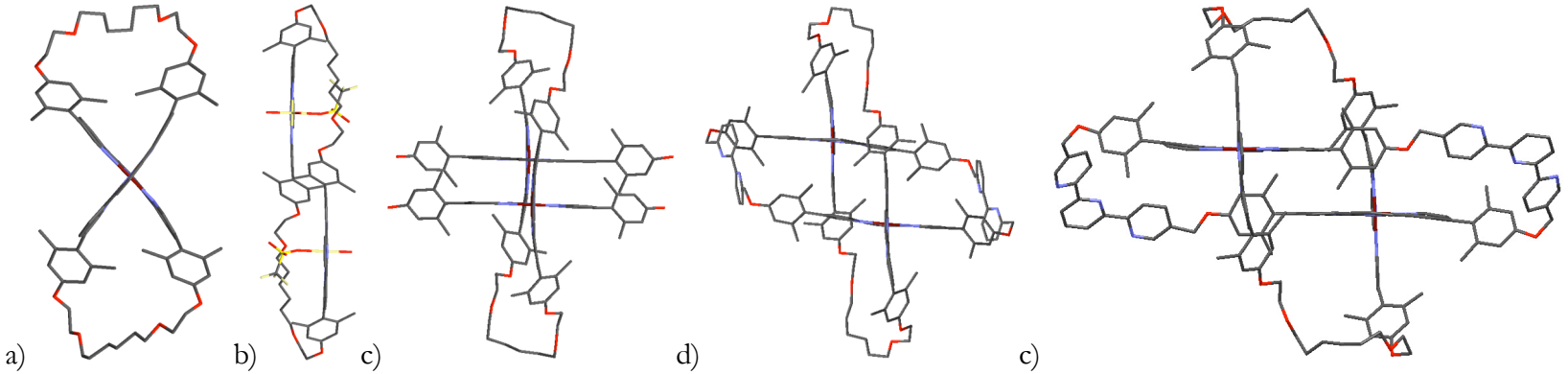

Figure 5.26 Off-set of ring one complexes a) **213**; b) **214**; c)**199**; d) **200**[38]; and e) **205**.

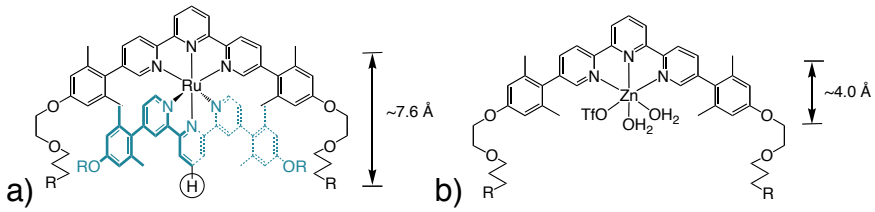

Figure 5.27 Pocket size requirements for coordinating (a) Ruterpy and (b) Zn(OTf)

Second, the first ring does not resist compression as hypothesized earlier,[38,43] but adapts itself to the size and shape of the second ring (Figure 5.25 and 5.26). In the solid state, the first ring prefers a compressed structure, **214**, but nevertheless is able to open up and accommodate the threading of the second ring, **199** and **200**. In the absence of any cap, the terminal phenols of **199** are separated by ~8.2 Å, an ideal distance for the *cis*-configuration of dimethyl-bipyridine. After capping with dimethyl-bipyridine, the second ring (Figures 5.25d and 5.26d) reorganizes to its preferred geometry and ring one adapts to the larger circumference (O-O distance ~10.7 Å). When methyl terpyridine is used as the cap, the semi-rigid second ring acquires a rhomboid shape and the first ring adapts to the new geometry (Figures 5.25e and 5.26e). Unfortunately, x-ray crystallography is only frozen snapshot and cannot address the equilibrium structure in solution. Do the free terpyridines rock in and out of the plane of the second ring? Is the rhomboid locked, or can it tilt from side to side, momentarily increasing the volume of the pockets? There is, however, a limit to the first ring. It cannot stretch far enough to accommodate the width required for bis-ethynyl terpyridine **204** or the intermediate transition state.

Switching to a terpyridine cap has also opened a second, and very promising, route to the Borromean link. Employing a heteroleptic, polypyridine complex as pre-threaded cap circumvents the difficulties of threading and presents a more convergent approach. Despite the recent interest in performing "organic" transformations on

"inorganic" compounds,[72] the effects of the coordinated metals are not always beneficial. The benzylic bromides of 5,5"-bis(bromomethyl)-terpyridine are further activated upon complexation and require regeneration and special care in choosing reaction conditions for subsequent transformations. 5,5"-Dibromoterpyridine presents a more robust scaffold and the possibility to modulate the pocket depth (Scheme 5.23). Lengthening the alkyne tail from the three carbon propynyl to butyyl or pentynyl linker would extend the pocket and the increased flexibility could be helpful as well. Alternatively, other longer, but not wider caps could be equally beneficial. The failure of thermodynamic controlled copper(I) templated threading with the extended phenanthroline cap **201**, argues for a ligand capable of making kinetically stable, preformed complex (Figure 5.27).

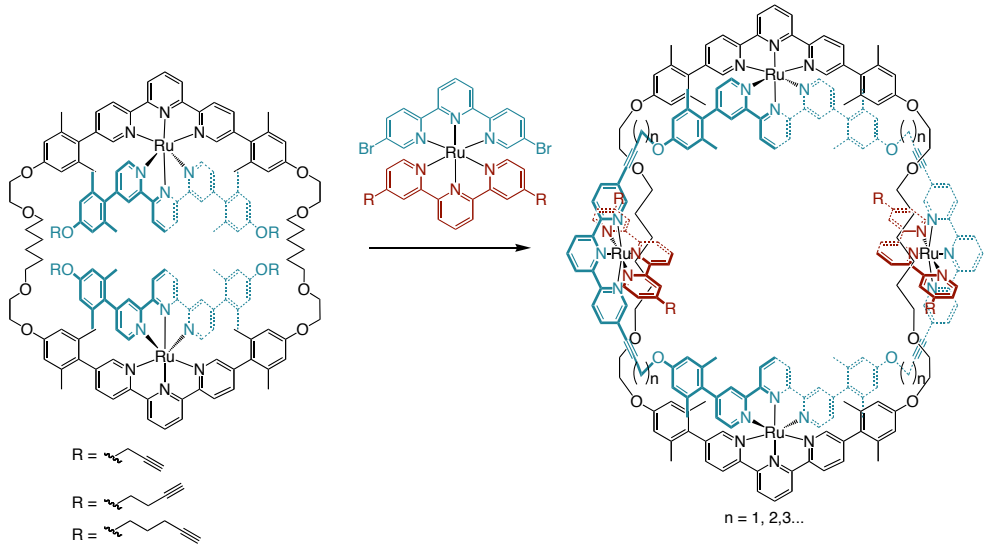

Scheme 5.23 Control of pocket depth by lengthening of the alkynyl chain.

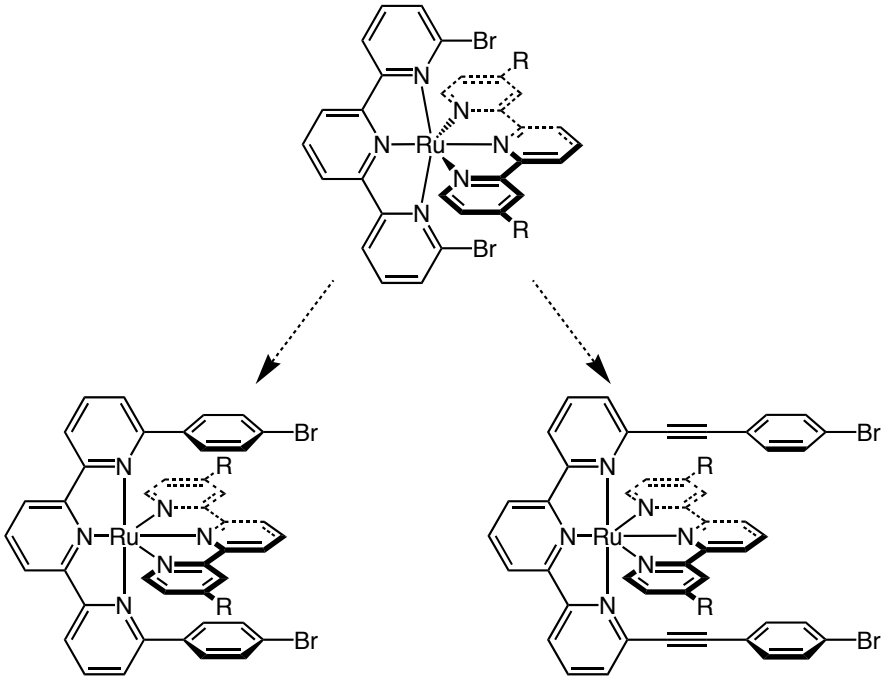

Figure 5.27 Potential heteroleptic pre-complexes with large pocket depths.

5.2.5 Conclusions

The many flashy successes of thermodynamic self-assembly are seductive, but the patience to slowly and systematically modify each component is ultimately more informative, especially in the realm of the nanometer. The ability of chemists to predict and the tertiary structure of increasingly large and complicated architectures is still maturing and a combination of solid state and solution state structural information combined with chemical reactivity is necessary to deduce the unseen equilibrium structure in solution. The synthesis of two new two-ring structures, **205** and **217**, both incorporating free terpyridine units, is an impressive leap forward in the pursuit of the directed synthesis of a Borromean link. The free terpyridines of two-ring complex **205** are each capable of coordinating different metal ions resulting in the tetra-metal complexes **207 – 209.** Solid state analysis of two-ring complexes **200** and **205**, in addition to simpler one-ring cognates **199**, **213**, and **214** shed new light upon the

flexibility of ring one and the importance in considering the possible conformations of ring two. To avoid the limitations of a strategy relying on the threading of a conformationally uncertain two-ring complex, a new approach relying on pre-formed polypyrdine complexes as building blocks was developed. The new structures and exploration of their reactivity add another dimension of understanding to the persnickety conformational constraints of a ring-in-a-ring system.

5.3 Experimental

Materials and Methods

^{1}H- and ^{13}C NMR spectra were recorded on Bruker 300, 400, 500, and 600 MHz spectrometers and were referenced to residual solvent: $CDCl_3$ (^{1}H-NMR: 7.26 ppm; and ^{13}C-NMR 77.00 ppm); CD_3CN (^{1}H-NMR: 1.94 ppm and ^{13}C-NMR: 1.39 ppm); $(CD_3)_2CO$ (^{1}H-NMR: 2.05 ppm and ^{13}C-NMR: 29.84 ppm); DMSO-d_6 (^{1}H-NMR: 2.50 ppm and ^{13}C-NMR: 39.52 ppm); or CD_2Cl_2 (^{1}H-NMR: 5.31 ppm and ^{13}C-NMR: 54.00 ppm).[73] Routine ESI-MS were recorded on a ThermoFinnigan Surveyor MSQ detector and hi-resolution MS measurements were performed by the Universität Zürich Mass Spectrum Facility. All experiments were carried out under normal atmosphere in reagent grade solvents unless otherwise noted. Commercial chemicals were used as supplied from Aldrich or Acros Chemical Co. Column chromatography was performed on neutral aluminum oxide (Brockmann III) and silica gel (230-425 mesh). Melting points are uncorrected and recorded on a Mel-Temp Laboratory Device. Dichlorotetrakis(dimethyl sulphoxide)ruthenium(II),[74] dichloro(1,5-cyclooctadien)platinum(II),[69] 5,5”-bis-(4-methoxy-2,6-dimethyl-phenyl)-2,2’:6’,2”-terpyridine, 5,5”-bis-(4-hydroxy-2,6-dimethyl-phenyl)-2,2’:6’,2”-terpyridine, 5,5”-bis-(4-methoxy-2,6-dimethyl-phenyl)-2,2’:6’,2”-terpyridine,[75] 2-trimethylsilyl-ethynyl)tributylstannane,[76] were prepared according to literature procedures.

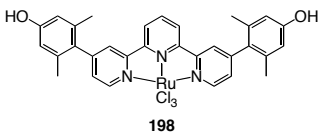

198

Ru[4,4”-bis-(4-hydroxy-2,6-dimethyl-phenyl)-2,2’:6’,2”-terpyridine]Cl_3

Prepared according to literature procedures.[38,77] Brown solid (0.496 g, 86%). ESI-MS: *m/z* for $[M + Na]^+$ calc 704.9, found 704.9.

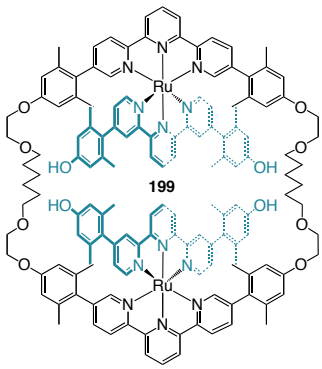

199

bis(5’5”-bis-(4-(2-(propoxy-ethoxy)-2,6-dimethyl-phenyl)-2,2’:6’,2”-terpyridine)macrocycle⊂bis-[Ru(II)[4,4”-bis-(4-hydroxy-2,6-dimethyl-phenyl)-2,2’:6’,2”-terpyridine]]$[PF_6]_4$

Prepared from modified literature procedures.[38] A 3:3:2 solution of dichloroethane : ethanol : ethylene glyclol (15 mL) containing 5,5”-bis-[2,6-dimethyl-4-(2-propoxy-ethoxy)-phenyl]-2,2’:6’,2”-terpyridine macrocycle **197** (0.100 g, 7.78×10^{-5} moles) and Ru[4,4”-bis-(4-hydroxy-2,6-dimethyl-phenyl)-2,2’:6’,2”-terpyridine}Cl_3 **198** (0.110 g, 1.63×10^{-4} moles) was heated at 125 ºC for 24 h. The reaction was cooled to room temperature and the dichloroethane and ethanol evaporated. The addition of aqueous potassium hexafluorophosphate induced precipitation of a red solid that was filtered over celite and washed with water and diethyl ether. The precipitate was dissolved with acetone into a clean flask, concentrated and diluted with methylene chloride. After drying over magnesium sulfate, filtering, and the solvent was removed to yield a red solid. The crude solid was purified by column chromatography on silica gel with

CH_3CN : H_2O : aq. KPF_6 (92: 8 : 0.8) as eluant to afford a red crystalline solid (0.166 g, 71%). Spectra matched literature values. ^{1}H NMR (500 MHz, $(CD_3)_2CO$, δ): 9.17 (4H, d, *J* = 8.4 Hz), 8.95 (4H, d, *J* = 8.4 Hz), 8.93 (4H, d, *J* = 8.4 Hz), 8.65 (2H, t, *J* = 8.4 Hz), 8.57 (4H, d, *J* = 1.2 Hz), 8.42 (2H, s), 8.27 (2H, t, *J* = 8.4 Hz), 7.99 (4H, dd, *J* = 8.4, 1.8 Hz), 7.89 (4H, d, *J* = 6 Hz), 7.60 (4H, d, *J* = 1.2 Hz), 7.23 (4H, ds, *J* = 6.0, 1.8 Hz), 6.63 (8H, s), 6.61 (8H, s), 4.07 (8, t, *J* = 4.8 Hz), 3.71 (8H, t, *J* = 4.8 Hz), 3.47 (8H, t, *J* = 6.6 Hz), 1.86 (24H, s), 1.63 (24H, s), 1.55 (8H, m), 1.37 (8H, m); ESI-MS: *m*/*z* for $[M]^{4+}$ calc. 609.2, found 609.1; *m*/*z* for $[M + PF_6^-]^{3+}$ calc. 860.6, found 860.9.

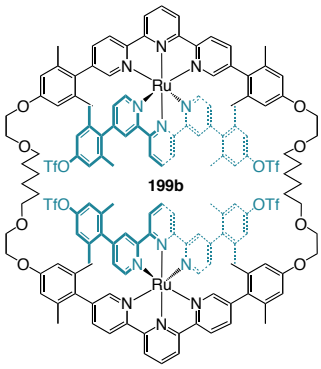

199b

[bis(5'5''-bis-(4-(2-(propoxy-ethoxy)-2,6-dimethyl-phenyl)-2,2':6',2''-terpyridine) macrocycle ⊂ bis-(Ru (4,4''-bis-(4-trifluoromethanesulfonyloxy -2,6-dimethyl-phenyl) -2,2':6',2''- terpyridine))][PF_6]$_4$

Prepared according to literature procedures.[38] Red solid (0.135 g, 85%). Spectra matched literature values. ^{1}H NMR (300 MHz, CD_3CN, δ): 8.84 (4H, d, *J* = 8.1 Hz), 8.61 (4H, d, *J* = 8.1 Hz), 8.60 (4H, d, *J* = 8.1 Hz), 8.48 (2H, t, *J* = 8.1 Hz), 8.31 (4H, d, *J* = 1.2 Hz), 8.19 (2H, t, *J* = 8.1 Hz), 7.82 (4H, dd, *J* = 8.1, 1.8 Hz), 7.57 (4H, d, *J* = 5.7 Hz), 7.19 (8H, s), 7.11 (4H, d, *J* = 1.2 Hz), 7.09 (4H, ds, *J* = 6.0, 1.8 Hz), 6.58 (8H, s), 4.01 (8, t, *J* = 4.5 Hz), 3.66 (8H, t, *J* = 4.5 Hz), 3.43 (8H, t, *J* = 6.6 Hz), 1.92 (24H, s), 1.60 (24H, s), 1.52 (8H, m), 1.32 (8H, m); ESI-MS: *m*/*z* for $[M]^{4+}$ calc. 737.7, found 737.6.

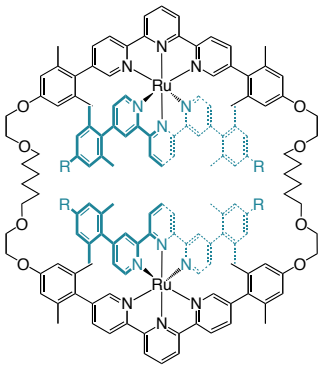

199c
R = CCTMS

[bis(5'5"-bis-(4-(2-(propoxy-ethoxy)-2,6-dimethyl-phenyl)-2,2':6',2"-terpyridine) macrocycle ⊂ bis-(Ru (4,4"-bis-(4-(2-(trimethylsilyl)ethynyl) -2,6-dimethyl-phenyl) -2,2':6',2"- terpyridine))][PF_6]$_4$

To an anhydrous solution of [bis(5'5"-bis-(4-(2-(propoxy-ethoxy)-2,6-dimethyl-phenyl)-2,2':6',2"-terpyridine) macrocycle ⊂ bis-(Ru (4,4"-bis-(4-trifluoromethanesulfonyloxy -2,6-dimethyl-phenyl) -2,2':6',2"- terpyridine))][PF_6]$_4$ **199b** (0.046 g, 1.30 × 10^{-5} moles) and $PdCl_2$(dppf) (0.008 g, 1.03 × 10^{-5} moles) in DMF (3 mL) was added (2-trimethylsilyl-ethynyl)tributylstannane[76] (0.043 g, 1.10 × 10^{-4} moles). The reaction was heated at 80 ºC under a nitrogen atmosphere for 24 h. The addition of aqueous potassium hexafluorophosphate induced precipitation of a red solid that was filtered over celite and washed with water and diethyl ether. The precipitate was dissolved with methylene chloride into a clean flask. After drying over magnesium sulfate, filtering, and the solvent was removed to yield a red solid. The crude solid was purified by column chromatography on silica gel with CH_3CN : H_2O : aq. KPF_6 (92: 8 : 0.8) as eluant to afford a red crystalline solid (0.039 g, 92%). mp = 283 ºC dec.; ^{1}H NMR (500 MHz, CD_3CN, δ): 8.82 (4H, d, *J* = 8.0 Hz), 8.62 (4H, d, *J* = 8.5 Hz), 8.61 (4H, d, *J* = 8.5 Hz), 8.46 (2H, t, *J* = 8.5 Hz), 8.28 (4H, d, *J* = 1.0 Hz), 8.17 (2H, t, *J* = 8.5 Hz), 7.83 (4H, dd, *J* = 8.5, 1.5 Hz), 7.52 (4H, d, *J* = 5.5 Hz), 7.23 (8H, s), 7.11 (4H, d, *J* = 1.5

Hz), 7.06 (4H, dd, J = 7.5, 1.5 Hz), 6.57 (8H, s), 4.01 (8, t, J = 4.5 Hz), 3.66 (8H, t, J = 4.5 Hz), 3.43 (8H, t, J = 6.5 Hz), 1.85 (24H, s), 1.60 (24H, s), 1.51 (8H, m), 1.31 (8H, m), 0.22 (36H, s); ^{13}C NMR (125 MHz, CD_3CN, δ): 159.92, 159.15, 157.53, 156.29, 156.42, 156.29, 153.80, 153.73, 151.60, 141.53, 140.70, 138.45, 136.92, 132.59, 132.37, 131.73, 129.38, 129.23, 128.59, 126.00, 125.27, 125.12, 124.65, 124.20, 114.75, 105.55, 95.73, 71.93, 69.94, 68.43, 30.46, 26.83, 20.95, 20.57, 0.03; ESI-MS: m/z for $[M]^{4+}$ calc. 689.5, found 690.3; m/z for $[M + PF_6^-]^{3+}$ calc. 967.6, found 968.3.

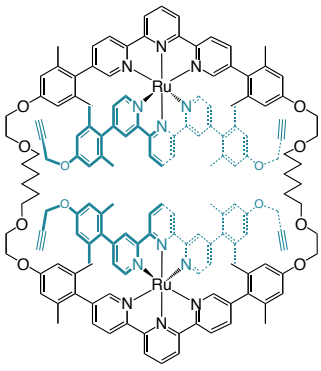

199d

[bis(5'5"-bis-(4-(2-(propoxy-ethoxy)-2,6-dimethyl-phenyl)-2,2':6',2"-terpyridine) macrocycle ⊂ bis-(Ru (4,4"-bis-(4-(ethynyloxy) -2,6-dimethyl-phenyl) -2,2':6',2"-terpyridine))][PF_6]$_4$

To an anhydrous solution of [bis(5'5"-bis-(4-(2-(propoxy-ethoxy)-2,6-dimethyl-phenyl)-2,2':6',2"-terpyridine) macrocycle ⊂ bis-(Ru (4,4"-bis-(4-hydroxy-2,6-dimethyl-phenyl) -2,2':6',2"- terpyridine))][PF_6]$_4$ **199** (0.061 g, 2.03 × 10^{-5} moles) and cesium carbonate (0.102 g, 1.62 × 10^{-4} moles) in DMF (3 mL) was added propargyl bromide (0.015 g, 1.22 × 10^{-4} moles). The reaction was stirred under a nitrogen atmosphere at room temperature for 12 h. The addition of aqueous potassium hexafluorophosphate induced precipitation of a red solid that was filtered over celite and washed with water and diethyl ether. The precipitate was dissolved with methylene chloride and acetonitrile into a clean flask. After drying over magnesium sulfate, filtering, and the

solvent was removed to yield a red solid. The crude solid was purified by column chromatography on silica gel with CH_3CN : H_2O : aq. KPF_6 (95: 5 : 0.5) as eluant to afford a red solid (0.057 g, 89%). mp = 237 – 243 ºC; ^{1}H NMR (400 MHz, CD_3CN, δ): 8.82 (4H, d, *J* = 8.0 Hz), 8.62 (4H, d, *J* = 8.4 Hz), 8.60 (4H, d, *J* = 8.4 Hz), 8.45 (2H, t, *J* = 8.4 Hz), 8.29 (4H, d, *J* = 1.2 Hz), 8.17 (2H, t, *J* = 8.4 Hz), 7.82 (4H, dd, *J* = 8.4, 1.2 Hz), 7.52 (4H, d, *J* = 6.0 Hz), 7.23 (8H, s), 7.17 (4H, d, *J* = 1.2 Hz), 7.10 (4H, dd, *J* = 7.8, 1.6 Hz), 6.64 (8H, s), 4.35 (8H, s), 4.01 (8H, t, *J* = 4.4 Hz), 3.66 (8H, t, *J* = 4.4 Hz), 3.43 (8H, t, *J* = 6.6 Hz), 2.24 (4H, t, *J* = 2.0 Hz), 1.83 (24H, s), 1.57 (24H, s), 1.50 (8H, m), 1.32 (8H, m); ^{1}C NMR (100 MHz, CD_3CN, δ): d): 159.02, 158.34, 157.46, 156.88, 155.60, 153.01, 152.50, 152.10, 140.63, 140.11, 136.97, 136.51, 136.28, 136.05, 129.44, 128.51, 126.02, 125.87, 124.24, 124.11, 123.82, 114.73, 114.55, 113.81, 79.82, 77.06, 71.90, 69.05, 67.85, 55.78, 29.57, 25.85, 19.79, 19.73. ESI-MS: *m*/*z* for $[M]^{4+}$ calc 647.2, found 647.2; *m*/*z* for $[M + PF_6]^{4+}$ calc 911.1, found 911.3.

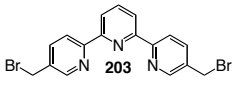

203

5,5”-bis(bromomethyl)-[2,2’:6’:2”]terpyridine

Prepared from modified literature procedures.[78] A carbon tetrachloride solution (40 mL) containing 5,5”-bis-methyl-[2,2’:6’:2”]terpyridine (0.500 g, 1.916×10^{-3} moles), *N*-bromosuccinimide (1.705 g, 9.579×10^{-3} moles), and catalytic benzoyl peroxide was placed in a hot oil bath at 80 ºC and heated for 3 h. The hot solution was filtered and the precipitate washed with carbon tetrachloride. Upon cooling the filtrate, a white precipitate forms and was collected, dissolved in methylene chloride, and washed with aqueous sodium thiolsulfate. The organic layers were combined, dried over magnesium sulfate, filtered and the solvent removed to give a white solid (0.413 g, 51%). Spectra matched the literature values. ^{1}H NMR (600 MHz, $CDCl_3$, δ): 8.71 (2H, d, *J* = 2.8 Hz),

8.60 (2H, d, J = 8.4 Hz), 8.46 (2H, d, J = 7.8 Hz), 7.96 (1H, t, J = 7.8 Hz), 7.90 (2H, dd, J = 8.4, 2.4 Hz), 4.56 (4H, s); ESI-MS: m/z for $[M+Na^+]^+$ calc. 442.1, found 442.1.

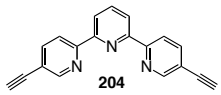

204

5,5''-bis(ethynyl)-[2,2':6':2'']terpyridine

Prepared from modified literature procedures.[79] 2-Bromo-5-(trimethylsilylethynyl)pyridine (1.430 g, 5.63×10^{-3} moles) was dissolved in THF (100 mL) and cooled to -78°C. To this was added n-BuLi (3.67 mL of a 1.6 M sol in hexanes) and the solution stirred for 10 min. A THF solution (50 mL) of $ZnCl_2$ (0.823 g, 6.05×10^{-3} moles) was cannulated into the reaction flask. The solution was stirred, allowed to warm to room temperature, and then cannulated into a THF solution (50 mL) of 2,6-dibromopyridine (0.423 g, 1.79×10^{-3} moles) and $Pd(PPh_3)_4$ (0.206 g, 1.79×10^{-4} moles). The resulting solution was heated at reflux 4 h. After cooling to room temperature, the solvent was removed and the solid was dissolved in diethyl ether and extracted with a saturated aqueous EDTA solution basified with sodium bicarbonate. The organic layer was separated, dried over magnesium sulfate, filtered, and evaporated to give an off-white solid. The crude solid was purified by column chromatography on alumina oxide with hexanes : methylene chloride (9 : 1) as eluant to afford a white solid (0.502 g 80%). Spectra matched the literature values. ^{1}H NMR (300 MHz, $CDCl_3$, δ): 8.80 (2H, d, J = 1.8 Hz), 8.59 (2H, d, J = 8.4 Hz), 8.47 (2H, d, J = 7.8 Hz), 7.97 (1H, t, J = 7.8 Hz), 7.93 (2H, dd, J = 8.1, 2.1 Hz), 3.31 (2H, s). ESI-MS: m/z for $[M + Na^+]^+$ calc. 304.3, found 304.3.

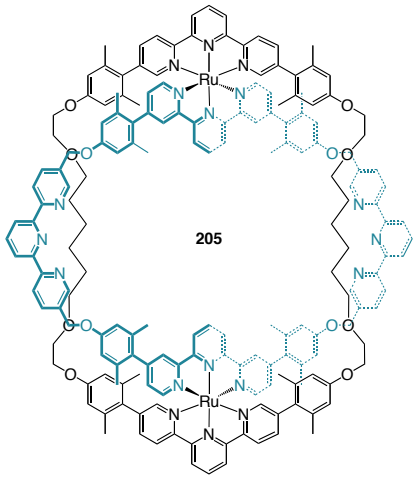

[bis-(5'5"-bis-(4-(2-(propoxy-ethoxy)-2,6-dimethyl-phenyl)-2,2':6',2"-terpyridine) macrocycle] ⊃ bis-(Ru(II)(*N,N'',N'''*-4,4"-bis-(4-oxy-2,6-dimethyl-phenyl)-2,2':6',2"-terpyridine-5,5"-bis(methyl)-2,2':6',2"-terpyridine macrocycle)][PF_6]$_4$

Cesium carbonate (0.096 g, 2.96 × 10^{-5} moles) was added to an anhydrous acetonitrile solution (40 ml) of bis Ru(II) tetraphenol macrocycle **199** (0.089 g, 2.96 × 10^{-5} moles), 5,5"-bis(bromomethyl)-2,2':6',2"-terpyridine (0.026 g, 6.21 × 10^{-5} moles), and tri(ethylene glycol) dimethyl ether (0.100 mL). The contents were heated at reflux for 48 h then cooled to room temperature. The solution was concentrated and aqueous potassium hexafluorophosphate was added until a deep red precipitate formed. The precipitate was filtered over celite, washed with water and diethyl ether and dissolved into a clean flask with methylene chloride and acetonitrile. The red solution was dried over magnesium sulfate, filtered and solvent evaporated to yield a red solid. The crude solid was purified by column chromatography on silica gel with CH_3CN : H_2O : aqueous KPF_6 92 : 8 : 0.08 as the eluant to yield a red crystalline solid (0.063 g, 60%). m.p. > 350 °C. ^{1}H NMR (600 MHz, (CD_3CN, δ): 8.82 (4H, d, *J* = 7.8 Hz), 8.80 (4H, d, *J* = 1.8 Hz), 8.62 (4H, d, *J* = 9.0 Hz), 8.60 (4H, d, *J* = 8.4 Hz), 8.54 (4H, d, *J* = 8.4 Hz), 8.47 (2H, t, *J* = 8.4 Hz), 8.47 (4H, d, *J* = 7.8 Hz), 8.22 (4H, d, *J* = 1.2 Hz), 8.11 (2H, t, *J* = 7.8 Hz), 8.05 (2H, t, *J* = 7.8 Hz), 7.94 (4H, dd, *J* = 8.4, 2.4 Hz), 7.80 (4H, dd, *J* = 8.4,

1.8 Hz), 7.49 (4H, d, J = 6.0 Hz), 7.11 (4H, d, J = 1.8 Hz), 7.08 (4H, dd, J = 6.0, 1.8 Hz), 6.83 (8H, s), 6.56 (8H, s), 5.31 (8H, s), 3.98 (8H, t, J = 4.8 Hz), 3.65 (8H, t, J = 4.8 Hz), 3.44 (8H, t, J = 6.6 Hz), 1.86 (24H, s), 1.59 (24H, s), 1.53 (8H, m), 1.34 (8H, m); ^{13}C NMR (125 MHz, CD_3CN, δ): 159.88, 159.17, 158.99, 157.57, 156.68, 156.48, 156.35, 156.30, 153.71, 153.55, 152.46, 149.74, 141.45, 140.74, 139.43, 138.48, 138.11, 137.11, 136.54, 134.72, 131.19, 129.89, 128.64, 126.92, 125.23, 124.94, 124.63, 122.09, 121.72, 115.28, 114.74, 71.91, 69.86, 68.45, 67.63, 30.97, 30.40, 26.77, 20.94, 20.90. ESI-MS: m/z for $[M]^{4+}$calc. 737.9, found 738.1; m/z for $[M + PF_6]^{3+}$ calc. 1032.2, found 1032.3.

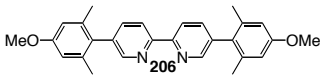

5,5'-bis-(4-methoxy-2,6-dimethyl-phenyl)-2,2'-bipyridine

Prepared according to literature procedures.[43,75] White crystalline solid (0.775 g 50%). Spectra matched the literature values. ^{1}H NMR (300 MHz, $CDCl_3$, δ): 8.48 (2H, d, J = 2.4 Hz), 8.47 (2 H, d, J = 7.8 Hz), 7.64 (2H, dd, J = 7.8, 2.4 Hz), 6.70 (4H, s), 3.82 (6H, s), 2.06 (12H, s); ESI-MS: m/z for $[M + H^+]^+$ calc. 425.2, found 425.3.

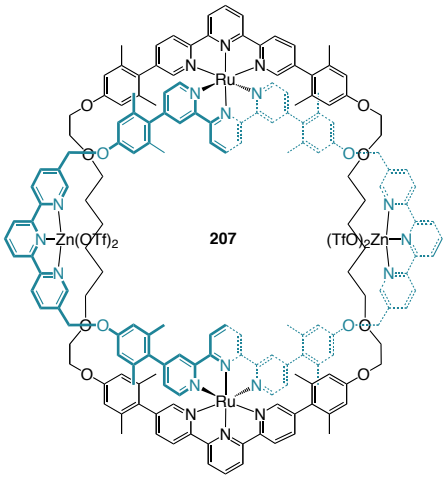

[bis-(5'5"-bis-(4-(2-(propoxy-ethoxy)-2,6-dimethyl-phenyl)-2,2':6',2"-terpyridine) macrocycle] ⊃ bis-(Ru(II)(*N,N'',N'''*-4,4"-bis-(4-oxy-2,6-dimethyl-phenyl)-2,2':6',2"-terpyridine-5,5"-bis(methyl)-2,2':6',2"-terpyridine macrocycle) ⊃ bis-Zn(OTf)$_2$][PF$_6$]$_4$

Prepared using an analogous procedure.[67] A solution of zinc triflate (0.003 g, 8.50 × 10^{-6} moles) in acetonitrile (0.5 mL) was added drop wise to a solution of two ring complex **205** (0.015 g, 4.25 × 10^{-6} moles) in acetonitrile (0.5 mL). The red solution was stirred for 3 h at room temperature before removing the solvent to yield a red crystalline solid (0.017 g, 94 %). m.p. > 350 °C ^{1}H NMR (600 MHz, (CD_3CN, δ): 8.86 (4H, d, *J* = 7.8 Hz), 8.85 (4H, d, *J* = 1.8 Hz), 8.7 - 8.4 (22H, series of m), 8.25 (4H, d, *J* = 1.2 Hz), 8.19 (2H, t, *J* = 7.8 Hz), 8.18 (2H, t, *J* = 7.8 Hz), 7.80 (4H, dd, *J* = 8.4, 1.8 Hz), 7.52 (4H, d, *J* = 6.0 Hz), 7.14 (4H, d, *J* = 1.8 Hz), 7.13 (4H, dd, *J* = 6.0, 1.8 Hz), 6.88 (6H, s), 6.58 (10H, s), 5.39 (8H, s), 3.99 (8H, t, *J* = 4.8 Hz), 3.65 (8H, t, *J* = 4.8 Hz), 3.43 (8H, t, *J* = 6.6 Hz), 1.92 (24H, s), 1.62 (24H, s), 1.54 (8H, m), 1.34 (8H, m); ^{13}C NMR (125 MHz, CD_3CN, δ): 161.52, 160.01, 159.48, 157.46, 157.00, 156.36, 156.29, 155.27, 154.21, 153.26, 151.64, 150.35, 145.29, 142.22, 139.40, 138.48, 138.1, 137.22, 135.37, 134.79, 130.77, 128.90, 128.64, 127.53, 126.12, 124.84, 124.13, 122.26, 121.83, 115.20, 114.94, 72.58, 69.82, 68.55, 66.93, 31.18, 30.68, 26.02, 20.96, 20.9. ESI-

MS: m/z for [M - 4OTf + $3H_2O$]$^{8+}$ calc. 392.04, found 392.2; m/z for [M - 3OTf]$^{7+}$ calc. 464.0, found 464.4; m/z for [M - 2OTf]$^{6+}$ calc. 568.1, found 563.2.

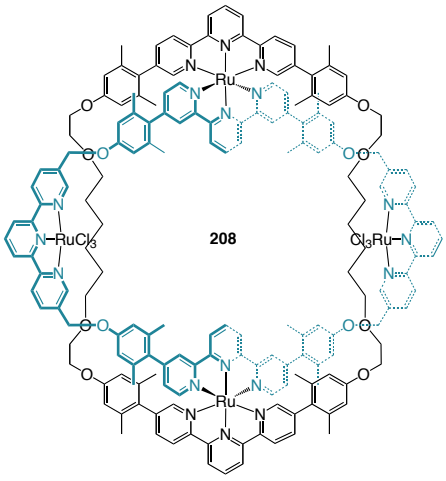

[bis-(5'5"-bis-(4-(2-(propoxy-ethoxy)-2,6-dimethyl-phenyl)-2,2':6',2"-terpyridine) macrocycle] ⊃ bis-(Ru(II)(*N,N",N"'*-4,4"-bis-(4-oxy-2,6-dimethyl-phenyl)-2,2':6',2"-terpyridine-5,5"-bis(methyl)-2,2':6',2"-terpyridine macrocycle) ⊃ bis-$RuCl_3$][PF_6]$_4$

Ruthenium(III) trichloride hydrate (0.005 g, 2.04 × 10^{-5} moles) and two ring complex **205** (0.018 g, 5.10 × 10^{-6} moles) were combined in a 2:1 solution (1.5 mL) of ethanol : dichloroethane. The red solution was heated for 16 h at reflux before reducing the solvent and adding aqueous potassium hexafluorophosphate until a dark red-brown precipitate formed. The precipitate was filtered over celite, washed with water and diethyl ether and dissolved into a clean flask with acetonitrile. The brown-red solution was dried over magnesium sulfate, filtered and solvent evaporated to yield a brown solid (0.020 g, 99%). m.p. > 350 °C; ESI-MS: m/z for [M - 4Cl + 4ACN]$^{6+}$ calc. 564.8, found 565.3; m/z for [M - 3Cl + 3ACN]$^{5+}$ calc. 676.6, found 676.6; m/z for [M]$^{4+}$ calc. 841.2, found 840.6.

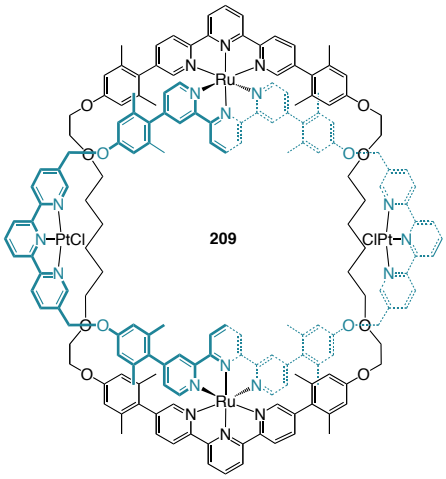

[bis-(5'5"-bis-(4-(2-(propoxy-ethoxy)-2,6-dimethyl-phenyl)-2,2':6',2"-terpyridine) macrocycle] ⊃ bis-(Ru(II)(*N,N'',N'''*-4,4"-bis-(4-oxy-2,6-dimethyl-phenyl)-2,2':6',2"-terpyridine-5,5"-bis(methyl)-2,2':6',2"-terpyridine macrocycle) ⊃ bis-PtCl][PF_6]$_6$

Prepared using an analogous procedure.[69] Solid silver(I)tertrafluoroborate (0.003 g, 1.59 × 10^{-5} moles) was added to solution of dichloro (1,5-cyclooctadiene)-platinum(II)[80] (0.003 g, 7.55 × 10^{-6} moles) in acetone (0.250 mL) and the solution filtered through a celite pad into a solution of two ring complex **205** (0.013 g, 3.68 × 10^{-6} moles) in acetonitrile (1.0 mL). The red solution was stirred for 30 min at room temperature before adding a 10% solution of hydrochloric acid to cause a red precipitate. The precipitate was filtered over celite, washed with water and diethyl ether and dissolved into a clean flask with acetonitrile. Aqueous potassium hexafluorophosphate was added until a deep red precipitate formed and the precipitate was filtered over celite, washed with water and diethyl ether and dissolved into a clean flask with acetonitrile. The red solution was dried over magnesium sulfate, filtered and solvent evaporated to yield a red solid (0.011 g, 70 %). m.p. 320 °C dec.; ^{1}H NMR (600 MHz, (CD_3CN, δ): 9.08 (4H, d, *J* = 1.8 Hz), 8.62 (4H, d, *J* = 6.6 Hz), 8.62 (4H, d, *J* = 8.4 Hz), 8.5-8.4 (8H, m), 8.35-8.25 (8H, m), 8.19 (2H, t, *J* = 7.8 Hz), 7.80 (4H, dd, *J* = 8.4, 1.8 Hz), 7.52 (4H,

d, J = 6.0 Hz), 7.16 (4H, d, J = 1.8 Hz), 7.14 (4H, dd, J = 6.0, 1.8 Hz), 6.86 (6H, s), 6.60 (10H, s), 5.30 (8H, s), 4.00 (8H, t, J = 4.8 Hz), 3.66 (8H, t, J = 4.8 Hz), 3.44 (8H, t, J = 6.6 Hz), 1.93 (24H, s), 1.61 (24H, s), 1.53 (8H, m), 1.33 (8H, m); ^{13}C NMR (125 MHz, (CD_3CN, δ): 162.34, 160.73, 159.02, 157.89, 156.89, 156.05, 155.97, 155.23, 154.31, 154.17, 151.02, 150.47, 145.68, 142.04, 140.19, 138.35, 138.12, 137.68, 135.49, 134.93, 131.21, 128.23, 128.01, 127.26, 126.24, 124.43, 124.04, 122.21, 121.90, 116.35, 115.27, 71.89, 70.66, 68.38, 66.23, 32.04, 30.73, 26.54, 21.01, 20.98. ESI-MS: m/z for $[M]^{6+}$ calc. 568.8, found 569.2.

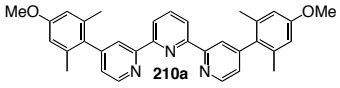

210a

4,4''-bis-(4-methoxy-2,6-dimethyl-phenyl)-2,2':6',2''-terpyridine

2-iodo-4-(4-methoxy-2,6-dimethyl-phenyl) pyridine **B3** (2.00 g, 5.90×10^{-3} moles) was dissolved in THF (75 mL) and cooled to -78°C. To this was added n-BuLi (2.71 mL of a 2.25 M sol in hexanes) and the solution stirred for 10 min. A THF solution (40 mL) of $ZnCl_2$ (0.829 g, 6.10×10^{-3} moles) was cannulated into the reaction flask. The solution was stirred, allowed to warm to room temperature, and then cannulated into a THF solution of 2,6-dibromopyridine (0.464 g, 1.97×10^{-3} moles)) and $Pd(PPh_3)_4$ (0.228 g, 1.97×10^{-4} moles). The resulting solution was heated at reflux overnight. After cooling to room temperature, a tan precipitate was filtered and washed with cold THF before drying. The precipitate was dissolved in methylene chloride and extracted with a saturated aqueous EDTA solution basified with sodium bicarbonate. The organic layer was separated, dried over magnesium sulfate, filtered, and evaporated to give an off-white solid (0.700 g, 71%). Spectra matched literature values.[75] ^{1}H NMR (600 MHz, $CDCl_3$, δ): 8.73 (2H, d, J = 4.8 Hz), 8.56 (2H, d, J = 7.8 Hz), 8.33 (2H, d, J

= 1.2 Hz), 8.00 (1H, t, J = 7.8 Hz), 7.11 (2H, dd, J = 4.8, 1.2 Hz), 6.69 (4H, s), 3.82 (6H, s), 2.05 (12H, s); ESI-MS: m/z for $[M + Na^+]^+$ calc. 524.2, found 524.3.

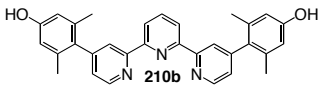

4,4''-bis-(4-hydroxy-2,6-dimethyl-phenyl)-2,2':6',2''-terpyridine

Prepared according to literature procedures.[38] Tan solid (0.410 g, 99%). Spectra matched literature values. ^{1}H NMR (600 MHz, DMSO-d_6, δ): 9.38 (2H, s), 8.74 (2H, d, J = 4.8 Hz), 8.48 (2H, d, J = 4.8 Hz), 8.21 (2H, d, J = 1.2 Hz), 8.14 (1H, t, J = 7.8 Hz), 7.27 (2H, dd, J = 4.8, 1.2 Hz), 6.55 (4H, s), 1.94 (12H, s); ESI-MS: m/z for $[M + Na^+]^+$ calc. 596.2, found 596.2.

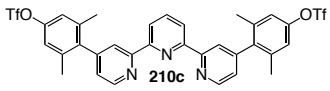

4,4''-bis-(4-trifluoromethanesulfonyloxy-2,6-dimethyl-phenyl)-2,2':6',2''-terpyridine

Prepared according to literature procedures.[43] Purified on Aluminum oxide with chloroform as eluant to give a white solid (0.452 g, 80%). Spectra matched literature values. ^{1}H NMR (600 MHz, $CDCl_3$, δ): 8.79 (2H, d, J = 4.8 Hz), 8.56 (2H, d, J = 7.8 Hz), 8.29 (2H, d, J = 1.2 Hz), 8.02 (1H, t, J = 7.8 Hz), 7.11 (2H, dd, J = 4.8, 1.2 Hz), 6.55 (4H, s), 2.10 (12H, s); ESI-MS: m/z for $[M + Na^+]^+$ calc. 794.1, found 794.1.

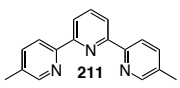

5,5''-dimethyl-2,2':6':2''-terpyridine

Prepared according to literature procedures.[78] White solid (2.200 g, 59%). Spectra matched literature values. ^{1}H NMR (300 MHz, $CDCl_3$, δ): 8.53 (2H, dd, J = 1.5, 0.9 Hz), 8.50 (2H, d, J = 7.8 Hz), 8.39 (2H, d, J = 7.8 Hz), 8.14 (1H, t, J = 7.8 Hz), 7.27 (2H, dd, J = 8.1, 1.2 Hz), 2.42 (6H, s); ESI-MS: m/z for $[M]^+$ calc. 261.1, found 261.1.

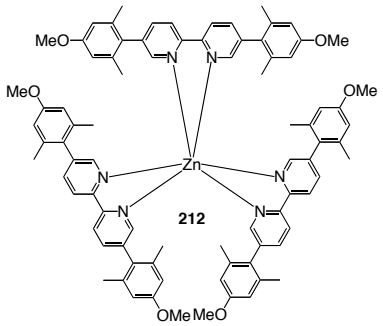

[Zn(5,5'-bis-(4-methoxy-2,6-dimethyl-phenyl)-2,2'-bipyridine)$_3$][PF$_6$]$_2$

Zinc triflate (0.014 g, 3.93 × 10^{-5} moles) in ethanol (5.0 mL) was added drop wise to 5,5'-bis-(4-methoxy-2,6-dimethyl-phenyl)-2,2'-bipyridine (0.050 g, 1.18 × 10^{-4} moles) in methylene chloride (5.0 mL) and stirred for 5 h at room temperature. The solvent was removed and the white solid dissolved in acetonitrile and aqueous potassium hexafluorophosphate was added until a white precipitate formed. The precipitate was filtered over celite, washed with water and diethyl ether and dissolved into a clean flask with methylene chloride and acetonitrile. The colorless solution was dried over magnesium sulfate, filtered and solvent evaporated to yield a white solid (0.044 g, 69%). mp = 340 ºC dec.; ^{1}H NMR (600 MHz, $CDCl_3$, δ): 8.56 (6H, d, J = 7.8 Hz), 8.04 (6H, dd, J = 8.4, 2.1 Hz), 7.64 (6H, d, J = 7.8, 2.4 Hz), 6.66 (6H, s), 6.64 (6H, s), 3.77 (18H, s), 1.66 (18H, s), 1.60 (18H, s). ^{13}C NMR (125 MHz, CDCl3, δ): 160.75, 156.32, 149.96, 138.56, 138.70, 137.14, 130.73, 121.52, 114.46, 114.52, 55.86, 21.03, 20.72. ESI-MS: m/z for $[M]^{2+}$ calc. 668.3, found 668.3.

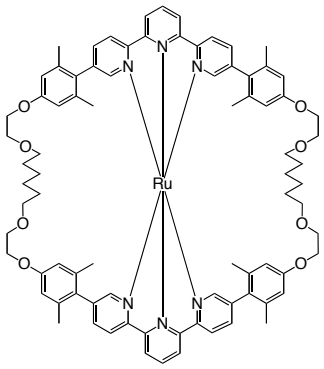

213

[Ru(5'5"-bis-(4-(2-(propoxy-ethoxy)-2,6-dimethyl-phenyl)-2,2':6',2"-terpyridine) macrocycle)][PF_6]$_2$

A 10:4:1 solution of ethylene glyclol: dichloroethane: ethanol (15 mL) containing 5,5"-bis-[2,6-dimethyl-4-(2-propoxy-ethoxy)-phenyl]-2,2':6',2"-terpyridine macrocycle **197** (0.024 g, 1.87 × 10^{-5} moles) and dichlorotetrakis(dimethyl sulphoxide)ruthenium(II) (0.005 g, 9.33 × 10^{-6} moles) was heated at 125 ºC for 16 h. The reaction was cooled to room temperature and the dichloroethane and ethanol evaporated. The addition of aqueous potassium hexafluorophosphate induced precipitation of a red solid that was filtered over celite and washed with water and diethyl ether. The precipitate was dissolved with acetone into a clean flask, concentrated and diluted with methylene chloride. After drying over magnesium sulfate, filtering, and the solvent was removed to yield a red crystalline solid (0.030 g, 96%). mp 295 ºC dec.; ^{1}H NMR (600 MHz, CD_3CN, δ): 8.70 (4H, d, *J* = 8.4 Hz), 8.52 (4H, dd, *J* = 8.4, 0.6 Hz), 8.32 (2H, t, *J* = 8.4 Hz), 7.72 (4H, dd, *J* = 8.4, 1.2 Hz), 7.33 (4H, dd, *J* = 1.8, 0.6 Hz), 6.86 (4H, bs), 6.60 (8H, bs), 4.44 (4H, m), 4.04 (4H, m), 3.59 (8H, m), 3.30 (4H, m), 3.13 (4H, m), 1.94 (12H, s), 1.26 (8H, m), 1.22 (12H, s), 1.08 (8H, m); ^{13}C NMR (125 MHz, CD_3CN, δ): 160.27, 157.29, 156.37, 153.94, 141.59, 141.31, 137.95, 137.33, 128.13, 125.02, 124.66, 117.88, 114.83, 73.28, 72.75, 68.26, 31.29, 28.04, 22.00, 20.86; ESI-MS: m/z for $[M]^{2+}$ calc. 694.3, found 694.2.

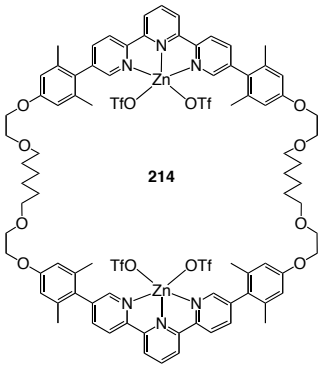

5'5"-bis-(4-(2-(propoxy-ethoxy)-2,6-dimethyl-phenyl)-2,2':6',2"-terpyridine) macrocycle ⊃ $Zn(OTf)_2$

Zinc triflate (0.014 g, 3.89×10^{-5} moles) in ethanol (5.0 mL) was added drop wise to 5,5"-bis-[2,6-dimethyl-4-(2-propoxy-ethoxy)-phenyl]-2,2':6',2"-terpyridine macrocycle **197** (0.025 g, 1.94×10^{-5} moles) in methylene chloride (5.0 mL) and stirred for 6 h at room temperature. The solvent was removed to yield a white solid (0.038 g, 97 %). mp 195 – 201 °C; ^{1}H NMR (400 MHz, CD_3CN, δ): 8.65 -8.50 (14H, m) 8.33 (4H, dd, J = 8.4, 1.2 Hz), 6.86 (8H, s), 4.15 (8H, t, J = 4.8 Hz), 3.75 (8H, t, J = 4.8 Hz), 3.51 (8H, t, J = 6.6 Hz), 2.61 (24H, s), 1.60 (8H, m), 1.40 (8H, m); ^{13}C NMR (100 MHz, CD_3CN, δ): 160.16, 156.92, 156.11, 149.95, 139.28, 138.63, 137.99, 138.25, 131.14, 121.80, 121.68, 114.56, 71.21, 69.42, 67.39, 29.59, 25.78, 21.21; ESI-MS: m/z for $[M - 4OTf]^{4+}$ calc. 354.6, found 354.7; m/z for $[M - 4OTf + 2ACN]^{4+}$ calc. 375.1, found 375.2; m/z for $[M - 3OTf]^{3+}$ calc. 527.8, found 528.1; m/z for $[M - 4OTf + OH]^{3+}$ calc. 478.5, found 478.2.

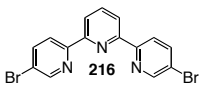

5,5"-bromo-2,2':6':2"-terpyridine

Prepared according to literature procedures.[81] White solid (0.950 g, 73%). Spectra matched literature values. ^{1}H NMR (300 MHz, $CDCl_3$, δ): 8.71 (2H, d, J = 1.8 Hz), 8.48

(2H, d, J = 7.8 Hz), 8.40 (2H, d, J = 7.8 Hz), 7.93 (1H, t, J = 7.8 Hz), 7.95 (2H, dd, J = 7.8, 1.8 Hz); ESI-MS: m/z for $[M + Na^+]^+$ calc. 414.1, found 414.2.

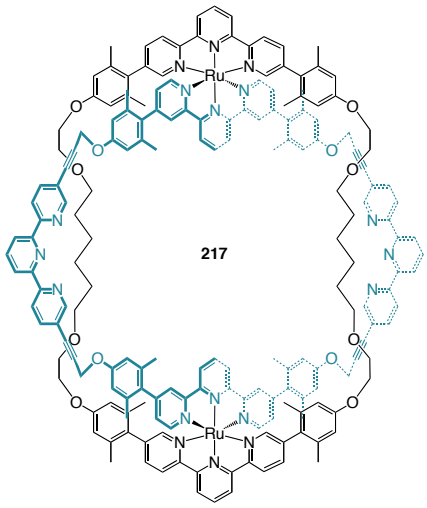

[bis-(5'5"-bis-(4-(2-(propoxy-ethoxy)-2,6-dimethyl-phenyl)-2,2':6',2"-terpyridine) macrocycle] ⊃ bis-(Ru(II)(*N,N'',N'''*-4,4"-bis-(4-prop-1-ynyl-2-oxy-2,6-dimethyl-phenyl)-2,2':6',2"-terpyridine-5,5"-bis(methyl)-2,2':6',2"-terpyridine macrocycle)][PF_6]$_4$

To a solution of [bis(5'5"-bis-(4-(2-(propoxy-ethoxy)-2,6-dimethyl-phenyl)-2,2':6',2"-terpyridine) macrocycle ⊂ bis-(Ru (4,4"-bis-(4-(ethynyloxy) -2,6-dimethyl-phenyl) -2,2':6',2"- terpyridine))][PF_6]$_4$ (0.021 g, 6.63 × 10^{-6} moles) in DMF (10 mL) was added triethylamine (5 mL), 5,5"-dibromo-2,2':6',2"-terpyridine (0.007 g, 1.66 × 10^{-5} moles), and $Pd(PPh_3)_4$ (0.002 g, 1.33 × 10^{-6} moles). The reaction was heated to 80 ºC and stirred under a nitrogen atmosphere for 24 h. The reaction mixture was cooled to room temperature and a second aliquot of 5,5"-dibromo-2,2':6',2"-terpyridine and $Pd(PPh_3)_4$ was added and the reaction was heated to 80 ºC and stirred under a nitrogen atmosphere for another 24 h. After cooling to room temperature, the addition of aqueous potassium hexafluorophosphate induced precipitation of a red solid that was filtered over celite and washed with water and diethyl ether. The precipitate was

dissolved with acetonitrile into a clean flask, concentrated and diluted with methylene chloride. After washing with 2M HCl, aqueous potassium hexafluorophosphate and water, the organic layer was separated, dried over magnesium sulfate, filtered, and the solvent was removed to yield a red solid (0.018 g, 75%). ^{1}H NMR (400 MHz, (CD_3CN, δ): 8.81 (4H, d, J = 7.8 Hz), 8.80 (4H, d, J = 1.8 Hz), 8.61 (4H, d, J = 9.0 Hz), 8.59 (4H, d, J = 8.4 Hz), 8.53 (4H, d, J = 8.4 Hz), 8.47 (2H, t, J = 8.4 Hz), 8.46 (4H, d, J = 7.8 Hz), 8.19 (4H, d, J = 1.2 Hz), 8.10 (2H, t, J = 7.8 Hz), 8.06 (2H, t, J = 7.8 Hz), 7.93 (4H, dd, J = 8.4, 2.4 Hz), 7.83 (4H, dd, J = 8.4, 1.8 Hz), 7.51 (4H, d, J = 6.0 Hz), 7.12 (4H, d, J = 1.8 Hz), 7.08 (4H, dd, J = 6.0, 1.8 Hz), 6.71 (8H, s), 6.66 (8H, s), 4.31 (8H, s), 3.99 (8H, t, J = 4.8 Hz), 3.66 (8H, t, J = 4.8 Hz), 3.45 (8H, t, J = 6.6 Hz), 1.86 (24H, s), 1.59 (24H, s), 1.53 (8H, m), 1.34 (8H, m); ESI-MS: m/z for $[M]^{4+}$ calc. 761.8, found 762.1.

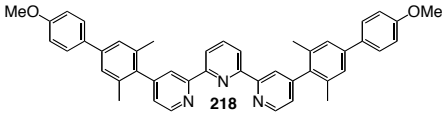

218

4,4”-bis-(4-(4-methoxyphenyl)-2,6-dimethyl-phenyl)-2,2’:6’,2”-terpyridine

A THF solution (5 mL) of 4-Bromoanisole (0.440 g, 2.34×10^{-3} moles) was cooled to -78°C. To this was added n-BuLi (1.17 mL of a 2.10 M sol in hexanes) and the solution stirred for 10 min. A THF solution (5 mL) of $ZnCl_2$ (0.331 g, 2.44×10^{-3} moles) was cannulated into the reaction flask. The solution was stirred, allowed to warm to room temperature, and then cannulated into a THF solution of 4,4”-bis-(4-trifluoromethanesulfonyloxy -2,6-dimethyl-phenyl)-2,2’:6’,2”-terpyridine **210c** (0.580 g, 1.97×10^{-3} moles) and $Pd(PPh_3)_4$ (0.091 g, 7.86×10^{-5} moles). The resulting solution was heated at reflux overnight. After cooling to room temperature, a white precipitate was filtered and washed with cold THF before drying. The precipitate was dissolved in methylene chloride and extracted with a saturated aqueous EDTA solution basified

with sodium bicarbonate. The organic layers were separated, dried over magnesium sulfate, filtered, and evaporated to give an off-white solid (0.361 g, 70% yield). mp 262 - 264 ºC ^{1}H NMR (500 MHz, $CDCl_3$, δ): 8.76 (2H, d, *J* = 4.8 Hz), 8.59 (2H, d, *J* = 7.8 Hz), 8.42 (2H, d, *J* = 0.6 Hz), 8.02 (1H, t, *J* = 7.8 Hz), 7.53 (4H, d, *J* = 8.4 Hz), 7.31 (4H, s), 7.16 (2H, dd, *J* = 4.8, 1.2 Hz), 6.95 (4H, d, *J* = 8.4 Hz), 3.86 (6H, s), 2.10 (12H, s). ^{13}C NMR (125 MHz, $CDCl_3$, δ): 159.20, 156.54, 155.71, 150.28, 149.45, 140.50, 138.00, 137.87, 135.94, 133.38, 128.16, 126.04, 124.89, 121.72, 121.56, 114.59, 55.35, 21.06. ESI-MS: *m*/*z* for $[M+Na]^+$ calc. 676.3, found 676.3. HRMS *m*/*z*: calc. for $[M]^+$ $C_{45}H_{39}N_3O_2$: 653.3042; found: 653.3031. X-ray quality crystals grown from methylene chloride. See attached crystallographic data.

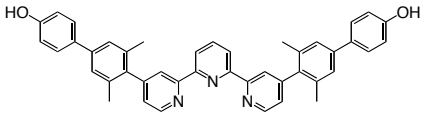

4,4''-bis-(4-(4-hydroxyphenyl)-2,6-dimethyl-phenyl)-2,2':6',2''-terpyridine

Neat pyridine hydrochloride (1.238 g, 1.08 × 10^{-2} moles) and 5,5'-bis-(4-methoxy-2,6-dimethyl-phenyl)-2,2'-bipyridine (0.190 g, 2.91 × 10^{-4} moles) were heated to 185 °C for 4 h. The hot solution was quenched with boiling water (40 mL). The resulting yellow precipitate was filtered, washed thoroughly with water and dried under vacuum overnight to yield a tan solid (0.140 g, 77%). m.p. = 307 – 310 °C dec. ^{1}H NMR (500 MHz, DMSO-d_6, δ): 9.53 (2H, bs), 8.80 (2H, dd, *J* = 4.5, 0.5 Hz), 8.52 (2H, d, *J* = 8.0 Hz), 8.32 (2H, d, *J* = 0.5 Hz), 8.16 (1H, t, *J* = 8.0 Hz), 7.47 (4H, d, *J* = 8.5 Hz), 7.35 (2H, dd, *J* = 4.5, 1.0 Hz), 7.34 (4H, s), 6.83 (4H, d, *J* = 8.5 Hz), 2.05 (12H, s). ^{13}C NMR (125MHz, DMSO-d_6, δ):157.23, 155.61, 154.96, 149.83, 149.37, 139.75, 138.69, 138.01, 135.02, 132.01, 127.66, 125.33, 125.09, 121.26, 121.20, 115.65, 20.51. ESI-MS *m*/*z*: 648.1 $[M + Na]^+$, 626.2 $[M + H]^+$. HRMS: *m*/*z* calc. for $[M]^+$ $C_{43}H_{35}N_3O_2$: 625.2729; found: 625.2778.

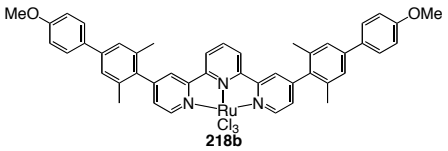

218b

Ru(4,4''-bis-(4-(4-methoxyphenyl)-2,6-dimethyl-phenyl)-2,2':6',2''-terpyridine)Cl_3

Prepared using an analogous procedure described by Sullivan *et. al.*[77] To a solution of 4,4''-bis-(4-(4-methoxyphenyl)-2,6-dimethyl-phenyl)-2,2':6',2''-terpyridine 2,2':6',2''-terpyridine (0.100 g, 1.60×10^{-4} moles) in absolute ethanol (15 mL) was added $RuCl_3$•''$3H_2O$'' (0.063 g, 2.40×10^{-4} moles) and heated at reflux for 5 h. The reaction was cooled to room temperature and the solvent reduced. Water was added to induce precipitation of a brown solid that was filter through a Büchner funnel, washed with copious amounts of water and dried in under vacuum overnight to yield a tan powder (0.115 g, 86%). The brown powder was used without further purification in the subsequent reaction. m.p. >350 ºC ; ESI-MS: *m/z* for $[M - Cl - ACN]^+$ calc. 866.2 , found 866.7.

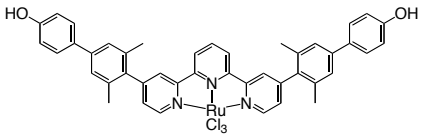

Ru(4,4''-bis-(4-(4-hydroxyphenyl)-2,6-dimethyl-phenyl)-2,2':6',2''-terpyridine)Cl_3

Prepared using an analogous procedure described by Sullivan *et. al.*[77] To a solution of 4,4''-bis-(4-(4-hydroxyphenyl)-2,6-dimethyl-phenyl)-2,2':6',2''-terpyridine 2,2':6',2''-terpyridine (0.160 g, 2.56×10^{-4} moles) in absolute ethanol (25 mL) was added $RuCl_3$•''$3H_2O$'' (0.100 g, 3.84×10^{-4} moles) and heated at reflux for 4 h. The reaction was cooled to room temperature and the solvent reduced. Water was added to induce precipitation of a brown solid that was filtered through a Büchner funnel, washed with copious amounts of water and dried in under vacuum overnight to yield a brown

powder (0.160 g, 75%). The brown powder was used without further purification in the subsequent reaction. m.p. >350 ºC; ESI-MS: *m/z* for $[M - Cl + ACN]^+$ calc. 838.1, found 840.4; *m/z* for $[M + Na]^+$ calc. 857.0, found 857.1.

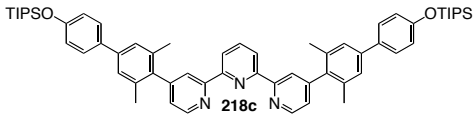

4,4”-bis-(4-(4-Triisopropylsilyloxyphenyl)-2,6-dimethyl-phenyl)-2,2’:6’,2”-terpyridine

Imidazole (0.065 g, 9.60×10^{-4} moles) and 4,4”-bis-(4-(4-hydroxyphenyl)-2,6-dimethyl-phenyl)-2,2’:6’,2”-terpyridine (0.200 g, 3.20×10^{-4} moles) were combined in DMF (5.0mL) and cooled to 0 ºC. Neat chlorotriisopropyl silane (0.130 g, 6.72×10^{-4} moles) was added via syringe. The temperature was maintained at 0 ºC for 1h after which it was slowly allowed to warm to room temperature overnight. The reaction was diluted with methylene chloride and washed with water. The organic layers were combined, dried over magnesium sulfate, and the solvent removed to give a dirty solid. The crude solid was purified by column chromatography on neutral alumina oxide methylene chloride as the eluant to yield a white solid (0.212 g, 71%). mp = 143 - 145 ºC ^{1}H NMR (600 MHz, $CDCl_3$, δ): 8.76 (2H, dd, *J* = 4.8, 1.0 Hz), 8.59 (2H, d, *J* = 7.8 Hz), 8.42 (2H, dd, *J* = 1.0, 0.6 Hz), 8.02 (1H, t, *J* = 7.8 Hz), 7.45 (4H, d, *J* = 8.4 Hz), 7.31 (4H, s), 7.15 (2H, dd, *J* = 4.8, 1.2 Hz), 6.95 (4H, d, *J* = 8.4 Hz), 3.86 (6H, s), 2.11 (12H, s), 1.28 (6H, m), 1.13 (36H, d, *J* = 6.6 Hz); ^{13}C NMR (150 MHz, $CDCl_3$, δ): 156.57, 155.70, 150.44, 149.29, 140.57, 137.92, 137.87, 135.94, 133.52, 128.12, 126.06, 124.87, 121.62, 121.62, 120.12, 114.18, 21.05, 18.06, 12.94; ESI-MS: *m/z* for $[M+H]^+$ calc. 938.5, found 939.5; HRMS *m/z*: calc. for $[M]^+$ $C_{61}H_{75}N_3O_2Si_2$: 937.5398 ; found: 937.5312.

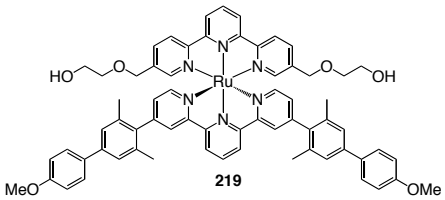

219

Ru[(4,4''-bis-(2,6-dimethyl-4-(4-methoxyphenyl)phenyl)-2,2':6',2''-terpyridine)(5,5''-bis(ethoxy-2-ol-methyl)-2,2':6',2''-terpyridine)][PF_6]$_2$

A ethylene glycol (3 mL) solution of Ru[(4,4''-bis-(2,6-dimethyl-4-(4-methoxyphenyl)phenyl)-2,2':6',2''-terpyridine]Cl_3 **218b** (0.100 g, 1.16×10^{-4} moles) and 5,5''-bis-bromomethyl-2,2':6',2''-terpyridine **203** (0.051 g, 1.22×10^{-4} moles) was heated at 125 ºC for 20 h. Aqueous potassium hexafluorophosphate was added until a deep red precipitate formed. The precipitate was filtered over celite, washed with water and diethyl ether and dissolved into a clean flask with methylene chloride. The red solution was dried over magnesium sulfate, filtered and solvent evaporated to yield a red solid (0.144 g, 87%). m.p. 205 – 208 °C. ^{1}H NMR (600 MHz, CD_3CN, δ): 8.74 (2H, d, *J* = 4.8 Hz), 8.73 (2H, d, *J* = 4.8 Hz), 8.51 (2H, d, *J* = 8.4 Hz), 8.42 (2H, dd, *J* = 1.8 Hz), 8.40, (1H, t, *J* = 8.4 Hz), 8.37 (1H, t, *J* = 8.4 Hz), 7.94 (2H, dd, *J* = 8.4, 1.2 Hz), 7.6 (4H, d, *J* = 9.0Hz), 7.40 (4H, s) 7.38 (4H, dd, *J* = 8.4, 1.2 Hz), 7.05 (2H, dd, *J* = 6, 1.8 Hz), 7.02 (2H, d, *J* = 9.0 Hz), 4.35 (4H, s), 3.46 (4H, t, *J* = 4.8 Hz), 3.29 (4H, t, *J* = 4.58 Hz), 1.98 (12H, s); ^{13}C NMR (150 MHz, CD_3CN, δ): 160.76, 159.54, 158.06, 156.78, 156.55, 153.36, 152.51, 151.88, 141.98, 140.64, 137.79, 136.98, 136.89, 136.71, 133.64, 129.42, 129.05, 126.90, 126.76, 125.27, 124.95, 124.50, 115.43, 73.70, 69.56, 61.91, 56.21, 21.00; ESI-MS: *m*/*z* for $[M]^{2+}$calc. 568.2, found 568.3;, *m*/*z* for $[M + PF_6^-]^+$ calc. 1281.3, found 1281.7.

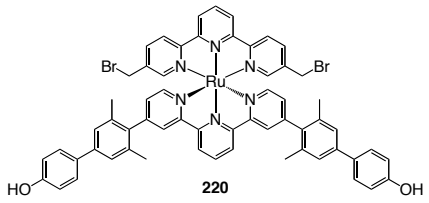

220

Ru[(4,4''-bis-(2,6-dimethyl-4-(4-hydroxyphenyl)phenyl)-2,2':6',2''-terpyridine)(5,5''-bis(bromo-methyl)-2,2':6',2''-terpyridine)][PF_6]$_2$

To solution of Ru[(4,4''-bis-(2,6-dimethyl-4- (4-methoxyphenyl)phenyl)- 2,2':6',2''-terpyridine)(5,5''-bis(ethoxy-2-ol-methyl)-2,2':6',2''-terpyridine)][PF_6]$_2$ **219** (0.140 g, 9.83 × 10^{-5} moles) in methylene chloride at -78 ºC was added boron tribromide (0.196 g, 7.86 × 10^{-4} moles). The solution was stirred and allowed to warm to room temperature over six h. Water was added to quench the reaction and the organic layer separated. The solvent was removed and the red solid diluted in acetonitrile. Aqueous potassium hexafluorophosphate was added until a deep red precipitate formed. The precipitate was filtered over celite, washed with water and diethyl ether and dissolved into a clean flask with methylene chloride. The red solution was dried over magnesium sulfate, filtered and solvent evaporated to yield a red solid (0.133 g, 94%). m.p. 340 °C dec.; ^{1}H NMR (600 MHz, $CDCl_3$, δ): 8.78 (2H, d, *J* = 4.8 Hz), 8.77 (2H, d, *J* = 4.8 Hz), 8.52 (2H, d, *J* = 8.4 Hz), 8.44 (2H, dd, *J* = 1.8 Hz), 8.43, (1H, t, *J* = 8.4 Hz), 8.42 (1H, t, *J* = 8.4 Hz), 8.02 (2H, dd, *J* = 8.4, 1.2 Hz), 7.52 (4H, d, *J* = 9.0Hz), 7.46 (2H, d, *J* = 1.8 Hz), 7.38 (2H, d, *J* = 6.0 Hz), 6.37 (4H, s), 7.05 (2H, dd, *J* = 6, 1.8 Hz), 6.89 (4H, d, *J* = 9.0 Hz), 4.33 (4H, s), 1.98 (12H, s); ^{13}C NMR (150 MHz, $CDCl_3$, δ): 159.42, 158.75, 158.16, 156.83, 156.26, 153.49, 153.31, 152.59, 142.01, 139.92, 139.67, 137.21, 136.99, 136.36, 132.81, 129.50, 129.20, 126.86, 126.64, 125.44, 125.16, 125.13, 116.78, 28.91, 20.96; ESI-MS: *m*/*z* for $[M]^{2+}$ calc. 572.9, found 572.9; *m*/*z* for $[M + PF_6^-]^+$ calc. 1290.9, found 1290.2.

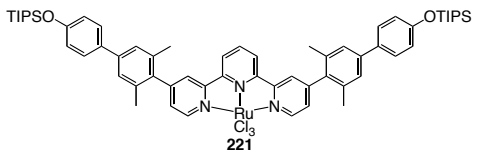

221

Ru[4,4''-bis-(4-(4-Triisopropylsilyloxyphenyl)-2,6-dimethyl-phenyl)-2,2':6',2''-terpyridine]Cl_3

Prepared using an analogous procedure described by Sullivan *et. al.*[77] To a solution of 4,4''-bis-(4-(4-Triisopropylsilyloxyphenyl)-2,6-dimethyl-phenyl)-2,2':6',2''-terpyridine 2,2':6',2''-terpyridine (0.068 g, 7.25×10^{-5} moles) in absolute ethanol (4 mL) was added $RuCl_3$•''$3H_2O$'' (0.028 g, 1.09×10^{-4} moles) and heated at reflux for 4 h. The reaction was cooled to room temperature and the solvent reduced. Water was added to induce precipitation of a brown solid that was filter through a Büchner funnel, washed with copious amounts of water and diethyl ether, and dried in under vacuum overnight to yield a brown powder (0.060 g, 72%). The brown powder was used without further purification in the subsequent reaction. m.p. >350 °C; ESI-MS: m/z for $[M + Na]^+$ calc. 1168.9, found 1169.3.

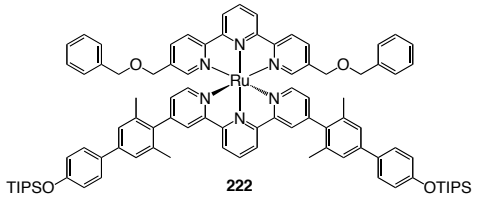

222

Ru[(4,4''-bis-(4-(4-Triisopropylsilyloxyphenyl)-2,6-dimethyl-phenyl)-2,2':6',2''-terpyridine)(5,5''-bis-((benzyloxy)methyl)-2,2':6',2''-terpyridine)][PF_6]$_2$

A benzyl alcohol (2 mL) solution of Ru[4,4''-bis-(4-(4-Triisopropylsilyloxyphenyl)-2,6-dimethyl-phenyl)-2,2':6',2''-terpyridine]Cl_3 **221** (0.055 g, 4.80×10^{-4} moles) and 5,5''-bis-bromomethyl-2,2':6',2''-terpyridine **203** (0.021 g, 5.04×10^{-5} moles) was heated at 125 °C for 20 h. Diethyl ether was added until a red precipitate formed. The precipitate was filtered over celite, washed with diethyl ether and dissolved into a clean flask with

methylene chloride. The red solution was washed with aqueous potassium hexafluorophosphate, dried over magnesium sulfate, filtered and solvent evaporated to yield a red solid (0.075 g, 87%). m.p. 210 -214 °C. ^{1}H NMR (600 MHz, CD_3CN, δ): 8.77 (2H, d, *J* = 4.8 Hz), 8.73 (2H, d, *J* = 4.8 Hz), 8.52 (2H, d, *J* = 8.4 Hz), 8.41 8.40, (1H, t, *J* = 8.4 Hz), 8.40 (2H, dd, *J* = 1.8 Hz), 8.33 (1H, t, *J* = 8.4 Hz), 7.93 (2H, dd, *J* = 8.4, 1.2 Hz), 7.54 (4H, d, *J* = 9.0Hz), 7.45 – 7.30 (16H, m) 7.16 (4H, m,), 7.05 (2H, dd, *J* = 6, 1.8 Hz), 6.98 (2H, d, *J* = 9.0 Hz), 4.36 (8H, s), 1.93 (12H, s), 1.30 (6H, m), 1.12 (36H, d, *J* = 6.6 Hz); ^{13}C NMR (150 MHz, CD_3CN, δ): 159.02, 158.12, 156.88, 156.54, 153.82, 153.01, 151.82, 142.00, 140.73, 138.02, 137.72, 137.21, 136.99, 136.64, 133.64, 129.42, 129.07, 128.32, 128.11, 127.05, 126.97, 126.90, 125.03, 125.33 124.56, 120.37 115.21, 73.70, 73.70, 21.07, 18.12, 12.61; ESI-MS: *m*/*z* for $[M]^{2+}$ calc. 756.3, found 756.5.

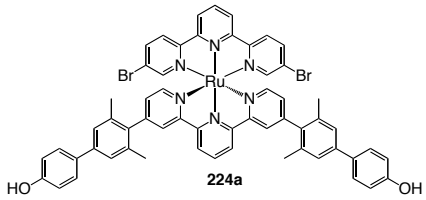

224a

Ru[(4,4''-bis-(2,6-dimethyl-(4-hydroxyphenyl)-phenyl)-2,2':6',2''-terpyridine)(5,5''-dibromo-2,2':6',2''-terpyridine)][PF_6]$_2$

A ethylene glycol (2 mL) solution of Ru[(4,4''-bis-(2,6-dimethyl-4-(4-hydroxyphenyl)phenyl)-2,2':6',2''-terpyridine]Cl_3 (0.100 g, 1.20×10^{-4} moles) and 5,5''-dibromo-2,2':6',2''-terpyridine **216** (0.049 g, 1.26×10^{-4} moles) was heated at 125 ºC for 20 h. Aqueous potassium hexafluorophosphate was added until a deep red precipitate formed. The precipitate was filtered over celite, washed with water and diethyl ether and dissolved into a clean flask with methylene chloride. The red solution was dried over magnesium sulfate, filtered and solvent evaporated to yield a red solid. The crude solid was purified by column chromatography on silica gel with CH_3CN : H_2O :

aqueous KPF_6 92 : 8 : 0.08 as the eluant to yield a red crystalline solid (0.089 g, 53%). m.p. 330 °C dec.; ^{1}H NMR (600 MHz, CD_3CN, δ): 8.77 (2H, d, *J* = 8.4 Hz), 8.76 (2H, d, *J* = 8.4 Hz), 8.43 (2H, d, *J* = 8.4 Hz), 8.42 (2H, dd, *J* = 1.8 Hz), 8.41, (1H, t, *J* = 7.8 Hz), 8.40 (1H, t, *J* = 7.8 Hz), 8.15 (2H, dd, *J* = 8.4, 1.2 Hz), 7.52 (4H, d, *J* = 9.0Hz), 7.48 (2H, d, *J* = 1.8 Hz), 7.38 (4H, s), 7.33 (2H, d, *J* = 6.0 Hz), 7.05 (2H, dd, *J* = 7.8, 1.8 Hz), 7.04 (2H, s), 6.89 (4H, d, *J* = 9.0 Hz), 2.01 (12H, s); ^{13}C NMR (150 MHz, CD_3CN, δ): 159.41, 158.08, 158.01, 156.80, 156.13, 154.39, 153.53, 152.64, 142.10, 137.30, 137.02, 136.97, 136.41, 132.83, 129.52, 129.16, 127.62, 126.81, 126.80, 125.30, 125.20, 123.95, 116.83, 20.92; ESI-MS *m/z* for $[M]^{2+}$ calc. 558.9, found 559.0.

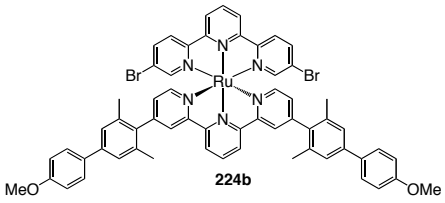

224b

Ru[(4,4''-bis-(2,6-dimethyl-(4-methoxyphenyl)-phenyl)-2,2':6',2''-terpyridine)(5,5''-dibromo-2,2':6',2''-terpyridine)][PF_6]$_2$

A ethylene glycol (2 mL) solution of Ru[(4,4''-bis-(2,6-dimethyl-4-(4-methoxyphenyl)phenyl)-2,2':6',2''-terpyridine]Cl_3 (0.050 g, 5.81 × 10^{-5} moles) and 5,5''-dibromo-2,2':6',2''-terpyridine **216** (0.024 g, 6.10 × 10^{-5} moles) was heated at 125 ºC for 12 h. Aqueous potassium hexafluorophosphate was added until a deep red precipitate formed. The precipitate was filtered over celite, washed with water and diethyl ether and dissolved into a clean flask with methylene chloride. The red solution was dried over magnesium sulfate, filtered and solvent evaporated to yield a red solid. The crude solid was purified by column chromatography on silica gel with CH_3CN : H_2O : aqueous KPF_6 92 : 8 : 0.08 as the eluant to yield a red crystalline solid (0.095 g, 89%). m.p. > 350 °C. ^{1}H NMR (600 MHz, $CDCl_3$, δ): 8.77 (2H, d, *J* = 8.4 Hz), 8.76 (2H, d, *J* = 8.4 Hz), 8.44 (2H, d, *J* = 8.4 Hz), 8.43 (2H, dd, *J* = 1.8 Hz), 8.41, (1H, t, *J* = 7.8 Hz),

8.40 (1H, t, J = 7.8 Hz), 8.12 (2H, dd, J = 8.4, 1.2 Hz), 7.53 (4H, d, J = 9.0 Hz), 7.48 (2H, d, J = 1.8 Hz), 7.37 (4H, s), 7.33 (2H, d, J = 6.0 Hz), 7.04 (2H, dd, J = 7.8, 1.8 Hz), 6.94 (4H, d, J = 9.0 Hz), 3.87 (6H, s), 2.09 (12H, s); ^{13}C NMR (150 MHz, $CDCl_3$, δ): 159.87, 158.65, 157.46, 156.20, 155.81, 153.97, 153.20, 152.10, 141.66, 136.88, 136.76, 136.02, 135.83, 132.02, 129.39, 128.61, 127.54, 126.30, 126.23, 124.87, 124.07, 123.49, 115.74, 20.54; ESI-MS: m/z for $[M]^{2+}$ calc. 573.0, found 572.04, m/z for $[M + PF_6]^+$ calc. 1290.9, found 1290.8.

5.4 Crystal Structure Data

Methods and Materials

All measurements (except **205**) were made on a *Nonius KappaCCD* area-detector diffractometer[82] using graphite-monochromated Mo *K*a radiation (λ = 0.71073 Å) and an *Oxford Cryosystems Cryostream 700* cooler. Single crystals of the two ring complex 205 was measured at SLS synchrotron (beamline PX) using radiation of wavelength λ = 0.800 Å and a MarResearch 225 detector 80 mm from the crystal. Data reduction was performed with *HKL Denzo* and *Scalepack*.[83] The intensities were corrected for Lorentz and polarization effects, but not for absorption. The structures were solved by direct methods using *SIR92*,[84] which revealed the positions of all non-hydrogen atoms. The non-hydrogen atoms were refined anisotropically. All of the H-atoms were placed in geometrically calculated positions and refined using a riding model where each H-atom was assigned a fixed isotropic displacement parameter with a value equal to $1.2U_{eq}$ of its parent atom ($1.5U_{eq}$ for the methyl groups). Refinement of the structure was carried out on F^2 by using full-matrix least-squares procedures, which minimized the function $Sw(F_o^2 - F_c^2)^2$. The weighting scheme was based on counting statistics and included a factor to downweight the intense reflections. Neutral atom scattering factors for non-hydrogen atoms were taken from Maslen, Fox and O'Keefe,[85] and the scattering factors for H-atoms were taken from Stewart, Davidson and Simpson.[86] Anomalous dispersion effects were included in F_c;[87] the values for f' and f'' were those of Creagh and McAuley.[88] The values of the mass attenuation coefficients are those of Creagh and Hubbel.[89] All calculations were performed using the *SHELXL97*[90] program.

Table 5.1 Crystallographic Data for **199**

Crystallised from	CH_2Cl_2 / Et_2O
Empirical formula	$C_{148}H_{152}Cl_8F_{24}N_{12}O_{12}P_4Ru_2$
Formula weight [g mol^{-1}]	3356.78
Crystal colour, habit	red, plate
Crystal dimensions [mm]	0.05 × 0.32 × 0.35
Temperature [K]	160 (1)
Crystal system	triclinic
Space group	$P\bar{1}$ (#2)
Z	1
Reflections for cell determination	267018
2θ range for cell determination [°]	4 – 50
Unit cell parameters a [Å] = 15.0040(5)	α [°] = 98.402(2)
b [Å] = 15.1525(4)	β [°] = 98.012(1)
c [Å] = 21.5611(7)	γ [°] = 108.321(2)
V [Å^3]	4513.0(3)
F(000)	1720
D_x [g cm^{-3}]	1.235
μ(Mo $K\alpha$) [mm^{-1}]	0.399
Scan type	ϕ and ω
$2\theta_{(max)}$ [°]	50
Transmission factors (min; max)	0.856; 0.987
Total reflections measured	77052
Symmetry independent reflections	15899
R_{int}	0.101
Reflections with $I > 2\sigma(I)$	11436
Reflections used in refinement	15899
Parameters refined; restraints	930; 271
Final $R(F)$ [$I>2\sigma(I)$ reflections]	0.0690
$wR(F^2)$ (all data)	0.1886
Weights: $w = [\sigma^2(F_o^2) + (0.1103P)^2 + 1.4163P]^{-1}$ where $P = (F_o^2 + 2F_c^2)/3$	
Goodness of fit	1.035
Final Δ_{max}/σ	0.001
$\Delta\rho$ (max; min) [e Å^{-3}]	0.54; -0.50
$\sigma(d_{(C-C)})$ [Å]	0.006 – 0.007

199

The structure of $[Ru_2(C_{144}H_{144}N_{12}O_{12})^{4+}] \cdot 4PF_6^- \cdot 4CH_2Cl_2$ has been solved and refined successfully. In the structure, the cation sits across a crystallographic centre of inversion, while there are two PF_6^- anions in general positions, thereby giving the required 1:4 cation:anion ratio. One of the anions is disordered and two orientations of the PF_6^- octahedron were employed in the model for this anion, while the geometry was restrained in order to retain proper octahedral geometry. The asymmetric unit also contains sufficient space for several solvent molecules, which, from the arrangement of residual electron density peaks, appear to be predominantly CH_2Cl_2, although inclusion of some diethyl ether at the solvent sites is possible, as this solvent was also used in the crystallisation solution. The disorder of the solvent molecules could not be modeled adequately. Therefore, the contribution of the solvent molecules to the intensity data was removed by using the *SQUEEZE* routine of the *PLATON* program. Omission of the solvent molecules leaves a single cavity of 1450 $Å^3$ per unit cell. The number of electrons contributing to the void in the structure was calculated by the *SQUEEZE* routine to be approximately 154 e, although this may be an underbound. Allowing for four CH_2Cl_2 molecules per cavity yields 168 e and this was used in the subsequent calculation of the empirical formula, formula weight, density, linear absorption coefficient and $F(000)$. Replacing any CH_2Cl_2 molecule with diethyl ether does not change the electron count as both molecules have the same number of electrons.

One of the symmetry-independent hydroxy groups in the cation forms hydrogen bonds with F-atoms from a disordered anion. The other hydroxy group on the same ligand forms an intermolecular hydrogen bond with one of the ether O-atoms in an adjacent cation. The corresponding hydroxy group in the same part of this second cation forms a corresponding hydrogen bond back to the original cation. However, the centrosymmetric nature of the cation means that each cation donates two hydrogen bonds of this type which then link the cations into extended double-bridged chains.

Table 5.2 Crystallographic Data for **205**.[91]

Crystallised from		benzonitrile/benzene
Empirical formula		$C_{178}H_{168}F_{24}N_{18}O_{12}P_4Ru_2$
Formula weight [g mol^{-1}]		3533.40
Crystal colour, habit		red, plate
Crystal dimensions [mm]		0.00 × 0.00 × 0.00
Temperature [K]		
Crystal system		orthorhombic
Space group		*Pnnn* (#48)
Z		4
Unit cell parameters	*a* [Å] = 22.824(1)	α [°] = 90
	b [Å] = 22.583(1)	β [°] = 90
	c [Å] = 47.813(1)	γ [°] = 90
V [Å^3]	24644(1)	
F(000)		7288
D_x [g cm^{-3}]		0.952
μ(Mo *K*α) [mm^{-1}]		0.212
Scan type		ω
$2\theta_{(max)}$ [°]		55
Total reflections measured		93055
Symmetry independent reflections		13465
R_{int}		0.048
Reflections with $I > 2\sigma(I)$		9271
Reflections used in refinement		13465
Parameters refined; restraints		1040; 788
Final $R(F)$ [$I > 2\sigma(I)$ reflections]		0.2454
$wR(F^2)$ (all data)		0.6022
Weights: $w = [\sigma^2(F_o^2) + (0.1000P)^2]^{-1}$ where $P = (F_o^2 + 2F_c^2)/3$		
Goodness of fit		5.051
Final Δ_{max}/σ		6.73
$\Delta\rho$ (max; min) [e Å^{-3}]		1.59; -0.85

Table 5.3 Crystallographic Data for **212**.

Crystallised from	CH_2Cl_2 / Et_2O
Empirical formula	$C_{88}H_{94}F_{12}N_6O_7P_2Zn$
Formula weight [g mol^{-1}]	1703.05
Crystal colour, habit	colourless, prism
Crystal dimensions [mm]	0.20 × 0.30 × 0.32
Temperature [K]	160(1)
Crystal system	monoclinic
Space group	$P2_1/c$ (#14)
Z	4
Reflections for cell determination	129715
2θ range for cell determination [°]	4 – 55
Unit cell parameters a [Å] = 21.9374(2)	α [°] = 90
b [Å] = 16.6216(2)	β [°] = 97.7884(6)
c [Å] = 23.8100(2)	γ [°] = 90
V [Å^3]	8601.9(1)
F(000)	3552
D_x [g cm^{-3}]	1.315
μ(Mo $K\alpha$) [mm^{-1}]	0.405
Scan type	ϕ and ω
$2\theta_{(max)}$ [°]	55
Transmission factors (min; max)	0.842; 0.928
Total reflections measured	169800
Symmetry independent reflections	19726
R_{int}	0.073
Reflections with $I > 2\sigma(I)$	14506
Reflections used in refinement	19725
Parameters refined	1019
Final $R(F)$ [$I>2\sigma(I)$ reflections]	0.0525
$wR(F^2)$ (all data)	0.1495
Weights: $w = [\sigma^2(F_o^2) + (0.0862P)^2 + 1.5362P]^{-1}$ where $P = (F_o^2 + 2F_c^2)/3$	
Goodness of fit	1.045
Secondary extinction coefficient	0.0019(2)
Final Δ_{max}/σ	0.002
$\Delta\rho$ (max; min) [e Å^{-3}]	0.50; -0.59
$\sigma(d_{(C-C)})$ [Å]	0.003 – 0.004

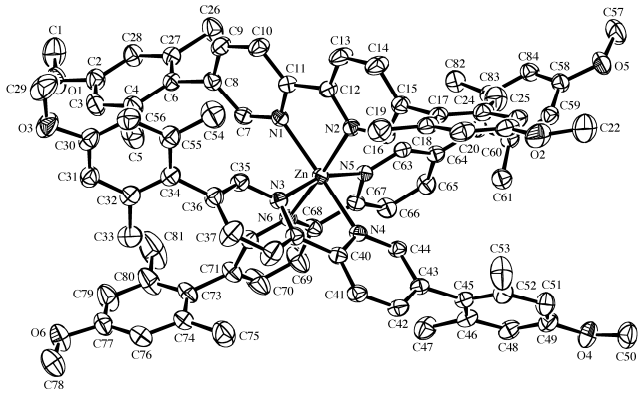

Figure 5.28 ORTEP diagram of [Zn(5,5'-bis-(4-methoxy-2,6-dimethyl-phenyl)-2,2'-bipyridine)$_3$][PF_6]$_2$ **212**.

212

The structure of [$Zn(C_{28}H_{28}N_2O_2)_3^{2+}$] ·2$PF_6^-$ ·Et_2O (JKK-IV-136) has been solved and refined successfully . The structure was solved by direct methods using *SIR92*[5], which revealed the positions of all non-hydrogen atoms. The asymmetric unit contains one cation, two PF_6^- anions and one disordered molecule of diethyl ether. The disorder of the solvent molecule could not be modeled adequately, but it was assumed that the solvent was diethyl ether, because, although the complex was crystallized from a mixture of Et_2O and CH_2Cl_2, both of which have the same number of electrons, the magnitudes and positions of the residual electron density peaks were more consistent with a molecule of Et_2O than with a molecule of CH_2Cl_2. The contribution of the solvent molecules to the intensity data was removed by using the *SQUEEZE*[6] routine of the *PLATON*[7] program. Omission of the solvent molecules leaves four cavities of 1018 Å^3 per unit cell. The number of electrons contributing to each the void in the structure was calculated by the *SQUEEZE* routine to be approximately 44 e. Allowing for one Et_2O molecule per cavity yields 42 e and this was used in the subsequent calculation of the empirical formula, formula weight, density, linear absorption coefficient and *F*(000). The non-hydrogen atoms were refined anisotropically. All of the H-atoms were placed in geometrically calculated positions and refined using a riding model where each H-atom was assigned a fixed isotropic displacement parameter with a value equal to 1.2U_{eq} of its parent atom (1.5U_{eq} for the methyl groups). Refinement of the structure was carried out on F^2 using full-matrix least-squares procedures, which minimized the function $Sw(F_o^2 - F_c^2)^2$. The weighting scheme was based on counting statistics and included a factor to downweight the intense reflections. Plots of $Sw(F_o^2 - F_c^2)^2$ versus F_c / F_c(max) and resolution showed no unusual trends. A correction for secondary extinction was applied. One reflection, whose intensity was considered to be an extreme outlier, was omitted from the final refinement.

Table 5.4 Crystallographic Data for **213**.

Crystallized from	MeCN / Et_2O
Empirical formula	$C_{90}H_{102}F_{12}N_{10}O_8P_2Ru$
Formula weight [g mol^{-1}]	1842.78
Crystal color, habit	red, prism
Crystal dimensions [mm]	0.07 × 0.20 × 0.32
Temperature [K]	160(1)
Crystal system	monoclinic
Space group	$P2_1/n$ (#14)
Z	4
Reflections for cell determination	257183
2θ range for cell determination [°]	4 – 50
Unit cell parameters a [Å] = 20.3614(3)	α [°] = 90
b [Å] = 15.5902(3)	β [°] = 94.4504(9)
c [Å] = 30.5936(5)	γ [°] = 90
V [Å^3]	9682.3(3)
F(000)	3832
D_x [g cm^{-3}]	1.264
μ(Mo $K\alpha$) [mm^{-1}]	0.274
Scan type	ϕ and ω
$2\theta_{(max)}$ [°]	50
Transmission factors (min; max)	0.871; 0.987
Total reflections measured	141740
Symmetry independent reflections	17083
R_{int}	0.111
Reflections with $I > 2\sigma(I)$	10493
Reflections used in refinement	17083
Parameters refined; restraints	1455; 4388
Final $R(F)$ [$I > 2\sigma(I)$ reflections]	0.1034
$wR(F^2)$ (all data)	0.3166
Weights: $w = [\sigma^2(F_o^2) + (0.1819P)^2 + 18.3927P]^{-1}$ where $P = (F_o^2 + 2F_c^2)/3$	
Goodness of fit	1.027
Final Δ_{max}/σ	0.001
$\Delta\rho$ (max; min) [e Å^{-3}]	1.91; -0.74
$\sigma(d_{(C-C)})$ [Å]	0.004 – 0.01

213

The structure was solved by direct methods using *SIR92* [5], which revealed the positions of all non-hydrogen atoms. The asymmetric unit contains one cation, two highly disordered anions distributed over three partially occupied sites, and an estimated four MeCN molecules. The disorder of the solvent molecules could not be modelled adequately, so the contribution of the solvent molecule to the intensity data was removed by using the *SQUEEZE*[6] routine of the *PLATON*[7] program. Omission of the solvent molecule leaves two main cavities of 841 $Å^3$ per unit cell (total void volume in the unit cell is 1810 $Å^3$). The number of electrons contributing to each void in the structure was calculated by the *SQUEEZE* routine to be approximately 149 e, although this may be an underestimate. This corresponds with 6.8 MeCN molecules per cavity or 3.4 per asymmetric unit. Therefore, it is estimated that there are in reality four MeCN molecules per asymmetric unit and this was used in the subsequent calculation of the empirical formula, formula weight, density, linear absorption coefficient and *F*(000).

In the cation, significant disorder is present in one of the alkyl ether chains and one of the immediately adjacent dimethylphenyl rings. Two positions were defined for the relevant atoms, starting with all atoms of the disordered dimethylphenyl ring and proceeding along the alkyl ether chain up to the ether O-atom, O(4), adjacent to the dimethylphenyl ring at the other end of the chain. Refinement of a common site occupation factor led to a value of 0.612(7) for the major conformation. Similarity restraints were applied to the chemically equivalent bond lengths and angles involving all disordered atoms. In addition, the C–C and C–O bond lengths were restrained to the usually observed values for these bonds in similar chemical environments and the atoms each conformation of the dimethylphenyl ring were restrained to be coplanar. Neighbouring atoms within and between each disordered conformation were restrained to have similar atomic displacement parameters.

The two PF_6^- anions in the asymmetric unit are highly disordered and statistically distributed over three partially occupied sites. The site occupation factors of these sites were refined while restraining their sum to 2.0. This yielded occupation factors of 0.698(3), 0.496(2) and 0.806(3) for the three sites. The P–F and F···F distances within each symmetry-independent site for the anions were restrained, so as to maintain octahedral geometry and uniform P–F bond lengths, while neighbouring atoms within and between each disordered orientation were restrained to have similar isotropic atomic displacement parameters. Additional disorder may be present within the sites of each anion, but no attempts were made to model such disorder further.

Table 5.5 Crystallographic Data for **214**.

Crystallised from	MeCN / Et_2O
Empirical formula	$C_{102}H_{130}F_{12}N_{10}O_{26}S_4Zn_2$
Formula weight [g mol^{-1}]	2399.17
Crystal colour, habit	colourless, plate
Crystal dimensions [mm]	0.13 × 0.30 × 0.30
Temperature [K]	160(1)
Crystal system	triclinic
Space group	$P\bar{1}$ (#2)
Z	1
Reflections for cell determination	82449
2θ range for cell determination [°]	4 – 50
Unit cell parameters a [Å] = 11.0301(2)	α [°] = 76.878(1)
b [Å] = 12.3939(4)	β [°] = 78.788(2)
c [Å] = 21.8715(7)	γ [°] = 87.305(2)
V [Å^3]	2856.3(1)
F(000)	1252
D_x [g cm^{-3}]	1.395
μ(Mo $K\alpha$) [mm^{-1}]	0.587
Scan type	ϕ and ω
$2\theta_{(max)}$ [°]	50
Transmission factors (min; max)	0.821; 0.963
Total reflections measured	43549
Symmetry independent reflections	10055
R_{int}	0.060
Reflections with $I > 2\sigma(I)$	7931
Reflections used in refinement	10053
Parameters refined; restraints	783; 165
Final $R(F)$ [$I > 2\sigma(I)$ reflections]	0.0533
$wR(F^2)$ (all data)	0.1380
Weights: $w = [\sigma^2(F_o^2) + (0.0559P)^2 + 4.8510P]^{-1}$ where $P = (F_o^2 + 2F_c^2)/3$	
Goodness of fit	1.051
Secondary extinction coefficient	0.0022(5)
Final Δ_{max}/σ	0.001
$\Delta\rho$ (max; min) [e Å^{-3}]	0.97; -0.65
$\sigma(d_{(C-C)})$ [Å]	0.005 – 0.008

214

The structure of $[Zn_2(C_{82}H_{90}N_6O_8)\ (CF_3SO_3)_2(H_2O)_4^{2+}]\cdot 2\ (CF_3SO_3^-)\cdot 4CH_3CN\cdot 2Et_2O$ has been solved and refined successfully. The cation sits across a crystallographic centre of inversion, while the asymmetric unit contains, in addition, one uncoordinated triflate anion in a general position, two MeCN molecules and one molecule of diethyl ether. The coordinated triflate anion is disordered. Two sets of overlapping positions were defined for the F-, O- and C-atoms of the disordered triflate anion and the site occupation factor of the major conformation refined to 0.606(8). Similarity restraints were applied to the chemically equivalent bond lengths and angles involving all disordered atoms, as well as the F···F distances, while neighbouring atoms within and between each conformation of the disordered trfilate anion were restrained to have similar and pseudo-isotropic atomic displacement parameters. The non-hydrogen atoms were refined anisotropically. The water ligand H-atoms were placed in the positions indicated by a difference electron density map and their positions were allowed to refine together with individual isotropic displacement parameters, while restraining the lengths of the O–H bonds. All remaining H-atoms were placed in geometrically calculated positions and refined using a riding model where each H-atom was assigned a fixed isotropic displacement parameter with a value equal to $1.2U_{eq}$ of its parent C-atom ($1.5U_{eq}$ for the methyl groups). Refinement of the structure was carried out on F^2 using full-matrix least-squares procedures, which minimised the function $Sw(F_o^2 - F_c^2)^2$. The weighting scheme was based on counting statistics and included a factor to downweight the intense reflections. Plots of $Sw(F_o^2 - F_c^2)^2$ versus $F_c / F_c(\max)$ and resolution showed no unusual trends. A correction for secondary extinction was applied. Two reflections, whose intensities were considered to be extreme outliers, were omitted from the final refinement.

At each Zn-atom in the cation, one of the coordinated water molecules forms hydrogen bonds with an ether O-atom in the terpy ligand (almost on the opposite side of the ligand) and with an uncoordinated triflate anion. The other coordinated water molecule forms hydrogen bonds with the same uncoordinated triflate anion and the ether O-atom of a neighbouring diethyl ether molecule.

Table 5.6 Crystallographic Data for **218**.

Crystallised from	$CHCl_3$ / Et_2O
Empirical formula	$C_{45}H_{39}N_3O_2 \cdot CHCl_3$
Formula weight [g mol^{-1}]	773.20
Crystal colour, habit	colourless, plate
Crystal dimensions [mm]	0.07 × 0.22 × 0.25
Temperature [K]	160 (1)
Crystal system	triclinic
Space group	$P\bar{1}$ (#2)
Z	2
Reflections for cell determination	6738
2θ range for cell determination [°]	4 – 50
Unit cell parameters a [Å] = 9.9817(3)	α [°] = 68.288(2)
b [Å] = 14.8308(4)	β [°] = 71.494(2)
c [Å] = 15.1499(5)	γ [°] = 72.658(2)
V [Å^3]	1933.9(1)
F(000)	808
D_x [g cm^{-3}]	1.328
μ(Mo $K\alpha$) [mm^{-1}]	0.280
Scan type	ω
$2\theta_{(max)}$ [°]	50
Total reflections measured	28476
Symmetry independent reflections	6825
R_{int}	0.078
Reflections with $I > 2\sigma(I)$	4619
Reflections used in refinement	6825
Parameters refined; restraints	531; 51
Final $R(F)$ [$I>2\sigma(I)$ reflections]	0.0774
$wR(F^2)$ (all data)	0.2484
Weights: $w = [\sigma^2(F_o^2) + (0.0784P)^2 + 4.5774P]^{-1}$ where $P = (F_o^2 + 2F_c^2)/3$	
Goodness of fit	1.106
Secondary extinction coefficient	0.020(3)
Final Δ_{max}/σ	0.001
$\Delta\rho$ (max; min) [e Å^{-3}]	0.32; -0.27
$\sigma(d_{(C-C)})$ [Å]	0.006 – 0.007

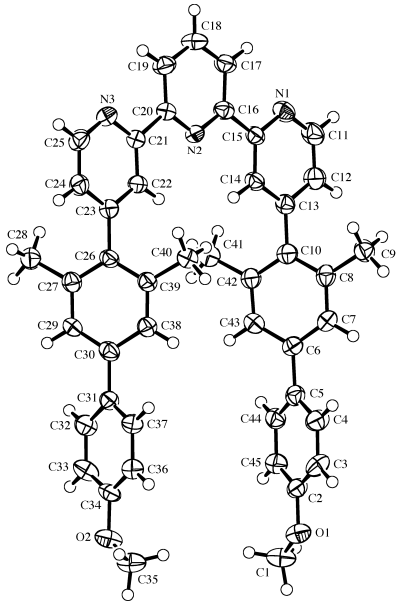

Figure 5.29 ORTEP diagram of 4,4”-bis-(4-(4-methoxyphenyl)-2,6-dimethyl-phenyl)-2,2’:6’,2”-terpyridine **218**.

218

The structure of $C_{45}H_{39}N_3O_2 \cdot CHCl_3$ has been solved and refined successfully. The asymmetric unit contains one terpyridine molecule and one molecule of chloroform which is disordered by inversion through a point approximately coincident with its centre of gravity. Two sets of positions were defined for all atoms of the chloroform molecule. The site occupation factor of the major conformation refined to 0.59(1). All of the C–Cl bond lengths were restrained to a common value. Furthermore, neighbouring atoms within and between each conformation of the disordered groups were restrained to have similar atomic displacement parameters. The non-hydrogen atoms were refined anisotropically. All of the H-atoms were placed in geometrically calculated positions and refined using a riding model where each H-atom was assigned a fixed isotropic displacement parameter with a value equal to 1.2Ueq of its parent atom (1.5Ueq for the methyl groups). The pyridyl N-atoms lie in an *anti*-configuration.

Table 5.7 Crystallographic Data for **224a**.

Crystallised from	MeCN / MTBE
Empirical formula	$C_{66}H_{56}Br_2F_{12}N_{10}O_2P_2Ru$
Formula weight [g mol^{-1}]	1571.97
Crystal colour, habit	red, tablet
Crystal dimensions [mm]	0.07 × 0.30 × 0.32
Temperature [K]	160(1)
Crystal system	monoclinic
Space group	$P2_1/c$ (#14)
Z	4
Reflections for cell determination	245834
2θ range for cell determination [°]	4–55
Unit cell parameters a [Å] = 10.1057(1)	α [°] = 90
b [Å] = 32.1920(4)	β [°] = 95.4410(6)
c [Å] = 22.2445(3)	γ [°] = 90
V [Å^3]	7204.0(2)
F(000)	3160
D_x [g cm^{-3}]	1.449
μ(Mo $K\alpha$) [mm^{-1}]	1.454
Scan type	ϕ and ω
$2\theta_{(max)}$ [°]	55
Transmission factors (min; max)	0.741; 0.917
Total reflections measured	133229
Symmetry independent reflections	16485
R_{int}	0.080
Reflections with $I > 2\sigma(I)$	11933
Reflections used in refinement	16485
Parameters refined; restraints	937; 2441
Final $R(F)$ [$I > 2\sigma(I)$ reflections]	0.0668
$wR(F^2)$ (all data)	0.1752
Weights: $w = [\sigma^2(F_o^2) + (0.08P)^2 + 11.881P]^{-1}$ where $P = (F_o^2 + 2F_c^2)/3$	
Goodness of fit	1.049
Final Δ_{max}/σ	0.001
$\Delta\rho$ (max; min) [e Å^{-3}]	0.80; -0.64
$\sigma(d_{(C-C)})$ [Å]	0.006–0.01

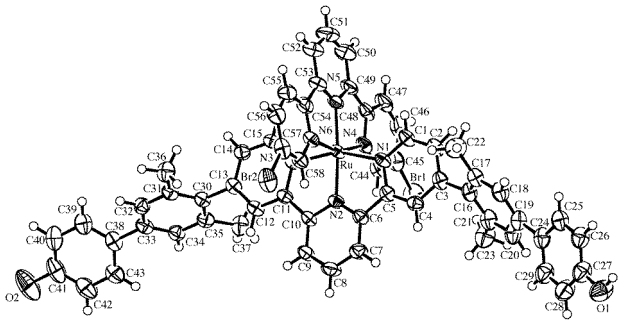

Figure 5.30 ORTEP diagram of Ru[(4,4''-bis-(2,6-dimethyl-(4-hydroxyphenyl)-phenyl)-2,2':6',2''-terpyridine)(5,5''-dibromo-2,2':6',2''-terpyridine)][PF_6]$_2$ **224a**.

224a

The asymmetric unit in the structure of [Ru($C_{15}H_9Br_2N_3$)($C_{43}H_{35}N_3O_2$)$^{2+}$] ·2PF_6^- ·4CH_3CN contains one cation, two highly disordered anions, with one of these distributed over two partially occupied sites, and an estimated four MeCN molecules. The disorder of most of the solvent molecules could not be modeled adequately, so the contribution of the solvent molecule to the intensity data was removed by using the *SQUEEZE*[6] routine of the *PLATON*[7] program. Omission of the solvent molecule leaves two cavities of 857 Å^3 per unit cell. The number of electrons contributing to each void in the structure was calculated by the *SQUEEZE* routine to be approximately 138 e, although this may be an underestimate. This corresponds with 6.25 MeCN molecules per cavity or 3.125 per asymmetric unit. One of the sites for a MeCN molecule overlapped with that of a partially occupied disordered PF_6^- anion, so its contribution could not be removed by the *SQUEEZE* procedure. This MeCN molecule was modelled and its site occupation factor refined to 0.605(4), which brings the total number of MeCN molecules per asymmetric unit to 3.73. Therefore, it is estimated that there are in reality four MeCN molecules per asymmetric unit and this was used in the subsequent calculation of the empirical formula, formula weight, density, linear absorption coefficient and *F*(000).

The two PF_6^- anions in the asymmetric unit are disordered, with one of these distributed over two partially occupied and slightly overlapping sites. Two orientations were defined for four of the F-atoms of one anion and refinement of the site occupation factor led to a value of 0.63(2) for the major orientation. Two sites that are displaced quite significantly from one another were defined for all atoms of the second anion and refinement of the site occupation factor led to a value of 0.605(4) for the most occupied site. The F-atoms of the most occupied site were then split further into two positions each and their site occupation factors refined to 0.302(2). The lesser occupied PF_6^- site is alternately occupied by a MeCN molecule. The P–F and F···F distances within each symmetry-independent site for the anions were restrained, so as to maintain octahedral geometry and uniform P–F bond lengths, while neighbouring atoms within and between each disordered orientation were restrained to have similar and pseudo isotropic atomic displacement parameters. A similar suite of restraints was applied to the atoms of the MeCN molecule that shares its site with a PF_6^- anion. Additional disorder may be present within the sites of each anion, but no attempts were made to model such disorder further.

5.5 References

(1) Cromwell, P.; Beltrami, E.; Rampichini, M. *Math. Intelligencer* **1998**, *20*, 53-62.

(2) Naynes, O. *Am. Math. Monthly* **1993**, *100*, 786-789.

(3) Tait, P. G. *Trans. R. Soc. Edinburgh* **1876**.

(4) Aravind, P. K. In *Potentiality, Entanglement and Passion-at-a-Distance*; Cohen, R. S., al., e., Eds.; Kluwer Academinc: London, 1997, pp 53-59.

(5) Austin, S. M.; Bertsch, G. F. *Sci. Am.* **1995**, *272*, 62-67.

(6) Zhukov, M.; al., e. *Phys. Lett.* **1993**, *231*, 151-199.

(7) Ruzmaikin, A.; Akhmetiev, P. *Phys. Plasmas* **1994**, *1*, 331-336.

(8) Baez, J.; Munian, J. P. *Gauge Fields, Knots and Gravity*; World Scientific, 1994; Vol. 4.

(9) Siegel, J. S. *Science* **2004**, *304*, 1256-1258.

(10) Schalley, C. A. *Angew. Chem. Int. Ed.* **2004**, *43*, 4399-4401.

(11) Frisch, H. L.; Wasserman, E. *J. Amer. Chem. Soc.* **1961**, *83*, 3789-3795.

(12) Wasserman, E. *Sci. Am.* **1962**, *207*, 94-102.

(13) van Gulick, N. *N. J. Chem.* **1993**, *17*, 619-625.

(14) Walba, D. M. *Tetrahedron* **1985**, *41*, 3161-3212.

(15) Dietrich-Buchecker, C. O.; Sauvage, J.-P. In *Bioorganic Chemistry Frontiers*; Dugas, H., Ed.; Springer-Verlag: Berlin, 1991; Vol. 2, pp 195-248.

(16) Walba, D. M.; Homan, T. C.; Richards, R. M.; Haltiwanger, R. C. *N. J. Chem.* **1993**, *17*, 661-681.

(17) Liang, C.; Mislow, K. *J. Math. Chem.* **1994**, *16*, 27-35.

(18) Liang, C.; Mislow, K. *J. Math. Chem.* **1995**, *18*, 1-24.

(19) Lehn, J.-M. *Angew. Chem. Int. Ed., Eng.* **1988**, *27*, 89-112.

(20) *Templated Organic Synthesis*; Diederich, F.; Stang, P. J., Eds.; Wiley-VCH: Weinheim, 2000, p 410.

(21) Chambron, J.-C.; Dietrich-Buchecker, C.; Sauvage, J.-P. *Top. Curr. Chem.* **1993**, *165*, 131-162.

(22) Amabilino, D. B.; Stoddart, J. F. *Chem. Rev.* **1995**, *95*, 2725-2828.

(23) *Molecular Catenanes, Rotaxanes, and Knots: A journey through the world of molecular topology*; Sauvage, J.-P.; Dietrich-Buchecker, C., Eds.; Wiley-VCH: Weinheim, 1999, p 368.

(24) As it is physically impossible for a three-dimensional Borromean link to consist of perfectly circular rings, stonecarvers often altered the crossing pattern, presumably for aesthetical purposes. See the following reference for a mathematical proof.

(25) Lindström, B.; Zetterström, H.-O. *Am. Math. Monthly* **1991**, *98*, 340-341.

(26) Fox, R. H. In *Topology of 3-manifolds and Related Topics*; Fort, M. K., Ed.; Prentice-Hall, Inc.: 1962, pp 120-167.

(27) Armstrong, K. *A History of God*; Vintage: London, 1993, p 511.

(28) Reeves, M.; Hirsch-Reich, B. *The Figurae of Joachim of Fiore*; Clarendon Press: Oxford, 1972, p 376.

(29) Didron, A. N. *Christian Iconography: the History of Christian Art in the Middle Ages*; Frederick Ungar: New York, 1968.

(30) Davidson, H. R. E. *Gods and Myths of Northern Europe*; Penguin Books: Baltimore, 1964, p 256.

(31) Sturluson, S. *Skáldskaparmál*; University Press of Southern Denmark: Copenhagen, 1987; Vol. 4, p 210.

(32) Cromwell, P. *Math. Intelligencer* **1995**, 3-4.

(33) Brunn, H. *Sitzung-berichte der Bayerischer Akad. Wiss. Math-Phys. Klasse 22* **1892**, 77-99.

(34) Tauber, S. J. *J. Res. Natl. Bur. Stand. A* **1963**, *67A*, 591-599.

(35) Mao, C.; Sun, W.; Seeman, N. C. *Nature* **1997**, *386*, 137-138.

(36) Seeman, N. C. *Angew. Chem. Int. Ed.* **1998**, *37*, 3220-3238.

(37) Seeman, N. C. In *Molecular Catenanes, Rotaxane, and Knots*; Dietrich-Buchecker, C. O., Sauvage, J.-P., Eds.; Wiley-VCH: Weinheim, 1999, pp 323-356.

(38) Loren, J. C.; Yoshizawa, M.; Haldimann, R. F.; Linden, A.; Siegel, J. S. *Angew. Chem. Int. Ed.* **2003**, *42*, 5702-5705.

(39) In one of his many musings upon chemical templating, Darryl Busch published a similar strategy based on Stoddart's pi-pi and a hydrogen bonding template. See the following reference.

(40) Hubin, T. J.; Kolchinski, A. G.; Vance, A. L.; Busch, D. H. *Adv. Supramolec. Chem.* **1999**, *5*, 237-357.

(41) Constable, E. C. *Adv. Inorg. Chem. Radiochem.* **1987**, *30*, 69-121.

(42) Howard, S. T. *J. Amer. Chem. Soc.* **1996**, *118*, 10269-10274.

(43) Loren, J. C., University of California, San Diego, 2004.

(44) Lindsey, J. S. *N. J. Chem.* **1991**, *15*, 153-180.

(45) Whitesides, G. M.; Mathias, J. P.; Seeta, C. T. *Science* **1991**, *254*, 1312-1319.

(46) Lehn, J.-M. *Angew. Chem. Int. Ed., Eng.* **1990**, *29*, 1304-1319.

(47) Chichak, K. S.; Cantrill, S. J.; Pease, A. R.; Chiu, S.-H.; Cave, G. W. V.; Atwood, J. L.; Stoddart, J. F. *Science* **2004**, *304*, 1308-1312.

(48) Huc, I.; Lehn, J.-M. *Proc. Nat. Ac. Sci.* **1997**, *94*, 2106-2110.

(49) Klekota, B.; Hammond, M. H.; Miller, B. L. *Tetrahedron Lett.* **1997**, *38*, 8639-8642.

(50) Polyakov, V. A.; Nelen, M. I.; Nazarpack-Kandlousy, N.; Ryabov, A. D.; Eliseev, A. V. *J. Phys. Org. Chem.* **1999**, *12*, 357-363.

(51) Cousins, G. R. L.; Poulson, S. A.; Sanders, J. K. M. *Chem. Comm.* **1999**, 1575-1576.

(52) Following the nomenclature of catenanes, Stoddart has proposed the term Borromeate to indicate Borromean ring compounds containing metals and the term Borromeand to indicate the metal-free compound.

(53) Peters, A.; Chichak, K. S.; Cantrill, S. J.; Stoddart, J. F. *Chem. Comm.* **2005**, 3394-3396.

(54) Pentecost, C. D.; Peters, A. J.; Chichak, K. S.; Cave, G. W. V.; Cantrill, S. J.; Stoddart, J. F. *Angew. Chem. Int. Ed.* **2006**, *45*, 4099-4104.

(55) Dobrazanska, L.; Raubenheimer, H.; J., B. L. *Chem. Comm.* **2005**, 5050-5052.

(56) Carlucci, L.; Ciani, G.; Proserpio, D. M.; Rizzato, S. *Cryst. Eng. Comm.* **2003**, *5*, 190-199.

(57) Carlucci, L.; Ciani, G.; Proserpio, D. M.; Rizzato, S. *Coord. Chem. Rev.* **2003**, *246*, 247-.

(58) Tong, M.-L.; Chen, X.-M.; Ye, B.-H.; Ji, L.-N. *Angew. Chem. Int. Ed.* **1999**, *28*, 2237-2240.

(59) Leznoff, D. B.; Xue, B.-Y.; Batchelor, R. J.; Einstein, F. W. B.; Patrick, B. O. *Inorg. Chem.* **2001**, *40*, 6026-6034.

(60) Muthu, S.; Yip, J. H. K.; J., V. J. *J. Chem. Soc., Dalton Trans* **2002**, 4561-4568.

(61) Suh, M. P. S.; Choi, H. J.; So, S. M.; Kim, B. M. *Inorg. Chem.* **2003**, *42*, 676-678.

(62) Metrangolo, P.; Neukirch, H.; Pilati, T.; Resnati, G. *Acc. Chem. Res.* **2005**, *38*, 386.

(63) Liantonio, R.; Metrangolo, P.; Pilati, T.; Resnati, G. *Crystal Growth & Design* **2003**, *3*, 355-361.

(64) Liantonio, R.; Metrangolo, P.; Meyer, F.; Pilati, T.; Navarrini, W.; Resnati, G. *Chem. Comm.* **2006**, 1819-1821.

(65) Liang, C.; Mislow, K. *J. Amer. Chem. Soc.* **1994**, *116*, 11189-11190.

(66) Liang, C.; Mislow, K. *J. Amer. Chem. Soc.* **1995**, *117*, 4201-4213.

(67) Hamann, C.; Kern, J.-M.; Sauvage, J.-P. *Inorg. Chem.* **2003**, *42*, 1877-1883.

(68) McMillin, D. R.; Moore, J. J. *Coord. Chem. Rev.* **2002**, *229*, 113-121.

(69) Lowe, G.; Vilaivan, T. *J. Chem. Res., S.* **1996**, 386-387.

(70) Morgan, G. T.; Burstall, F. H. *J. Chem. Soc.* **1934**, 1498.

(71) Under ESI-MS conditions, weakly coordinating anions, such as hexafluorophosphate anions, are often removed sequentially, giving [MX3-X]+, [MX2-2X]2+, [MX-3X]3+, and [M-4X]4+ in the case of a tetracation. Typically, the peak corresponding to the naked cation is the strongest and higher peaks decreasing in intensity.}

(72) Tor, Y. *Synlett* **2002**, *7*, 1043-1054.

(73) Gottlieb, H. E.; Kotlyar, V.; Nudelman, A. *J. Org. Chem.* **1997**, *62*, 7512-7515.

(74) Evans, I. P.; Spencer, A.; Wilkinson, G. *J. Chem. Soc., Dalton Trans* **1973**, 204-209.

(75) Loren, J. C.; Siegel, J. S. *Angew. Chem. Int. Ed.* **2001**, *40*, 754-757.

(76) Dallaire, C.; Brook, M. *Organomet.* **1993**, *12*, 2332-2338.

(77) Sullivan, B. P.; Calvert, J. M.; Meyer, T. J. *Inorg. Chem.* **1980**, *19*, 1404-1407.

(78) Schubert, U. S.; Eschbaumer, C.; Hochwimmer, G. *Synthesis* **1999**, 779-782.

(79) Grave, C.; Lentz, D.; Schäfer, A.; Samori, P.; Rabe, J. P.; Franke, P.; Schlüter, A. D. *J. Amer. Chem. Soc.* **2003**, *125*, 6907-6918.

(80) McDermott, J. X.; White, J. F.; Whitesides, G. M. *J. Amer. Chem. Soc.* **1976**, *98*, 6521-6528.

(81) Colasson, B.; Dietrich-Buchecker, C.; Sauvage, J.-P. *Synlett* **2002**, *2*, 271-272.

(82) Hooft, R. *KappaCCD Collect Software* Delft, The Netherlands, 1999, p Nonius BV.

(83) Otwinowski, Z.; Minor, W. In *Methods in Crystallography*; Carter, C. W., Sweet, R. M., Eds.; Academic Press: New York, 1997; Vol. 276, pp 307-326.

(84) Altomare, A.; Cascarano, G.; Giacovazza, C.; Guagliardi, A.; Burla, M. C.; Polidori, G.; Carmalli, M. *Journal of Applied Crystallography* **1994**, *27*, 435.

(85) Maslen, E. N.; Fox, A. G.; O'Keefe, M. A. In *International Tables for Crystallography*; Wilson, A. J. C., Ed.; Kluwer Academic Publishers: Dordrecht, 1992; Vol. C, pp 477-486.

(86) Stewart, R. F.; Davidson, E. R.; Simpson, W. T. *J. Chem. Phys.* **1965**, *42*, 3175-3187.

(87) Ibers, J. A.; Hamilton, W. C. *Acta Chrystallographica* **1964**, *17*, 781-782.

(88) Creagh, D. C.; Auley, W. J. In *International Tables for Crystallography*; Wilson, A. J. C., Ed.; Kluwer Academic Publishers: Dordrecht, 1992; Vol. C, pp 219-222.

(89) Creagh, D. C.; Hubbell, J. H. In *International Tables for Crystallography*; Wilson, A. J. C., Ed.; Kluwer Academic Publishers: Dordrecht, 1992; Vol. C, pp 200-206.

(90) Sheldrick, G. M.; University of Göttingen, Germany: Göttingen, 1997.

(91) All measurements were made at the SLS synchrotron (beamline PX) using radiation of wavelength ª = 0.800 Å and a MarResearch 225 detector 80 mm from the crystal.